UNIVERSITY OF LONDON

IMPERIAL COLLEGE OF SCIENCE AND TECHNOLOGY

PHYSICS DEPARTMENT

APPLIED OPTICS SECTION

Studies on the Neodymium Glass Laser as a Coherent Pulsed Light Source

by

IAN NORMAN ROSS M.A.

Thesis submitted for the Ph.D. degree of the University of London

1974

CONTENTS

Abstract

Chapter 1 Introductory Remarks

1.1 Introduction 1.1

1.2 Source Requirements 1.3

1.3 Aims 1.6

1.4 Synopsis 1.6

Chapter 2 Review of Pulsed Lasers

2.1 Introduction 2.1

2.2 Important parameters of laser operation 2.2

2.3 Ruby and Neodymium lasers 2.5

2.4 Coherence 2.24

2.5 Polarization effects 2.27

2.6 Symmary of neodymium laser 2.28

2.7 Dye lasers 2.28

Chapter 3 Analysis of Nd:glass laser

3.1 Abstract 3.1

3.2 Choice of Q-switch 3.3

3.3 Operation of rotating mirror Q-switch 3.14

3.4 Pumping efficiency and inversion distribution 3.31

3.5 System design 3.38

Chapter 4 Experimental Appraisal of Nd:glass laser

4.1 Introduction 4.1

4.2 Threshold investigations 4.2

4.3 Distribution of inversion 4.16

4.4 Efficiency curve 4.18

4.5 Time-integrated measurements 4.21

4.6 Time-resolved measurements 4.24

Chapter 5 Coherence

5.1 Abstract 5.1

5.2 Coherence theory 5.2

5.3 Resonator theory 5.6

5.4 Examples 5.14

5.5 Coherence measurement 5.29

5.6 Coherence control 5.54

5.7 Coherence improvement of Nd:glass laser 5.82

Chapter 6 Second Harmonic Generation

6.1 Abstract 6.1

6.2 Theory of Second Harmonic Generation 6.3

6.3 Experimental investigations 6.24

Chapter 7 Conclusions

Appendix I

Appendix II

Appendix III

Appendix IV

Appendix V

Appendix VI

Bibliography

Acknowledgements

ABSTRACT

This thesis assesses the neodymium in glass laser as a possible source for applications in optical measurement. It presents those aspects of a programme of research in the use of laser sources in optical measurement techniques (such as holography) which relate to this type of laser.

A comparative assessment of possible laser media for this application shows the advantages of Nd:glass and indicates the disadvantages which must be overcome.

The principal shortcoming relates to the coherence of the laser output. This topic is treated at some length with particular reference to the theory of laser resonators. A holographic technique, particularly useful for measuring pulsed laser coherence functions, is described, with several experimental examples. A critical discussion of methods of controlling laser coherence is given, followed by a description of the application of proposed techniques to the Nd:glass laser. Experimental evidence is again presented.

Considerable attention has also been paid to other aspects of laser design. The rotating mirror has been selected as Q-switch and some theory and computation of its operation are given. An integrated laser optimisation procedure is presented. Inorder to apply this to Nd:glass a computation of the optical pumping of this material was carried out.

Experimental measurements have been made on the Nd:glass laser to determine parameters required in the theory and to describe the performance of the laser. One or two novel aspects of laser diagnostic technique are discussed.

For most applications the Nd:glass laser needs a nonlinear process for transfering energy from its output wavelength at 1060nm to a visible wavelength. A theory of second harmonic generation is given and some experiments to improve the second harmonic generation from the Nd:glass laser are described.

CHAPTER 1

Introductory Remarks

1.1	Introduction	The need for pulsed light sources, and lasers in particular.	1.1
1.2	Source requirements	Choice of a specification for a useful pulsed laser light source.	1.3
1.3	Aims of the work reported in this thesis		1.6
1.4	Synopsis of the thesis.		1.6

1.1 Introduction

Short duration light sources have long been used to monitor moving or changing events. Bulk transport problems and the propagation of disturbances form the majority of these events, and there follows a short list of these which is intended just to give an idea of the range of application.

Bulk transport problems are those in which the interest lies in the movement of mass or in the state of mass as it moves. This mass might be a projectile or its exploded parts (Lankford 1970, Swift 1972), or it might be droplets in a raincloud (Pavitt et al 1970) or charged particles in a bubble chamber. (Withrington 1968, Welford 1966)

Propagation of disturbances involves on the other hand, the changes in the properties of matter produced by certain phenomena; these include shock waves, deformations of objects due to stress, shock, vibration, and temperature variations. Into this category, for example, comes the study of high speed motion in wind tunnels (North 1966, Beamish 1969), plasma diagnostics (Jahoda 1971, Alcock 1971, Smigielski et al 1970), tests on engineering components (Surget 1970, Aprahamian et al 1971), and combustion in fuel engines.

While the above problems need a light source of short duration, there are also applications which require the property which goes with short duration: high intensity. This further category includes ranging and many types of scattering experiment in which there are very high attenuations between source and detector and in which the observed mechanism may be highly intensity dependent.

The need for sufficient intensity is one of many conditions on the source arising out of the particular monitoring techniques used. Such techniques include interferometry, spectroscopy, holography and absorption and scattering measurements, and these impose restrictions on the spectral width, wavelength and optical waveform, as well as the pulse length and intensity of the light output.

With the development of the pulsed laser has come an alternative source for many of the above applications. It can be asserted that, in general, the more stringent the restrictions on the form of the output, the more favourably the pulsed laser compares with conventional incoherent sources. Table 1 gives a comparison between the output from a typical high intensity incoherent source and a simple Q-switched ruby laser pumped by such a source. The overall laser energy efficiency is taken to be only 0.1%, but it can be seen that for most of the figures quoted it has a substantial advantage. Take for example the range finding application in which it is important, in order th achieve high signal to noise in detection, to confine the output to as small as possible a solid angle. The relevant parameter is then the power per steradian, and the laser typically gives a factor of 5×10^7 improvement over the flash lamp. If the application is holography, in which a high coherence is necessary, then the energy output per steradian per Angstrom indicates the usefulness of the source. In this case a factor of 10^7 can be gained by using the laser, and indeed the problems of using conventional sources for such applications are so great that it is not practicable to do so.

Pulsed holography is just an example of a considerable class of applications which place such stringent requirements on the source that only lasers can be used. Requirements for power densities greater than a megawatt/cm^2, pulses of less than 1 μs, or high coherence outputs come into this category, which extends up to the present limits of laser operation, that is to say, up to 10^{12} W/cm^2 down to picoseconds and through to complete coherence.

So far the light source has been considered as a monitoring beam. It also can be used to initiate or create events, both high speed and static. In this more active role it can still be used to monitor what is happening. Many of these events also

come into the latter category above; that in which a laser must be used. The initiation of a spark (Pendleton and Guenther 1965) or creation of a high temperature plasma (DeMichelis 1969, 1970) generally requires power densities greater than 10^9 W/cm^2 since it is only then that the gas can be ionised or the material vaporised. Furthermore it is often important that the event be timed very precisely and it is, in consequence, important that the pulse be very short. The field of non-linear optical phenomena is an important one, supplying as it does valuable information on the atomic and molecular structure of matter, and is by its very nature one requiring high power densities either to reach a threshold or to obtain a detectable signal. This field includes Raman (Eckhardt 1966), Brillouin (Aleksandrov et al 1966) and Rayleigh scattering (Akhmanov 1968) (or photon-phonon and photon-electron interactions) optical harmonic generation, parametric oscillation and other multiphoton interactions (Terhune and Maker 1966), self-focussing, (Kelley 1965) optical breakdown (DeMichelis 1969). Of the scattering experiments the minimum power density so far required to get a substantial effect has been 1 MW/cm^2 for stimulated Raman scattering in benzene (Aleksandrov 1966). Efficient second harmonic generation requires at least 1 MW/cm^2 while the threshold for self focussing is 50 MW/cm^2 in benzene (Wang 1966). It has to be remembered that these phenomena generally also require a spectrally narrow source or one with low divergence.

To round off this brief look at the various uses for pulsed sources, and lasers in particular, it is worth noting that in many circumstances in which a continuous light source is used a singly or repetitively pulsed source might even be an improvement by making the measurement more quickly and more efficiently, and by relaxing the need for stability. Alignment, static holography and interferometry, along with many others, might well be considered with profit.

1.2 Source Requirements

All applications of pulsed sources impose requirements on the output from the source, and the above discussion serves to indicate the significance of some of them. Before proceeding with any development of lasers it is necessary to specify the requirements placed on the light source by the application.

The relevant properties can be listed as follows:-

a) Pulse length.

b) Energy and Power.

c) Coherence: transverse coherence (angular distribution)
temporal coherence (spectral distribution)

d) Output wavelength

e) Efficiency: size and weight.

f) Cost

The holography of diffusely reflecting objects places the most stringent requirements on the source, and may require pulse lengths measured in picoseconds, coherence lengths of many meters, complete transverse coherence, and many joules of energy (but not of course all at the same time).

a) For our purposes we will confine ourselves to the pulse length limitations imposed by normal laser Q-switching methods. These reduce the pulse length to, at best, the time for light to make a few transits of the laser cavity and for typical resonator lengths this is of the order of several nanoseconds. An object moving at 10km/s moves less than 100μm in this time and can thus be photographed without appreciable blurring. An object moving at 100m/s, on the other hand, moves less than 1μm (about a wavelength) and a reflection hologram is now possible.

b) A low-to-medium energy requirement is chosen. An output measured in fractions of a joule is quite sufficient for the majority of applications. Take, for example, the case in which a recording is made on slow holographic plates which may have a sensitivity of perhaps $100mJ/m^2$ (Agfa-Gaevert 8E75). A laser emitting 100mJ is capable of exposing a square centimeter when there is an attenuation by a factor as high as 10,000. Generally the attenuation is less than this and larger holograms can be recorded.

Whereas the energy is the important quantity for holography, the power must be considered if it is the intention to use a non-linear process, the efficiency of which is power dependent. With the neodymium glass laser, second harmonic generation must be used to convert at least 1% of the fundamental at a wavelength of 1.06μm to its second harmonic at a wavelength of 0.53μm in the visible. The minimum power required to achieve this efficiency is in the region of a megawatt and since this is achieved by

a pulse of 30mJ in 30ns, the energy requirement is the more difficult to meet.

c) The second harmonic efficiency also depends upon quantities such as the spectral distribution, and the transverse distribution of the output of the laser, all of which come under the term 'coherence' as applied to the source. This is not surprising in view of the coherent nature of the process for achieving optimum second harmonic generation. The dependence is complex and more detailed comment will be found in Chapter 6. The qualitative conclusion however is that both the efficiency and the reproducibility of the process increase with an increase in the coherence of the source. This is not to say that high coherence is necessarily essential since a reasonable conversion efficiency can usually be obtained without it. The overall efficiency of laser plus second harmonic generator and the reproducibility are however the important quantities and they are generally greatest when the laser has fairly high coherence. In the laser system chosen this coherence requirement is not as difficult to meet as that imposed by the holography of diffusely reflecting objects.

The great majority of useful applications of pulsed holography, and interferometry, do not need coherence lengths greater than 50cm, nor do they require complete transverse coherence over the entire wavefront. The degree of transverse coherence required for holography is one giving a visibility of the fringes forming the hologram which leads to an adequate holographic reconstruction efficiency. That we do not need complete transverse coherence from the source is significant since the efficiency of the laser is then higher. This type of output may not of course be suitable if say a maximum focussed power density is wanted.

d) The question of choosing a desirable output wavelength is linked to the type of detection system used. Visual observation and recording on present day photographic emulsion have peak sensitivity in the green. Our chosen laser system, that of Neodymium-doped glass, emits at 1.06μm and by virtue of the process of second harmonic generation this can be converted to a wavelength of 0.53μm in the green.

e) A further requirement is the efficiency. Up to this point it has merely been stated that it should be sufficient to supply enough output energy. We might however achieve this, but have to put up with a very large power supply. A maximum efficiency is therefore very desirable, since the size and cost of the system is then a minimum.

The importance of achieving a minimum size and cost is considered to be very high, particularly for applications in hostile environments and in competition with other light sources, and the questions of efficiency, size and cost will always be considered when choosing between possible alternative modifications of the laser. Of possible ways of improving the coherence, for example, a bias will be shown towards those which by their simplicity tend to take up less space and are cheaper. Similarly, any proposal which can improve the laser or maintain its performance and at the same time relax some of the specifications on properties like the optical quality of the rod, the pumping distribution and the temperature control, will receive favourable considera tion.

1.3 AIMS

Pulsed laser systems in present use and development tend to be combinations of high power, relative simplicity, and lack of coherence or low power, high complexity and high coherence. This last combination of high complexity and high coherence do not necessarily go together as has often been the underlying assumption; moreover the design of systems of minimum size and cost for applications such as those considered here, in which relatively low power is required, has not been fully explored. We attempt to make some progress in these fields as well as investigating the potential of the Neodymium:glass laser system, in comparison with the other possible laser sources, for meeting the above requirements.

1.4 SYNOPSIS

We have attempted to show some of the reasons for choosing a pulsed laser as a light source. The chosen laser system has been defined with an indication of its possibilities. Little has been said about other possible types of laser as it is intended to deal more fully with them in Chapter 2. It is the object of this thesis not only to assess the chosen system in the context of certain optical applications but also to discover if, for these applications, it is better than the alternatives.

In Chapter 2, a review of the properties of the other major pulsed laser systems is given, these being the ruby laser, the neodymium:crystal lasers, pulsed gas lasers and dye lasers. All these have properties which entitle them to compete for use in

the applications indicated above. Ruby has had the most development and is most widely used. Neodymium:crystal lasers require very little power to drive them. Pulsed gas lasers have an intrinsically high coherence and can be controlled readily, while dye lasers are undoubtedly the most flexible. A section is devoted to the properties of ruby so that a comparison of the relative merits of them all may be made. This comparison is largely devoted to the two which appear most suitable, namely neodymium: glass and ruby, although the tremendous potential of dyes must be remembered for possible lasers of the future. The conclusions to be drawn as this stage are that ruby is at present superior for applications requiring a high coherence, and that the second harmonic stage makes the neodymium:glass system more complex and somewhat unreliable. We attempt to investigate in later chapters whether or not these inadequacies can be corrected.

Within the framework of the type of laser that has been chosen, there is still a considerable measure of choice as to some of the parameters not as yet defined. Analysis of all systems with all geometries is not possible, so it is necessary to make an enlightened decision concerning some of them. Chapter three presents the arguments which govern the choice of Q-switch, pumping geometry and resonator geometry. To this aim, the chapter largely consists of three pieces of theory:-

a) A simplified pass-by-pass computer calculations of the output of a laser having a spinning mirror Q-switch. We show graphically some results for our neodymium: glass system.

b) the calculation of the distribution of the density of excited ions in a rod of neodymium:glass due to optical pumping.

c) The use of the results of b) to optimise a laser system. A practical example is taken to show how this optimisation works in practice.

The computation of a) above is for a spinning mirror Q-switch. A discussion on the relative merits of this and other types of Q-switch, along with some remarks to justify the particular one used, is also an important part of this chapter.

Having defined the initial system, the next step is a thorough investigation into its performance. Chapter 4 sets out in detail the steps taken to do this, and is divided into two parts:-

a) The first attempts to answer the question as to whether the system functions in the expected manner.

b) The second supplies information on properties of the system which cannot usefull be calculated. These properties include the variation of pumping inversion across the rod, optical distortions in the spinning prism, the losses and the coherence, both transverse and temporal.

The primary shortcoming of the neodymium:glass laser is its lack of coherence, especially that associated with its broad spectral width. Chapter 5 is concerned with the coherence problem. Possible methods are proposed for improving the coherence and from these we make a choice which is intended to be that most suited to our requirements. The following section of the chapter puts forward some theoretical analysis for our chosen methods, including a short computer programme to calculate the reflectivity curve for a resonant reflector. In the final section the results of the experimental realisation of these proposals are put forward, showing the measure of success we have had in producing a high coherence neodymium:glass laser.

The process of second harmonic generation, which is essential to the neodymium: glass laser in order that it can be useful optically, it treated in Chapter 6. A simplified form of analysis is given, which relates the efficiency to, for example, parameters such as the focussing of the infra-red and its coherence. Initial measurements on the second harmonic generation process are presented, the fundamental being supplied by the Nd-glass laser is its original unmodified form. Finally, we give the results of measurements on the second harmonic following several refinements to the system, and comment on the extent to which it now meets our requirements.

In Chapter 7, the final chapter, we sum up what, in various ways, has been achieved during the work presented here. In the light of this we can better appraise the Nd:glass laser in relation to ruby and other laser systems, particularly as to its usefulness for holography.

TABLE 1 Typical order of magnitude values of various output parameters of a Xenon flashtube and a simple ruby laser.

	INPUT	OUTPUT							
	ELECTRICAL ENERGY (JOULES)	RADIATED ENERGY (JOULES)	PEAK POWER (WATTS)	ENERGY PER STERADIAN (J/ster)	PEAK POWER PER STERADIAN (W/ster)	ENERGY PER WAVENUMBER (J/cm^{-1})	PEAK POWER PER WAVENUMBER (W/cm^{-1})	ENERGY PER STERADIAN PER WAVENUMBER ($J/ster/cm^{-1}$)	PEAK POWER PER STERADIAN PER WAVENUMBER ($W/ster/cm^{-1}$)
XENON FLASHTUBE	1000	500	10^{6}	10^{2}	2.10^{5}	$1.5x10^{-2}$	30	$3x10^{-3}$	6
RUBY LASER	1000	1	10^{8}	$4x10^{4}$	$5x10^{12}$	1	10^{8}	$5x10^{4}$	$5x10^{12}$

CHAPTER 2

Review of Pulsed Lasers

2.1 Introduction. Scope of this chapter. 2.1

Pulsed lasers that will be discussed and compared.

2.2 Parameters of laser operation which will be used as figures of merit. 2.2

2.2.1 Efficiency. 2.2

2.2.2 Gain. 2.5

2.2.3 Losses. 2.5

2.3 Discussion of these parameters in particular laser systems. 2.5

2.3.1 Ruby Laser 2.5

2.3.1.1 Threshold 2.6

2.3.1.2 Efficiency 2.7

2.3.1.3 Gain 2.10

2.3.1.4 Losses 2.12

2.3.2 Neodymium Lasers 2.14

2.3.2.1 Properties due to neodymium ion 2.14

2.3.2.2 Properties due to host material 2.17

2.4 Coherence. Description of coherence properties. 2.24

2.4.1 Ruby laser 2.24

2.4.1.1 Transverse coherence 2.26

2.4.1.2 Temporal coherence 2.26

2.4.2 Neodymium laser 2.27

2.4.2.1 Transverse coherence 2.27

2.4.2.2 Temporal coherence 2.27

2.5 Polarization Effects 2.27

2.6 Summary of Neodymium Laser Properties 2.28

2.7 Dye Lasers 2.28

2.7.1 Energy levels - similarities with neodymium. 2.29

2.7.2 Properties peculiar to dye lasers 2.29

2.7.2.1 Influence of triplet states 2.30

2.7.2.2 Effect of short decay time 2.31

2.7.2.3 Other properties 2.31

2.7.2.4 Overlap region of absorption-emission spectrum 2.32

2.7.3 Summary of dye laser properties 2.32

2.1 Introduction

The intention of this chapter is to present a comparative review of pulsed lasers. The properties and general characteristics will be given for those which are considered at the present time to have practical importance in applications requiring a coherent short pulse light source. The relevant advantages and disadvantages of the Nd: glass laser and these other lasers are discussed showing for what each is best suited and indicating their limitations. The Nd: glass system emerges from this analysis as a potential "best buy" if certain deficiencies in its performance can be rectified. It is the investigation of this last problem which forms the substance of this thesis.

The first laser to operate successfully was a pulsed ruby laser (Maiman 1960) and this active medium has remained in the forefront of solid state laser development and application ever since. As probably the most widely used of sources for pulsed coherent optical applications, the ruby laser will be taken as the basis against which to compare the Nd: glass and other systems. Cr^{3+} is the active ion in ruby and, with Nd^{3+}, has an almost complete monopoly in optically pumped solid state lasers. Unlike Cr^{3+} however the Nd^{3+} ion is compatible with several host materials. These are glass, first operated in 1961 (Snitzer), and a large number of crystals. The latter include calcium tungstate ($CaWO_4$) and yttrium aluminium garnet (YAG) and since the large majority of neodymium crystal lasers are one or other of these we will limit our discussion to them. First reported lasers of Nd:$CaWO_4$ and Nd:YAG were in 1961 and 1964 (Johnson and Nassau, Geusic et al). No qualitative differences exist between lasers of Nd in various crystal lattices and the quantitative differences are usually only small. We have merely picked the two commonest examples.

Short pulse techniques have also been applied successfully to gas lasers (Hattori and Goto 1968, Simmons 1970, Ericsson 1968) particularly those in which high gain coefficients can be established. The ease with which single

mode operation can be achieved is the best recommendation to the use of the output of these lasers for pulsed coherent applications. However, the available energy per pulse is often inadequate and the overall efficiency is low.

To complete this short list we must add those lasers under the general title of "dye" lasers. These consist of an active ion, the dye, dissolved in a solvent; they were first operated in 1966 (Sorokin and Lankard). Many combinations of dye and solvent are possible and much development is still required to single out the most promising, so it will be only the general characteristics that will be discussed, giving examples from published information where necessary. The dye laser combines the uniformity of the gas laser with the high gain of the solid state laser, while introducing various problems of its own. It has emerged only recently as a potentially important type of laser and at the present time does not seriously contend in our chosen field, although it is likely to do so in the near future. In this context it might be pointed out that some of the work presented here, in particular that on the control of the temporal coherence, is also applicable to the dye laser.

Values of some of the parameters discussed below are tabulated for the above types of laser in Table 2.

2.2 Before proceeding to a more detailed assessment of the above types of laser, it will be useful to formulate the parameters which control the operation of the laser in the Q-switched mode and to derive a relationship between these parameters and the basic laser properties.

2.2.1 The first of these parameters is the efficiency of the laser (η).

If E_i = the input energy into the flash tube; and E_o = the output energy

then $\eta = E_o/E_i$ 2.1

A relationship for the efficiency (η) is obtained as follows.

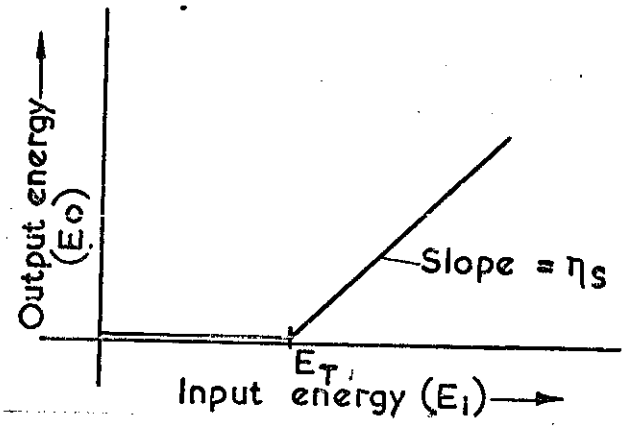
Of the input energy a fraction (say C_1) reaches the rod. Of this a fraction (say C_2) is absorbed per unit volume in it, C_2 being dependent upon the number and spectral breadth of the pumping bands, their absorption coefficients and the dimensions of the rod. Let the quantum efficiency for transfer of absorbed energy density into the upper laser level be c_3, and let a fraction c_4 of this be capable of radiative decay. We thus have a potentially useful energy density $= c_1c_2c_3c_4E_i$ in the upper laser level. Some of this however is wastefully employed in providing a sufficient positive gain to initiate laser action. This wasted energy density is given by $(N_4 + \frac{\ell n\,[1/S]}{2\sigma\ell}).h\nu$, where the first term is the population density in the lower laser level, which may depend upon the upper level population density; the second term is the threshold inversion, which is the inversion giving a gain sufficient just to offset the losses. (1-S = total loss per pass in the system; σ = stimulated emission cross-section; ℓ = rod length). The 'inversion' is defined as the excess population density of upper over lower laser level. If the efficiency of coupling stored energy out of the cavity is f, then the output energy becomes,

$$E_o = \int_{\text{volume}} f\left[c_1c_2c_3c_4E_i - h\nu\left(N_4 + \frac{\ln\,[1/S]}{2\sigma\ell}\right)\right] dV \qquad \ldots (2.2)$$

$$\therefore \text{ efficiency } \eta = \frac{E_o}{E_i} = \frac{1}{E_i}\int_{\text{volume}} f\left[c_1c_2c_3c_4E_i - h\nu\left(N_4 + \frac{\ln\,[1/S]}{2\sigma\ell}\right)\right]dV$$

A typical graph of output vs input is shown in Fig. 2.1 and the two most useful parameters are the input energy at which laser action begins called the threshold energy E_T and the slope of the line above threshold, called

FIGURE 2.1.



Typical laser input/output characteristic

the slope efficiency η_s.

As a comparative indication relating different lasers, these two parameters are more relevant than the overall efficiency. Their definitions in the general case are:-

$$\text{Threshold energy, } E_i \rightarrow E_T \quad \text{as} \quad E_o \rightarrow 0$$

$$\text{Slope efficiency, } \eta_s = \frac{\partial E_o}{\partial E_i} \quad \text{at} \quad E_i > E_T$$

The equation representing Fig. 2.1 is just:-

$$E_o = \eta_s (E_i - E_T) \quad \text{for } E_i \geq E_T$$

$$= 0 \qquad \text{for } E_i < E_T$$

and by comparison of this equation with Equ. 2.2 (and taking the case where none of the parameters vary with E_i) it is immediately seen that:-

$$E_T = \frac{h\nu}{c_1 c_2 c_3 c_4} \left[N_4 + \frac{\ln 1/S}{2\sigma\ell} \right] \qquad \ldots (2.3.a)$$

and

$$\eta_s = \int_V c_1 c_2 c_3 c_4 \, f \, d \, V \qquad \ldots (2.3.b)$$

The minimum threshold for any laser material occurs when the only losses are the intrinsic losses in that material. These are denoted by the material's loss coefficient β, and then $S = \exp(-2\beta\ell)$.

$$\therefore \quad \text{Minimum threshold } E_T = \frac{h\nu}{c_1 c_2 c_3 c_4} \left[N_4 + \frac{\beta}{\sigma} \right] \qquad \ldots (2.4.a)$$

or, since the upper level population density is $N_3 = \frac{c_1 c_2 c_3 c_4 \, E_i}{h\nu}$, minimum

threshold occurs when:-

upper level population density = lower level population density + $\frac{\beta}{\sigma}$

or $$N_3 = N_4 + \frac{\beta}{\sigma} \qquad \ldots (2,4,b)$$

2.2.2 The second parameter is the double pass gain (G) of the laser. Using previously defined quantities:-

$$G = S \exp 2\ell N\sigma = S \exp 2\ell\sigma \left[c_1 c_2 c_3 c_4 E_i/h\nu - N_4\right] \qquad 2.5$$

where N = inversion $= (N_3 - N_4)$

It is G which in a Q-switched laser primarily determines quantities such as the peak power and pulse length.

2.2.3 Finally a parameter or more correctly a class of properties which play an extremely important role in laser performance; these properties, which most come within the scope of the term "losses", generally hinder, modify and complicate the operation of the laser. The parameter directly dependent upon them is the loss term S, but they can also modify almost all the other quantities involved in the above equations. Thus for example, a temperature gradient in the laser material results in a gradient in the stimulated emission cross-section (σ) and introduces a misalignment which effectively reduces the coupling coefficient (f).

It can be seen that the three parameters are by no means independent. Consideration of the effect of any particular property on them, however, enables the relative merits of that property to be assessed.

Before proceeding, it is convenient to assume that the parameter $c_4 = 1$. There is no evidence to the contrary and we have only included it for completeness.

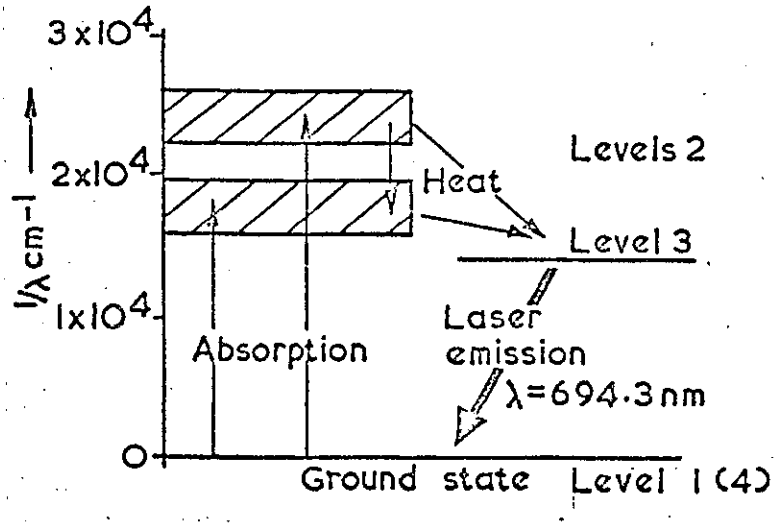
2.3.1 Ruby Laser

It is a remarkable fact that ruby will lase at all, let alone be such a useful medium. The reason for its success lies in the ability of a surprisingly favourable combination of several properties to overcome the

major disadvantage of its being a 3-level system.

2.3.1.1 This latter property is illustrated in Figure 2.2.

FIGURE 2.2.



Simplified energy level diagram of the Cr^{3+} ion in ruby.

A more detailed level diagram is given for example by Roess (1969), but for our purposes a simplified version is more suitable.

From equation 2.4 it can be seen that for a lossless material the minimum requirement for laser action is to achieve a population inversion, that is to get a higher population density in the upper laser level than in the lower. In terms of our diagram this means $N_3 > N_1$;

but for ruby $N_3 = N_o - N_1$ 2.6

where N_o = Number of Cr^{3+} ions/cc

i.e. the upper laser level lifetime is so long, in comparison with those of all other levels, that effectively all excited ions are in that excited state. Thus the minimum requirement is $N_3 > N_o - N_3$

or $N_3 > \frac{1}{2} N_o$ 2.7

At least half the atoms must be excited before there is a chance of laser action.

The likelihood of doing this is determined by the function $c_1 c_2 c_3$, since $N_3 = c_1 c_2 c_3 E_i / h\nu$. Of this function, only c_2 and c_3 depend on the laser material, but c_2 alone controls the upper level population density and hence the minimum threshold, since, for ruby, all the excited ions arrive

by decay processes at the upper laser level and the factor c_3 merely represents quantitatively the fact that energy is not conserved although the total number of excited ions must be. Now c_2 depends on the absorption spectrum of ruby (and also on the pump spectrum and the geometry), and increases for an increase in absorption coefficient, for an increase in the number of exciting photons of the right wavelength, and for an increase in the width of the absorption levels. The exact dependence has been calculated by Cook et al (1964), and we quote their results, whereas for Nd:glass the calculation is given in full in Chapter 3. The absorption spectrum of ruby is shown in Fig. 2.3. (Cooke et al 1964) along with the emission spectrum of a typical Xenon flash tube operating in the condition of complete ionization. (Edwards 1967).

Although conditions may not appear to suggest a high efficiency, the absorption levels are broad and the absorption cross-sections are high by comparison with other laser materials. As an example in a ruby rod 75 mm long and 6 mm diameter and of normal concentration (0.05% Cr^{3+}), an upper level population density of $\frac{1}{2} N_o$ is achieved for an incident energy of approximately 50J on the surface of the rod. For other laser materials it is usually difficult to pump even 10% of the ground state population.

Ruby is by no means a lossless material as assumed above. Thus the minimum threshold is also determined (Equ. 2.4.a) by the factor β/σ. Inclusion of this factor changes Equ. 2.7 to:-

$$N_3 = \tfrac{1}{2} N_o + \tfrac{1}{2} \beta/\sigma$$

From table 2, we see that, in a typical ruby,

$$\beta/\sigma = 0.8 \times 10^{18} = 0.05\ N_o.$$

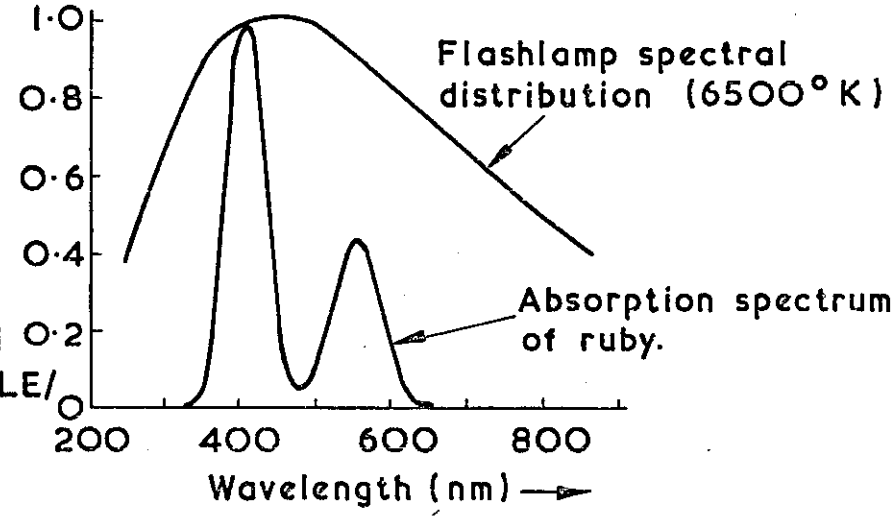
Thus the loss coefficient has a minor effect on the threshold.

2.3.1.2 The favourable absorption spectrum, which make it possible to achieve a positive gain in ruby, also contributes to making it

FIGURE 2.3

Spectral distribution of absorption in ruby and emission from flashlamp.

PEAK MOLAR EXTINCTION COEFFICIENT = 50 cm^{-1} / MOLE/ LITRE.



efficient once threshold has been passed. This efficiency, the slope efficiency, which is the incremental increase in output energy per unit input, is given in equation 2.3.b:-

$$\eta_s = \int_V c_1 c_2 c_3 c_4 f \, dV$$

The value of c_3 has real importance now as we are interested in the energy transfer rather than the build up of the upper level ion density, and we shall therefore consider it in more detail.

The quantum efficiency $c_3 = \frac{\text{energy density in upper level}}{\text{absorbed energy density}}$

Now absorbed energy exists initially as excited ions distributed among the levels in the absorption spectrum. Each ion then falls to the upper laser level with the release of an amount of heat corresponding to the difference between the two energy levels. If N_p is the initial population density in the absorption level p, then the absorbed energy density = $\Sigma_p N_p h\nu_p$ and since the energy density in the upper laser level = $N_3 h\nu_3$

$$c_3 = \frac{N_3 h\nu_3}{\Sigma_p N_p h\nu_p} \qquad 2.8$$

Now $N_3 = \Sigma_p N_p - N^1$ where N^1 = population density left in the absorption levels + that going to other levels

$$\therefore \quad c_3 = \frac{h\nu_3 \Sigma_p N_p}{\Sigma_p N_p h\nu_p} - \frac{N' h\nu_3}{\Sigma_p N_p h\nu_p} \qquad 2.9$$

For ruby $N^1 \ll N_2$ and we can neglect it

$$\therefore \quad c_3 = h\nu_3 \Big/ \frac{\Sigma_p N_p h\nu_p}{\Sigma_p N_p} = h\nu_3 / h\bar{\nu}_p \qquad 2.10$$

A high value of c_3 requires a value of the mean absorption level energy, or frequency, as close as possible to that of the upper laser level. It can be seen from Figure 2.2 that ruby is favourably situated in this respect; its quantum efficiency is 0.7 (Edwards 1967).

We also note here that the heat energy density released in this process

$$= (1-c_3)N_3h\nu/c_3 = N_3h\nu(1/c_3-1) \qquad 2.11$$

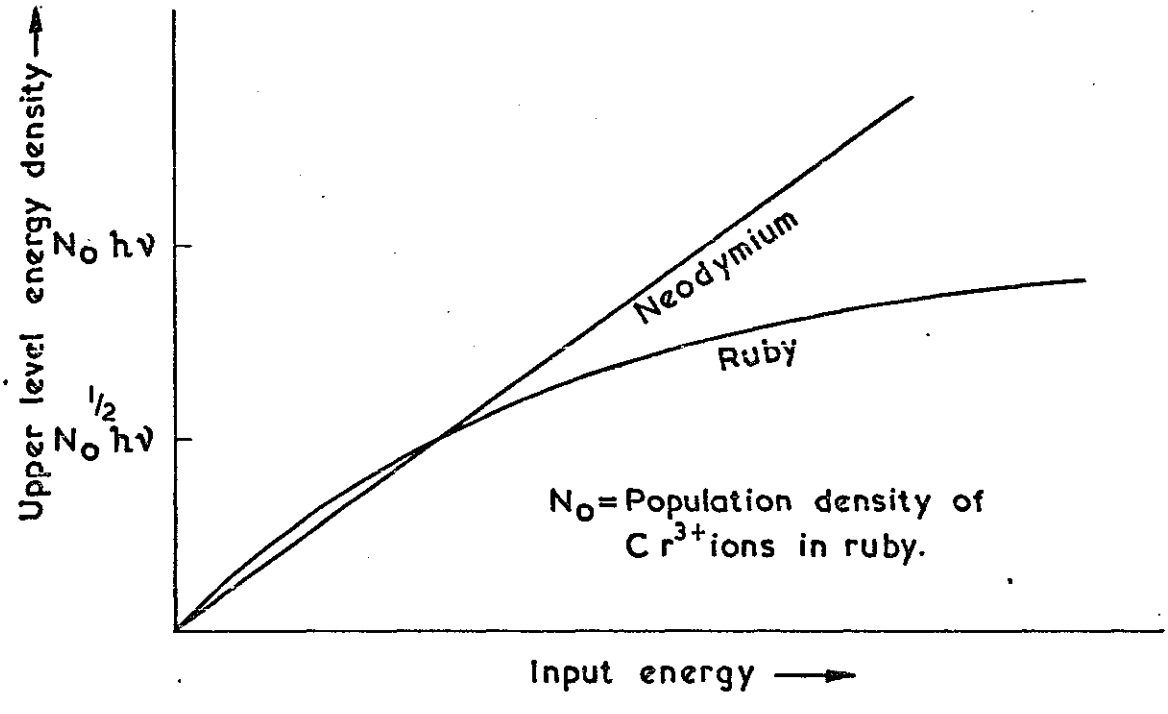
Another material parameter, apart from those included later in a discussion of the "losses", which can affect the slope efficiency by its influence on the output coupling term (f), is the lifetime (τ) of the upper laser level. This has a value of ~4ms for ruby. To achieve, in Q-switch operation, a low loss due to the spontaneous decay of the upper laser level, the duration of the pumping flash must be less than 4ms. Furthermore, this limitation itself limits the maximum energy it is possible to pass through a flashtube of given dimensions. For example, in a Xenon tube the breakdown energy is equal to $400\ r\ell\sqrt{t}$ (Edgerton et al 1964) (where t is the flash duration and r and ℓ the radius and length of the tube) and if, for a tube of length 100mm and radius 3.5mm, we limit the duration to 4ms, then the maximum energy that can be dissipated in it is 2800 joules.

The long spontaneous lifetime together with the high quantum efficiency and favourable absorption spectrum all promote a high slope efficiency in ruby. Three factors however help to limit the efficiency:-

(i) C_2 depends on the lower level population density, due to the dependence of the absorption coefficient on this density. Figure 2.4 gives qualitatively the relationship between the upper level energy density and the energy density falling on the rod. This results in a slope efficiency decreasing with increasing input energy from half its maximum value at the inversion point to zero for very large inputs.

(ii) The maximum possible energy density stored in the upper laser level = $N_o h\nu$. = 4.3 joules per cc for N_o = 1.5 x 10^{19} ions/cc, which is the usual 0.05% by weight concentration of Cr^{3+} in ruby. The concentration of Cr^{3+} cannot be varied very much - it cannot be increased to increase the efficiency and stored energy - since increasing or decreasing it would introduce spare ions or sites into the crystal lattice and result in optical defects in it. These and other defects contribute to the "losses" of the

FIGURE 2.4



Pumping efficiency of equivalent ruby and neodymium lasers.

laser.

(iii) The slope efficiency, in a Q-switched laser, depends upon the threshold inversion density (Wagner and Lengyel 1966), since the coupling factor f is then a function of the difference between the inversion and the threshold inversion. The higher the material can be pumped above the threshold the more efficient it is. In ruby the maximum inversion density is restricted by the relatively low ion density and consequently the slope efficiency is also limited.

2.3.1.3 The gain (G) of a laser has been defined by equation 2.4 as:-

$$G = S \exp 2\ell(N_3 - N_4)\sigma = S \exp 2\ell N\sigma$$

for ruby $$N_4 = N_1 = N_o - N_3$$

then, $$G = S \exp 4\ell(N_3 - N/2)\sigma \qquad \ldots (2.12)$$

The exponential term can be made to dominate by minimising the losses, and the product $N\sigma$(= 2 $[N_3 - N_o/2]\sigma$) is then the controlling factor. $N\sigma$ is called the gain coefficient, α. It is in fact a function of frequency. If the emission line has a Lorentz shape:-

$$\sigma = \frac{\sigma_0 \Delta^2}{(\nu^2 - \nu_0^2)^2 + \Delta^2}$$

where Δ = linewidth, σ_o = value at peak wavelength and ν = frequency Generally when no reference is made to frequency, σ is assumed to have the peak value σ_o. Some insight into σ, the stimulated emission cross-section, is given by the Fuchtbauer-Lundenberg relation:-

$$\sigma_0 = \frac{\lambda^2}{8\pi n^2} \frac{1}{\tau \Delta}$$

where τ = radiative decay lifetime, Δ = linewidth

λ = wavelength and n = refractive index.

Here again it is seen that the properties of ruby combine favourably, for although its fluorescent lifetime of ~ 4 ms is comparatively long the linewidth is very narrow, particularly at low temperatures, and the wavelength is long. σ_o for ruby at room temperature = 3×10^{-20} cm^2, and it has, therefore, a gain coefficient α of 0.2 cm^{-1}/joule/cc. This high gain of ruby per unit pumped energy density above inversion has several direct consequences:-

1. Extra losses in the laser can easily be overcome and result in a relatively small loss in energy output. From equation 2.2 we see that the loss in stored energy density due to the lumped loss term S is $h\nu \ln(1/s) 2\sigma \ell$ (where 1-S = extra loss per pass) and is small for large σ.

Thus in ruby an extra loss of 50% gives, for a rod of length 10 cms, a loss of 0.25 joules/cc stored.

2. When Q-switching is being used, the high gain results in a very fast build up of the output pulse, leading to a short pulse of high peak power.

On the debit side however:-

3. A normal specification on the output Q-switched pulse usually results in a high gain before switching. It may then be difficult to prevent prelasing, due to an incomplete quenching of the Q (there is nearly always some feedback due to poor quality Q-switching crystals or stray reflections); and superradiance, which is increased fluorescence by amplification in a single transit of the rod, may lead to a considerable loss in efficiency. Superradiance results in a greater rate of loss of inversion than that expected fron normal spontaneous fluorescence or, in other words, the effective decay time is reduced.

4. High gain results in short Q-switched pulses of high peak power for a given energy. This high peak power is useful in many applications such as

the observation of non-linear effects, but it does bring with it a high risk of damage to all surfaces and media involved.

2.3.1.4 The "losses" have a strong influence on two important factors, the loss factor S and the output coupling factor f, and they can make all the difference to the suitability or not of a laser material.

These losses can be put into the following categories:-

i) Those contributing to absorption losses.

ii) Those contributing to scattering losses.

iii) Those contributing to losses arising from other optical distortions.

iv) Those contributing to losses arising from other spatial inhomogeneities.

Ruby being a crystal, has certain crystal defects. Imperfections in the formation of the lattice lead to discontinuities in it and hence a certain amount of loss by scattering and diffraction. Impurities both increase absorption, (which, by being localised, reduces the damage threshold) and form scattering centres. Crystals are rarely free of strain, ruby being no exception, and this effectively introduces irregular optical distortions. Strain is also accompanied by strain birefringence which increases the losses by coupling energy from the efficient polarization to the inefficient one. Further, all crystal defects weaken the lattice and increase thereby the possibility of breakdown. Although very good rubies can now be grown, they still have residual defects and they are expensive.

Getting the action ion, Cr^{3+} in this case, into the lattice presents some difficulties. Firstly, very little latitude is possible for the concentration of chromium since any significant departure from the optimum increases the defects. This optimum for ruby is 0.05% by weight, much lower than one would like for maximum efficiency. Secondly, there inevitably arise concentration gradients, an inhomogeneity leading, via nonuniform

pumping, to nonuniform gain and temperature gradients. The latter contribute to optical distortion while the former is in category (iv) above and leads to inefficient energy extraction from the material and increased diffraction losses.

A large contribution to optical distortion losses is derived from non-uniform heating effects. We have already shown that the heat release per unit volume in the pumping process (equation 2.11) is $(N_3 h\nu)(1/c_3-1)$ and this is a measure of the average phonon energy released in the relaxation from the pumping bands to the upper laser level, see Fig. 2.2. For ruby, $(1/c_3-1)\sim 0.3$ (Edwards 1967) which is low for a laser material.

The heating, to have a detrimental effect must, as stated above, be nonuniform and this arises from a nonuniform distribution of pumping energy as well as inhomogeneities in the crystal. The effect of the former can, by suitable design of the pumping configuration, (Roess 1964) and optical compensation, (Stickley 1966) be eliminated while this is not possible in the latter case.

Similar heating effects can arise fron non-fluorescent decay processes from the upper laser level. The fluorescent efficiency of this level in ruby is 1.0 and these heating effects are negligible.

Finally, optical distortion can also arise from the nonuniform absorption of pump light and light at the lasing wavelength by atoms already in the upper laser level (Riedel and Baldwin 1967) Two forms of this distortion are possible-that due to heat emitted after this absorption process and the refractive index changes which accompany the resonant absorption at the laser wavelength.

Before transferring our attention to other materials we should mention that although a lot of development has gone into recording materials at 694nm, the output wavelength of a ruby laser, this wavelength has disadvantages. A large range of materials is still not available, the visual response and

most photodetector responses at 694nm are low, and the intrinsic resolving ability at this wavelength is less than shorter visual wavelengths.

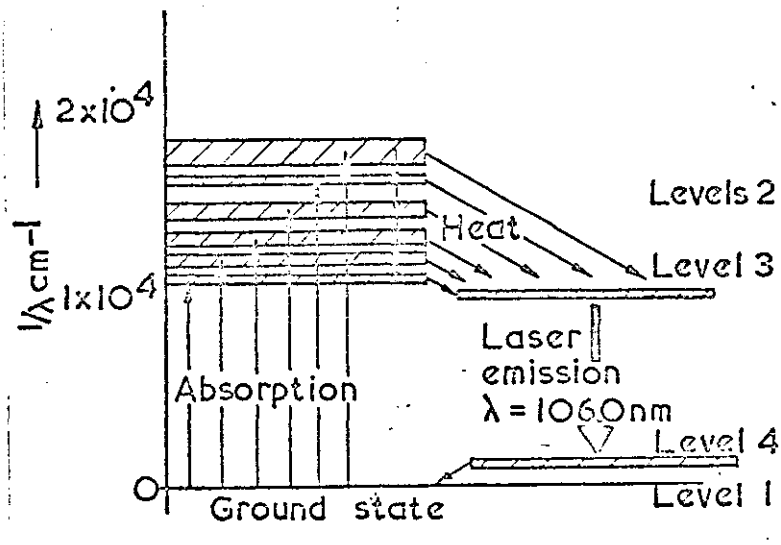
2.3.2. NEODYMIUM LASERS

As has been previously stated, the Nd^{3+} ion in a host material is the only solid state laser which can at present seriously compete with ruby in the coherent optical applications envisaged here. The properties of these lasers as determined by the Nd^{3+} ion will be considered initially and those determined by the host will be discussed subsequently. The former are of course those properties common to all neodymium lasers while the latter are peculiar to the host material.

2.3.2.1. Figure 2.5 illustrates the properties of the neodymium ion which are important to it as a possible laser material.

FIGURE 2.5.

Simplified energy level diagram of the Nd^{3+} ion



Detailed energy level diagrams for neodymium in various host materials are given by Roess (1969) and Patek (1970).

First and foremost neodymium is a 4-level laser material; the lower laser level is not the ground state but is a level higher in energy than the ground state by 0.25 eV (equivalent to 2000 cm^{-1}). The significance of this excited terminal state is demonstrated by considering the primary criterion for achieving laser action, that of bringing about a population inversion. In mathematical terms and referring to Figure 2.5:-

$$N_3 > N_4$$

The three sources of atoms in the lower laser excited state are

(a) thermal excitation (b) absorption of radiation at 2000 cm^{-1}

(c) decay of upper laser level

(a) is negligible since eV >> kT (kT ≈ 0.025 at room temperature)

(b) is 0.0016 x that at the peak wavenumber for a typical black body pumping source (Xenon at 6500°K). This low level of pumping and the high absorption coefficient at 2000 cm^{-1} in the host material results in a negligible contribution to N_4.

(c) The rate equation for the lower laser level is, assuming negligible direct pumping:-

$$\frac{dN_4}{dt} = \frac{N_2}{\tau_3} - \frac{N_4}{\tau_4}$$

where τ_3 = decay time of upper level

τ_4 = decay time of lower level

The steady state solution of this is:- $N_4 = N_3 \frac{\tau_4}{\tau_3}$;

now τ_3 varies between 100μs and 1ms depending on the host material and τ_4 ~100ns (Magnante 1972) i.e. $10^{-4} < \tau_4/\tau_3 < 10^{-3}$; thus we can again neglect this contribution to N_4.

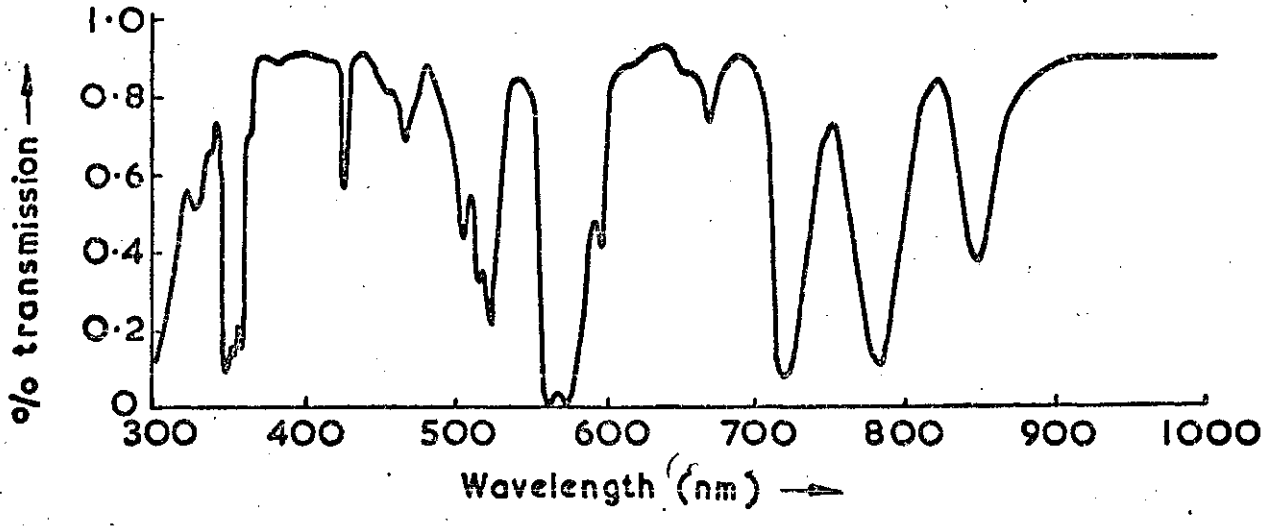
The minimum requirement for laser action now becomes $N_1 > 0$

i.e. an inversion is achieved as soon as the pump is initiated.

This fact probably represents the biggest advantage the neodymium laser has over ruby, in which half the chromium ions have to be excited (Equation 2.7) to achieve a population inversion.

The absorption spectrum for 2% concentration of Nd in glass is shown in Fig. 2.6.

FIGURE 2.6



ABSORPTION SPECTRUM OF Nd: GLASS. 6mm SAMPLE OF 6% LN6.

As can be seen, there are many narrow absorption bands throughout the visible and near infra-red. The important quantity, the ratio of the absorbed energy per unit volume to the incident energy, or C_2 as previously defined, is in fact very comparable to that of ruby for normal neodymium concentrations (e.g. 0.026 for a 3" x 1/4" 2% Nd:glass rod as compared to 0.010 for a similar ruby rod), and will be computed in chapter 3. It should be pointed out however that for a given incident energy roughly equal number densities of atoms in the excitedstate required 10 times the concentration of neodymium as compared to that of chromium in ruby. In other words, if we excite most of the atoms in ruby then under similar conditions only about 1/10 of the neodymium atoms are excited. The decrease in pumping efficiency as the ground state of ruby becomes depleted does not then occur in neodymium since one does not generally reduce the ground state population by more than a small fraction. Fig. 2.4 compares this property for ruby and neodymium under conditions (not unlikely) in which the upper level population densities are equal at the zero inversion point for ruby. The limit to the inversion of neodymium depends not upon this property but upon the breakdown limit of the flashtube or breakdown of the laser material itself.

The absorption spectrum shown in Fig. 2.6 is for 2% neodymium in glass. The width and height of each line does depend to some extent upon the host material; usually they are narrower and taller for crystals, but the effect upon the factor c_2 is small and the previous remarks are in no way invalidated as a qualitative comparison.

Figure 2.5 also enables a similar comparison of the heat released during relaxation from the absorption levels to the upper laser level. We recall equation 2.11 which is used with Figure 2.5 to give this heat.

Thus:- heat released/unit volume = $N_3 h\nu(1/c_3 - 1)$ = H say

where $c_3 = \dfrac{\text{energy density in upper laser level}}{\text{absorbed energy density}}$ and is given by

Equation 2.9 $H_{Nd}/H_{Ruby} \approx 1.9$ for typical case and assuming equal stored energy above threshold.

The laser transition in neodymium corresponds to a wavelength around 1.06μm, that is, in the infra-red. It is not visible and can only just be recorded by low resolution photographic material. The neodymium laser is made useful optically by converting the 1.06μm to 0.53μm in a non-linear material. The problems of this extra process, principally the reliability and efficiency, are to some extent alleviated by the favourability of 0.53μm as a wavelength for visible and optical applications.

To sum up, neodymium has advantages by virtue of being a 4-level laser and disadvantages in that it requires an extra loss process to produce an output of suitable wavelength.

2.3.2.2. The properties of a laser which are influenced by the host lattice can be separated into two classes: those electronic properties of the active ion which are affected by the electric field seen by it and those properties of the host material itself which modify the laser performance. The former category contains the spontaneous lifetime (τ), the cross-section for stimulated emission (σ), and the spontaneous linewidth (Δ);

while the latter includes the passive and dynamic optical distortion, the absorption and scattering losses, and the dimensional limitations to and cost of laser rods.

As before, the properties will be considered as to their effect on certain parameters.

One of the primary parameters, and considered in some detail for ruby, is the slope efficiency (η_s), where $\eta_s = \int c_1 c_2 c_3 c_4 \, dV$ ... 2.3b

As indicated in the previous section the factors c_2 and c_3 depend little on the host and are similar in value to those of ruby. c_1 is independent of the rod material and c_4 for neodymium:glass = 0.6 (De Shazer and Komai 1965), and for neodymium:crystal = 0.7 (Brandewie and Telk 1967) as opposed to a value of 1.0 for ruby. If also the flash duration is constrained to be less than the spontaneous lifetime then the factor f is also not dissimilar in value. Thus consideration of the slope efficiency does not lead one to favour anyone in particular of ruby, Nd:glass or Nd:crystal.

The spontaneous lifetime (τ) for Nd:glass varies from 200 μs to 700 μs, for Nd:YAG ≈ 200 μs and for Nd:$CaWO_4$ ≈175 μs (Thornton et al 1969). Since for the efficient coupling of stored energy into output energy we require a flash duration less than τ, and since the maximum loading on the flashtube is proportional to flash duration, the maximum output is limited by the above values of the lifetimes. By inserting maximum flash tube loading into calculations of the absorption of pumping radiation, as for example in chapter 3, we can determine a figure for the maximum stored energy per cc. This gives a value of 8 joules/cc for Nd:glass, and 5 joules/cc Nd:YAG and Nd:$CaWO_4$. For ruby the maximum stored energy/cc is 4.3 joules/cc and is really determined by the number of Cr^{3+} ions present per cc. The limits given above for Nd:crystal are in practice not achieved since there is a lower limit due to superradiance which, as will be discussed later,

becomes severe under high gain conditions.

Both a higher slope efficiency and higher maximum output would, on the face of it, result from an increase in the concentration of Neodymium in the host. As with chromium in ruby, YAG and tungstate become lossy and less durable for such an increase while for glass there is much greater flexibility (although an increase in concentration lowers the fluorescent lifetime). It can be shown (chapter 3) that there is often an optimum concentration dependent upon the geometry and the design requirements.

Equation 2.4 gives the gain of a laser as $G = S \exp 2\ell(N_3-N_4)\sigma$.

For neodymium lasers $N_4 \approx 0$. $\therefore$ $G = S \exp 2\ell N_3 \sigma$

The significant material parameter is the gain coefficient $\alpha = N_3 \sigma$

Now $N_3\sigma = N_3 h\nu(1/h\nu)\sigma$ = (stored energy density) $(1/h\nu)\sigma$

$\therefore$ α = constant (stored energy density) (stim. emis. X-section)

Previous remarks concerning the stored energy density also apply then to the gain coefficient, which it will be remembered, determines the length and peak power of a Q-switches pulse along with other properties such as the losses due to superradiance.

It is valuable, having already considered the relative merits of the solid state materials in achieving a useful stored energy density, to consider the gain coefficient per unit stored energy density. This quantity highlights the differences between the hosts for neodymium and between these neodymium lasers and ruby. From above:-

$$\frac{\text{gain coefficient}}{\text{unit stored energy density}} = \frac{\sigma}{h\nu}$$; and it will be remembered that the Fuchtbauer-Landenberg relation gives $\sigma = \frac{\lambda^2}{8\pi n^2} \frac{1}{\tau\Delta}$

In comparison with ruby which has a value of $\sigma/h\nu$ of 0.1 cm^{-1}/joules per cc; Nd:YAG has a value 4.6 cm^{-1}/ joules per cc (Kushida et al 1968) and Nd:$CaWO_4$ has a value 2.1 cm^{-1}/joules per cc (Arnold and Hanna 1968).

These high values for Nd:crystal coupled with the very low threshold make it ideal for cw operation and high repetition rate pulsing but at the same time not so good for single shot Q-switched operation. The later shortcoming arises from the effective shortening of the already short spontaneous decay time, by superradiance. Thus there is either a significant fraction of the pumped energy lost before Q-switching or, if the flash length is reduced accordingly, the maximum input energy before breakdown of the flashtube is reduced. The overall effect is a limitation on the maximum inverted energy density which is such as to limit the Q-switched output to a rather low value. (e.g. 0.2 joules/cc in a typical rod of YAG).

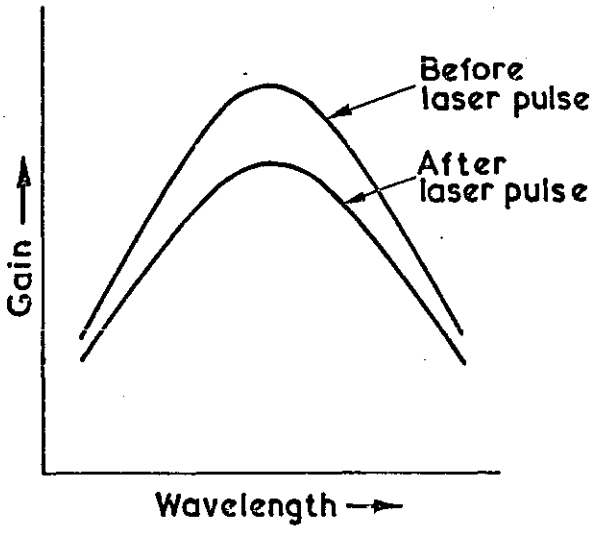
$\delta/h\nu$ for 6% Nd:glass = 0.1 $cm^{-1}/J/cc$ (Edwards 1968) and this low value is primarily due (Fuchtbauer-Landenberg relation) to its very large spontaneous linewidth. As a result Nd:glass is especially useful for obtaining high energy Q-switched pulses. For an energy of less than a joule, which is our requirement, and which can be supplied without difficulty by ruby, Nd:glass with its lower gain removes some problems (see above for ruby). This advantage is however not usually of great significance at this modest energy requirement. Of greater significance is the effect of the losses in the two types of laser and, as discussed more fully later, there is a considerable advantage to be gained by using Nd:glass, if dynamic effects can be overcome.

The large spectral linewidth in Nd:glass is due to asymmetries in the glass matrix. Not being an ordered structure like a crystal, glass does not have specific sites which can accept doping ions, all of which experience identical fields from the surrounding atoms. Instead, the neodymium ions in the glass are randomly situated and "see" fields, which have magnitudes varying randomly over a certain range. The surrounding field modifies and broadens the energy levels of the doping ion and shifts the wavelength and transition probability of any radiative transition. In media like crystals these effects are identical for all atoms with the result

that for any transition, the laser transition for example, the mean wavelength and linewidth is identical for all atoms. The laser line is homogeneously broadened. In glass however the varying fields cause the neodymium ions to have different laser transition wavelengths - the effective linewidth for each ion does not in fact vary much - with the result that the fluorescent linewidth is very much broader than that for a crystal host. The line is inhomogeneously broadened. The linewidths for Nd:glass and Nd:YAG are in the ratio 60. The significance of this broadening effect in Nd:glass may not just be to give it a high stored energy density per unit gain. It may prevent the extraction of a large part of the stored energy, as follows. If a pulse of wavelength near the peak gain wavelength passes through a material like ruby or Nd:crystal having a homogeneously broadened line the pulse experiences a certain gain which decreases as the wavelength difference between it and the peak gain wavelength increases and all the excited ions in the material are equally likely to emit. All the stored energy is available to that pulse. In a medium such as Nd: glass having an inhomogeneously broadened line the situation is different. The gain experienced by the pulse is given by the average effect over all the ions, (as it is also for a material with a homogeneous line) but only a fraction of the ions have an appreciable chance of emitting since, for only a fraction, is the pulse wavelength sufficiently close to the natural wavelength for the transition probability to be appreciable. To put it another way, the pulse effectively only stimulates ions having transition wavelengths no further away than the characteristic linewidth of each ion (the "homogeneous" linewidth). The fraction of the excited population that can emit is thus roughly in the ratio of the "homogeneous" linewidth to the "inhomogeneous" linewidth (fluorescent linewidth of whole). For Nd:glass this ratio can be 1:10 (Smitzer and Young 1968). The gain vs. wavelength curve, after the pulse,

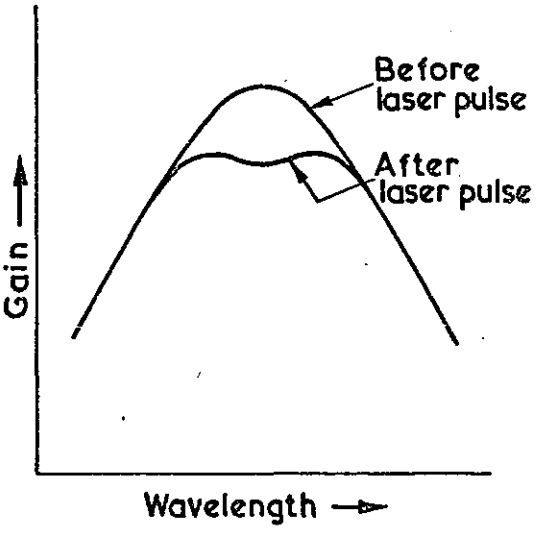
has the same shape as that prior to it for a material with a homogeneous line (Figure 2.7) whereas for a material with an inhomogeneous line (Figure 2.8) there is, after the pulse, a dip in the line of width roughly equal to the 'homogeneous' linewidth. The term "spectral hole burning" is used for this effect. As soon as spectral hole burning begins, a further process called "cross relaxation" tends to redress the balance. The above curve (Figure 2.8) returns to its initial shape. The hole is filled in. Cross relaxation is a 2-stage interaction in which an excited ion with a particular upper state energy exchange states and an unexcited ion, the latter becoming excited at a slightly different upper state energy. The energy released, a phonon, is then absorbed in a similar interaction in which the upper state energy difference just equals this phonon energy. The equilibrium distribution of excited ions (in terms of transition wavelength) is reestablished at a rate characterized by a certain time constant. The cross-relaxation time is a vital property in that it determines the efficiency with which stored energy can be extracted from the laser material. If it is much shorter than the laser pulse the transition is effectively homogeneous and all the stored energy can be coupled out; if it is much longer then the most that can be coupled out is a fraction of the order of the homogeneous linewidth divided by the inhomogeneous linewidth. The cross relaxation time depends upon the extent of the interaction between neighbouring ions of the laser element; it depends upon the spacing between these ions, or the doping concentration, and also upon the type of glass. Michon (1966) measured a time longer than Q-switched pulse lengths for 2% glass, but most 2% glasses and all 6% glasses can, for normal Q-switch pulse durations, be considered as having homogeneously broadened transitions. Inhomogeneity of the line broadening does, regardless of cross relaxation, have another consequence; a favourable one this time. The energy levels of atoms at room temperature are predominantly Doppler broadened, resulting in a highly temperature dependent

FIGURE 2.7



Effect of laser action on gain curve for a 'homogeneously' broadened line.

FIGURE 2.8



Effect of laser action on gain curve for an 'inhomogeneously' broadened line.

linewidth and peak transition probability. In materials with homogeneously broadened lines the linewidth is equal to that of each atom, and thus both it and the gain are temperature dependent. In materials with inhomogeneously broadened lines the linewidth depends only very marginally on that of each ion and in consequence it and the gain are practically temperature independent.

The "losses" associated with crystals doped with neodymium have the same forms as those of ruby. In general Nd:crystals are inferior to ruby. This comes about partly from the greater development effort concentrated on ruby and partly from the greater complexity of the crystals themselves. Some consequences of this are that:-

(a) The maximum volume of Nd:crystal of optical quality is much less than that of ruby.

(b) Nd:YAG is very expensive at present due to its slow growth rate.

(c) Nd:crystals have lower fracture thresholds.

(d) They are subject to more severe stress birefringence.

Ruby would appear therefore to be a more suitable material for a Q-switched laser and Nd:crystals more suitable for a cw or quasi-cw laser. This conclusion was also reached when considering the gain and efficiency parameters.

Apart from favourable properties arising from its being a 4-level material, and its high stored energy per unit gain, Nd: glass also suggests itself by virtue of the following:-

(i) Glass can be made completely free from static optical distortion.

(ii) It can be fabricated to any size or shape and is cheap.

(iii) The distribution of neodymium can be made very uniform.

(iv) There is almost no limit on the concentration of neodymium, imposed by the effect on the losses of changing the concentration. Increasing the concentration does, however, reduce the fluorescent lifetime due to the closer proximity between the neodymium ions and it is this that sets the limit.

(v) The physical properties of the glass are flexible in that they depend upon the composition of the glass and to a large extent this can be adjusted to suit the application. Other properties such as the loss coefficient, the fluorescent lifetime and the stimulated emission X-section can also be controlled to some extent in this way.

On the debit side the following effects must be taken into consideration:-

(vi) the dynamic optical distortion. This is the most serious contribution to the losses. As shown by Riedel and Baldwin 1967, this type of distortion increases with an increase in the temperature coefficients of length and refractive index and with a decrease in the termal conductivity. Glass is much inferior to ruby or Nd: crystals in all these respects, see Table 2, and its distortion is increased further by the greater fraction of absorbed energy which is released as heat in the relaxation from the pumping levels to the upper laser level. These properties, along with the fact that the thermal fracture point of Nd:glass occurs at a relatively low mean power dissipation, make it difficult to achieve cw or quasi-cw operation. In pulsed operation extra care may have to be taken to ensure symmetrical pumping, and efficient cooling may be necessary to operate at faster than say 1 ppm. While static optical distortion tends to be irregular and impossible to correct, dynamic optical distortion can at least be made regular so that compensating optics can be used.

2.4 COHERENCE

2.4.1 Ruby

We have not as yet introduced the effect on the laser performance of any requirements on the coherence of its output. More detail and theory will be devoted to this topic in a later chapter. It will be sufficient here to indicate the parameters which are important when considering

coherence and to say how the performance of the laser is affected when they are used in its control.

It is convenient to consider two coherence functions; transverse and temporal. The former represents the phase correlation across the output wavefront and the latter the temporal phase correlation (or spectral distribution). The general coherence function is not strictly separable into these two components but to do so is a very good approximation when considering lasers where the resonator length >> beam diameter.

Factors affecting the coherence are simply those which contain either a transverse dependence or a wavelength, or temporal, dependence. These are usually contained either in the output coupling term f and the loss term S or in the loss term S and gain coefficient α respectively.

Before proceeding, it is useful to introduce the concept of cavity modes when dealing with coherence. As with a microwave cavity, a vibrating drum membrane, or a "particle in a box", the photons or radiation within an optical cavity can only exist in certain discrete energy states which correspond to certain energy distributions within the cavity. (Kogelnik and Li 1966). Each state or distribution is termed a mode and is independent of all other modes unless an interaction is specifically introduced. Each mode is specified by a transverse distribution in two dimensions and an axial distribution and is denoted by TEM_{mnq} (as in microwave cavities), where m and n are integers specifying the transverse mode and q is the integer specifying the axial mode. For completeness it should be added that, strictly, there are two polarization modes for each of the modes TEM_{mnq} but in practice one polarization can be made to predominate without detrimental effect to the laser performance. From the fact that all modes are independent of each other we can infer ((Chapter 5) that the greater their number the greater the state of disorder, the lower the time averaged correlation between different points in the

in the energy distribution within the cavity (or indeed, emitted from it) and consequently the lower the coherence. The transverse coherence depends then upon the number of transverse modes while the temporal coherence depends, for the normal situation in which the cavity length is very much greater than the transverse dimension, upon the number of axial modes.

2.4.1.1 Transverse Coherence

All properties which have spatial dependence affect the transverse coherence or the number of transverse modes having appreciable energy. These include various loss terms as well as the resonator geometry. A judicious choice of the latter or introduction of the former can always reduce this number to one to obtain complete coherence. The important factor however is the loss in output which must be sustained to do this. Commonly accepted techniques of complete transverse mode control limit the output from a Q-switched ruby oscillator to a small fraction of a joule (typically 20 mjoules) whereas the same laser may emit half a joule without these techniques. This large loss is due to the non-uniformities caused by static optical distortion, heat dissipation and other losses, which result in only a small volume of the rod being able to operate single mode, and, while it is not accepted that this loss (or the necessity of ensuring single mode operation) is inevitable, the size of it and its causes are a measure of the difficulties involved.

2.4.1.2 Temporal Coherence

The minimum coherence of a ruby laser is determined by the spectral width of the gain coefficient which is itself limited by the fluorescent linewidth. For ruby this is 6 cm^{-1}. Techniques such as the use of a resonant output reflector introduce a wavelength dependent reflectivity, which can ensure single axial mode operation of the ruby laser. The resonant reflector need only consist of two flat and parallel plates to do this, and while a single axial mode is not infinitely narrow due to the limited

build-up time of the Q-switched pulse and due to time dependent changes within the laser, its width of typically ~ 0.002 cm^{-1} is quite adequate for the large majority of applications. Moreover, such resonant reflector techniques do not severely reduce the efficiency of the laser, as do transverse coherence techniques.

2.4.2 Neodymium

2.4.2.1 Transverse Coherence

The loss terms are a guide to the difficulty in achieving high transverse coherence. Thus the Nd:crystals tend to suffer a greater loss than ruby except in cases where only a small useful volume is required; in coherent applications we see again that they are more suitable as cw sources. Nd:glass should suffer a lower loss than ruby because of its superior static optical quality. This is however offset by its inferior dynamic optical quality and no a priori advantage can be said to lie with one or the other.

2.4.2.2 Temporal Coherence

Considering the Nd:crystal lasers first again: their fluorescent linewidths are generally similar to that of ruby (25 cm^{-1} for tungstate; 9 cm^{-1} for YAG) and the control of the temporal coherence is consequently no great problem.

Nd:glass has a fluorescent linewidth of about 200 cm^{-1} making a sufficient control of the temporal coherence of this type of laser difficult, very much more so than for ruby. This is a major disadvantage of Nd:glass in a useful coherent light source and must be overcome before it can be acceptable. Later sections show how sufficient coherence might be achieved, and give results of experimental attempts to achieve it.

2.5 POLARIZATION EFFECTS

The lossy effect of stress birefringence and static birefringence has already been noted for ruby. The birefringence couples energy from one

polarization to the other and this process represents a loss, since one of the polarizations has a very much lower gain than the other. In materials such as glass and cubic crystals like YAG there is no preferential gain for either polarization and these two birefringence effects need not constitute a loss. In $CaWO_4$, which has probably the highest birefringence of the materials so far mentioned, well over half the stored energy can be lost when used in a configuration which polarizes the output. Such a configuration may for example include an electro-optic Q-switch.

2.6 SUMMARY OF Nd LASERS

Nd:crystals are suitable for cw and low energy work, having a high gain and very low threshold. The quality of the crystals makes the transverse coherence poor and they are expensive.

Nd:glass is cheap and convenient and has good optical quality. High energy per unit gain indicate a good material for Q-switching particularly in view of the 4-level nature of the neodymium ion. Large bandwidth gives coherence problems and some difficulties are posed by high dynamic distortions.

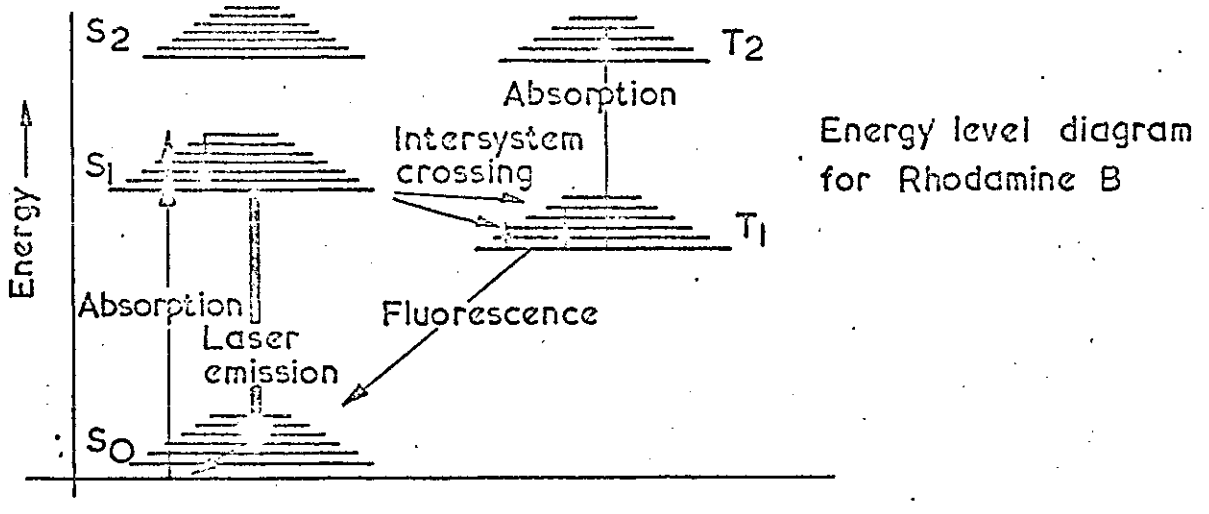
2.7 DYE LASERS

The term 'dye laser' was originally accurate in that it described lasers consisting of an organic dye dissolved in a solvent. It has now come to refer to all organic compounds which, when in solution, are capable of laser action. There are now a very large number of dye lasers, not so much due to the discovery of a great many suitable compounds but because very rapid excitation is now possible and many more compounds then become suitable. A few of these have emerged into general usage and they are those which offer the highest efficiency or convenience for a variety of output wavelengths. Table 2 shows some of the principal properties of these dyes. The general properties of dye lasers have been treated in several papers (Snavely 1969; Weber and Bass 2969) in some detail. A short

review of their characteristics will be given here to demonstrate certain aspects relevant to this thesis.

2.7.1 Figure 2.9 is the energy level diagram for a rhodamine B molecule, showing those levels relevant to laser operation, and Fig 2.10 shows the absorption and fluorescence spectra for the same molecule. These figures

FIGURE 2.9



are typical of dyes. Two similarities to the Nd;glass system are immediately apparent:-

(i) Dyes are four-level materials and, since the lower laser level is never appreciably populated, the inversion criterion, like neodymium, becomes $N_3>0$. Thus dyes have low energy thresholds.

(ii) The fluorescence spectrum is typically hundreds of angstroms wide and the problems of, and techniques for, overcoming this, when single frequency is required, are entirely comparable with those used with Nd:glass.

2.7.2. In other respects however, dyes operate in a very different way, due principally to the following three properties:-

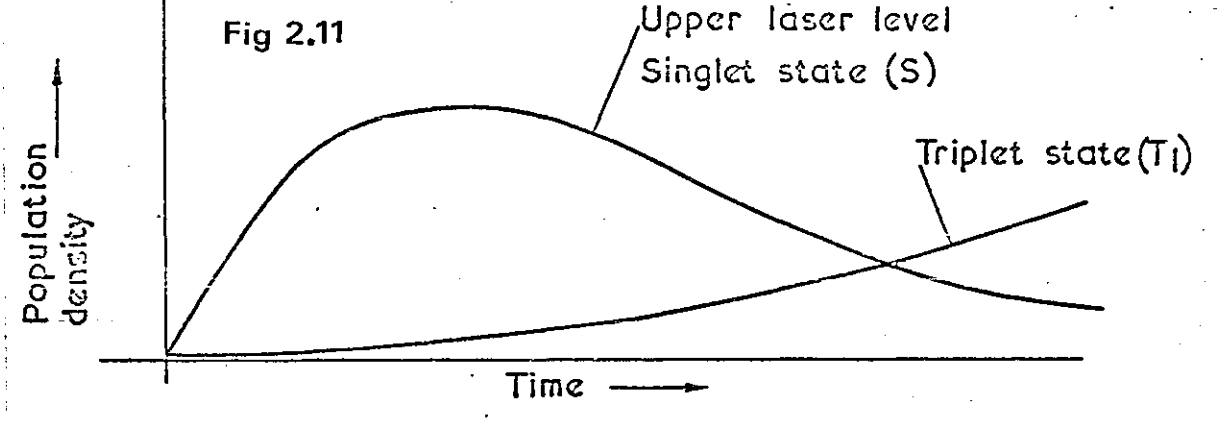
(a) The existence of the triplet complex as shown in Fig 2.9.

(b) The comparative simplicity of the absorption spectrum and, in particular, the existence of the overlap region of the two spectra shown in figure 2.10.

(c) The shortness of the upper level decay time; typically a few nanoseconds.

2.7.2.1. The influence of the triplet state is two-fold and arises from the probabilities of the two transitions $S_1 \rightarrow T_1$ and $T_1 \rightarrow S_o$. The first of these is very high, comparable to the laser transition spontaneous fluorescent probability, and results in a significant fraction of the upper level population being bled off into the triplet complex. This waste of excited molecules reduces the laser efficiency although laser action itself induces a greater fraction of the excited state population to decay via the laser transition. The $S_1 \rightarrow T_1$ transition, then, populates the triplet states while the $T_1 \rightarrow S_o$ transition depopulates them back to the ground state (S_o).

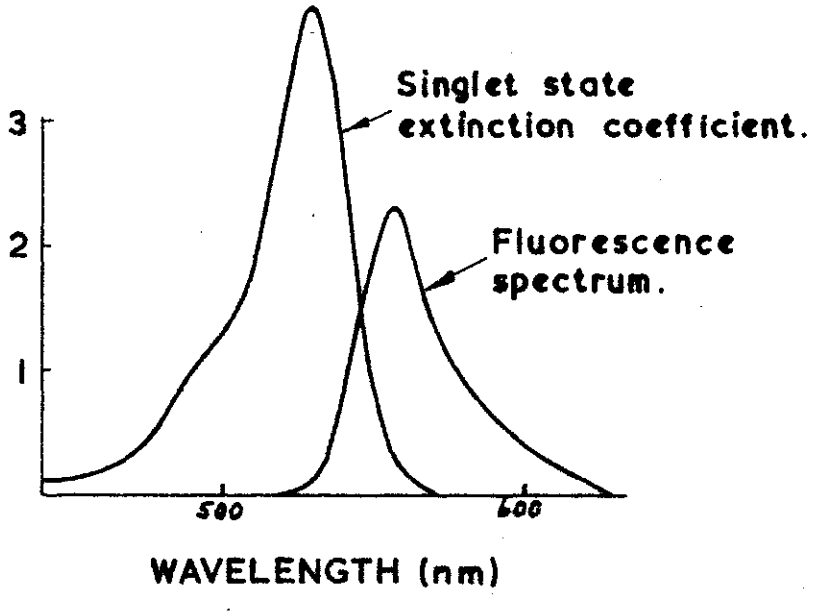
This $T_1 \rightarrow S_o$ transition is however usually slow and any atoms which arrive in the triplet state are effectively lost as far as laser action is concerned since they take a very long time to decay to the ground state for recirculation. There is, furthermore, a continuous buildup of atoms in the triplet state by virtue of the fact that a fraction of all pumped atoms arrive there and the fact that, to significantly populate the upper laser level, the rate of excitation of ground state atoms always exceeds the rate of decay from the triplet state back to the ground state. Figure 2.11 shows, in a typical case, the temporal variation of the upper laser level (or excited state) and triplet state populations for a constant pumping rate.



Temporal variation of singlet and triplet state densities under constant pumping rate conditions

FIGURE 2.10

ABSORPTION AND
'LUORESCENT SPECTRA
)F RHODAMINE 6G IN
O^{-4} MOLAR ETHANOL
OLUTION.



The drop in singlet state population when the triplet state has an appreciable population is not only a result of a depleted ground state giving a reduced absorption coefficient but also a consequence of the not inconsiderable absorption from the lowest triplet state into higher triplet states.

2.7.2.2 One effect of having a very short decay time for the upper laser level (or excited singlet state S_1) see (c) above, is that, since suitable flash lamps have pulse durations much greater than this decay time, it is only possible to reach threshold in a time long compared to this decay time. Consequently, to overcome the continuous fluorescent loss, a high pumping rate must be achieved to reach threshold. In a typical flash-lamp pumped dye laser the rate might be 1 MW into the lamp and the lamp would then fail if the pulse length were in the nanosecond regime. At this high pumping rate the rate of buildup in the triplet state is high and very rapidly the triplet population becomes so high that threshold is no longer possible. There is evidently no improvement in having a pump pulse longer than the time to reach this situation. For example, the maximum pulse length for Rhodamine 6G is several μs, and for anthracene about 50 ns. A further requirement on the pump pulse also follows. The faster its rise to the threshold level, the lower the loss to the triplet state.

2.7.2.3 In conclusion then, dye lasers require a flash lamp with a fast-rise high-intensity short-duration pulse. The maximum flashlamp energy is limited by breakdown of the flashlamp and generally does not exceed a hundred joules or so. The laser efficiency is limited by losses to the triplet state, and by spontaneous emission (the spontaneous decay time being very much less than the pulse length), but can be high by laser standards since the absorption spectrum (Fig 2.10) provides a very efficient absorption of energy from the pumping field. For Rhodamine 6G, for example, the overall laser efficiency can be 1.2% (Anliker et al 1972).

The emission from dye lasers, pumped conventionally, is comparable to

that of non-Q-switched solid state lasers but with an emission time of only up to a few μs in general. Longer pulses have been obtained (and even cw operation using an argon laser as pump) by so called "quenching" of the triplet state. This involves an additive which drastically speeds up the $T_1 \rightarrow S_o$ transition, so reducing the bottle-neck effect of the triplet complex and allowing the pump to maintain threshold for very much longer. Oxygen has been partially successful as also has been cyclooctatetraene C_8H_8 (COT)(Marling 1970).

The general time scale of dye laser action and the high spontaneous decay losses prevent Q-switching when pumping with flash lamps. Much higher pumping rates have been achieved using solid state lasers (second harmonic of an Nd:laser) and gas lasers (argon laser), but one has to remember the low efficiencies of these pumping sources.

2.7.2.4 The significance of property (b) above has partially been indicated, that the absorption spectrum makes for efficient pumping, efficient enough to overcome the intersystem singlet-triplet and the spontaneous decay losses. The other and more interesting significance arises from the presence of the overlap region. Weber and Bass (1969) among others deal with this effect in detail and calculate in particular the consequences for Rhodamine 6G and Anthracene. The effect of the overlap is to provide self-absorption of the fluorescence which is dependent both on wavelength and pumping and in consequence the dye has a gain versus wavelength curve which changes both its shape and the wavelength of maximum gain as the pumping is changed. The result is an emission wavelength which varies in time, and which depends upon the losses in the resonator, since these determine the minimum gain for laser action. This latter property offers the possibility of a fairly crude control on the output wavelength.

2.7.3. Dyes can have very high gain coefficients due to their efficient pumping and their high concentration. The concentration is an even more

flexible parameter in dyes than in the Nd:glass laser and since the medium is merely a liquid solution the uniformity is as good. The static optical quality is excellent, but the dynamic distortions constitute a serious disadvantage, more so even than in Nd: glass, and they can in practice curtail laser action even more severely than the triplet state effects. Dynamic distortions are also detrimental to the transverse coherence. Permanent damage and the need for cooling under high repetition rate conditions cause little difficulty on the other hand since the dye is usually circulated at such a rate that consecutive shots do no use the same sample.

At the present time then dye lasers are of medium power and high gain giving, for flash lamp pumping, spiking emission up to several μs in duration. Cw dye lasers pumped by argon lasers are also being increasingly used. The coherence of pulsed dye lasers is intrinsically lower than even Nd:glass but the laser is tuneable over several hundred angstroms. Several different dyes separately or in the same solution supply an output wavelength tuneable over very nearly the entire visible spectrum (Shank et al 1970). A recent review paper by Bradley (1971) gives the present state of dye laser technology.

TABLE 2 Some properties of laser materials.

	RUBY	ND:GLASS	ND:YAG	RHODAMINE 6G IN ETHANOL
MATERIAL	UNIAXIAL CRYSTAL	ISOTROPIC SOLID	ISOTROPIC CRYSTAL	LIQUID
ELECTRONIC TYPE	3-LEVEL	4-LEVEL	4-LEVEL	3-LEVEL
WAVELENGTH (λ)	694nm	1060nm	1065nm	590nm
LINEWIDTH ($\Delta\lambda$)	0.6nm	15nm	0.3nm	40nm
CONCENTRATION OF ACTIVE ION	0.05% 1.6×10^{19} ions/cc	VARIABLE 6%=3×10^{20} ion/cc	1% 1.9×10^{20} ion/cc	VARIABLE 10^{-3}M/L=6×10^{16} ion/cc
REFRACTIVE INDEX (n)	1.76	1.5-1.6	1.82	1.36
THERMAL CONDUCTIVITY	0.09Cal/s.cm.°C	0.002Cal/s.cm.°C	0.03Cal/s.cm.°C	0.0004Cal/s.cm.°C
EXPANSION COEFFICIENT	5.8×10^{-6}	10×10^{-6}	6.9×10^{-6}	1120×10^{-6}
$d\lambda/dT$	0.006nm/°C		0.005nm/°C	
dn/dT	1.3×10^{-5}/°C	-2.1×10^{-6}/°C	7.3×10^{-6}/°C	500×10^{-6}/°C
LOSS COEFFICIENT	2%/cm	0.2%/cm	1%/cm	
STATIC OPTICAL QUALITY	λ/inch	0.1λ/inch	2λ/inch	0.1λ/inch
COST OF TYPICAL ROD (3"x 1/4")	£ 300	£ 150	£ 500	
SPONTANEOUS LIFETIME (τ)	3000μs	500μs	200μs	0.007μs
X-SECTION OF STIM. EMISSION	2.5×10^{-20}cm^2	3×10^{-20}cm^2	8.8×10^{-19}cm^2	1.6×10^{-16}cm^2
STORED ENERGY PER UNIT GAIN	10J/cc/cm^{-1}	10J/cc/cm^{-1}	0.5J/cc/cm^{-1}	0.002J/cc/cm^{-1}
STORED ENERGY AT COMPLETE INVERSION	4.3J/cc	60J/cc	40J/cc	0.02J/cc
PRACTICAL MAX. STORED ENERGY	4.3J/cc	10J/cc	1J/cc	
TYPICAL THRESHOLD (REL)	30	10	1	1
MAX. SLOPE EFFICIENCY(APPROX)	1%	9%	5%	1.5%

CHAPTER 3

Analysis of the Optically-Pumped Q-switched Nd:glass Laser

3.1 Abstract 3.1

3.2 The Choice of Q-switch 3.3

3.2.1 Types of Q-switch and their operation 3.3

3.2.1.1 Electro-optic cell 3.3

3.2.1.2 Passive Q-switch 3.4

3.2.1.3 Rotating optical element 3.5

3.2.2 Performance parameters of a Q-switch. Comparison of the three types of Q-switch 3.6

3.2.2.1 Q Time-function and pulse build-up function 3.6

3.2.2.2 Coherence effects 3.8

3.2.2.3 Synchronization 3.9

3.2.2.4 Optical quality 3.10

3.2.2.5 Cost, complexity and convenience 3.11

3.2.2.6 Damage resistance 3.11

3.2.2.7 Repetitive pulsing capability 3.12

3.2.3 The Acousto-Optic Q-switch 3.13

3.3 Analysis of Operation of Rotating Mirror Q-switch 3.14

3.3.1 Threshold Considerations 3.16

3.3.1.1 Derivation of the threshold condition 3.16

3.3.1.2 Calculation of the number of available transits 3.18

3.3.1.3 Geometric optimization of number of transits 3.19

3.3.1.4 Other information from geometric representation 3.21

3.3.2 Calculation of resonator flux build-up 3.23

3.3.2.1 Flux increase in $(N+1)^{th}$ transit 3.24

3.3.2.2 Calculation of the gain at N^{th} transit 3.24

3.3.2.3 Rod depletion in $(N+1)^{th}$ transit 3.25

3.3.2.4 Ray matrix of resonator 3.26

3.3.2.5 Fluorescence 3.27

3.3.2.6 Summary 3.28

3.3.2.7 Some examples of computed results 3.29

3.4 Pumping Efficiency and Pumped Inversion Distribution 3.31

3.4.1 Calculation of the inversion distribution 3.32

3.4.1.1 Incident intensity 3.32

3.4.1.2 Calculation for specular surface of rod 3.33

3.4.1.3 Calculation for diffuse surface of rod 3.36

3.4.2 Some computed solutions and comments 3.37

3.5 Application to System Design 3.38

3.5.1 Formulation of laser operation as a product of efficiencies 3.39

3.5.2 Derivation of input/output equation 3.42

3.5.3 Optimization of the output 3.44

3.5.4 Solution for a typical case 3.48

CHAPTER 3

3.1 Abstract

A Q-switched laser consists of 4 parts:-

Rod: Q-switch: Resonator: Pumping chamber. Thus far only the rod material has been specified, that being Nd:glass.

Our concern now is to establish in more concrete form the laser system upon which the investigations are to be carried out.

A rough guide to the size of the rod is that its volume must be such as to enable sufficient energy to be stored to give an output of one joule. As it is reasonable to expect around one joule output per c.c., a rod volume of 1 c.c. is indicated. The rod used, American Optical 75 × 10 mm clad rod, has an active volume of 2.6 c.c. but the effective active volume is considerably less.

As stated, this is but a rough guide. Optimization of the rod parameters cannot in a proper analysis be considered in isolation since their effect on the laser is modified by the other three parts of the system. Before, however, considering the complete system it is necessary to put on a mathematical basis the achievement of a population inversion in the rod by means of an optical pump, since the dependence of this inversion on the rod geometry and pumping arrangement is an essential initial step towards an optimization of the complete laser.

Further information is still necessary to the optimization. We need to know the output coupling factor ('f' of the previous chapter). This factor cannot be calculated without a knowledge of the Q-switch and the dependence of the pulse evolution on it. The factors which determine the choice of Q-switch are discussed and compared for the common types of switch, namely the rotating mirror, the Pockels cell, the passive Q-switch and the acousto-optic cell. In general no one type is an automatic choice and sc

one must depend to some extent on personal preference. The reasons for our choice of a rotating mirror are given, followed by simplified analysis of its Q-switch action. This analysis is a novel approach but one which is considered essential for a better understanding of this type of Q-switch.

The final section attempts to integrate the earlier results into an optimization of the laser, giving examples of how this works out in practice.

3.2 The Choice of Q-switch

Of the three major categories of Q-switch, the rotating optical element, the electro-optic crystal and the passive Q-switch, we have chosen a member of the first of these, namely the spinning mirror. To anyone approaching the subject of Q-switching there are many factors which must be considered and the following is an attempt to categorize them and discuss for each one the differences between the above types of switch. The most suitable type depends on both the individual requirements and the individual, and the various reasons for using the spinning prism will be given. Firstly however a brief description of what is meant by a Q-switch and how each type functions.

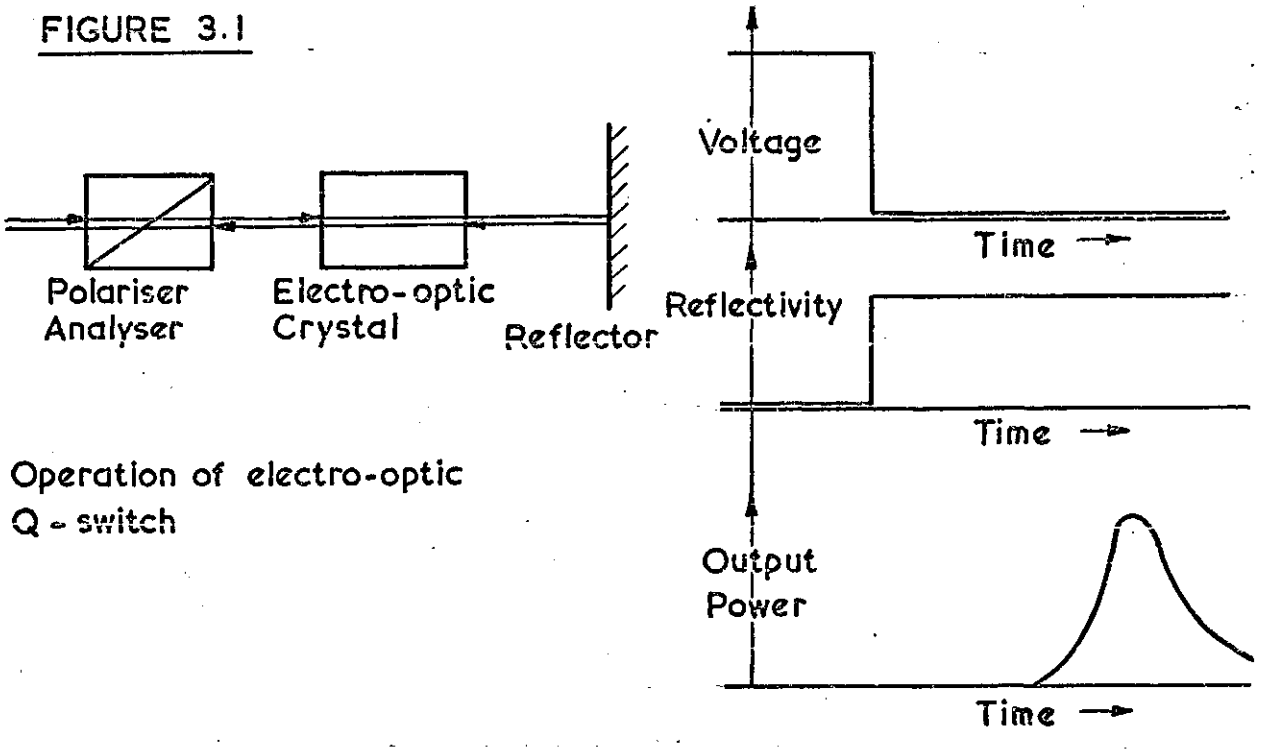
3.2.1 A Q-switch is a device which suddenly increases the Q of a laser resonator and it generally achieves the increase in Q by a rapid decrease in the loss per pass of light travelling up and down the resonator. The initial low Q enables attainment, by high pumping, of a high inversion within the rod without reaching laser threshold. When the Q increases, the threshold finds itself exceeded by a large amount and the consequent high gain per pass results in a rapid (light pulse) build-up and depletion of the inversion. The 'giant pulse' is generally between 10nS and 100nS in length.

3.2.1.1 The electro-optic switch is represented by the Pockels cell, first proposed and used by McClung (1962). This depends upon the transverse linear electro-optic effect by which a potential applied across the crystal induces a retardation of one polarization of light passing through it relative to the other polarization. It is generally used as in Fig. 3.1. The $\lambda/4$ voltage is applied so that, given the correct orientation, polarized light passing through the polarizer is rotated by 90° in a double transit of the crystal and cannot then pass back through the polarizer. This is the

low Q mode. The laser rod is pumped. Removal of the $\lambda/4$ voltage at the appropriate time restores the Q at the instant of max. inversion and a giant pulse results.

Figure 3.1

FIGURE 3.1

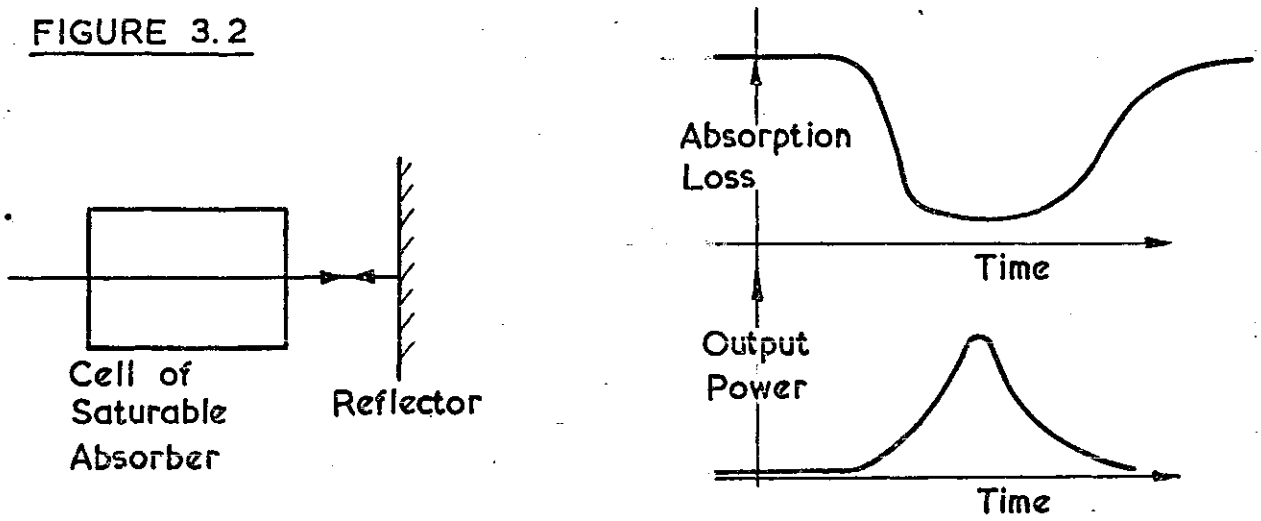


Operation of electro-optic Q - switch

3.2.1.2 The passive Q-switch is represented by a saturable absorber and was first used by Bret and Gives (1964). This is a material having an absorption transition at the laser wavelength which bleaches for power densities of the order of that reached by a non Q-switched laser. If for this power density effectively all the atoms in the lower level of the transition are removed by excitation the absorption section falls rapidly to zero. This sudden drop in absorption inside the resonator or sudden increase in Q initiates a giant pulse. (FIG. 3.2).

Figure 3.2

FIGURE 3.2

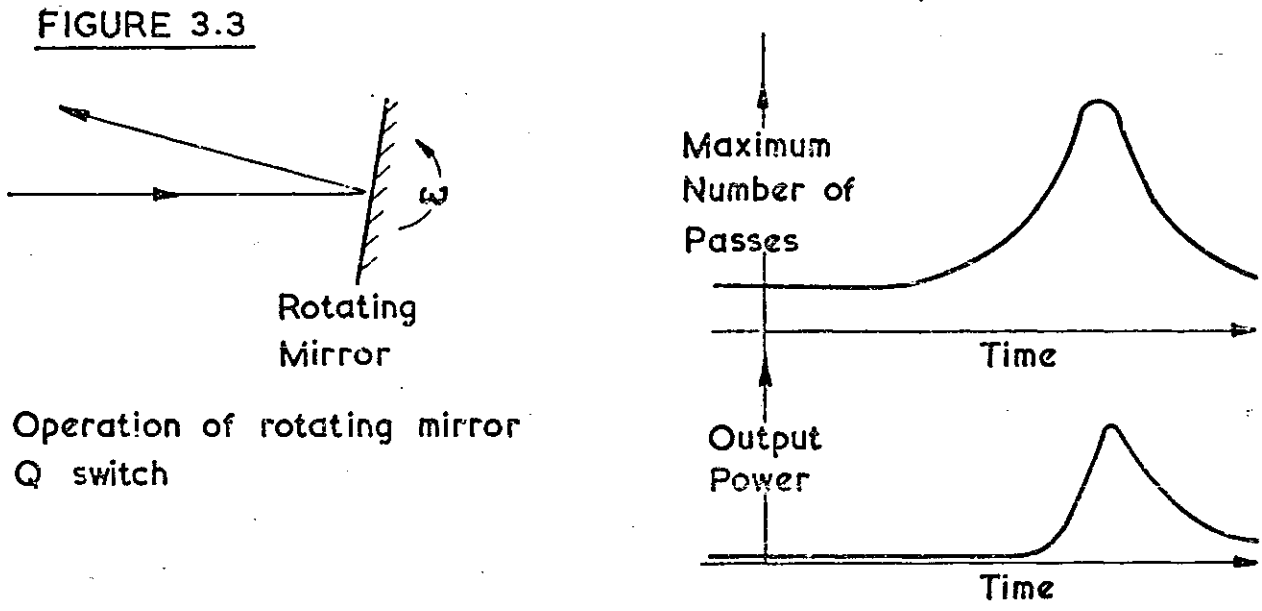


Operation of saturable absorber
Q switch

3.2.1.3 The most common type of rotating optical element (Collins et al (1962) is the spinning mirror. One of the end reflectors of the laser resonator is spun about an axis parallel to its own plane. While it is not parallel to the other end reflector, initially axial rays are reflected out of the system after very few passes and a pulse has no chance to build up. When the reflector comes into line a large number of passes is suddenly available (the Q is now high) and a giant pulse builds up. (Fig. 3.3).

Figure 3.3

FIGURE 3.3



Operation of rotating mirror
Q switch

3.2.2 When assessing the performance of Q-switches it is useful to consider in turn the following factors:-

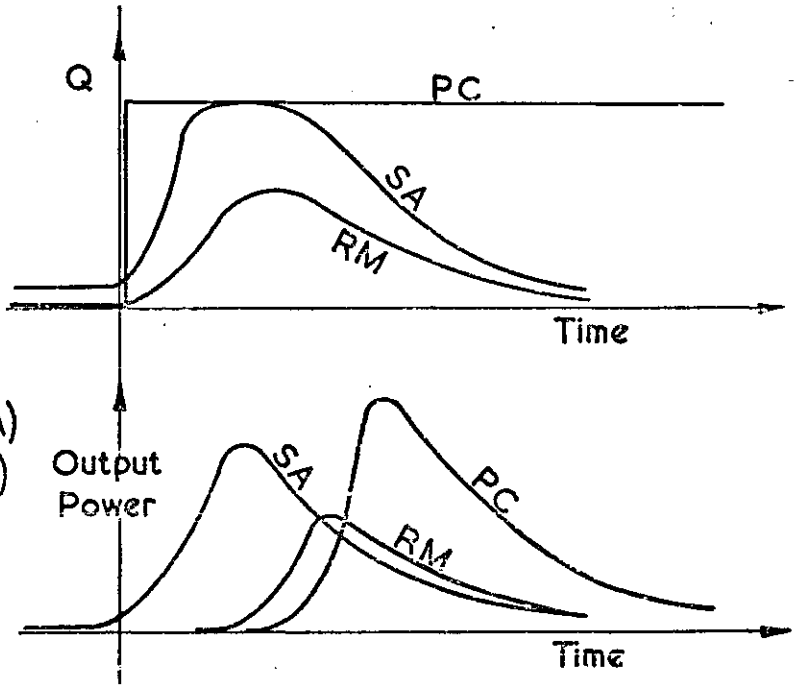
1. Q-switch action, which includes the time function for the Q change and the pulse build-up function.
2. 'Coherence effects' which are interactions such as mode-locking and transverse mode coupling.
3. Ability to synchronise with an event. Timing jitter and pulse repeatability are included here.
4. Optical quality.
5. Cost, complexity and convenience.
6. Damage resistance.
7. Repetitive pulsing capability.

To save repetition, the Q-switches will be referred to by their initial letters.

3.2.2.1 Fig. 3.4 compares typical curves of Q variation and pulse build-up for the three types of switch.

Figure 3.4

FIGURE 3.4



Comparative Q-switching of Pockel's Cell (PC), Saturable Absorber (SA) and Rotating Mirror (RM)

PC can be switched on in $\sim$ 1ns which is usually less than the time for light to make a double pass of the resonator. It is consequently an instantaneous switch resulting in a maximum pulse build-up rate and maximum depletion of the excited energy. Pulsing under these conditions is treated by Wagner and Lengyel (1966) and Wenzel (1967).

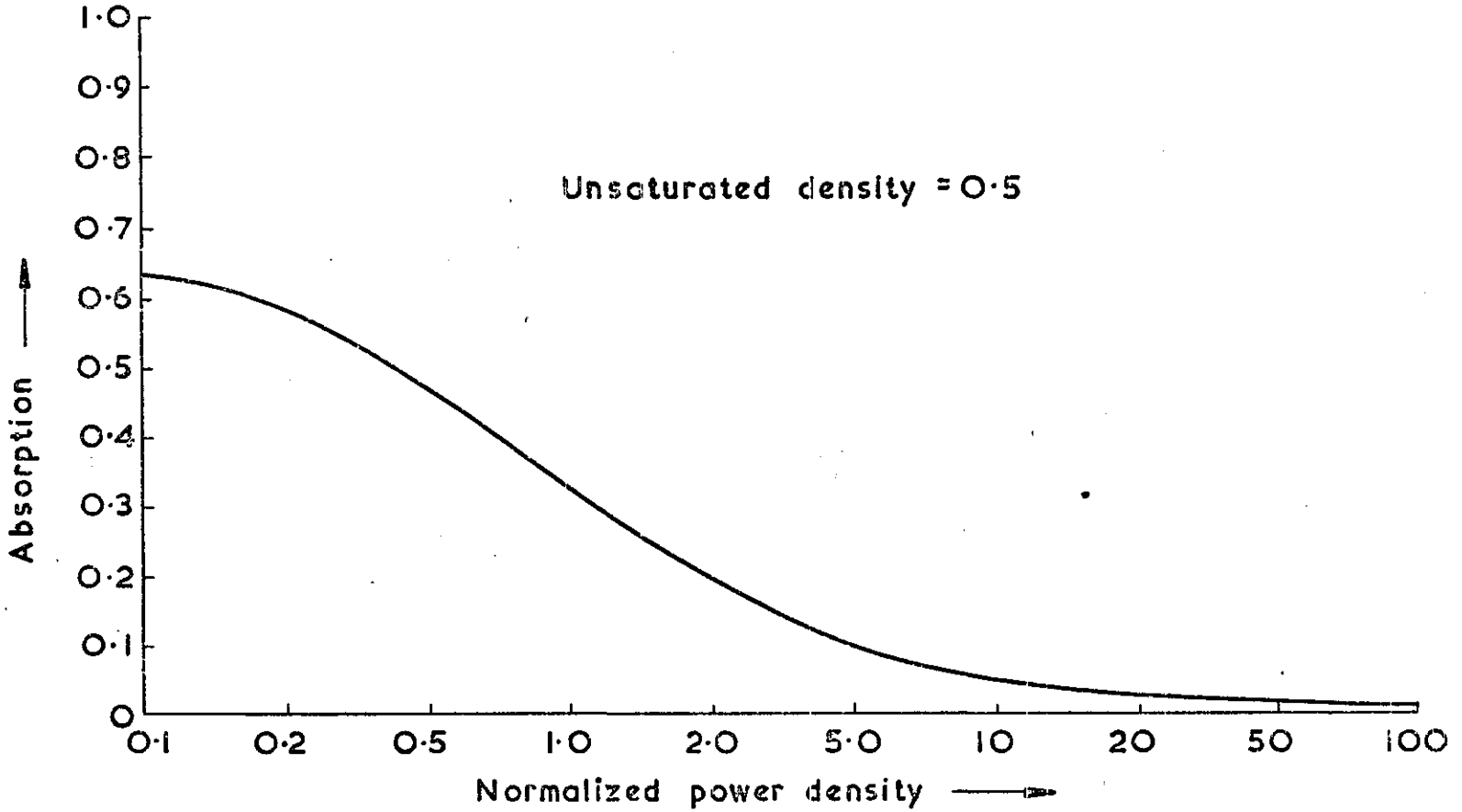
SA, unlike the other two types, is self-actuating. Laser action begins and can only begin when threshold for the low Q situation is exceeded. The dye concentration is usually adjusted to a maximum subject to laser action still occurring, since this gives the highest Q change. The initial build-up of the laser pulse then occurs under low gain and is slow. When the intensity in the SA reaches a certain level, it bleaches, the gain becomes high and the rest of the pulse proceeds rapidly. The 'switch' automatically closes when the intensity drops below the level which saturates the absorption of the dye. Since the rise time of the Q may be only a few nanoseconds, the pulse, following the slow build-up, has the same form as for PC (see Wagner and Lengyel 1966). RM has a relatively slow opening rate and a limited open period and the pulse has very different characteristics to that generated by PC and SA. For a RM it is more realistic to consider the number (N) of available resonator transits for a paraxial ray, rather than the resonator Q. Instead of considering a limited gain over an unlimited number of transits we consider a constant high gain over a limited number of transits. Two thresholds can be defined for RM Q-switched lasers. The first is the conventional one (of overall gain > 1). The second is arbitrarily defined as being reached when the

gain is sufficient for significant depletion to occur in the maximum number of passes available for that RM. Fig. 3.4 shows an optimized RM, where the RM speed is adjusted so that, for the gain available, the laser pulse peak occurs at the in-line position. A sufficiently slower speed gives a double pulse while a much faster speed reduces the maximum number of transits (open period) such that significant depletion cannot occur (threshold is not reached). The process is dealt with in greater detail later in this chapter.

3.2.2.2 With multimode operation the PC does not impose any coupling between the oscillating resonator modes and furthermore, since the pulse build-up is shortest, other constraints and interactions introduced into the laser have the least effect.

The SA has two distinct coherence effects. The first is a result of the long build-up period of the pulse, the longest of the three Q-switches. In the presence of differential mode constraints in the resonator the SA gives maximum discrimination between modes. If for example the mirror reflectivity for two modes A and B is R_A and R_B respectively, the resulting intensity ratio at the pulse peak is $(R_A/R_B)^N$, where N = number of transits during build-up = pulse build-up time/resonator transit time. Hence maximum discrimination occurs at maximum build-up time. The second coherence effect in a SA is a result of the intensity dependence of the absorption in it. This only approximates to a step function, as suggested in the simplest picture, and in reality FIG. 3.5 might be a more accurate representation. The SA then has a lower loss (higher Q) for field distributions giving higher intensity within it and there is consequently a discrimination against field distributions giving low intensities. This

FIGURE 3.5



FRACTION OF INCIDENT ENERGY ABSORBED AS A FUNCTION OF INCIDENT POWER DENSITY FOR A PERFECT SATURABLE ABSORBER.

preference for certain fields constitutes a coupling between resonator modes, both transverse and axial. The latter coupling can for example lead to 'mode locking' in which the resulting field distribution is a very short very high intensity pulse travelling up and down the resonator; the output is then a series of these pulses with length equal to the reciprocal bandwidth of the output and with separation equal to the double transit time of the resonator. For a mathematical explanation of the coherence effects in SA, the reader is referred to Sooy 1965 and Hercher 1967.

Multimode structure in a laser output is very often dependent upon local variations in the active medium. If either the material Livshitz and Tursunow 1967 or the beam within it is swept relative to the other, then local effects no longer exert so much influence and furthermore this mixing provides for coupling between modes. The RM, particularly when operated at high speed, sweeps the laser beam across the rod and thus appreciably affects the mode structure.

3.2.2.3 Since (FIG. 3.4) the Q-change for a PC is very short, perhaps 1nS, and since the PC is controlled by a voltage pulse, the system has maximum flexibility and repeatability. By this is meant that, given the right electronics, the PC can trigger or be triggered by an external event both precisely and with a very low timing jitter. The timing jitter relative to the pumping flash envelope is similarly very low and this helps give a consistent output pulse. (The optical quality also affects the repeatability as indicated below).

The SA is independent of any external event and cannot be synchronized or be used to synchronize. The timing jitter relative to the pump pulse initiation is large (e.g. several µs) for it operates at a time when the inversion of population reaches a particular value and this varies with

variations of pumping and variations in the SA from shot to shot. The latter variations also help to give large output pulse variations i.e. low repeatability.

The RM has high inertia and thus cannot easily be made to synchronize with another event. The use of optical, magnetic or electronic pick-ups enable the synchronization of both flash lamp pulse and external event to the RM. The jitter tends to decrease as the speed of rotation is increased and can be reduced to a value as good as that for the PC. Consequently the repeatability is good as far as this is affected by the jitter. Vibration can severely affect pulse consistency but can be eliminated by the use of air bearings.

3.2.2.4 The optical quality of the Q-switch may be of prime importance, particularly when large diameter single mode operation is required. An optical distortion amounting to a fringe per cm can have a serious effect under these conditions.

Complex crystals are difficult enough to grow to an adequate optical quality. When electric fiels are imposed on these crystals the quality is very much worse. Consequently the PC almost invariably puts significant optical distortion and loss into the resonator.

The SA also introduces optical distortions. Absorption is linked to refractive index and when the absorption saturates, as it does at the initiation of Q-switching, the refractive index is also changed. Assuming that the beam does not have uniform intensity across it, then the refractive index is also non-uniform, leading to optical distortion.

The RM is statically an optically uniform material being in general made from glass or fused silica. Furthermore the distortions introduced by rotational forces are, in almost all cases, negligible.

3.2.2.5 The PC is usually worst in the question of cost, complexity and convenience. Growing and polishing good optical quality crystals of sufficient size is expensive and as well as requiring two crystals (electro-optic and polarizer) also needed are the driving electronics which, for fast operation, are sophisticated and again expensive. Adjustment can often be rather critical in practice.

The SA is the opposite extreme - very cheap, simple and easy to use.

The RM is intermediate. Its cost varies greatly being very cheap for the slow electrically driven type and perhaps several hundred pounds for a very high speed air-turbine. The timing is run very simply and cheaply from an optical or magnetic pick-up and the system is easy to use particularly when the design of resonator is such that the positional or angular adjustments are non-critical.

3.2.2.6 Q-switches create high power density pulses and must be capable of withstanding these power densities. The PC not only tends to create the highest power density with a given laser system, but it also has the lowest damage threshold; a result of the presence of crystals with complex structures and defects. A good PC Q-switch may damage at 100MW/cm^2. This is provided by only 100mJ in a 10nS pulse of diameter ~3mm.

The SA suffers damage (chemical breakdown) easily but, when a liquid, can of course be quickly replaced. The necessity for constant replacement reduces the convenience of this Q-switch and may preclude its use in some cases i.e. high repetition rate lasers. SAs for the Nd:glass laser are also unstable even when not in use and can become inefficient only a short period after manufacture.

Damage to RM elements is not usually a result of poor materials since high quality silica and glass is commonly used. It is generally a result of imperfect workmanship e.g. poor roof-edges on retro-reflecting prisms,

poor quality high reflection and anti-reflection coatings etc. When operating without coatings the damage threshold can be above 1000MW/cm^2.

3.2.2.7 Being controlled electronically, the PC is the most flexible for repetitive Q-switching. Complex electronics may be required but essentially one can control precisely and at the turn of a knob the repetition rate and the Q-change for each pulse. The latter is particularly advantageous since it not only enables one to achieve equal intensity pulses (or pulses with particular energies) but it also enables the attainment of very high repetition rates where there may be negligible repumping of the rod between consecutive pulses. MHz repetition rates have been achieved (Rowlands 1969) and, although one must remember that the energy per pulse must be rather small in this case, the total output goes up with repetition rate so long as the losses do not also go up.

The SA gives multiple pulses if the rod is repumped to threshold after the first pulse. Since the operation of the SA depends upon a certain gain being reached in the rod, and since a given gain always occurs at the same stored energy, then the multiple pulses will ideally be of equal energy. The time taken to reach this gain depends upon the pumping rate which varies throughout the flash. Thus we have equal energy pulses with a variable frequency. In practice however the pulse energy also tends to vary due to the tendency of the SA not to operate reversibly at each pulse (chemical change). The repetition rate (and pulse energy) is varied by changing the dye concentration and can, for low concentrations, be very high.

Repetitive pulsing with RM (Gates, Hall and Ross 1968) has a precisely defined and controlled repetition rate, more controllable than SA and simpler to control than PC. Unlike the other two, its optical quality is not upset by the repetitive pulsing. On the debit side however the time available for each pulse to build-up decreases with increasing rotational

speed of the RM, thus requiring an increasing gain for a pulse to appear at all. Furthermore, if this 'threshold' gain is exceeded, more repumping than the other two Q-switches is required between pulses in order to reach threshold again. Hence there is a limitation on repetition rate. However, there are ways of reducing the effect of this limitation and the following are two examples:-

(a) Increasing the number of faces on a RM increases the repetition rate without increasing the rotational speed i.e. without increasing the 'threshold'.

(b) If a multiple faceted RM is used each face might select a different part of the rod, thus eliminating the need for rapid repumping between consecutive pulses.

Our choice of rotating mirror as the Q-switch is partly due to a need for a better understanding of its operation and partly due to the following points, which are taken from the above analysis:-

(a) It is of high optical quality and hence it is suitable for low transverse mode operation.

(b) It's damage resistance is high.

(c) It is more economic and simpler than the PC and more controllable than the SA.

3.2.3 Mention should be made of the acoustic-optic Q-switch, which is becoming increasingly common particularly in cw-pumped high repetition rate laser systems (Chesler et al 1970).

An ultrasonic field is induced in a block of transparent material (often glass or silica) using transducers cemented to its side face. The ultrasonic field results in a three-dimensional refractive index field in the medium which acts as a three dimensional diffraction grating. Inside

a laser cavity this grating constitutes a loss since it diffracts light away from the axial direction. Removal of the ultrasonic field removes the loss, thus acting as a Q-switch.

The advantages of the system are:-

(a) Low cost and compactness. Power requirements are around 1 watt, and the low voltage requirement as compared to PC lends the device to small scale transistorization.

(b) High flexibility of selection of repetition rate and triggering. In this respect it is even better than PC because of the lower voltage requirement.

(c) Low insertion loss (can be negligible for anti-reflection coated low absorption glass or silica), low optical distortion and very high damage resistance.

Disadvantages are:-

(a) Relatively slow change of Q. The rise time is limited by the aperture divided by the velocity of sound in the medium, and this means a practical limit of ~100nS (1mm aperture using glass).

(b) Limited loss. 75% loss has been claimed but in general the device is restricted to low gain (e.g. cw) systems or ones operating near threshold. Polarization effects are present but are not well explored as yet.

3.3 Analysis of the Rotating Mirror Q-switch

This work stems from the lack of an adequate formulation of the problem for the case of high rotation rates, that is to say, speeds for which the mirror movement in the time for light to travel up and down the resonator is not negligible. Previous analyses e.g. Midwinter 1965, Arecchi et al 1964, Barjot 1971 state or imply quasi-stationary operation and may give

erroneous results with high-speed operation. To give examples of the two extremes:-

(i) A slow mirror rotating at 50 Hz (3,000 rpm) moves 10^{-4} rad in 333.3nS and light moves up and down a 50 cm resonator 112 times in this time. The quasi-stationary solution might then be expected to work in this case.

(ii) A fast mirror rotating at 2000 Hz (120,000 rpm) moves 10^{-4} rad in 8.3nS and light only makes 3 double passes of the resonator in this time.

A more realistic analysis consists of a pass by pass calculation of the complete pulse build-up starting from noise. A complete analysis must include (i) diffraction (ii) transverse and axial distributions of field (iii) variation of gain with wavelength and other effects of having a distribution of frequency (iv) Doppler effects.

The simple calculation presented here neglects diffraction, axial distributions of inversion and field, the effects of finite initial spectral width, and Doppler effects. The first assumption implies high Fresnel number which is normally the case with a spinning mirror, since an aperture or angular limiting device not only reduces the Fresnel number but also reduces the number of available transits for build-up of the pulse thereby increasing the threshold. The second assumption makes a significant difference to the efficiency with which energy is coupled out of the rod but the pulse shape is not greatly affected. The difference made by this assumption in the case of fast rise Q-switching (e.g. Pockels cell) is seen by the difference between the analyses of Wagner and Lengyel (1966) and Wenzel (1967), the latter being the more rigorous, and we make the reasonable assumption that similar differences apply in the fast mirror situation.

The assumption that the spectral width can be neglected is valid if the gain is constant over the effective output spectral width (after pulse build-up) and if all the excited ions can be stimulated to emit at the output wavelength. The first condition is met when as in our laser the spectral width is narrowed to give appreciable temporal coherence. The second condition requires a homogeneously broadened laser transition line or an inhomogeneously broadened one with a fast rate of cross-relaxation (see section 2.3.2.2 chapter 2). Doppler effects in rotating Q-switches have been considered by Kafri et al (1971). The effect is a frequency shift of the laser beam resulting from the axial component of velocity of the rotating mirror. Since the mirror is rotating, different parts of the incident beam see different mirror velocities, and are subject to different frequency shifts. The result is a broadening of the output spectrum which increases with the mirror rotation speed and the beam diameter. An overall frequency shift of the spectrum also occurs if the mirror is not rotating in its own plane. The only possible effect on the Q-switch pulse dynamics occurs in an ideal single mode laser when the pulse length is given by the reciprocal of the spectral width. This occurs very rarely.

3.3.1 Threshold Considerations

Before proceeding with a calculation of the pulse build-up it is useful to consider what information can be obtained in a simple way about the spinning mirror situation.

3.3.1.1 First the threshold condition is calculated. Let us define the threshold condition as the situation in which the output power reaches a given value (say P_T). If the double pass gain of the laser resonator is G then:-

$$P_T = P_o G_T^{N_M} \qquad \ldots (3.1)$$

where P_o = output due to fluorescence, T = value at threshold,

and N_M = Maximum available number of cavity passes

Now $G = RS \exp 2\ell(\alpha-\beta)$

where α = gain coeff. β = loss coeff.

R = output mirror reflectivity

$1 - S$ = total of other losses per pass

ℓ = rod length

$$\left[RS \exp 2\ell(\alpha_T-\beta)\right]^{N_M} = \frac{P_T}{P_o}$$

Taking natural logarithms of both sides:-

$$\ln R + \ln S + 2\ell(\alpha_T - \beta) = \frac{1}{N_M} \ln (P_T/P_o \qquad \ldots (3.2)$$

Now $\alpha_T = \sigma N_T' = \sigma f(E_T)$; where E_T = input energy at threshold;

N_T' = inversion density at threshold

$$\text{Hence } \sigma f(E_T) = \frac{1}{2\ell N_M} \ln (P_T/P_o) - \frac{1}{2\ell} \ln R - \frac{1}{2\ell} \ln S + \beta \qquad \ldots (3.3)$$

thus enabling $f(E_T)$ to be calculated for a given pumping system, if N_M, R, S, β are known.

This equation is useful in two ways:

(i) With spinning mirror stationary ($N \to \infty$) and parallel to the output mirror, a graph of E_T vs.-ln R can be obtained experimentally. The extrapolated value of -ln R at $E_T = 0$ gives a value of the losses ($2\ell\beta$-ln S) while the shape of the curve gives information on f(E) (to be compared to that calculated).

(ii) An experimental graph of E_T vs. ω, the angular speed of the rotating prism, can be compared to a calculated graph resulting from a calculation of N_M as a function of ω.

A calculation of N follows, along with a novel geometric optimization procedure to obtain N_M which provides more than just the threshold information.

3.3.1.2 Calculation of N

Consider a plane mirror rotating at ω from an initial angle of α_o. The angle (Θ) which a ray makes to the axis is given by:-

$$\Theta_{N+1} = \Theta_N + 2(\alpha_o + N\omega\tau) \quad \text{where } \tau = \text{time for light to make a double transit of the resonator}$$

$$\therefore \Theta_{N+1} = \Theta_o + \sum_{0}^{N} 2(\alpha_o + N\omega\tau) = \Theta_o + 2(N+1)\alpha_o + N(N+1)\omega\tau$$

$$= \Theta_o + 2\alpha_o + (2\alpha_o + \omega\tau)N + \omega\tau N^2 \qquad \ldots (3.4)$$

The lateral distance (x) of the ray from the axis is given by:-

$$x_{N+1} = x_N + 2L'\Theta_{N+1} \quad \text{where } L' = L - \frac{\mu-1}{\mu}\ell. \text{ and } L = \text{resonator length}$$

ℓ = rod length

μ = rod index

$$\therefore \quad x_{N+1} = x_N + 2L' \left(\Theta_o + 2\alpha_o + [2\alpha_o + \omega\tau]N + \omega\tau N^2\right)$$

$$= x_o + \sum_0^N \left[2L'\Theta_o + 4L'\alpha_o + 2L'(2\alpha_o + \omega\tau)N + 2L'\omega\tau N^2\right]$$

$$= x_o + 2L' \left(\Theta_o + 2\alpha_o\right)(N+1) + L'(2\alpha_o + \omega\tau)N(N+1)$$

$$+ 2L'\omega\tau \tfrac{1}{3}N(N+\tfrac{1}{2})(N+1)$$

$$\boxed{x_{N+1} = \frac{2}{3} L'\omega\tau N^3 + 2L'(\alpha_o + \omega\tau)^2 N^2 + 2L'\left(\frac{2}{3}\omega\tau + 3\alpha_o + \Theta_o\right)N + 2L'(\Theta_o + 2\alpha_o) + x_o} \quad \ldots (3.5)$$

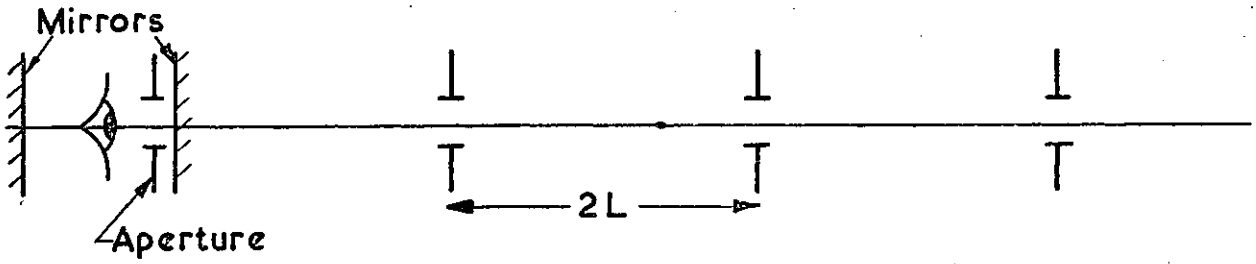
The number of available passes is the minimum value of N satisfying the above equation when $x_{N+1} = \pm R$, where R = radius of aperture. This N could then be maximised with respect to the variables α_o, Θ_o and x_o for any values of L', ω and R, by standard but rather ponderous methods.

3.3.1.3 A geometric method suggests itself from the physical nature of the problems, i.e. two mirrors facing each other.

Consider what is seen through an end mirror by a transparent observer positioned inside the resonator. If the mirrors are parallel and stationary he sees a set of concentric apertures going away into the distance. (Fig. 3.6A)

Figure 3.6A

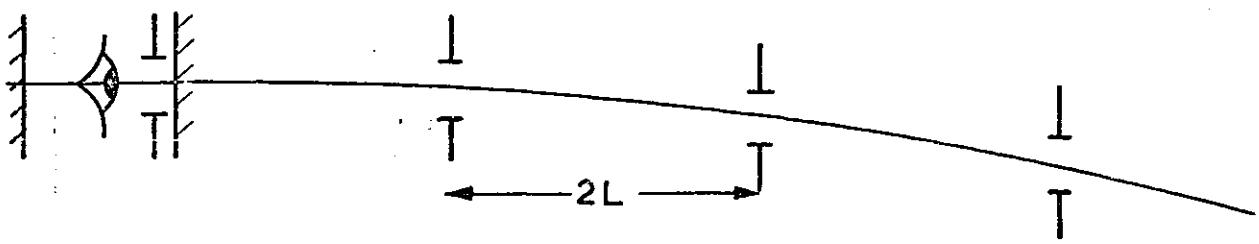
FIGURE 3.6A.



If one mirror is rotated through an angle (say φ), the observer sees, not concentric apertures, but apertures ever more rapidly disappearing out of the field of view as they go into the distance. (Fig. 3.6B)

Figure 3.6B

FIGURE 3.6B



If $\varphi \ll 1$ then all apertures can be considered parallel to the first and the perpendicular separation between consecutive apertures is 2L.

The same sequence of apertures but with a different locus of aperture centres occurs if one mirror is spinning. The locus in this case is given by the negative of Equation 3.5 with $x_o = \theta_o = 0$. Also $\alpha_o = 0$ (mirrors initially parallel) i.e.

$$-x_{N+1} = \frac{2}{3} L'\omega\tau N^3 + 2L'\omega\tau N^2 + \frac{4}{3} L'\omega\tau N$$

$$= \frac{2}{3} L'\omega\tau \left[N^3 + 3N^2 + 2N\right] \qquad \ldots (3.6)$$

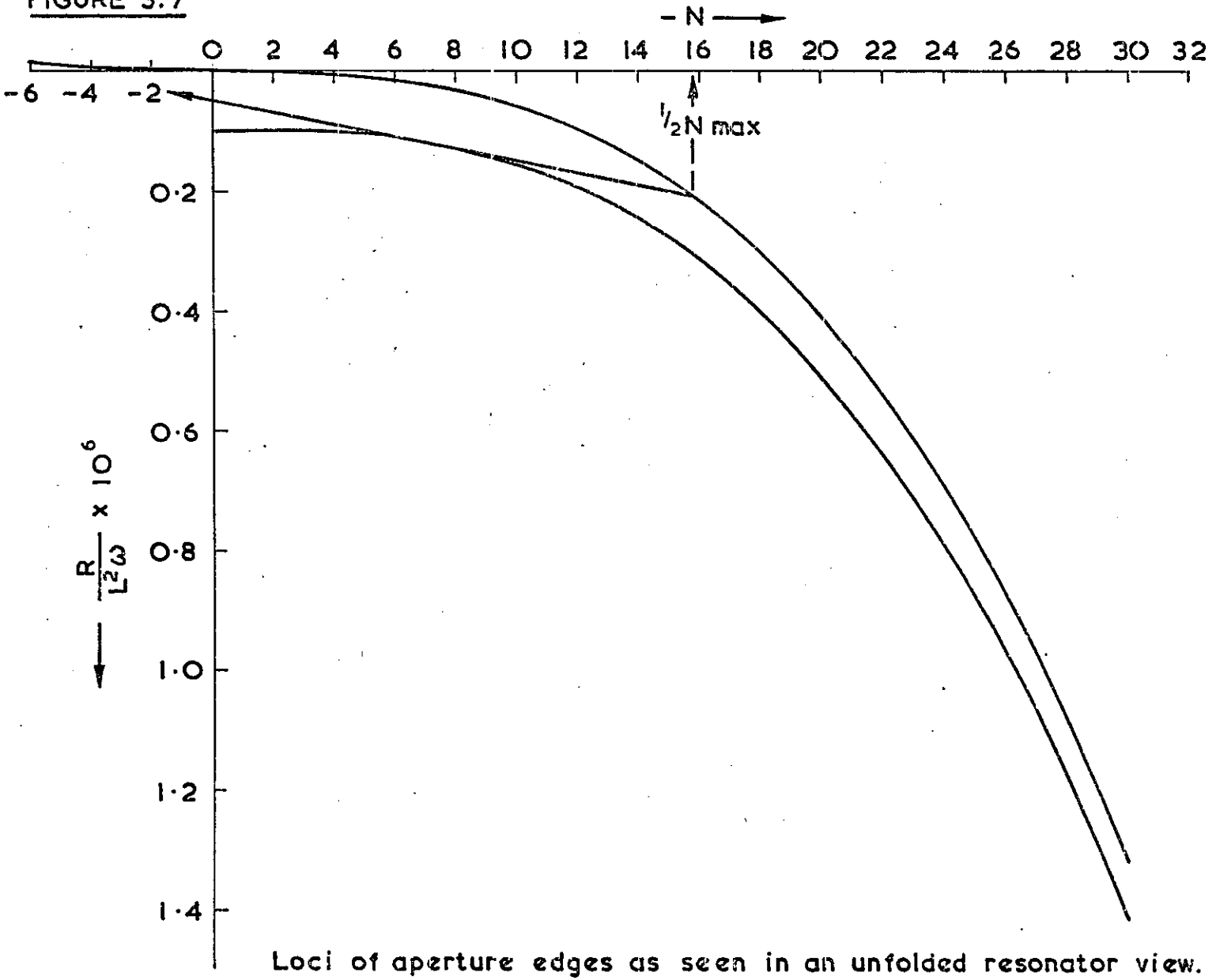
Looking in one direction represents the positive time direction (ω + ve) and looking in the opposite direction corresponds to the negative time extension of the resonator (ω -ve in Equation 3.5).

Figure 3.7 plots the loci of the aperture edges in one direction (for a typical value of $R/(L'^2\omega)$). Since this represents the 'view' of the aperture as seen by an observer inside the resonator all light rays travel in straight lines on this representation. The number of passes available to a ray with any initial parameters can quickly be obtained by drawing a straight line from the appropriate initial point (given by α_o and x_o) in the appropriate initial direction (given by θ_o) and observing where it first crosses one of the aperture edge loci. In particular the maximum number of passes is seen by inspection to be achieved by a ray passing through the origin and just grazing the convex locus line. Changing the aperture, mirror rotation speed or cavity length so that the product $R/(L'^2\omega)$ changes just corresponds to moving the aperture edge loci out or in. A plot of the maximum number of available passes as a function of $R/(L'^2\omega)$ is shown Fig. 3.8.

3.3.1.4 Further information can be obtained from the unfolded resonator representation.

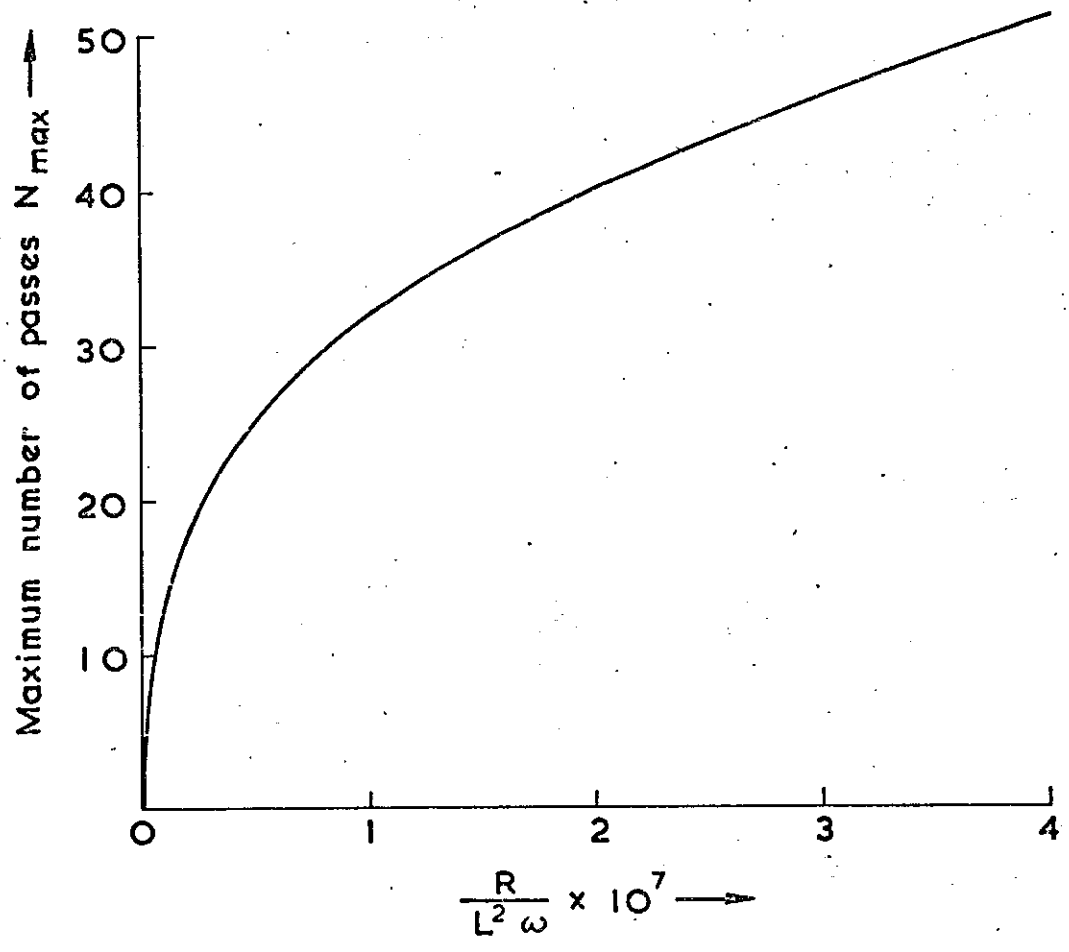
(i) For pumping above threshold, where the number of passes to reach a significant depletion of the material is less than N_M, the initiation of laser action can be determined. Inspection quickly indicates the first ray with a sufficient number of passes. Furthermore, during build-up of the pulse (before depletion is significant) the exact form of the output in angle and position can be determined.

FIGURE 3.7



Loci of aperture edges as seen in an unfolded resonator view.

FIGURE 3.8

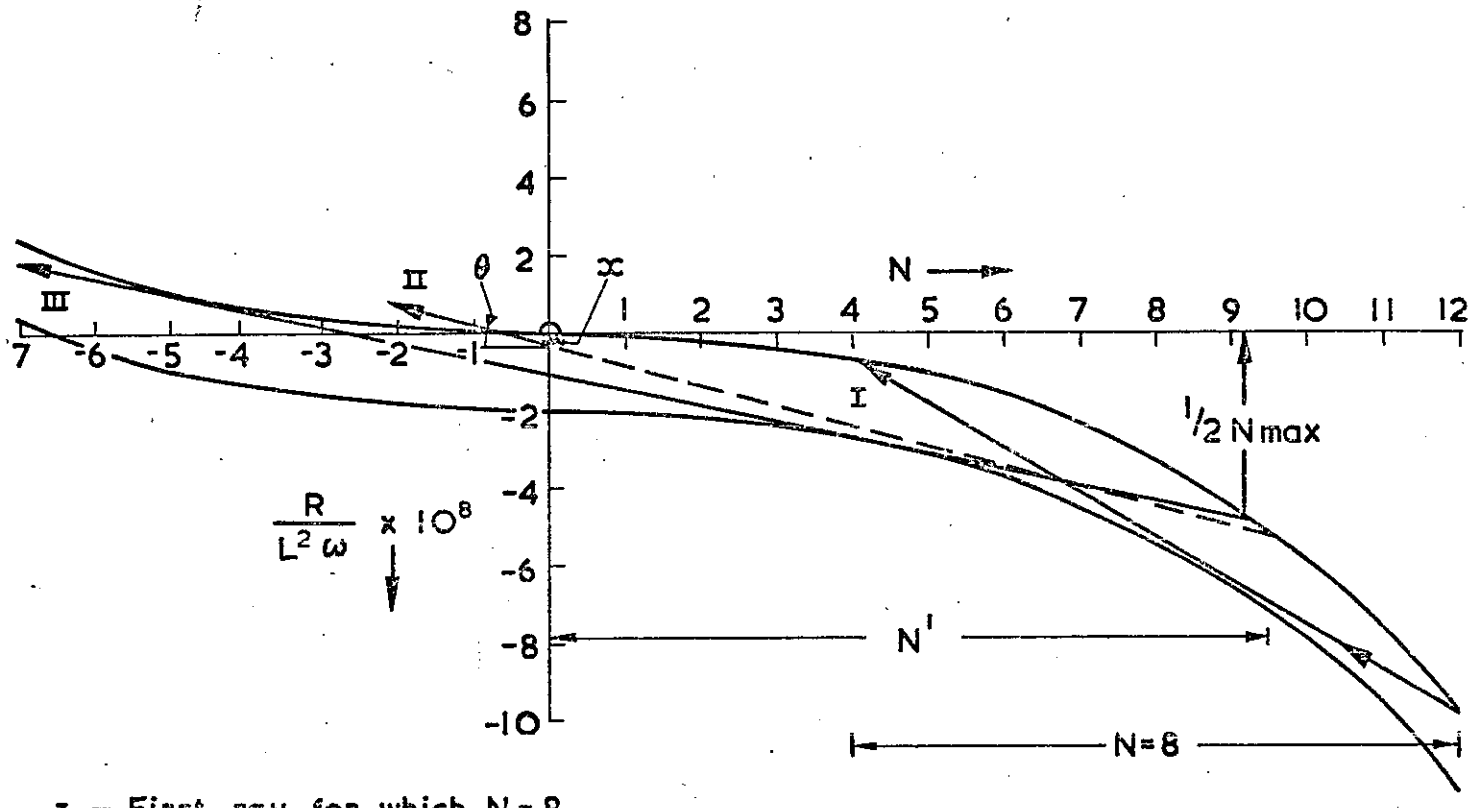


Variation of Q - switch open time with aperture (R), length (L) and angular velocity of spinning mirror (ω).

EXAMPLE Take the situation as shown by Figure 3.9, where $N_M = 18$. Let the pumping be increased so that the number of passes required to reach saturation is only 8. The first ray for which this is possible is shown and is seen to have originated at $N = -12$ or time = - 42 nS, before mirror parallelism. The output starts therefore to become appreciable at $N = -4$ ($t = -14$ nS). The distribution at say $N = 0$ is calculated as follows; the output at any position and angle at that time is given by $\phi_o G^{N'}$ where ϕ_o = fluorescence and G = double pass gain and where N' = number of passes of the ray of that position and angle drawn backwards to the first point of intersection of an aperture locus. For ray drawn in Fig. 3.9, $N' = 9.5$.

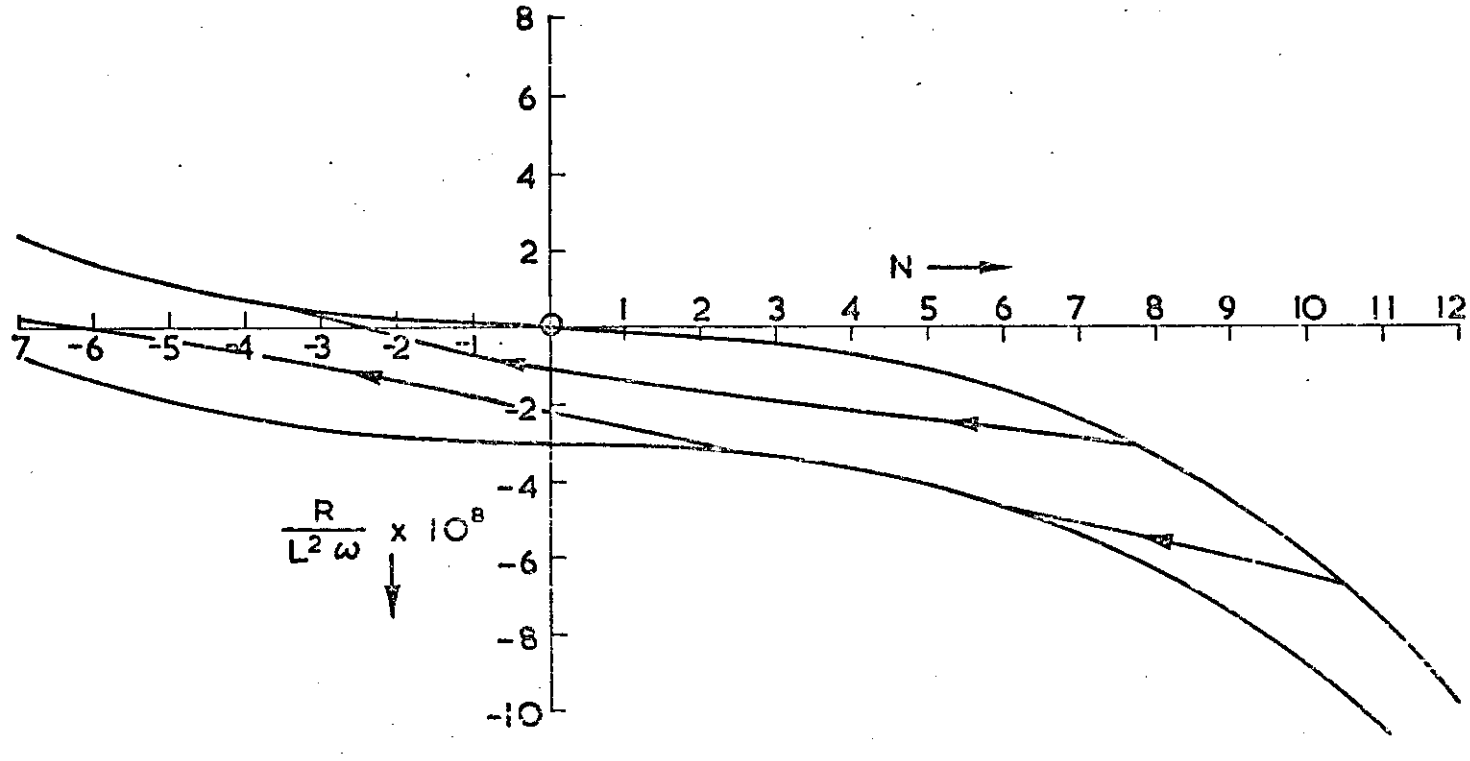
(ii) The above ray approach must necessarily be only an approximation, since we assume no diffraction loss or, in other words, the presence of a large number of modes with no loss. It is possible with the geometric representation to consider the diffraction losses of individual modes. Every ray considered previously can be considered as the direction of a mode with the same number of passes. All modes and all mode diameters are possible. The losses of the modes can be calculated, and quite easily for the important ones, which have significant diffraction losses at only one or two points in their path. The optimum mode diameter can be calculated for each mode and the optimum loss calculated at a function of mode. Thus at any time during the pulse (position on our graph) we can ascertain the mode (and its diameter) with minimum loss and we also know the other most likely modes together with an idea of the discrimination against them.

FIGURE 3.9



I = First ray for which N = 8
II = Ray arriving at (x, θ) when the mirrors are parallel.
III = Ray giving maximum number of passes.

FIGURE 3.10



Gaussian mode propagation up and down spinning mirror resonator.

EXAMPLE

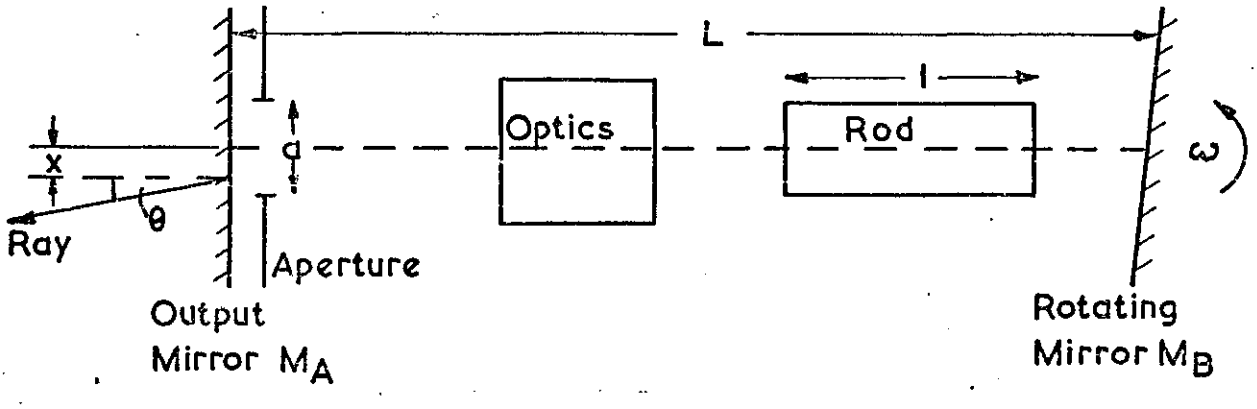
The ray in the last example, which has an output = $\phi_o G^{N'}$ has in reality an output = $\phi_o G^{N'} \Pi_p (D_M^p)$; where D_M^p = 1 - (loss of mode M at p^{th} aperture along the ray). Thus for example the mode shown in Fig. 3.10 has appreciable loss at two positions ($\Pi_p D_M^p = D_M^1 \times D_M^2$).

A mode starting as a gaussian does not in general come out as one since it is obscured unsymmetrically by the aperture edges.

3.3.2 The Calculation

Figure 3.11

FIGURE 3.11



3.3.2.1 Let the spatial and angular flux distribution at M_A after N double transits be $\phi(x, \theta)_N$ photons per sec. in dx and $d\theta$. The problem is essentially one dimensional since we only consider effects dependent upon the rotation of the mirror and this confines the sweep to a single dimension.

The distribution after N+1 double transits is given by

$$\phi(x', \theta')_{N+1} = RSG_N.\phi(x,\theta)_N + \phi(x',\theta')_o \qquad \ldots (3.7)$$

where G_N is a spatially dependent operator specifying the gain of the rod at the N^{th} double transit,

(x', θ') are new coordinates defined by the operation on (x, θ) of the operator O_N which specifies the resonator optics at that moment (including the effect of the spinning mirror)

$\phi(x', \theta')_o$ = distribution due to spontaneous emission,

R = reflectivity of the output mirror,

and 1-S = total fractional lumped losses.

Equation 3.7 enables a pass by pass calculation of the temporal, spatial and angular characteristics of the Q-switch pulse to be made.

3.3.2.2 Calculation of the Gain

The round trip gain of the rod is given by:-

$$G(x,\theta)_N = \exp 2\ell\left[\sigma N'(x)_N - \beta\right] \qquad \ldots (3.8)$$

where ℓ = rod length

β = loss coefficient of rod

$N'(x)_N$ = Number density of excited ions at coord x.

As shown by Equ. 3.8 the time and spatial dependence of the gain is determined by the variation of the excited population density with time and position.

This variation can be calculated from pass to pass using the following iterative relation:-

$$N'(x)_{N+1} = N'(x)_N - D.\phi(x)_N \qquad \ldots (3.9)$$

(Valid for plane parallel resonator and for θ small.)

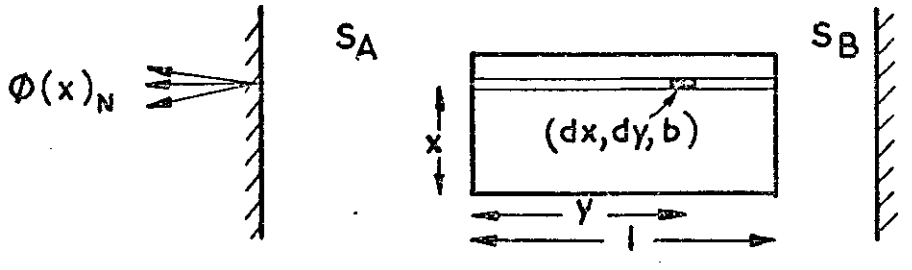
$$\text{where } \phi(x)_N = \sum_{\theta} \phi(x,\theta)_N$$

and $D.\phi(x)_N$ = depletion occurring on the N^{th} pass.

3.3.2.3 Calculation of D:-

Figure 3.12

FIGURE 3.12



$(1-S_A)$ and $(1-S_B)$ are the fractional losses on the two sides of the rod and $S_A S_B = S$

The depletion of the element shown is the sum of two contributions, travelling in opposite directions.

Consider the output as lumped into discrete amounts at times separated by the round trip time of the resonator. Then the number of photons at pass N in the element dx is $\tau \times \phi(x)_N$ and the depletion of the element at (dx, dy) is given by

$$RS_A\tau\phi(x)_N \left[(\exp(\sigma N(x)_N-\beta)y.)\sigma N(x)_N dy + S_B(\exp(\sigma N(x)_N-\beta)(2\ell-y))\sigma N(x)_N dy\right]$$

$\therefore$ total depletion of element at dx is given (integrating over length ℓ) by

$$\frac{RS_A\tau\phi(x)_N\sigma N(x)_N}{(\sigma N(x)_N-\beta)} \left[\exp \ell(\sigma N(x)_N-\beta)-1-S_B \exp \ell(\sigma N(x)_N-\beta) + S_B \exp 2\ell(\sigma N(N(x)_N-\beta)\right] \quad \ldots (3.10)$$

Let $S_B = 1$ $S_A = S$.

$\therefore$ depletion of element dx $= \dfrac{RS\tau\phi(x)_N}{(1-\beta/\sigma N(x)_N)} \left[\exp 2\ell(\sigma N(x)_N-\beta)-1\right]$

but volume of element = dx.ℓ.b where b = depth of rod taking part in laser action.

$$D\phi(x)_N = \frac{RS\tau\left[\exp 2\ell(\alpha-\beta)-1\right]}{dx.\ell b.(1-\beta/\alpha)} \cdot \phi(x)_N \quad \ldots (3.11)$$

where α = gain coefficient = $\sigma N'(x)_N$

β = loss coefficient.

3.3.2.4 Operator (O_N)

This is the operator characteristic of the spinning mirror and any resonator optics which enables calculation of the change of coordinates of a ray in pass $N \rightarrow N+1$.

The equation relating the coordinates before and after the $(N+1)^{th}$ pass is

$$\begin{bmatrix} x' \\ \theta' \\ 1 \end{bmatrix}_{N+1} = O_N \begin{bmatrix} x \\ \theta \\ 1 \end{bmatrix}_N \qquad \ldots (3.12)$$

where O_N is a 3×3 matrix operator.

The usual 2×2 matrix representation is not adequate for optical systems containing elements, such as a tilted mirror, which deviate an axially directed ray.

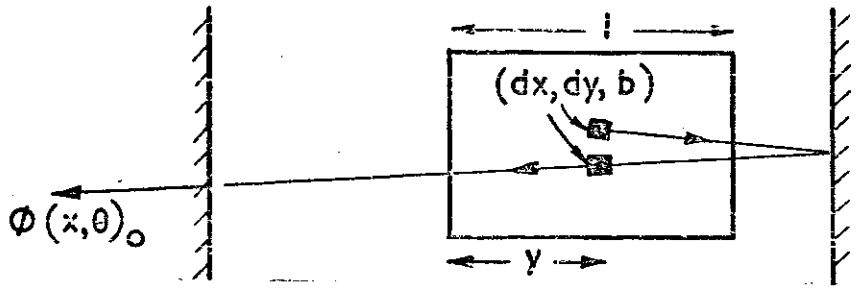
For our simple resonator with a plane mirror rotating with angular velocity ω from an initial $(N = 0)$ angle of α_o towards the normal position, the use of the matrix method offers no advantage since the coordinate transformation equations are just:-

$$\begin{aligned} \theta' &= \theta + 2(\alpha_o + \omega[t - \tfrac{1}{2}\tau]) \\ &= \theta + 2(\alpha_o + \omega\tau[N - \tfrac{1}{2}]) \qquad \ldots (3.13) \\ x' &= x + (L - \frac{\mu - 1}{\mu}\ell)(\theta + \theta') \qquad \ldots (3.14) \end{aligned}$$

3.3.2.5 Initial flux $\phi(x,\theta)_o$ due to fluorescence

Figure 3.13

FIGURE 3.13



Assuming the rotating mirror is effectively normal to the axis there are two contributions to $\phi(x,\theta)_o$ from elements at y

$$\text{thus } d\phi(x,\theta)_o = \frac{N(x)_o}{T} \cdot dxdyb \cdot \frac{d\theta\Omega}{4\pi} \cdot [\exp(\alpha-\beta)y + \exp(\alpha-\beta)(2\ell-y)]$$

where T = fluorescent decay time;

Ω = divergence angle of radiation in plane perpendicular to plane of θ.

We again assume $S_A = S$ and $S_B = 1$. Integrating over y, gives

$$\phi(x,\theta)_o = \frac{b\Omega N(x)_o}{4\pi T} \cdot dxd\theta \cdot \frac{(\exp 2\ell(\alpha-\beta)-1}{(\alpha-\beta} :$$

$$\text{or } \phi(x,\theta)_o = \frac{b\Omega dxd\theta}{4\pi T} \frac{\exp 2\ell\,[(\sigma N'(x)_o-\beta)-1]}{[\sigma-\beta/N'(x)_o]} \qquad \ldots (3.15)$$

3.3.2.6 <u>To sum up</u>:-

At $t=0$ ($N=0$), the flux distribution at the output mirror is that due to fluorescence, namely,

$$\phi(x,\theta)_o = \frac{b\Omega[\exp 2\ell(\alpha-\beta)-1]}{4\pi T\sigma[1-\beta/\alpha]} \cdot dxd\theta$$

and the inversion density distribution $N'(x)_o$ and other relevant parameters are chosen to apply to the particular spinning mirror laser system.

Thereafter the following set of equations (from 3.7 and 3.8, and 3.9 and 3.11) enable a pass by pass calculation of the pulse build-up to be carried out:-

Equ. 3.7 and 3.8 give:-

$$\phi(x',\theta')_{N+1} = \phi(x',\theta')_o + RS \exp 2\ell\,[\sigma N(x)_N-\beta]\phi(x,\theta)_N \quad \ldots (3.16)$$

while Equ. 3.9 and 3.11 give:-

$$N(x)_{N+1} = N(x)_N - \frac{RS\tau\,[\exp 2\ell(\sigma N[x]_N-\beta)-1]}{dx.\ell b.(1-\beta/\sigma N[x]_N)} \phi(x)_N \qquad \ldots (3.17)$$

where $$\phi(x)_N = \sum_{\theta} \phi(x,\theta)_N$$

and (Equ. 3.13) $$\theta' = \theta + 2(\alpha_o + \omega\tau[N-\tfrac{1}{2}])$$

(Equ. 3.14) $$x' = x + 2(L - \frac{\mu-1}{\mu}\ell)\,(\theta + [\alpha_o + \omega\tau(N-\tfrac{1}{2})])$$

3.3.2.7 Appendix I lists the computer program, together with an explanatory flow diagram.

We merely present here some examples of the computer output against which it will be useful to compare the experimentally obtained data on our laser.

The laser parameters used in the calculation were as follows:-

Size of rod = 10 × 0.5 × 0.5 cms; its refractive index (μ) = 1.5;

Stimulated emission cross-section (σ) = 3×10^{-20} cm^2; Loss coefficient (β) = 0.007 cm^{-1};

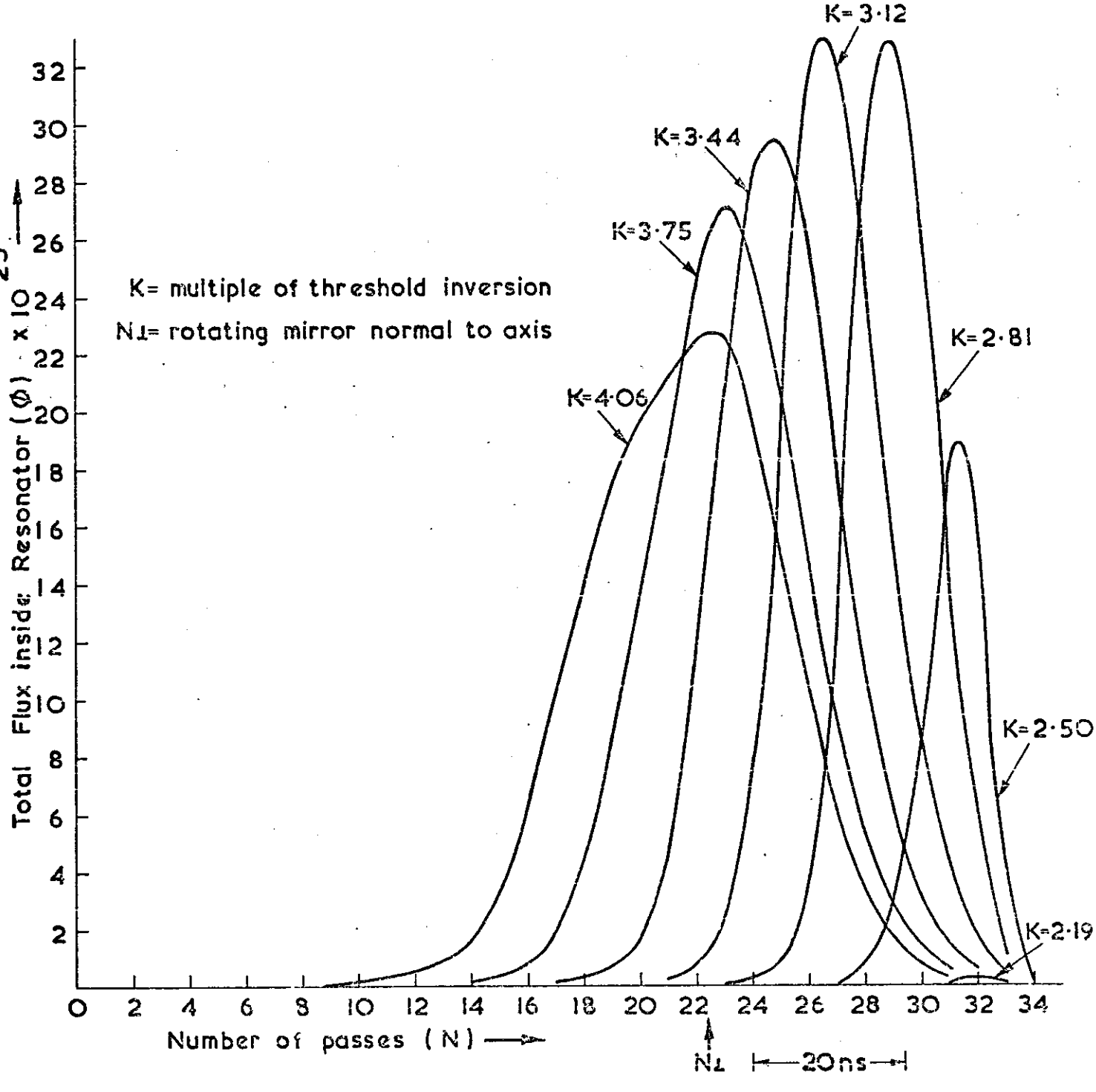
Fluorescent lifetime (T) = 500 μs;

Cavity length (L) = 50 cms; Reflectivity (R) = 50%;

Other losses = 10% = 1 - S.

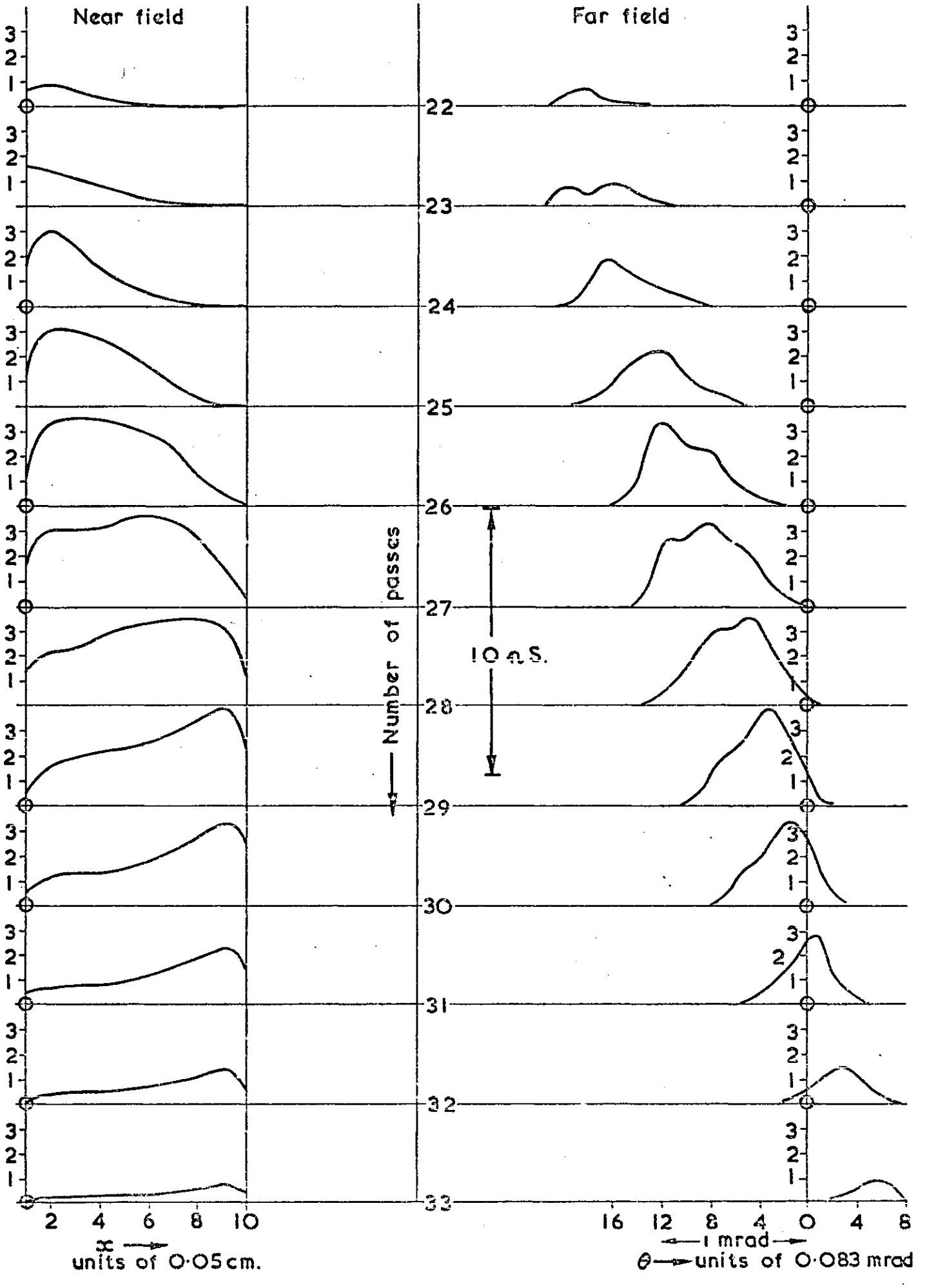
Figure 3.14 shows the output pulse form for different pumping levels at a mirror speed of 6000 rad/s. Other information available is exemplified by Figs. 3.15, 3.16 and 2.17, showing the far-field and near-field over one entire pulse, the effect on divergence at pulse peak of changing the pumping level, and the efficiency curve. Fig. 3.18 is a curve showing the dependence of integrated output on reflectivity, and Fig. 3.19 shows the dependence of threshold on mirror rotation speed.

FIGURE 3.14



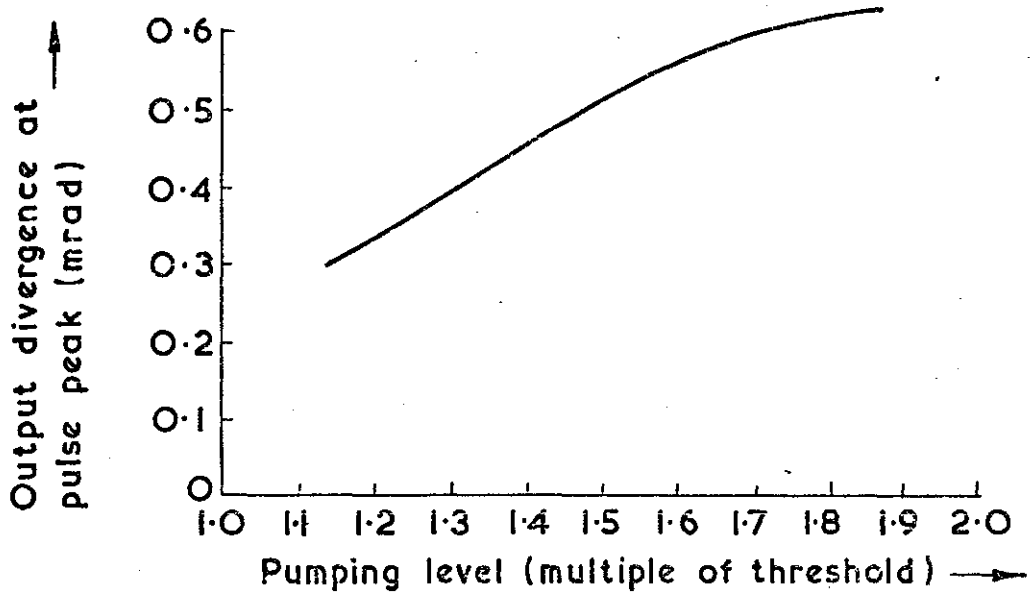
Pulse evolution in a spinning mirror Q-switched laser.

FIGURE 3.15



Temporal evolution of near field and far field during a Q-switch pulse.

FIGURE 3.16



EFFECT ON FAR-FIELD DISTRIBUTION OF VARYING LASER INPUT.

FIGURE 3.17

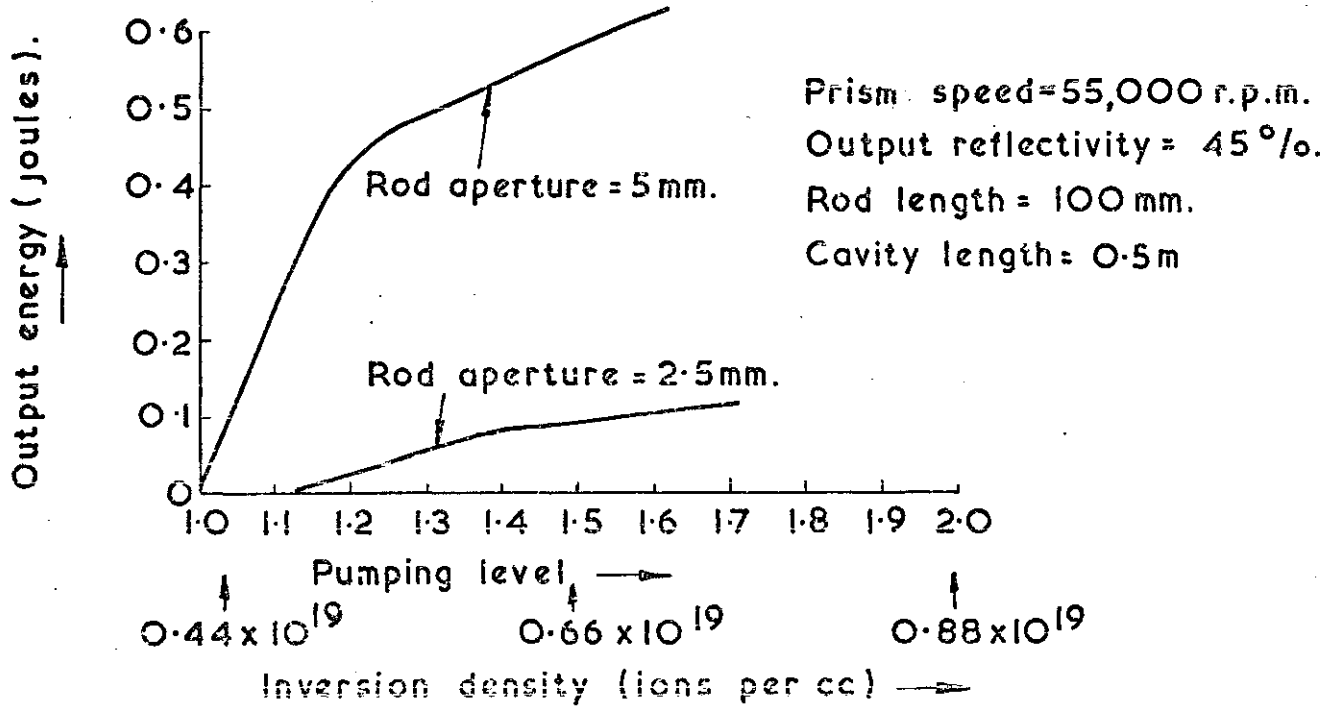
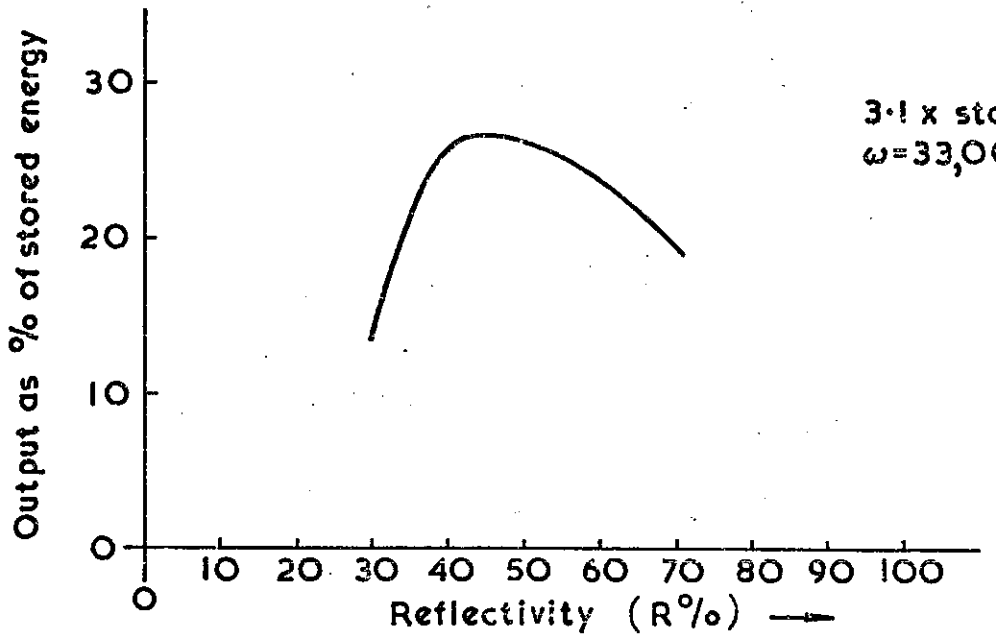
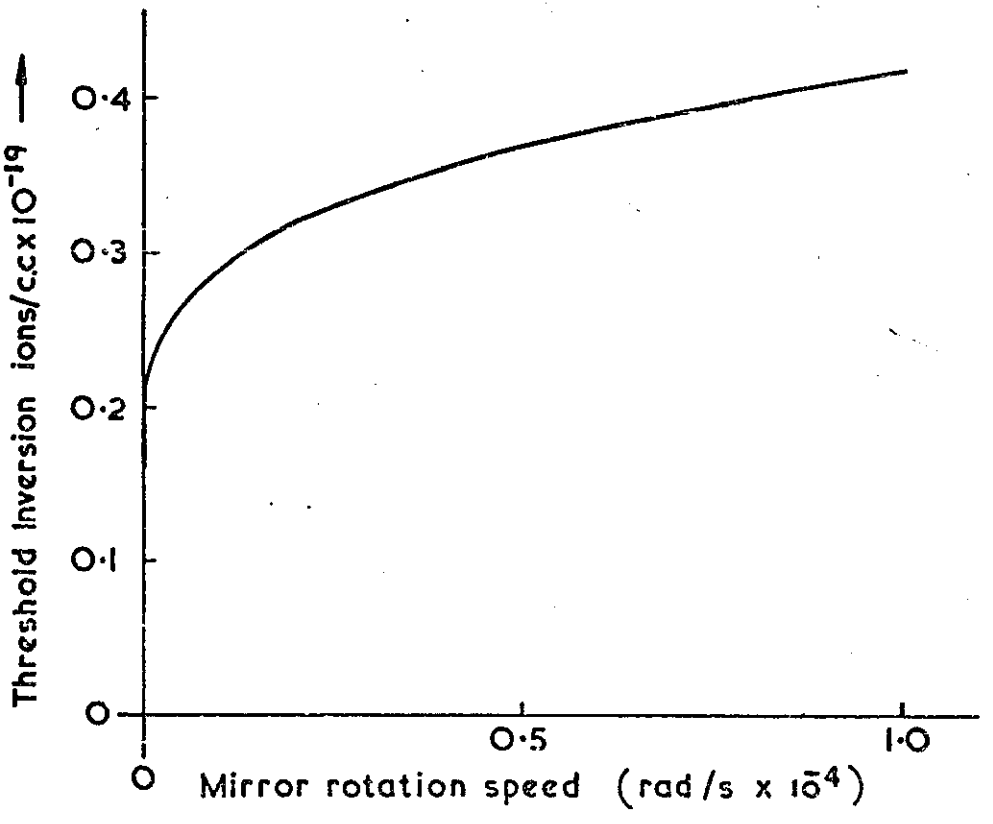


FIGURE 3·18



Effect of reflectivity on output for a given mirror speed and pumping level

FIGURE 3·19



Variation of Threshold with Mirror Speed

Some interesting points emerge from the results of the calculation

(i) The variation of threshold inversion with mirror rotation speed (Fig. 3.19) can be compared with the results of the threshold considerations, as given by Fig. 3.8, which plots the maximum number of available passes as a function of mirror rotation speed. Since the total gain in N passes must be constant at threshold (to raise output from fluorescence to a given threshold output level) and since this gain is proportional to $\exp(2\ell\sigma N \times [\text{inversion-inversion at } N = \infty])$ then it follows that (threshold inversion-threshold inversion at $N = \infty$) $\times$ maximum number of available passes is invariant. This product was calculated from Figs. 3.8 and 3.19 for a range of values of ω and was found to be constant to within 5%.

(ii) The temporal evolution of the pulse in the near and far field, as shown by Fig. 3.15, demonstrates clearly that there is considerable sweeping both in position and angle during the pulse and consequently that the quasi-stationary view of the spinning mirror is certainly not valid in this case. The sweeping is moreover not small since, in the example, the divergence of the emitted light does not exceed ~ 0.7 m rad although it is swept through ~ 2 mrad. The question arises as to which of these two figures for the divergence is the realistic one in practice when consideration may be given to obtaining the smallest possible focussed spot or to specifying the laser coherence. In both these cases the smaller value is likely to be the more valid since a beam swept simultaneously both in position and angle can to a first approximation be transformed into a beam swept only in position or one swept only in angle whichever is required, and the value of the fixed parameter in these two situations is just the instantaneous value for either the near or the far field as shown in Fig. 3.15.

(iii) Fig. 3.14 of the output pulse shape as a function of pumping level shows that the spinning mirror Q-switch at a given speed is optimum for one pumping level only (in this case; $k \simeq 3$). For excessive pumping, the Q-switch is too slow, resulting in increasing pulse width and low peak power, and for insufficient pumping, it is too fast, resulting in reduced peak power and inefficient operation. The efficiency curve of Fig. 3.17 also demonstrates this low efficiency at low pumping levels. Another significant fact shown by Fig. 3.14 is that the pulse peak under optimum operation occurs sometime after the spinning mirror is normal to the laser axis. This is contrary to the widely accepted view that the peak, under optimum operation, should occur simultaneously with the mirror arriving at the normal position.

(iv) Fig. 3.18, the optimization curve for reflectivity, is typical of such curves, giving an optimum reflectivity for the situation taken of 45%. This is close to the peak reflectivity (40%) of a two plate silica resonant reflector as described and designed in Chapter 5.

3.4 Pumping Efficiency and Distribution of Inversion

We now turn our attention to another important part of the laser process, the pumping of the laser rod. The calculation of the efficiency with which radiation incident on a Nd:glass rod is converted into a density of ions in the excited laser level (inversion population density) and into heat, and of how these depend upon the position in the rod has not been adequately treated in the literature although Borrelli and Charters (1965) provide some information and Cooke et al (1964) do the calculation for ruby. In filling this gap, we have investigated how the distribution of inversion density depends upon factors, such as the pumping wavelength, the rod radius, the refractive index of the Nd:glass, the doping level of Nd in the glass and the surface finish on the rod.

3.4.1 The Calculation

The calculation of the inversion and heat density as a function of radial position is performed as an integration both in three dimensions and over the pumping spectrum, and is carried out using a KDF9 digital computer.

All possible situations could not be encompassed in a limited time, necessitating a choice in respect of some of the variables.

The first choice concerns the incident radiation on the rod, and this we take to be uniformly distributed and to have a black body spectrum corresponding to a temperature of 6500°K. This spectrum corresponds roughly to that of a Xenon flash tube (Edwards 1967), while the temperature is approximately optimum for pumping neodymium. Information on the effect of wavelength is obtained by dividing this spectrum up into 4 parts, which roughly fit the regions of high and low absorption for Nd in glass, and doing the calculation on these parts separately before adding them together to give the pumping due to the entire spectrum.

Two forms of surface finish on the rod are considered; completely diffuse and highly polished (specular). Any other surface can be regarded as a combination of these two.

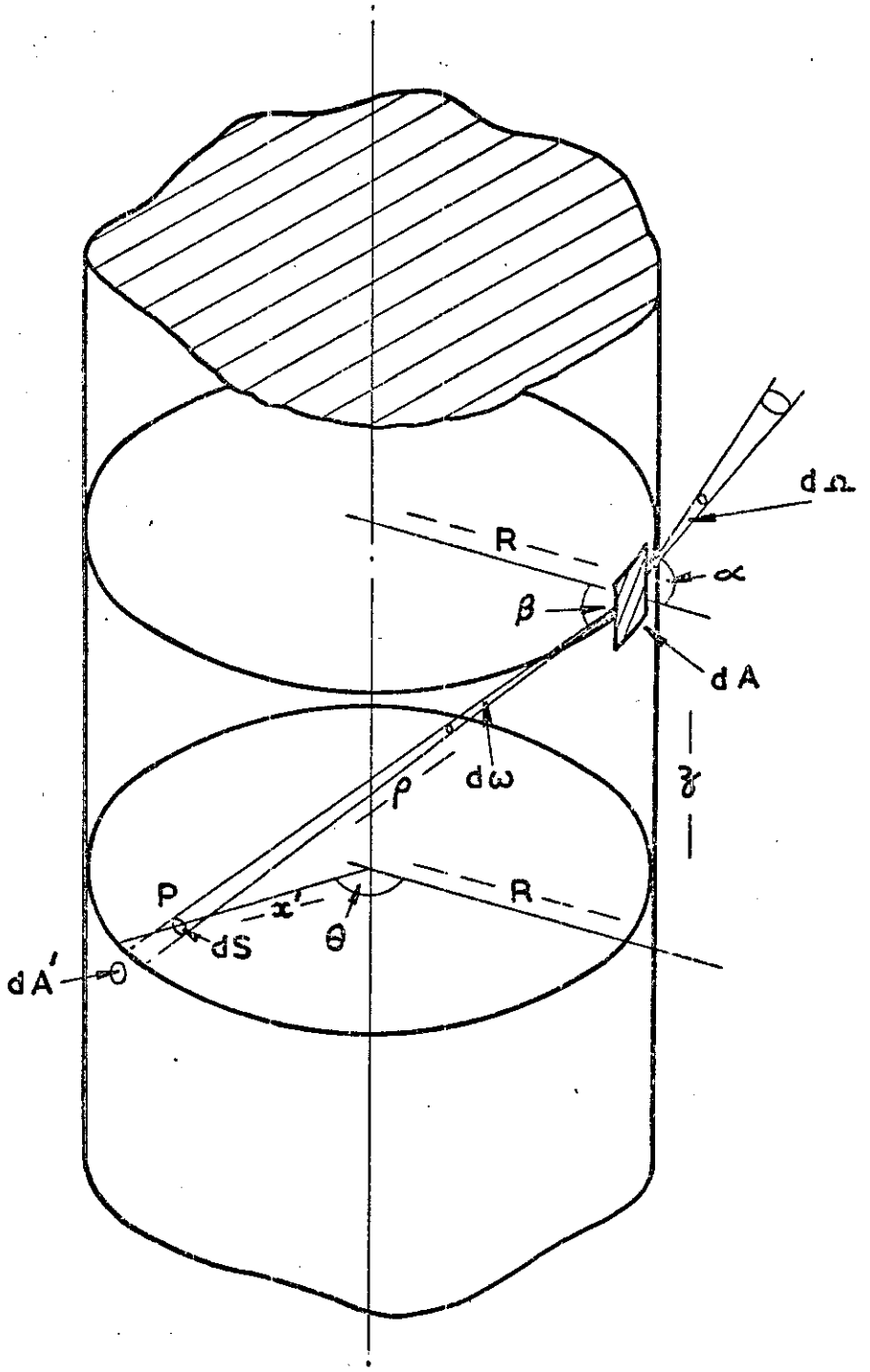
For the above specified cases the upper level population density and the heat density are calculated at ten points along the radius as a function of the radius, the concentration of Nd and the refractive index of the glass.

3.4.1.1 Fig. 3.20 represents a section of the rod.

Let energy incident on an element dA of the rod surface at an angle α to the normal and in the solid angle $d\Omega$ be $dW(dA,d\Omega,\alpha)$

Then $$dW(dA,d\Omega,\alpha) = I_o dA \cos\alpha \; d\Omega \qquad \ldots (3.18)$$

FIGURE 3.20



where I_o = the incident intensity and is in general a function of wavelength (λ), position on the rod surface and angle to the surface normal (α). Our assumption makes I_o independent of the last two, so we can write $I_o(\lambda)\,d\lambda$ for I_o, and we must then replace $dW(dA,d\Omega,\alpha)$ by $dW(dA,d\Omega,\alpha,\lambda)d\lambda$. By integrating over all angles we obtain the energy per unit area on surface $W(\lambda)d\lambda$

where $$W(\lambda)d\lambda = \int_{\alpha,\Omega} dW = \pi I_o(\lambda)d\lambda \qquad \ldots (3.19)$$

3.4.1.2 Specular Surface

In the case of a rod with a specular surface the element of energy given by Equ. 3.18 passes through the surface with transmission $T(\beta)$ into a solid angle $d\omega$ at an angle β to the surface normal;

Thus $$T(\beta)dW(dA,d\Omega,\alpha,\lambda) = dW(dA,d\omega,\beta,\lambda)$$

where $$\sin\alpha = n \sin\beta \qquad \ldots (3.20)$$

and $$\cos\alpha\, d\Omega = n^2 \cos\beta\, d\omega \qquad \ldots (3.21)$$

$$\therefore\ dW(dA,d\omega,\beta,\lambda) = T(\beta)I_o(\lambda)\, dAn^2 \cdot \cos\beta d\omega d\lambda \qquad \ldots (3.22)$$

where Eq. 3.22 results from a combination of Equ. 3.18, 3.20 and 3.21, and if the energy at P crossing the area dS normal to the beam and coming from dA is $dW(P,dA,dS,\lambda)$

then $$dW(P,dA,dS,\lambda) = dW(dA,d\omega,\beta,\lambda)e^{-g\rho} = \frac{T(\beta)I_o(\lambda)dAn^2\cos\beta dS e^{-g\rho}d\lambda}{\rho^2}$$

$$\ldots (3.23)$$

where ρ = distance from P to the surface element dA

and g = absorption coefficient of the material (Nd + glass)

and where we have used the identity $d\omega = dS/\rho^2$

g is a function of wavelength (λ), and concentration (c) of Nd, but to keep the equations simpler, this dependence is not explicitly stated. Since the useful absorbed energy density is the energy per unit area multiplied by the absorption coefficient of Nd, the element of energy absorbed by Nd in $d\lambda$ per unit volume at P and coming from dA is just $dW(P,dA,dS,\lambda)h(\lambda)$ and substituting for $dW(P,dA,dS)$ from Equ. 3.23

$$dW(P,dA,dS,\lambda)h(\lambda) = \left[\frac{T(\beta)W_o(\lambda).n^2\cos\beta e^{-g\rho}.d\lambda dA}{\pi\rho^2}\right]h(\lambda) \quad \ldots (3.24)$$

where $h(\lambda)$ is the absorption coefficient of the Nd ions at wavelength λ and where, using Equ. 3.19 $I_o(\lambda)$ has been replaced by $W_o(\lambda)/\pi$. Now if the total energy absorbed by the Nd ions per unit volume at P and in $d\lambda$ is $W(P,\lambda)$:-

$$W(P,\lambda) = \int_{dA} dW(P,dA,dS,\lambda)h(\lambda) = \frac{n^2W_o(\lambda)h(\lambda)d\lambda}{\pi}\int_A \frac{T(\beta)e^{-g\rho}}{\rho^2}\cos\beta dA \quad \ldots (3.25)$$

This absorption must be multiplied by λ/λ_o to give the absorbed energy into the upper laser level in $d\lambda$ at λ, where $\lambda_o = 1.06\mu$.

$\therefore$ W(P), the total energy density in the upper laser level due to absorption is given by

$$W(P) = \int_{\lambda} \frac{\lambda}{\lambda_o} W(P,\lambda)d\lambda = \frac{n^2}{\pi\lambda_o} \int_{\lambda} \lambda W_o(\lambda)h(\lambda) \int_{\theta}\int_{\beta} \frac{T(\beta)\sin\beta e^{-grR}.d\beta d\theta d\lambda}{\sqrt{r^2 \sin^2\beta - x^2\sin^2\theta}} \quad \ldots (3.26)$$

where dA has been expressed in terms of the angular variables β and θ and using $x = \frac{x'}{R}$ where x' = radius coordinate of dS,

R = rod radius

$$\text{and} \quad r = \frac{\rho}{R} = \frac{1 - x\cos\theta}{\cos\beta}$$

The contribution to the energy absorption at P made by radiation reflected one or more times within the rod can be shown to be equal to W(P) multiplied by a factor

$$\sum_{m=1}^{\infty} \frac{[R'(\beta)\exp(-gr_oR)]^M}{(1+Mr_o/r)^2}$$

where r_o = (length of the line from dA through P to the rod surface)/R

$= \rho_o/R$

and $R'(\beta)$ = reflection coeff. of the surface at an angle β.

A rough estimate of the contribution of internal reflections shows it to be less than 1% and we consequently neglect it.

$$T(\beta) \text{ for a specular surface} = \frac{(n+1)\cos\alpha(\cos\alpha+\cos\beta)}{(n\cos\alpha+\cos\beta)(\cos\alpha+n\cos\beta)}$$

this being the average over both polarizations.

3.4.1.3 Diffuse Surface

We assume that the surface of the rod is perfectly diffuse and has a transmission of $\frac{1}{2}$.

Using previous notation $dW(dA,d\omega,\beta,\lambda)$ the energy in $d\lambda$ leaving the area dA at the angle β in the solid angle $d\omega$ is given by

$$dW(dA,d\omega,\beta,\lambda) = \frac{W_o(\lambda)dA\cos\beta d\omega d\lambda}{2\pi} \qquad \ldots (3.27)$$

We now proceed just as in the specular case.
$dW(P,dA,dS,\lambda)$, the energy in $d\lambda$ crossing an area dS normal to the beam at P and coming from dA is now given by

$$dW(P,dA,dS,\lambda) = \frac{W_o(\lambda)dA\cos\beta dS e^{-g\rho}d\lambda}{2\pi\rho^2} \qquad \ldots (3.28)$$

and $W(P)$, the upper level energy density per unit volume at P is given by

$$W(P) = \frac{1}{2\pi\lambda_o}\int_{\lambda}\lambda W_o(\lambda)h(\lambda)\int_{\theta}\int_{\beta}\frac{\sin\beta e^{-grR}d\beta d\theta d\lambda}{\sqrt{r^2\sin^2\beta - x^2\sin^2\theta}} \qquad \ldots (3.29)$$

To include internal reflections we must modify $W_o(\lambda)$ to take into account light reaching the surface from the inside and being reflected diffusely inwards again. From Equation 3.28, by putting $\rho = \rho_o$ and $dS = dA' \cos\beta$, the total energy in $d\lambda$ incident on dA' from the inside is

$$\frac{dA'W_o'(\lambda)d\lambda}{2\pi}\int_A \frac{e^{-g\rho_o}\cos^2\beta\, dA}{\rho_o^2} = W_o'(\lambda)d\lambda I(\lambda)dA'$$

where we have introduced $I(\lambda) = \frac{1}{2\pi}\int_A \frac{e^{-g\rho_o}\cos^2\beta}{\rho_o^2}\,dA$ and where

$W_o'(\lambda)$ is now the total energy density incident on surface from both sides

$\therefore W_o'(\lambda) = W_o(\lambda)$ from outside $+ W_o'(\lambda)I(\lambda)$ from inside

$$\text{or } W_o'(\lambda) = \frac{W_o(\lambda)}{1-I(\lambda)} \qquad \ldots (3.31)$$

Since $I(\lambda)$ is not negligible in comparison with 1, we cannot ignore it and $W(P)$, the absorbed energy per unit volume into the upper laser level at P is correctly given by

$$W(P) = \frac{1}{2\pi\lambda_o}\int_\lambda \frac{\lambda W_o(\lambda)h(\lambda)}{1-I(\lambda)}\int_\theta\int_\beta \frac{e^{-grR}\sin\beta\, d\beta\, d\theta\, d\lambda}{\sqrt{r^2\sin^2\beta - x^2\sin^2\theta}} \qquad \ldots (3.32)$$

where $$I(\lambda) = \frac{1}{2\pi}\int_\theta\int_\beta \frac{e^{-grR_o}\sin\beta\cos\beta\, d\beta\, d\theta}{\sqrt{r_o^2\sin^2\beta - \sin^2\theta}}$$

Note that this integral for $I(\lambda)$ (apart from the addition of an extra $\cos\beta$) is equal to that of Equation 3.32 with $x = 1$ and $r = r_o = \frac{1-\cos\theta}{\cos\beta}$

3.4.2 Evaluation of equations 3.26 and 3.32 is carried out on a KDF9 computer for various positions along the radius (various values of x between 0 and 1), various radii (R) and concentrations (c) and two values of refractive

index (n). Further, by substituting for $\frac{\lambda h(\lambda)}{\lambda_o}$ a factor $g(\lambda) - \frac{\lambda h(\lambda)}{\lambda_o}$ the heat distribution within the rod was also calculated. The absorption coefficients $g(\lambda)$ and $h(\lambda)$ were measured for LN6 Nd:glass material using an SP700 spectrophotometer.

Typical calculated distributions are shown (Fig. 3.21) for two concentrations of Nd^{3+}, splitting each up into contributions from four spectral regions. Also shown is the curve (Fig. 3.22) indicating how the inversion at the centre depends upon the concentration for a $^3/_8$" diameter rod.

Integration of the inversion density versus radius curve gives the total inversion of the rod.

The following three points are useful when considering the results.

(i) Since $h(\lambda) = ch_o(\lambda)$ and $g(\lambda) = ch_o(\lambda) + j(\lambda)$

where c = the percentage concentration of Nd

$h_o(\lambda)$ = the Nd absorption coefficients for 1% concentration

$j(\lambda)$ = the glass absorption coefficient

the inversion distribution is not a function of cR only. However for most of the spectrum $j(\lambda) \sim 0$ and then inversion distribution at radial position (ρ) = cx function of cR.

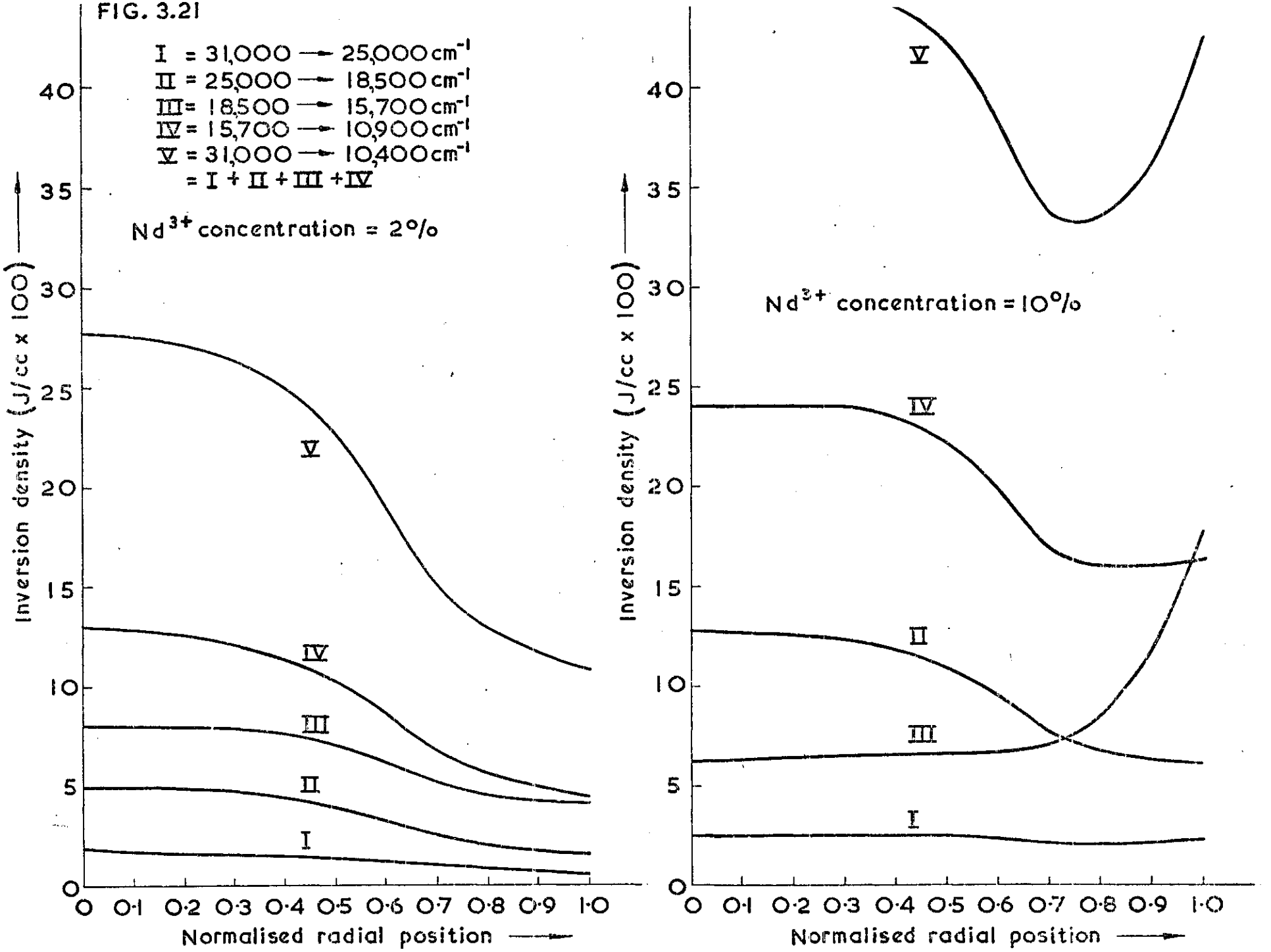
(ii) The calculation gives the inversion density in joules/cm^3 for an incident energy of 1 joule/cm^2 on the rod surface.

(iii) No account is taken of depletion processes such as spontaneous emission. The figures give the change in energy density in the upper laser level due solely to pumping.

3.5 Application to System Design

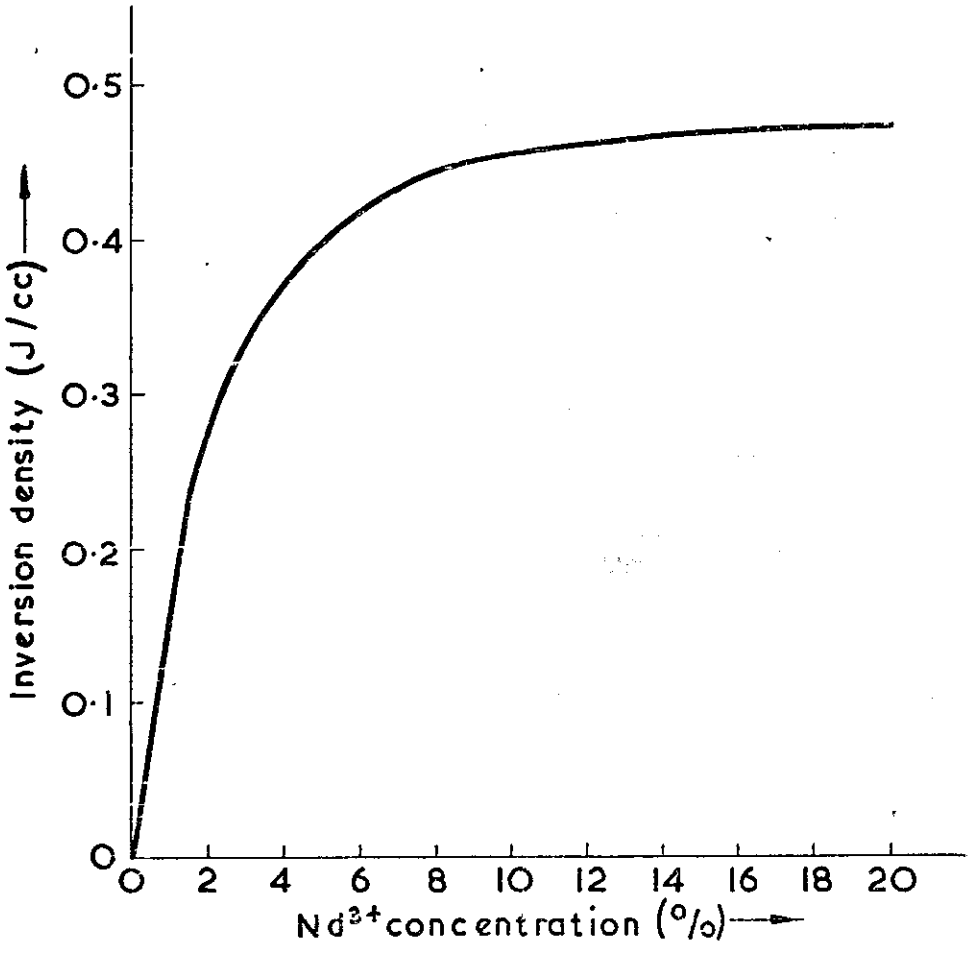
When trying to optimise a laser one is faced with achieving a best compromise between factors such as the following:-

FIG. 3.21



CALCULATED INVERSION VARIATION ACROSS PUMPED Nd: GLASS ROD

FIGURE 3·22



VARIATION OF INVERSION DENSITY ON AXIS WITH THE DOPING CONCENTRATION

(i) In a pulsed laser system the maximum permissible energy into the flash tube as determined by failure of the tube increases with the pulse length, suggesting that a long pulse is advantageous.

(ii) Too long a pumping pulse however is inefficient since the upper laser level is continuously being depleted at a rate inversely proportional to the lifetime.

(iii) High concentration improves the inversion (computed result);

(iv) but high concentration is linked with a low upper level lifetime and thus is contrary to the requirement as indicated by (i) and (ii) above.

A rational treatment of all the factors, some of which, as shown above, are interdependent, is obviously required and this entails a mathematical formulation of the complete pumping and lasing system such as to include them all. Optimisation is then carried out.

3.5.1 The formulation is just that of forming the product of the efficiencies of each element of the laser process at which losses occur.

These parts are:-

(i) The pumping source. Let the lamp efficiency, defined as the energy radiated divided by the electrical energy dissipated, be H.

(ii) The pumping reflector system. Let G be the fraction of the energy leaving the source which reaches the rod.

(iii) The rod absorption. The pumping efficiency, which we have calculated for the case of the Nd: glass rod subjected to uniformly distributed pumping radiation, we denote by F. This is the increase of energy density in the upper laser level in joules/cc as a result of a pumping energy of one joule per square centimeter on the rod surface.

(iv) Unless the pump pulse is very short in comparison with the decay rate of the upper laser level, less than 100% of the atoms pumped into this

level contribute to lasing action. Let the useful fraction be J. Thus if a cw pump gives a rate of increase of energy density of $h\nu dN/dt$ in the upper laser level, where N = number of ions/cc in this level, then a power density $h\nu N_c/\tau$ is lost due to spontaneous emission, where N_c = threshold inversion and τ = lifetime of the upper laser level. In the case of Q-switch action where the pump pulse is often very closely approximated by a half-sine wave (Edwards 1968) of length t_o, and Q-switching takes place at maximum inversion,

$$J = \frac{\text{maximum inversion}}{\text{maximum inversion for } \tau >> t_o} = \frac{\pi}{2} \cdot \frac{\tau}{t_o} \sin \frac{\pi t_1}{t_o} \qquad \ldots (3.33)$$

where t_1 is the time of maximum inversion and is given by the solution of:-

$$[1+(\pi\tau/t_o)^2] \sin \pi t_1/t_o = \pi\tau/t_o e^{-t_1/\tau} + \sin \pi t_1/t_o - \pi\tau/t_o \cos \pi t_1/t_o \qquad \ldots (3.34)$$

(v) Laser action does not couple all the useful stored energy out of the cavity. A certain fraction, say K, is released into the cavity and a fraction equal to (to a close approximation) logR/logRS (Edwards 1968) of this is coupled out of the cavity, where R = output mirror reflectivity and S = 1 - fraction lost to all other losses. The fraction K above depends upon the mode of operation of the laser: and with non-Q-switched operation for example, can be approximated by the fraction of useful pumped energy which is not employed in raising the laser to threshold and maintaining it at threshold.

We now combine all these elements for the case of a pulsed laser. If the energy input to the flash tube = E joules, then from (i) above, the radiated energy from the flashtube = HE joules.

From (ii), the energy reaching the rod = GHE joules $\therefore$ Energy density on rod $= \dfrac{GHE}{2\pi r_o \ell_o}$ joules/cm^2 where r_o = rod radius; ℓ_o = rod length and

from (iii), Pumped energy density in upper laser level $= \dfrac{FGHE}{2\pi r_o \ell_o}$

from (iv), Useful pumped energy density $= \dfrac{JFGHE}{2\pi r_o \ell_o}$ joules/c.c.

from (v), Output from laser $= \dfrac{\ell n\ R}{\ell n\ RS} \dfrac{KJFGHE}{2\pi r_o}$ joules/cm^2

or, total energy emitted $= \dfrac{\ell n\ R}{\ell n\ RS} \dfrac{JGHE}{2\pi r_o} \int_o^{r_o} KF 2\pi\rho d\rho$ ... (3.35)

where the integral contains only those functions dependent upon ρ, the radial position in the rod.

The functions in this equation depend on several variables as follows:-

$H \equiv H(r,\ell)$: $G \equiv G(r, \ell, r_o, \ell_o)$

$J \equiv J(r/t_o)$ see equations 3.33 and 3.34

$F \equiv cF'(\rho, cr_o)$ see section 3.4.2

$K = \dfrac{N_i - N_f}{N_i}$ where N_i, N_f are the inversions before and after the laser pulse

and where N_f is a function of $N_i = \dfrac{JFGHE}{2\pi r_o \ell_o h\nu}$

and the threshold inversion $N_c = \dfrac{-\ell n\ RS}{2\sigma\ell_o}$

$$\therefore \quad K \equiv K\left[\frac{JFGHE}{2\pi r_o \ell_o h\nu}, \quad \frac{-\ell n\, RS}{2\sigma \ell_o}\right]$$

The variables referred to are flashtube radius (r), flashtube length (ℓ), rod radius (r_o), rod length (ℓ_o), spontaneous lifetime (τ), flash duration (t_o), concentration (c), radial position in rod (ρ), and stimulated emission cross-section (σ).

3.5.2 The laser output will be optimized by inserting simple functions which closely approximate the actual functions into Equation 3.35. Certain assumptions have to be made for a solution to be possible and feasible analytically and these will be pointed out as they arise.

(i) Let $G = G_o \frac{r_o}{r}$, where G_o = efficiency of imaging of the flash lamp by the cavity. This is valid for a reasonably good image-producing pumping cavity in which $r_o \leq r$ and for rod length (ℓ_o) = flash lamp length (ℓ). If $r_o > r$, then $G = G_o$, but this case is rejected on the grounds that our pumping calculation becomes invalid and that the efficiency must drop as r_o increases above r since less energy will reach the volume having radius r and the rest of the volume has lower inversion and is not likely to contribute to the output.

(ii) Let H = constant = H_o say. On published data (Gonez 1966, Edwards 1967, Roess 1969, Jones and Wall 1971, Noble et al 1971, Edgerton 1970) the form of H is not certain, but this appears to be a reasonable approximation.

(iii) Let the pumping pulse shape be a half-sine wave. The solution for J of Equations 3.33 and 3.34 is given, to within 5%, by

$$J = \frac{1}{1+0.5t_o/\tau}.$$

(iv) The optimization of E_{OUT} in its integral form is complex and would require a great deal of computer time. We assume that $F'(cr_o,\rho)$ is separable $[F'(cr_o,\rho) \equiv F'_1(cr_o)F'_2(\rho)]$ and that $F'_1(cr_o) = F'(cr_o,0)$ and $F'_2(\rho) = 1; \quad \rho \leq kr_o$

$= 0; \quad \rho > kr_o$. where K is a constant between 0 and 1. Furthermore we replace $F'(cr_o,0)$ by the function $0.28\ c/(1+1.05cr_o)$ which approximates (to within 5%) to the computed functions (see Fig. 3.22) over at least the range $0.85 < cr_o < 5$. This analytic function does not preserve dimensions, since the constants replace variables which have dimension.

(v) For the case of a fast Q-switch (Wagner and Lengyel, Wenzel) $K(N_i,N_c) \equiv K(N_i/N_c)$ and replacement of $K(N_i,N_c)$ by $1-1.08/(N_i/N_c)^{1\cdot45}$ (Wenzel) is a very good approximation to the computed function.

(vi) The fluorescent lifetime depends on the concentration of neodymium in glass. Stroud (1968) has shown that $\tau \simeq 1.8e^{-c/4}$ ms is a reasonable approximation for a glass type such as LN6 and we have used this to eliminate τ from the equation. For other glass types the constant (1.8) is different. With all these functions substituted the output equation becomes:-

$$E_{OUT} = \left(-\ell n\ R\right)\left(\tfrac{1}{2}k^2r_o^2\right)\cdot\left[\frac{G_o r_o}{r}\cdot\frac{H_o}{r_o}\cdot\frac{E}{(1+0.28t_o e^{c/4})(-\ell nRS)}\cdot\frac{0.28c}{(1+1.05cr_o)}\right]$$

$$\times\left[1-1.08\left(\frac{\pi h\nu}{\sigma}\cdot\frac{r}{G_o r_o}\cdot\frac{r_o}{H_o}\cdot\frac{(1+0.28t_o e^{c/4})(-\ell nRS)}{E}\cdot\frac{(1+1.05cr_o)}{0.28c}\right)^{1\cdot45}\right]$$

$$\therefore\ E_{OUT} = -M'k^2r_o^2\ell nR\left[F - \frac{N'}{F^{0\cdot45}}\right] \qquad \ldots\ (3.37)$$

$$\text{where } M' = 0.14; \quad N' = 36.0 \left(\frac{h\nu}{\sigma}\right)^{1.45}$$

$$\text{and } F = \frac{G_o H_o}{r_o r} \cdot \frac{E}{(1+0.28 t_o e^{c/4})} \cdot \frac{cr_o}{(1+1.05 cr_o)} \frac{1}{(-\ell nRS)}$$

and $-\ell nS = 2\beta\ell_o - \ell nD$.

3.5.3 E_{OUT} then is a function of the independent variables r (flash tube radius), r_o (rod radius), R (reflectivity), t_o (flash length), c (doping concentration), ℓ_o (rod length) and the optimum can be found by solving the simultaneous equations:-

$$\frac{\partial E_{OUT}}{\partial r} = 0; \quad \frac{\partial E_{OUT}}{\partial r_o} = 0; \quad \frac{\partial E_{OUT}}{\partial R} = 0; \quad \frac{\partial E_{OUT}}{\partial t_o} = 0; \quad \frac{\partial E_{OUT}}{\partial c} = 0; \quad \frac{\partial E_{OUT}}{\partial \ell_o} = 0$$

The number of equations can be reduced to four by inspection of Equation 3.37 as to its dependence on r and r_o.

The dependence on r reduces to:-

$$E_{OUT} = \frac{A_r}{r} - B_r (r)^{0.45}$$

(A_r and B_r being independent of r) and this, by inspection, is a maximum for minimum r; also the dependence on ℓ_o reduces to:-

$$E_{OUT} = \frac{A_{\ell_o}}{-\ell nRD + 2\beta\ell_o} - B_{\ell_o} (-\ell nRD + 2\beta\ell_o)^{0.45}$$

which by inspection is a maximum for minimum ℓ_o. These two requirements on the flash tube dimensions are incompatible with the requirement for a finite energy input and flash length since the tube would break down if its radius and length were to be reduced too far. The breakdown energy of Xenon flash tubes is given by:-

$$F_c = 800\ r\ \ell\sqrt{t_o}\ \text{joules (Edgerton et al 1964)} \qquad \ldots (3.38)$$

where, again, this is a good analytic approximation, which does not preserve dimensions.

From the above considerations it is evident that, for maximum efficiency, it is desirable to work as close as possible to this limit.

We therefore introduce the further constraint:-

$$E = b\ 800\ r\ell\sqrt{t_o}$$

where b = safety factor. Take $b = 0.5$ (Life of tube ~ 5000 shots)

$$\therefore \qquad r\ell\sqrt{t_o} = E/400 \quad \text{or} \quad r = E/(400\ell\sqrt{t_o}) \qquad \ldots (3.39)$$

We now consider the optimization with respect to r_o.
The dependence of E_{OUT} on r_o reduces to:-

$$E_{OUT} = \left[\frac{A_{r_o}}{(1+1.05cr_o)} - B_{r_o}\ (1.05cr_o)^{0.45}\right] r_o^{\,2}$$

which is a maximum for maximum r_o.

but Maximum $r_o = r$ (see paragraph 3.5.2)

$\therefore$ from Equ. 3.39, $r_o = E/(400)\, \ell\sqrt{t_o})$ where we have replaced ℓ by ℓ_o, since we are assuming $\ell = \ell_o$

These two substitutions into equation 3.37 gives:-

$$E_{OUT} = Mk^2 \frac{(-\ell nR)}{\ell_o^2 t_o} \left[F - \frac{N}{F^{0.45}} \right] E^2 \qquad \ldots (3.40$$

where $M = 3.50 \times 10^{-4}$; $N = 0.48 \times 10^{-2} \left(\frac{h\nu}{\sigma} \right)^{1.45}$

and $$F = \frac{G_o H_o c \ell_o \sqrt{t_o}}{(1+0.28 t_o e^{c/4}) \left(1 + \frac{2.63 \times 10^{-3} Ec}{\ell_o \sqrt{t_o}}\right) (-\ell nRS)} = \frac{G_o H_o \ell_o \sqrt{t_o}}{PQ(-\ell nRS)}$$

where $$P = 1 + 0.28\, t_o e^{c/4}$$

$$Q = 1 + \frac{2.63 \times 10^{-3}\, Ec}{\ell_o \sqrt{t_o}}$$

The simultaneous equations to be solved are now:-

$$\frac{\partial E_{OUT}}{\partial R} = 0; \quad \frac{\partial E_{OUT}}{\partial t_o} = 0; \quad \frac{\partial E_{OUT}}{\partial c} = 0; \quad \frac{\partial E_{OUT}}{\partial \ell_o} = 0$$

After differentiation and some rearrangement these four equations become:-

$$\frac{F^{1.45}}{N} = 1 + 1.45 \left[\frac{-\ell n\ R}{-\ell n\ S} \right] \qquad \ldots (3.41)$$

$$\frac{F^{1.45}}{N} = 1 + 1.45 \left[\frac{2Q-P}{2PQ-2Q+P} \right] \qquad \ldots (3.42)$$

$$Q = \frac{4P}{c(P-1)} \qquad \ldots (3.43)$$

$$\frac{F}{N} = 1 + 1.45 \left[\frac{(2Q-1)(-\ell nRS)-2\beta\ell Q}{(-\ell nRS)+2\beta\ell Q} \right] \qquad \ldots (3.44)$$

Equating the square brackets in Equ. 3.41 and 3.42 gives:-

$$\frac{-\ell nR}{-\ell nS} = \frac{2Q-P}{2PQ-2Q+P} \qquad \ldots (3.45)$$

or

$$\frac{-\ell nRS}{-\ell nS} = \frac{2PQ}{2PQ-2Q+P}$$

Equating the square brackets in Equ. 3.42 and 3.44 and substituting for (-ℓn RS) from Equ.3.45 gives, after some rearrangement:-

$$\beta \ell_o - \ell n\ D = \frac{\beta \ell_o P}{2Q(P-1)} \qquad \ldots (3.46)$$

again substituting for $(-\ell n\ RS)$ from Equ. 3.45, Equ. 3.42 becomes

$$\frac{2.9\ PQ}{2PQ-2Q+P} = \frac{1}{N}\left[\frac{G_o H_o c \ell_o \sqrt{t_o}(2PQ-2Q+P)}{2P^2Q^2(-\ell n\ S)}\right]^{1.45} + 0.45 \qquad \ldots (3.47)$$

where F has been inserted from Equ. 3.40.

We have now eliminated R from Equ. 3.41, 3.42 and 3.44 giving two equations (3.46 and 3.47) which, together with 3.43, form a set of three simultaneous equations in the variables t_o, c and ℓ_o.

Equation 3.43 can be solved for ℓ_o, by substituting for Q from Equ. 3.40:-

$$\ell_o = \frac{2.63 \times 10^{-3} Ec^2(P-1)}{\sqrt{t_o}\ (4P-cP+c)} \qquad \ldots (3.48)$$

3.5.4 The pair of simultaneous equations formed by substituting Equ. 3.48 in Equ. 3.46 and 3.47 were solved (for c and t_o) using a simple BASIC programme (APPENDIX II) through an on-line computer terminal. The programme also calculates the values of ℓ, R and E_{OUT} at the optimum.

As an example, the following values were used:-

Flash tube efficiency constant (H_o) = 0.3

Cavity efficiency (G_o) = 0.8

$\frac{h\nu}{\sigma}$ = 8.0 This value is that of ED-2 Nd:glass

β = 0.007 This value is that of ED-2 Nd:glass

$-\ell nD$ = 0.1 i.e. Other losses in the laser amount to ~ 10%

k = useful fraction of rod radius = 0.7. This roughly corresponds to the central high inversion area due to focussing of the pumping energy by refraction at the rod surface.

The optimum was calculated for various inputs (E) and plotted in Fig. 3.23.

For 100mJ output the optimum is seen to be as follows:-

E = 17.5 Joules

optimum c = 19.5; optimum t_o = 2.25 μs;

optimum ℓ_o = 10.1 cm; optimum R = 48%.

The only value not given is the rod radius (r_o) which can be easily calculated since $r_o = E/(400\ \ell_o \sqrt{t_o})$. For the case above r_o = 0.091 cms.

It is also of great interest to know how critically the output depends upon the various parameters in the region of the optimum.

The programme has been adapted to enable this to be done, and as an example the best that can be done with 6% Nd:glass (the usual max. concentration) was found.

For optimum E_{OUT} = 100 mJ; E = 25J

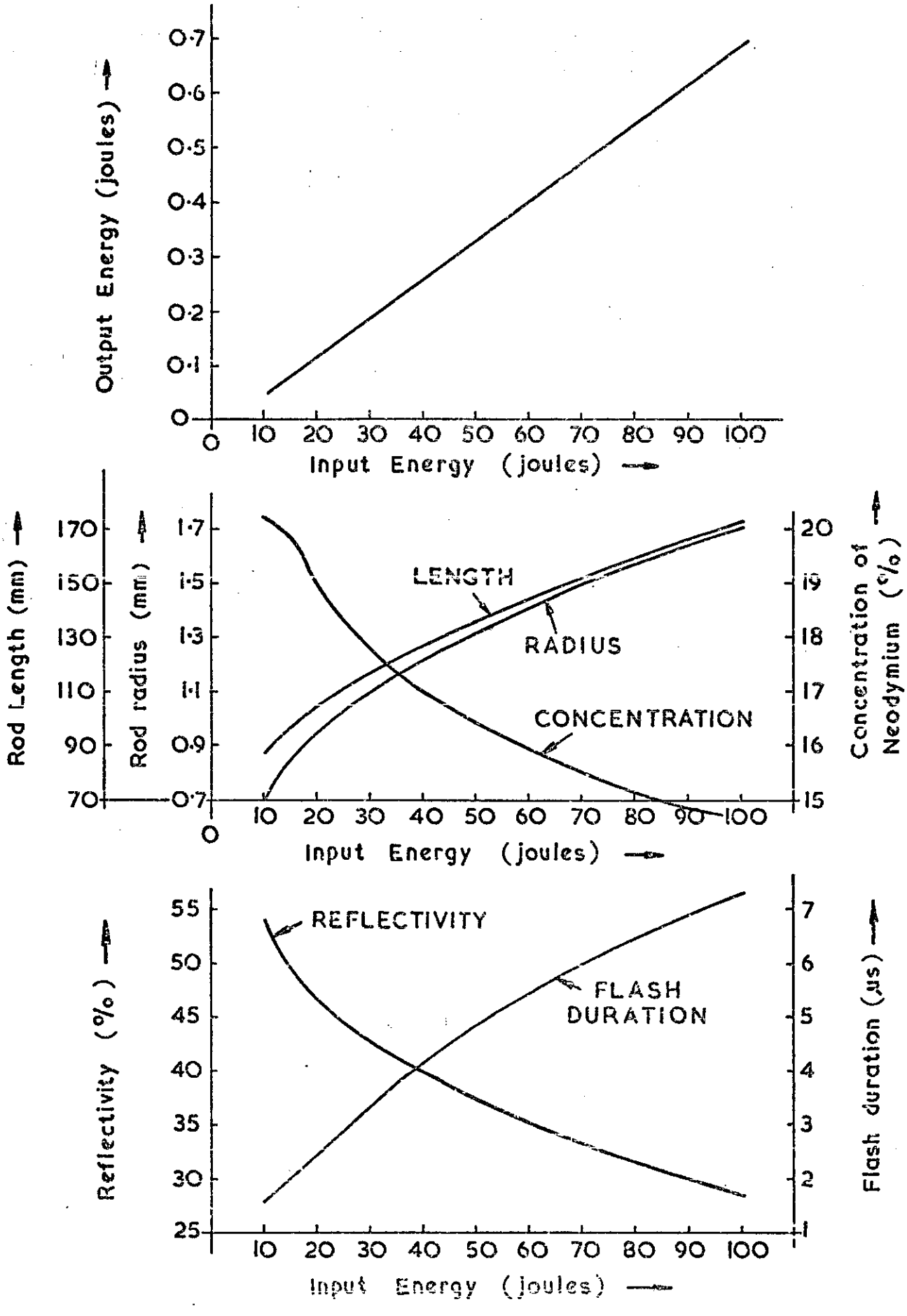
The two major uncertainties in the above analysis should be restressed.

(i) The flash tube efficiency and how it depends upon the flash tube parameters.

(ii) The approximation of the integral is not adequate in some cases. If k were allowed to vary with E, r, c, and R a more accurate assessment would be obtained.

The optimization programme developed above has been modified to include two new pieces of information. These are:-

FIGURE 3·23



Variation of Optimum Laser Output and other Laser Parameters with Input Energy

(a) a new and improved neodymium laser glass with different constant parameters. For our program to fit this glass three constants were changed. $\frac{h\nu}{\sigma}$ was reduced from 8.0 to 6.4 joules/c.c/cm^{-1}; the loss coefficient β was also reduced, from 0.007 to 0.006; and the fluorescent lifetime was reduced by a factor 2.37. As a direct comparison with the previous glass taken, the laser system was optimized for the new glass with 6% concentration and 20 joules input. The result was a 7% increase in output. Optimization for the new glass was also performed with the other new piece of information;

(b) the dependence of the pumping efficiency on the effective colour temperature of the flashtube. This has been calculated using the computation outlined in Section 3.4 of this chapter. In the example there a colour temperature of 6500°K was assumed in calculating the spectral content of the pumping radiation. A different colour temperature leads to a different intensity spectrum which will be a better or worse match to the absorption spectrum of neodymium in glass. A good match to the calculated dependence of pumping efficiency on colour temperature was found to be given (for colour temperatures > 6500°K) by the analytic expression $e^{-\frac{T^2}{C}}$, where T = colour temperature and C = constant. The formula is not valid below 6500°K because the efficiency does in fact begin to fall again below this temperature, contrary to the predicted continuing increase. The above analytic expression was included in the overall laser efficiency and the optimization computation repeated. The effect of this modification was considerable, biassing the optimum strongly in favour of long pulse durations and hence rods of lower concentration and larger volume. The laser output was greatly reduced.

For example, at 40 joules input the optimum output is 73mJ (250mJ) at a concentration of 8.3% (17%), a pulse length of 60 μs (4 μs)), a rod length of 17 cm (12.6 cm) and a rod diameter of 2.35 mm (2.44 mm), where the figures in brackets refer to the optimum values as previously calculated.

CHAPTER 4

Experimental Appraisal of Nd:glass Laser

4.1	Introduction	4.1
4.2	Threshold Investigations	4.2
4.2.1	Threshold vs. $-\log_e R$; measurement of losses.	4.4
4.2.1.1	Theoretical dependence of inversion on pumping.	4.5
4.2.1.2	Comparison of experimental and theoretical dependence	4.7
4.2.1.3	Discharge circuit losses. Flashlamp light output vs. capacitor energy	4.8
4.2.1.4	Neodymium fluorescent intensity vs. capacitor energy Effective input vs input	4.8
4.2.2	Threshold vs Q-switch rotation speed	4.10
4.2.2.1	Measurement of rod optical distortion and induced birefringence	4.12
4.3	Distribution of Inversion in the Rod	4.16
4.4	Output vs. Input	4.18
4.5	Time-integrated Output Distributions	4.21
4.5.1	Near-field distribution	4.21
4.5.2	Far-field distribution	4.23
4.5.3	Coherence	4.23
4.6	Time-resolved Output Distributions	4.24
4.6.1	Using photodetectors	4.25
4.6.2	Using streak techniques	4.26
4.6.3	A photodetector experiment	4.31

4.1 Introduction

This chapter describes the experimental investigation carried out on the chosen laser system in its initial unmodified form, this being an American Optical 'Aolux' 3" × $\frac{1}{4}$" Nd:glass rod pumped by a linear Xenon flashtube in an elliptic cavity and in a resonator consisting of an output mirror and a fully reflecting mirror. A rotating optical element, comprising a hollow spindle air-turbine and silica prism rotating element, is placed inside the resonator and is the Q-switch. FIGS. 4.1 and 4.2 show the system diagrammatically.

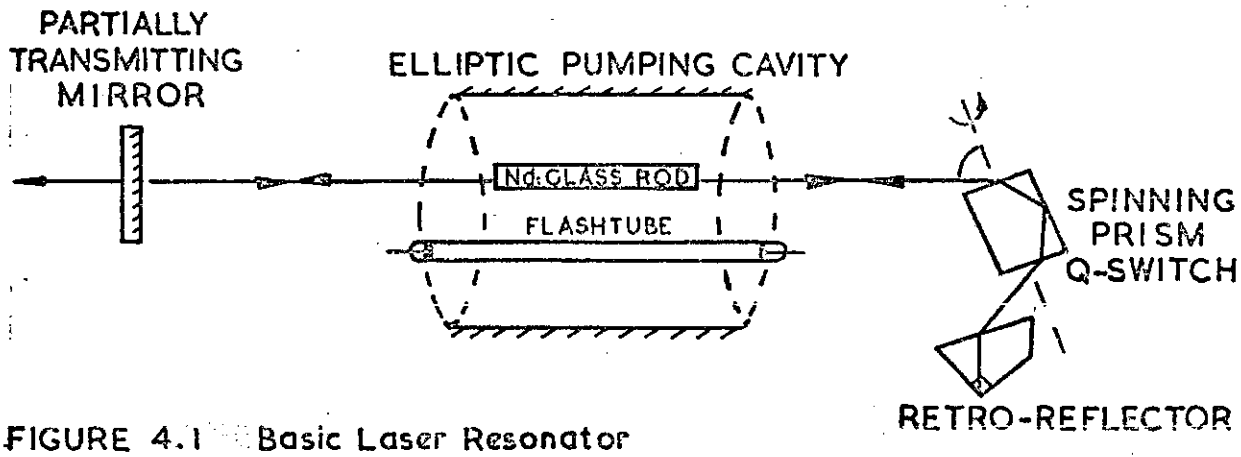
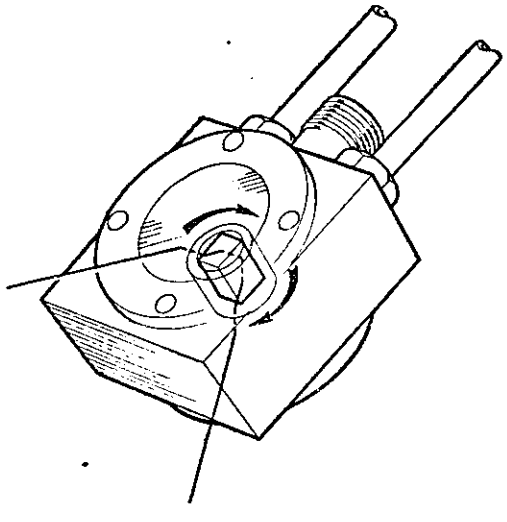


FIGURE 4.1 Basic Laser Resonator

FIGURE 4.2

Q-switch prism inside air-turbine drive unit



The following quantities are measured:- static and dynamic losses in the system, pumping efficiency, inversion distribution in the rod, rod distortions due to pumping, threshold investigations, input/output characteristic, spatial and temporal output characteristics, and coherence properties. Essentially, three types of measurement are involved, the measurement of quantities needed for calculations such as those in chapter 3: observations that show how the system matches up to those calculations: measurements of properties, such as distortions, which do not enter the calculation and may cause the system to operate differently from the expected performance.

In the course of making measurements on lasers one is often aware of a need for an improved or alternative technique. This chapter is also concerned with the diagnostic methods used with lasers and an important part of it will be concerned with discussing some of those we have used. In particular, those upon which new work has been carried out are; the time resolution of the spatial intensity distribution; the measurement of dynamic distortions; the measurement of coherence.

4.2 Threshold Investigations

Measurement of the variation of threshold with output mirror reflectivity and Q-switch rotation speed permits measurement of:-

(i) Static losses in the laser (Findlay and Fray 1966) and the form of the dependence of the inversion on the input energy.

(ii) The variation of the number (N) of available passes with the speed of rotation of the prism.

This follows immediately from the threshold equation (3.3) of Chapter 3:-

$$\sigma N_T = \sigma f(E_T) = \frac{1}{2\ell N_M} \ln \frac{P_T}{P_o} - \frac{1}{2\ell} \ln R \frac{1}{2\ell} \ln S + \beta \qquad \ldots (4.1)$$

(i) If the Q-switch is stationary, then $N = \infty$ and the equation becomes:-

$$\sigma f(E_T) = -\frac{1}{2\ell} (\ln R + \ln S) + \beta$$

$$= -\frac{1}{2\ell} \ln R + \beta_o \quad \text{say} \qquad \ldots (4.2)$$

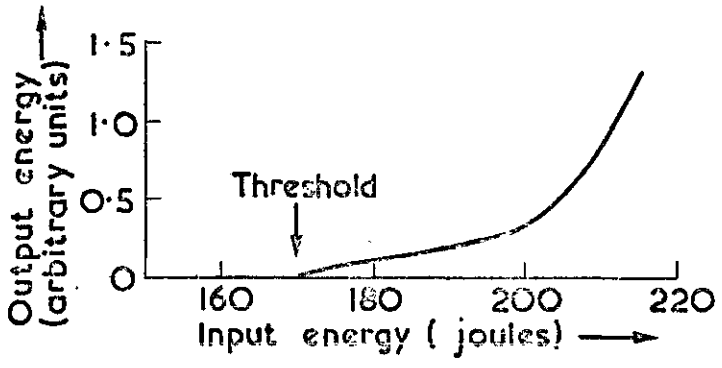
If E_T is measured as a function of R Then:- extrapolating back to $E_T = 0$ gives $\beta_o = \frac{1}{2\ell} \ln R$ and the shape of the curve gives the form of the variation of inversion with input energy.

(ii) Measurement of the variation of threshold with turbine speed enables, using the results of (i) above in equation 4.1, a calculation of the dependence of N upon the turbine speed.

Before making any measurements, it is important to define how the threshold is to be measured. This is most easily done by observing the input at which the output has sufficient energy density to burn polaroid print material. This energy density is quite clearly defined at $\sim$ 100 mJ/cm^2 (as compared to an output of $\approx$ 10 J/cm^2 at 1.5 $\times$ threshold) or, in other words, very little depletion of the rod has occurred at this point. An alternative but lengthier method is to determine, using a photo-detector, the output/input curve near threshold and extrapolate back to

zero output. FIG. 4.3 shows an example of this.

FIGURE 4.3



DETERMINATION OF LASER THRESHOLD

Comparison between the two methods shows that the error of the first method is small, smaller indeed than the errors due to instabilities of the laser system and the errors in measuring the input.

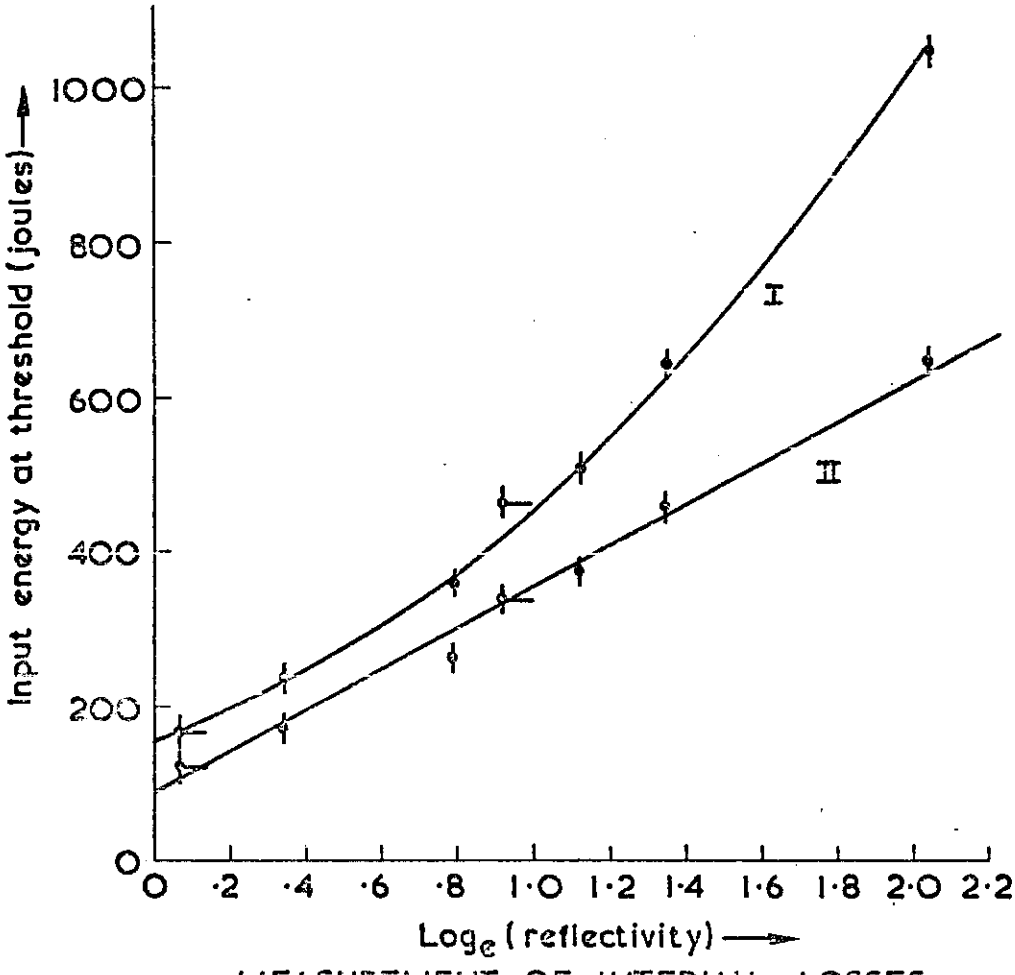
4.2.1 (i) The threshold was measured, by the second method above, as a function of output mirror reflectivity. The range of reflectivity was covered by various multilayer dielectric mirrors and various combinations of silica, glass and sapphire flats as resonant reflectors. The maximum reflectivity used was 93%, made up of one 71% coated reflector and a resonant reflector consisting of two silica flats, while minimum reflectivity of 13% was obtained using a single silica flat. Fig. 4.4 I is a graph of threshold input energy against -ln (reflectivity) = -ln R.

The value of -ln R at zero threshold input gives a value of the total effective loss coefficient (β_o) of 0.023 cm^{-1}. This is made up of the loss coefficient of the rod ($\simeq$ 0.005 cm^{-1}) and scattering and reflection losses at the various faces through which the beam has to pass. Subtracting 0.005 cm^{-1} from β_o gives 0.018 cm^{-1}. Setting this equal to $-\ln S/2\ell$ gives a value of S of 0.76. Thus the total of these scattering and reflection losses are 1 - S = 24% per double transit.

This figure is made up of:-

(a) a reflection loss from each end of the rod, giving a double transit loss of $\approx$ 16% (4 surfaces at 4% surface)

FIGURE 4.4



MEASUREMENT OF INTERNAL LOSSES

I– Capacitor stored energy

II– Energy into flashtube in first 1·4ms.

(b) a small loss at the 14 Brewster angle surfaces; a small loss from scattering in bulk media; and, since there is some induced birefringence in the rod, a small loss from reflection of the unfavoured polarization.

(c) a loss at the roof-edge retro-reflector, due to slight imperfection of the edge itself.

The fact that the curve of Fig. 4.4 I is not smooth must be due to the reflectivities not being as expected. The values taken for the multiple plate resonant reflectors may have been over-estimated since no effort was made to ensure that all the appropriate distances were in phase for the wavelength of peak gain. The error bars show the range over which these reflectivities could vary. Further discussion of resonant reflectors is left to chapter 5 where their use in coherence control is considered.

4.2.1.1 The shape of the curve gives information concerning the way input energy is converted into an inversion population. It is in fact the inverse of the function f in Equation 4.1 and we can calculate as follows what shape the curve should be.

Let the pumping pulse shape be a half-sine wave.

Then the rate of change of inversion population $\left(\frac{dN}{dt}\right)$ is equal to the increase due to pumping less the decrease due to fluorescence, or

$$\frac{dN}{dt} = N_o k \sin \pi t/t_o - \frac{N}{\tau} \qquad \ldots (4.3)$$

where N_o = population of ionic ground state ≃ constant.

t_o = pumping pulse length

τ = fluorescent lifetime

k = rate of pumping

Integrating and putting $N = 0$ at $t = 0$ gives

$$N = \frac{N_o k\tau}{1+(\pi\tau/t_o)^2}\left[\sin \pi t/t_o - \frac{\pi\tau}{t_o}\cos \pi t/t_o + \frac{\pi\tau}{t_o}e^{-t/\tau}\right] \quad \ldots (4.4)$$

Fig. 4.5 shows the pumping pulse and an example of the temporal evolution of N for $\tau/t_o = 0.5$ (which is the value in our own case).

Threshold occurs when the peak value of $N(\equiv N_{MAX})$ is just sufficient for the losses to be overcome.

At this point $dN/dt = 0$

$\therefore$ from Equ. 4.3:- $N_{MAX} = N_o k\tau \sin \pi t/t_o$. $\quad \ldots (4.5)$

Equating the right hand side of Equ. 4.4 and Equ. 4.5:-

$$N_o k\tau \sin \pi t/t_o = \frac{N_o k\tau}{1+(\pi\tau/t_o)^2}\left[\sin \pi t/t_o - \frac{\pi\tau}{t_o}\cos \pi t/t_o + \frac{\pi\tau}{t_o}e^{-t/\tau}\right]$$

$$\text{or} \quad (1+[\pi\tau/t_o]^2)\sin \pi t/t_o = \sin \pi t/t_o - \frac{\pi\tau}{t_o}\cos \pi t/t_o + \frac{\pi\tau}{t_o}e^{-t/\tau}$$

Since this equation does not contain k, the time at which maximum inversion occurs is independent of the pumping level. Let this time be t'; then from Equ. 4.5:- $N_{MAX} = N_o k\tau \sin \pi t'/t_o$

Now the input energy E_{IN} = constant $\times \int_o^{t_o} k \sin \pi t/t_o \, dt$

$$= \text{constant} \times 2kt_o/\pi$$

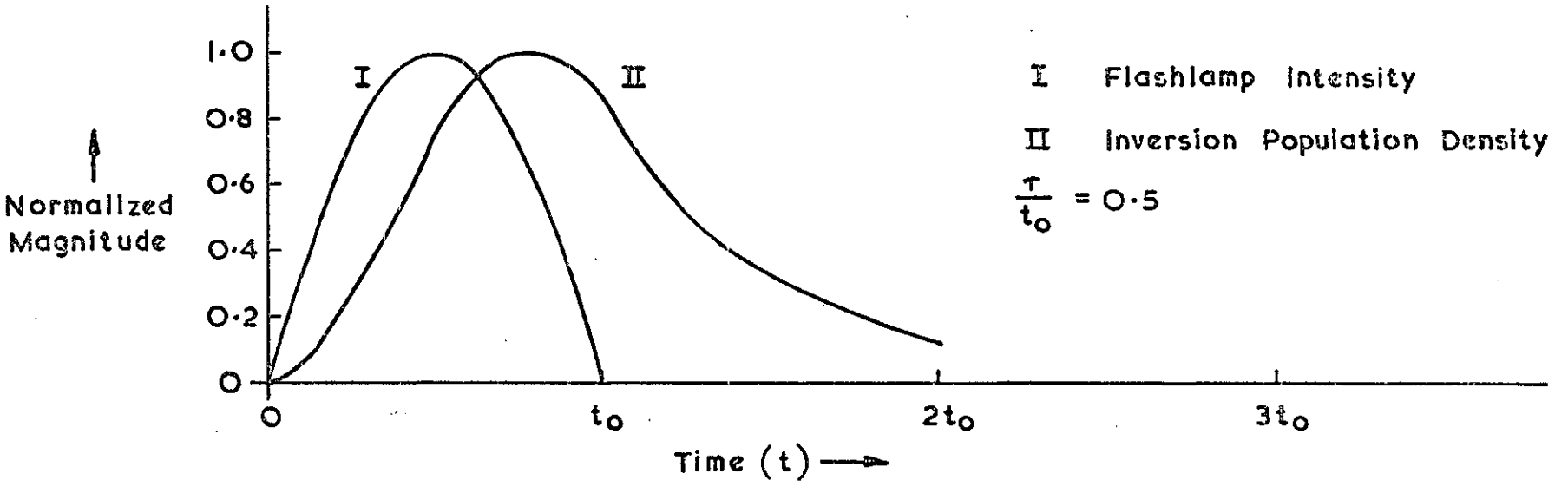


FIGURE 4.5 Pump Intensity and resulting Inversion Population Density for $\frac{\text{fluorescent lifetime}}{\text{flashlength}} = 0{\cdot}5$

so that we can substitute for N_{MAX} from above into this equation to get:-

$$- E_{IN} = \text{constant} \times \frac{2}{\pi N_o \sin \pi t'/t_o} \times N_{MAX}$$

$$= \text{constant} \times N_{MAX} .$$

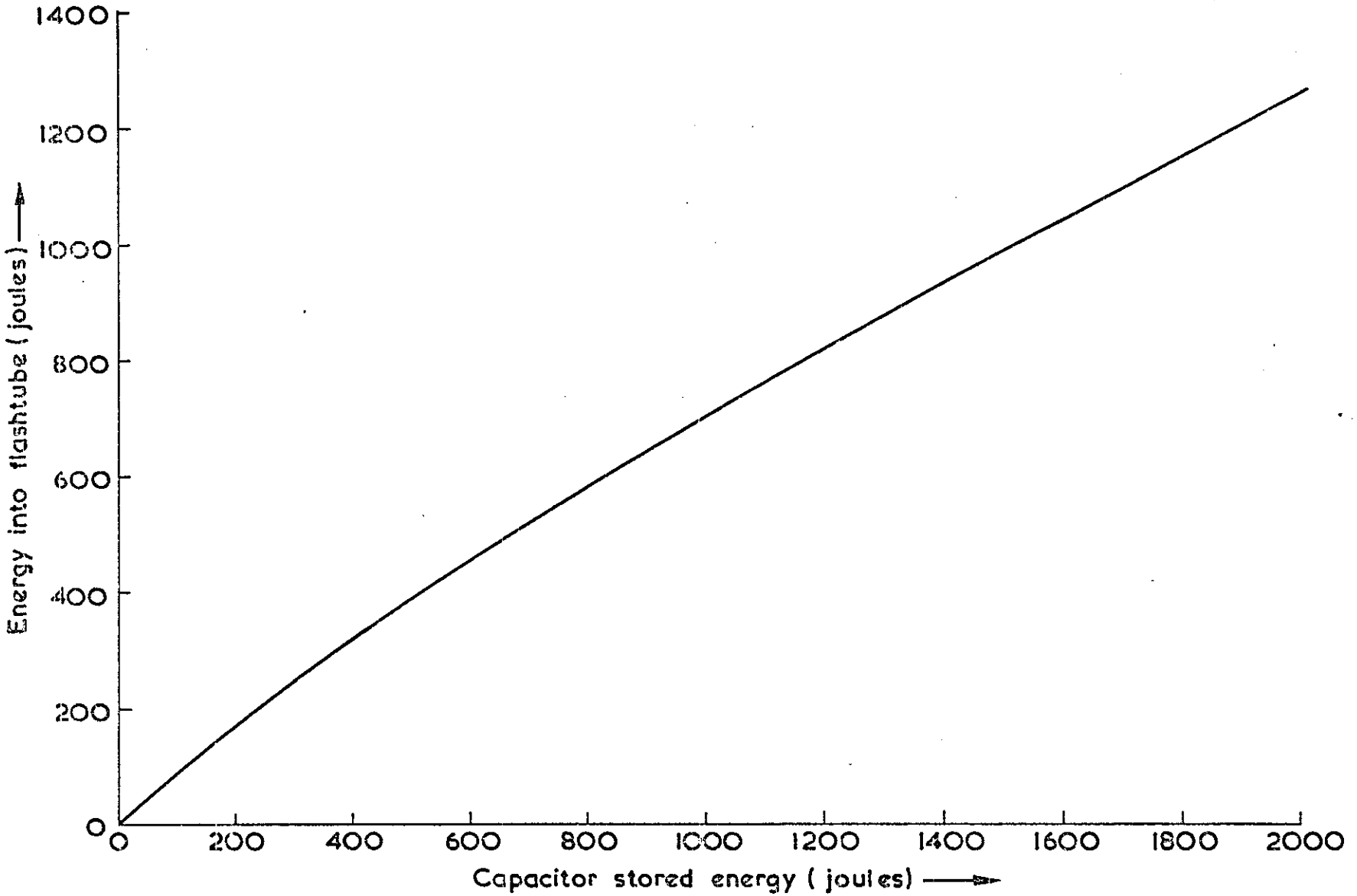
i.e. there is a linear relation between the peak inversion density and the input energy.

The variation of threshold input energy with -ln (reflectivity) should then (from Equ. 4.2) also be linear.

4.2.1.2 A glance at Fig. 4.4 I shows that this is not so. Moreover the experimental shape indicates a decrease in pumping efficiency at higher inputs. One possible contribution to this has been investigated and shown to have a considerable effect. This is the ohmic loss in the discharge circuit. Markiewicz and Emmett (1966) showed that the loss in efficiency due to ohmic losses depends on the input energy, and the fractional loss was calculated as a function of α, a circuit parameter given by $\alpha = \frac{k_o C^{\frac{1}{2}}}{(2EL)^{\frac{1}{4}}}$, where k_o is the resistance parameter of the flashtube, C = capacitance, L = inductance and E = initial stored energy in the condenser bank. Inserting the particular values of k_o, C and L for our discharge circuit into the equation for α enabled this parameter to be calculated for various values of stored energy. Using then the calculated curve of Markiewikz and Emmett and knowing the circuit resistance we obtain a curve of the fractional loss as a function of stored energy.

The circuit resistance was measured to be 0.40 Ω using a dc resistance bridge. Inserting this value into the above enabled Fig. 4.6 of the energy into the tube vs capacitor stored energy to be drawn.

FIGURE 4.6



EFFICIENCY OF ELECTRICAL DISCHARGE CIRCUIT
DETERMINED BY CALCULATION OF CIRCUIT LOSSES.

4.2.1.3 To try to verify this the flashtube light output was measured as a function of the stored energy in the capacitor. Using an SGD 100 photodiode in the circuit of Fig. 4.7, polaroid prints of the scope traces corresponding to different input energies were obtained.

Since an absolute intensity reading was not required, calibration of the detection system was not carried out. Linearity of the system was, however, necessary and tests were made which confirmed this for the range employed. The test simply involved repeating the above experiment with a density filter between flashtube and detector and observing that the resulting curve shape was the same. The area of the scope traces were a measure of the electrical energy dissipated in the flashtube and, as it is known that this energy tends to the capacitor stored energy as the input tends to zero, Fig. 4.8 could be drawn showing the variation of the energy into the flashtube with the stored energy in the capacitor bank. This curve compares well with Fig. 4.6, the curve obtained from ohmic loss considerations. Two implicit assumptions have been made; that the change in spectral distribution if any on increasing the input does not result in a change of detector response (the latter is not independent of wavelength); and that the flashtube efficiency is independent of input level. The same experimental curve was drawn with a narrow band spectral filter in front of the detector and the fact that the shape of the curve was unaltered indicated that our first assumption is reasonable. The justification for the second assumption is the agreement between Fig. 4.6 and Fig. 4.8.

4.2.1.4 A further step in the laser process was also tested, by measuring peak fluorescent intensity emitted by the rod at the laser wavelength vs capacitor input energy.

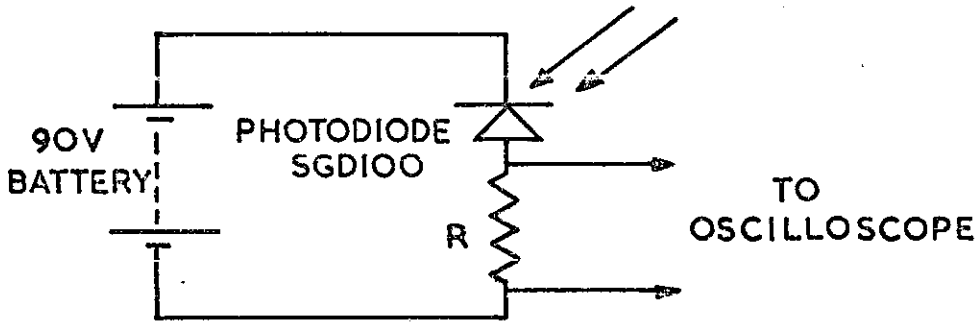
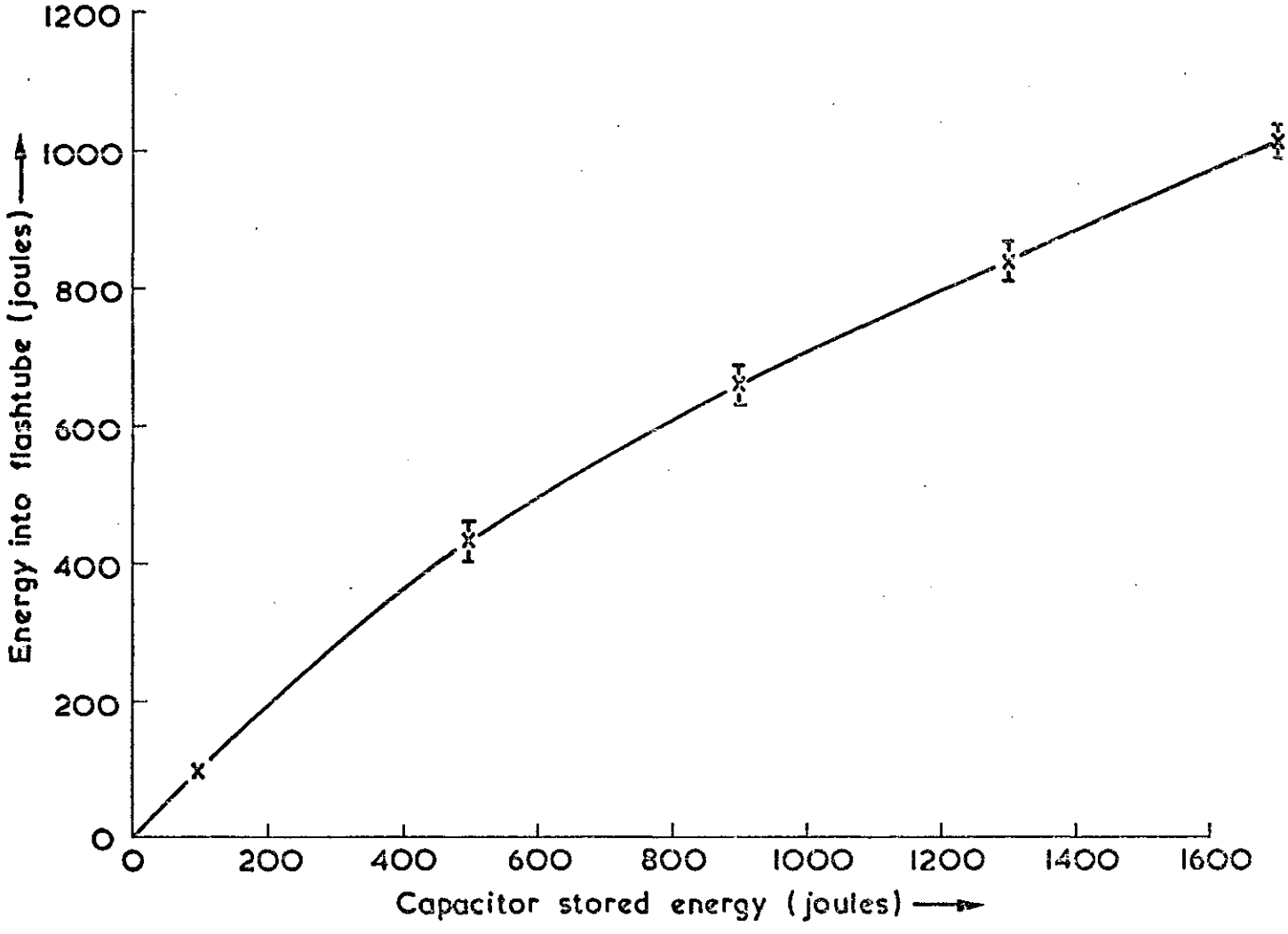


FIGURE 4.7 Circuit diagram for observation of pulses of light.

FIGURE 4.8



EFFICIENCY OF ELECTRICAL DISCHARGE CIRCUIT DETERMINED BY MEASUREMENT OF THE TOTAL LIGHT OUTPUT FROM THE FLASHLAMP.

Fig. 4.9 shows the arrangement used.

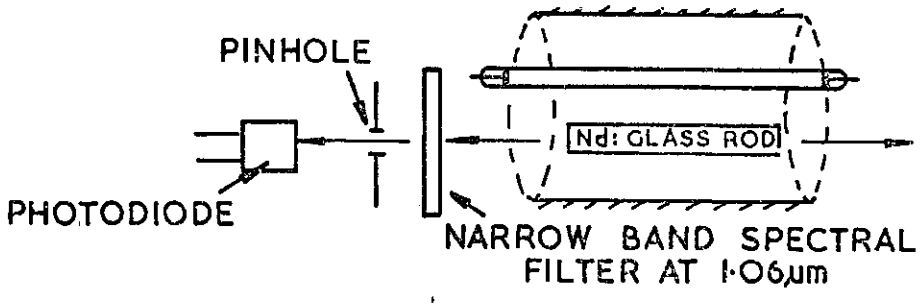


FIGURE 4.9 Arrangement for measuring the fluorescent output at 1·06μm from the flashlamp-pumped Nd:glass laser rod.

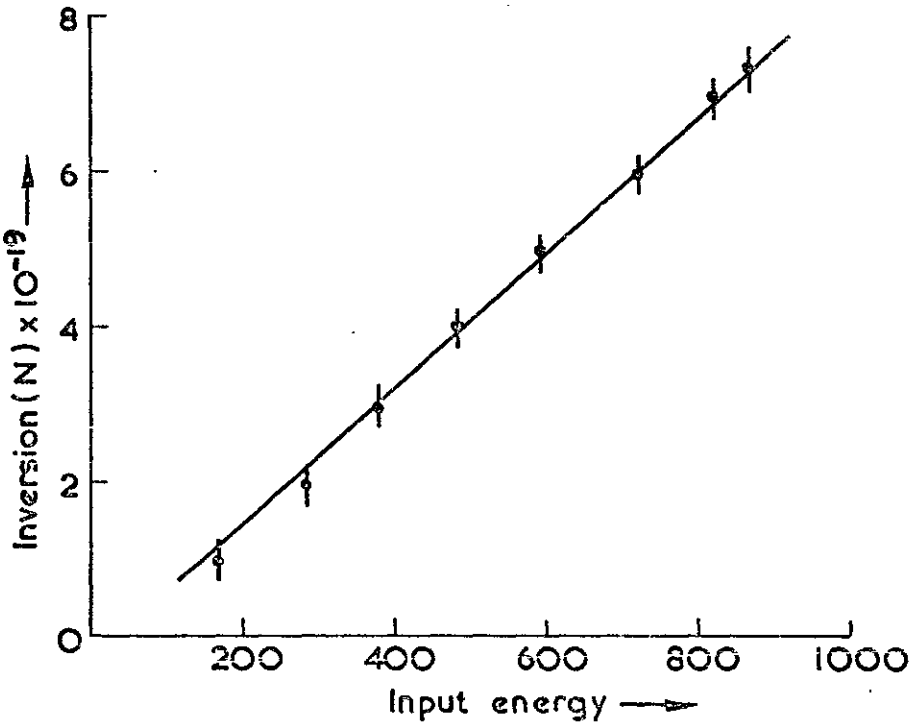
Since the fluorescent intensity φ_o is given by:

$$\varphi_o = \text{constant} \times \frac{[\exp 2\ell(\alpha-\beta)-1]}{(1-\beta/\alpha)}$$, see Equation 3.15, where $\alpha = \sigma x$

inversion density (N), it is possible (as shown in paragraph 4.3)to directly plot the inversion vs input energy. This is done in Fig. 4.10, where we have allowed for the inefficiency of the discharge circuit. This confirms the linearity of dependence of the inversion population on the flashtube output, indicating again that the spectral distribution is independent of input.

The above investigation enables a correction to be applied to the measurement of all quantities as a function of input energy. In all future measurements, for input read effective input where effective input is the energy dissipated in the flashtube as calculated from Fig. 4.8 and the inversion is then directly proportional to the effective input. A further point should be added for completeness. Since the flash envelope has a shape that alters with input energy and the laser action occurs before the flash is completed then the effective input should be the effective input in the time period from zero up to the point of laser

FIGURE 4.10



CALCULATED VARIATION OF INVERSION WITH INPUT ENERGY USING MEASURED VALUES OF ROD FLUORESCENCE.

action. In our case (see position of N_{MAX} in Fig. 4.5) this period is approximately the first 1.4 ms of the flash (since t_o = 1.75 ms), and, using the scope traces recorded above and measuring the area in the first 1.4 ms, equivalent curves for this area were drawn, thus enabling the correct effective input to be used. Fig. 4.11 shows the two effective input vs input curves and it can be seen that the difference, apart from a scaling factor, is small.

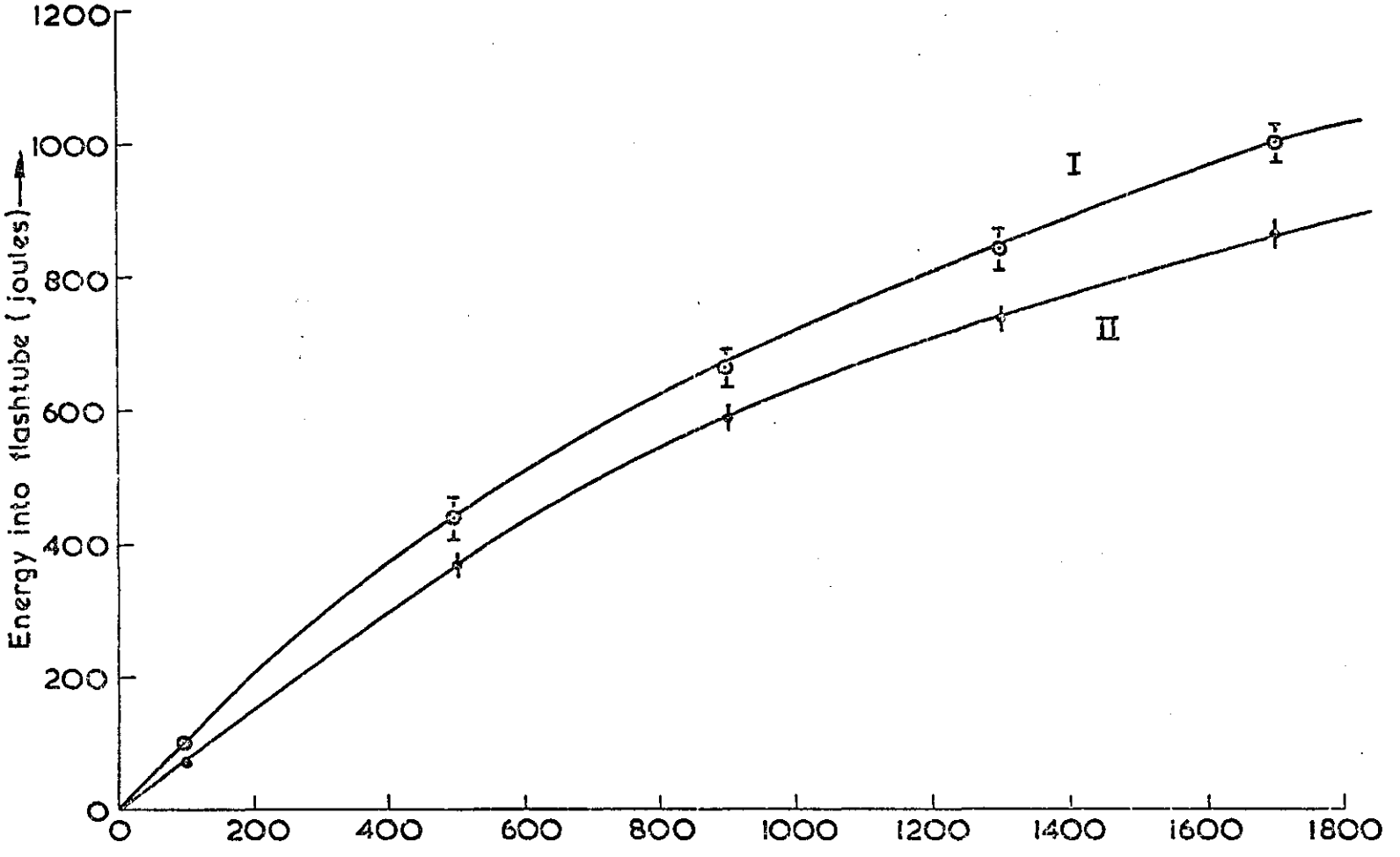
Curve II of Fig. 4.11 was used to derive curve II of Fig. 4.4, the variation of threshold with reflectivity. A straight line, as expected, was obtained and it was from this that the losses S were measured. (para. 4.2.1)

4.2.2 (ii) The dependence of the threshold (as measured in (i)) on turbine rotation speed was determined. An air pressure valve controlled the mirror rotation speed, which was measured by painting a semicircle of black paint on the top of the rotor and measuring the frequency of oscillation of reflected light using a tachometer. Fig. 4.12 is the experimental curve of threshold versus rotation frequency. Equation 4.1 shows that if the origin is shifted so as to intersect the curve at zero rotation speed Fig. 4.12 immediately becomes, apart from a scaling factor, a curve of (^{1}/Number of available double transits) vs (rotation speed). This can be immediately checked against Fig. 3.8 of Chapter 3, this being the theoretical curve. Considerable discrepancies (due to extra losses) are found to be present at the higher frequencies, and these require an explanation. The following possibilities exist:-

(a) Air turbulence around the turbine rotor could introduce optical distortions into the resonator.

(b) Dynamic distortion of the rotating prism at high speeds introduces

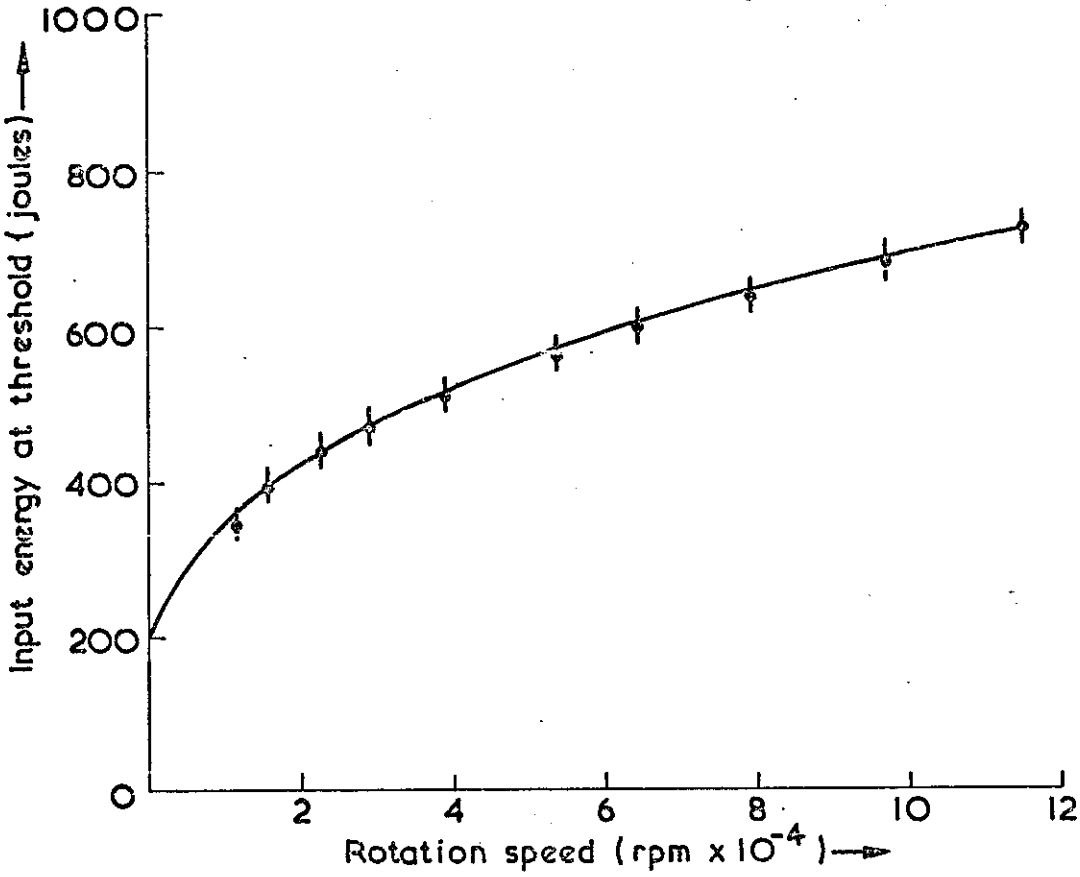
FIGURE 4.11



EFFICIENCY OF ELECTRICAL DISCHARGE CIRCUIT
MEASURING THE LIGHT OUTPUT FROM THE FLASHLAMP.

I Entire pulse.
II First 1·4 ms of pulse.

FIGURE 4.12



VARIATION OF LASER THRESHOLD WITH SPEED OF ROTATION OF Q-SWITCH.

two types of optical distortion, and attenuation due to induced birefringence which couples light out of the favoured polarization.

(c) Incorrect choice of parameters used in the theoretical calculation.

(d) Dynamic optical distortion and induced birefringence in the laser rod due to the nonuniformity of the inversion distribution and heat distribution in it when optically pumped.

(a) Air turbulence. This is likely to be very small for a rotating prism such as ours which is sealed into a cylinder which rotates about its axis. Any loss that does result from turbulence is likely to depend on the square of the rotation speed (ω). If we call this loss L_T, then $L_T = K_T\omega^2$ and this loss constitutes an extra term in Equ. 4.1:-

$$f(E_T) = \frac{1}{2\ell N_M} \ln \frac{P_T}{P_o} - \frac{1}{2\ell} \ln R - \frac{1}{2\ell} \ln S + \beta - \frac{1}{2\ell} \ln (1 - K_T\omega^2) \quad \ldots (4.6)$$

and the effect is to add a term $- \frac{\ln(1-K_T\omega^2)}{\ln P_T/P_o}$ to the theoretically calculated $1/N_M$. K_T can be chosen to make the two curves coincide at the origin and one other point but not to coincide over the entire curve.

(b) Appendix III describes the holographic method used to evaluate the dynamic distortions in the spinning prism as a function of rotation speed. Fig. 4.13 shows the single pass interference fringes of the optical distortion for two prism rotation speeds.

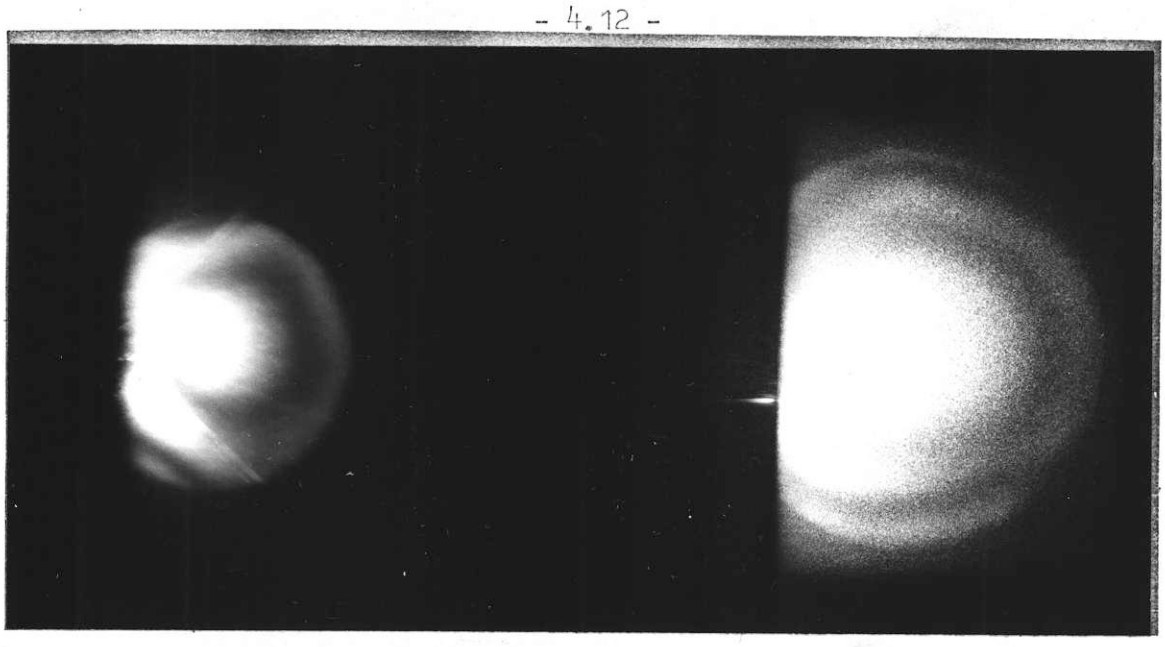


FIGURE 4.13 Holographic interferograms showing dynamic distortion in a spinning Q-switch prism.
(a) 90,000 r.p.m. (b) 120,000 r.p.m.

This distortion is uniformly distributed through the prism and is shown to be entirely a result of the centrifugal forces present. Furthermore, over the area used by the laser and for the optical path actually used, both the wavefront distortions and birefringence losses are shown to be very small.

(c) The threshold value of $^1/N$ depends only upon the product $L^2\omega/a$, where L = cavity length, a = effective aperture. This is implied by Equ. 3.6. An error in the choice of (L) or (a) results, therefore, in a scaling error in ω. A scaling factor can be found such that Figs. 4.12 and 3.8 coincide at two points but the curves still do not coincide over their entire lengths.

(d) It is not proposed to go into the theory of dynamic optical distortion induced in laser rods during the pumping cycle. This has been done by, for example, Riedel and Baldwin (1967), but in our case some important data, such as the non-uniform distribution of pumping radiation on the rod, is not known, and this would result in large uncertainties in the calculated distortion.

The alternative is an experimental measurement of the distortions, and this has been done as follows

Figs. 4.14 and 4.15 show diagrammatically the methods of measuring the optical distortion and induced birefringence respectively.

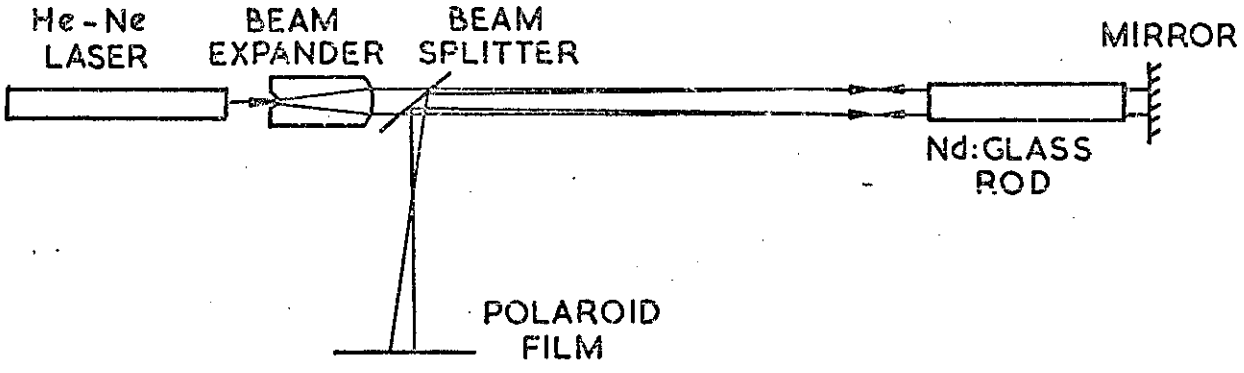


FIGURE 4.14 Measurement of Dynamic Distortion in Nd: glass Rod

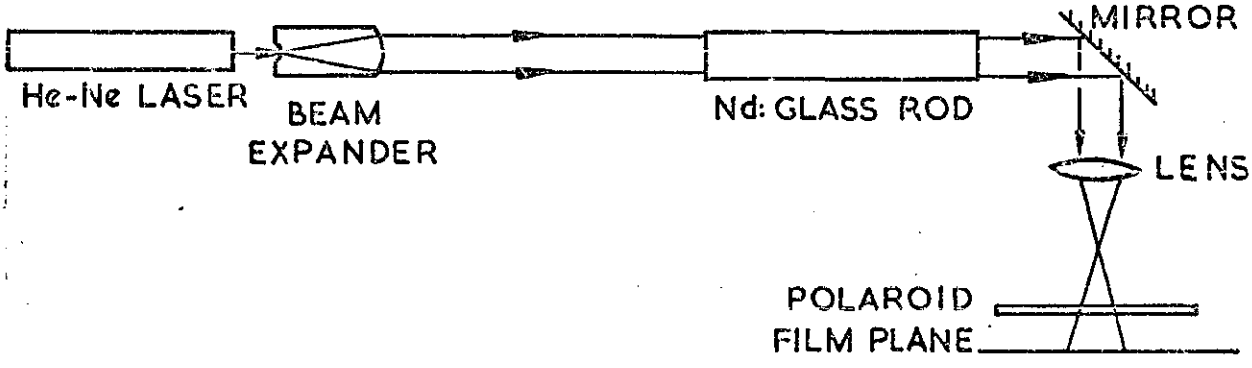


FIGURE 4.15 Measurement of Induced Birefringence in Nd: glass Rod

The former investigation consists in passing the expanded TEM_{∞} mode output from a He-Ne laser through the rod and recording the intensity distribution in the transmitted beam at a large distance from the rod. The distorted spot was recorded on polaroid 55P/N for several different input levels and Fig. 4.16 shows some examples.

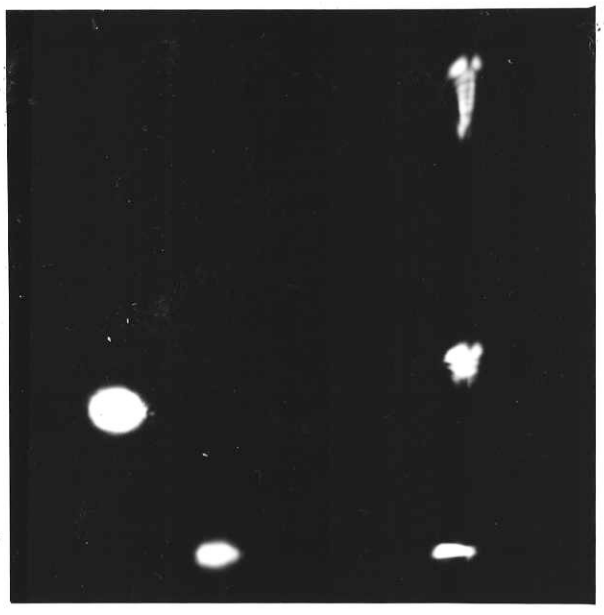
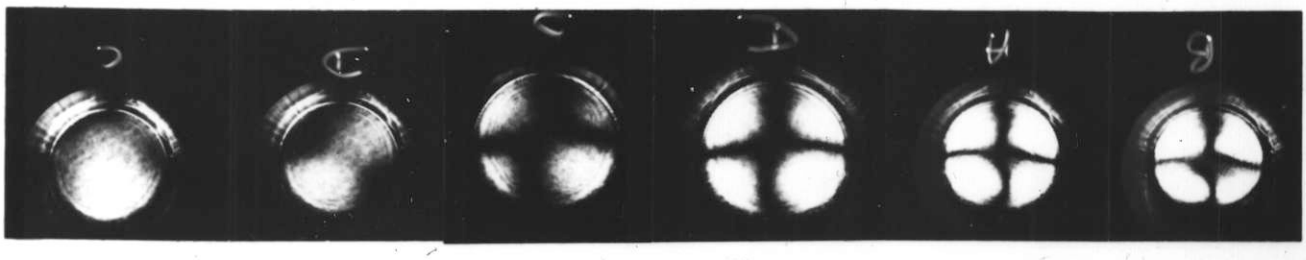


FIGURE 4.16 Distribution across light beam distorted by transmission through a pumped Nd:glass rod.

The distorted intensity pattern returned to being a gaussian distribution with a time constant of a few seconds, so that the pictures of Fig. 4.16 had to be recorded with a short exposure immediately after completion of the pumping cycle.

The birefringence measurement was made by inserting a piece of polaroid which had its polarization axis of maximum transmission crossed with the polarization of the gas laser beam. The unpumped undistorted rod gave a dark field on the recording material. Birefringence patterns for various pumping levels were recorded and Fig. 4.17 shows some examples of these.



Unpumped 76J 300J 680J 1200J 1800J

FIGURE 4.17 Birefringence of a pumped Nd:glass rod between crossed polarizers.

The first and most obvious feature of the above measurements is that the distortions are quite considerable and are not lens-like in form. It is likely that if their effect on the threshold were calculated we could satisfactorily explain the observed threshold variations. The problem of relating the observed patterns to the threshold is considerable owing to the complexity of the distortions. The only satisfactory method is to modify the computer program of Chapter 3. The equations which relate the ray positions and directions on consecutive transits would need to be adjusted to include the effect on the path of each ray due to the rod. Furthermore the effect on the number of available transits of the distortions in the

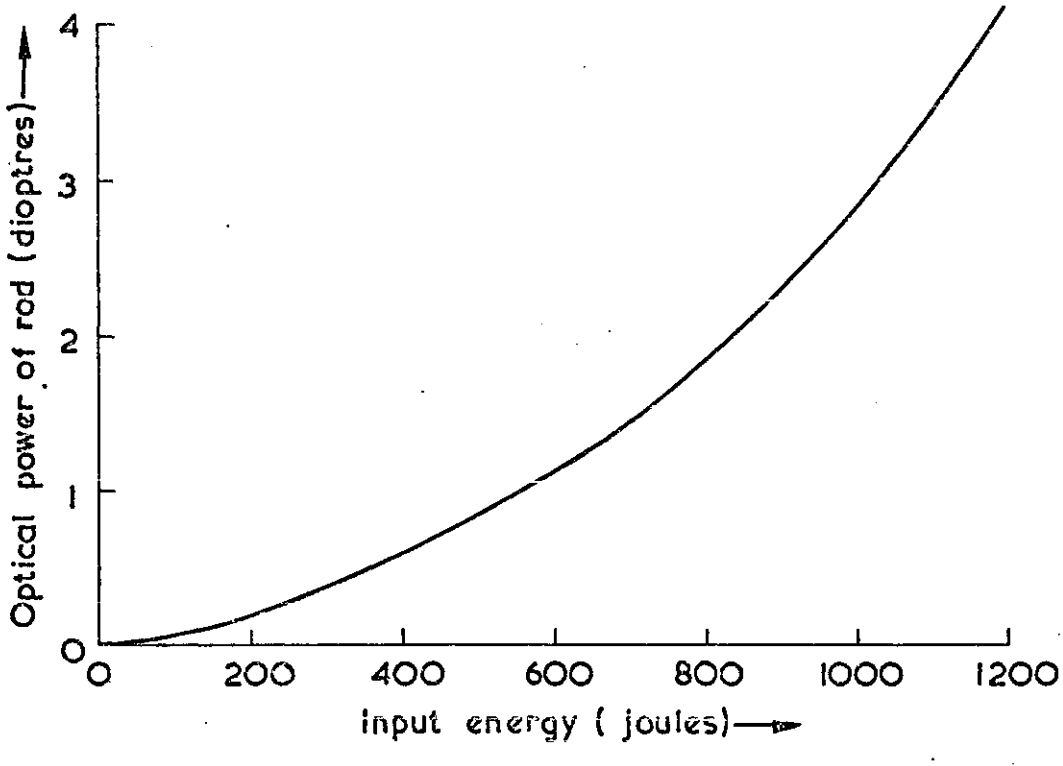
plane normal to that of the rotating mirror sweep must be included although this is likely to be small in most situations. These modifications to the programme are important to a full understanding of the laser process but are not included in this thesis as they are not considered to be crucial to the main theme.

One further comment on the distortion distributions should be made since it will be relevant at a later stage to the problem of transverse coherence, which is strongly dependent upon the shape of the wavefront transmitted by the rod. It has been stated that the distortions are not lens-like. The closest description relating to conventional optical components is that the rod roughly becomes a positive cylindrical lens of power depending upon input energy. This is calculated from the experimental measurements and is shown in Fig. 4.18.

Since the rod focuses in the plane of the rod and flashtube it follows that, with or without compensation for the distortions, the optimum orientation of the pumping cavity is such that the plane containing the rod and flashtube is normal to that of the rotating mirror sweep. In this orientation there is minimum distortion along the line swept out by the laser pulse. Less of the rod is used normal to this line with less need for good quality.

Dynamic optical distortions are a result of heating effects in the rod and as shown in the pumping calculation in Chapter 3 the heat distribution in the rod is closely linked with the distribution of inversion. Thus we come to the next measurement on the laser, which is required for the laser pulse calculation of Chapter 3 as well as providing another link to the distortion measurement above. This is the measurement of the inversion distribution in the rod.

FIGURE 4.18



CYLINDRICAL POWER OF PUMPED LASER ROD
AS A FUNCTION OF THE INPUT PUMPING ENERGY

4.3 Inversion Distribution in the Rod

Fig. 4.19 shows diagrammatically the method used for this measurement.

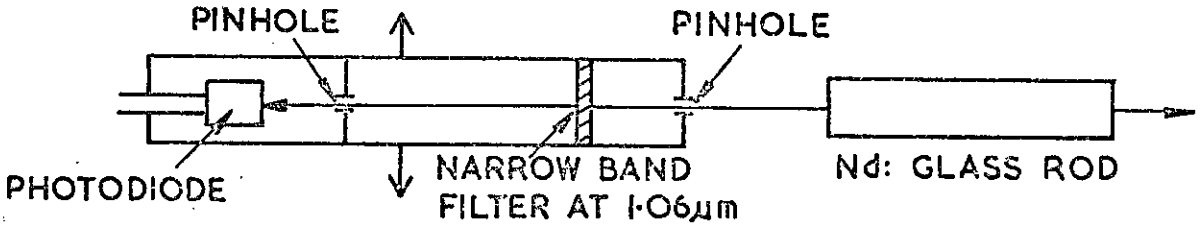
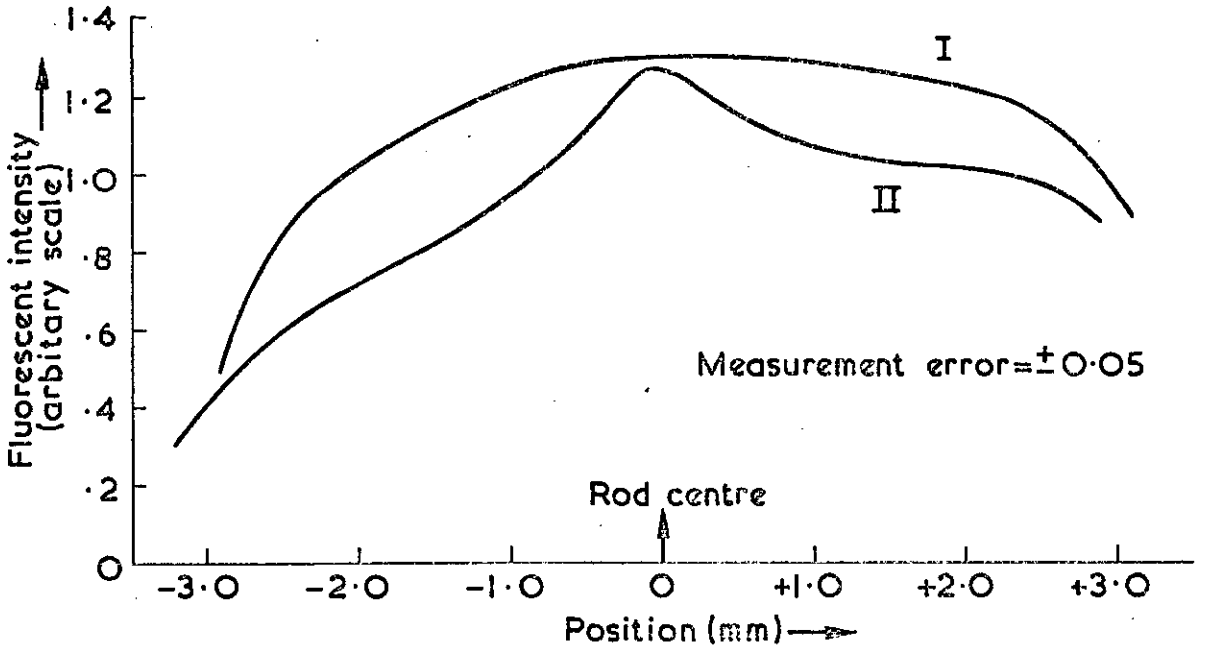


FIGURE 4.19 Inversion distribution across Nd: glass rod by measurement of filtered fluorescence at 1·06μm

The photocell and pinhole assembly measured the light leaving a small area of diameter 0.4 mm of the rod within a small angle of 3 mrad to the axis of the rod. A spectral filter restricted the wavelength being measured to 1.06μ ± 0.05μ. The resulting descrimination against flashlight was at worst ≈ 5:1. To measure the fluorescent intensity from different points on the rod diameter the photocell and pinhole assembly was racked across the face of the rod as a unit and in so doing ensured, that the origin of the measured light moved by the same amount along the rod diameter, that the measured rays were always along the rod axis and that the same area of the detector was used in all the measurements. A lamp input of 680 Joules was chosen and measurements were made along two perpendicular diameters of the rod, that along the plane of the rod and flashtube and that perpendicular to it. Fig.4.20 shows the resulting graphs of fluorescent intensity versus diametric position in the rod for both these diameters. The vertical scale is proportional to the integrated fluorescent intensity at the photodiode. The output of the photodiode was integrated in a capacitor and the voltage across it was displayed on an oscilloscope and recorded on polaroid film. The integrated fluorescent intensity can be related in the following way to

FIGURE 4.20

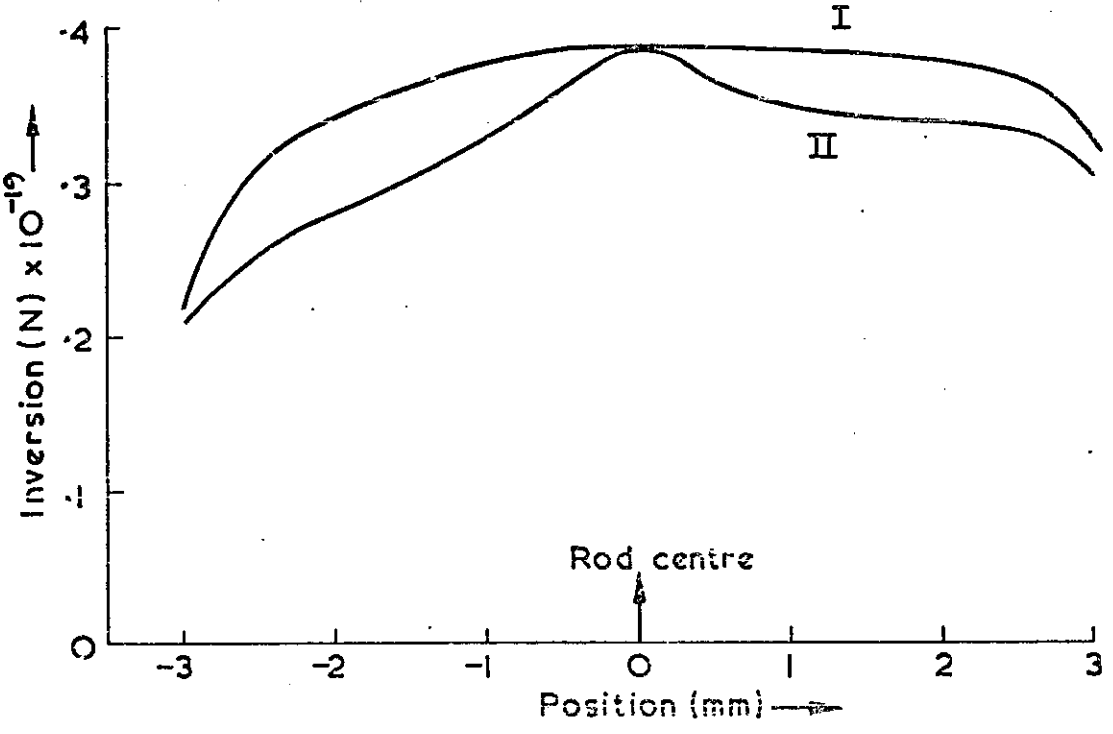


MEASURED VARIATION OF FLUORESCENT INTENSITY IN AN AXIAL DIRECTION WITH DIAMETRIC POSITION IN THE LASER ROD.

I – Measuring along a diameter normal to the line joining the rod and flashtube.

II – Measuring along a diameter along the line joining the rod and flashtube.

FIGURE 4.21



VARIATION OF INVERSION WITH DIAMETRIC POSITION AS CALCULATED FROM FIG. 4.20

the total number of atoms reaching the upper laser level (total inversion population) due to pumping:-

Equ. 3.15 of Chapter 3 is the claculated fluorescent intensity when there is a reflector behind the rod. When there is not the equation becomes:-

$$\text{fluorescent intensity } (\varphi) = \text{const. } x \frac{\exp \ell(\alpha-\beta)-1}{1-\beta/\alpha} \qquad \ldots (4.7)$$

where $\alpha = \sigma$ x inversion density $= \sigma N$.

The constant is determined by firstly reading the threshold value of $-\ln R$ at 680 Joules input from Fig. 4.4 II and inserting this value (1.42) together with the calculated value of 0.023 for β_o into Equ. 4.2 to calculate the value of α corresponding to an input of 680 Joules.

Equ. 4.2 gives:- $\sigma N = \alpha = \frac{1}{2\ell}(-\ln R)+\beta_o = 0.117$

This value of α corresponds to the peak value of the fluorescent intensity (φ) at 680 Joules input, as measured above. Inserting this value of φ and the value of α above into Equ. 4.7 enables the constant to be evaluated.

Since we also know β and ℓ Equ. 4.7 enables a graph of φ vs N to be drawn (where $N = \alpha/\sigma$), from which the value of N for any measured value of φ can be read.

Application of the above correction results in Fig. 4.21 which shows the variation of the normalized inversion across the rod along the two chosen diameters. These numbers can now be directly used in the Q-switching computation of Chapter 3.

Further, the results and conclusions of the distortion investigation above appear reasonable in the light of Fig. 4.21 since, in Chapter 3,

calculation showed that there is a close similarity between the heat distribution and the inversion distribution. It would be instructive at a future date to estimate a heat distribution on the basis of the above inversion distribution and from that heat distribution, using the theory of thermal optical distortion, calculate the distorted distribution in a gaussian light beam which has passed through the rod. This is of course exactly what has also been measured above.

4.4 Output/Input Measurements

Fig. 3.17 of Chapter 3 is the calculated efficiency curve for our laser according to a geometrical optics model. In view of the previous paragraphs concerning the effects of optical distortions etc (in effectively reducing the number of available transits for a pulse to build up) the laser would not be expected to follow this curve in detail. However it might be expected to follow this curve (i) at well above threshold when the number of double transits to reach saturation is less than the number available, (even when this available number is reduced by distortions), since the energy is then extracted before the beam is swept out of the aperture (ii) if the aperture used for the theoretical curve is assumed smaller than that used experimentally, since the optical distortions in effect cause a higher vignetting of the beam per pass. Fig. 3.17 of Chapter 3 shows the effect of reducing the aperture by 50%.

The output energy of the laser was measured using a beam-sampling photodiode unit, the diagram of which is shown in Fig. 4.22.

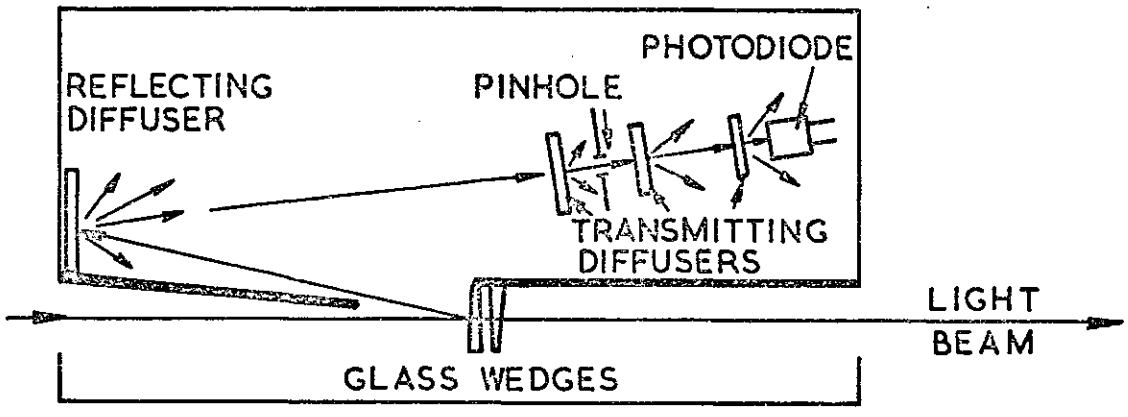
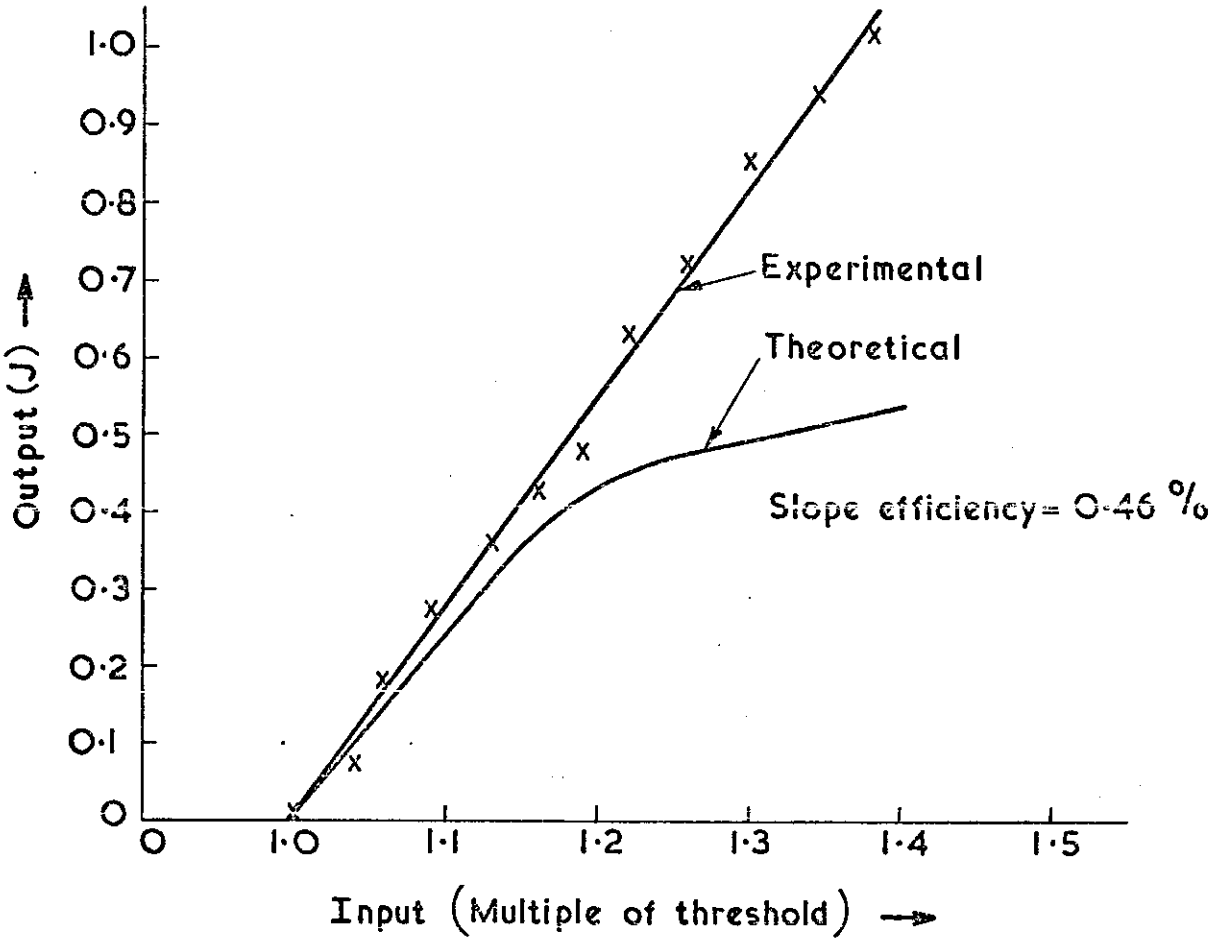


FIGURE 4.22 Accurate beam sampling photodiode unit; electronic circuit not shown.

This unit was constructed along the lines of a design proposed and used by J. G. Edwards (NPL). The design and performance of power and energy measuring devices for Q-switched lasers have been treated at some length by Edwards (e.g. 1969), and the one used has a time resolution of a few nanoseconds, with attenuation suitable for the power developed by our laser and with integrating capacitors suitable for conversion to the measurement of energy. The unit is accurate to around 5%. The energy calibration was performed by measuring the output of an fixed-Q Nd:glass laser against a cone calorimeter which has an absolute accuracy of 2%. The power calibration, which we shall require later, was performed by measuring, using an oscilloscope, the peak power in a Q-switched Nd:glass laser against a similar unit containing an ITT F4000 biplanar photodiode. The power calibration of the latter can be calculated from its energy calibration while that of our unit cannot, since for short pulses (< 1 μs) the response consists of two parts, an accurate shape record of the pulse plus an exponential tail which has a time constant of several microseconds and contains up to half the total charge released.

FIGURE 4.23



EXPERIMENTAL AND THEORETICAL EFFICIENCY CURVES FOR Nd. GLASS LASER WITH ROTATING MIRROR Q-SWITCH.

Fig. 4.23 shows the experimental curve of output energy vs effective input energy (energy dissipated in flashtube before the moment of Q-switching). Also plotted is the theoretical curve as calculated for an aperture size of 5 mm.

The experimentally determined slope efficiency (0.46%) is higher than expected from the theory particularly at higher input levels. This is thought to be a result of the dynamic optical distortion in the rod which, as we have already seen (para. 4.2.2), increases the threshold considerably but which does not reduce to the same extent the output at well above threshold.

The measurement also indicates that the slope efficiency (= 0.5%) does not appear to be significantly reduced by slow spectral cross-relaxation. Cross-relaxation is, as explained in Chapter 2, a process involving absorption and emission of phonons by which excited ions with one excitation energy transfer their excitation to other ions which thereby become excited at a slightly different energy. If cross-relaxation does not occur in materials such as Nd:glass, in which the spectral line is inhomogeneously broadened, then there is no mechanism by which excited ions with excitation energies at the extremes of the line can contribute to the Q-switch pulse, which has a narrow spectral band-width centred around the middle of the spectral line. Not all the excited ions can take part in laser action. If the ratio of homogeneous to inhomogeneous line width is Δ_h/Δ_{inh} and if the spectral width of the pulse is less than Δ_h and no cross-relaxation occurs, then the expected slope efficiency is roughly reduced by the factor Δ_h/Δ_{inh}. For Nd:glass $\Delta_h/\Delta_{inh} \simeq 0.15$. In our case the slope efficiency is not significantly reduced indicating that the time constant associated with cross-relaxation is very much less than our Q-switched pulse length.

4.5 Time-integrated Output Distributions

4.5.1 Near-field distribution

Three methods of measuring the near-field distribution have been used, the choice depending upon how much information is required. In all cases, the material was placed close to or in an image plane of the laser output reflector.

The first is to burn the distribution into unexposed but developed polaroid print material. The edges of the recorded mark are the contours of equal energy density, the value of this energy density being ~100 mJ/cm^2. Successive pictures with different density filters in the beam or different beam expansion can be used to build up a contour map of the distribution. This method is simple and has good repeatability and an adequate resolution in spite of the necessarily small size of image.

The second method used an image recording panel. It requires operation in the dark, is fairly rapid and has some dynamic range. Furthermore it is more sensitive, having a lower threshold of ~ 1 mJ/cm^2, and thus allowing a larger image with better resolution. The panel has a doped semi-conductor surface which is maintained at just below its fluorescing threshold by a d.c. voltage of 72 volts across the panel. When a sufficient intensity of radiation is incident on any part of the surface the threshold is exceeded and fluorescence is emitted from that area. The emitted fluorescence is a replica of the incident illumination distribution. Since it is visible it can either be directly inspected or be recorded photographically on fast polaroid material. The image is not seriously degraded if recorded within a minute or two of its formation. Fig. 4.24 shows an example of the near-field recording, recorded on polaroid 3000 material by imaging of the image retaining panel.

FIGURE 4.24

Near-field distribution of Q-switched Nd:glass laser, showing effect of roof edge.



The third method is a direct photographic recording and gives most information. However, at 1.06 μm, IZ plates, presensitised in ammonia solution, must be used. The time including processing required per exposure is more than 30 minutes and in many cases did not warrant the use of this method.

Image converters have also been used but those available were not considered superior to the image recording panel.

The following comments can be made concerning the near-field distribution as shown in Fig. 4.24:-

(i) It has two lobes separated vertically. This is a result of losses occurring at the roof-edge retroreflector which acts as the 100% resonator mirror. These losses are caused by imperfect construction of the roof-edge (it has finite width); by using a gas laser beam of similar size to that emitted by the Nd:glass laser and measuring the incident, transmitted and reflected intensities, it was determined that ~ 10% of the beam was lost at the edge.

(ii) The transverse dimensions of the pattern are ~ 2-3 mm indicating that the optical distortions in the rod reduce the effective aperture to about this value.

4.5.2 Far-field distribution

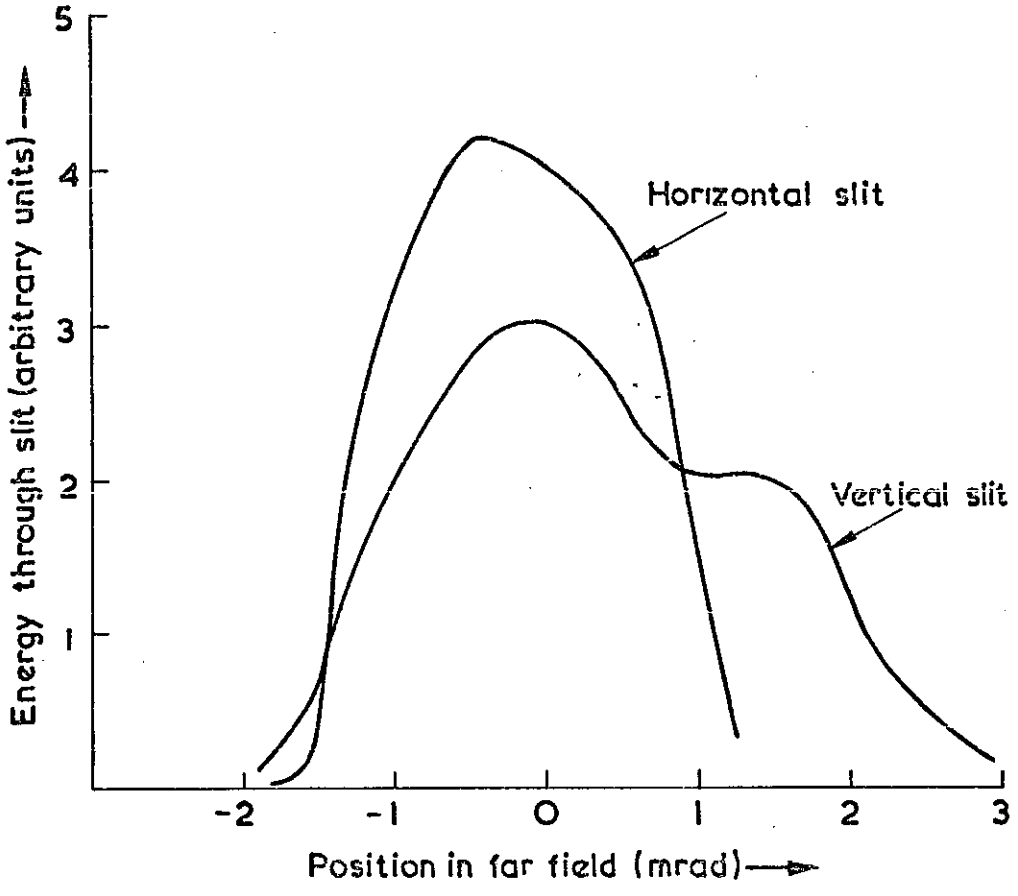
The techniques of measurement are the same as those used for the near-field distribution. The recording plane is now, however, in the focal plane of a lens, the power of which is chosen to result in the best size of image.

A further technique has been used for far-field recording. It could equally be used for the near-field but is a little less accurate then due to the generally greater intensity fluctuations in the near-field. A narrow slit or small aperture is moved across the required plane and for each position the integrated light transmission through the slit or aperture measured using a calibrated photodiode unit. In spite of some shot to shot intensity variations this method gives the most quantitative intensity distribution figures. Fig. 4.25 shows a curve plotted from measurements through a slit in the far-field of the Nd:glass laser. Since the far-field represents the angular intensity distribution it is plotted as such by simply dividing the position readings by the focal length of the lens used (100 cms). Measurement using a photodiode also enables a time-resolved picture of the distribution to be built up.

4.5.3 Coherence

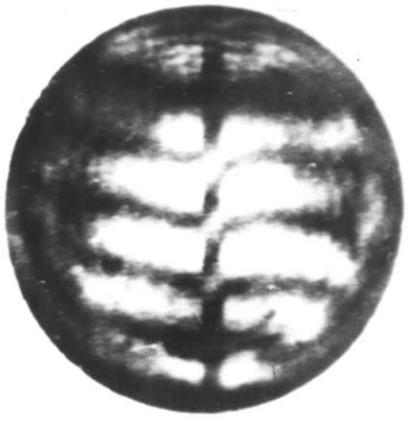
Coherence will be discussed in some depth in the following chapter. At this stage, without explaining the methods used, two examples indicating the coherence of our laser are shown in Fig. 4.26.

FIGURE 4.25

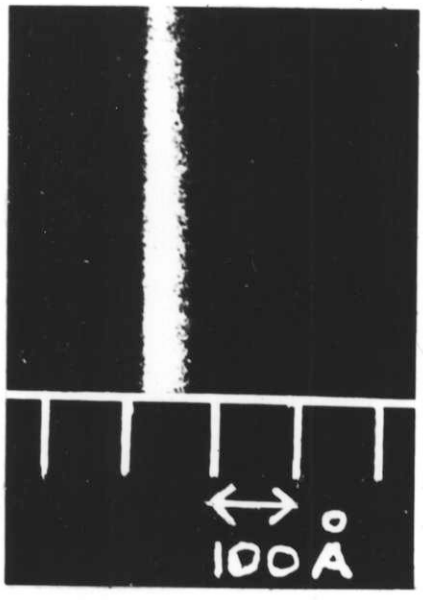


FAR - FIELD DISTRIBUTION OF Nd: GLASS LASER

FIGURE 4.26



Transverse Coherence of Nd:glass laser recorded in reversing interferometer.



Temporal Coherence of Nd:glass laser recorded in prism spectrograph.

The first Fig. 4.26(a) is a recording of transverse coherence using a reversing interferometer which shows a considerable fringe visibility at points well away from the line of inversion and indicating a transverse coherence of $\simeq 0.65$. The second Fig. 4.26(b) is a prism spectrograph recording of the spectral output distribution of the laser with a coated output reflector. A spectral width of $\simeq 50$ Å is shown indicating a poor temporal coherence (coherence length $\simeq 0.02$ cm).

4.6 Time Resolved Output Distributions

Time resolution is of great importance since it yields information on (i) Q-switching process, perhaps leading to an improved mathematical model (ii) Internal interactions and loss mechanisms in the laser resonator, as functions of time. These exert considerable influence on properties such as the coherence. (iii) the capability of the laser for second harmonic generation, or other non-linear process, which depends non-linearly on the fundamental intensity.

With pulse durations of 20 ns or more, any time sequence must be capable of much better resolution than this. A figure for the resolving

power of ≃ 1 ns enables much useful information to be obtained although it is possible that significant information is still un-resolved.

Ideally one would like to obtain time records of the near and far-field distributions and coherence distributions. The tool for this is the high speed image converter streak and framing camera, which in the streak mode with one dimensional spatial resolution can have a resolution limit of 2 ps (Bradley 1972) and in the framing mode with two dimensional spatial resolution can give frame separations of < 1 ns. However this instrument is a costly and complex device and much useful information can still be achieved using simpler methods. Moreover one was not available for continuous use. We have concentrated on other methods of obtaining time-resolved records and a discussion of these, with some results obtained using them, will take up the remainder of this chapter.

The methods divide into two: fast photodetector techniques and streak techniques using rotating reflectors.

4.6.1 Photodetectors

Biplanar vacuum photocells using 1 to 2 KV can have rise times as short as 0.3 ns (ITT F4000 for example) and in combination with a fast oscilloscope (Tektronix 519 for example) can give a rise time for the system of around 0.5 ns (Edwards 1969).

Rise times of other detectors such as photomultipliers (> 1 ns) and photodiodes (> 2 ns) are greater, but they have better sensitivity and in the case of photodiodes they run off lower voltages, are cheaper and can be packed into compact units.

Both vacuum photocells and photodiodes have been incorporated into units as shown in Fig.4.22, and have been used extensively in power and energy measurements on the laser output, and also as output monitors while carrying out other

experiments with the laser. The vacuum photocell has normally been used, in conjunction with a 519 oscilloscope, when detailed time records have been required. Calibration has been carried out from time to time against the cone calorimeter as indicated in para 4.4.

The basic measurement of photodetectors, that of the variation of incident intensity with time, may be extended beyond the measurement of the time dependence of the total intensity from the laser. By measuring the intensity transmitted by movable apertures in either the near or far-field planes, the time-dependence of these two distributions may be built up from successive recordings with the aperture in different positions. Although convenient and providing a recording which is simple to interpret, it is time consuming, and, more important, the assumption must be made that the distribution being measured remains constant from shot to shot. Further, the overall intensity in the output must be measured simultaneously to be able to correct for shot to shot variations in laser output energy.

In an attempt to obtain more temporal information about a laser pulse during each pulse, it was considered worthwhile to look at the possibility of using simple means of providing a streak record.

4.6.2 Streak Recording

If an output distribution can be represented as $\varphi(x,y,t)$, the photodetector method records during one pulse the variation of $\varphi(x,y,t)$ with t. The streak method records, during a pulse, $\int_x \varphi(x,y,t)dx$ or $\int_y \varphi(x,y,t)dy$ as a function of y and t or x and t respectively, the alternative being determined by the direction of streaking.

Up to the present, optical streaking, as opposed to electronic streaking, has not been considered for the time scale of a Q-switched laser pulses. This has been mainly due to the necessity of a combination of a very high

rotational speed for the optical element and a long optical arm to give a reasonable streaking speed. However the very high rotational speeds achieved by our rotating prism air turbine Q-switch suggest that we may already have a suitable candidate for the job. The resolution limit of a rotating optical reflector is calculated as follows:-

Let aperture diameter of reflector = a

Then angular resolution limit = $1.22\ \lambda/a$

If the angular velocity of the reflected beam is ω then the time resolution limit $dt = d\theta/\omega = \frac{1.22\lambda}{a\omega}$.

Our Q-switch prism has an aperture = 10 mm, has a maximum rotation speed of 4000 π rad/sec and is best used in double pass at Brewster angle to the incident and reflected beams as shown in Fig. 4.27. The angular speed of the reflected beam is then $4000\ \pi \times 4 \sin \hat{\beta} = 1600\ \pi \sin 57^\circ$ rad/s

$\therefore$ at 1.06 μm, the resolution limit $= \frac{1.22 \times 1.06 \times 10^{-3}}{10 \times 16{,}00\ \pi \sin 57^\circ} = 3.07$ ns.

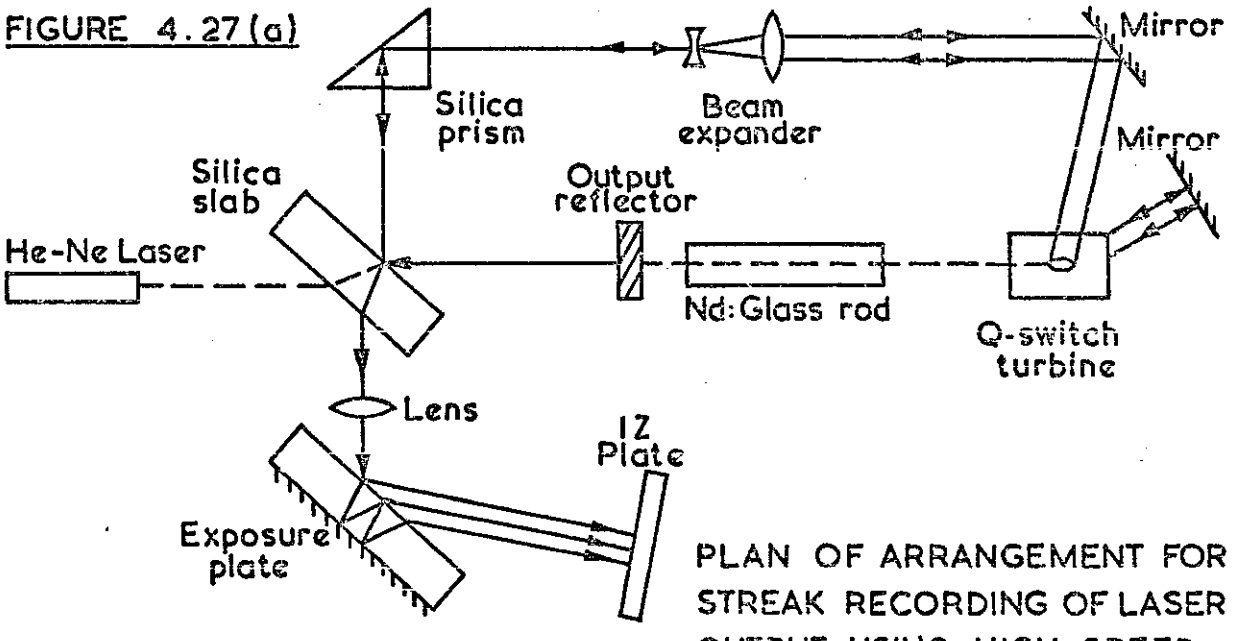
Although not as low as is ideal this figure offers a considerable amount of information content in the streak record. There is the possibility of reducing this figure by passing the beam back through the prism to further increase the rate of deflection. Improvement cannot however be achieved by increasing either the prism rotation speed or the prism aperture since, as indicated in Appendix III, this would bring the silica of the prism too close to its mechanical yield point for comfort. A stronger glass or a metal prism using the external reflection offer possibilities for increasing the resolution. Steel and beryllium prisms have been run at high enough rotational speeds for this.

Another major deterrent to the use of optical streaking lies in the need for very good synchronization of the pulse to be streaked with the streaking element; synchronization of the element to the pulse is not possible since the inertia of the element prevents its position being adjusted quickly from

outside. The allowable jitter for the image to remain on the photographic material might typically be a microsecond. Again we find that this is no problem in our case since the Q-switching prism can only be in one position at the time the Q-switch pulse is emitted: it is then parallel to the laser output mirror. Setting up the streaking arrangement is greatly facilitated by this fact, since the Q-switch prism can be set up in the exact position simply by one of the normal alignment methods used on fixed Q or cw lasers.

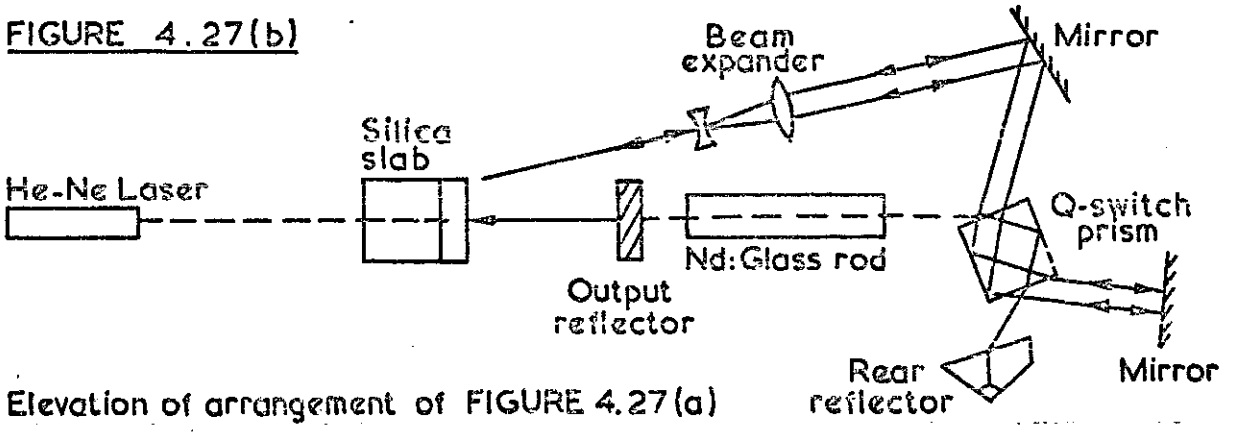
Fig. 4.27 show a diagrammatic plan and elevation of the arrangement used.

FIGURE 4.27(a)



PLAN OF ARRANGEMENT FOR STREAK RECORDING OF LASER OUTPUT USING HIGH SPEED Q-SWITCHING PRISM.

FIGURE 4.27(b)



Elevation of arrangement of FIGURE 4.27(a)

A gas laser beam, set along the laser axis and normal to the output reflector, was used to align the optics and although some dispersion does occur the method was adequate enough to be able to make final adjustments using the laser output.

Two additional optical elements were designed for use in this streak camera. Fig. 4.28 shows a thick glass plate (also seen in Fig. 4.27) with reflecting coatings on each side such that consecutive reflections have an intensity ratio of 0.5.

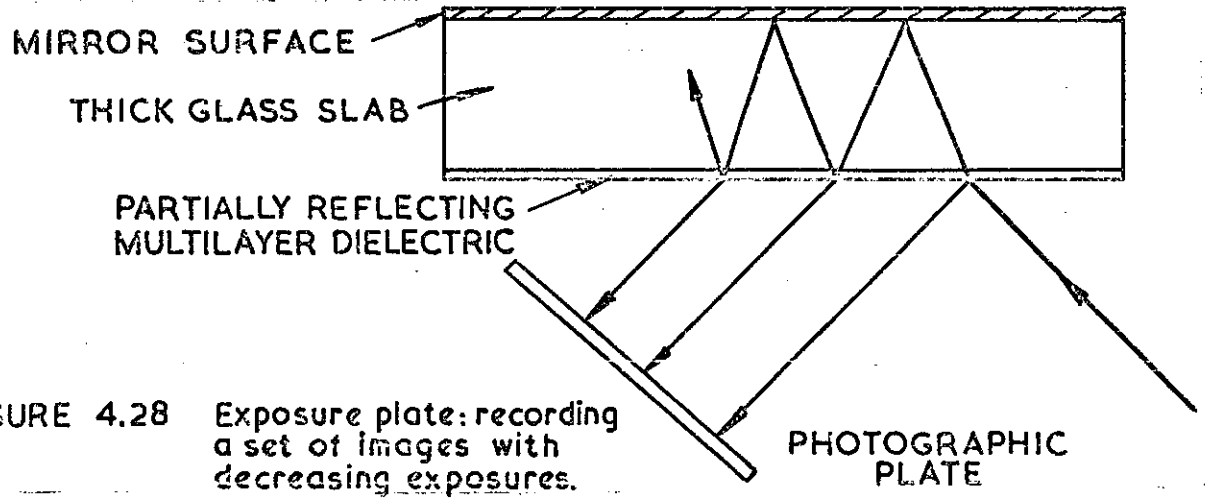


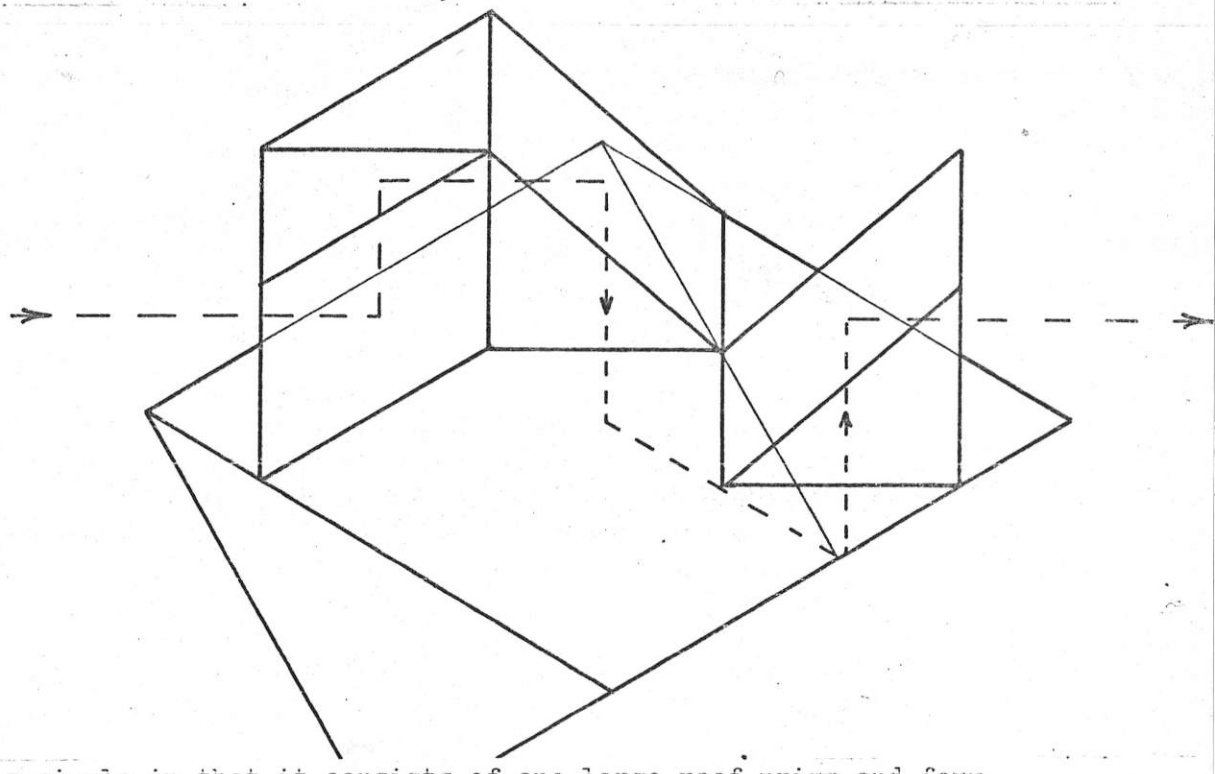
FIGURE 4.28 Exposure plate: recording a set of images with decreasing exposures.

Introduction of this plate into any photographic recording set-up results in several images of different intensities being recorded. One of these images will have the correct exposure.

If a photographic plate is placed normal to the beams reflected from the 'exposure' plate, and the angle of incidence on the exposure plate is 49°, all of each image is in focus; all images are in focus and there is a maximum separation between the images. The mathematical proofs are given in Appendix IV.

Fig. 4.29 shows a prism which was designed and constructed for the purpose of rotating the light distribution through 90° so that the beam can be swept in the perpendicular direction.

FIGURE 4.29



The prism is simple in that it consists of one large roof prism and four smaller roof prisms fixed together with an index matching cement. This was carried out by the glass workshop and resulted in a prism with little distortion and a high transmission.

Fig. 4.30 shows a streak record of the near-field of the Q-switched output from the Nd:glass laser, the direction of sweep being in the plane of the Q-switch sweep.



FIGURE 4.30

Streak photograph of the near-field of a Nd:glass laser.
Streak rate = 5.3ns/mm.
Second distribution is a later Q-switch pulse.

The prism speed was 100,000 rpm giving a theoretical resolution limit of 3.7 ns and the rate of sweep at the photographic plate was 5.3 ns/mm. Two consecutive pulses have been recorded and are separated spatially by a prism which moves the image on a circle, the tangent to the circle corresponding to a horizontal line in the laser. Fig.4.30 shows (i) that the pulse duration is approx. 30 ns, (ii) that the output beam diameter of the laser expands from 1.5 mm initially to a maximum of 4.5 mm after approx. 17 ns. (iii) that the effect of the roof edge loss is sufficient to prevent laser action on a line parallel to this edge and passing through the rod axis.

4.6.3 Finally there is a short description of a time resolution experiment on the laser using apertures and fast photodetectors.

Fig. 4.31 shows the system used.

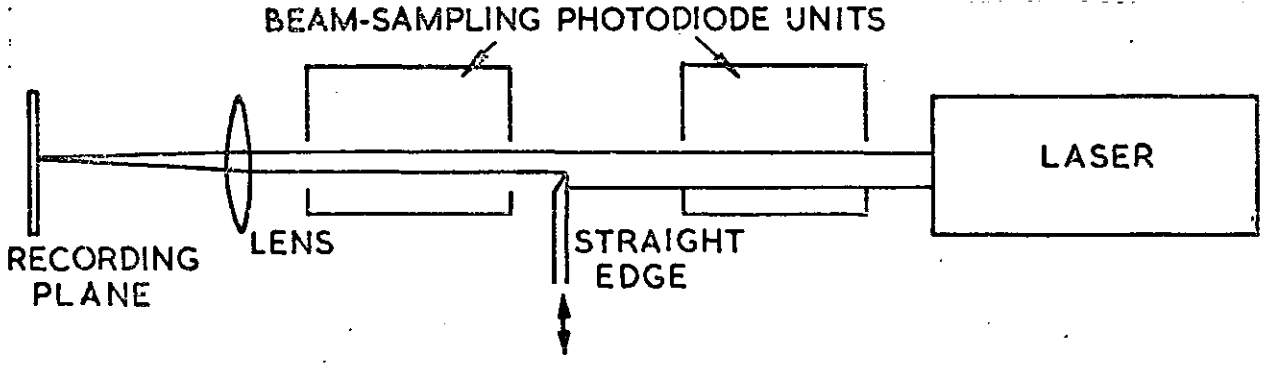


FIGURE 4.31 Experiment supplying information on the correlation between the time evolution of the laser pulse and its transverse and angular distributions.

The laser input was maintained at a constant level and the total output was monitored using photodiode unit No. 2. The sharp metal edge was moved successively across the near-field in the direction of sweep of the Q-switching prism. At each laser pulse (i) both oscilloscope beams were triggered from the monitor recording total output; (ii) the intensity profile of the sample and of the total output were recorded by the two oscilloscope beams. (iii) The sample was focussed onto polaroid print material to record by means of the resulting burn pattern the approximate size and distribution in the far-field.

Measurement of the far-field and scope traces yielded directly information on the power, pulse width, timing and divergence of the sample with respect to the whole output. Fig. 4.32 shows graphically some of these results. In particular it can be seen that the beginning of the pulse occurs successively later for progressive positions across the near-field and that the divergence increases with increasing sample of the near-field. It is concluded that the pulse is swept approximately linearly across the output mirror at a rate of $\simeq$ 0.50 mm/ns and that at the same time it is swept in angle at a rate of $\simeq$ 0.25 mrad/ns. The apparent centre of sweep is thus a distance from the steel edge back through the laser of $\frac{0.50}{0.25 \times 10^{-3}}$ mm = 2000 mm. This was checked by placing a cylindrical lens of known focal length (405 mm) in front of the laser and finding the position of best focus. This was 470 mm from the lens, and the calculated object distance for this image distance is 2800 mm, in reasonable agreement with the value above.

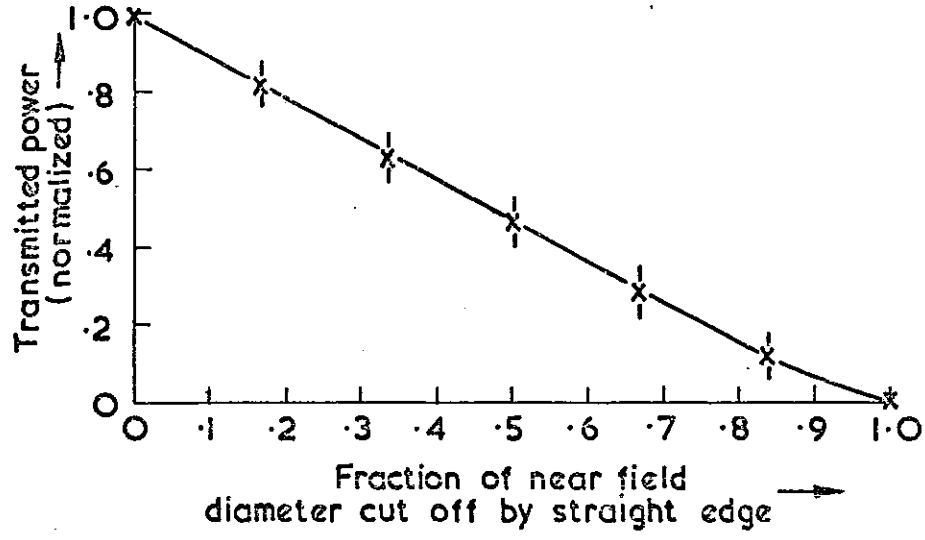
This cylindrical lens experiment also gave a figure of 0.9 mrad for the minimum possible divergence when compensation for angular sweep is introduced.

As expected, no sweeping was found to occur in the vertical direction, which is perpendicular to the sweep direction of the Q-switching prism.

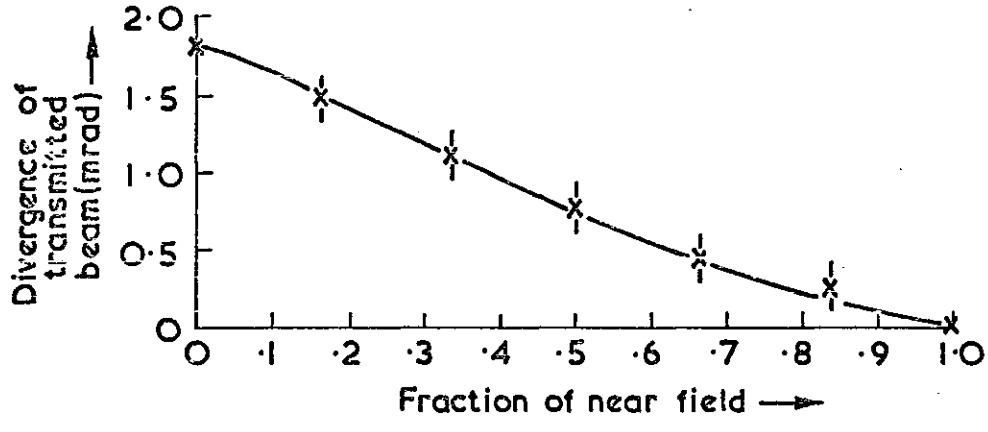
This result has also been compared with a computer-calculated curve corresponding to Fig. 4.32. This is shown in Fig. 4.33. The sweep rate of 0.62 mm/ns corresponds to our measured value of 0.50 mm/ns.

FIGURE 4.32

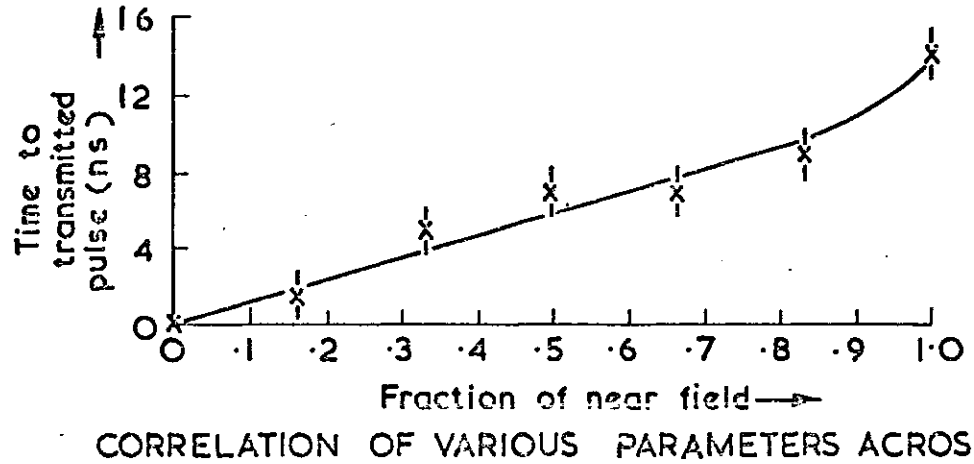
(a)



(b)



(c)



CORRELATION OF VARIOUS PARAMETERS ACROSS THE OUTPUT OF Nd: GLASS LASER WITH ROTATING MIRROR Q-SWITCH.

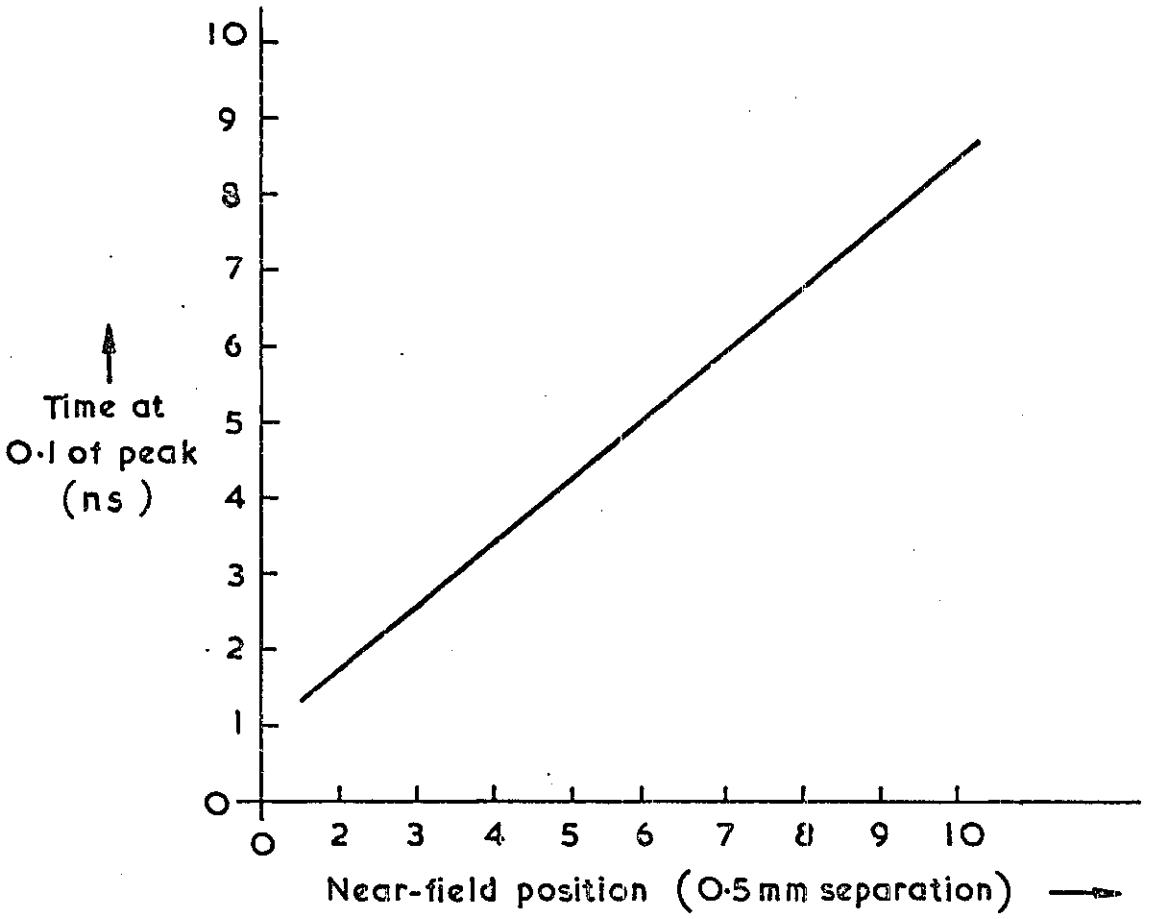


FIGURE 4·33 Computed dependence of the position in the near field of the leading edge of the pulse as a function of time.

CHAPTER 5

Coherence

5.1	Abstract	5.1
5.2	Theoretical Considerations of Coherence	5.2
	5.2.1 Definition of Coherence	5.2
	5.2.2 Formulae for Coherence	5.5
5.3	Resonator Theory	5.6
	5.3.1 Introduction	5.6
	5.3.2 Theory	5.7
	5.3.3 Solutions	5.9
	5.3.4 Resonator modes and coherence	5.13
5.4	Examples	5.14
	5.4.1 Mode Descrimination	5.14
	5.4.1.1 Example of axial mode discrimination	5.16
	5.4.1.2 Example of transverse mode discrimination	5.16
	5.4.2 Calculated Examples of Coherence Functions	5.17
	5.4.2.1 Laser operating TEM_{00} + TEM_{01}	5.17
	5.4.2.2 Laser operating with 5 axial modes	5.20
	5.4.3 General Remarks on Laser Coherence Functions	5.20
	5.4.4 Coherence and Holography	5.22
	5.4.4.1 Efficiency of thin amplitude holograms	5.23
	5.4.4.2 Coherence requirement for efficient holograms	5.25
	5.4.4.3 Coherence requirement vs energy requirement	5.26
	5.4.4.4 Pitfalls of a multimode laser for holography	5.28
	5.4.4.5 Conclusions	5.28

5.5 Coherence Measurement 5.29

5.5.1 Conventional Methods 5.29

5.5.1.1 Interferometric techniques 5.29

5.5.1.2 Spectroscopic techniques 5.31

5.5.1.3 Information capability of these methods 5.37

5.5.2 Holographic Methods 5.38

5.5.2.1 The Principle 5.39

5.5.2.2 Experimental arrangements 5.42

5.5.2.3 Experimental measurements 5.48

5.6 The Control of Coherence 5.52

5.6.1 Methods of Improving Transverse Coherence 5.54

5.6.1.1 Diffraction loss 5.54

5.6.1.2 Gain coefficient 5.58

5.6.1.3 Reflectivity 5.58

5.6.1.4 Enhancement of discrimination 5.56

5.6.2 Methods of Improving Temporal Coherence 5.61

5.6.2.1 Gain coefficient 5.61

5.6.2.2 Reflectivity 5.62

5.6.2.3 Internal loss 5.65

5.6.2.4 Enhancement of discrimination 5.67

5.6.3 Selection of a Method of Controlling Transverse Coherence 5.70

5.6.3.1 Selection criteria 5.70

5.6.3.2 Aperture 5.71

5.6.3.3 Length 5.72

5.6.3.4 Intracavity galilean telescope 5.72

5.6.3.5 Confocal parameter 5.72

5.6.3.6 'Unstable' resonator 5.73

5.6.3.7 Methods of enhancing discrimination 5.73

5.6.4 Selection of a Method of Controlling Temporal Coherence 5.74

5.6.4.1 Resonant reflector 5.74

5.6.4.2 Resonant rejector or intracavity etalon 5.78

5.6.4.3 Wavelength stability 5.81

5.7 Coherence Control of the Nd:glass Laser 5.82

5.7.1 Temporal Coherence 5.82

5.7.1.1 Theoretical design 5.82

5.7.1.2 Experimental measurements 5.88

5.7.2 Transverse Coherence 5.92

5.7.2.1 Existing transverse coherence 5.92

5.7.2.2 Aperture method to improve coherence 5.92

5.7.2.3 Galilean telescope method 5.94

5.7.2.4 Compensating optics method 5.96

5.7.2.5 'Unstable' resonator method 5.97

5.7.2.6 Conclusion 5.98

CHAPTER 5

5.1 Abstract

This chapter deals with all the aspects of coherence which are relevant to this thesis.

Firstly, the topic is discussed theoretically. The classical coherence theory of Born and Wolf (1959) is the basis, and is related to the laser output which has been shown (Fox and Li 1961, Kogelnik 1966 etc.) to consist of a limited number of discrete resonator modes. The effect of limited pulse duration is also discussed. The nature of laser coherence functions is shown to be more complex in general than classical light sources, and it becomes necessary to think more carefully about the criteria for coherence requirements as well as to devise new ways of assessing coherence. The former is discussed with particular reference to holography and a new coherence measurement which is holographic in nature is included among other more conventional means.

Having related degree of coherence to numbers of resonator modes, ways of controlling coherence are found by looking into the process of laser action to find parameters which depend upon the resonator mode and which can themselves be controlled. Following a comparison of the available methods, proposals are made for controlling both transverse and temporal coherence. These are developed theoretically and investigated experimentally for our laser system, and from the results it is shown that high temporal coherence can be achieved without loss in output and that the transverse coherence can be quite adequate, again without a severe drop in output.

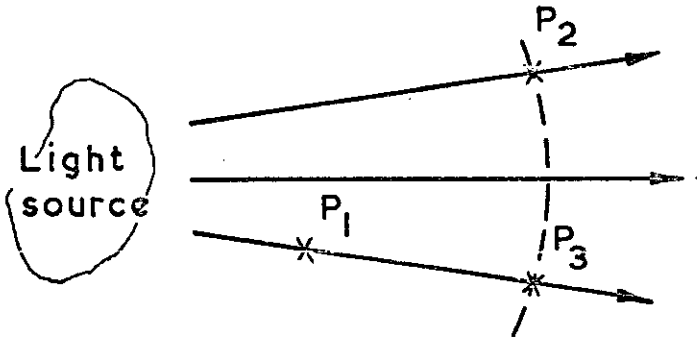
5.2 Theoretical Considerations of Coherence

The concept of coherence is not an easy one and although the term is in constant use in the discussion of lasers and laser optics, the meaning of coherence as applied to lasers is often rather vaguely understood and its effect, when various applications are being considered, is often not sufficiently well thought out.

5.2.1 Definition

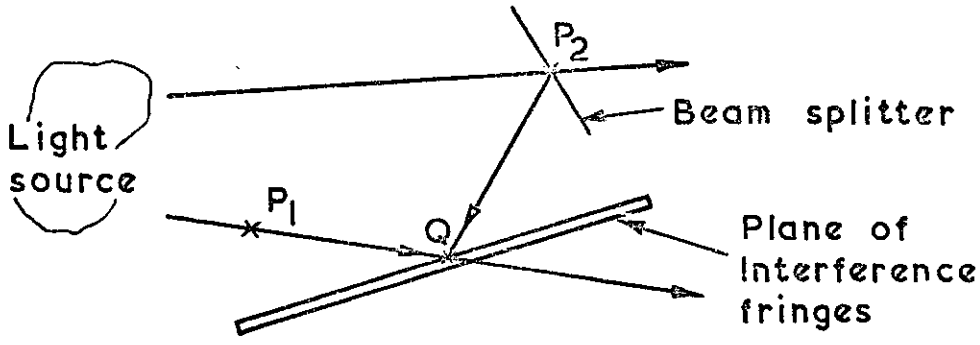
(i) Consider the light source in Fig. 5.1 and the electro-magnetic waves originating from the source which pass through the points P_1, P_2 and P_3.

FIGURE 5.1



The two extremes of coherence can be defined thus:-
a completely coherent source is one resulting in identical phase disturbances at P_1 and P_2, while an incoherent source is one giving rise to uncorrelated disturbances at these two points. All sources lie between these two extremes and are partially coherent to a greater or lesser degree. The degree of coherence is defined by its physically observable effect, that of forming an interference pattern when the two disturbances are mixed, as shown in Fig. 5.2 for example.

FIGURE 5.2



This interference pattern is specified by the depth of modulation, or visibility, of the fringes forming it, and it is this visibility which is used as a measure of the coherence. Two types of coherence may be distinguished. The coherence between the disturbances at two points such as P_1 and P_3, which receive light from the same point of the source, is termed 'temporal coherence'. The two points are such that the disturbance at the point nearer the source (P_1 in this case) travels away from the source through the second point (P_3) and thus the only difference between the two disturbances is that due to a time delay. Hence the nomenclature used.

The coherence between two points such as P_2 and P_3, which are equidistant from the source and not therefore subject to a relative time delay, is known as 'transverse coherence'. The word used is transverse since the two points lie in a surface transverse to the direction of propagation.

Although the coherence between P_1 and P_2 is not necessarily separable into two components, a temporal component between P_1 and P_3 and a transverse component between P_2 and P_3, it is often so to a good approximation and the problems of measurement, analysis and control of coherence are very much simplified by always endeavoring to keep them separate.

(ii) A mathematical definition is desirable so that calculations of coherence functions and the effects, for example, of constraints can be evaluated. Born and Wolf form the basis of the following. Starting with the observable quantity, the fringe visibility (V), this is defined as:-

$$V = \frac{E_{MAX} - E_{MIN}}{E_{MAX} + E_{MIN}}$$ where E_{MAX} and E_{MIN} are the energy densities in the bright and dark fringes ... (5.1)

The use of 'energy densities' in the definition is preferred to the more usual 'intensities', since all methods of measuring the fringes do in fact rely upon an energy density. The energy density is the intensity integrated over a characteristic time which may be the response time for a photocell or just the exposure time of a photographic emulsion. A further recommendation to the use of energy density is that the mathematical analysis is more straightforward.

Let the visibility of fringes formed by mixing the disturbances at P_1 and P_2 of Fig. 5.1 be V_{12}.

For coherent disturbances at P_1 and P_2 of amplitude a_1 and a_2

$$E_{MAX} = \int (a_1 + a_2)^2 \, dt \quad \text{and} \quad E_{MIN} = \int (a_1 - a_2)^2 \, dt$$

and assuming that the ratio between a_1 and a_2 remains constant with time,

$$\therefore \quad V_{12} = \frac{2\sqrt{E_1}\sqrt{E_2}}{E_1 + E_2}$$ where E_1 and E_2 are the energy densities of each beam on its own. ... (5.2)

If V_{12} is less than this then the beams are not completely coherent and we put

$$V_{12} = \frac{2\sqrt{E_1}\sqrt{E_2}}{E_1 + E_2} |\gamma_{12}| \qquad \ldots (5.3)$$

so defining $|\gamma_{12}|$, the degree of coherence between P_1 and P_2.

There is another characteristic of the fringes which depends upon the coherence, this being their absolute position (or phase). The intensity distribution in the fringes is given by:-

$$E = (E_1 + E_2)\,(1 + V_{12} \cos [\varphi - 2\pi \underline{\sigma} . \underline{r}]) \qquad \ldots (5.4)$$

where σ is the fringe spatial frequency and φ gives their absolute position (or phase).

It can be seen then that both aspects of coherence can be included together if the 'coherence function' γ_{12} is complex, where the modulus $|\gamma_{12}|$ is defined as above and the argument is defined by:-

$$\arg \gamma_{12} = \varphi \quad \text{i.e.} \quad \gamma_{12} = |\gamma_{12}| e^{i\varphi}$$

5.2.2 The next step is to relate γ_{12} to fundamental parameters of the disturbances at P_1 and P_2. Appendix V sets out this proof, based on that of Born and Wolf.

The result is that if the complex disturbances at P_1 and P_2 are $A_1(t)$ and $A_2(t)$ then:-

$$\gamma_{12} = \frac{\int A_1(t) A_2^*(t)\,dt}{\sqrt{\int A_1(t) A_1^*(t)\,dt}\ \sqrt{\int A_2(t) A_2^*(t)\,dt}} \qquad \ldots (5.5)$$

and further, if the coherence is considered separable into a temporal coherence γ_{13} between P_1 and P_3 and into a transverse coherence γ_{23} between P_2 and P_3 then:-

$$\gamma_{13} = \frac{\int G(\nu) e^{-2\pi i \nu \tau} d\nu}{\int G(\nu) d\nu} \qquad \ldots (5.6)$$

where $G(\nu)$ = spectral density

τ = time for light to travel from P_1 to P_3.

and

$$\gamma_{23} = \frac{\int A_3(t) A_2^*(t) dt}{\sqrt{\int A_3(t) A_3^*(t) dt} \sqrt{\int A_2(t) A_2^*(t) dt}} \qquad \ldots (5.7)$$

These equations can be used, as shown later, to calculate coherence functions from a knowledge of the output spectral distribution and a knowledge of the amplitude and phase distribution across the output wavefront.

5.3 Resonator Theory

5.3.1 Any discussion on the coherence of lasers must involve some form of theory which attempts to predict the coherence of a laser and tries to relate the coherence to the independent parameters of the laser (such as the geometry and the optics). This theory, known as resonator theory, was first developed by Fox and Li (1961), and applied to plane parallel resonators with strip mirrors. Other forms of resonator have been studied by these and many other authors; for example Collins 1964, Boyd and Kogelnik 1962, Fox and Li 1963, Siegman and Arrathoon 1967, Toraldo di Francia 1966.

In essence the problem is similar to that of a microwave cavity or the 'particle in a box' of wave mechanics. A solution of the appropriate wave

equation shows the existence of discrete energy states or eigen-values along with a complete set of wave functions or eigenmodes. For the laser resonator, as with the microwave cavity, the eigenmodes are termed 'modes' and are designated TEM_{mnq}, the subscripts specifying the precise mode.

The properties of the eigenmodes or 'modes' are such that:-

(i) A single mode is a stationary state and thus has a phase and amplitude distribution which remains constant with time apart from a scaling factor. A laser operating single mode is completely deterministic and must in consequence be **perfectly coherent,** apart from the perturbing influence of coupling light out of the laser.

(ii) Modes are independent states with no inter-correlation. They are mathematically orthogonal. A laser operating multimode has, then, a certain randomness of phase and amplitude and this lack of correlation of phase from time to time is evidenced by a lack of coherence. The laser is partially coherent.

(iii) The modes form a complete set; i.e. any light distribution can be represented as the sum of this set of modes. The output from a white light source of large size, when represented in this form, contains significant contributions from all modes resulting in a minimum correlation between disturbance at two points in the field. The source is an incoherent one, as is well known.

The above serves to illustrate that an increasing number of modes is synonymous with a decreasing degree of coherence, a fact which might be proved mathematically by inserting a mixture of mode distributions into the coherence equation 5.5.

5.3.2 A condensation of the resonator theory which calculates the mode functions and their energy states is given below:-

The equation to be solved can be written down from the property of a mode, that its form is unchanged, bar a scaling factor for every round trip

of the resonator.

If the amplitude and phase distribution at one mirror is $\varphi_1(xy)$ and the amplitude and phase distribution at the other mirror is $\psi_2(x'y')$ then in the stationary state these two distributions are related by the Kirchhoff equation as follows:-

$$A_1 \varphi_1(xy) = \int_2 K(xyx'y')\, \psi_2(x'y')dx'dy'$$

and ... (5.8)

$$A_2 \psi_2(x'y') = \int_1 K(x'y'xy)\, \psi_1(xy)dxdy$$

where the kernel $K = \frac{ik}{4\pi}.\frac{e^{-ikR}}{R}.(1 + \cos\theta)$

and $R^2 = (x'-x)^2 + (y' - y)^2 + L^2$; $\cos\theta = L/R$; L = length of resonator and is therefore a function depending upon the geometry of the resonator; and where A_1 and A_2 are complex constants.

Substitution of one equation into the other results in an eigenvalue equation, the solutions of which are the eigenmodes or 'modes', $\varphi_{mnq}(xy)$, and the corresponding eigenvalues γ_{mnq} are $= A_1A_2 = D_{mnq}e^{i\varepsilon_{mnq}}$ say. The significance of the eigenvalues is that the square of the modulus $(=D^2)$ is just 1 - diffraction loss per double pass, and the argument (ε) is just the overall phase change per double pass which must be a whole number of half wavelengths in order that there is a node at the end mirror. Thus:-

Diffraction loss/double pass $= 1 - D^2$ ... (5.9)

Phase change/double pass $= \varepsilon = q\pi$ ... (5.10)

Since ε is a function of wavelength, EQU 5.10 determines the allowed resonator wavelengths (λ_{mnq}).

Simplification of the resonator equation is achieved by suitable choice of mirror shape and coordinate geometry. Thus with infinite strip and rectangular mirrors or apertures and using rectangular coordinates the equation separates into two independent one-dimensional equations, while with circular mirrors or apertures cylindrical coordinates also yield a separation into one-dimensional equations.

5.3.3 The solution of these equations has taken several forms in the literature. An exact solution is only possible for the confocal resonator, as shown by Boyd and Gordon (1961), others (Fox and Li 1961 for example) have used iterative methods and others have used perturbation techniques. Fox and Li used an iterative method with some physical significance. An arbitrary initial amplitude and phase distribution was postulated and the progress of this wave up and down the cavity was calculated by repetitive use of the Kirchhoff integral. The distribution of amplitude and phase eventually settles into that of a mode. This calculation has the added advantage that it shows how long it takes, under given conditions, for a mode to establish itself; an important aspect in Q-switched lasers where pulse build-up times correspond to perhaps only 20 double transits of the resonator.

Fig. 5.3 shows, for infinite strip mirrors, how many passes are required, with a Fresnel number of 6.25, for the distribution to settle into a mode.

Solution, one way or another, of the resonator equation quickly shows that every possible resonator does not lead to a different set of modes with different losses per pass and different characteristic frequencies.
A considerable degeneracy exists and can be stated as follows:-

All resonators, having equal shaped apertures and spherical mirrors, and also having a given value of i) $g = (1 - {}^{L}/_{R_1})(1 - {}^{L}/_{R_2})$, called the 'confocal parameter' and ii) $F = w_1 w_2/\lambda L$ called the 'Fresnel number',

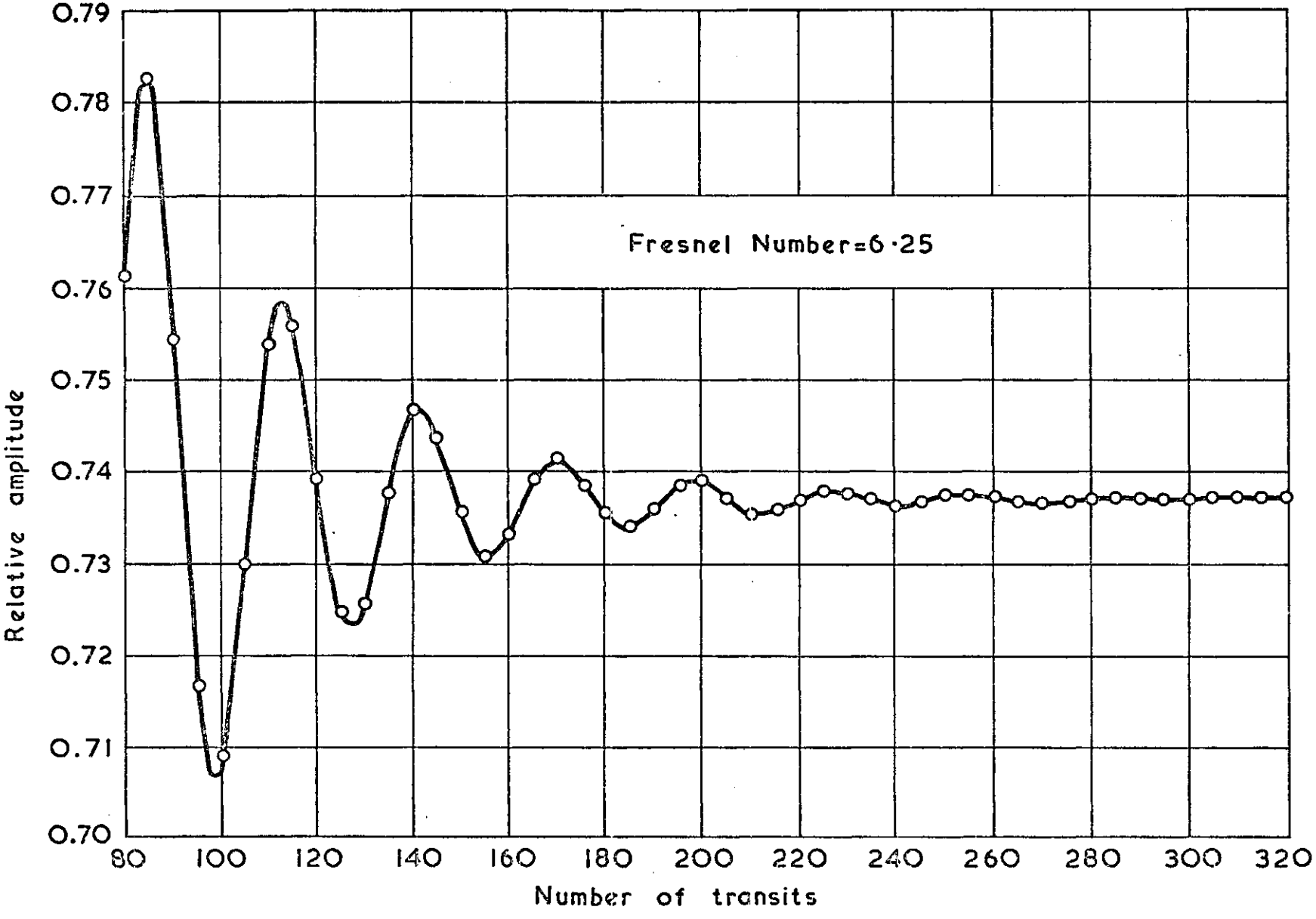
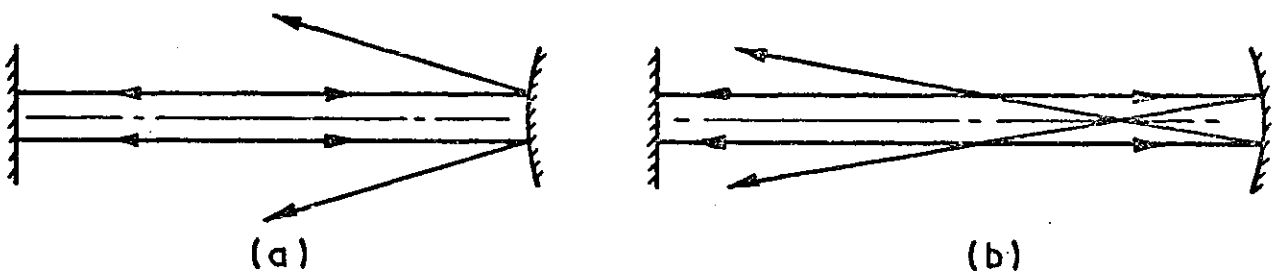


FIG. 5·3 FLUCTUATION OF FIELD AMPLITUDE AT x=0.5 AS A FUNCTION OF NUMBER OF TRANSITS. (THE INITIALLY LAUNCHED WAVE HAS A UNIFORM DISTRIBUTION.)

(where L = resonator length; R_1 and R_2 are the mirror radii of curvature; w_1 and w_2 are mode radii at the mirrors) are equivalent and have the same modes, the same losses and the same resonant frequencies. The only differences lie in differences of mode profile in the axial direction. Examples of resonators are 'confocal' ($g = 0$), 'plane parallel' and 'concentric' ($g = +1$).

Examples of the dependence of mode losses on Fresnel number (F) and confocal parameter (g) (as calculated in the literature) are shown in Figs. 5.4. This enables a comparison of losses and mode discriminations characteristic of different resonator configurations. It is noted particularly that losses for large F rise sharply above $|g| = +1$. The cause of this is simply that the propagation of a mode up and down the cavity becomes a diverging process as indicated in Fig. 5.5.

FIGURE 5.5



TWO EXAMPLES OF 'UNSTABLE' RESONATORS

The mode is no longer confined laterally and losses occur whatever the aperture. Resonators such as these are termed 'lossy' or 'unstable'. Fig. 5.6 is the stability diagram, having axes $1 - L/R_1$ and $1 - L/R_2$ respectively, and any resonator is a point on this diagram.

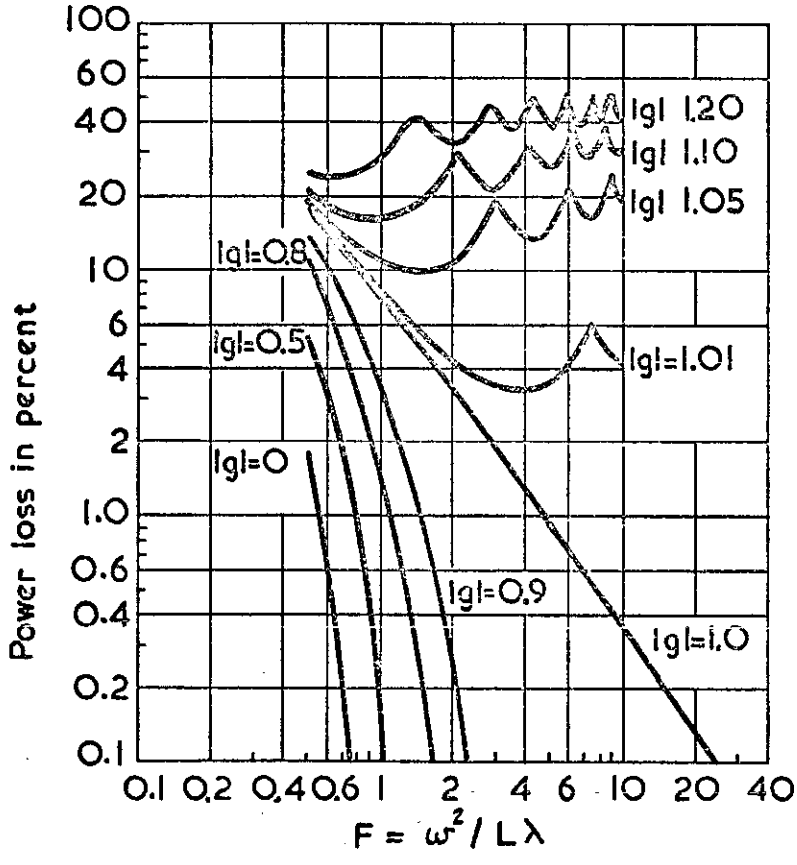
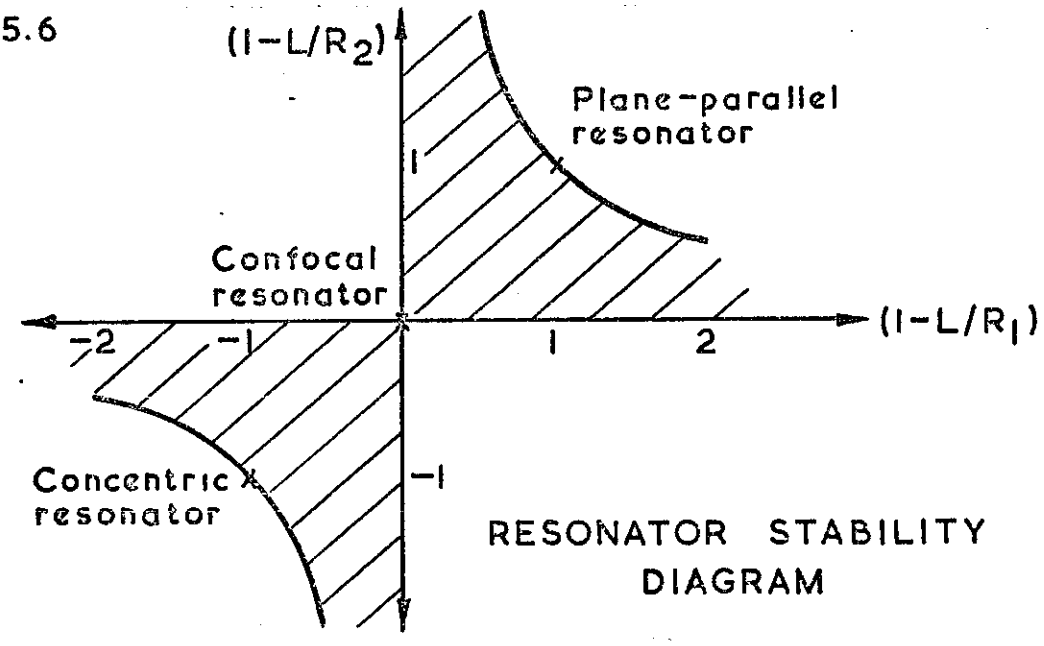


FIG. 5.4 EFFECT OF FRESNEL No (N) AND CONFOCAL PARAMETER (|g|) ON THE POWER LOSS PER TRANSIT OF THE TEM_{00} MODE IN A RESONATOR WITH STRIP MIRRORS

FIGURE 5.6



By calculating the ray transfer matrix of a resonator, stable configurations, in which any arbitrary ray remains confined, are shown to be those with a value of confocal parameter g between 0 and 1. These requirements are met by all resonators lying within the shaded area of the stability diagram. All resonators outside are 'unstable' or 'lossy'.

Fig. 5.7 is an example of the calculated phase shifts (ε) as a function of Fresnel number and confocal parameter, for the TEM_{oo} mode. Other modes have similarly shaped curves with different vertical scale. For sufficiently large Fresnel number (linear region of Fig. 5.7)

$$\varepsilon = \frac{2\pi L}{\lambda} - (m + n + 1) \cos^{-1} \sqrt{g}$$

but $\varepsilon = q\pi$ (resonance condition)

$$\therefore \text{ Resonance frequency } = \frac{c}{\lambda} = \left[q + \frac{1}{\pi} (m + n + 1) \cos^{-1} \sqrt{g} \right] \frac{c}{2L}$$

... (5.11)

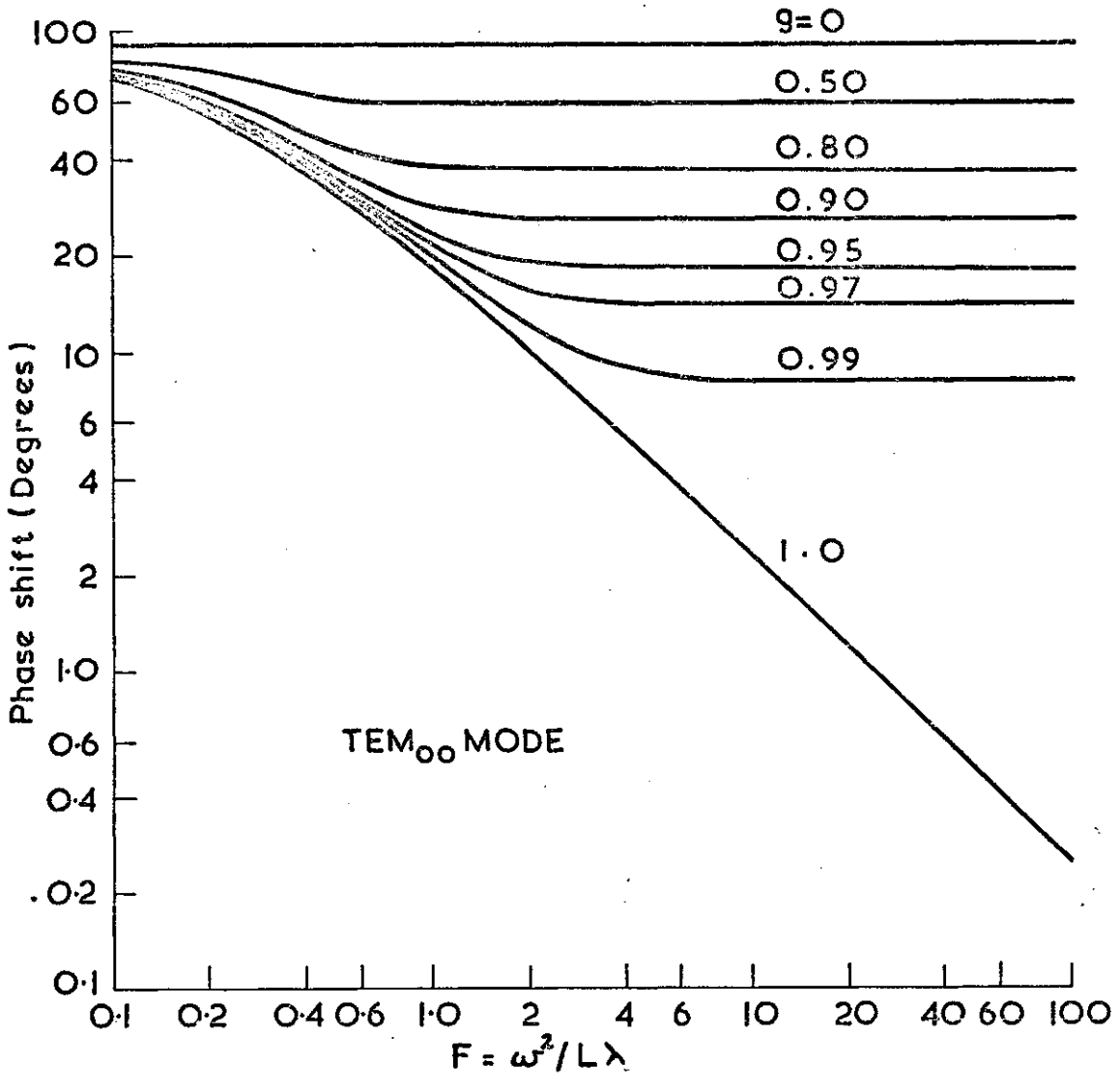


FIG. 5.7 PHASE SHIFT PER TRANSIT FOR THE TEM_{00} MODE OF A STABLE RESONATOR WITH CIRCULAR MIRRORS

The difference in resonance frequency between the TEM_{00} and TEM_{01} modes is plotted in Fig. 5.8 as a function of confocal parameter. For high Fresnel number this difference extends from 0 for the plane parallel resonator to half the axial mode frequency separation for the confocal resonator.

As examples of solutions to the eigenvalue equation, take the confocal and the plane parallel resonator. There is an analytic solution to the former, for which the mirrors coincide with the phase front; and the modes are approximated, for square aperture, by Hermite-Gauss functions (the approximation becomes exact for large Fresnel number). These are:-

$$\psi = H_m\left(\sqrt{2}\frac{x}{w}\right) e^{-x^2/w^2} \; H_n\left(\sqrt{2}\frac{y}{w}\right) e^{-y^2/w^2} \; e^{-i\varphi} \quad \ldots (5.12)$$

where w = beam radius

$$\varphi = \text{phase shift/transit} = \frac{2\pi L}{\lambda} - \frac{(m+n+1)}{} \times \frac{\pi}{2}$$

where L = mirror separation

and where H_m is a Hermite polynomial of order m and

$H_0(x) = 1$; $H_1(x) = x$; $H_2(x) = 4x^2-2$; $H_3(x) = 8x^3 - 12x$; ...

From the phase shift, the resonant frequencies can be calculated to be:-

$$\nu = \left[(q + 1) + \tfrac{1}{2}(m + n + 1)\right] c/2L \quad \ldots (5.13)$$

Fig. 5.9 plots $H_m(x/w)e^{-x^2/w^2}$ for $m = 0$ to 2 showing the form of the Hermite-Gaussian and showing that an aperture must give a greater loss for the higher order modes which spread further from the axis. The exact

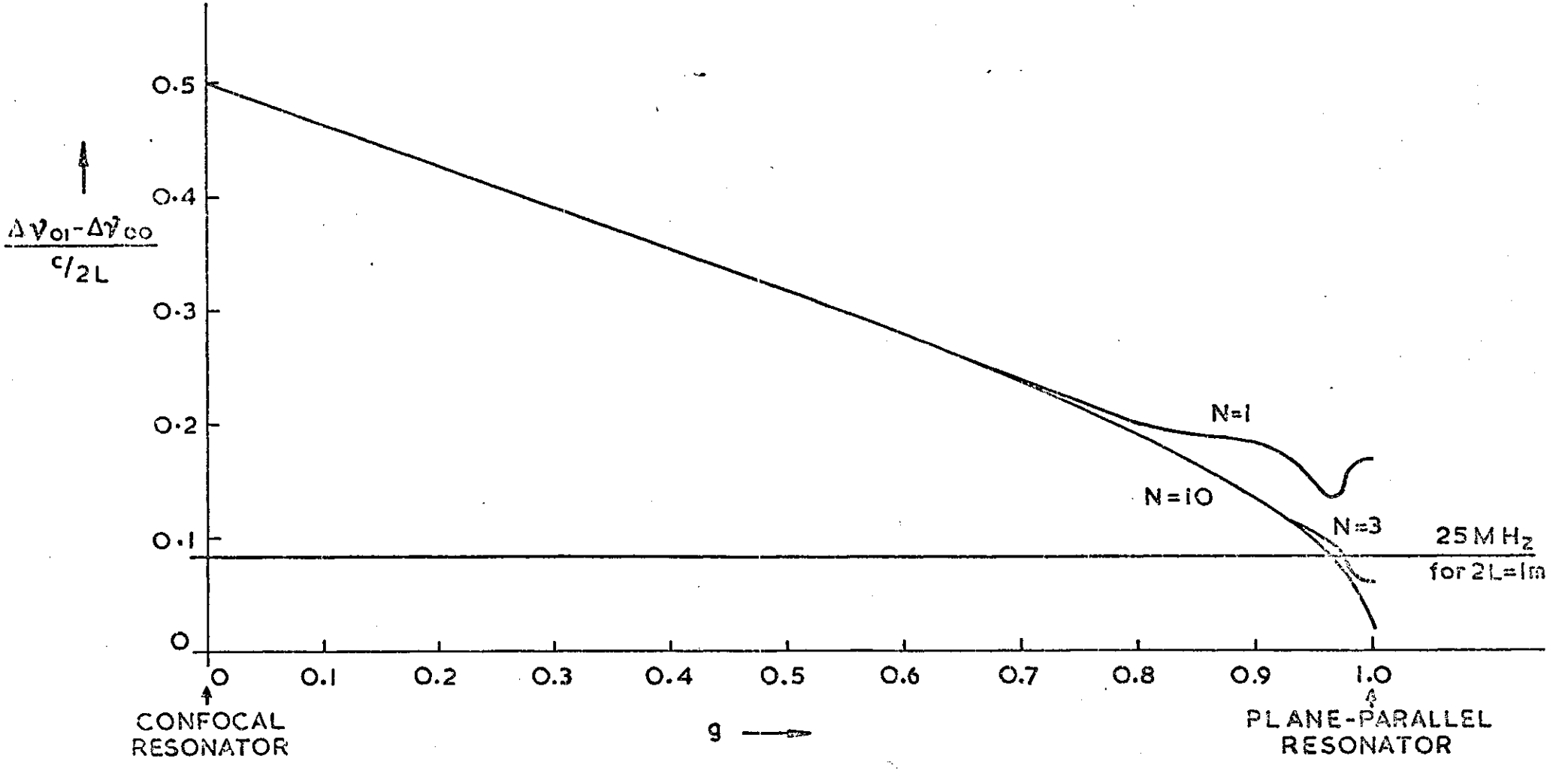
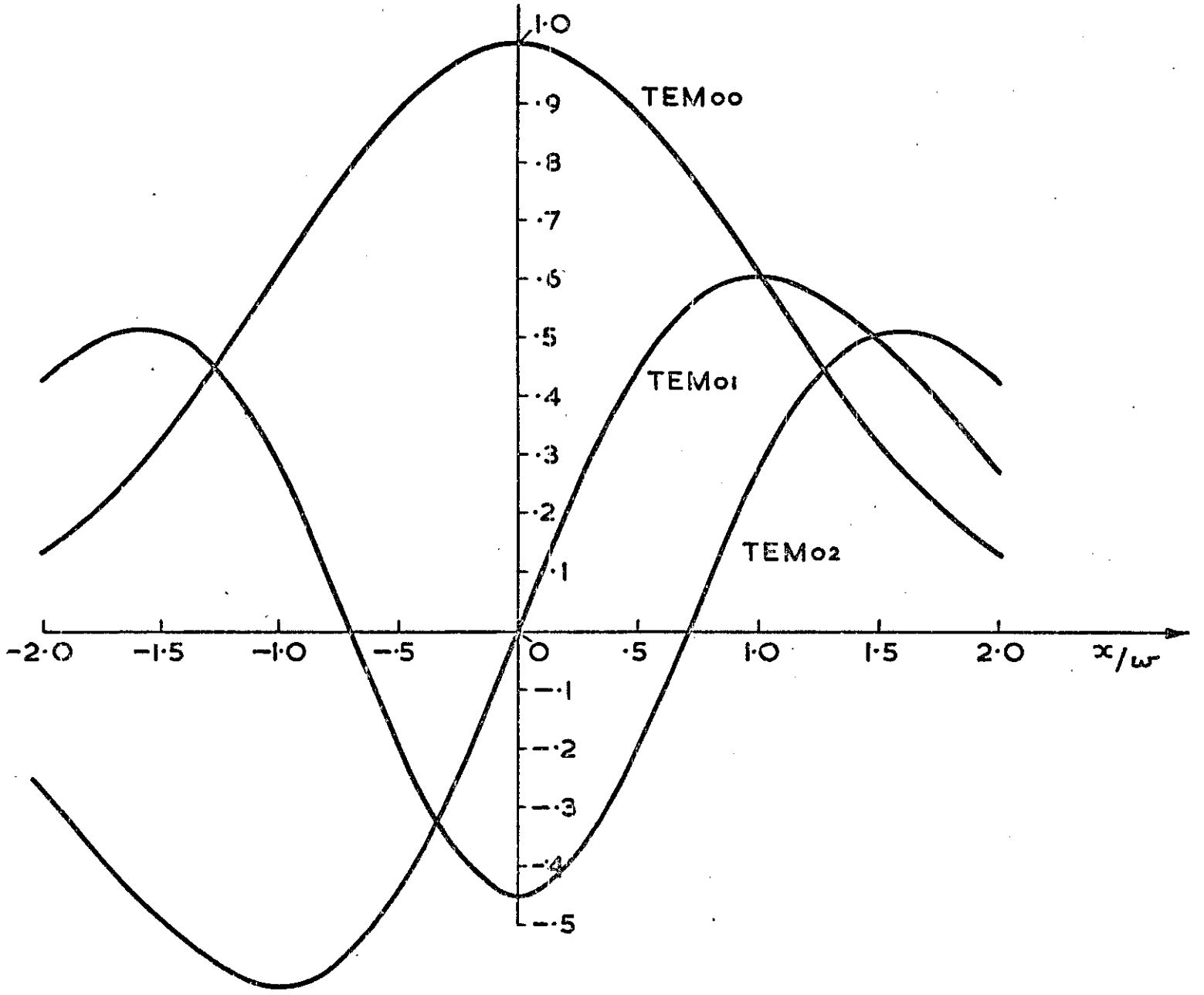


FIGURE 5.8 Frequency separation of TEM_{00} and TEM_{01} modes as a function of the confocal parameter (g) for various values of Fresnel number (N)



AMPLITUDE DISTRIBUTIONS OF THE THREE HIGHEST ORDER MODES OF A CONFOCAL RESONATOR WITH CONSTANT ENERGY PER MODE

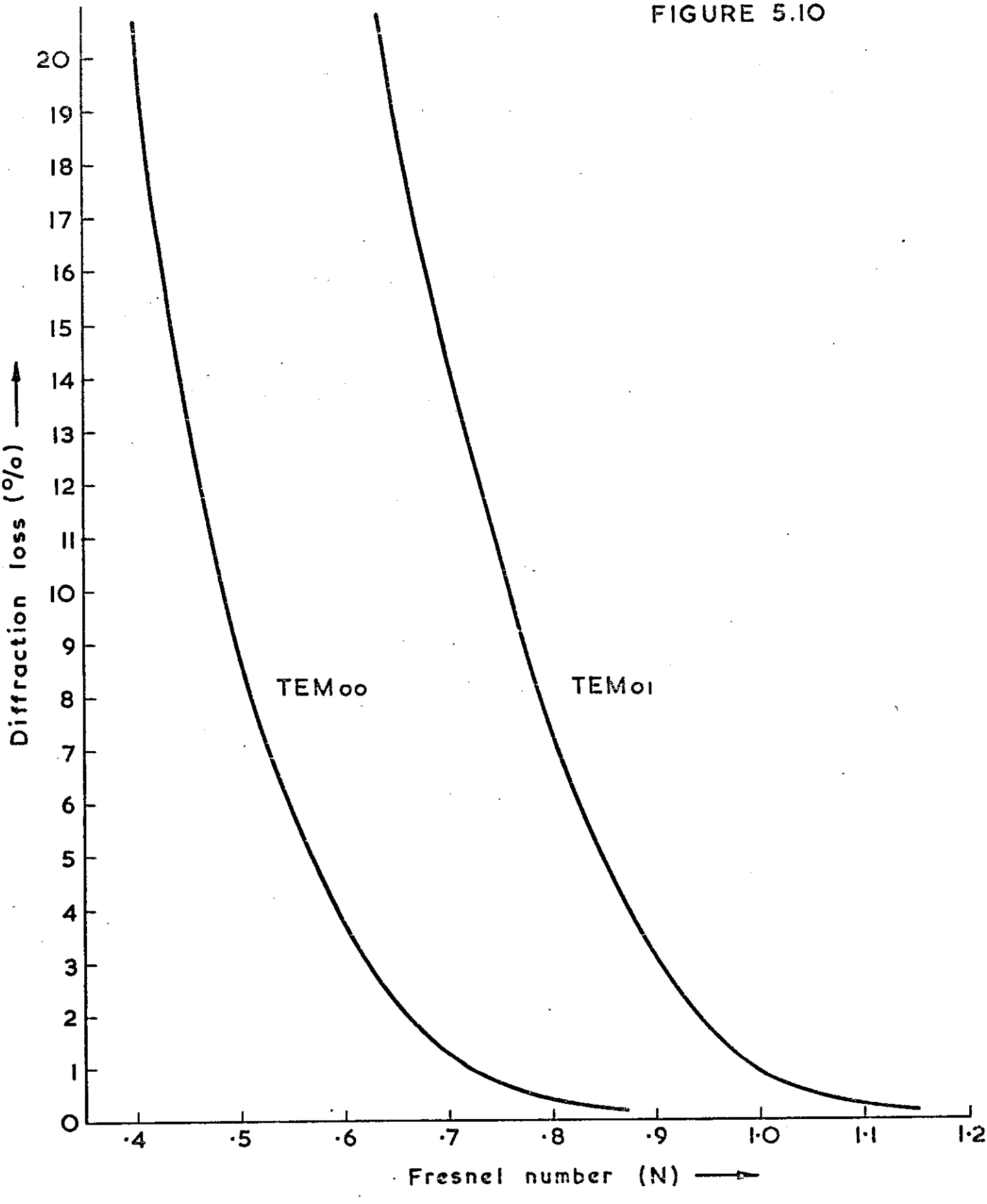
solution for small Fresnel numbers calculates this loss and this is shown in Fig. 5.10 as a function of Fresnel number for two modes.

Solutions for non-confocal resonators are, as previously stated, found by iterative computational methods. Fig. 5.11 shows typical calculated mode distributions for a plane parallel resonator. The modes are of similar general form but the mirrors no longer coincide with phase fronts and the profile no longer has such a simple form.

5.3.4 The mode distribution in a long thin resonator is separable into two parts: the first part (called the 'transverse' mode) characterises a stationary distribution of amplitude and phase in a plane normal to the resonator axis and the second part (the 'axial' mode) specifies a distribution along the resonator axis. Axial modes can be thought of in terms of standing waves along the axis, different axial modes having different numbers of half wavelengths between the end mirrors. The wave number separation between different axial modes (having the same transverse distribution) is consequently $\frac{1}{2L}$ cm^{-1}, where L is the resonator length. Since axial modes are specified by purely axial distributions they do not come into the determination of transverse coherence. Transverse modes can be thought of similarly, the transverse pattern having (as shown in Fig. 5.9) different numbers of zeros across it. Increasing transverse mode number (increasing numbers of zeros) is associated with increasing transverse complexity and increasing angle to the axis (decreasing collimation). Transverse modes are separated in wavenumber by $\frac{1}{\pi}\cos^{-1}\sqrt{g}$ cm^{-1} (as also shown above,) and as this is often very much less than the axial mode separation, they play little part in the determination of the spectral width or temporal coherence of the laser.

It can be stated then that:-

FIGURE 5.10



DIFFRACTION LOSSES OF THE TWO LOWEST ORDER MODES FOR A CONFOCAL RESONATOR

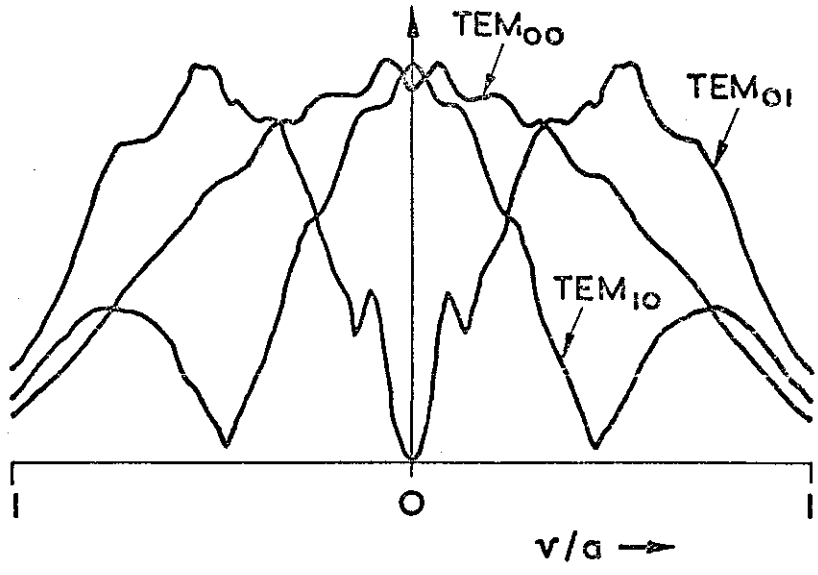


FIG. 5.11 RELATIVE FIELD DISTRIBUTIONS OF FOUR OF THE LOW ORDER MODES OF A FABRY-PEROT RESONATOR WITH (PARALLEL-PLANE) CIRCULAR MIRRORS (N=10).

(i) the axial mode distribution or spectral distribution generally determines the temporal coherence

(ii) the transverse mode distribution determines the transverse coherence

(iii) the far-field, or angular, distribution is a measure of the transverse mode distribution and is consequently also a measure of the transverse coherence.

5.4 Practical Examples

5.4.1 The question now arises as to what determines the distribution of modes in a laser?

Not all modes are evident in the output of a laser because there is discrimination between them and this discrimination leads to the dominance of just a few. The process of discrimination can be stated simply: Let the double pass gain of a mode be G_{mnq}, where m, n and q specify mode TEM_{mnq}. If the initial intensity for mode (m, n, q) is ${}_oI_{mnq}$, then the mode intensity $I_{mnq} = {}_oI_{mnq}\, G_{mnq}^{N}$ where N = number of double passes to reach this intensity.

The mode, say (m', n', q'), with maximum gain, evidently has the maximum intensity after a given number of passes (N), and the relative intensity in any other mode (m, n, q) is given by:-

$$\frac{I_{mnq}}{I_{m'n'q'}} = \frac{{}_oI_{mnq}}{{}_oI_{m'n'q'}} \left[\frac{G_{mnq}}{Gm'n'q'} \right]^N \qquad \ldots (5.14)$$

i.e. relative intensity = relative fluorescent intensity $\times$ (relative gain)^N. All modes with fluor. int. $\times$ (rel. gain)$^N \ll 1$ make a negligible contribution to the output. There is one exception however. If the gain for different modes is derived from different sets of excited ions, the energy store for

the lower gain mode is not prematurely depleted by the higher gain mode. The minor mode still has a low intensity at the time the high gain mode has reached its peak but its intensity can still go on rising and reach the same peak intensity after a greater number of passes. Situations in which this can occur are:-

(i) Transverse modes operating in different regions of the rod.

(ii) Axial modes operating with a large frequency separation when the following conditions apply. The laser ions have partially inhomogeneously broadened spectral lines and this frequency separation is greater than the homogeneous linewidth. The spectral cross-relaxation rate is slower than the intensity rise-time. All these conditions might occur simultaneously in a Nd: glass laser as has been suggested in Chapter 4.

Returning to the normal case in which modes can be regarded as eliminated if rel. fl. int. × (rel. gain)^N $\ll 1$; since in general $N \gg 1$, the effect of any difference in fluorescent intensity is negligible and the inequality becomes:-

$$(\text{relative gain})^N \ll 1 \quad \text{or} \quad \left[\frac{G_{nmq}}{Gn'm'q'}\right]^N \ll 1. \qquad \ldots (5.15)$$

Now, $G = RS \exp 2\ell(\alpha-\beta)$

where R = output reflectivity; $1-S$ = total of other resonator losses

ℓ = rod length; $\alpha = \sigma N$ = gain coefficient

β = loss coeff. of rod material

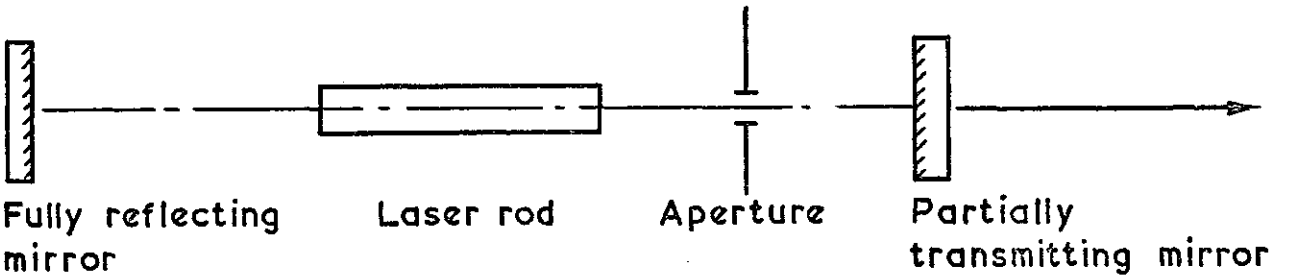
$\therefore$ the condition for mode elimination becomes:-

$$\left(\frac{R_{mnq}}{R_{m'n'q'}}\right)^N \left(\frac{S_{mnq}}{S_{m'n'q'}}\right)^N \exp 2\ell N\left[(\alpha_{mnq} - \alpha_{m'n'q'}) - (\beta_{mnq} - \beta_{m'n'q'})\right] \ll 1$$

$$\ldots (5.16)$$

5.4.1.1 Let Fig. 5.12 represent a simple example.

FIGURE 5.12



LASER OPERATING WITH TRANSVERSE MODE SELECTING APERTURE AND WITH NO AXIAL MODE SELECTION

Consider the axial mode distribution. Of all the parameters in EQU 5.16 only the gain coeff. is dependent upon the axial mode. The equation becomes:- $\exp 2\ell N (\alpha_q - \alpha_q') \ll 1$. Let us find how many modes have intensities more than 1% of maximum. In a typical Q-switching case N may be $\approx 30\ \alpha_q' \approx 0.15\ cm^{-1}$ and $\ell = 10$ cm

$$\therefore \quad \exp 600 \times 0.15\ (\alpha_q/\alpha_q' - 1) = 0.01$$

$$\text{or} \quad 1 - \frac{\alpha_q}{\alpha_q'} = \frac{1}{90} \log_e 100 = 0.051 \quad \therefore \quad \alpha_q/\alpha_q' = 0.95$$

If, also, the curve of gain vs wavenumber is a Gaussian of form $\exp-(\bar{\nu}^2/\Delta^2)$ it has a value of 0.95 at $\bar{\nu} = 0.226\Delta$. The Nd: glass laser with $\Delta \approx 100\ cm^{-1}$, has output spectral width of $0.452 \times 100 = 45\ cm^{-1}$ under these conditions, and the number of axial modes present is 45 ÷ axial mode separation or $45 / \left(\frac{1}{2 \times \text{cavity length}}\right)$. For a cavity of length 50 cm, there are 4500 axial modes. For a ruby laser there may be 200 while for a gas laser there may be only 2 or 3.

5.4.1.2 For the transverse mode distribution, EQU 5.16 reduces to:- $[S_{mn}/S_{m'n'}] \ll 1$ since the only transverse mode dependent parameter is the diffraction loss (D) at the aperture and this is included in S. In fact

$S = S'(1-D)$, and if we again look for modes with more than 1% of the peak intensity, we get:- $[1-D_{mn}/1-D_{m'n'}]^N = 0.01$.

Putting $N = 30$:- $1-D_{mn}/1-D_{m'n'} = (0.01)^{1/30} = 0.86$

The resonator theory gives the loss for each mode (D_{mn}) under any configuration of resonator, and examples of the dependence of this loss on confocal parameter (g) and Fresnel number (F) were shown in Fig. 5.4. The same calculations can also be used to plot $(1-D_{mn})/(1-D_{m'n'})$. Fig. 5.13 shows the variation of $(1-D_{01})/(1-D_{00})$ with confocal parameter and Fresnel number. All points on these curves, below the line drawn at 0.86, are cavity configurations for which the output is at least 99% single mode.

Analysis of the loss curves (Fig. 5.4) shows that it is the Fresnel number which primarily controls the transverse mode discrimination. The confocal parameter merely modifies this calculation. Further, single mode operation occurs in general close to a value of Fresnel number of unity. This is not at all surprising when one remembers that if the central lobe of the diffraction pattern of an incoherently illuminated aperture of radius a_1 exactly fills a second aperture of radius a_2 at a distance L from the first aperture, then the system defines a Fresnel number of 0.61. It is quite reasonable then to find that significant diffraction losses occur in a resonator when the Fresnel number is reduced below about unity.

5.4.2 To give an idea of the type of coherence function typical of a laser, two examples are chosen and the coherence function calculated.

5.4.2.1 A laser operating in the two lowest order transverse modes of the same axial mode. These modes are the TEM_{00} (Gaussian) and TEM_{01} modes and their amplitude distributions across the output reflector are approximated by -

$a_{00}\, e^{-(x^2+y^2)/w^2}\, e^{i2\pi\nu_{00}t}$ and $a_{01}\frac{x}{w}\, e^{-(x^2+y^2)/w^2}\, e^{i(2\pi\nu_{01}t+\delta)}$ respectively.

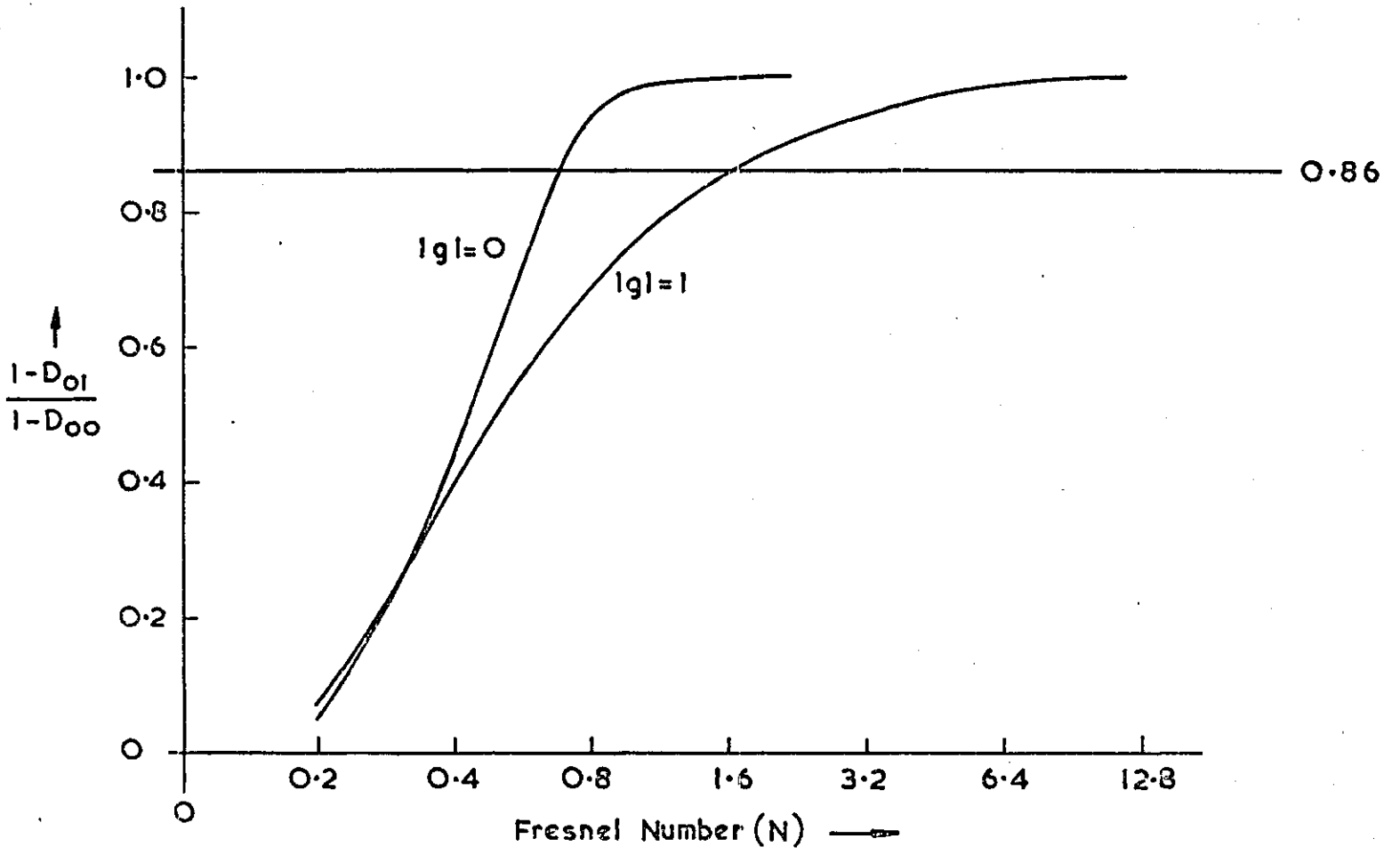


FIGURE 5.13 Discrimination factor between TEM_{00} and TEM_{01} modes as a function of Fresnel number (N) for two resonator configurations; confocal ($|g|=0$) and plane-parallel ($|g|=1$)

where x and y are the transverse coordinates measured from the axis and δ is the phase difference at $t = 0$.

These are exact when the resonator is confocal and the aperture large. By the law of superposition the combined amplitude at the output mirror is:-

$$A = \left[a_{00} + a_{01}\frac{x}{w}e^{i(2\pi\delta\nu t+\delta)}\right]e^{-(x^2+y^2)/w^2}\, e^{i2\pi\nu_{00}t} \qquad \ldots (5.17)$$

where we have put $\nu_{01} = \nu_{01} + \delta\nu$.

As an example let us calculate the coherence between two points at the output reflector having coordinates $(x_1\ 0)$ and $(x_2\ 0)$, and amplitudes A_1 and A_2 respectively. Equation 5.7 can now be used to calculate the transverse coherence between these two points and we get:-

$$\gamma_{12} = \frac{a_{00}^2 + a_{01}^2\frac{x_1x_2}{w^2} + a_{00}a_{01}\int_T\left(\frac{x_1}{w}e^{i\delta}\, e^{i2\pi\delta\nu t} + \frac{x_2}{w}e^{-i\delta}\, e^{-i2\pi\delta\nu t}\right)\frac{dt}{T}}{\sqrt{\left[a_{00}^2+a_{01}^2\frac{x_1^2}{w^2}+2a_{00}a_{01}\frac{x_1}{w}\int_T\cos(2\pi\delta\nu t+\delta)\frac{dt}{T}\right]\left[a_{00}^2+a_{01}^2\frac{x_2^2}{w^2}+2a_{00}a_{01}\frac{x_2}{w}\int_T\cos(2\pi\delta\nu t+\delta)\frac{dt}{T}\right]}}$$

$$\ldots (5.18)$$

where T = time interval of interest

The coherence is evidently a function of the integration time or pulse length. We take the two extremes:-

a) $T \gg 1/\delta\nu$ (or T = integral multiple of $1/\delta\nu$)

Then all the integrals are zero since the average value of sine and cosine is zero over an integral number of cycles, or as $T \to \infty$

$$\therefore \quad \gamma_{12} = \frac{a_{00}^2 + a_{01}^2 x_1 x_2/w^2}{\sqrt{\left(a_{00}^2 + a_{01}^2 x_1^2/w^2\right)\left(a_{00}^2 + a_{01}^2 x_2^2/w^2\right)}} \qquad \ldots (5.19)$$

Figure 5.14 plots γ_{12} as a function of x_2/w for the case with $\frac{x_1}{w} \equiv -1.0$, and with equal energy per mode ($a_{00} = a_{01}/\sqrt{2}$)

b) $T \ll 1/\delta\nu$

Then the integrands do not change appreciably over the period of integration (T).

$$\therefore \gamma_{12} = \frac{a_{00}^2 + a_{01}^2 x_1 x_2/w^2 + a_{00} a_{01}(x_1/w + x_2/w)\cos\delta + i a_{00} a_{01}\left(\frac{x_1}{w} - \frac{x_2}{w}\right)\sin\delta}{\sqrt{\left[a_{00}^2 + a_{01}^2 \frac{x_1^2}{w^2} + 2a_{00} a_{01}\frac{x_1}{w}\cos\delta\right]\left[a_{00}^2 + a_{01}^2 \frac{x_2^2}{w^2} + 2a_{00} a_{01}\frac{x_1}{w}\cos\delta + \delta\right]}} \qquad \ldots (5.20)$$

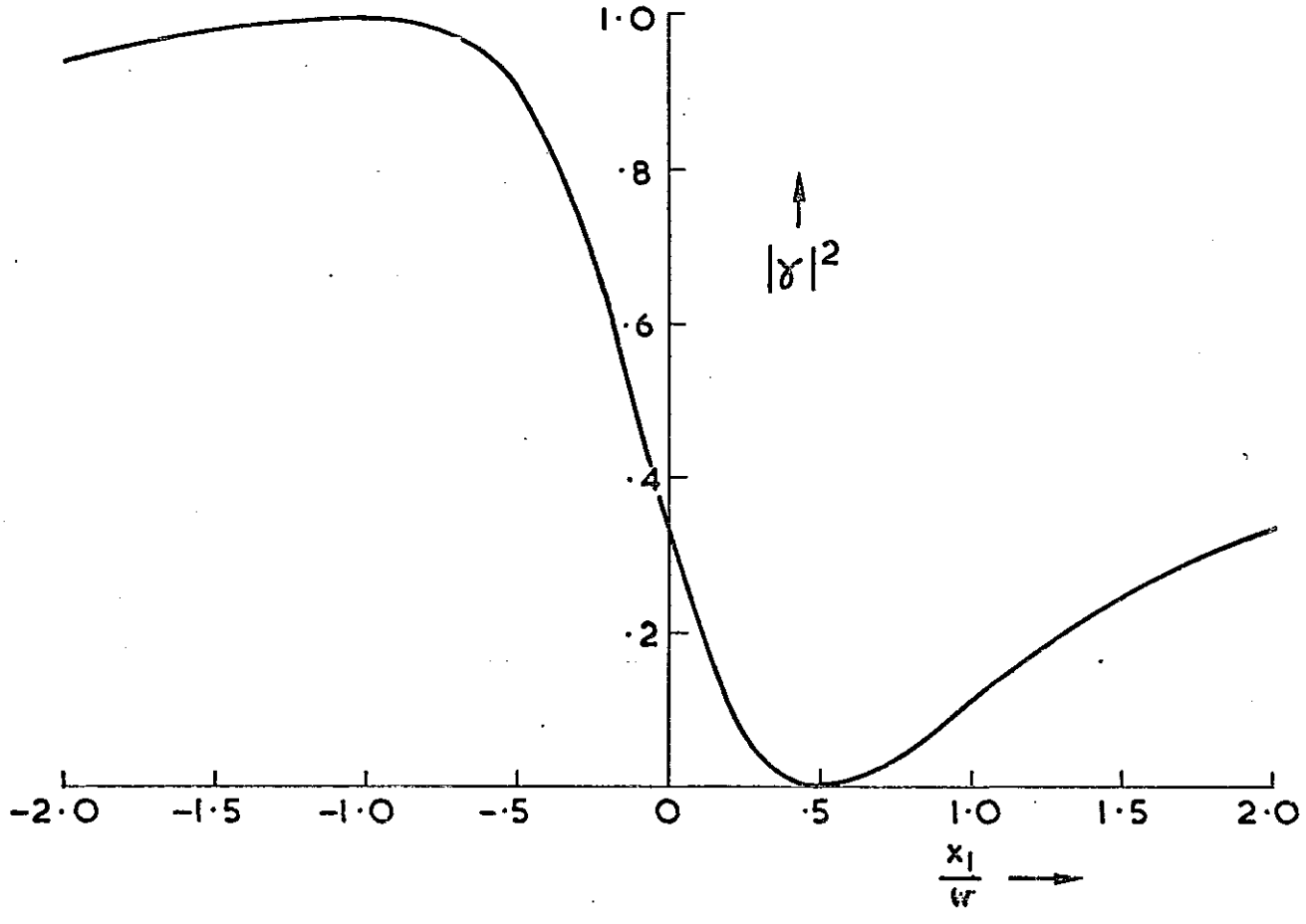
and this reduces to $\gamma_{12} = e^{i\phi}$

where ϕ = phase angle given by:-

$$\tan\phi = \frac{a_{00} a_{01}\left(\frac{x_1}{w} - \frac{x_2}{w}\right)\sin\delta}{a_{00}^2 + a_{01}^2 x_1 x_2/w^2 + a_{00} a_{01}(x_1/w + x_2/w)\cos\delta}$$

This very different situation is quite possible in practice since $\delta\nu$, the frequency separation of the modes, can be very small especially for a plane parallel resonator. Fig. 5.8 plotted $\delta\nu$ as a function of the confocal parameter. In the case of a Q-switched pulse of 20 ns a high

FIGURE 5.14



TRANSVERSE COHERENCE WITH RESPECT TO $^{x_1}/_{w}=1$ OF A LASER OPERATING SIMULTANEOUSLY IN THE TWO MODES TEM_{00} AND TEM_{01} EQUAL ENERGY PER MODE

coherence still exists between the two lowest modes for a confocal parameter range of $0.98 \leq g \leq 1$ (Fresnel number > 3).

5.4.2.2 A laser operating in several (say 5) axial modes of the same transverse mode. Let the frequencies of the 5 modes be $\nu+2\delta\nu$, $\nu+\delta\nu$, ν, $\nu-\delta\nu$ $\nu-2\delta\nu$, where, as shown in EQU 5.13, $\delta\nu = c\delta\bar{\nu} = c/2L$. and let their spectral densities be G_1, G_2 ... G_5.

To calculate the temporal coherence of the output we make use of Equation 5.6. Inserting the above and rearranging we get:-

$$\gamma(\tau) = \frac{\left[G_1 e^{-2\pi i(2\delta\nu)\tau} + G_2 e^{-2\pi i(\delta\nu)\tau} + G_3 + G_4 e^{+2\pi i(\delta\nu)\tau} + G_4 e^{+2\pi i(\delta\nu)\tau}\right] e^{-2\pi i\nu\tau}}{G_1 + G_2 + G_3 + G_4 + G_5} \quad \ldots (5.21)$$

Take as a practical example a spectral profile giving:-

$$G_1 = G_5 = G \quad G_2 = G_4 = 3G \quad G_3 = 4G$$

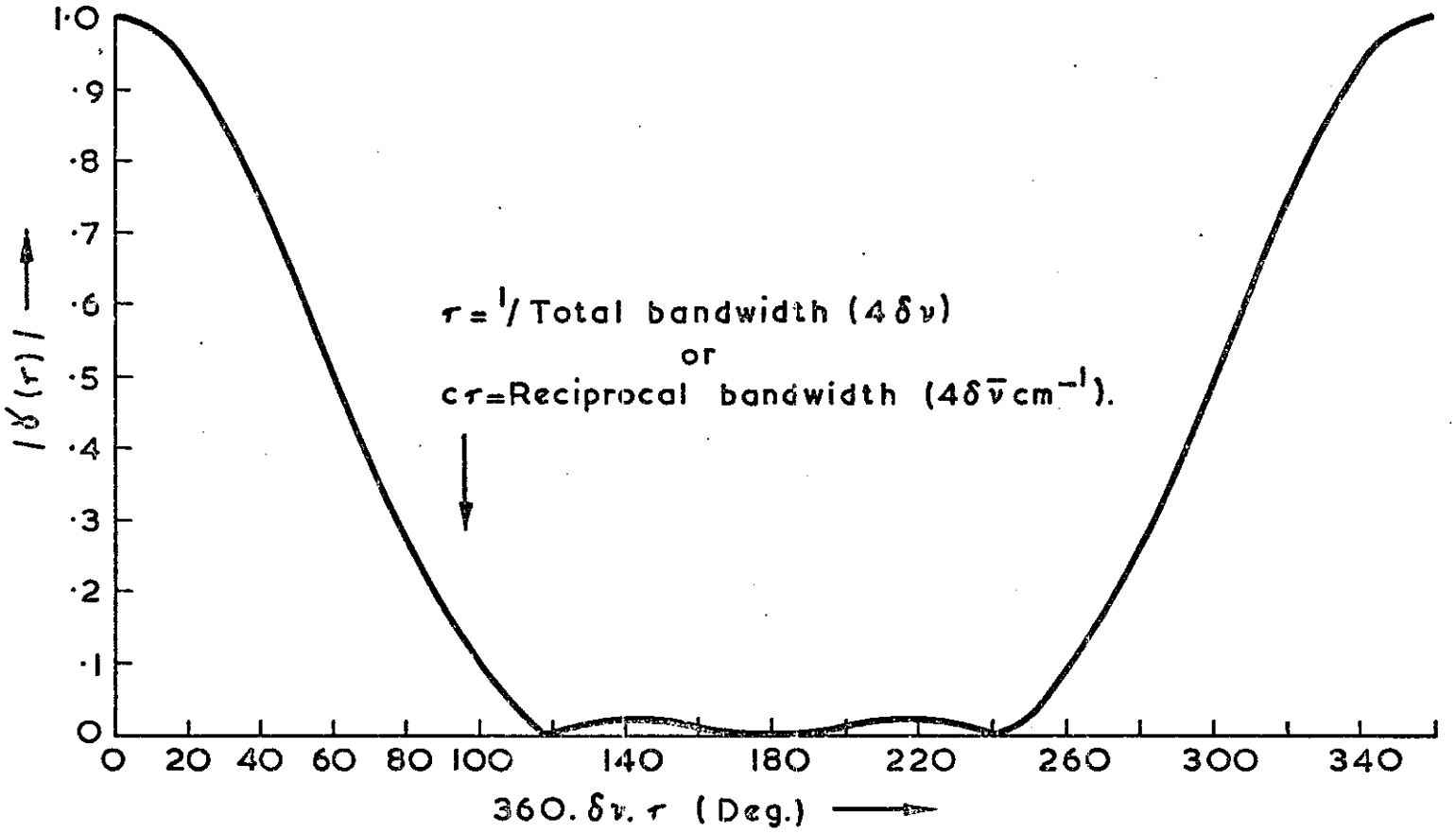
$\therefore$ The coherence reduces to:-

$$\gamma(\tau) = \frac{1}{6}\left[2 + 3\cos 2\pi\delta\nu\tau + \cos 4\pi_1\nu\tau\right] e^{-2\pi i\nu\tau} \quad \ldots (5.22)$$

Fig. 5.15 plots $|\gamma(\tau)|$ vs τ.

5.4.3 The coherence functions just calculated are seen to be very different from the more familiar curves of other sources, examples of which are calculated in Born and Wolf and measured by Michelson and others. The differences are a result of the discrete mode nature of lasers, and, in particular, of the fact that the modes form a finite ordered progression. (The axial modes for example form an arithmetic progression with respect to frequency and their number is often quite small).

FIGURE 5.15



VARIATION OF COHERENCE WITH PATH DIFFERENCE FOR FIVE CONSECUTIVE AXIAL MODES (MODE SEPARATION = $\delta\nu$ Hz)

The following states the important differences between the coherence functions of lasers and other sources:-

Laser coherence functions are usually more complex in that they are not single-valued and monotonic. A low measured value does not indicate the coherence limit, since the coherence may rise significantly under apparently more adverse situations. These coherence functions may also vary rapidly with a change of coordinate, it is evidently important to either record continuously over the range or record the coherence at a large number of coordinate points. The need for a more extensive measurement to obtain adequate coherence information has prompted the investigation of possible methods of measurement which might prove more effective than conventional means. This is discussed later. It is sometimes particularly important to remember that a single figure specifying the coherence length or effective incoherent source size is not sufficient for laser coherence. The only exceptions are a laser operating single mode (transverse and axial) or one operating in a very large number of transverse and axial modes. An equivalent incoherent source may be a valuable concept but it has a non-uniform intensity distribution which must be specified as well as the size.

A further property of the laser temporal coherence function stresses again its difference from other sources. The constant axial mode separation ($= \frac{1}{2L}$ cm^{-1}) results in a periodic coherence function, as exampled in the calculation above, the path difference between consecutive coherence maxima being just 2L cm. This property can be and is often used, in making holograms for example, when it is more convenient to operate at a path difference between reference and signal of an integer multiple of 2L. Coherence of lasers can as shown in paragraph 5.4.2.1 be a function of the pulse duration.

What becomes apparent from the above is that:-

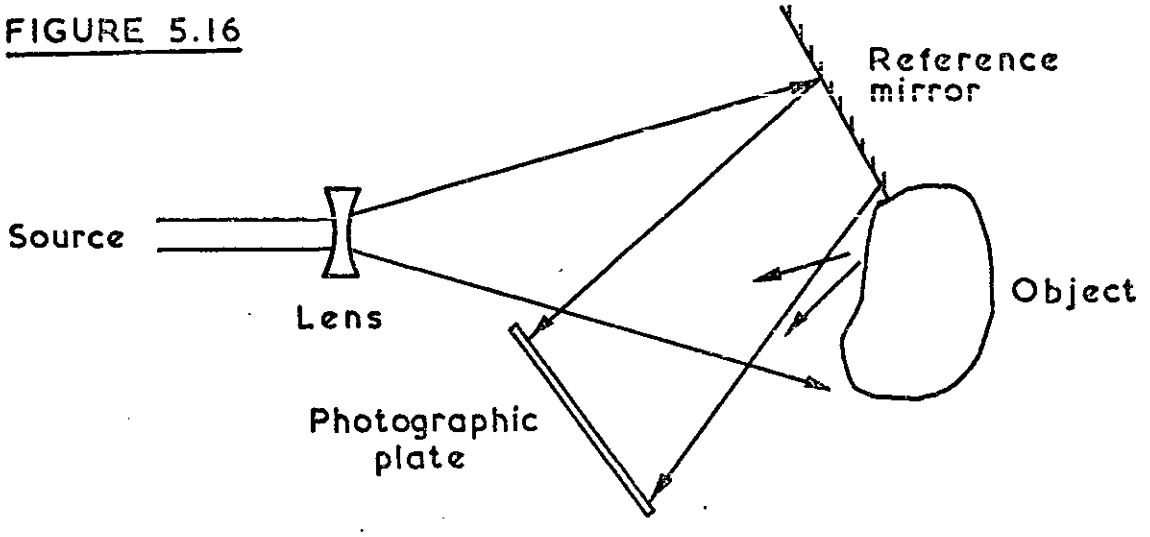
(i) New methods of measuring coherence are desirable.

(ii) A single figure cannot completely specify coherence. Some alternative needs to be found.

(iii) The coherence requirements for any particular application require careful consideration. The shape of the coherence function is important as well as the magnitude of it.

5.4.4 These points will now be illustrated in the context of holography, and it is necessary to explain briefly this recording technique and derive a relationship which tells us how it depends upon the coherence of the light used. Two beams, a 'reference' wave of simple form (usually plane or spherical) and an 'object' wave, are superposed on a recording medium. Fig. 5.16 is a typical arrangement.

FIGURE 5.16



Simple arrangement for recording a hologram

The interference pattern so recorded is called the hologram and contains all the information of the amplitude and phase of the wave coming from the object, (the 'object' wave). This information can be recovered without loss and in its original form, simply by replacing the 'reference' wave on the developed hologram plate. The plate acts as a complex diffraction grating, the first order diffracted image being a replica of the 'object' wave. More description of the process need not be given here since it

is only necessary to establish the relationship of the coherence between the two recording beams to intensity in the image reconstructed by the hologram.

5.4.4.1 The analysis which follows is for thin amplitude holograms and is similar to that used by Biedermann (1970)

Let two plane waves of amplitude $A_1 e^{i\phi_1}$ and $A_2 e^{i\phi_2}$, and with an angular separation θ, form a simple grating hologram. The intensity distribution (I) on the hologram is given by:-

$$I = (I_1+I_2) \times [1 + V \cos (\phi_1 - \phi_2)] = \bar{I}[1 + V \cos (\phi_1 - \phi_2)] \quad \ldots (5.23)$$

where $I_1 = A_1^2$; $I_2 = A_2^2$; V = fringe visibility; $\bar{I}$ = mean intensity.

$$\therefore \text{ Exposure } E = \int Idt = \bar{E}\left[1 + V \cos (\phi_1 - \phi_2)\right] \quad \ldots (5.24)$$

For linear recording; the amplitude transmittance (τ) of the developed hologram should be a linear function of exposure E at the mean exposure level i.e.

$$\tau = \tau(\bar{E}) + \beta(\bar{E}).\Delta E \quad \ldots (5.25)$$

where ΔE is the exposure excursion from $\bar{E}$, and is $E-\bar{E}$, and $\beta(\bar{E}) = {}^{d\tau}/dE$ at the mean exposure level.

Taking into account the modulation transfer function (MTF) which reduces the visibility to an effective visibility = $M(\nu)V$ and substituting for ΔE from Equ. 5.24, the amplitude transmittance becomes:-

$$\tau = \tau(\bar{E}) + \beta(\bar{E}).\bar{E}.V.M(\nu).\cos (\phi_1-\phi_2) \quad \ldots (5.26)$$

where ν = fringe spatial frequency.

If, now, the reconstructing beam is equal to $A_3.e^{i\phi_1}$, the transmitted amplitude is just $A_3 e^{i\phi_1} \times \tau$, and the reconstruction of the object field is

the term of this function having the correct phase term ($e^{i\phi_2}$). Simple calculation yields this term to be:-

$$\tfrac{1}{2}\, A_3 . \beta(\bar{E}) . \bar{E} . V . M(\nu) . e^{i\phi_2}$$

and the reconstructed intensity, $I_r = I_3 \left[\tfrac{1}{2} . \beta(\bar{E}) . \bar{E} . V . M(\nu)\right]^2$

or the efficiency of reconstruction $\eta = \tfrac{1}{4} \left[\beta(E) . \bar{E} . V . M(\nu)\right]^2$ ... (5.27)

now

$$\beta(\bar{E}) . \bar{E} = \frac{d\tau}{d\bar{E}} \bar{E} = \log e . \frac{d\tau}{d(\log E)}$$

let $\dfrac{d\tau}{d \log E}$ (= slope of τ - log E curve at $\bar{E}$) = $\alpha(\bar{E})$

$$\therefore \eta = 0.047 \left[\alpha(\bar{E}) . V . M(\nu)\right]^2 \qquad \ldots (5.28)$$

The efficiency of reconstruction is proportional to (visibility)^2 up to the point at which density variations are such that the assumption of linear recording no longer holds. For present emulsions this point occurs at an effective visibility (V.M(ν)) of about 0.4. Above this value, the hologram begins to diffract appreciable energy into two other terms and the first order term (that of the correct reconstruction) rises progressively more slowly with increase in visibility until it passes through a maximum and begins to fall. The two other terms mentioned are:-

(i) Higher order terms with phase $e^{i2\phi_2}$, $e^{i3\phi_2}$ etc. resulting from non-linearity of the τ-E curve. These reconstructions lie at offset angles $2\phi_2$, $3\phi_2$ etc. and may or may not obstruct the first order reconstruction depending on the value of ϕ_2 and

the size of the object. The efficiency into these higher order images also depends upon the effective visibility, $V \times M(\nu)$.

(ii) Intermodulation noise. This results from having too high an intensity in the signal beam (that arriving from the object) such that the reference beam to signal beam ratio (I_1/I_2) approaches unity. In this case cross terms in the reconstructed field, which have an intensity proportional to $I_2 \times \frac{I_2}{I_1}$, contain appreciable energy in relation to the first order term, which has an intensity proportional to I_2. These cross terms appear as haloes around the various reconstructed orders, including the first order. Hence, the use of the term 'noise'.

The analysis presented is for a 'thin' emulsion having only amplitude variations. The efficiency is increased if the emulsion is thicker and if there are phase variations, but the main conclusion still holds that the reconstruction efficiency increases with increasing visibility (and consequently coherence), the variation being a square law for $V.M(\nu) < 0.4$.

5.4.4.2 Let Maximum efficiency occur at an effective visibility of 0.6. and let $M(\nu) = 0.7$ (Biederman 1969)

$$\text{Now } V = \frac{2\sqrt{E(1)E(2)}}{E(1)+E(2)} |\gamma(1,2)| \qquad \ldots (5.3)$$

$$\therefore V = \frac{2\sqrt{E(1)E(2)}}{E(1)+E(2)} |\gamma(1,2)| = \frac{0.6}{0.7} = 0.86$$

The minimum coherence (γ) for which this is true is for the case of equal intensity beams, and the value of the minimum coherence is then $= 0.86$.

Thus for maximum efficiency of holographic recording it is not essential to have a source of coherence > 0.86. Furthermore if, as is often the case, there are good reasons for wanting a reconstruction in which the intensity distribution is proportional to that of the original object, it is essential to record linearly.

$\therefore$ Maximum $V = \dfrac{0.4}{M(\nu)} = 0.57$, for $M(\nu) = 0.7$, and by the same argument as before, the hologram is as efficient as possible even for a coherence as low as 0.57.

5.4.4.3 Against this low coherence requirement there is a higher energy requirement. The relationship between coherence and total energy is derived as follows:-

For constant holographic efficiency the fringe visibility (V) must remain constant. From Equ. 5.3,

$$V = \frac{2\sqrt{E(1)E(2)}}{E(1)+E(2)} |\gamma(1,2)|$$

$$\therefore \quad \frac{2\sqrt{E(1)E(2)}}{E(1)+E(2)} \gamma = \text{constant} = C \text{ say} \qquad \ldots (5.29)$$

where $E(1)$ = reference beam energy density at plate.

$E(2)$ = object beam energy density at plate.

γ = coherence between these two = $|\gamma(1,2)|$

Let $E(1) = kE(2)$; Energy output from laser = E;

and let $E = p(1)E(1) + p(2)E(2)$, $p(1)$ and $p(2)$ being attenuation factors in the reference and object beams respectively.

$$\therefore \quad E = [kp(1) + p(2)]E(2) \qquad \ldots (5.30)$$

Inserting $kE(2)$ for $E(1)$ in equation 5.29 above gives:-

$$\frac{2\sqrt{k}}{1+k}\,\gamma = C \qquad \ldots (5.31)$$

As well as requiring constant visibility for constant holographic efficiency, it is also necessary to maintain constant energy density on the photographic plate.

$$\therefore \quad E(1) + E(2) = (k+1)E(2) = \text{constant} = D \text{ say} \qquad \ldots (5.32)$$

Eliminating $E(2)$ from Equ. 5.32 and 5.30:-

$$E = \frac{[kp(1) + p(2)]D}{(k+1)} \qquad \ldots (5.33)$$

Eliminate k from Equ. 5.33 and 5.31:-

$$2\gamma\sqrt{(p(2)D-E)(E-p(1)D)} = [p(2)-p(1)]\,CD \qquad \ldots (5.34)$$

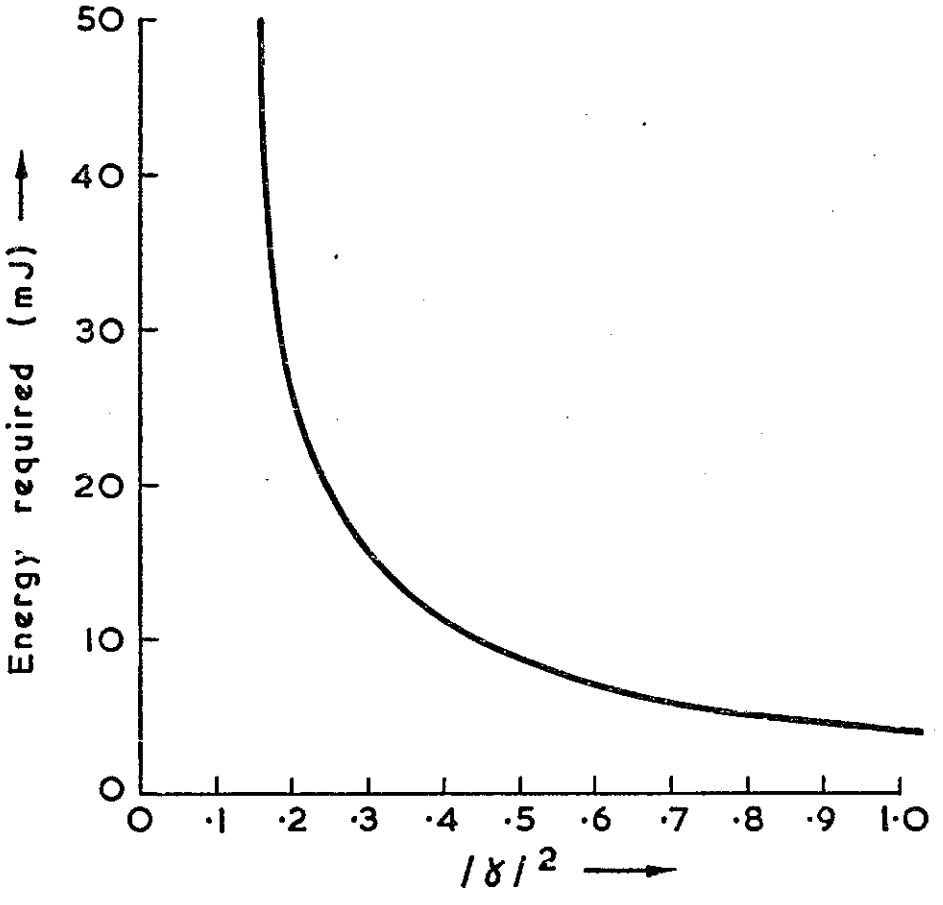
Take a practical example in diffuse reflection holography, in which the attenuation in the object beam is very much greater than that in the reference beam i.e. $p(2) \gg p(1)$.

Let $p(2) = 2$ mJ/mJ/m^2

also let $D = 50$ mJ/m^2 and $C = 0.4$.

Fig. 5.17 plots the dependence of E upon $|\gamma|^2$ for this example.

FIGURE 5.17



VARIATION OF ENERGY REQUIRED FROM LASER FOR HOLOGRAPHY WITH COHERENCE OF THE SOURCE. FRINGE VISIBILITY = 0·4; EXPOSURE = 50 m J/m^2; OBJECT BEAM ATTENUATION = 0·5 mJ/m^2 PER mJ.

One could also plot, for a given laser and a given method of improving its coherence, a curve relating E and γ. This curve arises from the usually adverse affect on the output of an attempt to improve the coherence. The two curves could then be used to decide, for example, how best to operate the laser to result in maximum holographic efficiency. This might well be under neither the maximum nor the minimum coherence configurations. If recording ratios near 1 to 1 are envisaged account must be taken of the adverse effects of intermodulation noise.

5.4.4.4 There are possible pitfalls to recording holographically with a multimode or partially-coherent laser. These pitfalls lie in holographic applications involving double exposure interference techniques. Holography can be used to perform and extend the function of an interferometer by recording a double hologram of the object in the two conditions one wishes to compare. Each exposure reconstructs an image wave. The two reconstructed image waves interfere to give fringes characteristic of the difference between the two conditions of the object. It is important to the assessment of these fringes that there is no possibility of a significant loss of contrast of the fringes or of any other sets of fringes appearing. This possibility exists in a multimode output, if the mode distribution does change from one pulse to the next, and is more likely to occur the greater the number of contributing modes. (i.e. the lower the coherence).

Two criteria of holography have been considered in their determination of a coherence requirement. This requirement is affected more or less by the dependence these criteria have on the exact form of the holographic method, but it can be concluded that a maximum coherence is desirable (but not necessary) within the confines of achieving an adequate holographic efficiency. By referring back to Fig. 5.17, it follows that methods of

improving the coherence must be found which do not lead, as is often the case, to a very large decrease in output from the laser.

5.5 Coherence Measurement

All coherence measurements are aimed at measuring independently the transverse and temporal coherence. This simplifies the measurements and greatly assists the checking of them against other measurements and against theoretical calculation.

5.5.1 Conventional Methods

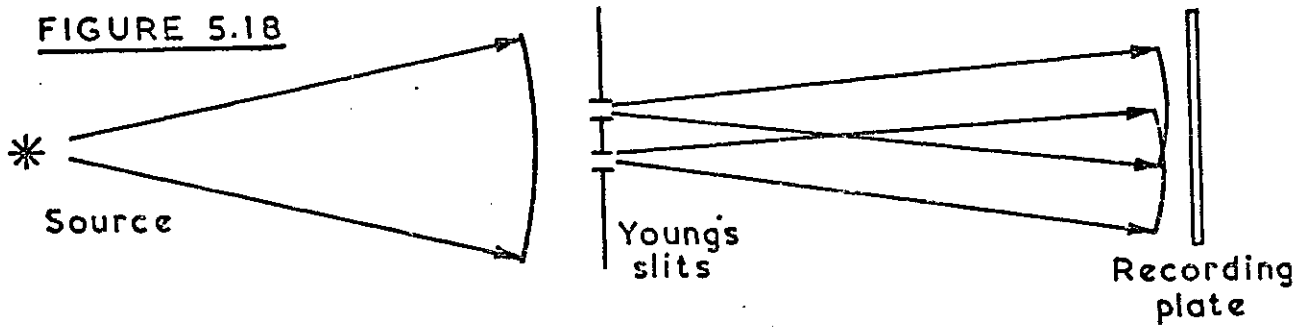
5.5.1.1 Interferometric techniques

Interference fringes are obtained using particular designs of interferometer. The visibility of these fringes is measured either by direct photoelectric detection or by recording on a photographic plate and using a densitometer on the developed image. From Equ. 5.3

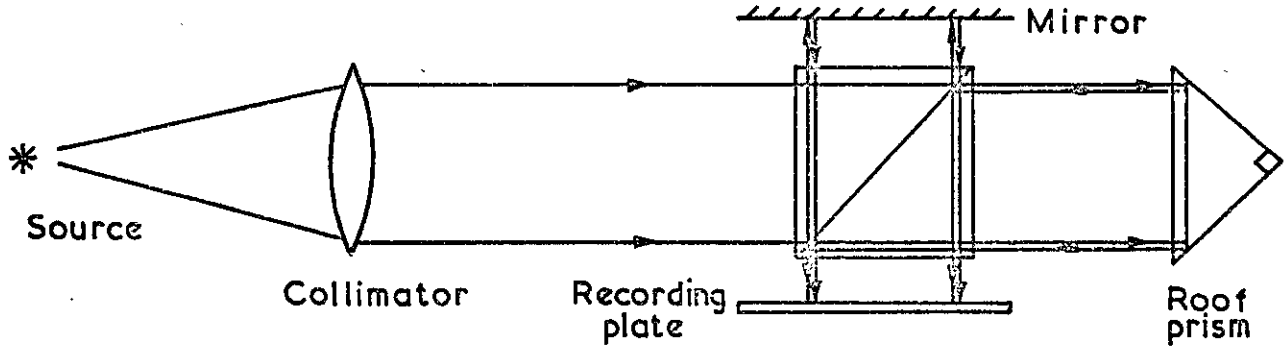
that $V = \dfrac{2\sqrt{E(1)E(2)}}{E(1)+E(2)} |\gamma(1,2)|$, and knowing the energy densities in the two interfering beams, the coherence (γ) can be calculated.

Fig. 5.18 shows three examples of this technique.

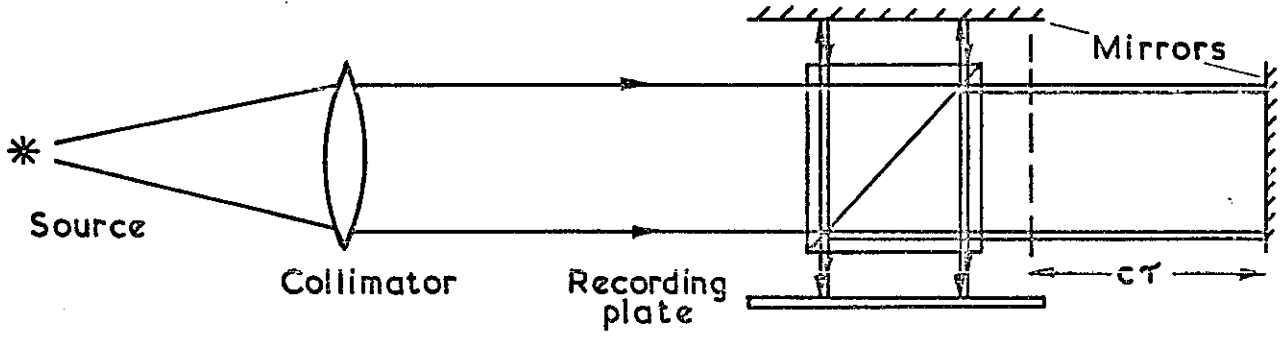
FIGURE 5.18



(a) Measurement of Transverse Coherence by Young's slits method.



(b) Measurement of Transverse Coherence using modified Twyman-Green interferometer



(c) Measurement of Temporal Coherence using Twyman-Green interferometer

The first is a Young's slit experiment which, if the fringes are recorded in the region of zero path difference, measures the transverse coherence between pairs of points in the wave field which lie opposite each other on the two slits.

The second also measures transverse coherence. One flat mirror of a Twyman-Green interferometer is replaced by an optically high quality roof-prism, which serves to reverse one of the wavefronts with respect to the prism roof-edge. Tilt fringes are obtained by adjustment with the two

interferometer arms equalised and these then result from interference between all points in the wave front and all points which lie an equal distance from the line of reversal and on the opposite side of this line.

The third is the classical experiment of Michelson to measure the temporal coherence of a source. Tilt fringes are obtained by adjustment of a Twyman-Green interferometer. The visibility of the fringes so formed is measured as a function of the difference in path between the two arms of the interferometer. Each set of fringes provides a single point on the temporal coherence curve. If however one flat mirror is replaced by a stepped mirror, several points on this curve can be obtained simultaneously.

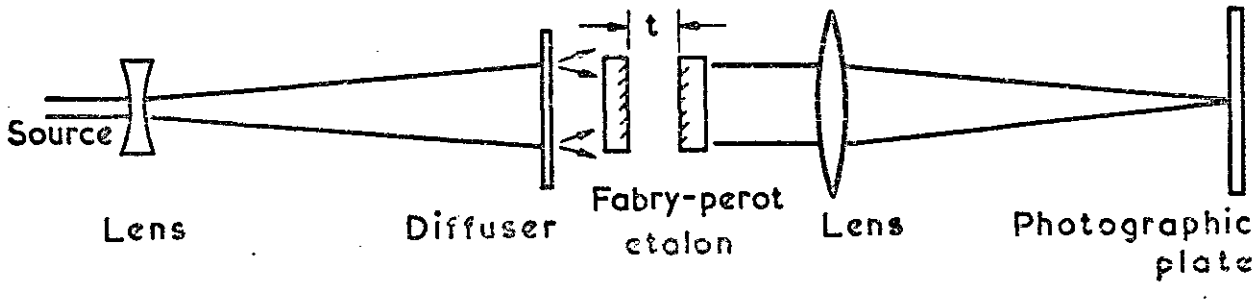
5.5.1.2 Spectroscopic Techniques

As shown by Born and Wolf and reproduced earlier in this chapter, see Equ. 5.6, the temporal coherence curve can be calculated from a curve of spectral profile.

Initial testing can be carried out using a spectrograph but its resolving power is not adequate when trying to measure the coherences achievable with lasers. The Fabry Perot etalon is generally used for the high resolution measurement of laser spectral output curves. The principles of its operation are well established. The technique we have used with lasers is as follows:-

Fig. 5.19 shows a typical arrangement.

FIGURE 5.19



SPECTRAL ANALYSIS USING
A FABRY-PEROT INTERFEROMETER

The laser beam is expanded to the size of the aperture of the etalon and diffused, and the ring pattern at the focus of a long focus lens recorded photographically. The etalon spacing (t) is adjusted such that the instrument has the required resolving power. The limit of resolution ($d\bar{\nu}$) of a Fabry-Perot etalon is given by:-

$$d\bar{\nu} = (\text{order separation/finesse}) \text{ cm}^{-1} \quad \ldots (5.35)$$

$$\text{where order separation } (\Delta\bar{\nu}) = \frac{1}{2t} \text{ cm}^{-1} \quad \ldots (5.36)$$

$$\text{finesse } (F) = \frac{\pi\sqrt{R}}{1-R} \quad \ldots (5.37)$$

R being the single surface reflectivity.

Thus, in order to calculate the correct spacing, it is necessary to know the finesse. This has been measured by observing visually the interference rings obtained from a He-Ne laser operating in several axial modes, and increasing the etalon spacing (t) until the modes are just resolved. Since the mode separation is $\frac{1}{2L}$ where L = He-Ne cavity optical length, the finesse is calculated from:-

$$\text{Finesse} = \frac{1}{2t} \div \frac{1}{2L} = \frac{L}{t} \quad \ldots (5.38)$$

Having adjusted the etalon spacing it is necessary to measure it and this can be done again using a He-Ne gas laser. A stationary ring pattern is recorded photographically, and the pattern measured so as to plot a graph of the square of the ring diameter (D) vs. the order number (p) of the ring, counting from the centre. The angular radii (θ) of the bright rings are given by $2t \cos\theta = n\lambda$, where n = integer, and this is very well approximated, for the small angles used, by $2t(1-\theta^2/2) = n\lambda$; now the ring

diameter $D = 2f \tan\theta (\approx 2f\theta$ for small angles) where f = focal length of the lens at wavelength λ.

$$\therefore \quad 2t(1 - D^2/8f^2) = n\lambda \qquad \ldots (5.39)$$

Let the true order number n of a ring be $n_o - p$ where n_o = order number of the ring from which measurements begin.

If this ring has diameter D_o, then $2t(1 - D_o^2/8f^2) = n_o\lambda$.

Subtracting these two equations gives:-

$$D^2 - D_o^2 = p \cdot \frac{4f^2\lambda}{t} \qquad \ldots (5.40)$$

and the slope of the curve of D^2 vs $p = 4f^2\lambda/t$

Having measured the focal length (f) and knowing that $\lambda = 632.8$ nm for the He-Ne laser, enables calculation of the etalon spacing t.

Remembering to refocus the lens for the different wavelength of the pulsed laser, its ring pattern is recorded. Fig. 5.20 shows a typical example.

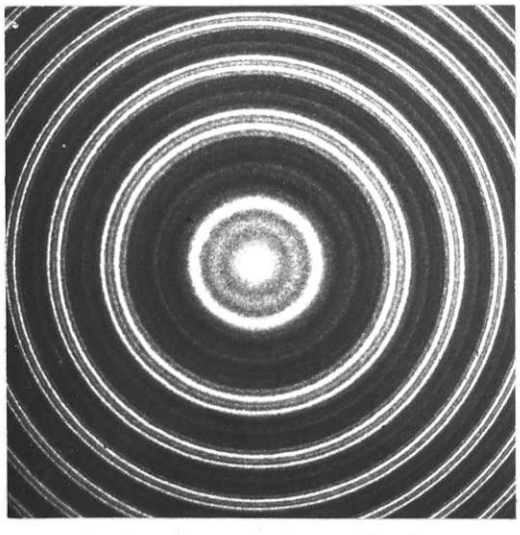


FIGURE 5.20

Typical Fabry-Perot interferogram of a multimode laser.

The parameters of interest are (i) the number of each component (ii) the spectral width of each component (iii) the component separations (iv) the absolute wavelength of one of the components. The separation in wavenumbers $\delta\bar{\nu}$ of two closely-spaced components is given by the standard equation:-

$$\delta\bar{\nu} = \frac{D_{1b}^2 - D_{1a}^2}{D_{2a}^2 - D_{1a}^2} \cdot \frac{1}{2t} \qquad \ldots (5.41)$$

where D_{1b} and D_{1a} are the diameters of the two components in one ring order, and D_{2a} and D_{1a} are the diameters of one of the components in the same and next ring order. This equation follows from Equ. 5.39. If, as can easily occur in practice, the nearest rings of the two components do not belong to the same ring order, then Equ. 5.41 becomes:-

$$\delta\bar{\nu} = \frac{bD_1^2 - aD_1^2}{aD_2^2 - aD_1^2} \frac{1}{2t} + q. \frac{1}{2t} \qquad \ldots (5.42)$$

where q = integer.

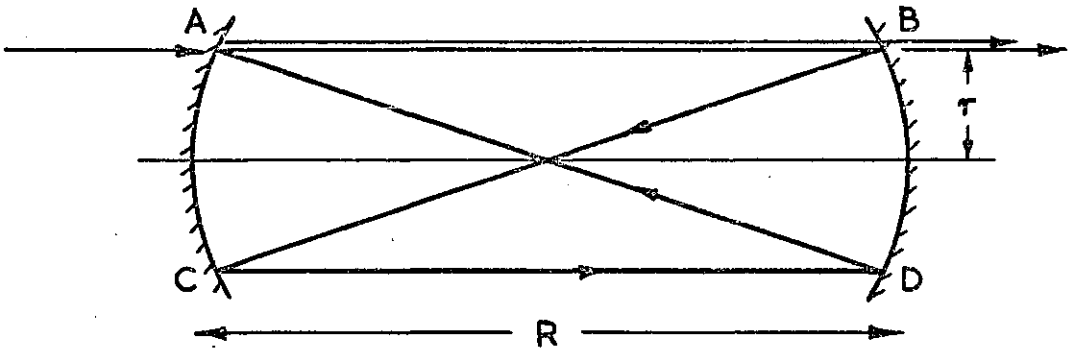
and it may be necessary to carry out the experiment for another etalon spacing in order to remove the ambiguity.

The same equation is used to calculate the widths of each component and any absolute wavelength change from shot to shot of the laser. One merely replaces D_{1b} and D_{1a} by the appropriate diameters. Absolute wavelength change measurements cannot be relied upon unless the etalon is continuously monitored for drifts in the spacing (t).

Very high resolution work is difficult. From Equ. 5.35 and Equ. 5.36 it requires high finesse and high etalon spacing. High finesse is limited by (i) the limited quality and reflectivity of the reflecting surfaces, (ii) their departure from flatness and parallelity and by (iii) the use of the instrument at angular radii greater than zero. This limit might typically be 50 for a high quality unit. Large etalon spacing adversely affects the finesse by increasing the degrading effects of (ii) and (iii) above, and it also results in a very small diameter for the interference rings.

A Fabry-Perot with all round better performance was originally proposed by Connes (1956) and recently analysed for pulsed laser work by Bradley et al (1968) and by Hercher (1968). This is the spherical Fabry-Perot (Fig. 5.21).

FIGURE 5.21



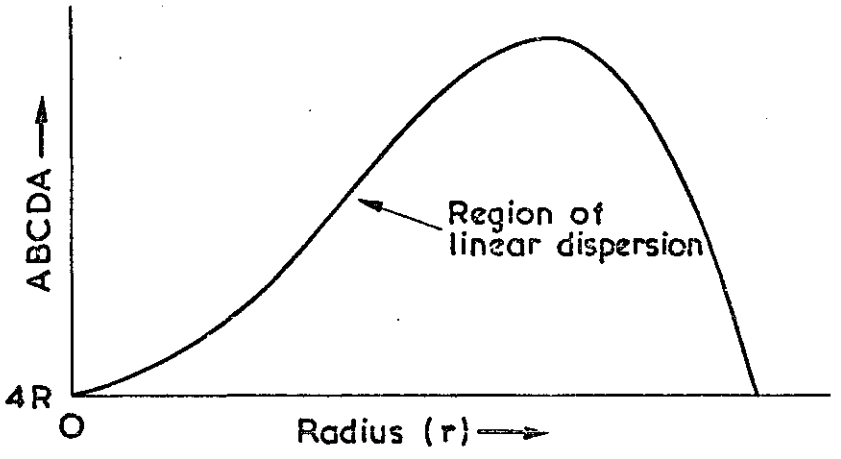
SPHERICAL FABRY — PEROT ETALON

If the spherical mirrors were spaced apart by their radius of curvature (R) as shown, the emitted rays corresponding to an initial distance (r) from the axis would have path differences equal to ABCDA. Now, ABCDA = $4R - \frac{r^4}{R^3}$ + higher order terms (negligible), and bright rings occur when $4R - \frac{r^4}{R^3} = n\lambda$. This fourth power dependence (due to spherical aberration) between ring radius and ring number is inconvenient and makes quantitative measurement difficult. By increasing the mirror spacing by a small amount, say Δ, a region of linear dispersion can be obtained. ABCDA now becomes $4(R+\Delta) + k'r^2 - kr^4$ and the bright rings occur at

$$4(R+\Delta) + k'r^2 - \frac{r^4}{R^3} = n\lambda. \text{ where } k' = -4\Delta/R^2 \qquad \ldots (5.43)$$

Fig. 5.22 plots ABCDA as a function of radius in a typical case with Δ small and negative, showing the region of approximate linear dispersion.

FIGURE 5.22



Since this region is defined by dn/dr = constant, differentiating Equ. 5.53 enables calculation of the correct defocusing quantity Δ. Other advantages of the defocussed spherical Fabry-Perot (abbreviated to DSFP) are:-

a) All rings are produced by rays parallel to the axis, thus eliminating the normal reduction in finesse due to walk-off occurring at finite angles.

b) Similar errors in the quality and alignment of the mirrors result in very much smaller losses of finesse.

c) It is equivalent to a normal Fabry-Perot of twice the length, since the path difference between successive reflections is 4 × mirror separation as opposed to 2 × this separation for the Fabry-Perot. Higher resolution can consequently be achieved.

d) The balancing of the defocus term and the spherical aberration term along with the choice of the radius of the region of linear dispersion enable a higher dispersion to be achieved for the same mirror separation.

With the DSFP finesses of ~ 4 × that of a normal Fabry-Perot of similar design have been achieved (Bradley 1968), Hercher 1968).

5.5.1.3 Let us consider the information content of the coherence measurement techniques so far discussed, and compare that with the total information necessary to completely describe a particular radiation field. This latter is the coherence between one point in the three dimensional field and any other point in the field. If there are N independent positions along each coordinate axis in the field, then each point can be paired with N^3 other points and this number of pairs exist for every point. Thus the total number of pairs or necessary bits of coherence information is $(N^3 \times N^3)/2 = N^6/2$, the factor 2 arising because each pair has been counted twice. As explained earlier however, the coherence function can generally be regarded as separable into the product of the transverse and temporal coherence. The transverse coherence is that across the area of the wave front and consequently requires $(N^2 \times N^2)/2 = N^4/2$ bits of coherence information for its complete specification. The temporal coherence is confined to that in the third dimension, the direction of propagation, and thus requires only $(N \times N)/2 = N^2/2$ bits of coherence information. Furthermore there is still a redundancy of information since the temporal coherence depends only upon the difference between the coordinates of the two points. (This is $c \times \tau$, where c = velocity of light, and τ = time difference between the two points). This reduces the number of bits of information required for the temporal coherence to N.

The Young's slit technique yields N bits of information per recording, while that using the reversing interferometer gives N^2 bits. A great many recordings are thus necessary for a complete measurement of the transverse coherence function.

The Michelson method for temporal coherence allows the coherence corresponding to only a single value of path difference to be measured. N such measurements are required. The alternative method of spectroscopy

for temporal coherence measurement does give all the information in one or two recordings, but it becomes difficult, because of the extreme resolution required, to obtain detailed information of coherence corresponding to path differences of 100 cm or more.

For conventional incoherent light sources the coherence functions, being simple in form, can be determined with very much less information than the maximum requirements above. One recording, using a method already noted, can be sufficient, but even if it is not the source is sufficiently stable to be able to rely on measurements made at different times.

The pulsed laser not only has a more complex coherence function but the output may not be the same from shot to shot. The need arises then for a method of measuring coherence which can record as much as possible if not all of the necessary information from a single pulse. This need is satisfied by the use of holography.

5.5.2 Holographic Methods

The idea of using holography for measuring coherence arises naturally from the fact that recording holograms is one of the major applications of lasers for which coherence is required. What better, to test a laser for its ability to record a hologram, than to make a hologram and observe how effective the laser is at doing so? Other disadvantages of the conventional interferometric methods are (a) that the measurement itself is inconvenient, since an accurate measurement of visibility requires several readings on the recorded fringes, and (b) that for this measurement to be possible the fringes must have a reasonable spacing and this measurement is then an average over a considerable area - the information content is again limited. These problems do not exist with the holographic method. In the first place the

observation is the intensity of reconstruction from the hologram and this intensity is a direct measure of the coherence; and in the second place the fringes which form the hologram can have spacings as low as $\lambda/2$ and if even 100 fringes are required to give an intensity which is an accurate measure of the coherence, the area required for this fringe spacing is still only 0.03 mm across. Further, a hologram is recorded whenever two beams, with some coherence between them, are incident upon a suitable recording medium. The lack of criticality on the angle between the beams - the only requirement being that the resolution limit of the recording medium should not be exceeded - and on the general arrangement is in sharp contrast to the problems of setting up an interferometer to obtain a suitable recording.

Several authors (Lurie 1968, Stetson and Powell 1966, Staselko et al 1969, McClung et al 1970, Siebert 1971) have performed experiments showing some of the possibilities of using holography as a coherence tester and have shown that the method works well in cases where the coherence function is a relatively simple one. No-one appears to have used the method to obtain quantitative measurements of the coherence function or mode structure of a laser, and the experimental arrangements used have not fully exploited the advantages of holographic recording.

5.5.2.1 The Holographic Method

We have already, in attempting to arrive at some criteria for coherence requirements, discussed how the intensity of reconstruction from a hologram depends upon the coherence of the recording beam. It will be useful to state the main points once again.

The hologram is a two-beam interference recording in which the two beams are, in general, derived from different points, say P_1 and P_2, in a wave field. Being the recording of an interference pattern, the hologram is

dependent upon the coherence, designated $\gamma(1,2)$, between P_1 and P_2. Mathematically, $\gamma(1, 2)$ is defined as the time averaged correlation between the disturbances at P_1 and P_2, where the averaging time is either a time long compared to $^1/c\Delta\bar{\nu}$, where $\Delta\bar{\nu}$ = spectral width in wavenumbers, or the pulse duration, whichever is the shorter. It is important to remember that, with Q-switched lasers, the pulse duration can be comparable to $^1/c\Delta\bar{\nu}$, and in these cases the coherence is dependent upon the pulse duration as well as the number of oscillating modes. Even in cases where the pulse duration is very much greater than $^1/c\Delta\bar{\nu}$, it may still be related to the coherence, since all modes present during the pulse may not be present for its entire duration - a part of the pulse may have fewer modes, and be more coherent, than the pulse complete.

The visibility of the interference pattern forming a hologram is given by:-

$$V = \frac{2\sqrt{E_1 E_2}}{E_1 + E_2} |\gamma(1, 2)| \qquad \ldots (5.3)$$

where E_1 and E_2 are the energy densities of the two beams at the plate and $|\gamma(1,2)|$ is the modulus of the coherence function.

The intensity of reconstruction I_r from a hologram is a function of the fringe visibility V, the mean energy density $\bar{E}$ and the spatial frequency ω, of the interference pattern, i.e.

$$I_r = \text{fn}\,(V\,\bar{E}\,\omega),$$

the function being dependent upon the emulsion and on the processing procedure. For visibilities less than 0.25, the dependence of the reconstructed intensity on V becomes (Equation 5.27), to a good approximation, a direct square law.

Thus $$I_r = V^2 \times \text{fn}\,(\bar{E}, \omega) \qquad \ldots (5.44)$$

We have chosen to work in this square law regime since, although the efficiency is limited, it is not then necessary to calibrate over the entire range of visibility and the noise in the reconstruction is minimized. One of the main difficulties in obtaining quantitative results is due to variations in intensity across the output beam of the source under test, and these variations are intentionally left undisturbed in order not to affect the coherence properties. Automasking techniques could be used to even up the intensity variations without upsetting the coherence properties and might result in a better measurement accuracy than the two ways we have used to correct for any intensity fluctuations. These two methods are as follows:-

(i) To measure them directly or by densitometry on the hologram. When doing this, it may be necessary to pre-expose the hologram so that the mean energy density (I) is nearly uniform (and easily controlled) and the intensity variations cause only changes in the visibility of the hologram interference fringes. This visibility is now given by:-

$$V = \frac{2\sqrt{E_1 E_2}}{E_1 + E_2 + E_o} |\gamma(1,2)| \qquad \ldots (5.45)$$

where E_o = pre-exposure level of energy density

and since the reconstructed intensity is now proportional to V^2 only, $\bar{E}$ being uniform, the correction can be carried out without recourse to the properties of the emulsion.

(ii) To obtain from the same or a similar hologram another reconstruction for which the source is effectively completely coherent.

The intensity in this other reconstruction then can be used as a normalising factor. It will be seen below how this can be done in practice.

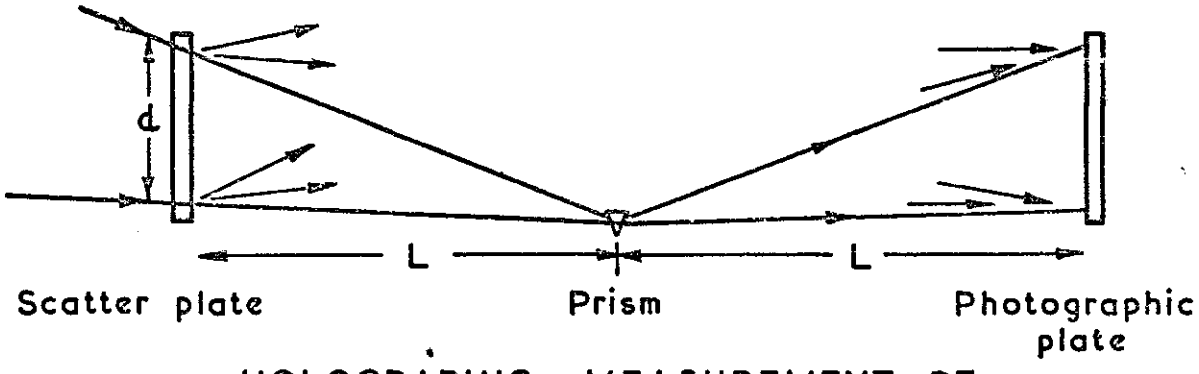
5.5.2.2 Experimental Methods

As stated previously, it is desirable to design experiments for measuring coherence which measure the transverse and temporal coherence separately. This is a major simplification, and we have tried to choose arrangements which further simplify the measurement process.

a) Transverse Coherence.

Fig. 5.23 shows the chosen method of measuring transverse coherence.

FIGURE 5.23



HOLOGRAPHIC MEASUREMENT OF TRANSVERSE COHERENCE

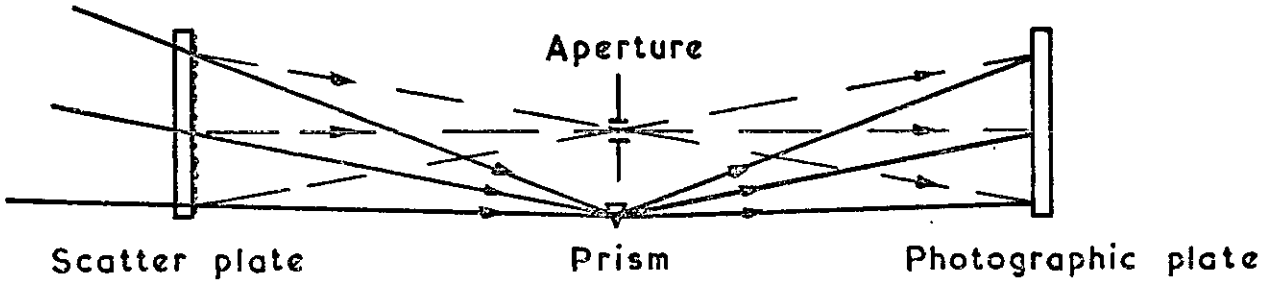
This method combines the ability to record all the transverse coherence as well as maintaining the maximum of simplicity. A scatter plate acts as beam-splitter by amplitude division, a fraction of the incident light passing through undisturbed and the rest scattered uniformly over a suitable angle. The hologram is recorded in a plane where each point of the plate receives, as reference, one ray of the undisturbed beam and, as signal, scattered light from the entire wave-front. Reconstructing through a small area at that point gives a reconstructed picture of the wavefront with an intensity distribution dependent upon the coherence between all points on the wavefront and the point of origin of the reference ray arriving at that reconstructing point. The prism ensures an off-axis reference

beam so that the two first order reconstructions do not overlap. As can be seen in Fig. 5.23 path differences do occur between reference and signal beam so that there is need for some temporal coherence. The maximum path difference between reference and signal beams is approximately d^2/L, while the maximum variation of signal beam path for any hologram point is approximately $d^2/2L$. By suitable adjustment of d and L, the maximum path difference can be reduced to a value very much less than $1/\Delta\bar{\nu}$ cm (where $\Delta\bar{\nu}$ = spectral width of source in wavenumbers), and then the temporal coherence is effectively unity for all possible measurements. In our own case, d = 2 cms and L = 50 cms.

∴ Maximum path difference requirement = $d^2/2L$ = 0.04 cm and the system can be used on all sources with spectral widths $<< 25\ cm^{-1}$.

If intensity variations exist across the beam, and a pre exposure has been given, the second of the methods previously suggested can be employed. This is shown by Fig. 5.24.

FIGURE 5.24



RECORDING OF TRANSVERSE COHERENCE HOLOGRAM SHOWING THAT ALL SIGNAL RAYS WHICH REQUIRE NO COHERENCE PASS THROUGH A SMALL APERTURE

All rays from the scatter plate which interfere, on the hologram plate, with reference rays originating from the same point on the scatter plate are shown. It can be seen that they intersect at the same point, this point being in the plane of the reference beam focus. A small aperture placed at this point (as shown in Fig. 5.24) during reconstruction picks out only those reconstructed rays for which we know the coherence to be unity. The

intensity distribution across the reconstruction is now independent of coherence and varies only due to intensity variations in the original recording wavefront.

To measure the coherence between points P_1 and P_2 of the wave field incident on the scatter plate, a reconstruction efficiency η is measured as described. Now $\eta \propto V^2$, where V is the fringe visibility in the hologram, and from Equ. 5.45:-

$$V = \frac{2\sqrt{E_1 E_2}}{E_1 + E_2 + E_0} \; |\gamma(1,2)|$$

Also measured are the efficiencies η_1 and η_2 at P_1 and P_2 in the apertured reconstruction, corresponding to fringe visibilities V_1 and V_2 in the hologram

Now $$V_1 = \frac{2\sqrt{E_1 E_1}}{E_1 + E_1 + E_0} = \frac{2E_1}{2E_1 + E_0} \quad \text{and} \quad V_2 = \frac{2E_2}{2E_2 + E}$$

and if we neglect terms such as $E_1^{\,2}$ in comparison with E_0^2, Equ. 5.45 becomes

$$V^2 = V_1 V_2 \; |\gamma(1,2)|^2$$

Since reconstructed efficiency is proportional to the square of the visibility, and the constant of proportionality is the same for V, V_1 and V_2, this equation can be written:-

$$\eta = \sqrt{\eta_1 \, \eta_2} \; |\gamma(1,2)|^2$$

and the coherence can be calculated.

If no pre exposure is given, the first of the correction methods is used, where the intensity variations across the beam are measured. The

correction is possible, despite the variation of the mean exposure level (E) over the hologram, since each set of coherence measurements across the reconstruction use one point of the hologram only.

In this case: $$V = \frac{\sqrt{E_1 E_2}}{E_1 + E_2} |\gamma(1,2)|$$

where E_1 is constant and E_2 varies and both are known at all points in the reconstruction.

Now reconstruction efficiency $\eta \propto V^2$

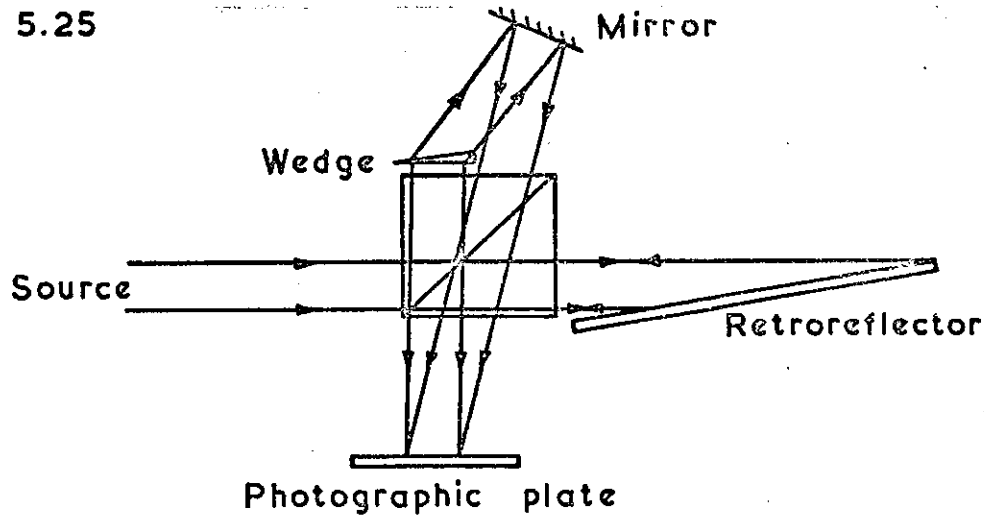
$$\therefore \eta = \text{const.} \frac{E_1 E_2}{(E_1 + E_2)^2} |\gamma(1,2)|^2$$

Making use of the fact that one point in the reconstruction has a coherence of unity ($P_1 \equiv P_2$) we can eliminate the constant and the coherence is determined.

b) Temporal Coherence

For the measurement of temporal coherence, the method which suggests itself at once is that of recording by holography an object which has depth (McClung et al 1970; Stetson and Powell 1966). Fig. 5.25 shows an adaptation of this method.

FIGURE 5.25



RECORDING OF TEMPORAL COHERENCE HOLOGRAM USING MODIFIED TWYMAN-GREEN INTERFEROMETER

A Twyman-Green interferometer is the basis, but one of the mirrors is replaced by a plane retroreflecting surface placed at an angle to the incident wavefront ('object with depth'). Also, the other mirror is slightly rotated to give a small but non-zero angle (θ) between the two interfering beams at the hologram plate, and the geometry is arranged such that, for a perfect retroreflector, these two interfering beams are exactly superposed. The consequence of these adjustments are:-

(i) The fringe spatial frequency comprising the hologram is sufficiently large that a meaningful reading of reconstructed intensity can be made from a small area of the hologram. The larger the spatial frequency the greater the number density of points on the measured coherence curve.

(ii) The fringe spatial frequency is sufficiently small to enable emulsions such as Polaroid 55 P/N to be used.

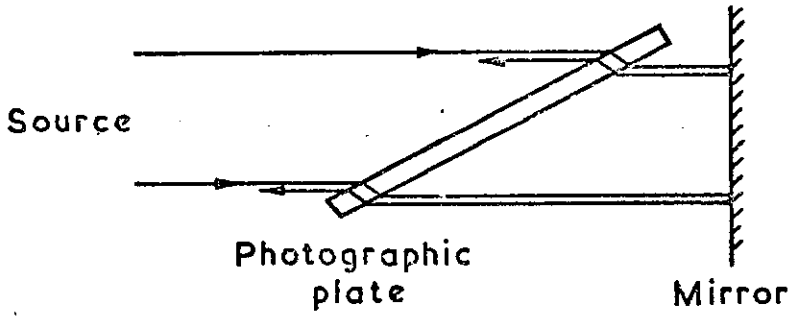
(iii) No transverse coherence is required.

Two retro-reflectors have been used. A blazed grating, which is a very efficient retroreflector, and a plane surface coated with a retro-reflecting material such as Scotchlite. The latter is generally very much

less efficient since only a small fraction of the 'retro-reflection' usually lies within a small enough angle to be spatially coherent with the reference beam. The grating method is not entirely satisfactory in that for the measurement of temporal coherence over large path differences the necessarily large gratings with high angles of blaze are expensive.

An alternative and simpler method has been investigated and shown to be very suitable. It is similar to methods for the optical production of gratings (Burch and Palmer 1961) which, for a grating with N elements, requires a high temporal coherence of the source over a range of path difference of $N\lambda$. For the purpose of measuring temporal coherence up to a path difference of say p, a grating of $N = p/\lambda$ elements is made and its diffraction efficiency is measured as a function of position on the grating. A grating is, of course, just a simple hologram with only one spatial frequency, and 'the diffraction efficiency of the grating' is equivalent to 'the reconstruction efficiency of the hologram'. Since the number of grating elements (N) is equal to p/λ, coherence measurements over large path differences (p) require gratings of large size and small element. Fig. 5.26 shows the simplest possible method.

FIGURE 5.26

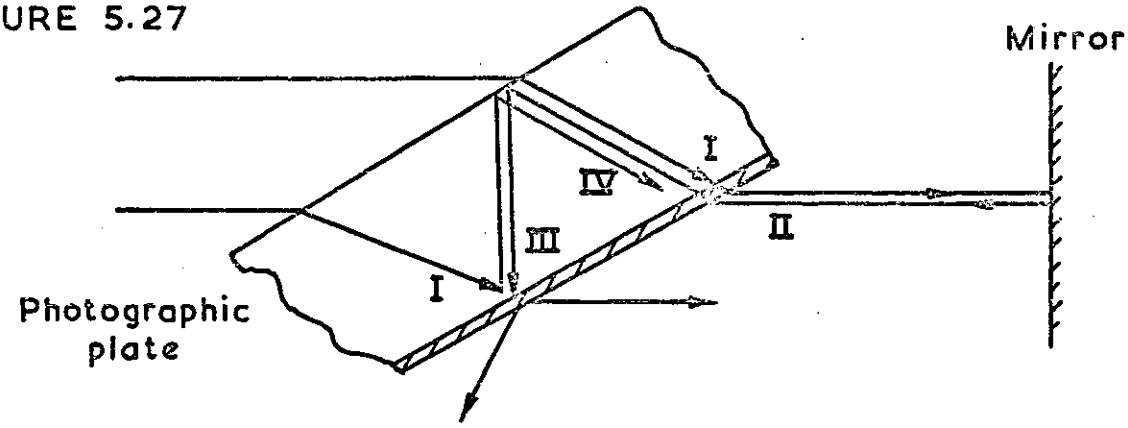


SIMPLE METHOD FOR RECORDING A TEMPORAL COHERENCE HOLOGRAM

Beams in opposite directions interfere in the emulsion to form a 180° Lipmann hologram (or grating). The fringe spacing is $\lambda/2$ necessitating the use of very high resolution emulsions such as Eastman Kodak 649F,

Agfa-Gaevert 10E or photo-resists. Unless the plate is orientated at the Brewster angle to the incident polarization, surface inter-reflections are present and these were at first thought to be an unwanted complication. It was realized however that they might be useful. Their effect, as illustrated in Fig. 5.27, is to form other holograms.

FIGURE 5.27



INTERREFLECTIONS IN PHOTOGRAPHIC PLATE DURING RECORDING OF A TEMPORAL COHERENCE HOLOGRAM

Beams I and III form a hologram which reconstructs more efficiently and in a more convenient direction than that of I and II and this hologram also contains the same temporal coherence information. Beams I and IV form a hologram which reconstructs with an efficiency independent of the temporal coherence, since the path difference between them is constant. This reconstruction is just that required for eliminating the effects of intensity variations.

5.5.2.3 Experimental Measurements

a) Transverse coherence.

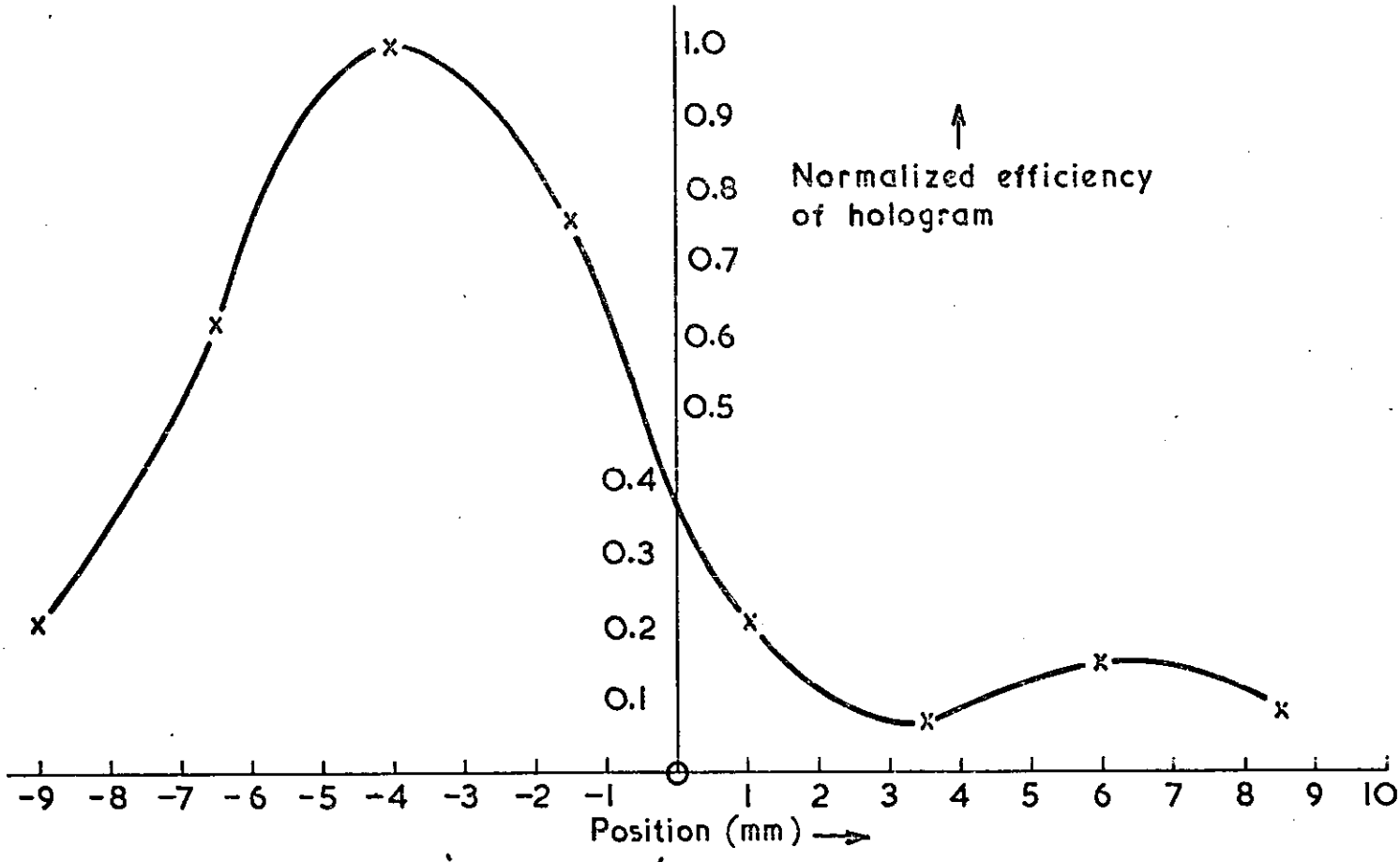
A quantitative test on the method was made using a gas laser operating simultaneously in the TEM_{00} and TEM_{01} modes (Stetson and Powell 1966). Earlier in this chapter the coherence function of such a laser was calculated and Equation 5.19 gives the result for the coherence between a fixed point ($x = x_0$, $y = 0$) and a variable point (x) along the line $y = 0$:-

$$\gamma = \frac{a_{00}^2 + \frac{a_{01}^2 x_0}{w^2}\, x}{\sqrt{a_{00}^2 + \frac{a_{01}^2 x_0^2}{w^2}}\ \sqrt{a_{00}^2 + \frac{a_{01}^2 x^2}{w^2}}}$$

where a_{00} and a_{01} are the amplitudes of the two modes and w their radius. This curve is plotted in Fig. 5.14 for typical parameters. A transverse coherence hologram was recorded by the method of Fig. 5.23. A probe reconstructing beam of diam. = 1.0 mm was introduced onto the hologram at the point $x = x_0$, $y = 0$. A small aperture (1.0 mm) was tracked along the x axis in the plane of the reconstruction and the intensity transmitted by this aperture was recorded using a suitable photodetector (Vickers M030500). Fig. 5.28 plots these measurements, which are still affected by the intensity distribution across the recording wavefront. As indicated before, it is possible to eliminate this effect by using all the hologram to reconstruct and by placing a small aperture in the plane of the reference focus to eliminate all components carrying coherence information. This was done and the reconstructed intensity distribution along the x-axis measured. The noise level was subtracted from this curve and from Fig. 5.28 and the ratio between the two resulting distributions is shown in Fig. 5.29. Fig. 5.29 shows a good agreement between experiment and theory, particularly when the reconstructed intensity is well above the noise level.

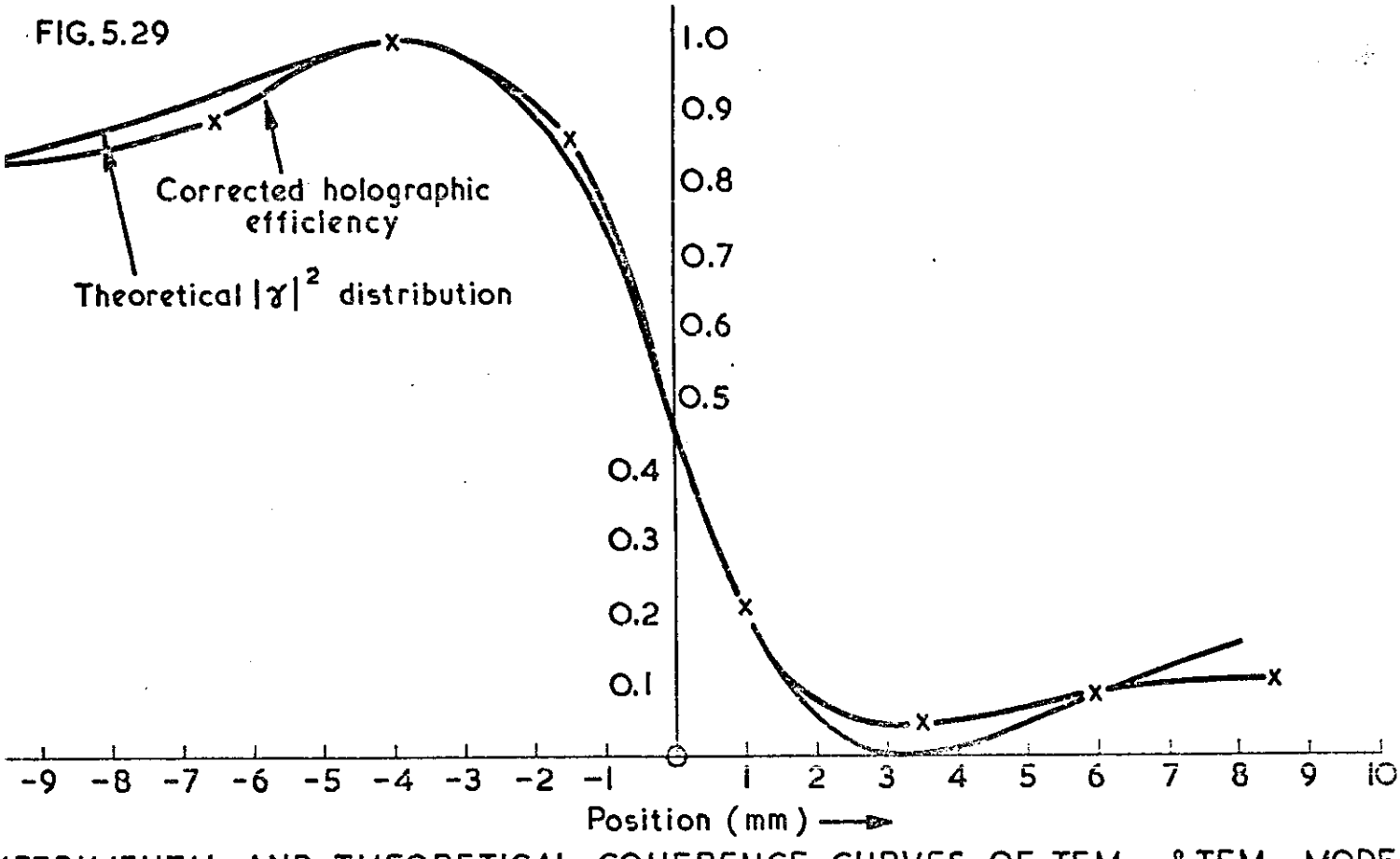
Using the same method, the transverse coherence of several pulsed lasers in addition to the one under investigation have been measured and examples of two of these are given here. The first is a laser similar in every way to our Nd:glass system except that the Nd:glass rod was replaced by one of ruby. Holographic recording using the 1.06 μ output of Neodymium lasers has not been achieved with present recording media. The ruby system

FIG. 5.28



EASURED EFFICIENCY OF 'COHERENCE' HOLOGRAM OF TEM_{00} & TEM_{01} MODE GAS LASER

FIG. 5.29

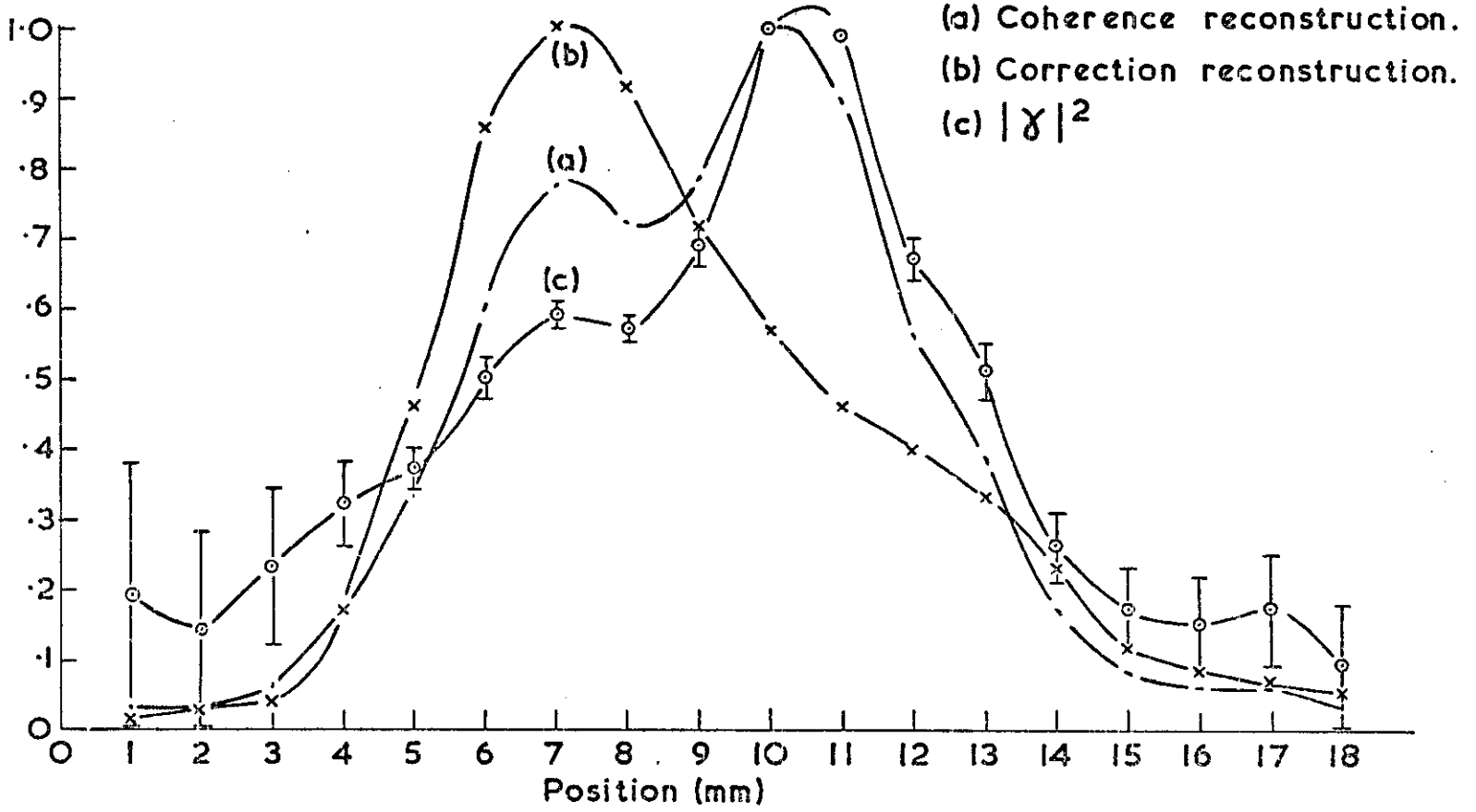


XPERIMENTAL AND THEORETICAL COHERENCE CURVES OF TEM_{00} & TEM_{01} MODE GAS LASER

however emits at 0.694 μm, which can be recorded holographically, so that we can obtain some information about the rest of the laser system by measuring the coherence in the fundamental of this laser. Fig. 5.30(a) shows the reconstructed intensity distribution using a small probe beam at the centre of hologram, this distribution containing information about the transverse coherence along a diameter of the wavefront with respect to its centre. Because the recording beam was not uniform, the reconstruction free of coherence effects was recorded. This is shown in Fig. 5.30(b). A visual comparison indicates that the laser has considerable coherence over the entire wavefront. In the same manner as for the two mode HeNe laser, the above two graphs were processed and a curve of $|\gamma|^2$ along the chosen diameter drawn, Fig. 5.30(c).

The other example given here is of the second harmonic component at 0.53 μm of the Nd:glass laser after the output has passed through a crystal with high non-linear coefficient; ammonium dihydrogen phosphate (ADP) in this case. Proceeding with the measurement in an identical way results in Figs. 5.31(a), (b) and (c) which correspond to Fig. 5.30(a), (b) and (c) respectively. With this and the previous example no coherence controls have been introduced into the resonator, and, with very little control already present, the quite considerable transverse coherence is at first sight rather surprising, particularly in view of the non-uniformity of the intensity distribution. Two factors must contribute to this interesting result; the mode coupling introduced by the rotating Q-switch, which acts as a spatial mixing device, and the short pulse duration, within which different transverse modes can be mutually coherent. It should be stressed here that, in the presence of phase distortions, a single mode laser can have a very complex intensity distribution. The presence of severe non-uniformities is not a certain indication of multimode operation.

FIGURE 5.30



TRANSVERSE COHERENCE ACROSS THE OUTPUT OF A RUBY LASER WITH RESPECT TO THE BEAM CENTRE.

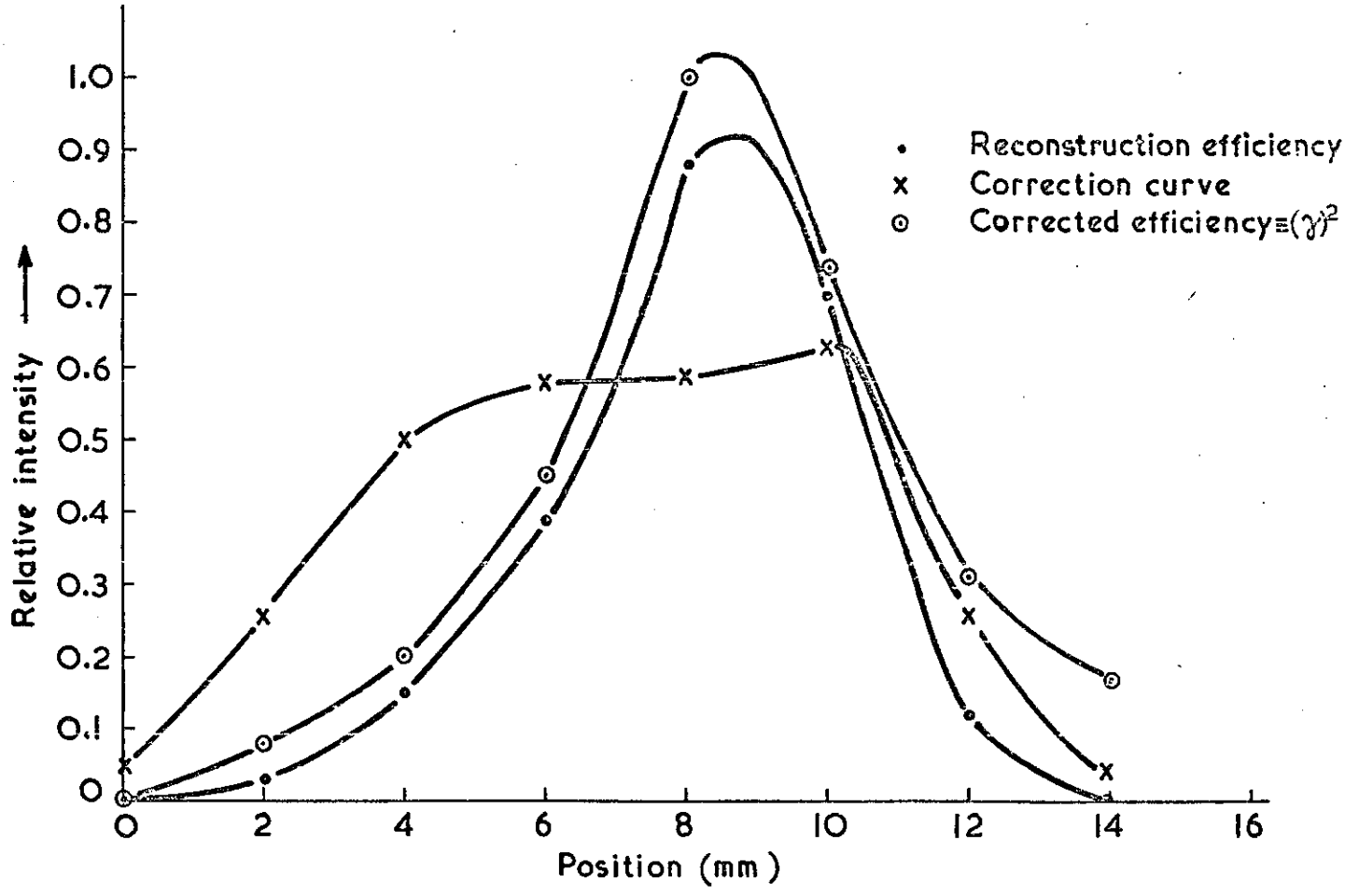


FIG. 5.31 TRANSVERSE COHERENCE ACROSS THE SECOND HARMONIC BEAM FROM A Nd: GLASS LASER WITH RESPECT TO THE BEAM CENTRE

b) Temporal Coherence

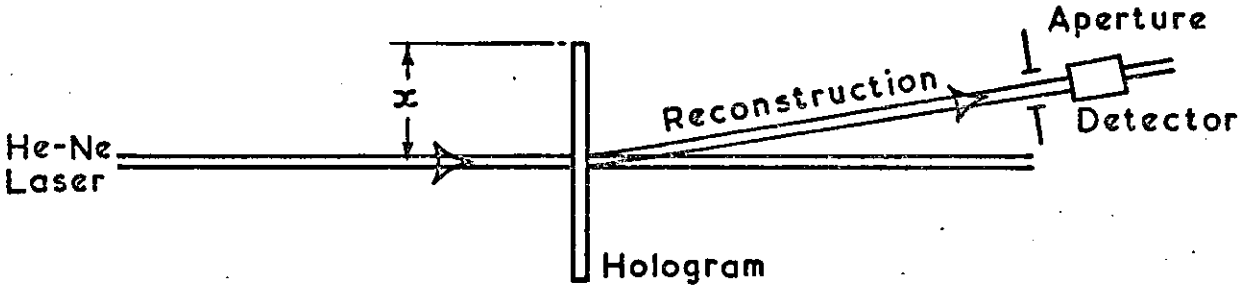
The temporal coherences of the two test lasers were measured by the two methods already described.

Fig. 5.25 shows the holographic arrangement using the grating Twyman-Green method. The grating used was a Bausch and Lomb 73 lines/mm grating, blazed at 63° and 8" long. Thus the maximum range of coherence measurement, which is the path difference between beams at the two ends of the grating, is $2 \times 20.3 \sin 63 = 36.1$ cms. In practice the maximum range was limited to ~ 24 cms by the limited size of the beamsplitter. The holographic plate was oriented to give a best match between the two incoming wavefronts, although distortions in the optics and particularly in the grating prevented a perfect match. The beams were incident on the plate at an angular separation of about 5° giving a fringe spatial frequency on the hologram of $\sin 5°/\lambda = 126$ lines/mm. Polaroid 55P/N with a resolution of ~ 250 lines/mm has been used successfully, but we have generally used Agfa-Gevaert 10E75 because of its higher efficiency.

Fig. 5.26 shows the holographic arrangement used in the other method. Eastman-Kodak 649F plates recorded the Lippmann holograms, and although the 9 cm × 12 cm plates gave a coherence range of only $2 \times 12 \times \sin 70 = 22.5$ cm, it is quite possible to use film which allows an unlimited path difference. Film has a further advantage in being thinner than the plates. The distortion introduced into the transmitted beam is then very much less allowing both a better matching between the interfering wavefronts and a better focus in the reconstructed beam.

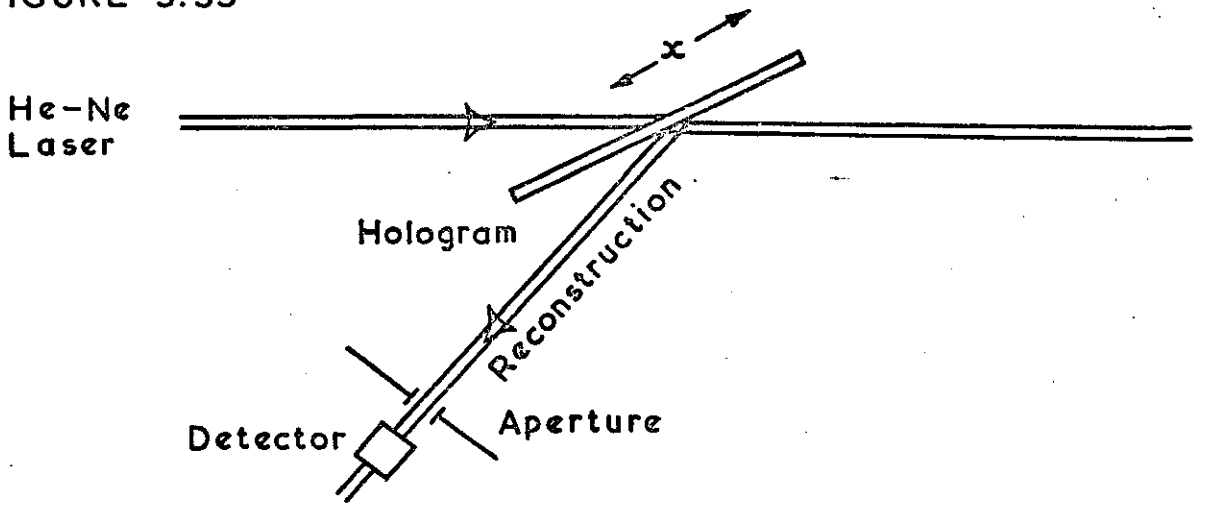
Fig. 5.32 and 5.33 also show the reconstructing arrangements for the two methods, a probe gas laser beam is tracked over the hologram, using a sensitive and linear photodetector, the reconstructed intensity is measured as a function of path difference.

FIGURE 5.32



MEASUREMENT OF TEMPORAL COHERENCE
FROM A HOLOGRAM RECORDED ON
MODIFIED TWYMAN - GREEN INTERFEROMETER

FIGURE 5.33



MEASUREMENT OF TEMPORAL COHERENCE FROM A HOLOGRAM RECORDED BY 'SIMPLE' TECHNIQUE

Fig. 5.34 shows examples of experimental graphs of $|\gamma|^2$ versus path difference, which compare the two methods above for a ruby laser with no spectral control. The same laser has also been subjected to a Fabry-Perot analysis, showing the spectrum to consist of 7 axial modes of differing intensities with separation = 0.11 cm^{-1}. This spectral distribution enables a calculation of $|\gamma|^2$ similar to one made earlier in this chapter. The resulting $|\gamma|^2$ curve is also shown in Fig. 5.34 and is seen to be in agreement with the other more direct measurements.

5.6 The Control of Coherence

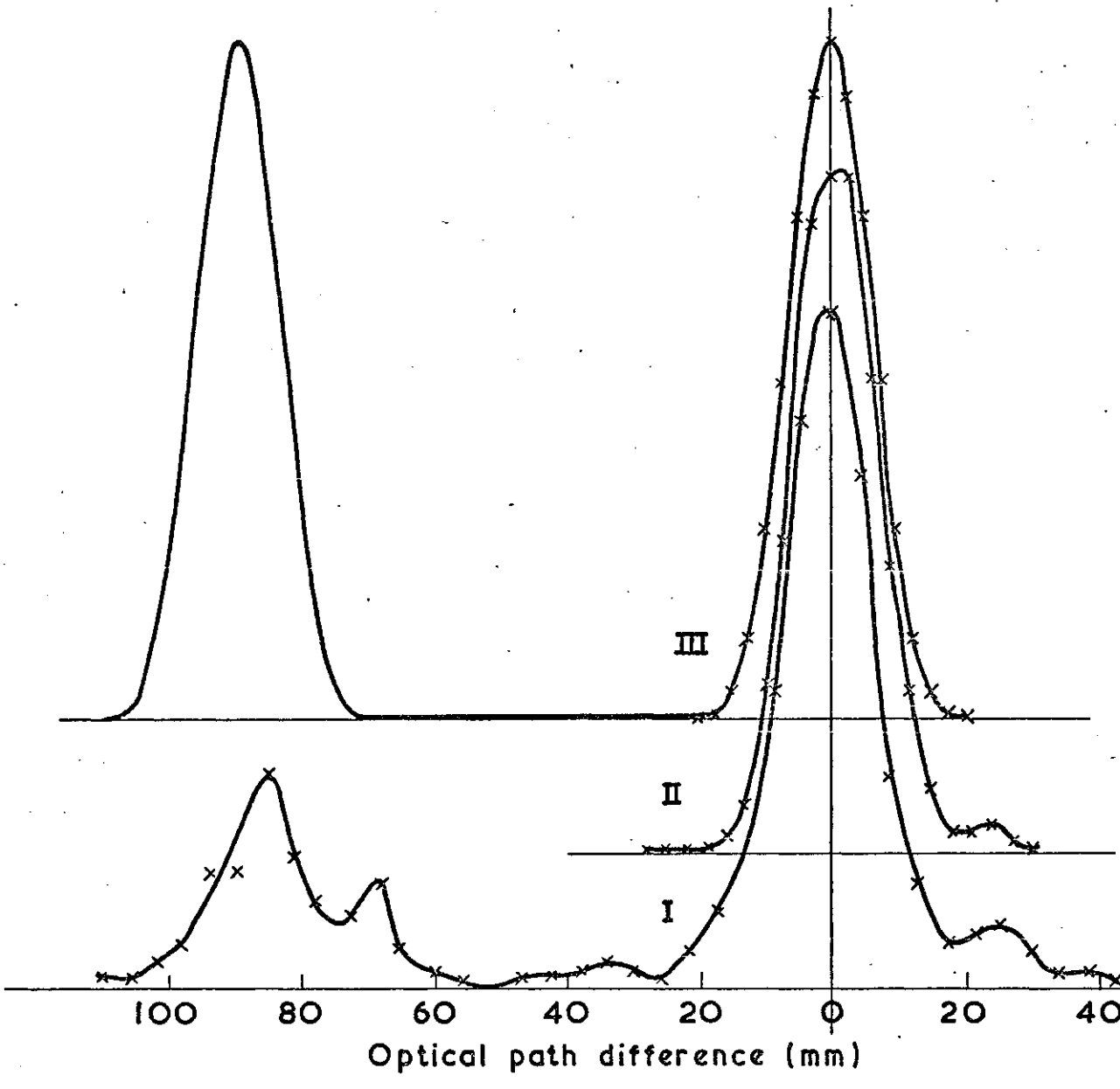
The principle of coherence control is simply that of reducing the number of independently oscillating modes by contriving that:-

(i) The round-trip gain of the laser resonator is mode dependent, and

(ii) The modes reaching their peak first extract all the available stored energy leaving none for other modes to reach their peak later.

To recall from paragraph 5.4.1, if the mode having maximum gain is

FIGURE 5.34



TEMPORAL COHERENCE OF SHORT-CAVITY RUBY LASER.

I FROM COHERENCE HOLOGRAM USING GRATING - TWYMAN-GREEN

II FROM COHERENCE HOLOGRAM USING MIRROR AND TILTED PLATE.

III CALCULATED FROM FABRY-PEROT SPECTRUM.

denoted by A, and another mode is denoted by B, then the condition for effective elimination of B is

$$\left[G_B / G_A\right]^N << 1$$

where N = Number of round trips to pulse peak

G = round trip gain

From this, Equ. 5.16 was obtained:-

$$\left(\frac{R_B}{R_A}\right)^N \left(\frac{S_B}{S_A}\right)^N \exp 2\ell N \left[(\alpha_B-\alpha_A) - (\beta_B-\beta_A)\right] << 1$$

where R = output mirror reflectivity

1 - S = cavity losses (diffraction, scattering, reflection etc.)

ℓ = rod length

α = gain coefficient = $\sigma \times$ inversion density

β = loss coefficient in laser rod.

It is apparent from this equation that the parameters which can control the coherence by being made mode dependent are the reflectivity of the output mirror, the cavity losses, the gain coefficient of the laser material and its loss coefficient. Furthermore the effectiveness of any differential that is introduced or is already present is dependent upon the other parameters in the equation and in particular the number of round trips to reach saturation.

We shall proceed by listing in some detail the possible methods of controlling the transverse and temporal coherence and follow this by making proposals as to the most profitable of these to use. Particular accent is placed, when making a choice, on those likely to be simple and reliable and which result in minimum loss in laser efficiency.

Many authors, for example Burch (1964), Hanna (1970), Magyar (1969), McMahon (1969), Roess (1966) have considered various possibilities for the improvement of coherence.

5.6.1 Ways of Controlling Transverse Coherence

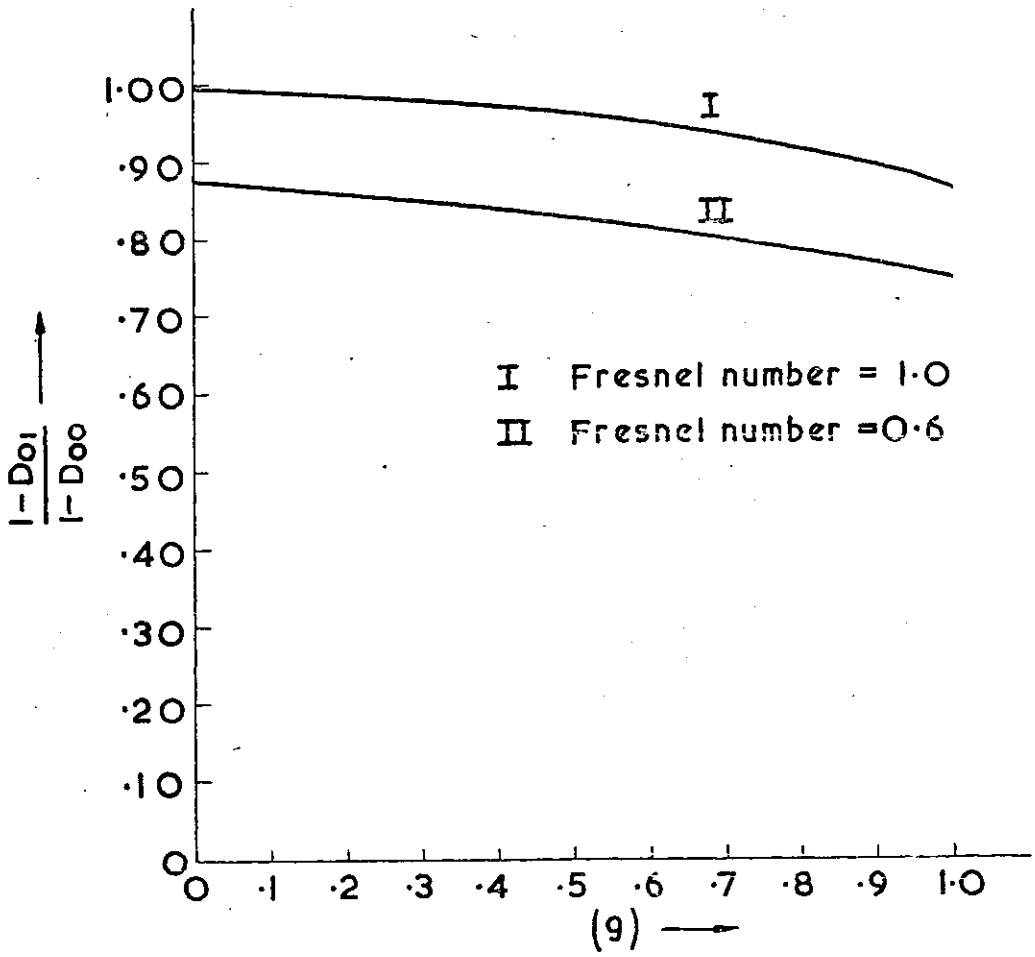
5.6.1.1 Diffraction loss

Different transverse modes are not spatially coincident in a transverse plane. An aperture placed in the resonator consequently results in a diffraction loss at its edge which varies according to the mode. From the Fox and Li resonator theory, the differential mode losses depend upon two parameters; the Fresnel Number, given by $a_1 a_2/\lambda L$, and the Confocal Parameter, given by $\left(1 - \frac{L}{R_1}\right)\left(1 - \frac{L}{R_2}\right)$.

Reduction of the Fresnel number always improves discrimination between modes and there is always a value, dependent upon the confocal parameter and the number N of round-trips, for which only one mode, the Gausian TEM_{00} mode, survives. Manipulation of the confocal parameter can enhance the mode discrimination at a particular Fresnel number, but it also affects other parameters of interest, such as the mode shape and the frequency separation of the transverse modes. We have already seen that all modes within a certain bandwidth can be considered coherent for the particular pulse duration characteristic of this bandwidth. Consequently it might be preferable to choose a confocal parameter for which a greater number of modes oscillate but over a total bandwidth which is smaller.

An example of the dependence on Fresnel number of the mode discrimination has been given and is shown in Fig. 5.13 for two values of confocal parameter. Fig. 5.35 shows how the discrimination varies with the confocal parameter for a given Fresnel number.

FIGURE 5·35



DISCRIMINATION BETWEEN TEMoo AND TEMoi MODES IS A FUNCTION OF CONFOCAL PARAMETER (g) FOR TWO VALUES OF FRESNEL NUMBER

Possible configurations which restrict the Fresnel number are:-

a) Introduction of small apertures. This is a direct limitation on the product $a_1 a_2$, to which the Fresnel number is directly proportional. As an example, if a Fresnel number of one is required for single mode operation (and this is often about right), and the cavity length (L) is 1m, then, for a ruby laser with $\lambda = 694$ nm,

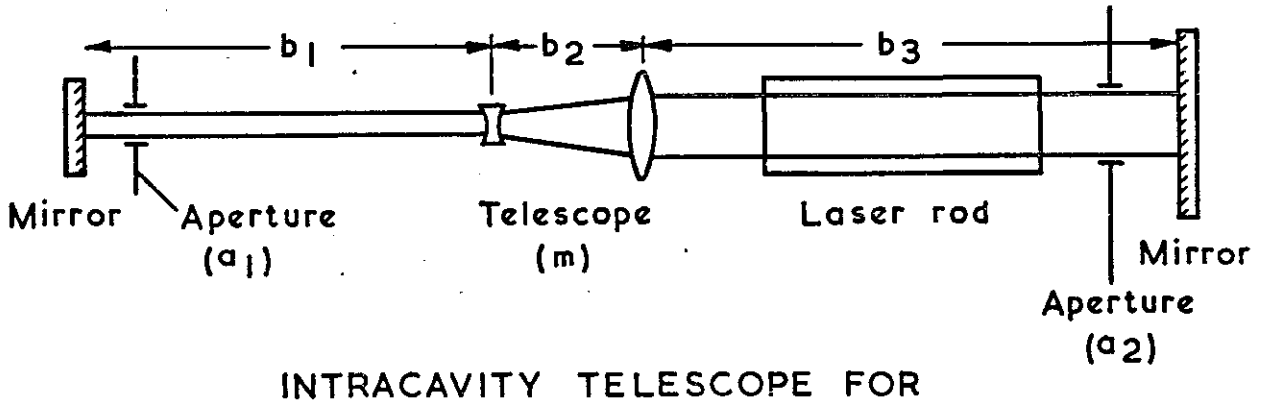
$$\frac{a_1 a_2}{\lambda L} = \frac{a_1 a_2}{694 \times 10^{-9} \times 1} = 1 \therefore a_1 a_2 = 0.694 \times 10^{-6}.$$

Thus aperture radii of 0.83 and 0.83 mm, or 1.66 and 0.415 mm, etc, are required.

b) Increase in resonator length (L).

c) Use of intra-cavity optics. Let a galilean telescope with angular magnification (m) be inserted inside a resonator with Fresnel number $a_1 a_2/\lambda L$ as shown in Fig. 5.36.

FIGURE 5.36



INTRACAVITY TELESCOPE FOR INCREASED MODE VOLUME IN ROD

The effective Fresnel number is changed by the presence of the telescope and is now given by

$$\text{Fresnel Number, } F = \frac{a_1 a_2}{\lambda(m b_1 + b_2 + b_3/m)} \quad \text{(Kogelnik 1965)}$$

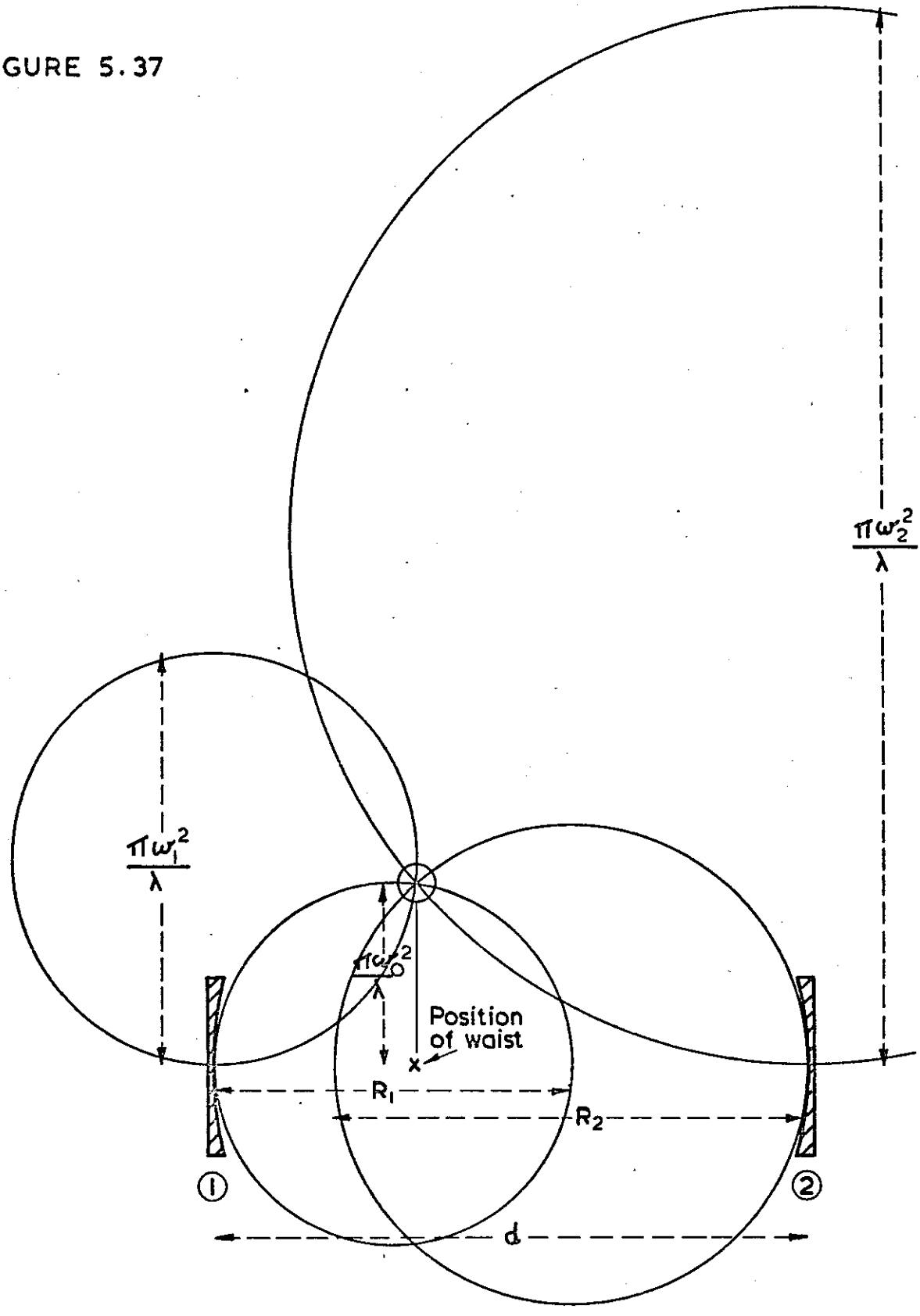
The shape of the lowest order Gaussian mode is also changed, a fact which may itself be of considerable use, as discussed later.

Configurations, which have a confocal parameter which allows a high Fresnel number and yet retains good mode discrimination, are:-

d) Arrangements with confocal parameter = $1 - \Delta$, where Δ is small. For example, a plane parallel resonator ($\Delta = 0$) of Fresnel number 4 has a discrimination equal to that of a confocal resonator with Fresnel number 1, but has poor mode stability since a small perturbation can lead to large changes in mode diameter. A graphical design procedure to give large and stable mode operation has been considered by Hercher following the graphical methods of Kogelnik 1966 and Collins 1964 and is as follows:-

Consider the resonator shown in Fig. 5.37 comprising two mirrors with radii of curvature R_1 and R_2 and separated by a distance d. The lowest order transverse mode of this resonator, the TEM_{00} gaussian mode, has a unique configuration and, using graphical methods, it is possible to very simply establish the principal parameters of this mode, these parameters being the radius and position of the waist and the radii at the two mirrors. To do this, two circles of diameter R_1 and R_2 are drawn tangentially to the two mirrors. A perpendicular from the point of intersection of these circles onto the resonator axis marks the position of the waist and the length of this perpendicular is just $\frac{1}{2}\frac{\pi\omega_0^2}{\lambda}$, where ω_0 is the beam radius at the waist and λ is the wavelength. Finally two more circles are drawn tangentially this time to the resonator axis at the two mirrors, and passing through the point of intersection of the circles already drawn. The diameters of these circles are then equal to $\frac{\pi\omega_1^2}{\lambda}$ and $\frac{\pi\omega_2^2}{\lambda}$ where ω_1 and ω_2 are the beam radii at the two mirrors. The proofs of these constructions are given in the literature cited above and Fig. 5.37 shows an example of a resonator with the four construction circles and perpendicular.

FIGURE 5.37



GEOMETRIC REPRESENTATION OF TEM_{00} MODE PARAMETERS IN A LASER RESONATOR

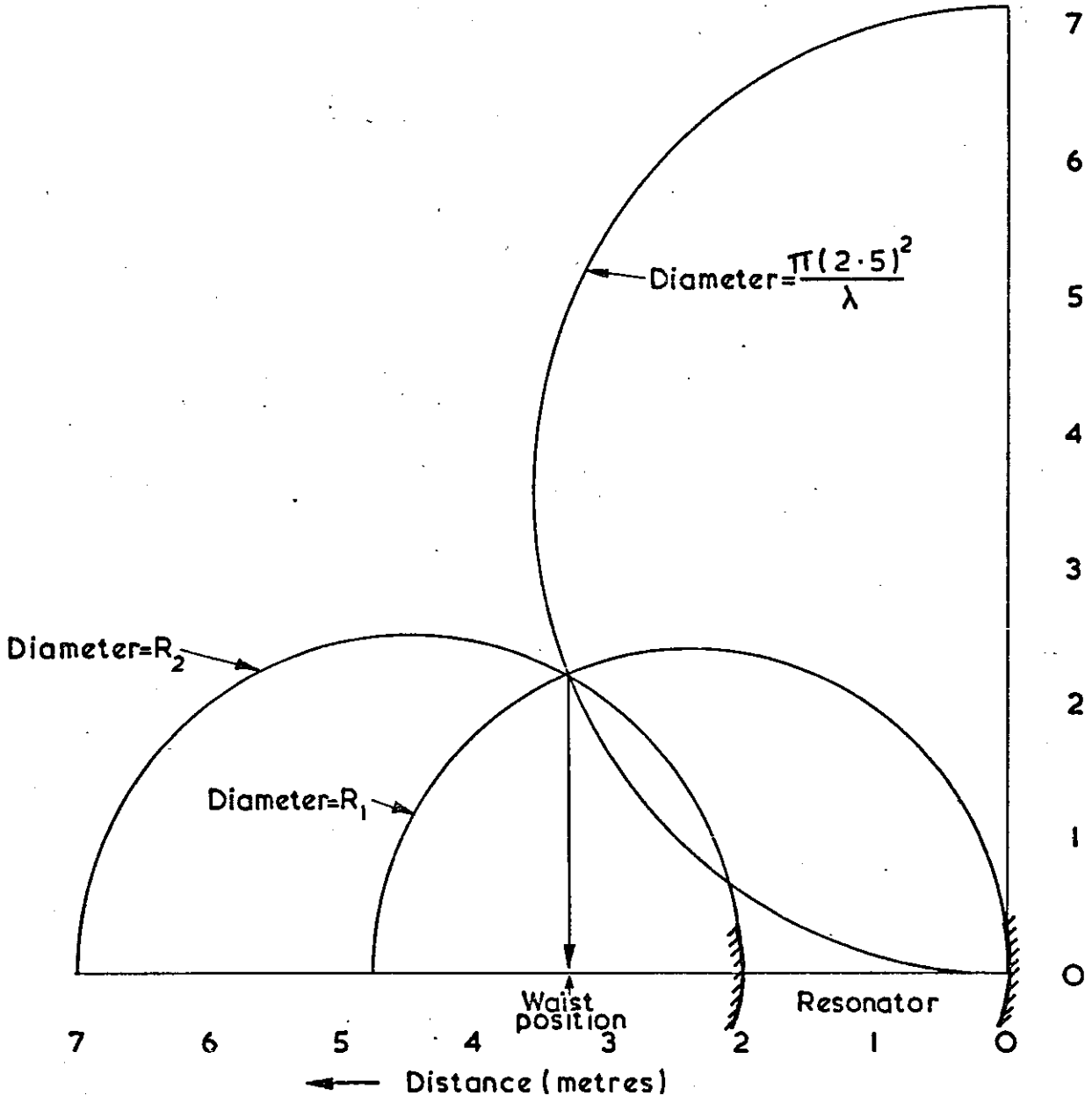
It is worth adding two comments. Firstly, the Fresnel number of the Gaussian mode is $\frac{\omega_1\omega_2}{\lambda d}$. Secondly, the mode stability can be considered as the sensitivity of the mode parameters to perturbations of the resonator curvatures. The graphical method can give information on this question either by making a small change in R_1 or R_2 and finding the change in ω_0, ω_1 and ω_2 by construction or simply by noting the angle between the circles of diameter R_1 and R_2 at their intersection. If this angle is small then the mode is unstable; if it is near 90° the mode is stable.

To design a resonator with say a mode radius of 2.5 mm in the rod (i.e. at one mirror), the circle of diameter $\frac{\pi(2,5)^2}{\lambda}$ is drawn and the two circles of diameter R_1 and R_2 are drawn to intersect on this circle and to intersect at a large angle (high mode stability) for a resonator of reasonable length. Fig. 5.38 shows an example of a reasonable design where the resonator length is chosen at 2m. The solution is not unique but is one giving good stability as can be seen by the large angle of intersection of the circles and the not too large radii of curvature of the mirrors (4.8 m and 5 m respectively.) The Fresnel number F of the Gaussian mode in this resonator is given by

$$F = \frac{\omega_1\omega_2}{\lambda d} = \frac{2.5 \times 1.6}{0.694\times10^{-3}\times2\times10^{3}} = 2.9$$

e) Resonators with confocal parameter < 0 and > 1. Resonator configurations of this type are classed as 'unstable' or 'lossy', since the propagation of a given mode up and down the cavity is a diverging process. Any mode must expand to fill the available volume, or alternatively, any ray within the resonator is not confined and must eventually be thrown out. The lossy resonator situation was proposed by Burch in 1963 and has since undergone considerable analysis by Siegman (1965), Kahn (1966),

FIGURE 5.38



LARGE DIAMETER TEM_{00} MODE PULSED RUBY LASER.

Siegman and Arrathoon (1967) and others. The conclusions of such analyses are that, although the 'lossy' resonator modes are more lossy than the modes of stable resonators, the discrimination is better and the mode diameter is larger.

5.6.1.2 Gain Coefficient

A spatial variation of the gain coefficient in the transverse plane will lead to mode discrimination since certain modes will be better matched to this distribution and this will result in these modes having a higher value of integrated gain coefficient. A typical distribution of gain within a pumped cylinder of laser material, as calculated in Chapter 3, is shown in Fig. 5.39. This is evidently a much better match to a Gaussian TEM_{00} mode than a TEM_{01} which has a central zero.

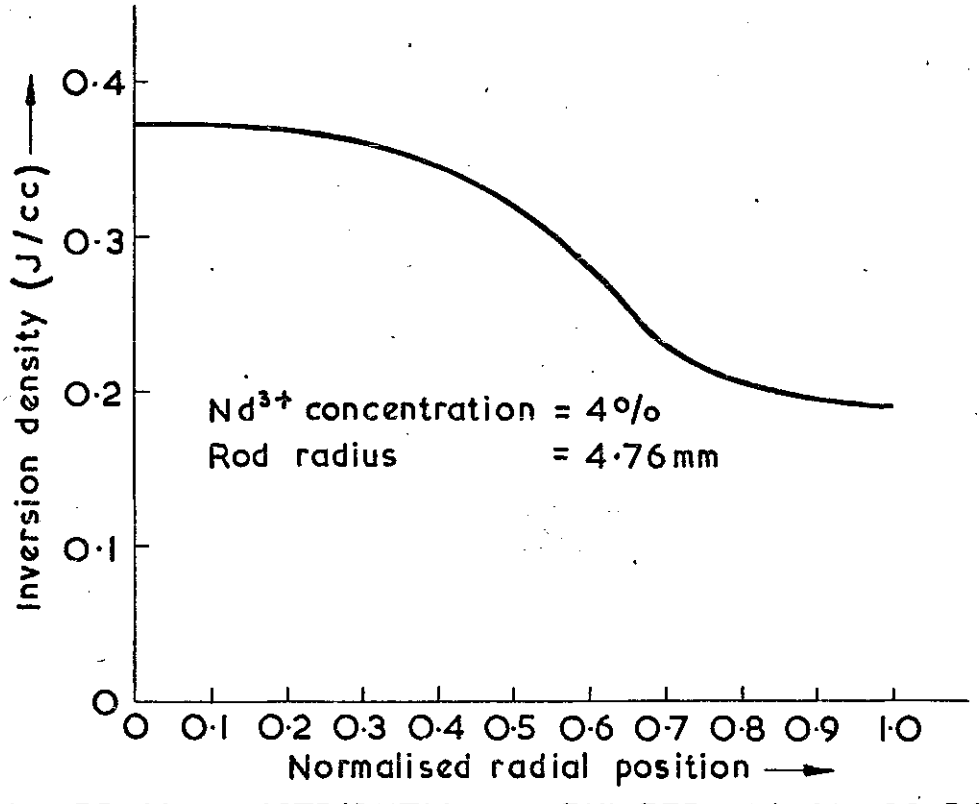
5.6.1.3 Reflectivity

In a similar way to that in the previous section, a transversely variable distribution of output mirror reflectivity will give a transversely integrated round-grip gain which is mode dependent (Kalinin et al 1969). A reflector with suitably optimised distribution of reflectivity is by no means impossible and, although not available as yet, may prove of significant value in the future.

5.6.1.4 Enhancement of Discrimination

Let us consider the effects of optical phase distortions in the laser resonator. They introduce a perturbation on the mode-forming behaviour of the resonator, this perturbation in general increasing the losses and reducing the discrimination between modes. This being the case, the discrimination of any method of transverse mode control can be enhanced by reducing (or changing) the phase distortions. Before discussing possible ways of bringing this about it is necessary to consider an important factor,

FIGURE 5·39



INVERSION DISTRIBUTION IN PUMPED Nd: GLASS ROD FOR 1 J/cm² INCIDENT ON SURFACE.

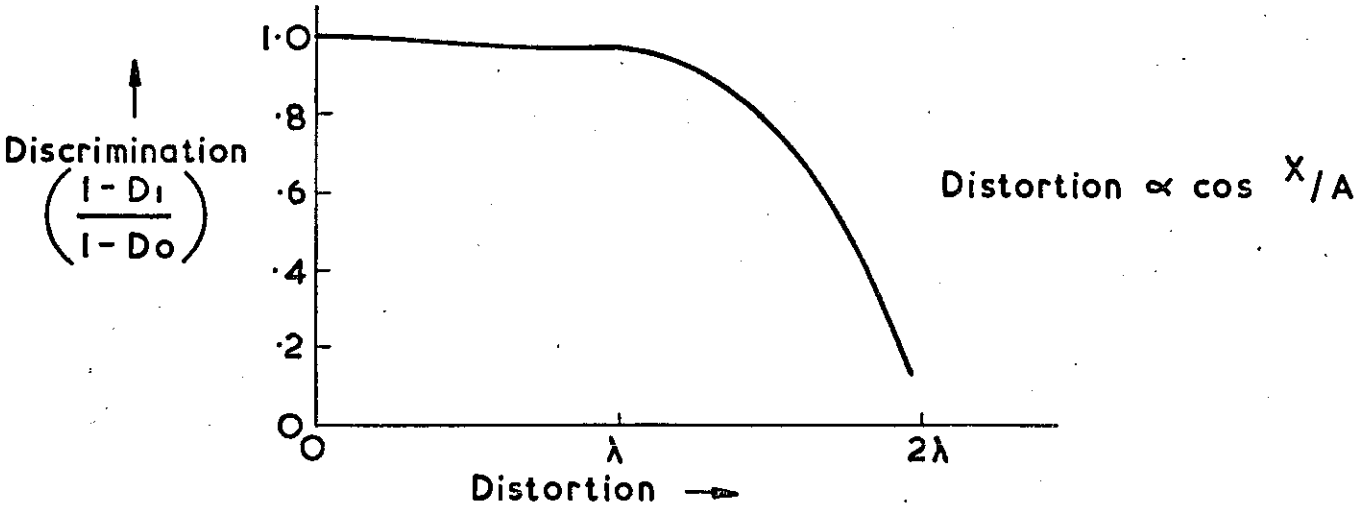
the sensitivity of the mode structure in a resonator to these distortions, or, as we also call it, the stability of the mode structure. A computer calculation of just this factor has been performed by Burch and we quote a few examples of his results. The case taken was a confocal resonator of Fresnel number 4, and various forms and magnitudes of phase distortion at the mirrors were introduced. Fig. 5.40 shows a typical example. Fig. 5.40(a) plots the variation of the mode discrimination with the magnitude of the phase distortion. The situation with zero distortion has no discrimination as one would expect, but losses become very considerable even for distortions of a wavelength and in general all types of distortion give considerable losses for phase disturbances greater than this. The other main result as exemplified in Fig. 5.40(b) is that the distribution in any mode is also a highly dependent parameter. Furthermore the mode discrimination and amplitude distribution are sensitive to changes in the form of the phase distortion. We can conclude from these calculations that:-

(i) elimination of phase disturbance is required to tight limits (at least $\lambda/4$) to eliminate their effect on the mode structure

(ii) a measured near-field intensity distribution which is highly non-uniform does not necessarily indicate poor transverse coherence. This distribution is possible even with single mode operation, in the presence of phase distortion. Some of our measurements of transverse coherence have also indicated this result.

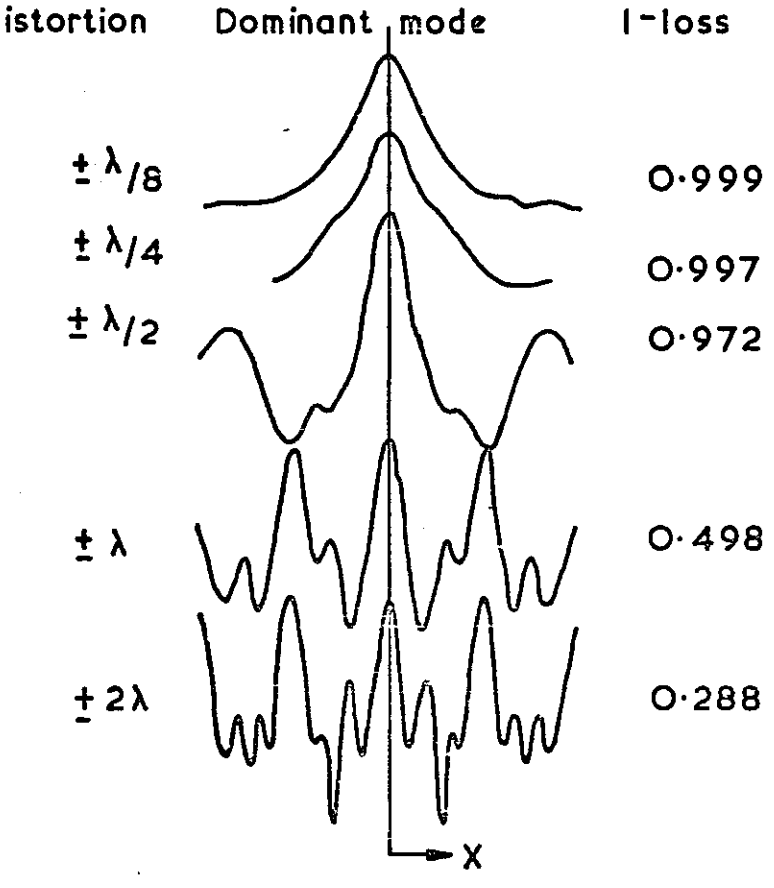
(iii) Both the mode discrimination and the amplitude distribution can be improved if there is sufficient control to be able to produce the right form of distortion, and if there is sufficient gain to overcome the increased loss.

FIGURE 5.40 (a)



DISCRIMINATION BETWEEN TWO DOMINANT MODES FOR VARIOUS MAGNITUDES OF RESONATOR DISTORTION.

IGURE 5.40(b)



AMPLITUDE DISTRIBUTION OF THE DOMINANT MODE FOR VARIOUS AMPLITUDES OF DISTORTION.

DISTORTION ∝ cos X/A.

The effects in resonators of other forms are different, of course, but the general conclusions are the same (see for example Schaak 1967). A further point should be made for resonators having very high Fresnel numbers and/or large distortions. In this case the laser may break up into small elements of small Fresnel number across which the phase distortion is small and between which there is no interaction and hence no correlation. This is known as filamentary laser action, and it occurs because the system is less lossy when operating in this way.

Methods of reducing the detrimental effects of optical phase distortions are:-

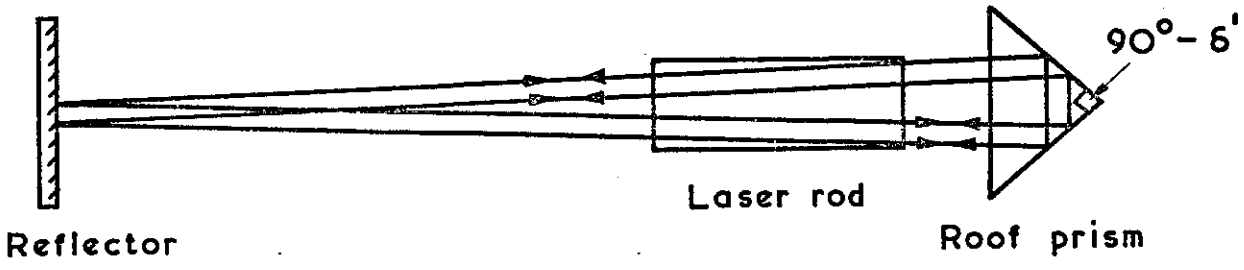
(i(i) Compensating optics. Spherical and cylindrical distortions can be eliminated using appropriate lenses. It is possible to completely compensate in this way, if the rod is very good quality and if the pumping is arranged so that the dynamic optical distortions have circular symmetry (Stickley 1966)

(ii) in situ holographic recording of the distortions. The hologram can be used in a properly designed resonator to eliminate the distortions whatever they may be. The drawbacks are that the resonator design is more complex, that the holograms damage more easily than the other components and that the correction only applies to one input level.

(iii) Arrangements which allow modes to average over the distorted phase distribution. To do this a mode must pass through different areas of the rod (where most distortion occurs) at different times. There is then an interaction between different areas and different modes. The spinning mirror, if running sufficiently rapidly, sweeps any lasing mode across the laser rod and might therefore be expected to result in an

improved transverse coherence. Measurements by Magyar (1970) and during the work presented here show this to be so. Also an arrangement as shown in Fig. 5.41 using a roof reflector with its roof angle slightly less than 90° does, as shown couple together two quite different regions of the rod.

FIGURE 5.41



ROOF PRISM WITH ANGLE NOT QUITE 90°

An improvement in transverse coherence should result, although the phase averaging occurs only over two positions, and it has been shown that this is the case. (Soncini and Svelto 1967).

5.6.2 Ways of Controlling Temporal Coherence

Possible laser parameters for doing this must vary with axial mode. They must, therefore, be frequency-dependent.

5.6.2.1 Gain Coefficient

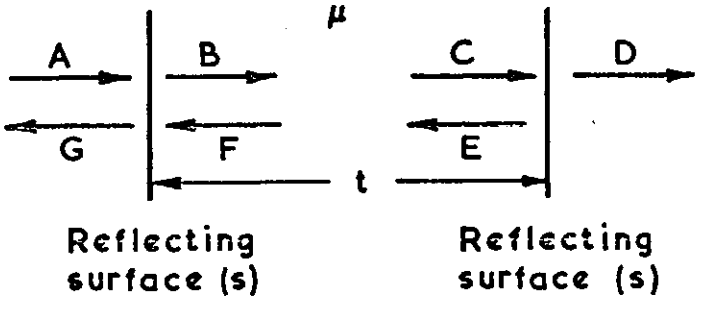
This is naturally dependent upon frequency. The gain linewidth and shape vary from material to material depending as they do upon the electronic structure of the ions and their interaction with the surrounding matrix. Nd:glass, for example, has a Gaussian line of width about 200 cm^{-1}. Given a particular laser the power spectrum can be calculated from Equ. 5.16. The width of this spectrum was calculated, see para 5.4.1.1., to be 45 cm^{-1} for a typical Q-switched Nd:glass laser at well above threshold.

5.6.2.2 Reflectivity

A reflector can be made to have a frequency-dependent reflectivity by ensuring that it has two or more parallel surfaces which contribute to the reflectivity and whose contributions have different optical delays. The 'resonant reflector' as it is called was proposed by Burch in 1964 and has since been subject to several analyses (Watts 1968, McClung and Weiner 1965, Hercher 1965). It is, in its simplest form, a plane parallel plate with or without reflecting coatings, and is just a Fabry-Perot etalon, the theory of which is well known. We give here a somewhat different approach to the theory, the basis of which is the calculation, as follows, of the reflectivity of the combination of two reflecting surfaces separated by a distance t in a medium of index μ.

Fig. 5.42 is a diagram of the resonant reflector.

FIGURE 5.42



RESONANT REFLECTOR

The letters represent amplitude components of the incident, reflected and transmitted waves at the two surfaces. We can immediately write down the continuity equations for the two surfaces:-

$$B = AT_1 + FR_1' \quad ; \quad E = CR_2'$$

and ... (5.46)

$$G = AR_1 + FT_1' \quad ; \quad D = CT_2'$$

where R and T are the amplitude reflection and transmission coefficients from the outside and R^1 and T^1 are those from the inside. For normal reflection from an uncoated dielectric surface in air (Fresnel reflection), for example, $R^1 = -R = \frac{(\mu-1)}{(\mu+1)}$ and $T^1 = \mu T = \mu.\frac{2}{\mu+1}$ where μ = index inside the surface.

We can also relate B and C, and E and F, by the phase factor corresponding to the optical separation of the surfaces (μT). Thus:-

$$C = B \exp i \frac{2\pi}{\lambda} \mu t \quad \text{and} \quad F = E \exp i \frac{2\pi}{\lambda} .\mu t \qquad \ldots (5.47)$$

Eliminating C and F from equations 5.46 gives:-

$$B = AT_1 + ER_1^1 \exp i \frac{2\pi}{\lambda} . \mu t \; ; \quad E = BR_2^1 \exp i \frac{2\pi}{\lambda} . \mu t$$

and $\qquad \ldots (5.48)$

$$G = AR_1 + ET_1^1 \exp i \frac{2\pi}{\lambda} . \mu t \; ; \quad D = BT_2^1 \exp i \frac{2\pi}{\lambda} \mu t$$

Solving these simultaneous equations for $\frac{G}{A}$, the amplitude reflectivity of the combination of surfaces, and $\frac{D}{A}$ its amplitude transmittance, gives:-

$$\frac{G}{A} = R_1 + \frac{T_1 T_1' R_2' \exp i \frac{2\pi}{\lambda}.2\mu t}{1-R_1' R_2' \exp i \frac{2\pi}{\lambda}.2\mu t} \qquad \ldots (5.49)$$

$$\frac{D}{A} = \frac{T_1 T_2' \exp i \frac{2\pi}{\lambda}.\mu t}{1-R_1' R_2' \exp i \frac{2\pi}{\lambda}.2\mu t} \qquad \ldots (5.50)$$

The intensity reflectivity (or just reflectivity) (ρ) and the intensity transmissivity (or just transmissivity) (τ) are then given by:-

$$\rho = \left(\frac{G}{A}\right)\left(\frac{G}{A}\right)^{*} \text{ and } \tau = \left(\frac{D}{A}\right)\left(\frac{D}{A}\right)^{*} \qquad \ldots (5.51)$$

noting that all Rs and Ts may be complex.

It can be seen that the reflectivity (ρ) varies with wavelength λ, the variation being periodic with a period ($d\lambda = \lambda_2 - \lambda_1$) given by:-

$$\frac{2\pi}{\lambda_1} 2\mu t - \frac{2\pi}{\lambda_2} 2\mu t = 2\pi \text{ or } \frac{d\lambda}{\lambda^2} = d\bar{\nu} = \frac{1}{2\mu t} \qquad \ldots (5.52)$$

and having a maximum for values of λ satisfying:-

$$\frac{2\pi}{\lambda} \cdot 2\mu t = 2n\pi + \phi_0 \qquad \ldots (5.53)$$

where ϕ_0 = phase term = π - phase change at first reflection.
All combinations of surfaces can be calculated by iterative use of the above equations, and this will be done for a complex resonant reflector in paragraph 5.7.1.1. Returning to the simplest case, that of an uncoated flat, the following relations can be used to simplify the reflectivity equation:-

$$R_1 = Re^{i\pi}; \quad R_1' = R; \quad R_2' = R; \quad R_2 = Re^{i\pi}$$

$$T_1 T_1' = T_2 T_2' = 1 - R^2; \quad T_1 = T_2; \quad T_1' = T_2'$$

Equation 5.51 then becomes:-

$$\rho = \left[\frac{-R(1-\delta)}{1-R^2\delta}\right]\left[\frac{-R(1-\delta)}{1-R^2\delta}\right] = 1 - \frac{(1-R^2)^2}{1+R^4-2R^2\cos\phi} \quad \ldots (5.54)$$

where $R = \frac{\mu-1}{\mu+1}$ and $\phi = \frac{4\pi\mu t}{\lambda}$ and $\delta = e^{i\phi}$

This is just the equation of the Fabry-Perot, with low reflectivity. Fig. 5.43 plots a typical curve which can be seen to be very close to sinusoidal.

5.6.2.3 Internal Loss

Several ways are possible of introducing a frequency dependent loss into the laser resonator:-

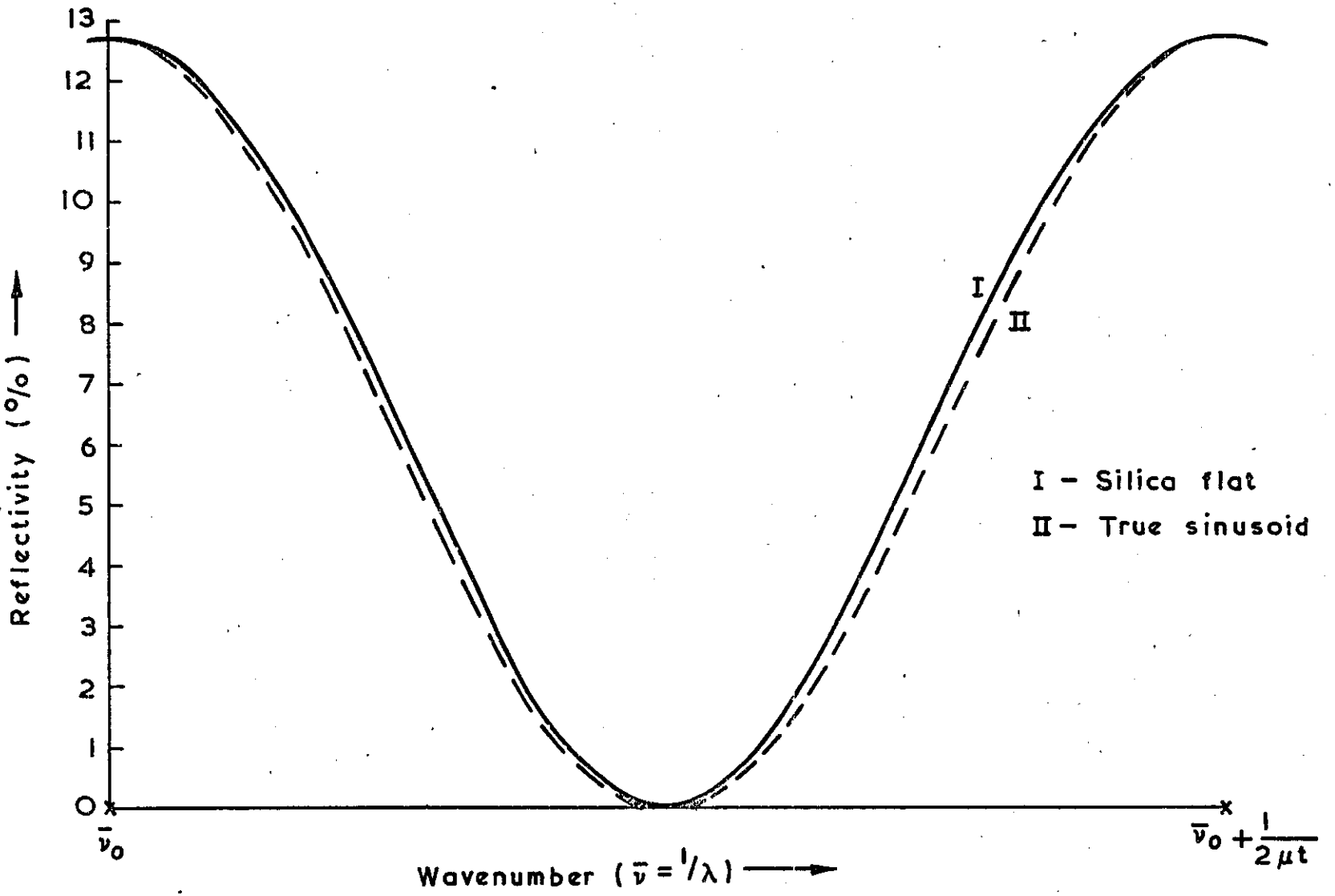
a) Resonant Rejector or rejector plate.

This is just a resonant reflector which is placed inside the resonator with its plane not quite normal to the laser axis (Hercher 1969). The reflection from this component is thrown out of the resonator and is therefore a loss. Since the reflection is frequency dependent we have a frequency dependent resonator loss. The parameter which determines the laser performance is S = 1 - loss, and in this case is the transmissivity of the rejector plate as calculated by Equation 5.51. Of particular note is that the plate introduces no loss for those wavelengths characteristic of maximum transmissivity of the plate, and that since the effective thickness of the plate is $2\mu t\cos\theta$, where θ = angle of refraction of the ray inside the plate, the wavelength with maximum transmissivity can be varied continuously by rotating the plate.

b) Birefringent Plate (Cirkovic et al 1968)

This method is effective in a polarization-selective resonator; i.e. one which exhibits a very much higher gain for one polarization. This

FIGURE 5.43



REFLECTIVITY OF A SILICA FLAT (THICKNESS t; REFRACTIVE INDEX μ) AS A FUNCTION OF WAVENUMBER

type of resonator is very common and includes all ruby lasers and all lasers with a Pockets cell Q-switch. The birefringent plate is introduced into the resonator with its axis at 45° to the preferred direction of polarization. Light of this polarization then separates into two equal components in the crystal, these components being orthogonally polarized and travelling with a different velocity. If the initial amplitude and phase of the components is $Ae^{i\phi}$ their amplitudes and phases on emerging from the crystal are $Ae^{i(\phi+\frac{2\pi}{\lambda}.\mu_1 t)}$ and $Ae^{i(\phi+\frac{2\pi}{\lambda}.\mu_2 t)}$, where μ_1 and μ_2 are the two indices of the crystal. Thus the amplitude of the component after transmission through the crystal having the preferred polarization is given by:-

$$B = Ae^{i(\phi+\frac{2\pi}{\lambda}\mu_1 t)} \cos 45° + Ae^{i(\phi+\frac{2\pi}{\lambda}\mu_2 t)} \cos 45°$$

$$= 0.707Ae^{i(\phi+\frac{2\pi}{\lambda}\mu_1 t)}\left[1 + e^{i\frac{2\pi}{\lambda}(\mu_2-\mu_1)t}\right]$$

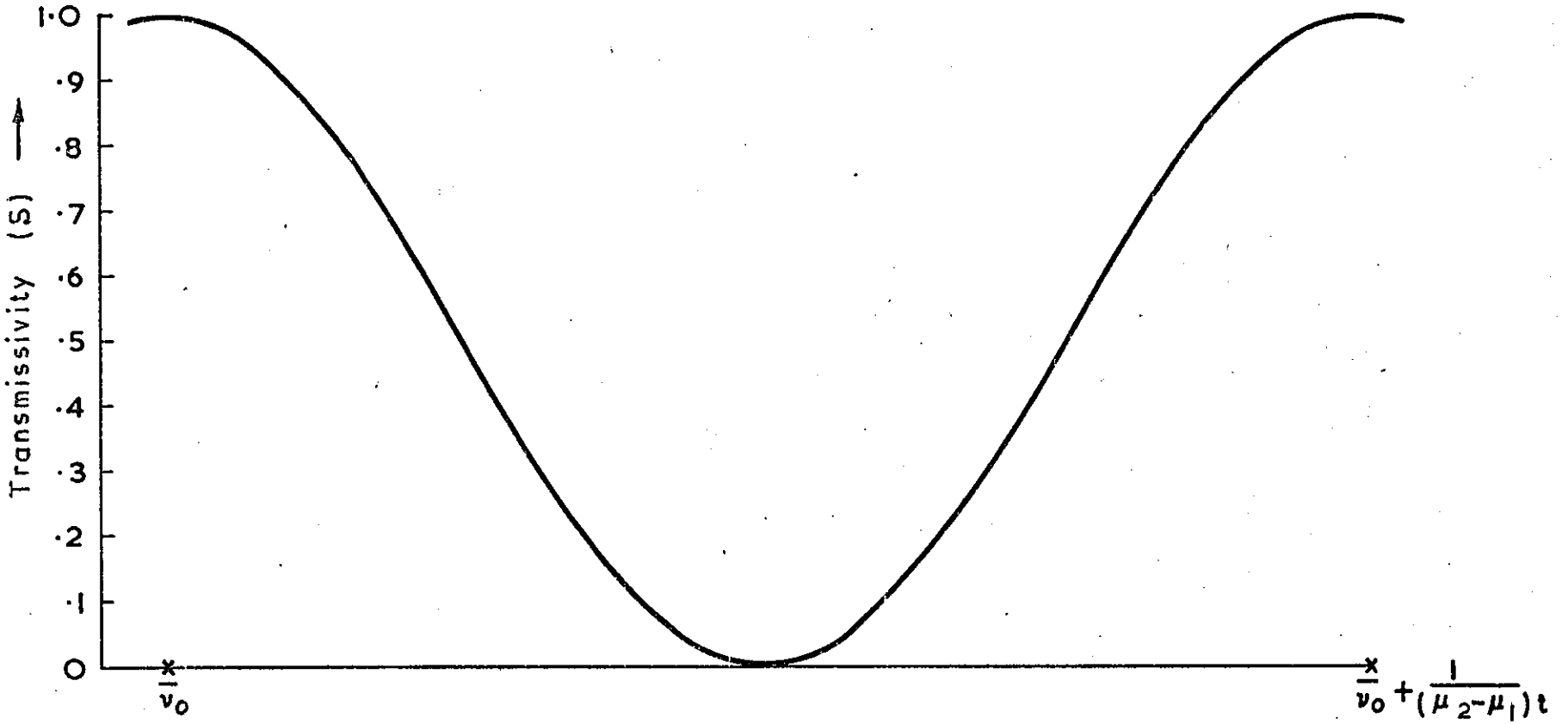
and the intensity in the preferred polarization is given by:-

$$BB^* = 0.5\,A^2\left[2 + 2\cos\frac{2\pi}{\lambda}(\mu_2 - \mu_1)t\right] = A^2\left[1 + \cos\frac{2\pi}{\lambda}(\mu_2-\mu_1)t\right] \quad \ldots (5.55)$$

$\frac{BB^*}{2A^2}$ = the fraction of the intensity not lost = 1 - loss = S.

Fig. 5.44 plots S as a function of wavenumber $\bar{\nu}\left(=\frac{1}{\lambda}\right)$. The wavenumber dependence is periodic with period $d\bar{\nu} = \frac{1}{(\mu_2-\mu_1)t}$. Wavelengths for which the loss is zero are given by:-

FIGURE 5.44



FRACTION TRANSMITTED BY A BIREFRINGENT PLATE IN ONE DIRECTION OF POLARIZATION
PLATE THICKNESS = t ; ORDINARY REFRACTIVE INDEX = μ_1 ; EXTRAORDINARY REFRACTIVE INDEX = μ_2

$$\frac{2\pi}{\lambda}(\mu_2-\mu_1)t = 2n\pi \quad \text{or} \quad n\lambda = (\mu_2-\mu_1)t \qquad \ldots (5.56)$$

The effect of the birefringent plate is very similar to that of a rejection plate of thickness t' and index μ' given by

$$2\mu' t' = (\mu_2-\mu_1)t \quad \text{or} \quad t' = \frac{(\mu_2-\mu_1)t}{2\mu'} \qquad \ldots (5.57)$$

Since $\mu_2-\mu_1/2\mu << 1$, the equivalent rejection plate thickness is small and it may be preferable to use the birefringent plate when a slow dependence of loss on wavelength is required.

c) Absorption line

A material with absorption lines in the region of the laser wavelength would, if placed inside the cavity constitute wavelength-dependent loss which might be used profitably in eliminating unwanted axial modes.

d) Highly absorbent film

Each axial mode exhibits a standing wave distribution down the resonator, this distribution being a series of nodes and antinodes with spacings of $\lambda/2$. The nodes of different axial modes will rarely coincide so that, if a highly absorbing film of thickness very much smaller than $\lambda/2$ is placed in the resonator normal to the axis, the loss introduced will only be small for those modes with nodes within the thickness of the film. This method has been tried with a metal film and shown to be feasible by Smith et al 1969.

5.6.2.4 Enhancement of Discrimination

Equ. 5.16 indicates that the selective effect of any mode-dependent parameter is controlled by the number N of passes during build-up of the

pulse. If two mode intensities are in a ratio p due to a selective reflector:-

$$\left(\frac{R_B}{R_A}\right)^N = p$$

If N were doubled, then this ratio would become

$$p' = \left(\frac{R_B}{R_A}\right)^{2N} = p^2$$

For example, let $p = 0.1$ $\therefore$ $p' = 0.01$

The contribution of the second mode is reduced from 10% to 1%, a considerable improvement.

An effective way of increasing N is to operate the laser closer to threshold, either by reducing the level of pumping or by increasing the losses. The round trip gain G is reduced, and the pulse takes longer to build-up (more round trips are required). Take as an example the effect on the spectral width of approaching threshold, assuming that the gain coefficient (α) is the only term which is wavelength-dependent. Let its dependence on wavenumber be a gaussian of form $e^{-\left(\frac{\bar{\nu}-\bar{\nu}_0}{\Delta}\right)^2}$,

where $\bar{\nu}_0$ = wavenumber of peak gain coefficient (α_0); 2Δ = width at $1/e$ points.

$$\therefore \quad \alpha(\bar{\nu}) = \alpha_0 \, e^{-\left(\frac{\bar{\nu}-\bar{\nu}_0}{\Delta}\right)^2} \qquad \ldots (5.58)$$

Now, at threshold, let $\alpha_0 = \alpha_t$ say

But at threshold, gain = 1 $\therefore$ RS exp $2\ell\ (\alpha_t - \beta)$ = 1 ... (5.59)

At k × threshold, $\alpha_o = k\ \alpha_t$

If we now assume that the total gain of the pulse build-up from fluorescence to saturation = G_o, we can immediately write down the equation for N:-

$$[RS \exp 2\ell\ (\alpha_o - \beta)]^N = G_o \qquad \ldots (5.60$$

Putting $\alpha_o = k\ \alpha_t$ and rearranging using the threshold identity:-

$$2\ell\ N\ \alpha_t = \frac{\ell n\ G_o}{K-1} \qquad \ldots (5.61)$$

This value of N can now be introduced into Equ. 5.16 which calculates the mode intensity ratio (say $p(\nu)$ in this case). Since we assume no selective reflector or internal loss, Equ. 5.16 becomes:-

$$\exp 2\ell N\ \alpha_o \left(-1 + \frac{\alpha(\nu)}{\alpha_o}\right) = p(\nu) \qquad \ldots (5.62)$$

where α_B is replaced by α_o and α_A is replaced by $\alpha(\bar{\nu})$

Eliminating N from Equ. 5.62 using Equ. 5.61 and Equ. 5.58 results in:-

$$p(\bar{\nu}) = \exp\left[\ell n\ G_o . \left(\frac{K}{K-1}\right)\left(-1 + \exp - \left[\frac{\bar{\nu}-\bar{\nu}_o}{\Delta}\right]^2\right)\right] \qquad \ldots (5.63)$$

We now define the output spectral width = $2(\bar{\nu}_w - \bar{\nu}_o)$; where $p(\bar{\nu}_w) = {}^1/_e$.

$\therefore$ Equation 5.63 becomes, after rearranging:-

$$\bar{\nu}_w - \bar{\nu}_o = \Delta \sqrt{-\ell n \left[1 - \left(\frac{1}{\ell n\, G_o}\right)\left(\frac{k-1}{K}\right)\right]} \qquad \ldots (5.64$$

For example, in a typical Q-switched Nd:glass laser,

$$\Delta = 100\ cm^{-1} \quad \text{and} \quad G_o = 10^{10}$$

Fig. 5.45 plots the calculated spectral width ($= 2[\bar{\nu}_w - \bar{\nu}_o]$) against the pumping level (k).

It will be recalled from chapter 3 paragraph 3.2.1.2 that the operation of the passive Q-switch is that of pulse build-up at very near threshold, followed by a sudden increase in Q due to a saturation of the dye absorption line, and resulting in a giant pulse. There is thus good mode selection in this type of Q-switch. Equally good mode selection from any other Q-switch can only be achieved at close to threshold and this represents a severe restriction on output energy. This restriction does not apply to the passive Q-switch.

5.6.3 Choice of Transverse Coherence Control

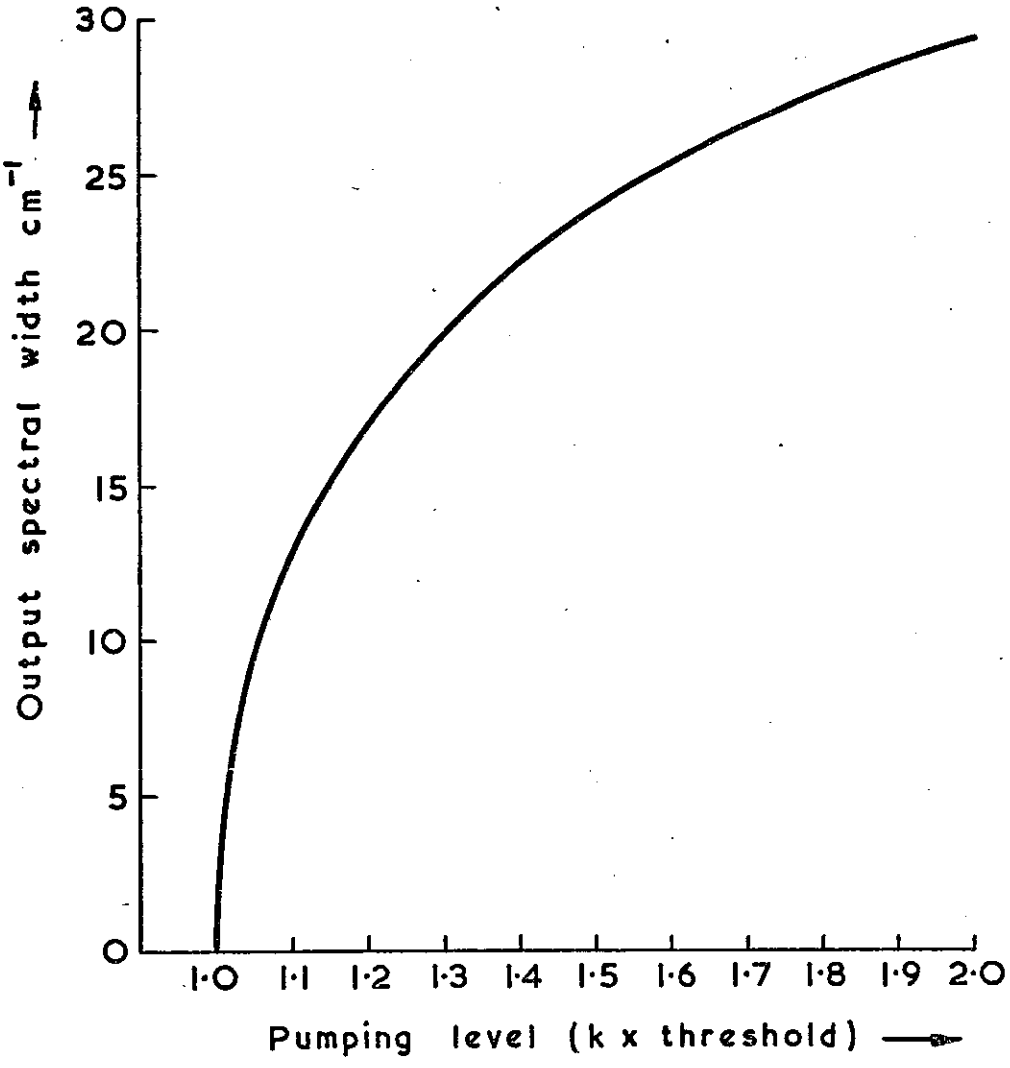
5.6.3.1 The criteria which determine this choice are:-

i) Maximum transverse coherence is required for minimum loss of efficiency. Considerations such as given in paragraph 5.4.4 enable a determination for any given method (with its resulting variation of coherence with efficiency) of the optimum requirement on the coherence control.

ii) There must be as little likelihood as possible of optical breakdown. Methods resulting in high power densities are to be avoided, particularly if these power densities occur within or near optical components.

iii) High mode stability is required thus rendering the laser reproducible from shot to shot.

FIGURE 5.45



OUTPUT SPECTRAL WIDTH OF Nd GLASS LASER FOR DIFFERENT LEVELS OF PUMPING. FLUORESCENT SPECTRAL WIDTH = 200 cms $^{-1}$

iv) Methods of greatest simplicity are favoured.

With these considerations in mind a choice can be made between the various methods of control. Before discussing this choice, however, two points must be remembered. Firstly, the actual variation of the laser efficiency with the degree of control imposed is dependent upon the details of the laser being used and in particular upon the phase distortions present in the laser. Measurements to determine this variation should, strictly, be made but it is still possible, without these measurements, to place the methods of control in an order of merit, in spite of the performance of each not being precisely known. Secondly, quantitative assessment of the mode stability is not possible for these same reasons but, again, an order of merit can be formulated and a choice made.

5.6.3.2 The most commonly used restraint on the transverse coherence, or number of transverse modes, is an aperture placed at a suitable position within a resonator. A Fresnel number of about 1 is usually required for restriction to a single mode. Although this is simple it results in a small mode diameter. The volume of active material available to the mode is small and hence the efficiency is low, and a high power density makes for a considerable risk of damage to the aperture, rod, mirrors or Q-switch. There is some trade-off available in that a larger mode diameter is possible in the rod if it is made smaller at some other point (since it is the product of the two diameters which is important). However the smaller diameter region is then under a much greater breakdown stress, since not only is the area reduced but there may also be a higher power. In its favour is the generally high stability of the mode induced by the aperture method. This is evident when we consider what makes a mode stable. In the first place, if its diameter is insensitive to optical perturbations of the resonator the mode is stable, and in the second place it is also stable

if the optical distortions across the mode are small. A small diameter mode is likely to be stable with respect to both these considerations.

The problem then is to find methods which increase the mode volume in the laser material and which also reduce the chances of optical damage, reduce the losses and maintain a high mode stability.

5.6.3.3 Increasing the cavity length is discarded as a possibility since the resonator becomes inconveniently long and the losses and criticality of adjustment are increased.

5.6.3.4 The use of an intra cavity galilean telescope (Fig. 5.36) is proposed as an effective method. It is equivalent, when placed at one end of the resonator with the rod, to increasing the cavity length without the drawbacks of that method. The mode diameter on the output end is now reduced, but not so much as it would be if the aperture method were used to give the same mode diameter in the rod. In a typical case, with $m = 9$, $b_1 = b_3 = 250$ mm, b_2 very small, a mode diameter of 10 mm in the rod requires, for a Fresnel number of one, a diameter at the other end of 1.1 mm with the telescope and 0.2 mm with just apertures.

5.6.3.5 The method, given in paragraph 5.6.1.1, of arranging that the confocal parameter is such as to give single mode for high Fresnel number, is a good one in that the mode diameter is large everywhere in the resonator and the laser is thus efficient. An example was given of the design of such a resonator. It does rely however upon having a small optical distortion across the mode diameter, so that the mode is not stable (single mode is more difficult to achieve than expected) other than for very high quality rods with compensation for optical distortions. This high sensitivity to optical imperfections makes this method less promising.

5.6.3.6 Operating the laser in the 'lossy' or 'unstable' configuration shows considerably more promise. As shown by the various analyses, operation in the unstable mode (confocal parameter < 0 and > 1) provides good mode discrimination if it is acceptable to have a considerable extra loss. The detrimental effect of this extra loss can be small in lasers where it can be used as the laser output and where there is ample gain to overcome it. The primary advantage over the method of the previous paragraph is the increased mode stability. Greater phase variations across the aperture are possible while maintaining single mode operation since the ever-expanding nature of the oscillating mode results in an averaging of these phase distortions.

5.6.3.7 Methods of enhancing the mode discrimination created by the above suggested arrangements are likely to result in considerable improvement.

Compensating optics, which correct for optical distortion of the laser rod, can be used if the improvement is not overshadowed by the insertion loss, and the difficulties in adjustment. The improvement may not be significant when the distortions prove not to have the right symmetry, but whether or not this is so can only be established by experiment.

The holographic method of compensating for optical distortions would require considerable development. It should not be forgotten however, since it provides complete compensation for large distortions.

As with compensating optics the beneficial effects of using a roof reflector having a roof angle less than 90° can only be assessed by experimentation since it depends upon the actual form of the optical distortions present. It has a further advantage, common to the use of a fast spinning mirror, and this is that, since the oscillating mode passes through different parts of the rod the energy available to that mode is increased in proportion to the increase in rod area seen by the mode. The laser is more efficient than it would otherwise be.

5.6.4 Choice of Temporal Coherence Control

5.6.4.1 The resonant reflector is a natural choice as a method of temporal coherence control. It not only provides sufficient axial mode discrimination, if designed correctly, but also does this without significant loss in laser efficiency, and, when made up of uncoated materials, can withstand very much higher power densities than a coated mirror of equal reflectivity. The design requirements of a resonant reflector will be considered in general terms now and will later be applied to formulating a suitable design for the Nd:glass laser.

Let us assume that it is necessary to reduce the output spectral width from Δ cm^{-1} to δ cm^{-1} and that the reflectivity must be reduced to X% of its maximum for a mode to be eliminated. The resonant reflector is required then to have a maximum reflectivity at a wavenumber near the centre of the laser gain line; to have at least $\Delta/2$ cm^{-1} between this maximum and the next maximum (the reflector, being a periodic structure, has a spectral reflectivity curve which repeats after a characteristic wavenumber interval) at which the laser gain has reduced to < X% of its maximum; to have between these maxima no value of reflectivity greater than X% of the maximum; and to have a falling off on either side of the reflectivity peak such that the reflectivity has dropped to less than X% of the peak value for a wavenumber shift of $\frac{\delta}{2}$ cm^{-1}. As a simple example take the single uncoated flat for which Fig. 5.43 is the reflectivity curve. The wavenumber separation of consecutive maxima is $1/2\mu t$ (Equ. 5.52). The position of the peak reflectivity depends upon the optical thickness (μt) of the plate and can be best thought of as shifting by one order ($1/2\mu t$ cm^{-1}) for a change in optical thickness of $\lambda/2$.

The other requirement concerns the rate at which the reflectivity drops on either side of a reflectivity maximum. This can be calculated quite straightforwardly from Equ. 5.54; $\rho = 1 - \frac{(1-R^2)^2}{1+R^4-2R^2\cos\phi}$. As an example, if $X = 95\%$ and the material is silica ($\mu = 1.449$ at 1.06μ), then a wavenumber interval around the peak over which the reflectivity is greater than 95% of the maximum is $\delta\bar{\nu}$, where $\delta\bar{\nu}$ = 0.158×order spacing

$$= 0.158 \times 1/2\mu t.$$

Looking back at the requirements, if $\delta > 0.158\,\frac{\Delta}{2}$, a single flat is sufficient; but if $\delta < 0.158\,\frac{\Delta}{2}$, it is not. In the latter case a greater number of coherent surfaces must be introduced into the reflector with different characteristic optical thicknesses so that more constraints can be placed upon the reflectivity vs. wavenumber curve. The design and operation becomes more complex as more surfaces are introduced mainly because of the problem of 'tuning' the various optical thicknesses. This tuning results from the fact that optimum operation only occurs when the reflectivity of the working wavelength is an absolute maximum for the system and this absolute maximum is achieved only when each and every pair of surfaces has a maximum reflectivity at that wavelength. This means that each optical thickness is required to have one of a set of values given by $2\mu t = n\lambda$, (where λ is the working wavelength and n is an integer) and can be required to maintain its value to a very small fraction of a wavelength. The criticality of the tuning of the components in a resonant reflector is of considerable importance in its design and the aim should always be to minimise it, since this may make the difference between whether the reflector is of practical use or not. A further requirement we have tried to follow, which is suggested by the fact that the greater the number of resonant surfaces the more complex the problem of analysis, and the more difficult, in general, the tuning problems, is to minimise the number of

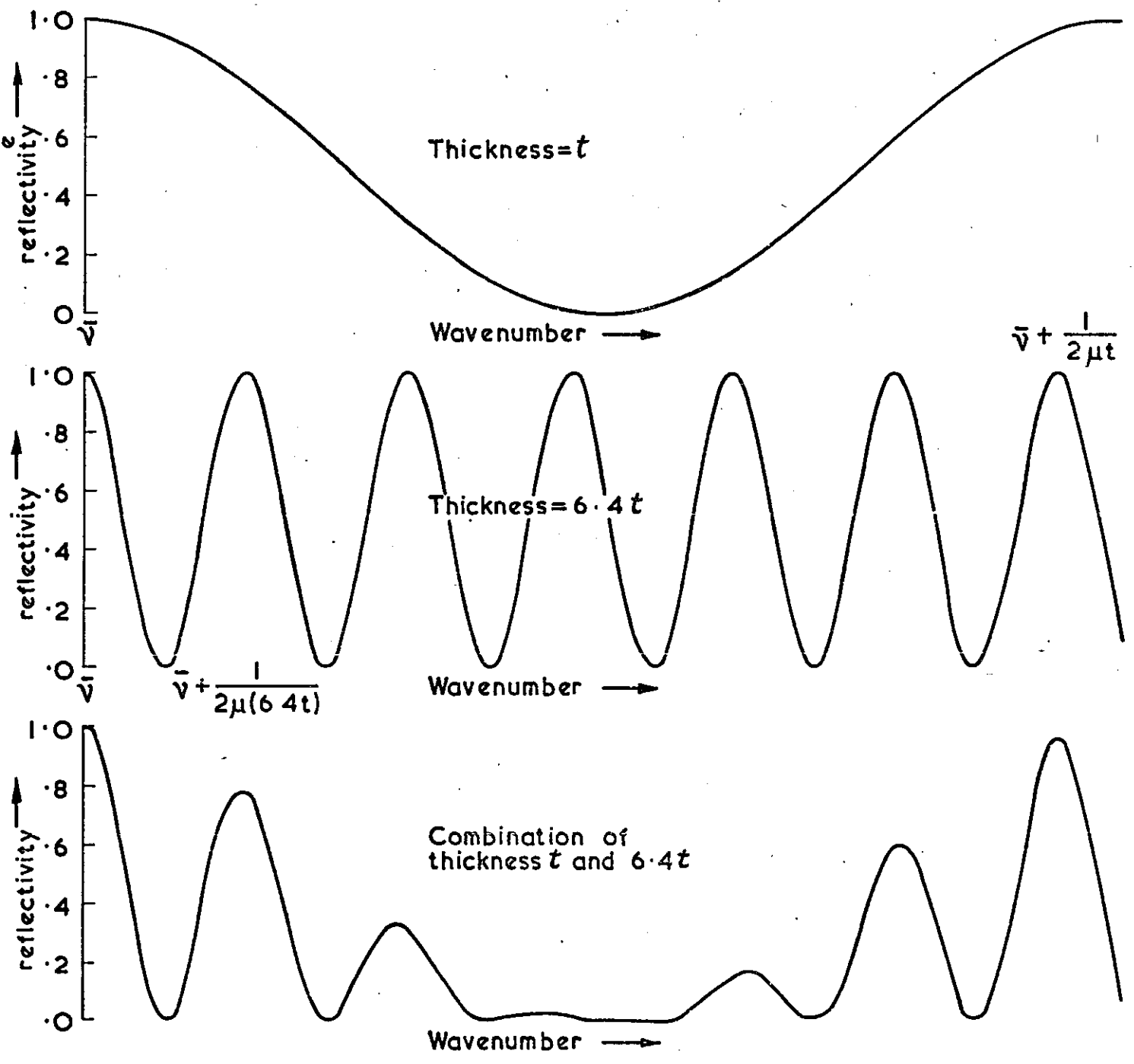
surfaces in the resonant reflector. As shown above, the reduction in total spectral width for a single etalon, if 95% is the fraction of the maximum reflectivity for mode elimination, is 12.7 to 1 (δ = 0.079 Å). This suggests that, in theory, two spacings have a spectral reduction of 12.7 × 12.7 = 162 to 1, and so on. Thus two spacings should reduce the output spectral width of ruby from ~ 1 cm^{-1} down to 0.0062 cm^{-1} and three spacings should reduce that of Nd:glass from ~ 50 cm^{-1} down to 0.024 cm^{-1}. In practice it is necessary, due to the need for insensitivity to small tuning errors, to design for a discrimination per spacing which is well within the capability of that spacing. The design of a reflector for Nd:glass will show this. There is one other requirement on a resonant reflector; that its working reflectivity be such that the operation of the laser is optimal. This may be in conflict with the previous requirement and has led researchers to have more surfaces in the resonant reflector than is strictly essential from mode control considerations. Although these reflectors will work quite well, it might well have proved simpler and cheaper either to consider boosting the reflectivity of a less complex unit by choosing higher index material, or by coating one or more surfaces, or by operating the laser at a lower output reflectivity - the performance of the laser is usually very tolerant of changes in this parameter.

To return to the problem of design, some general guide-lines can be suggested.

It is usually a good idea to keep to a design which can be largely worked out by hand, as opposed to using a brute-force computational technique. This requires an enlightened choice of certain parameters and might not necessarily be the very best that one could achieve, but it results in a reflector which works and in which the effect of small or large changes in the various parameters can be foreseen. That this is possible is suggested

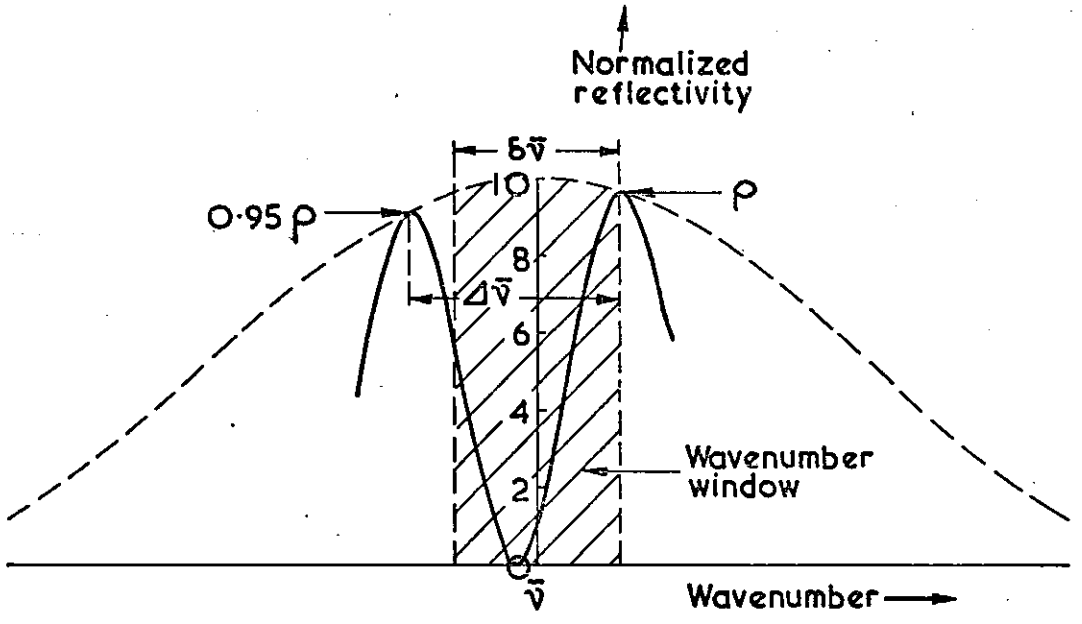
by the large discrimination achieved by a single silica plate, namely 12.7 to 1 assuming 95% of the peak reflectivity represents mode elimination. Let the output spectral width be 2Δ cm^{-1}. The optimum reduction with a single plate is achieved with one of thickness $t_1 = {}^1/2\mu\Delta$, when the width is reduced to $2\Delta/12.7$, and the next reflectivity maxima do not appear, being Δ cm^{-1} away. A second thickness (or spacing) t_2 can be introduced to reduce the width by a further factor 12.7. Its thickness must be ${}^1/(2\mu.\frac{\Delta}{12.7}) = t_1 \times 12.7$, and the resulting spectral width is now ${}^{2\Delta}/(12.7 \times 12.7)$. For a further reduction by a factor 12.7 the third spacing has thickness $t_3 = t_2 \times 12.7 = t_1 \times 12.7 \times 12.7$, and so on. A design of this type gives the required control with the minimum number of surfaces and by also relaxing the requirement on the discrimination per spacing, gives noncritical tuning. This design is indicated by Fig. 5.46, which shows the reflectivity curve of a resonant reflector with two spacings in the ratio 6.4 to 1 (i.e. half that to give maximum descrimination), along with the curves of each spacing. The tuning is the superposition of the peak of one and the peak of the other and gives maximum reflectivity in only one of the smaller width peaks. The wavenumber 'window' (the tuning tolerance) is indicated in Fig. 5.47 and if a small width peak lies within this interval (say $\delta\bar{\nu}$) the neighbouring peak gives a reflectivity < 95% of the maximum. If no peak lies in this interval, modes lying at the second highest peak have reflectivities > 95% of the maximum and are not eliminated. Thus, if no attempt is made at tuning the two spacings, there is a probability of correct operation of $\delta\bar{\nu}/\Delta\bar{\nu}$, where $\Delta\bar{\nu}$ = interval between neighbouring peaks. Taking as an example again the requirement of a drop of 95% of the maximum for mode elimination, Fig. 5.48 plots the dependence of the chance of random tuning success $(\delta\bar{\nu}/\Delta\bar{\nu})$ vs the ratio between the two spacings. In particular, a reduction of the ratio to 6.4 to 1 gives $\delta\bar{\nu}/\Delta\bar{\nu} = 0.76$. The problem of tuning is not great under

FIGURE 5.46



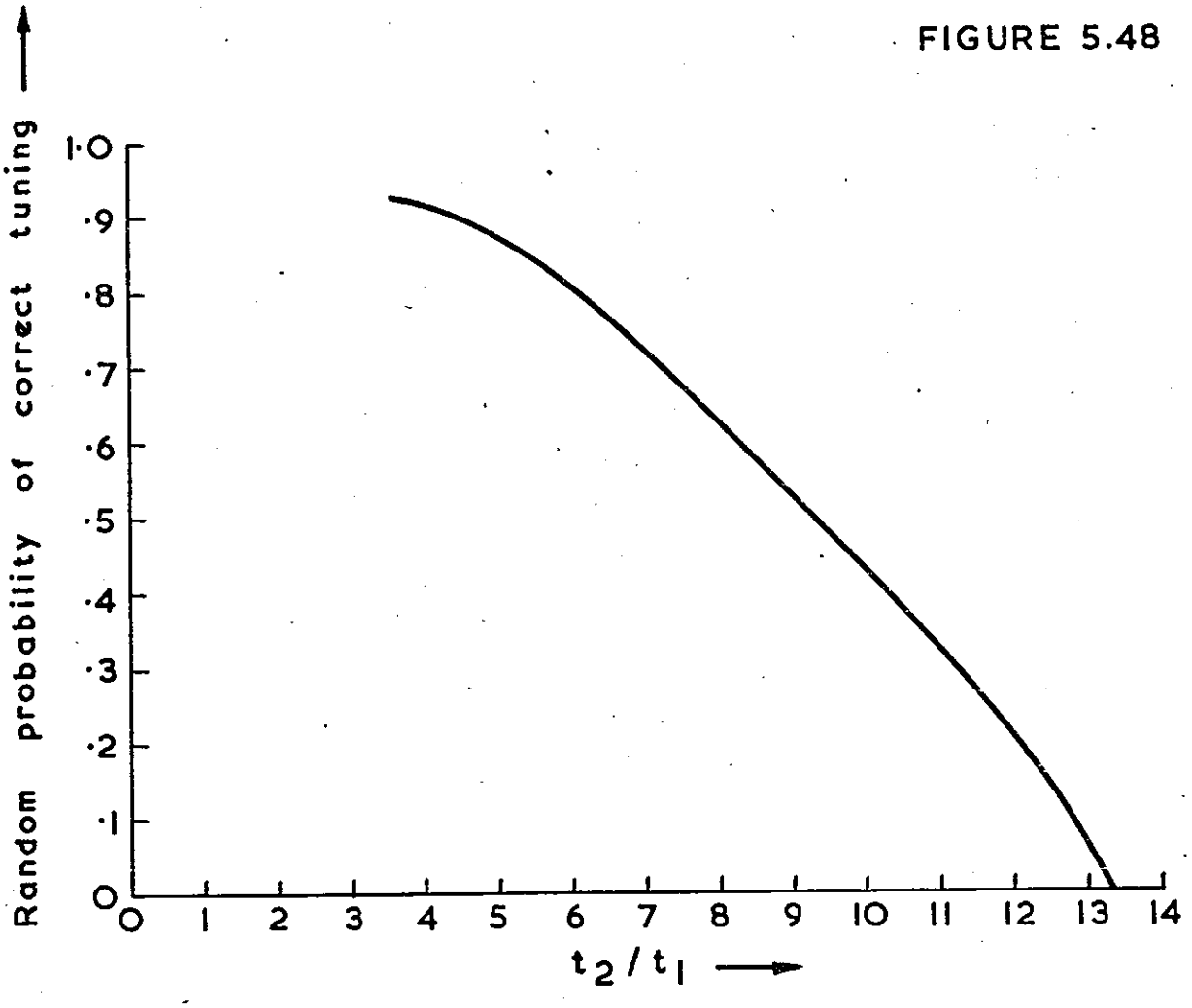
REFLECTIVITY CURVES FOR TWO THICKNESS RESONANT REFLECTOR. REFLECTOR IN TUNE.

FIGURE 5.47



REFLECTIVITY OF TWO THICKNESS RESONANT REFLECTOR
MAXIMUM OUT-OF-TUNE FOR SECONDARY PEAK
≤ 0·95 x PRINCIPAL PEAK

FIGURE 5.48



PROBABILITY OF CORRECT OPERATION OF A TWO COMPONENT RESONANT REFLECTOR.
THICKNESSES OF PLATES ARE t_1 AND t_2 RESPECTIVELY

these conditions and if one operates within the required tolerance, the peak reflectivity cannot drop below 96.5% of that available with perfect tuning. Furthermore if a rejector plate (paragraph 5.6.2.3) is used to eliminate the second highest peak no tuning of the resonant reflector is required at all, although, if several spacings are required in the reflector, several rejector plates would then be required.

5.6.4.2 The rejector plate eliminates the need to tune the resonant reflector but must itself be tuned into that reflector. Other methods of tuning the resonant reflector are possible: an air spacing can be tuned sensitively by control of either pressure or temperature, or by changing the forces on the spacer. The sensitivity of temperature tuning is calculated as follows:-

The wavelength of maximum reflectivity is given by:-

$$n\lambda = 2\mu t \qquad \ldots (5.65)$$

Differentiating with respect to temperature (T) gives:-

$$\frac{1}{\lambda}\frac{d\lambda}{dT} = \frac{1}{\mu}\frac{d\mu}{dT} + \frac{1}{t}\frac{dt}{dT}$$

$$= \frac{1}{\mu}\frac{d\mu}{dT} + \alpha$$

where α = linear coefficient of expansion

$$\therefore \frac{d\lambda}{dT} = \lambda\left(\alpha + \frac{1}{\mu}\frac{d\mu}{dT}\right) \qquad \ldots (5.66)$$

For an air gap, the value of $\frac{1}{\mu}\frac{d\mu}{dT}$ for air is inserted together with the value of α for the spacer. For a reflector plate, either the plate can be made correctly by monitoring during manufacture, or temperature control can be used for tuning and the above equation can again be used to determine how tight this control must be. An important point in connection with temperature tuning is that temperature affects all the resonant reflector spacings and if one is concerned with the tuning in of one spacing with another, it is the relative $d\lambda/dT$ which is the important parameter. It can be seen from Equ. 5.66 above that $d\lambda/dT$ is independent of the spacing (t). Consequently tuning can only occur between spacings consisting of different materials (e.g. air and glass). Conversely, and probably of greater significance, it is possible to minimise detuning due to temperature fluctuations by using the same material for all of the reflector plates.

As an example of temperature tuning take a silica flat working at a wavelength of 1.06μ.

$$\therefore \quad \frac{d\lambda_s}{dT} = (1.06 \times 10^{-4})(0.4 \times 10^{-6} + 5.9 \times 10^{-6})$$

$$= 0.067 \text{ Å}/^\circ\text{C}$$

but for air at constant pressure with a silica spacer

$$\frac{d\lambda_A}{dT} = (1.06 \times 10^{-4})(0.4 \times 10^{-6} - 1.0 \times 10^{-6})$$

$$= -0.0064 \text{ Å}/^\circ\text{C}$$

$\therefore$ tuning sensitivity,

$$\frac{d\lambda_s}{dT} - \frac{d\lambda_A}{dT} = 0.073 \text{ Å}/^\circ\text{C}.$$

The importance of the rejector plate has already been indicated. Its operation and design are similar to those of the resonant reflector and need not be discussed again. It is used as an alternative to adding another plate to the resonant reflector and it has significant differences.

(i) The reflectivity is not increased with the increased mode selectivity.

(ii) The analysis is very much simpler than that of an extra reflector plate, since only one spacing is introduced rather than two.

(iii) A further tuning method is available with the rejector plate, that of controlling its offset angle. This can be very sensitive for small angles, since differentiating the equation of the rejector plate gives:-

$$\frac{1}{\lambda}\frac{d\lambda}{d\theta} = \tan\theta \qquad \ldots (5.67)$$

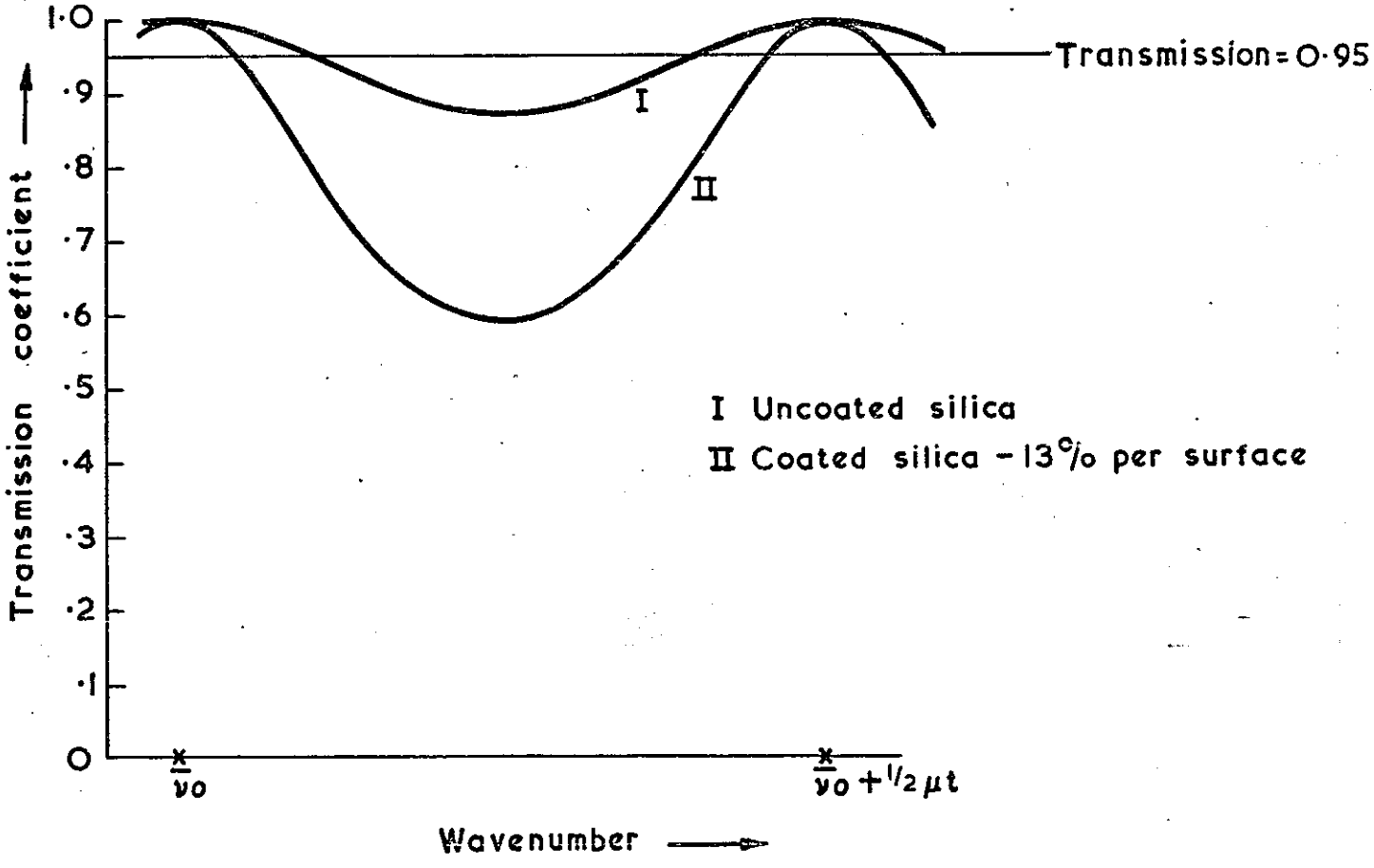
where θ = off-set angle

and $d\lambda/d\theta \to 0$ as $\theta \to 0$.

(iv) The discrimination achievable with a rejector plate depends on its peak reflectivity; that is to say, on the maximum loss it introduces. Fig. 5.49 shows the transmission curve for an uncoated silica plate (peak loss = 13%) and for a coated silica plate with peak loss = 50%. The bandwidths that can still lase are shown by drawing a line at a transmission of 95% (which is assumed to be the lasing limit). The difference in discrimination is immediately apparent.

It is not proposed to use any of the other suggested methods of

FIGURE 5.49



TRANSMISSION CURVES FOR TWO REJECTOR PLATES

controlling temporal coherence. The birefringent plate does the same job as a very much thinner resonant reflector spacing, but is likely to be optically inferior and hence introduce losses into the resonator. Both the 'absorption line' and 'highly absorbent film' methods present practical difficulties and are likely also to be lossy at the central lasing wavelength.

5.6.4.3 Stability of the selected wavelength

One of the advantages of the resonant reflector is that, in controlling the output spectrum (i.e. temporal coherence or axial mode distribution), wavelength variations due to variations in the active medium etc. are only allowed within the width and at the wavelength permitted by the reflector and being a passive item stabilization is simpler than with, say, the rod, which experiences dynamic changes. In trying to ensure invariance of the lasing wavelength, the primary concern is with the effects of temperature. Assuming that the reflector is kept tuned properly, so that the allowed bandwidth remains adequately narrow, Equ. 5.66 determines the change in selected wavelength with temperature. Thus, taking the example given, that of silica, $\frac{d\lambda}{dT} = 0.067$ Å/°C at 1.06μ. Since laboratory temperatures may vary by 5 to 10 °C, and assuming that wavelength shifts of 0.34 to 0.67 Å are not allowable, it will be necessary to do something to prevent the change. Three possibilities are open:-

(i) Use a temperature controlled oven to ensure constant temperature of the resonant reflector.

(ii) Introduce an adjustment on the reflector which is calibrated in terms of the measured temperature.

(iii) Make the reflector unit temperature self-compensating.

We suggest two possible ways of doing this. Firstly, mount the rejector plate on a bimetallic strip which operates on the plate angle.

Differentiating the rejector plate equation and putting $\frac{d\lambda}{dT} = 0$;

$$\tan\theta \frac{d\theta}{dT} = + (\alpha + \frac{1}{\mu}\frac{d\mu}{dT}), \qquad \ldots (5.68)$$

and the bimetallic strip must give this angular change with temperature. This method is quite feasible if it is ensured that the temperature of the bimetallic strip is equal to that of the rejector plate.

Secondly, a correct choice of materials can render a resonant reflector spacing or plate temperature-independent. Equating $\frac{d\lambda}{dT}$ to zero in equation 5. 66 gives:-

$$\alpha = -\frac{1}{\mu}\frac{d\mu}{dT} \qquad \ldots (5.69)$$

No plate material is known unfortunately which has this property but an air spacing at constant pressure requires of the spacer an expansion coefficient $\alpha = 1.0 \times 10^{-6}$ and this is quite feasible with a low expansion glass or with an 'invar' type alloy. Also a sealed air spacing (constant number of molecules) has a negligible value of $\frac{1}{\mu}\frac{d\mu}{dT}$ and might be used in conjunction with a zero expansion glass spacer, such as titanium silicate ($\alpha = 4 \times 10^{-8}/°C$).

5.7 Coherence Control of the Nd:Glass Laser

5.7.1 Temporal Coherence

5.7.1.1 Theoretical Design

Having indicated which methods of coherence control are preferred and having also suggested a design approach for the chosen methods, (the resonant reflector and resonant rejector) it is necessary to apply this to the Nd:glass laser and work out a suitable design for this laser.

Certain information is required, however, before this can be done. From paragraph 5.6.4.1, it can be seen that the examples given are based upon the assumption that a 95% drop in reflectivity (or round-trip gain) will eliminate a mode. In a real case, the required discrimination must be measured and this can be done by observing (i) the natural gain linewidth (i.e. the frequency width over which the gain coefficient of the material is greater than say 1/e of its maximum value) and (ii) the output linewidth under the operating conditions, but with reflectors with no spectral variation of reflectivity. The spectral gain profile is given by:-

$$\alpha = \alpha_o e^{-\left(\frac{\bar{\nu}-\bar{\nu}_o}{\Delta}\right)^2} \qquad \ldots (5.70)$$

where 2Δ = natural gain linewidth

$\bar{\nu}_o$ = wavenumber of peak gain coefficient.

At $2(\bar{\nu}-\bar{\nu}_o)$ = observed output linewidth, say 2δ, the gain coefficient has dropped to $\alpha = \alpha_o e^{-(\delta/\Delta)^2} = q\,\alpha_o$ say, but the output is effectively eliminated at this point ∴ the fraction of max. gain (q) giving mode elimination is just

$$q = e^{-(\delta/\Delta)^2} \qquad \ldots (5.71)$$

Δ has been measured for the Nd:glass used and is 140 cm^{-1}.

Using a prism spectrograph the output spectral width of the laser under investigation was measured. The resonator reflectors were a roof prism and a partially transmitting multilayer dielectric and consequently the only control on the output spectral width was that due to the gain profile. This width (at points at which the intensity is 0.5 of the maximum was measured to be 32 cm^{-1}.

Inserting the value of Δ and δ into Equations 5.71 gives a value of q of 95%. This is the figure used in the calculations of Paragraph 5.6.4.1. Hence the results shown there can be immediately used. The first result was that the maximum reduction in spectral width with a single silica plate is 12.7:1. The difficulty of correctly tuning a plate with this discrimination is very high. A compromise between tuning sensitivity and spectral reduction was chosen to be at a spectral reduction of 6.35:1 when the chance of tuning success with no application of tuning control is 0.76. It was shown also that with 'n' thicknesses increasing in geometrical progression by factors of 6.35, the total reduction in width is $(6.35)^n$:1. Thus with $n = 3$, the Nd:glass laser output reduces to $50/256 \simeq 0.195$ cm^{-1}, while with $n = 4$ the resultant spectral width is $50/1625 = 0.031$ cm^{-1}. A four-thickness resonant reflector should, therefore, provide sufficient control to achieve the requirement on coherence length of 25 cm. A four-thickness reflector is difficult since, unless one surface reflection is eliminated, there are always an odd number of thicknesses (n plate thickness + [n-1] air spacings). Tuning a four-thickness reflector has only a $(0.76)^4 = 0.33$ chance of random success and some control should really be applied. In view of these two points a two-plate reflector (2 plate thickness + 1 air thickness) together with a tilted etalon rejector plate has been chosen. The reflector requires only a crude method of tuning for correct operation and the fine tuning is accomplished by a tilt control of the rejector plate. Within this format then, the various thicknesses must be chosen to give the required selectivity with the maximum ease of tuning.

The rejector plate, if made of silica, can at best ensure that only one of seven equally-spaced spectral components has appreciable energy (the loss introduced by the plate is > 5% for all the other six). We choose

for two reasons to use it in this way rather than arrange for it to reduce the spectral width by a further factor. Firstly, the tuning of the resonant reflector is easier, as illustrated below, and secondly, if it were to control the minimum width then its thickness would be large and its discrimination reduced since the resonant action of a tilted resonant plate is reduced as the thickness increases (due to incomplete spatial matching of interreflected beams). The thickness of the tilted plate is determined by the separation of the several components which would be present in its absence.

Let us consider the resonant reflector. It must result in not greater than seven spectral components each having a width equal to the minimum width requirement. Since the temporal coherence required is 25 cms the spectral width must be ~ 0.04 cm^{-1}. Thus from paragraph 5.6.4.1 the maximum thickness t_{max} in the resonant reflector given by:-

$$0.04 \times 6.35 = \frac{1}{2\mu t_{max}}$$

$\therefore$ $t_{max} = 1.36$ cm, since $\mu = 1.449$ (silica).

Another thickness, the minimum thickness t_{min} must reduce the known output width of ~ 50 cm^{-1} by our factor of 6.35. Paragraph 5.6.4.1 enables the thickness for a reduction of 12.7 to be calculated. The thickness giving a 6.35 reduction is just half this value and is thus given by:-

$$\frac{1}{2\mu t_{min}} = 2 \times \frac{50}{2} = 50 \text{ cm}^{-1}$$

$\therefore$ $t_{min} = 0.01$ cm

where the minimum thickness is chosen to be the air gap in the two-plate reflector.

This thickness should reduce the width to $50/6.35 = 7.9\ cm^{-1}$. The third thickness (say t) reduces by another factor of 6.35. The calculation is just as for t_{min} but with $50\ cm^{-1}$ replaced by $7.9\ cm^{-1}$ and gives:-

$$t = 0.044\ cm$$

and this thickness is the second silica plate and it reduces the width to $\frac{7.9}{6.35} = 1.24\ cm^{-1}$. Finally the number of components of width $0.04\ cm^{-1}$ lying within this width can be calculated. These components are separated by $\frac{1}{2\mu t_{max}} = 0.25\ cm^{-1}$. Hence there are $1 + \frac{1.24}{0.25} = 6$ components, and the tilted silica plate should eliminate all but one.

The thickness (t_R) of this rejector plate can now be calculated. Fig. 5.50 shows how its reflectivity curve must match up to the six components in order that maximum discrimination against five should be achieved. It is seen that the period of its reflectivity curve $\left(= \frac{1}{2\mu t_R}\right)$ must be equal to about 3.5 × spacing of the components

$$\therefore \quad \frac{1}{2\mu t_R} = 3.5 \times 0.25$$

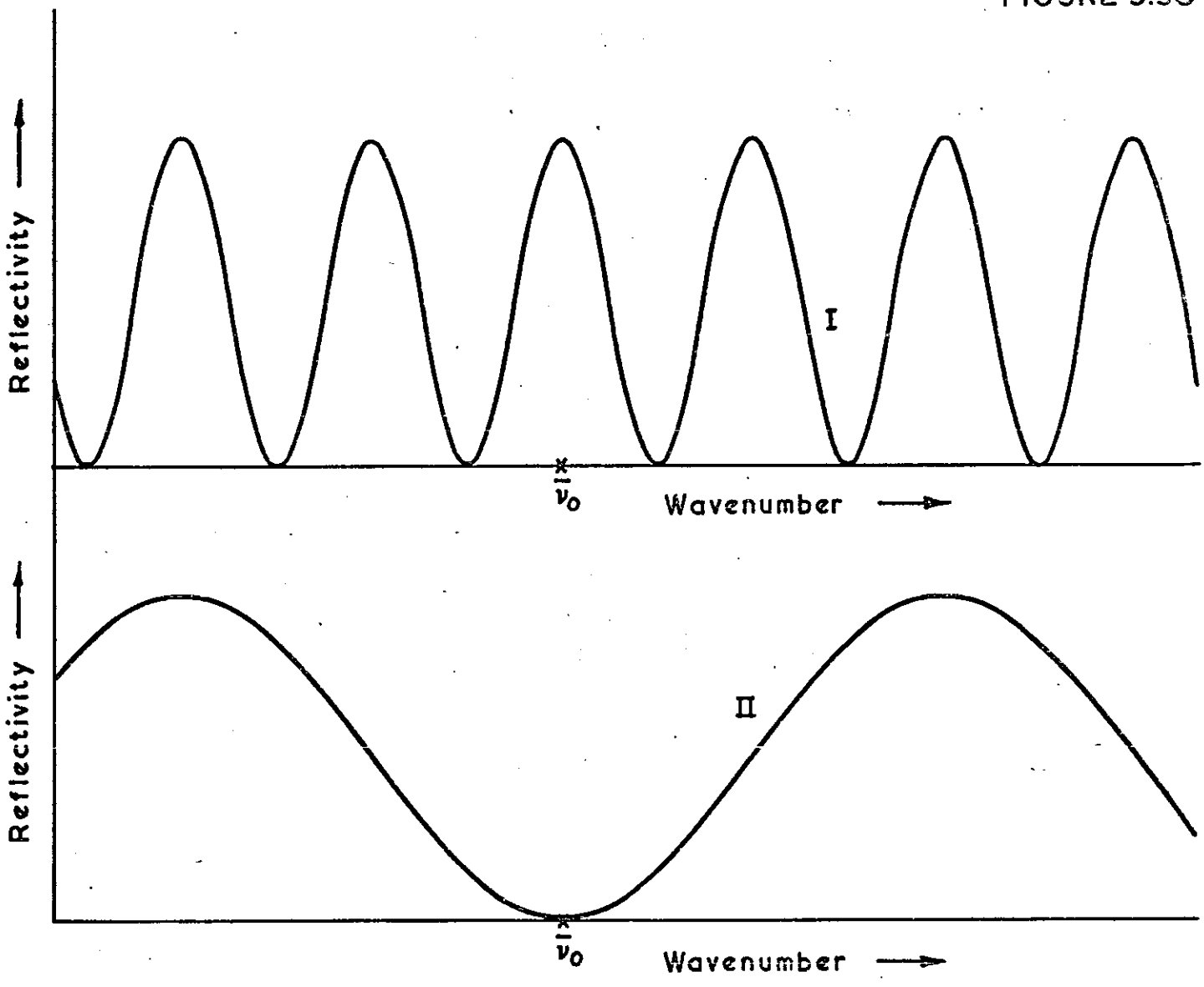
$$\therefore \quad t_R = 0.39\ cm$$

Since the reduction factor has been somewhat arbitrarily chosen at 6.35 and since the discrimination possible with the tilted rejector plate has not been fully used, the design can have some flexibility as to the precise thicknesses used. The resonant reflector which has been constructed has the following parameters:-

Plate thicknesses = 0.70 cm and 0.75 cm

Separation = 0.01 cm.

FIGURE 5.50



I — REFLECTIVITY CURVE OF RESONANT REFLECTOR GIVING 6 NEARLY EQUAL COMPONENTS

REQUIRED REFLECTIVITY CURVE OF INTRACAVITY TILTED ETALON TO ELIMINATE ALL BUT ONE OF THE 6 COMPONENTS

It will be noticed that the plates have nearly equal thickness instead of one large and one small as suggested above. The thickness chosen however are entirely equivalent to ones of 0.75 cm and 0.75-0.70 = 0.05 cm respectively, and these are similar to the design values above. The tilted plate has a thickness = 0.20 cm.

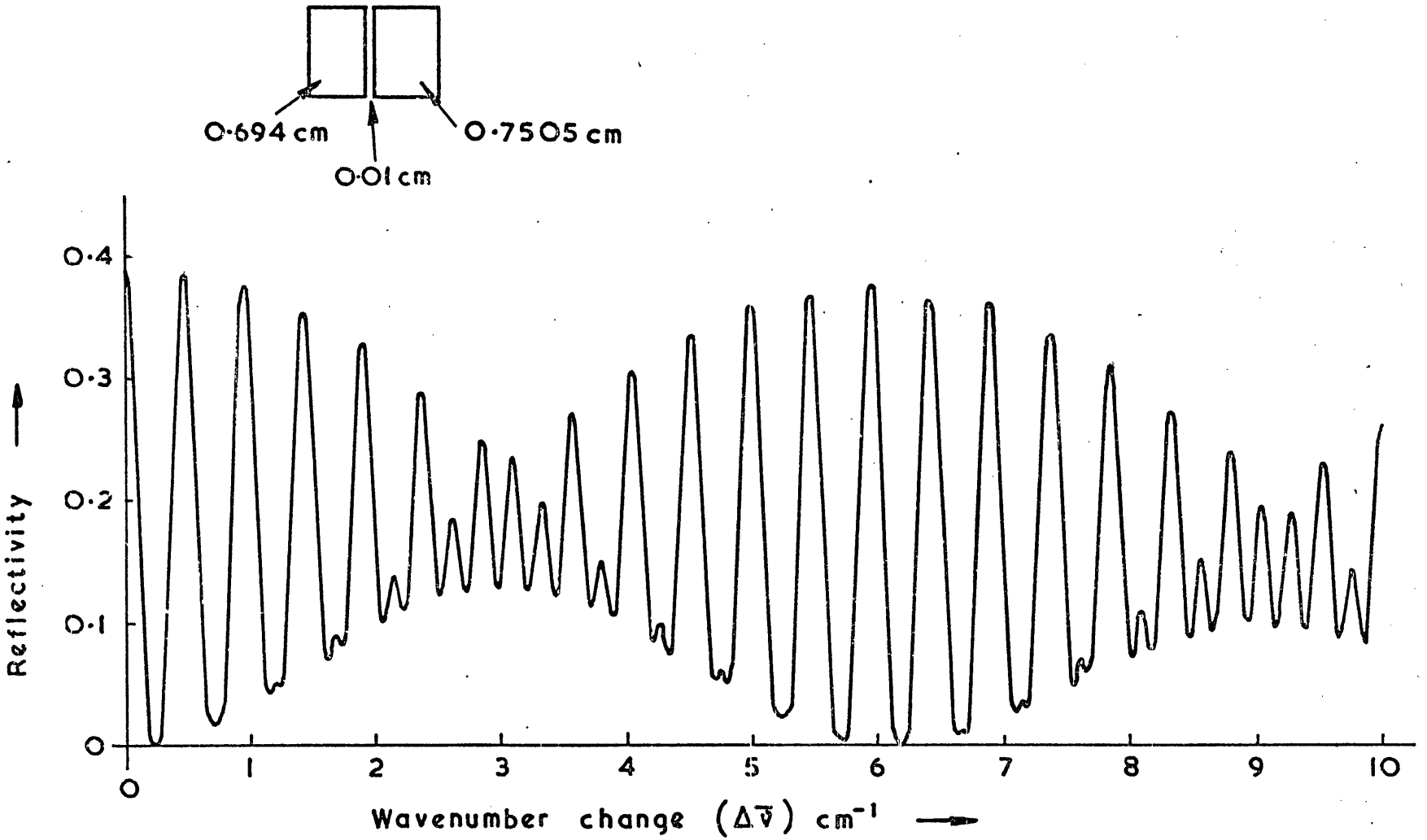
The performance of this reflector system has been measured experimentally and calculated theoretically (as a single unit) using the equations of paragraph 5.6.2.2, and writing a BASIC computer program which has been run from an on-line GPO terminal.

The formula for the reflectivity curve for the resonant reflector is calculated by inserting the reflectivity and transmissivity curves for two single plates of different thicknesses (Equation 5.54) into Equation 5.49. The resultant amplitude reflectivity curve has the form $\frac{A+iB}{C+iD}$ and the intensity reflectivity is then given by:-

$$\rho = \frac{A^2+B^2}{C^2+D^2} .$$

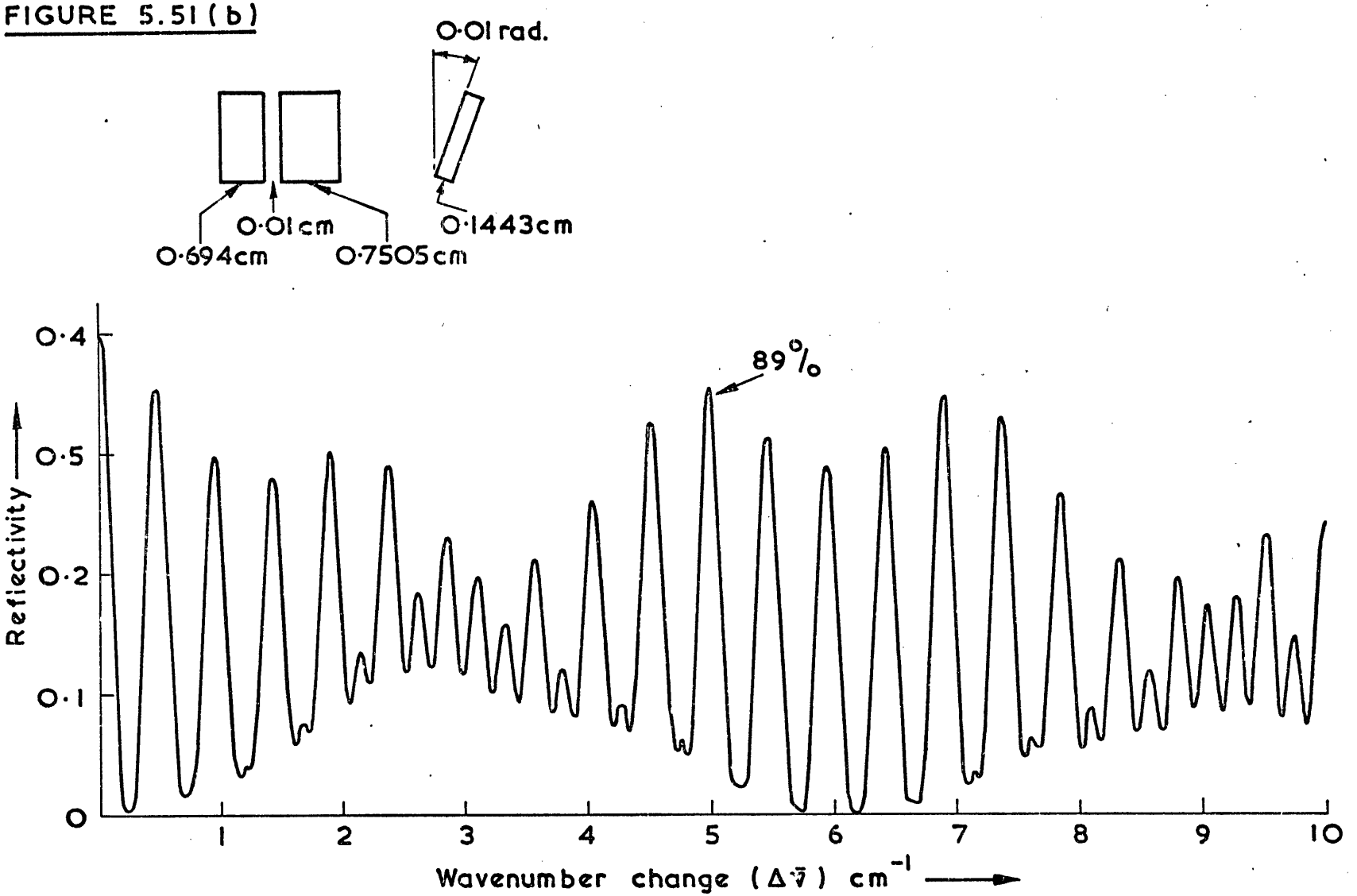
The full calculation is given in Appendix VI along with the BASIC program, which not only calculates this reflectivity but also multiplies it by the transmissivity of the rejector plate, given by Equ. 5.50 and 5.51.
Fig. 5.51 shows the reflectivity vs the wavenumber for (a) the resonant reflector (b) the reflector + rejector plate (c) the reflector + coated rejector plate with 45% reflectivity per surface. In all cases the thicknesses were assumed to be in tune at the origin of the wavenumber axis ($\Delta\bar{\nu} = 0$). Fig. 5.51(b) shows that no subsidiary peak is more than 95% of the maximum reflectivity and the width of the highest peak at the 95% points is 0.060 cm^{-1}. The coated rejector plate is seen to provide far more discrimination than is necessary, but as a result of this, its tuning is

FIGURE 5·51 a



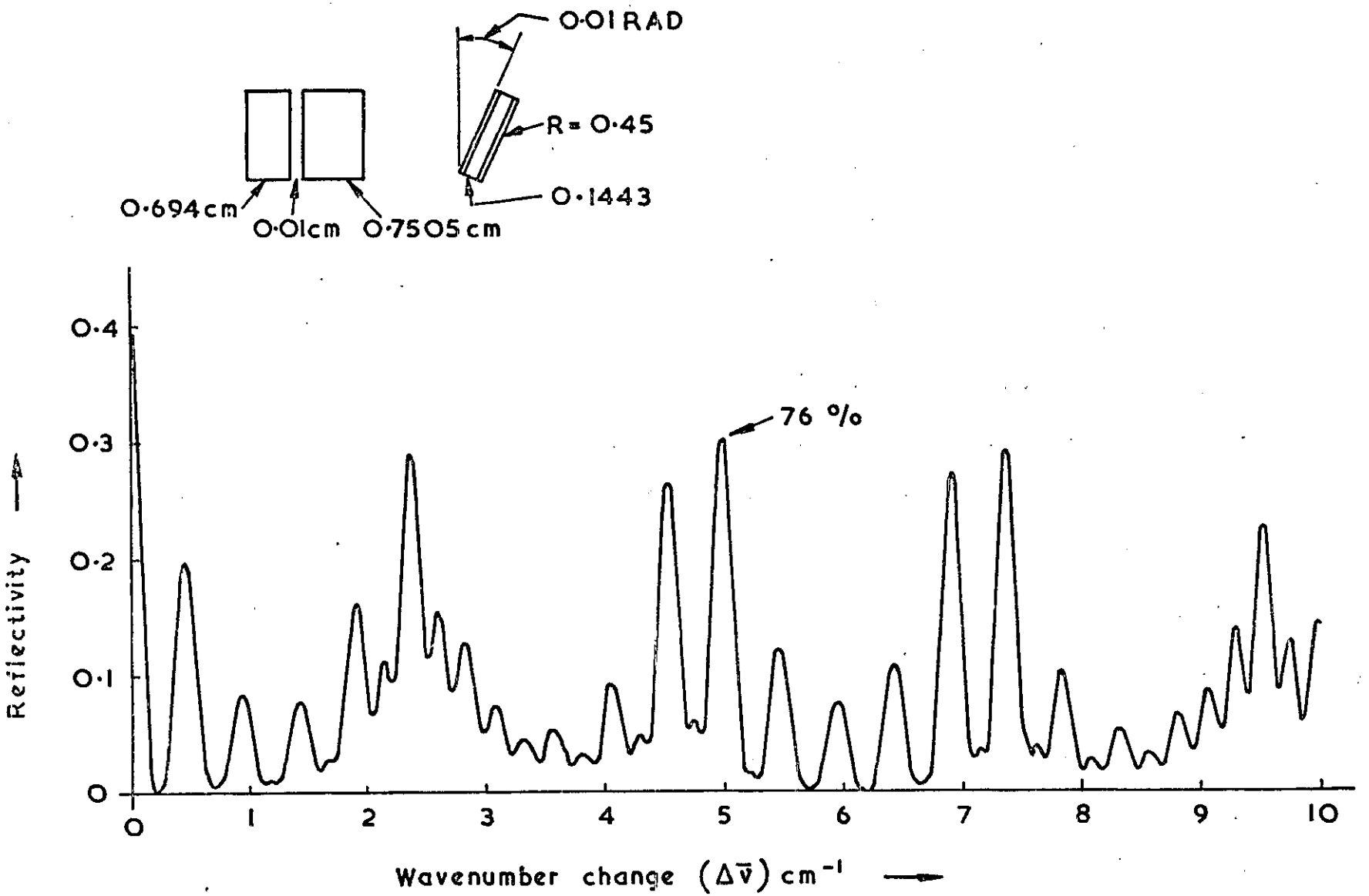
Reflectivity of Resonant Reflector (2 plate)

FIGURE 5.51 (b)



Reflectivity of Resonant Reflector (3 plate)

FIGURE 5·51(c)



Reflectivity of Resonant Reflector (3 plate)

very much less critical and correct operation of the reflector + rejector is easily achieved. The coated reflector we have tried has been very effective but there has been a tendency for the coatings to damage at high power densities (> 100 MW/cm^2). The wavenumber discrimination of the tilted etalon increases with the refractive index of the material (higher reflectivity per surface) so that a high index glass or crystal might be an alternative to the silica plate with coated surfaces. The use of different materials in the reflector + rejector system however was shown in paragraph 5.6.4.2, to lead to detuning with a change in temperature, and consequently a rejector plate of this form was not used.

5.7.1.2 Experimental Measurements

Spectral measurements on the output at 1.06μ of the Nd:glass laser were made using an adjustable spacing Fabry-Perot etalon in the manner previously described (para. 5.5.1.2). Fig. 5.19 showed the experimental arrangement. The etalon was adjusted using a He-Ne laser, as described in Paragraph 5.5.1.2. A correction for the change in focal length of the fringe-focussing lens with the change from 0.632μ to 1.06μ was calculated and introduced. IZ plates, hypersensitized in 4% ammonia solution, were used to record the Fabry-Perot rings at 1.06μ. Fig. 5.52 is the interferogram recorded with the two plate resonant reflector (specified above) as resonator output reflector, and working at 20% above threshold.

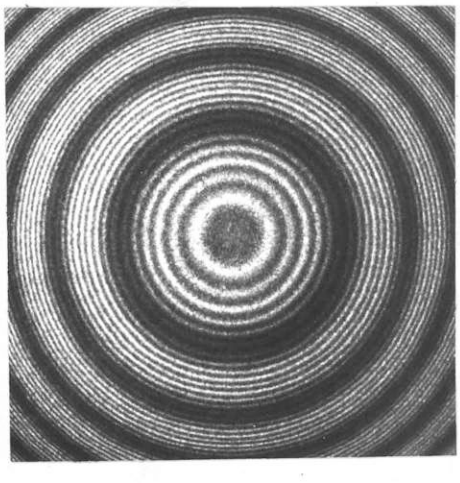


FIGURE 5.52

Fabry-Perot interferogram of a Nd:glass laser with a two-plate resonant reflector.

Plate thicknesses --- 7.0mm:7.5mm
Plate separation --- 0.10mm
Free spectral range --- 4.5cm^{-1}

Seven components are observed as compared to the expected number of six. Employing the method described in paragraph 5.5.1.2. the absolute wavelength of one component and the wavenumber separation of the components were found, by measurement of the interferogram, to be 1.06μ and 0.48 cm^{-1}, which agree with the expected values. The uncoated silica rejector plate was introduced at a known small angle (ϕ) and an interferogram recorded (Fig. 5.53).

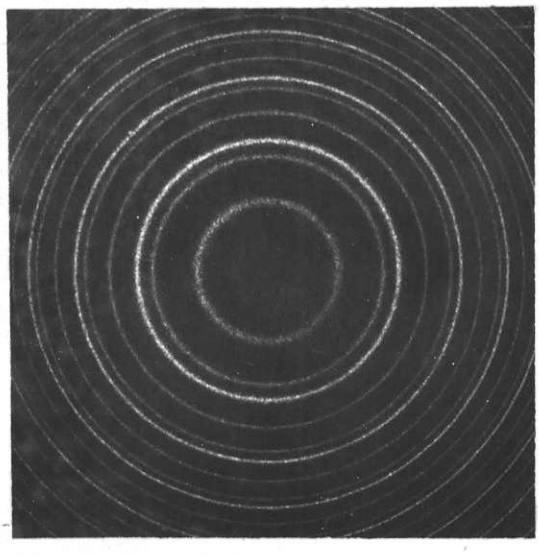


FIGURE 5.53

Fabry-Perot interferogram of a Nd:glass laser with a two-plate resonant reflector and a rejector plate at arbitrary angle.

Rejector plate thickness = 2.0mm
Free spectral range = 4.5cm^{-1}

From this and the interferogram of Fig. 5.52 the tuning error of the arbitrarily chosen angular setting of the rejector plate was calculated. Fig. 5.54 shows the power spectral distribution calculated from Figs 5.52 and 5.53. By correlation between these spectra, the position of the rejector plate minimum loss wavenumber was estimated to require a wavenumber shift of 0.48 cm^{-1}. The angular change required can now be calculated, since angle and wavenumber are related by:-

$$2t\cos\theta = (n+\tfrac{1}{2})\lambda \quad \text{for zero reflectivity.}$$

where t = plate thickness

n = integer

λ = wavelength = $1/\bar{\nu}$

θ = angular off-set of the refracted ray in the plate.

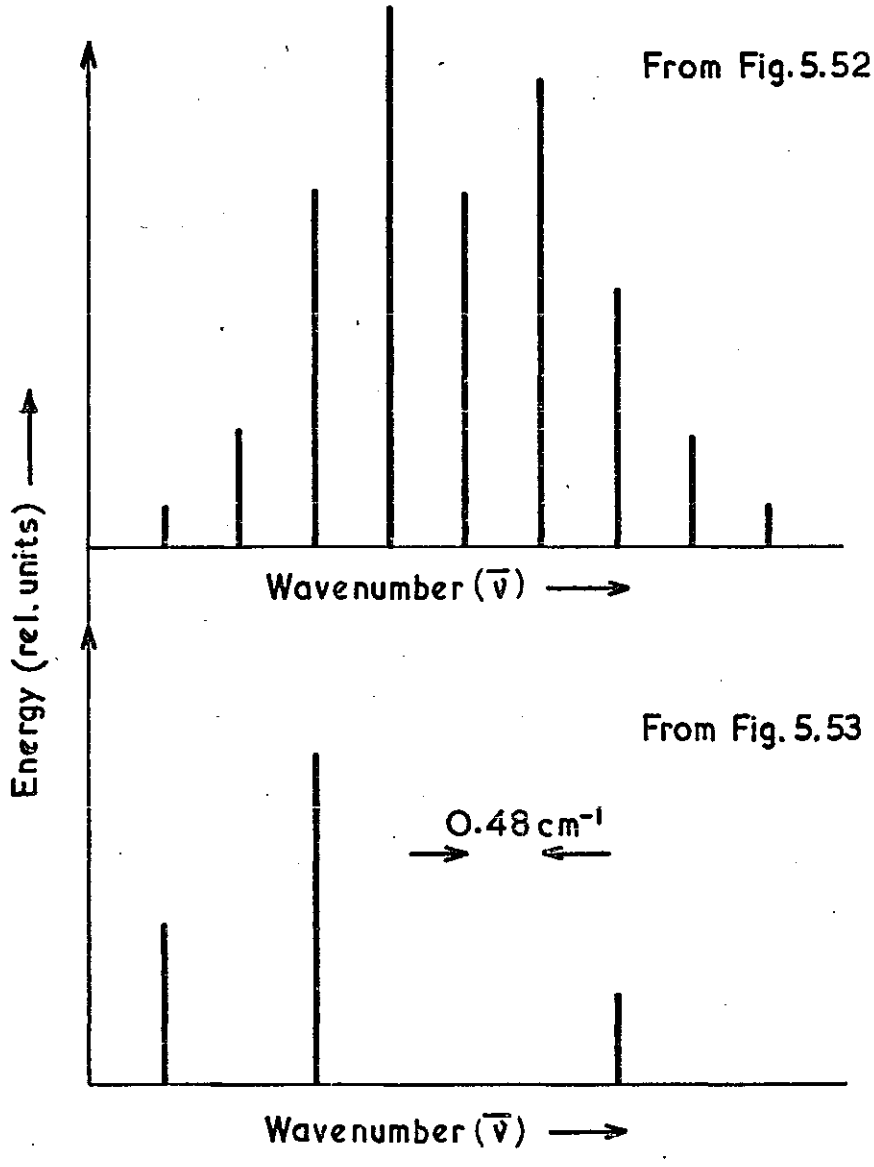


FIG. 5.54 SPECTRAL ANALYSIS OF FABRY-PEROT RINGS SHOWN IN FIG.5.52 AND FIG.5.53

for θ small:-

$$2t\left(1 - \frac{\theta^2}{2}\right) = (n+\tfrac{1}{2})\lambda \qquad \ldots (5.72)$$

Changing the angle slightly from θ to $\theta+\delta\theta$ results in a change of wavelength from λ to $\lambda+\delta\lambda$:-

$$\text{where} \quad 2t\left(1 - \frac{[\theta+\delta\theta]^2}{2}\right) = (n+\tfrac{1}{2})(\lambda+\delta\lambda) \qquad \ldots (5.73)$$

Subtracting 5.72 from 5.73 and dividing by t.

$$\frac{\delta\bar{\nu}}{\bar{\nu}} = -\frac{\delta\lambda}{\lambda}\,\frac{2\theta\delta\theta+(\delta\theta)^2}{2-\theta^2} \simeq \theta\delta\theta + \frac{(\delta\theta)^2}{2} \text{ for small } \theta. \qquad \ldots (5.74)$$

This equation enables the necessary angular tilt $(\delta\phi)$ of the rejector plate to be calculated from the required wavenumber change $(\delta\bar{\nu})$, since, for small angles, ϕ is related to θ by $\phi = \mu\theta$. Having made this tuning adjustment a Fabry-Perot interferogram was recorded and is shown in Fig. 5.55.

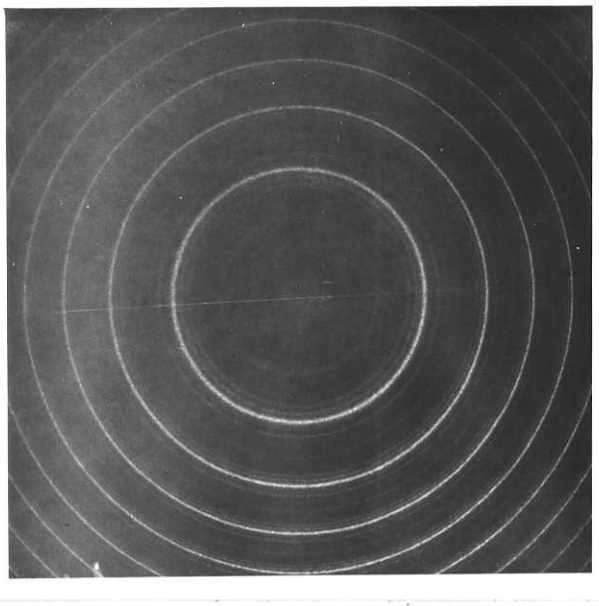


FIGURE 5.55

Fabry-Perot interferogram of a Nd:glass laser with a two-plate resonant reflector and a rejector plate at optimum angle.

Free spectral range = 4.5cm^{-1}

The output spectral purity was shown, by recording interferograms at different times and different laboratory temperatures, to be independent of temperature. This was predicted in paragraph 5.6.4.2.

The discrimination of both the resonant reflector and the rejector plate approaches but does not quite reach the theoretical limit. The two likely causes are:- (i) thickness variations of the flats across the working area. These might be about $\lambda/20$ (a flat worked to a tenth wave/cm and a working diameter of 5 mm) resulting in a shift of 1/20 of the order spacing of the reflectivity vs wavenumber curve of one part of the incident beam relative to another. If the thickness of one part of the flat is in tune with the other spacings, then another part is slightly out of tune and the latter selects a different spectral range to the former. In the above case with the extreme curves relatively displaced by 1/20 × order spacing, the sum of the spectral widths of all points in the beam is just increased by 1/20 of the order spacing. But the output spectral width of a perfect plate is 1/6.35 of the order spacing. Thus the imperfection results in a 32% increase in the output spectral width or a 32% decrease in the discrimination and:- (ii) A finite range of angles present in the laser beam. This range was always < 2 mrad. Its effect is entirely equivalent to a thickness change (δt) given by:-

$$2t\cos\delta\theta = 2(t-\delta t)\cos\theta \approx 2(t-\delta t).$$

where $\delta\theta$ = max. angle to the axis inside the flat

= $1/\mu$ × max. angle of incident rays

= $1/\mu \times \frac{1}{2}$ × angular range of incident beam

putting $\cos\delta\theta = 1-(\delta\theta)^2/2$ and rearranging:-

$$2\delta t = t(\delta\theta)^2 = \frac{t}{4\mu^2}\,(\text{angular range})^2$$

Let angular range = 2 mrad and $t = 10^4\lambda$

$$\therefore \qquad \delta t = \lambda/420$$

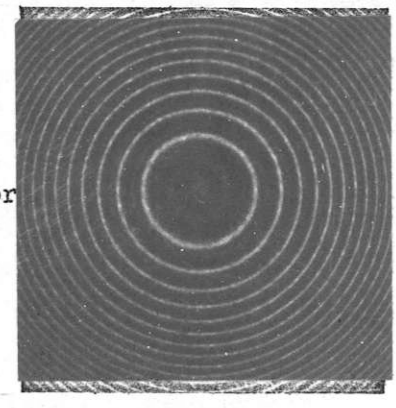
The effect of the angular range is negligible under these conditions.

To eliminate the small components present in the output spectrum, the uncoated silica rejector plate was replaced by one coated with a hard high index material. (Zirconium oxide-$\mu = 2.19$). The same tuning procedure was performed with a result shown in Fig. 5.56, in which only one component is visible.

FIGURE 5.56

Fabry-Perot interferogram of a Nd:glass laser with a two-plate resonant reflector and a coated rejector plate at optimum angle.

Free spectral range = $0.205 cm^{-1}$



The tolerance on tuning was found to be considerably higher, again as expected.

The spectral width of the single component of Fig. 5.56 was measured as indicated in paragraph 5.5.1.2. It was found to be $0.030\ cm^{-1}$ and, since this was about equal to the resolving limit of the Fabry-Perot, the actual width is likely to be considerably less than this.

5.7.2 Transverse Coherence

5.7.2.1 Fig. 5.31 (c) shows the transverse coherence, measured by the holographic technique, of one point with respect to the horizontal diameter across the output beam of the Nd:glass laser with second harmonic generation. There is a useful coherence over approximately 0.3 of the diameter. A

similar curve measured from the same hologram showed that along a vertical diameter the beam has appreciable coherence over about 0.5 of this diameter. Thus it follows that 0.3×0.5 of the output energy at 0.53 μm can be regarded as coherent (a coherent beam of this energy can be obtained by filtering). This is a high proportion for a laser with a plane parallel resonator of Fresnel number 10 particularly in view of the degradation of the transverse coherence in the second harmonic crystal (see chapter 6). As discussed previously this is probably due to the spatial averaging effects of the spinning prism Q-switch and to the shortness of duration of the laser pulse (for a plane parallel resonator the modes remain coherent with each other over an appreciable time - see Fig. 5.8). This coherence measurement is our datum point against which all methods of improving the transverse coherence can be compared. For each method we can measure the drop in output energy and the increase in coherence and calculate the energy that can be regarded as coherent. This must be more than the reference value for that method to be effective.

Four methods of improving the transverse coherence have been considered experimentally:

(i) Usual aperture method

(ii) Introduction of a Galilean telescope arrangement inside the resonator

(iii) Introduction of lenses inside the resonator to compensate for optical distortions in the laser-rod

(iv) Operation of the laser in an 'unstable' resonator configuration

Apart from the third method which just improves the mode discrimination processes already present, the methods chosen are those which give high stability of mode. This is important in the laser under investigation because the optical distortions are large (see chapter 4) and would prevent

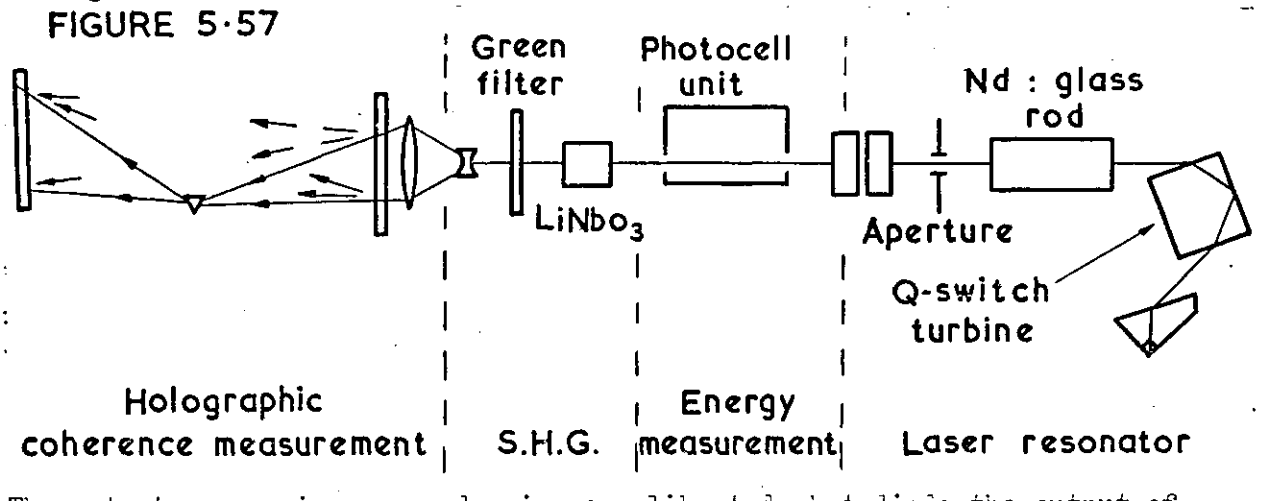
single mode operation in less stable situations. The price one has to pay for this mode stability is the increase in loss which the optical distortions give in these methods, and the decrease in output energy which results from this increased loss will dictate whether the method is worth employing.

5.7.2.2 Aperture Method

An aperture introduced into the resonator reduces the Fresnel number and so increases the discrimination against higher-order modes. As the aperture radius is reduced fewer modes have appreciable energy and the transverse coherence increases. However a smaller volume of the rod is available to the modes that do oscillate and there is a fall in the output energy. The other major effect of the reduction in aperture radius is that the mode stability increases due to the decrease in optical distortion across the aperture, the more so because it is possible to choose the part of the rod with least distortion). It is interesting to note that, even with high quality rods and uniform pumping geometry single mode beams of diameter more than 3 mm are very difficult to achieve.

The effect on the output energy and coherence of an intracavity aperture was investigated using the experimental arrangement shown diagrammatically in Fig. 5.57.

FIGURE 5·57



The output energy is measured using a calibrated photodiode the output of which is integrated in a suitable capacitor and the voltage across the

capacitor is displayed on an oscilloscope. The transverse coherence is measured using the holographic method of paragraph 5.52. The measurement is made on the second harmonic, generated by passing the infra-red output beam through a nonlinear phase-matched crystal. ($LiNbO_3$ in this case).

The measurements were made with no aperture in the resonator and with the laser at 35% above threshold with a Q-switch prism speed of 60,000 r.p.m. In this case the output energy at 1.06μ was 400 mJ and a measure of the transverse coherence is given by Fig. 5.31(c). The coherent fraction of the output is $0.15 \times 400 = 60$ mJ.

An aperture of 2.5 mm diameter was introduced in the resonator close to the output reflector. The output energy at the same input was now 84 mJ and Fig. 5.58 is the curve of transverse coherence which corresponds to Fig. 5.31(c). It can be seen that there is no increase in coherence to compensate for the large reduction in output energy. The coherent fraction of the output is now only $0.15 \times 84 = 13$ mJ. The large drop in output is due not only to the reduction in usuable rod volume but also to the increase in threshold that accompanies a smaller aperture in a laser with a spinning mirror Q-switch (Chapter 3). The failure of the aperture to improve the coherence probably arises because the beam passing up and down the unapertured resonator is already only 2.5 mm in diameter. The rod is already effectively apertured by optical distortions within it, these distortions causing rays passing near the edge of the rod to be lost in one round trip of the resonator. The output beam, integrated in time, appears however larger than 2.5 mm because it is swept across the output mirror by the Q-switch. This sweeping helps the beam to collect more energy from the rod (by passing through different volumes) and also may improve the coherence by averaging to some extent over the optical distortions in the rod.

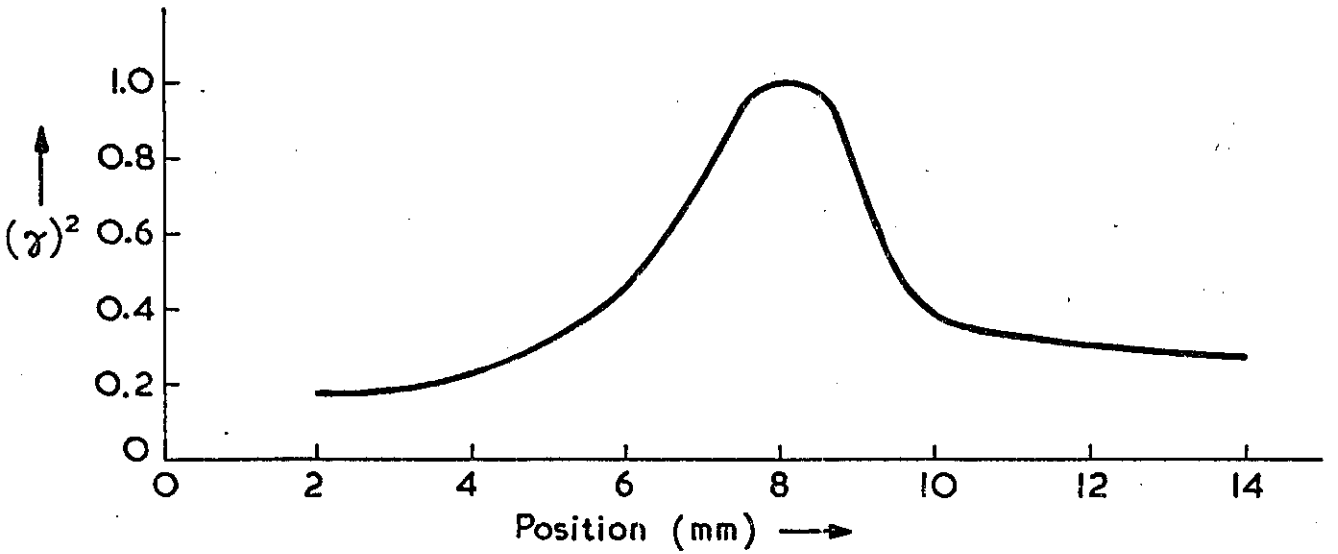


FIG. 5.58 TRANSVERSE COHERENCE ACROSS A HORIZONTAL DIAMETER WITH RESPECT TO THE CENTRE OF A Nd:GLASS LASER + SHG WITH 2·5mm INTRACAVITY ETALON.

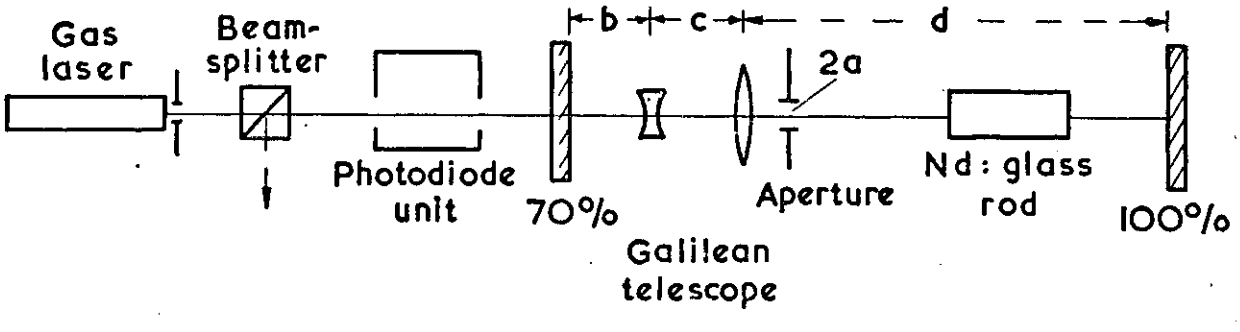
One final point on this method which further decreases its acceptability: damage was experienced to the surface of one of the silica resonant reflector plates when an aperture was present. This underlines the necessity of a transverse coherence control which does not significantly increase the power density near the resonator components.

5.7.2.3 Galilean Telescope

This method of transverse coherence control as discussed in paragraph 5.6.3.4, reduces the Fresnel number without decreasing the mode diameter in the laser rod and without increasing the resonator length. It should, therefore, be efficient. It should also give high mode stability but with increased loss, the amount of this loss depending upon the optical distortions in the laser rod.

The principle feature of an experiment investigating this method is to find out if the advantage of large mode volume in the rod outweighs the disadvantage of increased losses, and to do this a comparison is made against another method, such as the aperture method, where the mode volume and losses are smaller. Figure 5.59 shows the experimental arrangement used.

FIGURE 5·59



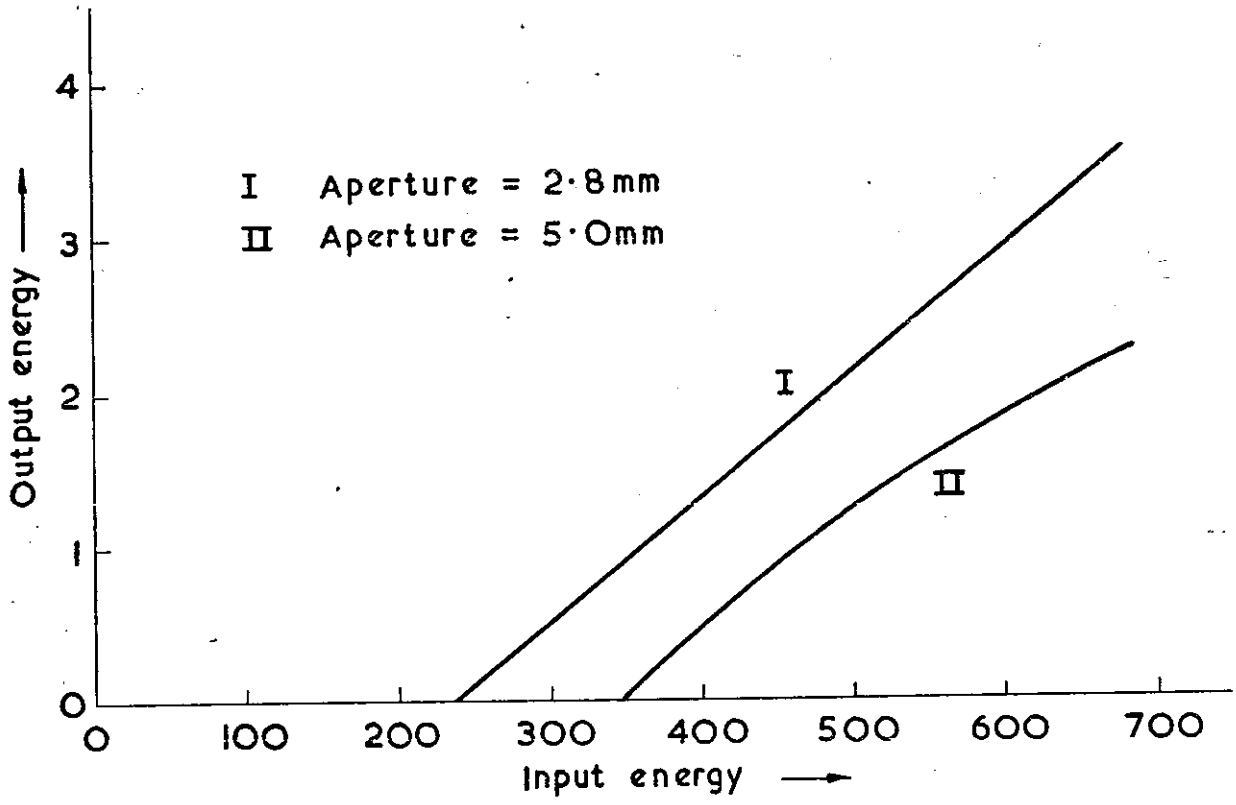
The gas laser and beamsplitter are used for aligning all the resonator components and, to remove the possibility of damage to them, are masked off when the laser is operated. The photodetector unit contains an integrating capacitor so that, when the output is displayed on an oscilloscope, a direct

reading of the output energy of the laser is obtained. The experiment is essentially that of translating the Galilean telescope down the resonator, maintaining the Fresnel number at 1.0 by introduction of an aperture of the correct size, and measuring the input-output curve of the laser. As the telescope is moved towards the rod (increasing b) the aperture size (at the rod end) for a Fresnel number of 1 increases giving a larger mode volume in the rod. By choosing a Fresnel number of 1 in a plane parallel resonator, single transverse mode operation is assured and the comparison between the different positions of the Galilean telescope is a valid one. Also, to ensure a valid comparison, the two lenses were adjusted for maximum output at about twice threshold. Figure 5.60 plots out the input-output characteristic for two values of mode diameter in the rod (2.8 mm and 5.0 mm). There is a significant increase in threshold as expected when the mode diameter in the rod is increased. For the considerable degree of rod distortion due to pumping with the elliptic cylinder configuration however this increased rod volume is not sufficient to result in increased output. This method is not a profitable one with the present rod and pumping geometry. It would prove otherwise for more uniform pumping of the laser rod.

5.7.2.4 Compensating Optics

The preceding paragraphs have shown that transverse mode selection techniques become inefficient when the optical distortions of the rod become large, as is the case with the Nd:glass rod pumped in an elliptic cylinder. Having measured the rod optical distortion (Chapter 4 paragraph 4.2.2.1), and having shown in particular that it is heavily asymmetric, it was not surprising that little success was achieved with the two techniques already described. It might be expected however that a first order compensation of the optical distortion would give a significant improvement, and we have attempted to do this both with and without the intracavity Galilean telescope.

FIGURE 5·60



EFFICIENCY CURVES FOR RESONATOR WITH GALILEAN TELESCOPE

The measurements in Chapter 4 show that to a first order the rod becomes a cylindrical lens with optical power given by Fig. 4.18. This showed that at 675 joules (roughly twice threshold for the Galilean telescope measurements of the preceding paragraph) the rod becomes roughly a cylindrical lens of power + 1.3 Dioptres. A lens of this power was introduced into the resonator (Galilean telescope included) in the correct orientation and adjusted to give maximum output at 675 joules. This output was however small compared to that without the cylindrical lens and it is concluded that the rod distortion is not uniform enough to be adequately approximated as a cylindrical error. Although the overall shape of a transmitted wavefront was improved the detailed shape over the small area used by the laser beam was probably degraded.

5.7.2.5 'Unstable' Resonator

Referring to paragraph 5.6.1.1, it is seen that the unstable resonator provides better transverse mode discrimination and a larger mode diameter (increased efficiency) but the laser threshold will be higher due to increased losses.

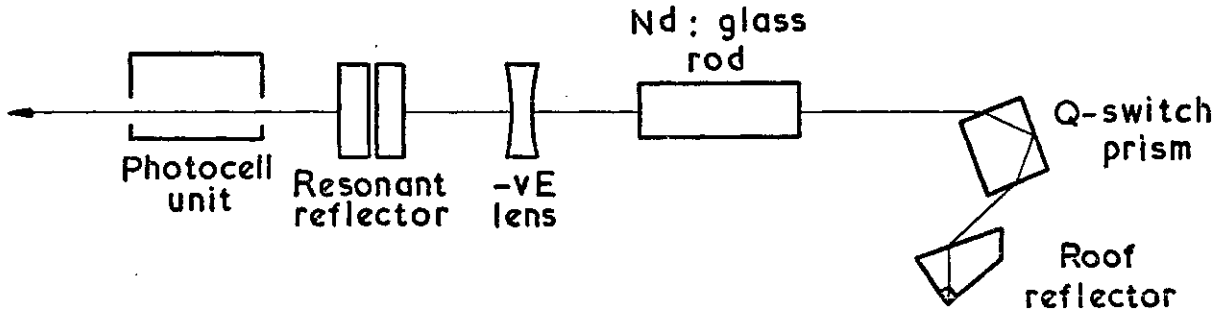
The important questions to be answered when considering this type of resonator with a particular laser system are:-

(i) what is the optimum confocal parameter?

(ii) At this optimum, does the increase in efficiency justify the increase in threshold?

We attempted to investigate these points with our Nd: glass laser by varying the confocal parameter in the unstable regime. The experimental arrangement is shown in Fig. 5.61.

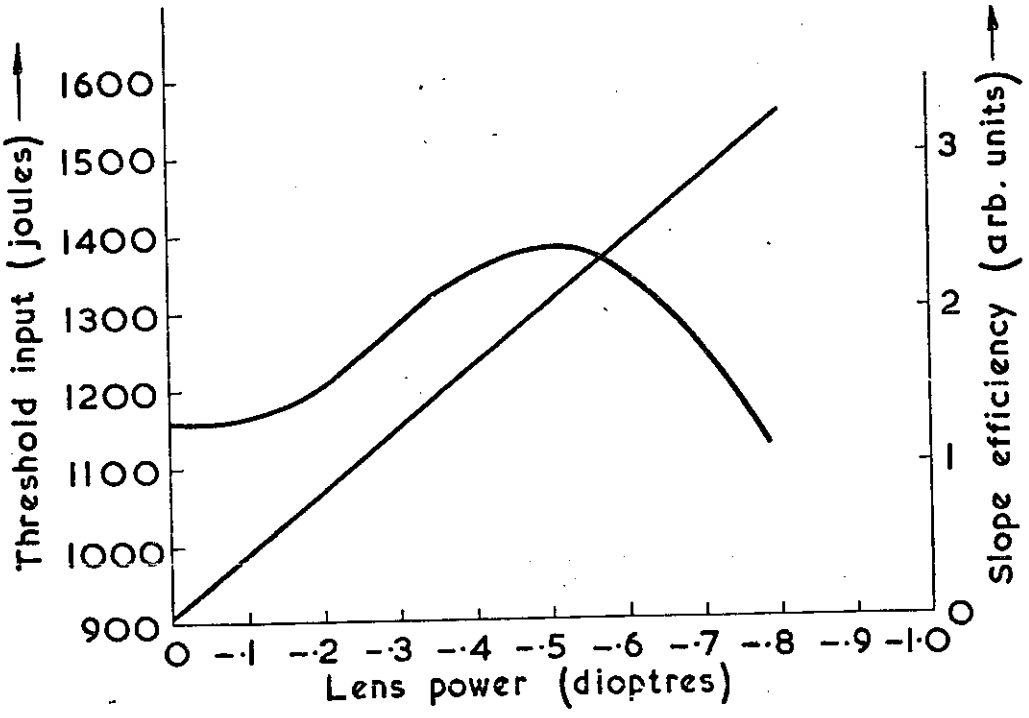
FIGURE 5·61



A negative lens is introduced inside the resonator to make it 'lossy' or 'unstable', and by increasing the power of the lens the confocal parameter is increased further into the unstable regime. Fig. 5.62 plots the threshold and slope efficiency as a function of lens power, these values being obtained directly from laser input/output curves measured for each intracavity diverging lens. It can be seen that at the optimum the slope efficiency has increased by about 100% while the threshold has risen by about 45%. A better way of expressing this is that this unstable resonator configuration has an higher 'overall' efficiency only at an input greater than 90% above the minimum threshold (occurring without any lenses). Since it is undesirable to operate the laser at such a high input level, this type of resonator must be regarded as unprofitable with this particular laser operating under the particular conditions prevailing.

5.7.2.6 Although the various methods of improving the transverse coherence (or the fraction of the output energy that can be regarded as coherent) have been largely unsuccessful, due principally to the severe nature of the optical distortions in the rod (which occur with the pumping geometry employed), only modest improvements in the uniformity of pumping would enable these techniques to be effective.

FIGURE 5·62


Threshold input (joules)
1600
1500
1400
1300
1200
1100
1000
900
Slope efficiency (arb. units)
3
2
1
0
0 -·1 -·2 -·3 -·4 -·5 -·6 -·7 -·8 -·9 -1·0
Lens power (dioptres)

CHAPTER 6

Second Harmonic Generation

6.1	Abstract	6.1
6.2	Theory of Second Harmonic Generation	6.3
6.2.1	Simplified Analysis	6.3
6.2.1.1	Solution for small conversion efficiency	6.5
6.2.1.2	Phase matching	6.9
6.2.1.3	Solution for phase matched crystal and appreciable conversion	6.12
6.2.1.4	Solution with absorption in the fundamental	6.14
6.2.1.5	Lateral displacement limit	6.16
6.2.1.6	Limitations of long crystals	6.16
6.2.1.7	Power and Energy conversion	6.17
6.2.1.8	Transverse mode conversion	6.18
6.2.1.9	Spectral conversion	6.20
6.2.1.10	Transverse coherence conversion	6.21
6.2.1.11	Intracavity conversion	6.21
6.2.1.12	Efficiency improvement by focussing	6.22
6.2.2	More Exact Analyses in the Literature	6.23
6.3	Experimental Investigations	6.24
6.3.1	Tolerance of phase matching angle	6.25
6.3.2	Second harmonic efficiency curve	6.26
6.3.3	Temporal evolution of fundamental and second harmonic	6.26
6.3.4	Methods of improving second harmonic efficiency	6.28
6.3.4.1	Focussing	6.28
6.3.4.2	Transverse mode control	6.30
6.3.4.3	$LiNbO_3$ outside the resonator	6.31
6.3.4.4	$LiNbO_3$ inside the resonator	6.32
6.4	Conclusions	6.33

CHAPTER 6

6.1 Abstract

The Nd:glass laser emits radiation at 1.06 μm. Since the eye and all photographic emulsions (and particularly those suitable for holography) are insensitive to this wavelength, it is essential, for this laser to have value in the field of optical measurement, to transfer as much as possible of the energy at 1.06 μm into energy at another more suitable wavelength. The only process capable of a high enough conversion efficiency is that of second harmonic generation in certain nonlinear crystals. This process converts some of the radiation at 1.06 μm into light at the very useful wavelength of 0.53 μm.

The first observation of any nonlinear optical effect was the second harmonic conversion of a free running ruby laser reported by Franken et al (1961). In the following years the phenomenon attracted a great deal of interest, particularly when significant conversion efficiencies were achieved following the discovery of Q-switching techniques in 1962. Since then a great deal of experimental evidence has become available for the second harmonic generation (SHG) of the outputs of all the common types of laser and some workers, notably Volosov (1969) with 65% in KDP and Hagen (1969) with 51% in KDP have achieved very high conversion efficiencies. The various techniques that have been used to achieve efficient conversion efficiencies are (i) to use phase-matchable crystals such as KDP (Maker et al 1962) (ii) to use more efficient crystals such as $LiNbO_3$ (Miller et al 1965), $Ba_2NaN_5O_{15}$ (Geusic et al 1968) and $LiIO_3$ (Nath et al 1969) (iii) to focus the fundamental into the crystal (Bjorkholm 1966), (iv) to place the crystal inside the resonator (Wright 1963, Smith 1970) (v) to improve the mode properties of the fundamental (Hagen 1969) (vi) to mode lock the

fundamental (Bass and Andringa 1967, Osterink and Foster 1968). Many workers have, right from the first reported observation in 1961, attempted to place the phenomenon on a sound theoretical basis. Some notable papers giving a general theory are by Armstrong et al (1962) Bloembergen (1965) Kleinman (1962), and Pershan (1966) while other authors, including those mentioned above, have concentrated on particular aspects of the process. Further information concerning the irreproducibility and low conversion efficiency when using a multimode fundamental has been obtained by for example Ducuing and Bloembergen (1964) and Grütter et al (1969) using statistical analyses. The problem with forming a satisfactory theoretical analysis of second harmonic generation, and other nonlinear optical effects, is that one is concerned with an interaction (with tensor character) of a crystal with an incident (often complex) radiation field. This complex situation must be simplified for the problem to be tractable. The tendency has been to simplify as little as possible and this has in general called for fairly sophisticated and somewhat unpalatable mathematics and it is sometimes difficult to see how the real situation is related to the theory. We have aimed in this chapter at the simplest possible approach and have been able to demonstrate most of the principal properties of second harmonic generation. In one or two instances in fact, much more quantitative information than expected is obtained, showing that for these properties the simpler approach is as accurate as and more effective than more detailed analyses.

An outline of the theory of second harmonic generation will be given including the derivation of the condition for phase matching and a discussion of the effects of focussing the fundamental (1.06 μm) into the crystal and the effects of the fundamental being multimode.

Measurements of the second harmonic conversion efficiency made on the Nd:glass laser in its original form will be described, the conversion taking

place in a crystal of ammonium dihydrogen phosphate (ADP) placed directly in front of the laser.

Following a discussion of these preliminary measurements, the various possibilities for improving the efficiency will be listed and a critical assessment of their various advantages and disadvantages given.

Several methods of improving the efficiency of second harmonic generation (SHG) will be investigated experimentally in an attempt to maximise the amount of green light available. Factors of importance, apart from the efficiency and how it depends upon the fundamental intensity, are the reproducibility of the green output, its spatial and angular distribution and its coherence.

6.2 The Theory of Second Harmonic Generation

It will be valuable to separate this section into two parts: one deals with the process of SHG (second harmonic generation) using a simplified treatment while the other comments on more rigorous treatments. The first part is intended to promote a better understanding of the physics of SHG and at the same time predict as much as possible of the operation of the process using very simple mathematics. It will be seen that it is possible to explain (i) the variation of the S.H. efficiency with the input intensity (ii) the phase matching condition (iii) the variation of the S.H. efficiency with the length of crystal and with its absorption (iv) the S.H. spectrum (v) some transverse mode effects and (vi) a qualitative measure of the effect of focussing the fundamental into the S.H. crystal. An exact mathematical theory must be formulated to give (i) the magnitude of the S.H. efficiency (ii) the effects on the S.H. efficiency of temperature and misalignment of the crystal (iii) the S.H. intensity distribution and coherence, and (iv) the quantitative effect of focussing on the S.H. process.

6.2.1 From Maxwell's equations one derives the wave equation for a non-magnetic and homogeneous medium:-

$$\nabla^2 \underline{E} = \frac{\mu_0}{c^2} \frac{\partial^2 \underline{D}}{\partial t^2} \qquad \ldots (6.1)$$

where $\underline{E}$ = electric field vector

$\underline{D}$ = electric displacement vector

Solution of this equation requires a knowledge of the material equation which relates the electric displacement to the electric field. This material equation is:-

$$\underline{D} = \varepsilon_0 \underline{E} + \underline{P} \qquad \ldots (6.2)$$

where P = 'polarization' = induced dipole moment per unit volume. The vector notation is dropped from here on, since we assume that $\underline{P}$ and hence also $\underline{D}$ is parallel to $\underline{E}$, and it then becomes redundant. This bulk dipole moment P arises by virtue of the electric field exerting forces on the elementary charged particles, causing displacements of those charges and hence elementary dipole moments (charge X displacement). The bulk moment P is proportional to the elementary moment which is related to E by the force-displacement law of the charged particles. If linearity is assumed, that the displacement is proportional to the force, then P is proportional to E or:-

$$P = \varepsilon_0 \chi E \qquad \ldots (6.3)$$

where $\varepsilon_0 \chi$ = constant and χ is called the 'susceptibility'. This is the assumption of classical electromagnetic theory and it leads to the well known propagation laws. The above assumption of linearity is a very valid one in all situations except those with extremely high electric fields. Only lasers can produce, without great difficulty, electric fields sufficient to make the classical theory invalid, and in this case the force-displacement

law becomes 'non-linear'.

In general this law can be expressed as a polynomial in increasing powers of E, the electric field. Thus:-

$$P = \varepsilon_0 [\chi E + \chi_2 E^2 + \chi_3 E^3 + \ldots] \qquad \ldots (6.4)$$

where χ_2 = 2nd order susceptibility

χ_3 = 3rd order susceptibility etc.

6.2.1.1 We will consider only the second order term which gives under the right conditions a very much larger effect that any higher order terms.

Thus we put

$$P = \varepsilon_0 [\chi E + \chi_2 E^2] \; . \qquad \ldots (6.5)$$

$\therefore$ from Equ. 6.2 and 6.5:-

$$D = \varepsilon_0 E + P = \varepsilon_0 (1+\chi) E + \varepsilon_0 \chi_2 E^2 \qquad \ldots (6.6)$$

and the wave equation (Equ. 6.1) becomes:-

$$\nabla^2 \underline{E} - \frac{\varepsilon_0 \varepsilon \mu_0}{c^2} \frac{\partial^2 E}{\partial t^2} = \frac{\mu_0 \varepsilon_0 \chi_2}{c^2} \frac{\partial^2}{\partial t^2} (E^2) \qquad \ldots (6.7)$$

where ε = permittivity = $(1 + \chi)$

As a first approximation, let the right hand side = 0. The equation now becomes just the linear wave equation. Take a typical plane wave solution of this linear equation:-

$$E = E_1 \cos (\underline{k}_1 . \underline{r} - \omega_1 t) \qquad \ldots (6.8)$$

and introduce it into the right hand side of the wave equation to obtain a next approximation. Equ. 6.7 becomes:-

$$\nabla^2 E - \frac{\varepsilon_0 \varepsilon \mu_0}{c^2} \frac{\partial^2 E}{\partial t^2} = \frac{\varepsilon_0 \chi_2 \mu_0}{c^2} \frac{\partial^2}{\partial t^2} \cdot \left[E_1 \cos(\underline{k}_1 \cdot \underline{r} - \omega_1 t)\right]^2$$

$$= \frac{\varepsilon_0 \mu_0 \chi_2 E_1^2}{2c^2} \frac{\partial^2}{\partial t^2} \left[1 + \cos 2(\underline{k}_1 \cdot \underline{r} - \omega_1 t)\right].$$

$$= -\frac{4k_1^2 \chi_2 E_1^2}{2\varepsilon_1} \cos(2\underline{k}_1 \cdot \underline{r} - 2\omega_1 t) \left[\text{using } \frac{c^2}{\varepsilon_0 \varepsilon \mu_0} = \frac{\omega^2}{k^2}\right]$$

... (6.9)

The solution of this equation must now contain a term at the second harmonic frequency ($2\omega_1 \equiv \omega_2$). Let the solution be:-

$$E = E_1 \cos(\underline{k}_1 \cdot \underline{r} - \omega_1 t) + E_2 \cos(\underline{k}_2 \cdot \underline{r} - \omega_2 t) \qquad \ldots (6.10)$$

Substituting for E and writing Equation 6.9 in the exponential form gives:-

$$\nabla^2 \left[E_1 \operatorname{expi}(\underline{k}_1 \cdot \underline{r} - \omega_1 t) + E_2 \operatorname{expi}(\underline{k}_2 \cdot \underline{r} - \omega_2 t)\right]$$

$$- \frac{\varepsilon_0 \varepsilon \mu_0}{c^2} \frac{\partial^2}{\partial t^2} \left[E_1 \operatorname{expi}(\underline{k}_1 \cdot \underline{r} - \omega_1 t) + E_2 \operatorname{expi}(\underline{k}_2 \cdot \underline{r} - \omega_2 t)\right]$$

$$= -\frac{4k_1^2 \chi_2 E_1^2}{2\varepsilon_1} \operatorname{expi}(2\underline{k}_1 \cdot \underline{r} - 2\omega_1 t) \qquad \ldots (6.11)$$

This equation now separates into two, one for each frequency:-

$$\nabla^2 [E_1 \exp i(\underline{k}_1 . \underline{r} - \omega_1 t)] - \frac{\varepsilon_0 \varepsilon_1 \mu_0}{c^2} \frac{\partial^2}{\partial t^2} [E_2 \exp i(\underline{k}_1 . \underline{r} - \omega_1 t)] = 0 \quad \ldots (6.12)$$

$$\nabla^2 [E_2 \exp i(\underline{k}_2 . \underline{r} - \omega_2 t)] \frac{\varepsilon_0 \varepsilon_2 \mu_0}{c^2} \frac{\partial^2}{\partial t^2} [E_2 \exp i(\underline{k}_2 . \underline{r} - \omega_2 t] = \frac{4k_1^2 \chi_2 E_1^2}{2\varepsilon_1} \exp i(2\underline{k}_1 . \underline{r} = 2\omega_1 t) \quad \ldots (6.13)$$

We are particularly interested in the second harmonic component, which is given by Equation 6.13. Remembering that we are considering a plane wave solution and assuming it to be travelling in the direction of $\underline{r}$, and allowing the electric field amplitudes to vary along the direction of propagation, the equation for the second harmonic component becomes, after differentiation:-

$$\frac{\partial^2 E_2}{\partial r^2} + 2ik_2 \frac{\partial E_2}{\partial r} = - \frac{4k_1^2 \chi_2 E_1^2}{2\varepsilon_1} \exp i(2\underline{k}_1 - \underline{k}_2) . \underline{r} \quad \ldots (6.14)$$

Assuming that the conversion is small and consequently that E_1 is approximately constant with respect to r and that the second derivative is very small, equation 6.14 becomes:-

$$\frac{\partial E_2}{\partial r} = i \frac{k_1^2 \chi_2 E_1^2}{k_2 \varepsilon_1} \exp i(2\underline{k}_1 - \underline{k}_2) . \underline{r} \quad \ldots (6.15)$$

Integrating with respect to r, putting in the boundary condition, that $E_2 = 0$ at $r = 0$, gives an expression for the second harmonic electric field:-

$$E_2 = \frac{k_1^2 \chi_2 E_1^2}{k_2 \varepsilon_1} \cdot \frac{[1-\exp i(\underline{\Delta k}.\underline{r})]}{\Delta k} \qquad \ldots (6.16)$$

where $\underline{\Delta k} = \underline{2k_1} - \underline{k_2}$

Since we are more interested in the intensities of fundamental and second harmonic, and since these are given by:-

$$I_1 = \sqrt{\varepsilon_1}\ E_1 E_1^* \quad \text{and} \quad I_2 = \sqrt{\varepsilon_2}\ E_2 E_2^*$$

Equation 6.16 can be quickly converted to give the relationship between intensities:-

$$I_2 = \frac{\sqrt{\varepsilon_2}}{\varepsilon_1} \left(\frac{k_2 \chi}{4\varepsilon_2} \right)^2 \cdot I_1^2 \cdot \left(\frac{\sin \frac{1}{2}(\underline{\Delta k}.\underline{r})}{\frac{1}{2}\Delta k} \right)^2$$

where we have also used the identity $\dfrac{k_1^2}{\varepsilon_1} = \dfrac{k_2^2}{4\varepsilon_2}$.

Finally since the refractive index $n = \sqrt{\varepsilon}$:-

$$I_2 = \frac{k_2^2}{16 n_1^2 n_2^3} \cdot \chi^2 \cdot I_1^2 \cdot \left[\frac{\sin \frac{1}{2}\Delta k r}{\frac{1}{2}\Delta k} \right]^2 . \qquad \ldots (6.17)$$

where the intensity I is Poynting's Vector and is 'power per unit area'. It has been shown that if the electric field is of sufficient magnitude to induce an appreciable nonlinear polarization then, as that electric field propagates through the medium, an appreciable fraction of it is converted into the second harmonic, and, at any point in the medium, the SH intensity is approximately given by Equation 6.17.

6.2.1.2 The salient features of this equation are:-

i) The S.H. intensity is proportional to the square of the fundamental intensity.

ii) The S.H. intensity is an oscillatory function of distance along the direction of propagation. The characteristic distance (r_c), which is that separating neighbouring peaks, is given by:-

$$r_c = 4\pi/\Delta k = 4\pi/(2k_1 - k_2) \qquad \ldots (6.18)$$

iii) As Δk gets smaller, two effects occur. The peak S.H. intensity rises and the characteristic distance also rises.

If $\underline{\Delta k} = 0$, Equation 6.17 becomes:-

$$I_2 = \frac{k_2^2}{16n^2n_2^3} \cdot \chi^2 \cdot I_1^2 \cdot r^2 \qquad \ldots (6.19)$$

and I_2 increases quadratically (and indefinitely) with r. Thus long crystals should give efficient SHG, if $\underline{\Delta k} = 0$ can be satisfied. This condition for efficient conversion is called 'phase-matching' and to discover what is required, replace $\underline{\Delta k}$ by $\underline{2k_1} - \underline{k_2}$ to give

$$2\underline{k_1} = \underline{k_2} \qquad \ldots (6.20)$$

Now $|k_1| = \frac{2\pi n_1}{\lambda_o}$ and $|k_2| = \frac{2\pi n_2}{(\lambda_o/2)}$

where λ_o = wavelength of the fundamental in vacuo.

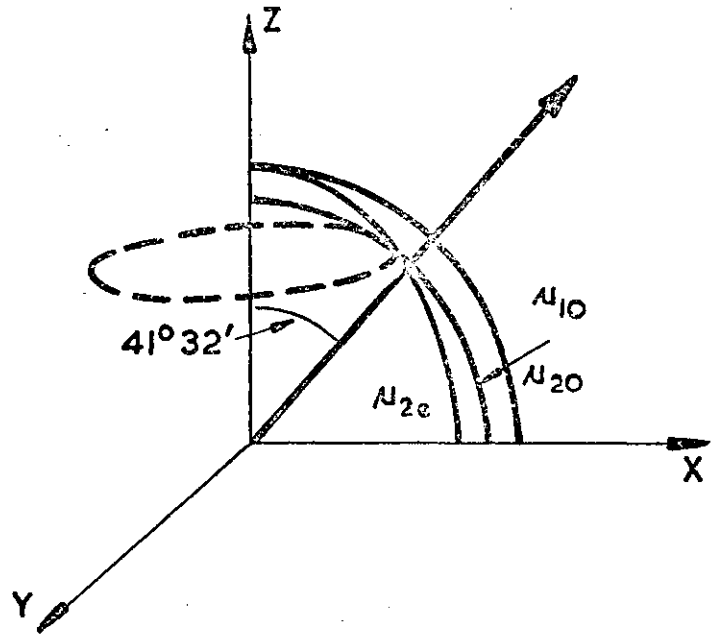
$\therefore$ the phase matching condition becomes:-

$$n_1 = n_2 \qquad \ldots (6.21)$$

and the fundamental and S.H. wave vectors must be in the same direction. Because of dispersion the condition $n_1 = n_2$ can only occur in a birefringent medium in which there are two refractive indices (an ordinary index n_o and an extraordinary index n_e) for each of the frequencies. For example, in a positive uniaxial crystal $(n_e > n_o)$ it is possible for n_{1e} to be equal to n_{2o} or in a negative uniaxial crystal for n_{1o} to be equal to n_{2e}. Fig. 6.1(a) demonstrates index matching in the negative uniaxial crystal ADP. It shows the loci of the two refractive index curves (ordinary and extraordinary) with respect to direction in the crystal for both the fundamental (1.06μ) and second harmonic frequencies (0.53μ) of the Nd:glass laser. A cone of directions at an angle of 41°32' to the optic axis satisfies the requirement that $n_{1o} = n_{2e}$. The requirement that the two relevant wave vectors must have the same direction is satisfied by cutting the entrance surface of the crystal normal to one of these directions i.e. at 90°-41°32' or 48°28' to the optic axis. Fig. 6.1(b) demonstrates the term 'Phase matching'. It shows the two fundamental and the two second harmonic wavefronts generated from a point on the surface. The extraordinary S.H. wavefront and the ordinary fundamental wavefront are seen to have a common tangent in the direction of propagation. This means that a plane wave at the fundamental, incident normal to the surface, generates a second harmonic plane wave which remains in step or in phase with it. The second harmonic wave is being continuously generated and it is expected that a maximum conversion is achieved when an already generated component is always in phase with a newly generated one. This is so in the situation shown in Fig. 6.1(b).

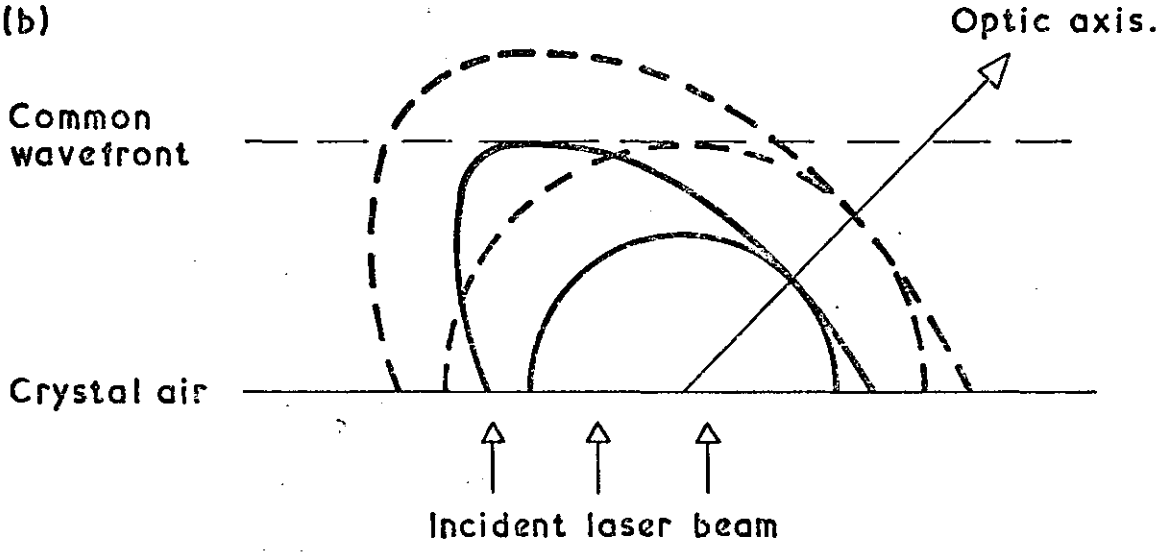
FIGURE 6·1

(a)



REFRACTIVE INDEX CURVES OF ORDINARY AND EXTRAORDINARY WAVES IN ADP AT 1·06 μ AND 0·53 μ SHOWING DIRECTION OF INDEX MATCHING.

(b)



– – – – Refers to ω_1

———— Refers to $2\omega_1$

Circles are ordinary wavefronts.
Ellipsises are extraordinary wavefronts.

WAVEFRONTS OF FUNDAMENTAL AND SECOND HARMONIC IN A SUITABLE NON-LINEAR CRYSTAL, SHOWING PHASE MATCHING.

A more general phase matching condition can be derived by extending the theory to cover the case of birefringent media. This extension differentiates between the two mutually perpendicular directions of polarization which characterise the ordinary and extraordinary waves.

Since, for phase-matched operation, an electromagnetic field polarized in one direction must generate a S.H. component in the other polarization and since that S.H. component can only be generated by a bulk dipole moment (P) having the same direction, there must be a nonlinear susceptibility which enables an electric field $E(\omega)$ of one polarization to create a bulk dipole moment ($P[2\omega]$ of the perpendicular polarization. Mathematically, if the two directions of polarization are indicated by subscripts x and y:-

$$P_y = \varepsilon_o \chi_{yx} E_x^2 \quad \text{where} \quad \chi_{yx} \neq 0 \qquad \ldots (6.22)$$

This equation is just the nonlinear part of Equ. 6.7 and leads to the same solution, this solution being that for the S.H. electric field polarized in the y-direction.

Equ. 6.22 can be extended to the general case, that there are susceptibilities, giving S.H. components, in all polarization directions arising from all possible pair products of electric fields in these directions.

$$\text{i.e.} \qquad P_y = \varepsilon_o [\chi_{yxx} E_x^2 + \chi_{yyy} E_y^2 + \chi_{yzz} E_z^2 + \chi_{yxy} E_x E_y + \chi_{yxz} E_x E_z + \chi_{yyz} E_y E_z] \qquad \ldots (6.23)$$

and similarly for P_x and P_z.

In our case $E_z = 0$, leaving three terms contributing to P_y (and similarly three more contributing to P_x). Disregarding the term in E_y^2 for which phase-matching cannot occur, let us turn our attention to the term $\varepsilon_0 \chi_{yxy} E_x E_y$. Use of this term as the nonlinear term in our wave equation for E_{zy} results in an alternative equation very similar to Equation 6.16; namely:-

$$E_{2y} = \frac{K_{1x}^2 \chi_{yxy} E_{1x} E_{1y}}{k_{2y} \varepsilon_{1x}} \frac{[1-\exp i\underline{k}.r]}{\Delta k} \qquad \ldots (6.24)$$

$$\text{where } \underline{\Delta k} = \underline{k}_{1x} + \underline{k}_{1y} - \underline{k}_{2y}$$

$\therefore$ the alternative phase matching condition becomes:-

$$\underline{k}_{1o} + \underline{k}_{1e} = \underline{k}_{2e} \text{ or } \underline{k}_{1o} + \underline{k}_{1e} = \underline{k}_{2o} \qquad \ldots (6.25)$$

For ADP, Equ. 6.25 can also be satisfied, but the direction of phase matching is now at 61°12' to the optic-axis and the entrance face must now be cut normal to this direction.

6.2.1.3 The analysis leading to Equ. 6.16 is not valid if significant conversion takes place and it is just this situation that is the most useful. The derivation of the generation of S.H., which takes account of the drop in fundamental intensity, is however not difficult under phase matched conditions. The differential equation to be solved is, by putting $\Delta k = 0$ in Equation 6.15, given by:-

$$\frac{dE_2}{dr} = i \frac{k_1^2 \chi_2 E_1^2}{k_2 \varepsilon_1} \qquad \ldots 6.26$$

we can also relate E_2 and E_1 by the 'conservation of energy': thus:-

$$I_o = I_1 + I_2 \quad \text{in a lossless medium}$$

where I_o = incident fundamental intensity.

$\therefore \quad \sqrt{\varepsilon_1} E_o E_o^* = \sqrt{\varepsilon_1} E_1 E_1^* + \sqrt{\varepsilon_2} E_2 E_2^*$ where Es are complex.

Now E_o and E_1 are real and E_2 is imaginary since Equ. 6.26 says that under phase matching all increments of the S.H. have a 90° phase shift from the fundamental.

$$\therefore \qquad \sqrt{\varepsilon_1} E_o^2 = \sqrt{\varepsilon_1} E_1^2 - \sqrt{\varepsilon_2} E_2^2 \qquad \ldots (6.27)$$

Eliminating E_1 from Equ. 6.26 using Equ. 6.27 gives:-

$$\frac{dE_2}{dr} = i \sqrt{\frac{\varepsilon_2}{\varepsilon_1}} A \left[E_o^2 \sqrt{\frac{\varepsilon_1}{\varepsilon_2}} + E_2^2 \right] \quad \text{where} \quad A = \frac{k_1^2 \chi_2}{k_2 \varepsilon_1} \qquad \ldots (6.28)$$

Integrating this equation gives:-

$$E_2 = \left(\frac{\varepsilon_1}{\varepsilon_2} \right)^{\frac{1}{4}} E_o \tan i \left[\left(\frac{\varepsilon_2}{\varepsilon_1} \right)^{\frac{1}{4}} x \, A E_o r \right] = i \left(\frac{\varepsilon_1}{\varepsilon_2} \right)^{\frac{1}{4}} E_o \tanh \left[\left(\frac{\varepsilon_2}{\varepsilon_1} \right)^{\frac{1}{4}} x \, A E_o r \right]$$

$\ldots (6.29)$

$$\therefore \quad \text{S.H. intensity} \quad I_2 = \sqrt{\varepsilon_2} E_2 E_2^* = I_o \tanh^2 \left(\frac{\varepsilon_2}{\varepsilon_1} \right)^{\frac{1}{4}} A E_o r$$

$\ldots (6.30)$

$$\therefore \qquad I_2 = I_o \left[1 - \frac{4}{e^{R} + e^{-R} + 2} \right] \qquad \ldots (6.31)$$

where $$R = 2 \left(\frac{\varepsilon_2}{\varepsilon_1} \right)^{\frac{1}{4}} \times AE_o r.$$

Fig. 6.2 plots the variation of the S.H. intensity with length of crystal. Also plotted is the fundamental intensity which is given by:-

$$I_1 = I_o - I_2 = \frac{4I_o}{(e^{R} + e^{-R} + 2)} \qquad \ldots (6.32$$

In particular at $\frac{1}{2}R = \left(\frac{\varepsilon_2}{\varepsilon_1} \right)^{\frac{1}{4}} \times AE_o r = 1$, $I_2 = 0.58I_o$. Thus for high S.H.G. efficiency, the crystal length must be of the order of r_c, where

$r_c = \frac{k_2 \varepsilon_1}{k_1^2 \chi_2 E_o} \left(\frac{\varepsilon_1}{\varepsilon_2} \right)^{\frac{1}{2}}$ and can be termed the characteristic conversion length.

For example, χ_2 for ADP $= 5.7 \times 10^{-3}$ M/volt

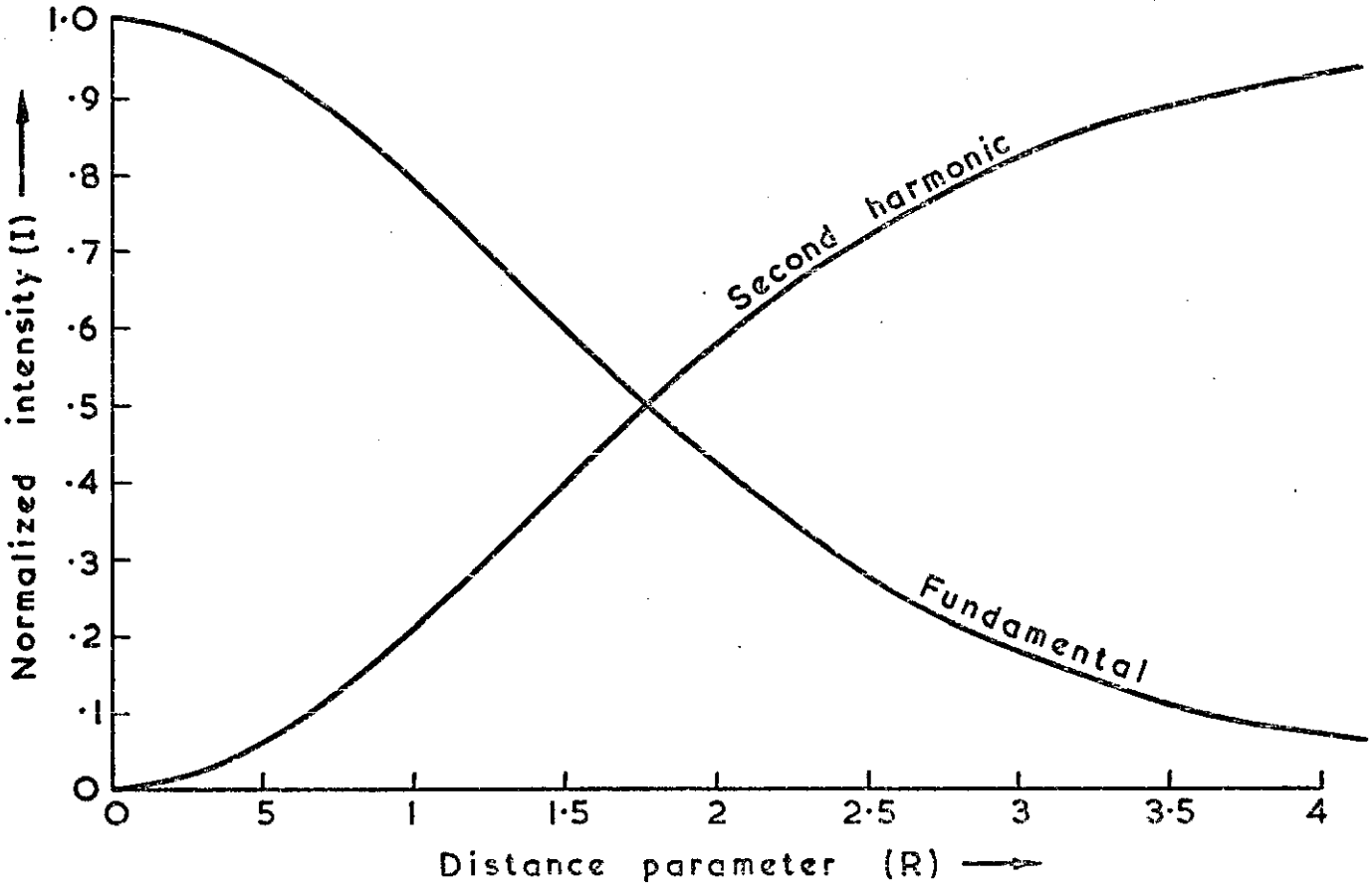
and $r_c = 6.3$ cm for an incident intensity of 100 MW/cm^2.

6.2.1.4 Absorption

The assumption made in the above analysis that the material is lossless is not valid for ADP which demonstrates a considerable loss at the fundamental. Such a loss at the fundamental can quite easily be included in the analysis since, if the loss coefficient $= \beta$, then the conservation of energy law has to be written:-

$$\frac{dI_1}{dr} = -\frac{dI_2}{dr} - \beta I_1 \qquad \ldots (6.33)$$

FIGURE 6.2



SECOND HARMONIC CONVERSION EFFICIENCY FOR DIFFERENT LENGTHS OF CRYSTAL

Substituting for I_1 from Equ. 6.26 gives:-

$$\frac{dI_1}{dr} = -\frac{dI_2}{dr} - \frac{\beta\sqrt{\varepsilon_1}}{iA}\frac{dE_2}{dr} \qquad \ldots (6.34)$$

and by integration:

$$I_1 = I_o - I_2 - \frac{\beta\sqrt{\varepsilon_1}}{iA} E_2 \qquad \ldots (6.35)$$

using this equation instead of:- $I_1 = I_o - I_2$ leads to an integrable equation the solution of which is:-

$$I_2 = I_o \left[\frac{Z}{\sqrt{1+D^2} + DZ} \right]^2 \qquad \ldots (6.36)$$

where $D = \dfrac{\beta\sqrt{\varepsilon_1}}{2A\sqrt{I_o}\varepsilon_2^{\frac{1}{4}}}$ and $Z = \tanh \dfrac{\varepsilon_2^{\frac{1}{4}} A}{\varepsilon_1^{\frac{1}{4}}} \sqrt{I_o^2 + D^2\sqrt{\varepsilon_1}.r}$

It can be seen that if the absorption parameter $D = 0$, this equation reduces to Equ. 6.31, which was derived assuming no loss.

In a particular case it would be interesting to compare the S.H. efficiencies (I_2/I_o) with and without loss.

The maximum efficiencies occur for very long crystals when $Z \to 1$

$$\text{and efficiency} = \frac{I_2}{I_o} = \frac{1}{1+2D^2+2D\sqrt{1+D^2}} \qquad \ldots (6.37)$$

for no loss, $D=0$ and <u>maximum efficiency = 1 (100%)</u>

with appreciable loss, take the case of ADP where the absorption depth

$(=1/\beta) \simeq$ a few centimeters, it requires a particularly high fundamental intensity for high conversion in this depth. Let the intensity be such that the lossless characteristic conversion length $r_c = 1/\beta$. For ADP, this intensity $\approx$ 100 MW/cm^2

$$\therefore \quad D = 0.5$$

$$\therefore \quad \underline{\text{maximum efficiency}} = \frac{1}{1+0.5+\sqrt{1.25}} = \underline{0.38(38\%)}$$

N.B. for lower fundamental intensities the maximum efficiency is even less.

6.2.1.5 Another important factor in the second harmonic process is indicated by Fig. 6.1(b). The direction of energy transfer in the S.H. generated beam is shown and is seen not to coincide with that of the fundamental generating beam. The two become laterally displaced and maximum conversion and independence of imperfections cannot occur since the S.H. field originating at some considerable distance into the crystal cannot then give a maximum amplitude addition with that originating at an earlier distance. The efficiency of SHG is reduced if $\ell\alpha \simeq d$ where

ℓ = length of crystal

α = angular displacement of S.H. beam

d = beam width.

6.2.1.6 It was shown by Equation 6.19 that for small S.H. component the efficiency of SHG varies as the square of the length of crystal thus suggesting that a maximum length of crystal should be used. In practice there is an optimum length of crystal. Increasing the length does not increase the SHG efficiency. Three effects reduce the efficiency of long crystals. The first is described in para. 6.2.1.5. The second arises from the inevitable optical imperfections of crystals, which place different phase errors in the

fundamental and S.H. beams such that, for long crystal, it is not possible to phase match over the entire length. These faults may also limit the useful cross-sectional area of the crystal. The third effect is the finite absorption of the crystal at the S.H. Losses at the fundamental reduce the efficiency of SHG but the maximum efficiency still occurs for very long crystals.

6.2.1.7 From Equation 6.17, $I_2 \propto I_1^2$, where 2 and 1 refer to S.H. and fundamental respectively, and I is the power per unit area or 'surface power density'. Generally it is the total power (P) or total energy (W) conversion which is important, and for these quantities Equation 6.17 becomes:-

$$P_2 = \int_A I_2 \, dA = C \times \int_A I_1^2 \, dA \qquad \ldots (6.38)$$

and

$$W_2 = \int_t P_2 \, dt = C \times \int_t \int_A I_1^2 \, dA . dt \qquad \ldots (6.39)$$

$$\ldots (6.39)$$

$$= C \times \int_A \int_t I_1^2 \, dt \, dA$$

where C is independent of A and t.

Let us look at an example:-

Let $I_1 = I_o \exp -\left(\frac{t-t_o}{\Delta_1}\right)^2$. The input pulse has a gaussian temporal distribution and all parts of the input beam have the same time variation. Substituting into Equation 6.39 gives:-

$$W_2 = C \int_A I_o^2 dA \int_t \exp -2\left(\frac{t-t_o}{\Delta_1}\right)^2 dt = C \times \Delta_1 \sqrt{\frac{\pi}{2}} \times \int_A I_o^2 dA$$

using Equation 6.38 in the above now yields

$$W_2 = \Delta_1 \sqrt{\frac{\pi}{2}} \times P_{2o} \quad \text{where} \quad P_{2o} = \text{peak power in the S.H.}$$

$$-\left(\frac{t-t_o}{\Delta_2}\right)^2$$

Let $P_2 = P_{2o} \exp$

$$\therefore \quad W_2 = \int_t P_2 dt = \Delta_2 \sqrt{\pi} \times P_{2o}$$

From these two equations it is immediately seen that $\Delta_2 = \Delta_1/\sqrt{2}$ i.e. the S.H. pulse width is $1/\sqrt{2}$ of the fundamental pulse width. Further, it follows that the energy conversion efficiency is $1/\sqrt{2}$ of the efficiency of conversion of the peak power.

6.2.1.8 Mode conversion. If the fundamental is a given mode or mixture of modes, it is possible to calculate the mode distribution of the S.H. As a simple example let the fundamental be the TEM_{10} mode in cylindrical coordinates. The amplitude distribution (or E_1) is given by:

$$E_1 = E_o r e^{-r^2}$$

where r = normalized coordinate = $\frac{R}{w}$

where w is the beam width.

From Equation 6.16:

$$\begin{aligned} E_2 &= \text{constant} \times E_1^2 \\ &= \text{constant} \times E_0^2 r^2 e^{-2r^2} \\ &= \text{constant} \times \left[(2r^2-1)e^{-2r^2} + e^{-2r^2}\right] \\ &= \text{constant}\ \left[TEM_{20}\ \text{mode} + \tfrac{1}{2} TEM_{00}\ \text{mode}\right] \end{aligned}$$

The fundamental TEM_{10} mode is seen to result in the S.H. being a combination of the TEM_{20} and TEM_{00} modes. This mode conversion is correct under a more exact analysis in which the modes are not assumed to be plane waves, although the proportion of each mode is then not necessarily 2 to 1. Let us also calculate the S.H. power and power conversion efficiency from Equation 6.38:-

$$P_2 = C \times \int_A I_1^2 dA = C_1 \times \int_r (E_0 r e^{-r^2})^4 r dr$$

$$\therefore \quad P_2 = C_2 \int_{-\infty}^{\infty} r^4 e^{-4r^2} r dr = \frac{15C_2}{512} = \frac{15C_1}{512} E_0^4$$

$$\text{Now} \quad P_1 = \int I_1 dA = E_0^2 \int r^3 e^{-2r^2} dr = \frac{3E_0^2}{16}$$

$$\therefore \text{ The power conversion efficiency } \frac{P_2}{P_1} = \frac{15}{512} \cdot \frac{16}{3} C_1 E_0^2 = \frac{240}{1536} C_1 E_0^2$$

A similar calculation for an assumed TEM_{00} mode fundamental gives:-

$$\frac{P_2}{P_1} = \frac{1}{2} C_1 E_0^2$$

$$\frac{\text{S.H. efficiency of } TEM_{00} \text{ mode}}{\text{S.H. efficiency of } TEM_{10} \text{ mode}} = \frac{1}{2} \cdot \frac{1536}{240} = 3.2$$

It can be concluded that it is important for the achievement of maximum S.H. efficiency to ensure that a laser oscillates in the gaussian TEM_{00} mode.

6.2.1.9 S.H. spectrum

Let the fundamental contain two frequencies, ν_1 and ν_1'. The induced dipole moment term in the wave equation (the R.H.S. of Equation 6.7) becomes:-

$$\frac{\varepsilon_0 \mu_0 \chi_2}{c^2} \frac{\partial^2}{\partial t^2} \left[E_1 \cos(k_1 r - \omega_1 t) + E_1' \cos(k_1' r - \omega_1' t)\right]^2$$

which reduces to:-

$$-\frac{\varepsilon_0 \mu_0 4\omega_1^2 \chi_2 E_1^2}{2c^2} \cos(2k_1 t - 2\omega_1 t) - \frac{\varepsilon_0 \mu_0 4\omega_1'^2 \chi_2 E_1'^2}{2c^2} \cos(2k_1' r - 2\omega_1' t)$$

$$-\frac{\varepsilon_0 \mu_0 (\omega_1 + \omega_1')^2 \chi_2 E_1 E_1'}{c^2} \cos([k_1 + k_1']r - [\omega_1 + \omega_1']t) - \frac{\varepsilon_0 \mu_0 (\omega_1 - \omega_1')^2 \chi_2 E_1 E_1'}{c^2} \cos([k_1 - k_1']r - [\omega_1 - \omega_1']t)$$

and there must be S.H. components at frequencies $2\omega_1$, $2\omega_1'$, $\omega_1 + \omega_1'$ and $\omega_1 - \omega_1'$ and the intensities of these components are proportional to

$$\frac{(2\omega_1 E_1)^2}{2}, \frac{(2\omega_1' E_1)^2}{2}, (\omega_1 + \omega_1')^2 E_1 E_1', (\omega_1 - \omega_1')^2 E_1 E_1'$$

i.e. there are components in the S.H. at all sum and difference frequencies. If $(\omega_1 - \omega_1') = \Delta\omega$, where $\Delta\omega \ll \omega$, the difference component is vanishingly small and the frequencies present in the S.H. are $2\omega_1$, $2\omega_1 - 2\Delta\omega$, $2\omega_1 - \Delta\omega$. A two component spectrum becomes one having three components and double the

frequency spread. The effect on the coherence is derived simply:-

Coherence length $\sim 1/\Delta\bar{\nu}$ where $\Delta\bar{\nu} = \Delta\nu/c$ = wavenumber spread

$\therefore$ Doubling the frequency spread, doubles the spread in wavenumber and halves the coherence length.

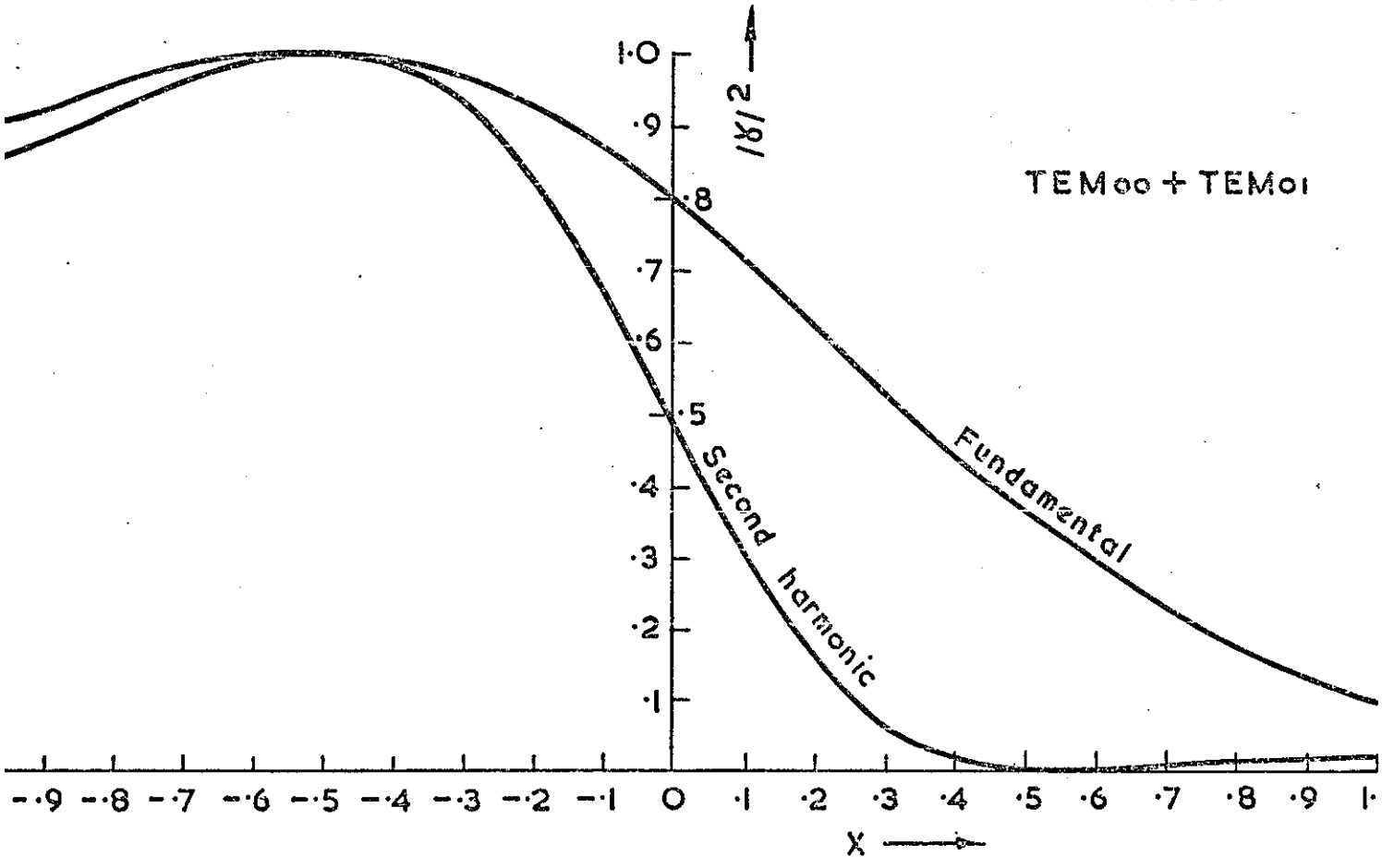
6.2.1.10 Transverse Coherence

The effect of the S.H. conversion on the transverse coherence follows immediately from the considerations of mode conversion. If for example the fundamental consists of the sum of the two lowest order modes, $TEM_{00}+TEM_{01}$, the transverse coherence of the fundamental can be calculated, see para. 5.4.2.1, Chapter 5. The second harmonic distribution is calculated as in para 6.2.1.8 and the coherence of the second harmonic is calculated in the same way as the fundamental. Fig. 6.3 plots the calculated coherence curves of fundamental and S.H. for this case, showing that the transverse coherence is also degraded by the S.H. process.

6.2.1.11 Intracavity Conversion

Since the power density inside the laser resonator is always higher than that outside and since radiation inside is travelling in both directions, then it is to be expected that a higher conversion can be achieved by placing the S.H. crystal inside. If for example the output mirror reflectivity is 50%, the internal fundamental power density travelling towards the output mirror is twice as high as that outside giving twice the efficiency of S.H.G. The internal fundamental intensity travelling away from the mirror is equal to that outside giving an equal efficiency of S.H.G. The total efficiency is thus improved by a factor 3. The crystal must of course be free of loss otherwise the fundamental will be reduced by its presence. If considerable conversion does take place intracavity, it constitutes a significant power dependent loss at the fundamental. This reduced overall gain at high

FIGURE 6.3



ANSVERSE COHERENCE OF FUNDAMENTAL AND SECOND HARMONIC FOR TEMoo + TEMoi MODE LASER.

HERENCE CALCULATED FOR ALL POINTS WITH RESPECT TO X=-0·5

powers lengthens the Q-switch pulse, reduces the peak-power and hence reduces somewhat the efficiency of S.H.G.

6.2.1.12 Focussing

To show the qualitative effects on S.H.G. of focussing the fundamental into the nonlinear crystal, let as make the following assumptions:-

The fundamental is a gaussian beam.

The majority of the S.H. is produced by a region near the fundamental beam focus within which the beam diameter (2w) remains essentially constant. A convenient length for this region (say 2b) is that for which the beam area lies within a factor of 2 of the area at the focus.

If $2b > \ell$, (where ℓ = length of crystal) the effective length of the crystal = ℓ. If, on the other hand, $2b < \ell$, the effective length of crystal = 2b.

From Equ. 6.19 and Equ. 6.38, the S.H. power P_2 is given by:-

$$P_2 = \text{const} \int I_1^2 \, \ell_1^2 dA$$

where I_1 = fundamental power density $= dP_1/dA \simeq P_1/A$

ℓ_1 = effective length of crystal.

Let $\int I_1^2 dA = \text{const } I_1^2 A_0$ where A_0 = min area of beam

$$\therefore \quad P_2 = \text{const} \frac{P_1^2}{A_0^2} \frac{\ell_1^2}{} . \; A_0 = \text{const} \frac{\ell_1^2}{w_0^2}$$

where w_0 = min radius of beam

$\underline{2b > \ell}$:- $P_2 = \text{const} \cdot \frac{\ell^2}{w_0^2}$ $\therefore$ Max P_2 requires $\underline{\text{min}}$. w_0

$\underline{2b < \ell}$:- $P_2 = \text{const} \cdot \frac{b^2}{w_0^2}$.

For a gaussian $b = \frac{\pi w_0^2}{\lambda}$ = (distance from focus at which $w = \sqrt{2}\, w_0$).

$\therefore P_2 = \text{const} \frac{w_0^4}{w_0^2} = \text{const} \cdot w_0^2$ $\therefore$ Max P_2 requires $\underline{\text{max.}}$ w_0

These two statements indicate that an optimum focussing is achieved for $2b = \ell$ e.g. $\ell = 10$mm requires $b = 5$mm or $w_0 \simeq 40\mu$m (beam convergence $\simeq 10$ mrad).

6.2.2 Some of the properties of S.H.G. have been discussed using simple formulae derived from first principles. These are based on assumptions which render the results quantitatively inexact but they provide valuable information and some insight into the physical processes involved. All the properties we have considered have been placed on a more exact mathematical basis by several authors.

A considerable number of papers on the general theory of S.H.G. have appeared in the literature. Armstrong, Bloembergen, Ducuing and Pershan (1962) first solved the wave equation (Equation 6.15) for the case of high conversion and under phase-matched conditions and the results of their calculation are just those of our rather simpler one, given in para. 6.2.13 and demonstrated by Fig. 6.2.

Weber et al (1966) tabulated all possible phase matching situations for KDP, ADP and $LiNbO_3$ at various wavelengths.

Bhawalkar et al (1970) and Kingston and McWhorter (1965) have treated in some detail the theory of mode conversion giving, in particular, the relative amplitudes in the different modes in the S.H. and in the fundamental mode.

Smith (1970) solves the problem of intracavity S.H.G. in a continuous wave laser showing how to optimize the efficiency and calculating the expected value of this maximum efficiency. Murray and Harris (1970) give solutions for the case of the Q-switched laser and make the particular point that the pulse length can be controlled by varying the coupling of fundamental into S.H.

The possibility of improved S.H.G. efficiency by focussing was first investigated theoretically by Bjorkholm (1966) and extended by Boyd and Kleinman (1968). Their computations are valid for a gaussian beam under the assumption of low conversion efficiency. Examples of their results are shown in Fig. 6.4 where it is seen that an optimum length of crystal exists for any degree of focussing of the gaussian beam. Bjorkholm's measured values using a cw He-Ne laser were in very good agreement with his theory.

6.3 Experimental Investigations

The experimental work concerned with the S.H. process has been concerned primarily with the achievement of an adequate efficiency. It has not been found necessary to explore the process in depth in order to optimise every aspect of it. The approach has been to take the laser in its early form, together with a crystal of ADP, measure the S.H. efficiency and other properties of the process and then having made various modifications which might reasonably be expected to significantly improve the performance, remeasure the efficiency and the other properties. Comments will be made from time to time on the experimental measurements particularly where they diverge from the simplified theory. Possible explanations of the observed effects will be given but will not be discussed at length or investigated further.

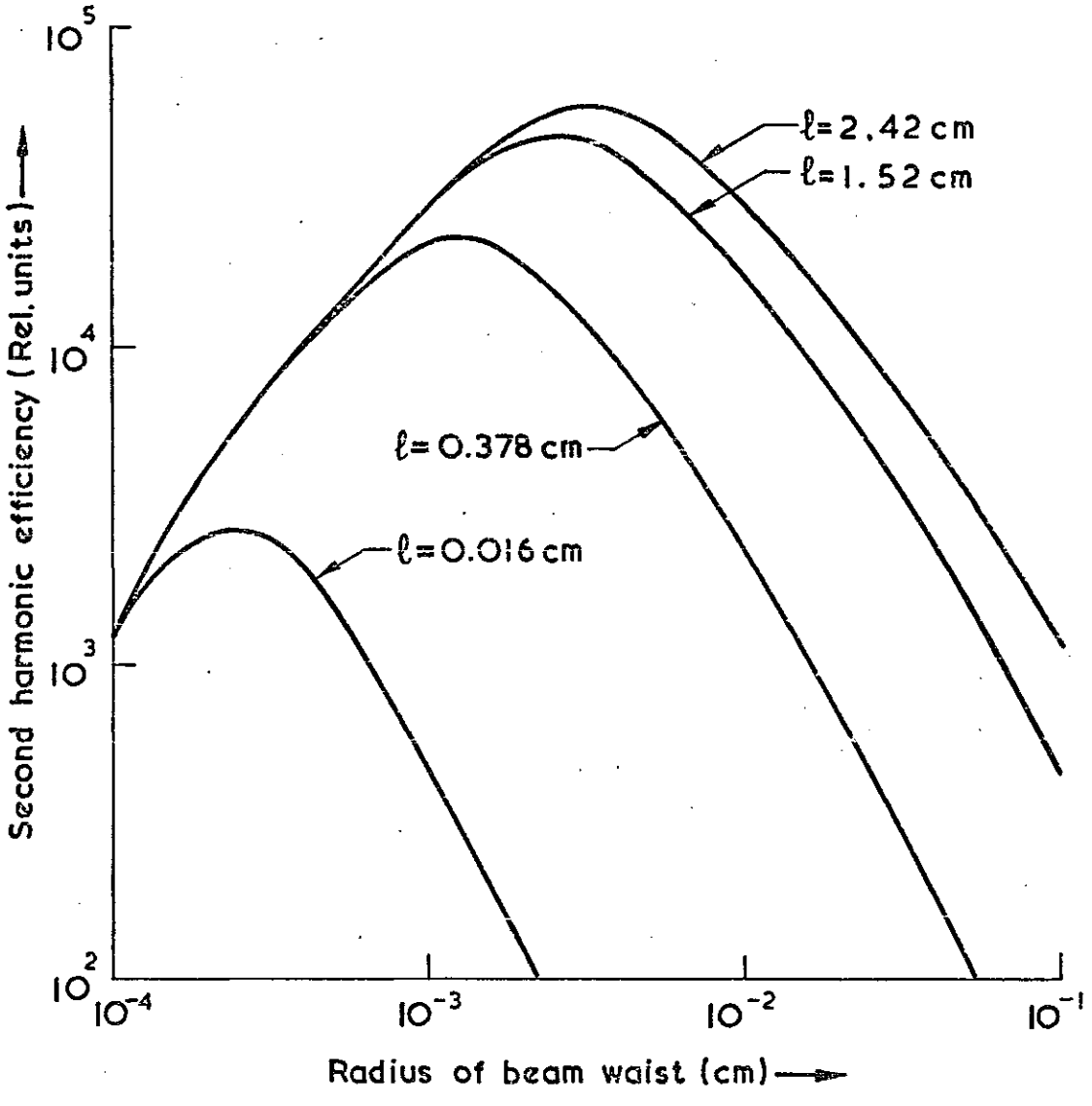
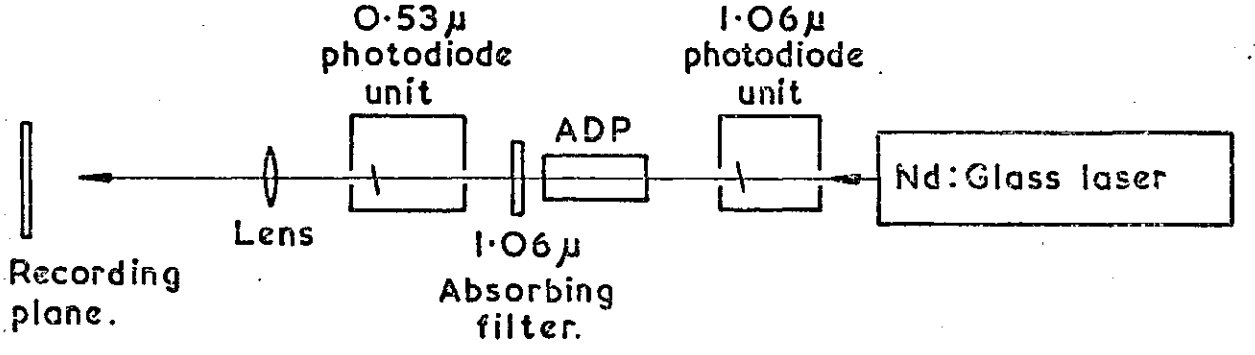


FIG. 6.4 CALCULATED DEPENDENCE OF SECOND HARMONIC EFFICIENCY ON DEGREE OF FOCUSSING (FROM BJORKHOLM 1966.)

Initially, as a basis for comparison, measurements were made on the laser with a crystal of ADP placed directly in the path of the infrared output and with no intervening optics. Fig. 6.5 shows the arrangement including the measuring detectors.

FIGURE 6.5



BASIC ARRANGEMENT FOR MEASUREMENTS ON SECOND HARMONIC GENERATION.

The parameters that have been measured are:-

The time resolved intensity and total energy in the infra-red fundamental; The time resolved intensity and total energy in the green S.H.; The transverse intensity distribution of the fundamental (just before the crystal) and S.H. (just after the crystal); and the near and far-field and spectral distribution of the fundamental.

6.3.1 It was necessary initially to establish the phase matching situation and observe how critical is the phase-matching angle. Measurements on the variation of efficiency with the setting of the angular control indicated that the angular half width was apparoximately 0.9 mrad in the critical plane and > 10 mrad in the non-critical plane. The literature (Hagen and Magnante 1969) indicates that a value of ~ 0.6 mrad should be obtained for the former and since the fundamental had a divergence of approximately 0.7 mrad, one

would then expect the angular half-width to be approximately $\sqrt{(0.7)^2+(0.6)^2} = 0.92$. The measured value was consequently capatible with the expected value.

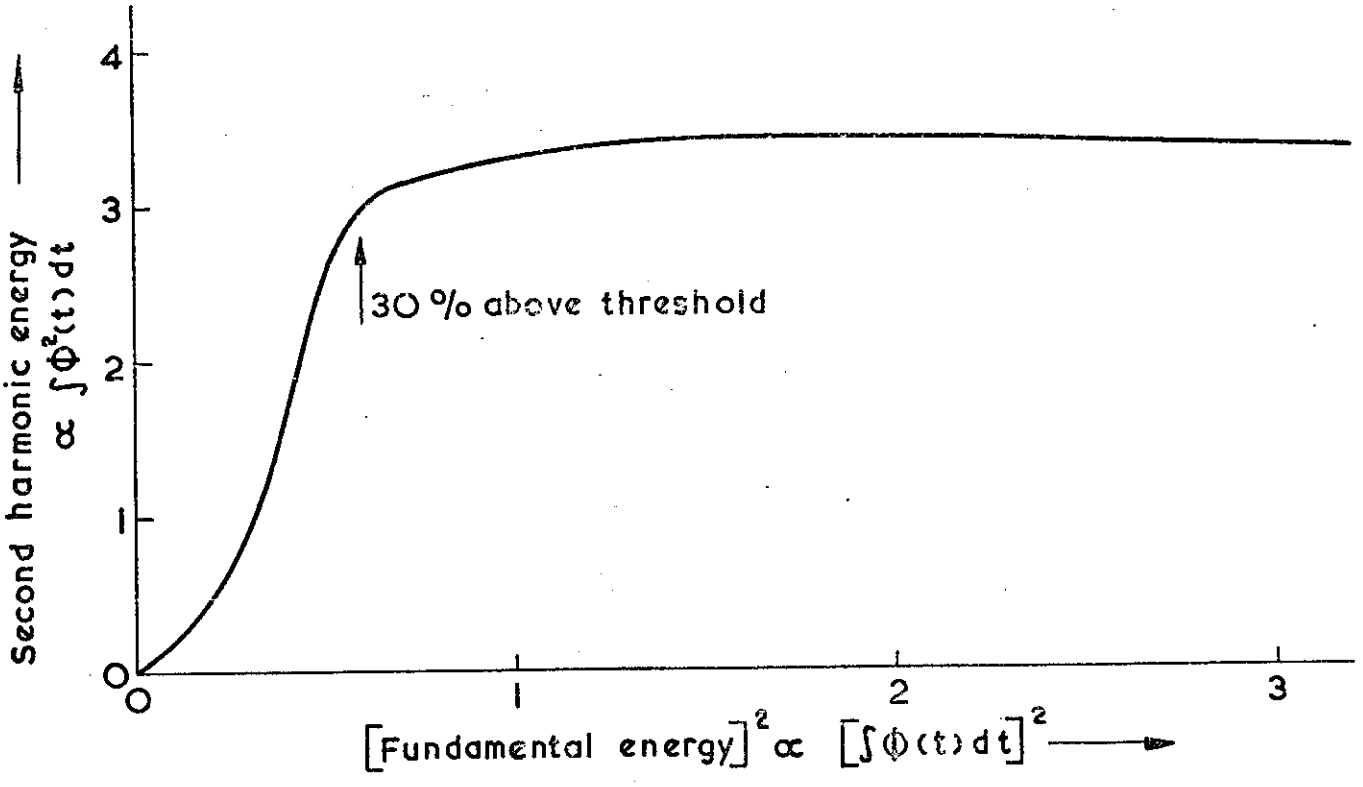
6.3.2 The next measurements were those of S.H. efficiency and its variation with the magnitude of the fundamental. Calibrated photodiodes were available for the measurement of energy at 1.06μm and energy at 0.53μm, and the first set of measurements were of the S.H. energy as a function of the fundamental energy. Fig. 6.6 plots the second harmonic energy as a function of energy in the fundamental. The main feature of this graph is that it does not follow a linear relationship. This is not very surprising in view of the likelihood of considerable changes in spatial and temporal distribution as the fundamental energy changes, or even from shot to shot at the same fundamental energy. The possible contribution to this non-linearity, of changes in temporal distribution (and, in particular, an increase in pulse width with increasing pumping), can be estimated theoretically from the spinning mirror Q-switch calculation of Chapter 3. In a typical case from those results, we have plotted Fig. 6.7 showing the variation of the integral over time of the square of the photon flux with the square of the integral over time of the photon flux.

$$\text{i.e. } \int \phi^2(t)dt \quad \text{vs} \quad \left[\int \phi(t)dt\right]^2.$$

Comparison of these graphs indicate that the change in temporal distribution can explain the overall flattening of the efficiency curve at high inputs. The large shot to shot jitter cannot however be explained and must be due to mode instabilities.

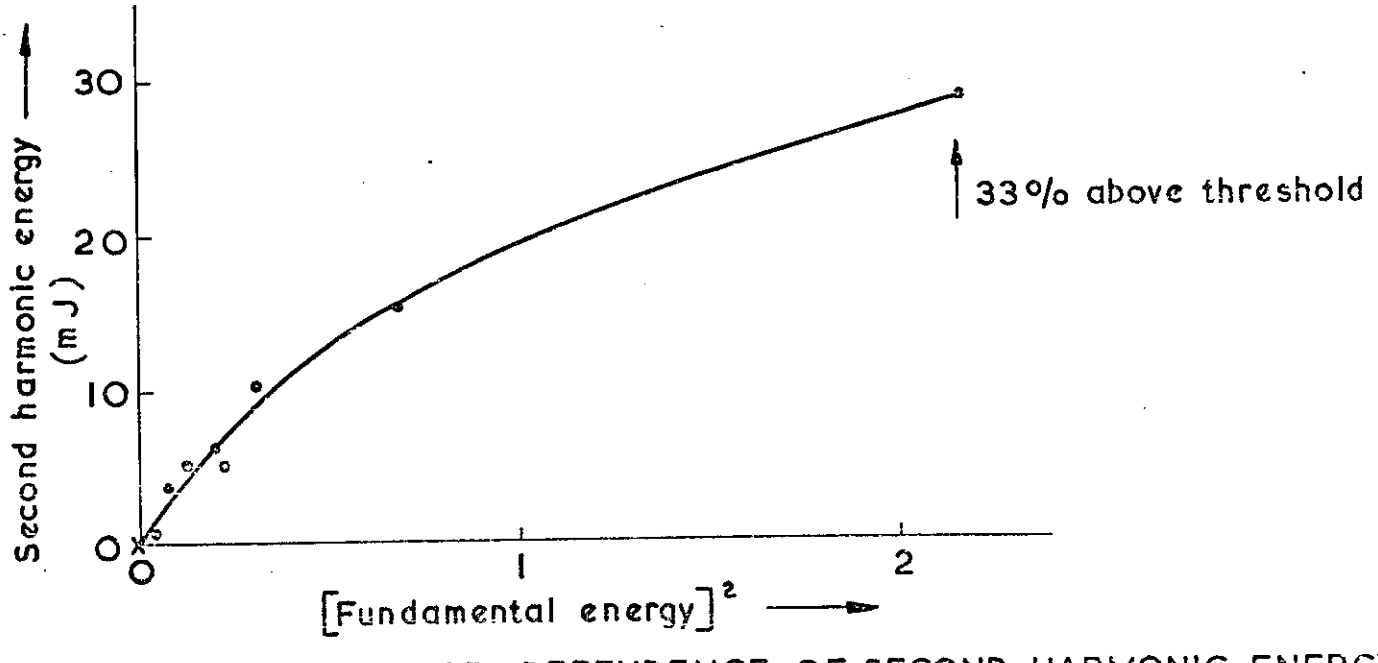
6.3.3 It was considered worthwhile to measure the temporal distribution in the fundamental and S.H. Two purposes were served; axial mode instabilities

FIGURE 6·7



THEORETICAL CURVE FOR DEPENDENCE OF SECOND HARMONIC ENERGY ON (FUNDAMENTAL ENERGY)²

FIGURE 6·6



EXPERIMENTAL CURVE FOR DEPENDENCE OF SECOND HARMONIC ENERGY ON (FUNDAMENTAL ENERGY)²

and mode interaction effects could be observed and the efficiency curve as measured from a single pulse could be plotted. The latter is not of course affected by shot to shot variations. Biplanar vacuum photocells coupled to a 519 Tektronix oscilloscope gave a temporal resolution better than 1ns. An electronic delay line enabled both pulses to be displayed on the same scope trace. Fig. 6.8 shows typical examples of the fundamental pulse followed by the S.H. pulse.

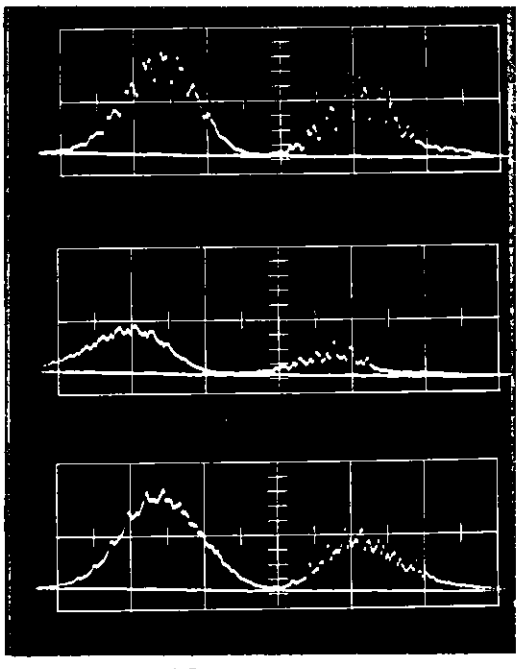


FIGURE 6.8

Oscillograms showing three examples of the time-evolution of the fundamental and second-harmonic pulses from a Nd:glass laser.

Second harmonic pulse delayed by 55ns.

Sweep speed = 20ns/square

Fig. 6.9 plots the S.H. power vs (fundamental power)^2 for the topmost pulses in Fig. 6.8, and is typical for these pulses. The majority of the graph is approximately linear, unlike the energy curve shown in Fig. 6.6. The curve is not linear however at low input powers and curious effects can be seen near the pulse peak. The explanation of the effects is probably related to mode competition effects occurring during the pulse and to sub-nanosecond structure in the fundamental and second harmonic which is not resolved by the photocell. A feature of the curves of Fig. 6.8 is the modulation of the envelope. This must be due to the presence of more than one axial mode. Now the beat frequency between consecutive axial modes = $c/2L$, where L = optical length of the resonator, and since L = 66 cm, $c/2L$ = 230 MHz and the period of the modulation = $2L/c$ = 4.4 ns. This is

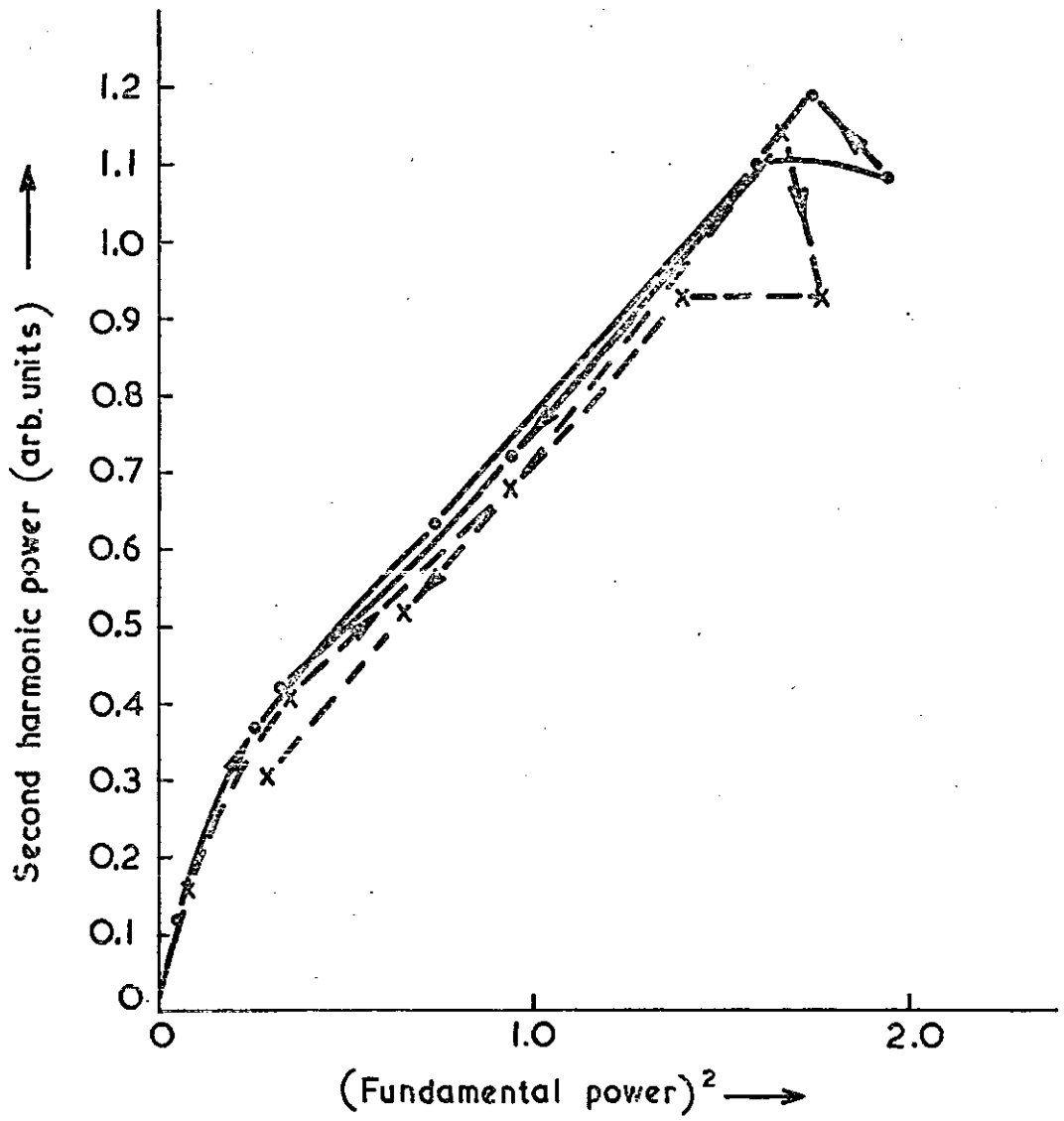


FIG. 6.9 MEASURED DEPENDENCE OF SECOND HARMONIC POWER ON SQUARE OF FUNDAMENTAL POWER OVER A SINGLE Q-SWITCHED PULSE. MEASUREMENTS MADE AT PEAKS OF TOP CURVES OF FIG. 6.8. CONTINUOUS AND DASHED CURVES REPRESENT DIFFERENT SETS OF OF PEAKS. ARROWS SHOW DIRECTION OF INCREASING TIME.

just the major modulation period on Fig. 6.8. The existence of higher modulation frequencies in the trace, and the changes in modulation during the pulse indicate the presence of more than two axial modes which are not mutually locked in phase.

6.3.4 In the theoretical section of this chapter several possible ways of improving the efficiency and stability of second harmonic generation were suggested. We have taken a brief experimental look at the effectiveness with our Nd:glass laser of:-

(i) focussing the fundamental into the second harmonic crystal

(ii) improving the mode structure in the fundamental

(iii) using a different second harmonic crystal

(iv) placing the crystal inside the resonator

6.3.4.1 From the analysis of Bjorkholm (1966), focussing condition for the maximum efficiency of second harmonic generation in a gaussian beam is given by:-

$$2b = \frac{\ell}{\pi} \quad \text{where } b = \text{confocal parameter and } \ell = \text{length of crystal}$$

b is just the axial distance from the beam waist at which the beam radius has increased by $\sqrt{2}$, and is given by:-

$$b = \frac{\pi w_0^2}{\lambda} = \frac{4\lambda}{\pi\theta^2} \quad \text{where } w_0 = \text{waist radius and } \theta = \text{divergence at infinity}$$

For the system being used:-

$$\ell = 40 \text{ mm}; \quad \lambda = 1.06 \times 10^{-3} \text{ mm}$$

$$\therefore \quad \theta^2 = \frac{4\lambda}{\pi b} = \frac{8\lambda}{\ell} = \frac{8 \times 1.06 \times 10^{-3}}{40} = 2.12 \times 10^{-4}$$

$$\therefore \quad \theta = 14.5 \text{ mrad}$$

Thus for optimum focussing a lens must be chosen giving a convergence angle of 14.5 mrad. Since the beam diameter at the lens position ≈ 2 mm and the incident beam is collimated, the focal length of the lens must be $2/14.5 \times 10^{-3} = 138$ mm.

A test was not carried out with this lens because the resulting power density in the S.H. crystal would certainly have been above the damage threshold. The S.H. efficiency with lenses of lower power was however measured as a function of lens focal length. This showed that instead of increasing with decreasing focal length the efficiency dropped steadily and at a focal length of 440 mm was down by approximately 40%. Even at this focal length the estimated peak power density in the crystal was ≈ 1 GW/cm^2 and damage was found to have occurred at the surface of the crystal. The failure to produce an improvement in efficiency is no doubt due primarily to the difference in profile between the beam actually present and a Gaussian distribution. Any departure from a gaussian reduces the fraction of the power in the focussed spot which is directed close enough to the axial direction to be within the angular tolerance for phase matching. The angular distribution is not so concentrated and the efficiency of conversion is reduced.

A more effective method of focussing is to use a cylindrical lens correctly orientated to the crystal axis such that the direction in which the angular spread is increased coincides with the direction in which phase matching is not critical with respect to angle. In this situation the

power density at the crystal is increased and all of the incident power can still satisfy the phase matching condition.

6.3.4.2 Paragraph 6.2.1.8 showed that the conversion efficiency of the TEM_{00} mode is higher than for the TEM_{01} mode with the same intensity. It can also be shown similarly that other modes are also unfavourable for second harmonic generation. There is the possibility then that improving the transverse mode structure of the laser output, although it may result in reduced total energy, may still lead to increased energy in the second harmonic. Furthermore the variability of S.H.G., which is largely due to shot to shot variations in output intensity distribution (itself a result of changing mode structure), is likely to be reduced by reducing the number of transverse modes and consequently stabilizing the mode structure.

A simple test experiment was carried out. The fundamental and second harmonic energies were measured both with and without an aperture of diameter 2.5 mm inside the resonator. Conditions were kept constant throughout and the transverse position of the aperture was adjusted for optimum operation. It was found that introduction of the aperture led to a high risk of damage to the other optical components in the resonator, and the peak power and hence the energy had to be restricted. The consequent restriction in second harmonic output was to a value less than could easily be achieved with no aperture. Furthermore, equal energies at the second harmonic necessitated a higher input when the aperture was present, because the increase in threshold and reduction in rod area were not offset by a sufficient rise in second harmonic efficiency. The small increase in this efficiency can be explained from measurements made on the near-field distribution at the fundamental, which show that the instantaneous distribution has dimensions of approximately 2.5 mm, no larger than the aperture used above.

6.3.4.3 The high non linear coefficient of $LiNbO_3$ in comparison with ADP (they are in the ratio 12:1 respectively) suggests that it will give more efficient second harmonic generation. Furthermore it can be phase matched at 90° to the c-axis by varying the temperature of the crystal. The implications of this are:-

(i) losses due to the walk-off effect (paragraph 6.2.1.5) do not occur.

(ii) the angular tolerances are much higher

(iii) the spectral tolerance is much tighter - a few cm^{-1} as compared to 100-200 cm^{-1} for ADP.

Several detrimental effects occur however:-

(a) The crystal damages easily - the damage threshold is of the order of $^1/_{10}$ of that of ADP

(b) It is difficult to produce good $LiNbO_3$ crystals and variations of birefringence across the crystal tend to limit the volume of crystal that can be phase-matched at one temperature.

(c) Temperature gradients create birefringence effects with the same effect as in (b). However the possibility exists of using temperature gradients to eliminate the effects of (b).

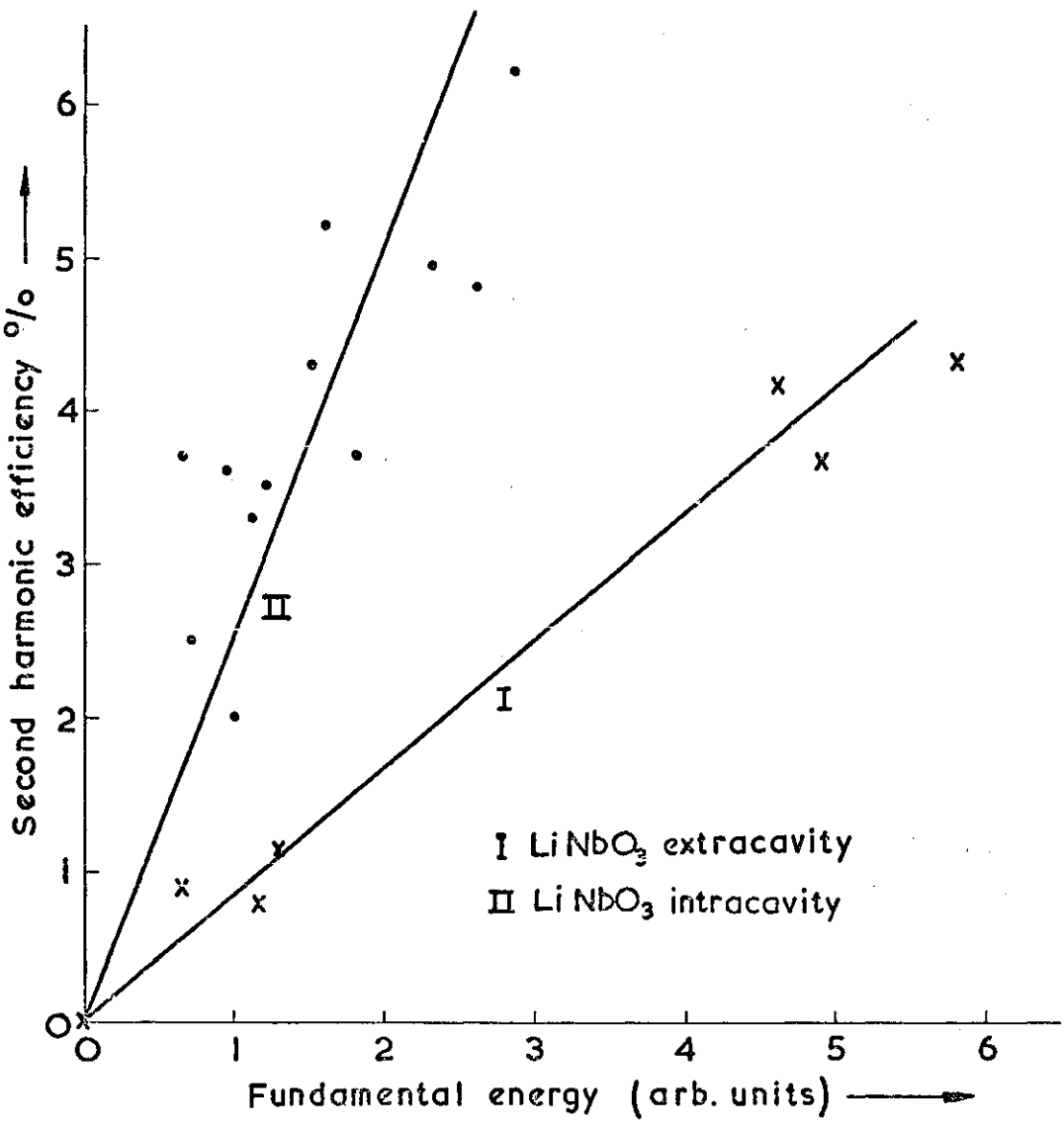
An 8 mm cube of $LiNbO_3$ was obtained, together with a suitable oven, and substituted for the ADP crystal in the unexpanded output beam of the Nd:glass laser. The temperature was adjusted for maximum efficiency and this efficiency measured as with ADP. The efficiency at 100 mJ energy in the fundamental, obtained by interpolation from efficiency measurements at energies near this value, was 3.9%. The value for ADP, obtained in the same way (see Fig. 6.9) was 4.2% and consequently is to be preferred. The power density in both crystals at this level of input was estimated to be

$\approx$ 100 MW/cm^2. This is well inside the damage threshold for ADP but it was a little surprising that damage did not occur at this level in the $LiNbO_3$. It was however found to have damaged at approximately 200 MW/cm^2.

That $LiNbO_3$ did not give a higher S.H. efficiency than ADP is due primarily to the presence of optical distortions in the crystal. These distortions are in part due to residual imperfections in the crystal and in part to thermal gradients. Another more severe cause is however likely to be present; so called 'optical' damage. High intensity illumination can cause optical distortion in crystals having an open structure and $LiNbO_3$ is particularly subject to this effect. Photographs of the intensity distribution in the fundamental and in the second harmonic supported the above explanation, since local intensity variations were present in the second harmonic that were not present in the fundamental and the form of these variations agree with that expected as a result of optical distortions in the crystal.

6.3.4.4 The final experimental test was to place the $LiNbO_3$ inside the resonator. Paragraph 6.2.1.11 showed that this should lead to increased efficiency with a crystal having no absorption at the fundamental wavelength. $LiNbO_3$ is such a crystal and we made comparative S.H.G. efficiency measurements with the crystal inside and outside the resonator. Fig. 6.10 shows the two sets of readings and we have plotted the energy efficiency against the fundamental energy. Again we see quite a spread to the points but it is clear that more efficient S.H.G. is obtained with the crystal inside the resonator as expected. An estimate of the increase in efficiency is obtained by drawing the best straight lines fitting the two sets of points and finding the ratio of their slopes. This ratio was 3.0, and this again is as expected from paragraph 6.2.1.11.

FIGURE 6·10



EFFECT OF AN INTRACAVITY SECOND HARMONIC CRYSTAL

There were however two problems to the use of $LiNbO_3$ intracavity:-

(i) It introduced losses either due to absorption at 1.06μ or due to optical distortion in the crystal. In spite of the increase in efficiency it was still necessary, at the output levels required, to use a higher input energy to the laser to obtain the same energy at 0.53μ.

(ii) Damage occurred in the crystal at a lower second harmonic energy than for extra-cavity operation.

6.4 Conclusions

We have shown that for our laser system the most efficient and reliable of the various techniques of S.H.G. we have tried is that of placing an ADP crystal in the unexpanded infra-red output beam of the laser. The best orientation of the crystal is that (Weber et al 1966) in which the phase-match angle is 61°12' to the optic axis and the incident plane of polarization is at 45° to the plane containing direction of propagation and the optic axis. The S.H.G. efficiency with respect to energy was more than 5% for fundamental energies greater than about 150 mJ and in particular 29 mJ of green second harmonic was obtained for an energy of 465 mJ in the infra-red.

CHAPTER 7

Conclusions

7.1	Principal achievements	7.1
7.2	Theoretical Aspects	7.1
7.3	Experimental Techniques	7.3
7.4	Experimental Results	7.4
7.5	Conclusion	7.5

Conclusions

7.1

This thesis sets out a study of the Nd:glass laser with second harmonic generation and presents theoretical and experimental work designed to improve this laser. It has been possible:-

(i) to achieve a better understanding of pulsed solid state lasers and in particular those with a rotating mirror Q-switch and those employing Nd:glass as the active medium.

(ii) to improve on laser design procedures.

(iii) to improve the design of the Nd:glass laser with second harmonic generation to make it more useful as a coherent source of light.

(iv) to suggest further improvements which can make it even more competitive with the ruby laser.

7.2 Theoretical aspects have divided themselves principally into five items which deserve comment here as having been new or presenting existing theory in a different way.

7.2.1 Analysis of spinning mirror Q-switch. A simple computer programme has been developed to describe this type of Q-switching which does not make the assumption, as has been the case previously, that the movement of the mirror is negligible over the entire duration of the laser pulse. The programme can be adapted without great difficulty to include diffraction effects and more complex optical designs of the resonator.

7.2.2 Calculation of the distribution of absorbed energy density in a rod of Nd:glass. Quantitative knowledge of this distribution, and how it varies with several parameters, is necessary to any calculation of optimum laser design, and has not previously been computed in a three dimensional form and taking into account the exact absorption spectrum of the Nd:glass. This has been done and the resulting computer program can be used to show quickly

the effects of changing the concentration of neodymium, the rod geometry, the type of glass and the operating conditions in the flashlamp.

7.2.3 Optimization of the laser. A method of optimization for use in the design of lasers is proposed, and demonstrated with an example for a Q-switched Nd:glass laser. An analytical approach is assumed using analytic functions to approximate, for example, the pumping efficiency as computed in the previous section and the efficiency of Q-switching. The only computational step is to solve a pair of simultaneous equations, and in the example the maximum output energy for various input energies is calculated along with the optimum values of neodymium concentration, rod and flashtube length and radius, pumping pulse duration and output mirror reflectivity. The major assumptions in this analysis are that the pumping distribution in the rod is a 'top hat' function as also is the output beam intensity profile. The use of a very much greater computational capacity can perform the calculation more exactly and has since been done by J.G. Edwards and R. Jefferies of this Laboratory for a gaussian beam profile and a better approximation to the pumping distribution. Their results show that the simple method is a valuable one and that it is quantitatively close to being an exact one.

7.2.4 Coherence Theory. It was felt, after looking at the way this topic has been treated in the literature, that there was a need to present an exact theory using the minimum of mathematics. It should also be in a form whereby it is possible to easily calculate the coherence of actual sources and the observable properties which depend on it. An attempt has been made to do this and particular accent has been placed on laser coherence functions and the effect of coherence on holography. From this it has been possible to show how the coherence of lasers can be improved and also to specify how much improvement is required.

7.2.5 The theory of second harmonic generation. This subject is also one that can be very involved mathematically and an attempt is made, similarly, to find a different presentation which is a balance between exactness and ease of application to practical situations. It is shown that several properties can be derived quite simply, and in particular efficient S.H.G. under phase matched conditions including the effect of absorption. As with coherence, there follows a discussion of the factors which affect the efficiency and this discussion gives the information which will enable a laser system to be suitably designed for a required performance.

7.3 On the experimental side it has been necessary to use many techniques in assessing and improving the performance of the Nd:glass laser. It has also been important to be critical of and to modify certain diagnostic methods which have shown deficiencies when applied to lasers. In two particular situations a novel approach has been adopted and shown to have advantages.

The first of these is the use of high speed rotating prisms for the streak recording of light distributions with a time resolution of a few nanoseconds. This method is of particular use to workers studying rotating mirror Q-switched lasers who do not have access to appropriate image converter cameras, since a suitable rotating prism is already in use in the laser and since this prism always has the same orientation at the moment of the Q-switched pulse.

The other technique which has been developed is the use of holography in the measurement of coherence. For light sources, such as pulsed lasers, having complex coherence functions which may change from shot to shot it is often desirable to record all the coherence information in one exposure. Only the holographic method can do this adequately. Experimental techniques for the measurement of both transverse and temporal coherence are proposed.

and tested and they are shown to be promising as suppliers of quantitative coherence information.

7.4 Much experimental data on the laser has been collected, and from it has come (a) a better understanding of the system and how it works (b) a check on some of the theoretical results, and (c) an assessment of various proposed modifications. These modifications have resulted from the need for a narrower spectral output width, a greater amount of coherent energy output, a reduction in the effects of dynamic optical distortion and an increase in the efficiency of S.H.G.

7.4.1 The design specification of a spectral width $< 0.04\ cm^{-1}$ has been achieved using a resonant reflector as output mirror coupled with a tilted intracavity etalon. It has been considered important to find a design which is non-critical in respect of initial adjustment and subsequent temperature variations.

7.4.2 The second task has proved more difficult. High efficiency has not been achieved in TEM_{oo} mode operation due to poor rod optical quality when pumped in the available pumping cavity. However, coherence measurements have shown that a surprisingly large fraction of the output can be regarded as coherent even under conditions of multimode operation when the laser is much more efficient. This is thought to be a result of mode coupling effects and of the shortness of duration of the pulse. Attempts to increase the amount of 'coherent' energy have been unsuccessful also due to the dynamic optical distortion of the rod. Reduction of this distortion by suitable design of pumping cavity to give a more uniformly pumped rod is expected to result in considerable improvements. A pumping cavity of the exfocal ellipsoid or close-coupled helical or double elliptic cylinder would all be suitable designs.

7.4.3 Second harmonic generation is also adversely affected by poor rod-optical quality and this has resulted in little increase in the efficiency of second harmonic generation when various modifications to the system have been introduced. Again, it is expected that more uniform pumping of the rod would lead to considerable improvements. The energy efficiency is, however, about 5% and the amount of green light available is still adequate for many forms of holography.

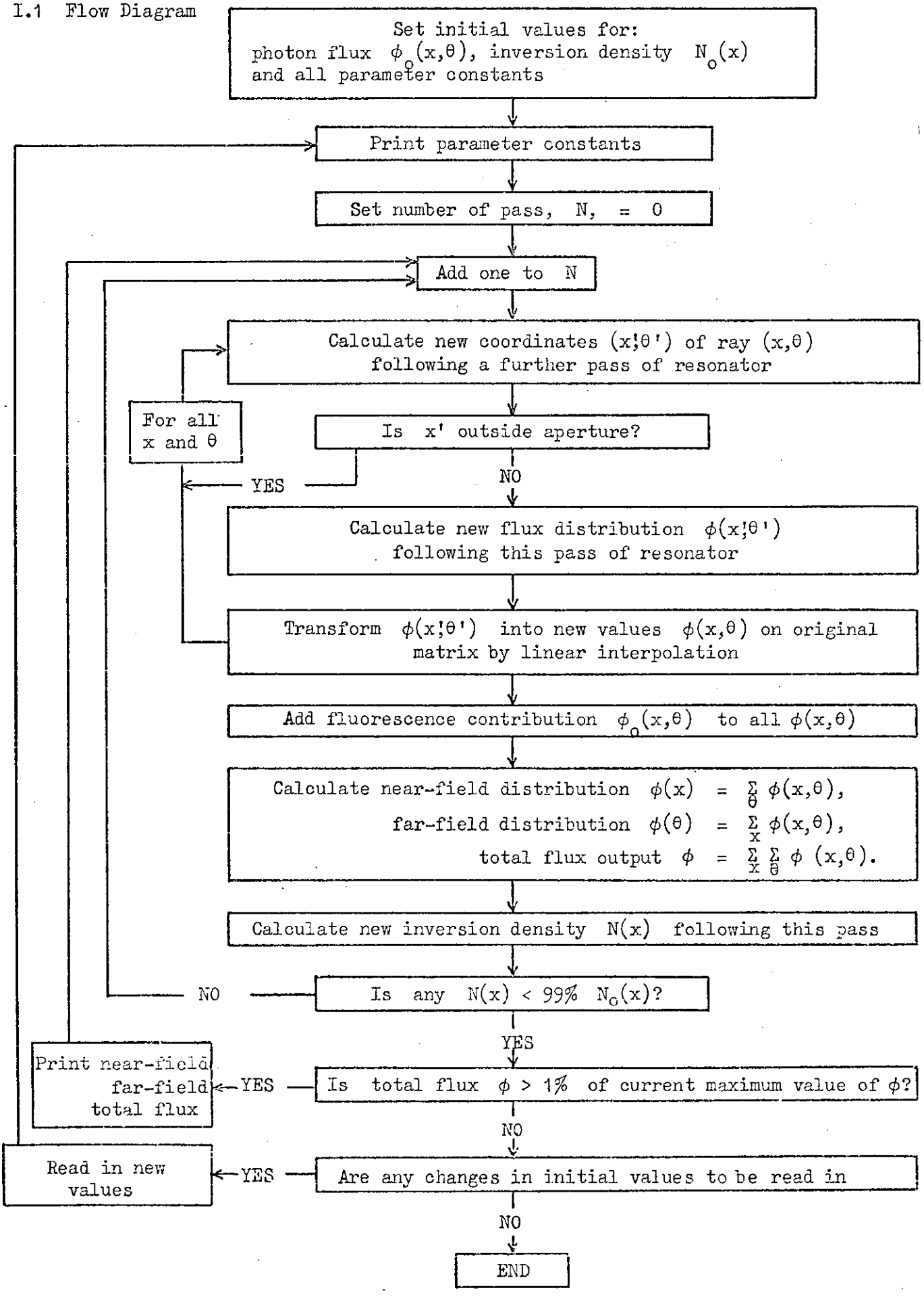
7.5 The Nd:glass laser with second harmonic generation has given approximately 30 mJ in 25 ns at 530 nm with a coherence length greater than 25 cm and a transverse coherence adequate for the holography of diffusely reflecting objects. A similar laser system with ruby instead of Nd:glass has given approximately 300 mJ in 25 ns at 694 and with a similar coherence. In all measurement techniques, except the holography of wide angular fields where a great effort has been put into producing fast red sensitive emulsions, the increase in sensitivity of the technique at 530 nm compensates for the difference in the energy output of the two lasers.

Applications requiring smaller lasers would favour ruby while those requiring larger lasers would favour Nd:glass as the active medium. Future improvements are likely to be greater for the Nd:glass laser particularly with respect to the rod optical distortion and this laser would then be more favourable for medium energy applications such as those upon which the work reported here is based.

APPENDIX I

Computer Program to Calculate Action of Spinning Mirror Q-switch

I.1 Flow Diagram



```
ORLASER1/T013/ROTQSWNDGL1/INR08030/5*          03/05/72    10.14.07

                *XEQ*
                *CARDLIST*
                *TABLES*

OR ORGANISER ENTERED  10.14.12          03/05/72
CHAIN1*                                                                IR00
IDENTIFIERMAIN*                                                        IR000010
FORTRAN*

GTRAN COMPILER          MARK NO. 30204          DATE    03/05/72          TIME    10.
  DO LOOP TO CALL CALCULATING,INPUT AND OUTPUT ROUTINES FOR EACH CAVITYIR00
  PASS UNTIL LASER PULSE IS OVER                                       IR00
      DIMENSION PHI(10,100),PHIO(10,100),PHIT(10,100),PHIPSX(100),PHIPSY
     2(10),AN(10),ANO(10)
 TO READ IN THE INPUT DATA                                             IR00
      READ    210,R,S,CL,SI,B,AO,W,SL,AM,C,CVX,CVY,ANN
      READ     220,(ANO(NX),NX=1,10)
      PRINT 400,(R,S,CL,SL,SI,B,AM,AO,CVY,CVX,W)                       IR000065
400   FORMAT (1H120X12HLASER OUTPUT//20HPARAMETER VALUES ARE/5X15HREFLECIR050070
     2TIVITY = ,E9.3/5X17HOTHER LOSSES = 1-,E9.3/5X16HCAVITY LENGTH = ,EIR050080
     29.3/5X13HROD LENGTH = ,E9.3/5X27HSTIM. EMISSION X-SECTION = ,E9.3/IR050090
     25X19HLOSS COEFFICIENT = ,E9.3/5X19HREFRACTIVE INDEX = ,E9.3/5X29HIIR050100
     2NITIAL MIRROR ORIENTATION = ,E10.3/5X12HUNIT OF Y = ,E9.3/5X12HUNIT
     2T OF X = ,E9.3/5X24HMIRROR ROTATION SPEED = ,E9.3)
   SET PHI = PHIO AND AN = ANO
      TAU=2.0*(CL+(AM-1.0)*SL)/C                                       IR000120
18    K=0
      DO 150 NX=1,10
      PH=(1.6*(EXP(2.0*SL*(SI*ANN*ANO(NX)-B))-1.0))/(CVX**2*CVY*SI)
      DO 160 NY=1,80
      PHIO(NX,NY)=PH
160   CONTINUE
150   CONTINUE
      PRINT 600, PHIO(5,10)
600   FORMAT (////6X,11HPHIO(5,10)=,E10.3)
      CALL AEQUB (PHI,PHIO)
      DO 140NX=1,10
      AN(NX)=ANN*ANO(NX)
140   CONTINUE
      PHISM=0.0                                                        IR000100
      N=0
20    N=N+1                                                            IR000130
      CALL PHIC (PHIT,PHIO,PHI,PHIPSX,PHIPSY,PHIS,AN,R,S,CL,SI,B,N,K,AO,IR000140
     2W,TAU,SL,AM,ANO,C,CVX,CVY,ANN)
      IF (K.LT.1) GO TO 20                                             IR000170
      IF (PHIS.GT.PHISM) PHISM=PHIS                                    IR000150
      IF (N.LT.-AO/(TAU*W)) GO TO 31
      IF (PHIS.LT.0.01*PHISM) GO TO 130                                IR000160
 TO WRITE OUT THE NEAR AND FAR FIELDAAND3TOTAL POWER EACH PASS         IR01
31    PRINT 300,N,(PHIPSX(NY),NY=1,80),(PHIPSY(NX),NX=1,10),PHIS
300   FORMAT (////10X25HOUTPUT AFTER PASS NUMBER ,I3///2X24HTHE ANGULAR IR050030
     2DISTRIBUTION,/10(E9.3,3X)/10(E9.3,3X)/10(E9.3,3X)/10(E9.3,3X)/10(E
     29.3,3X)/10(E9.3,3X)/10(E9.3,3X)/10(E9.3,3X)/2X24HTHE LATERAL DISTR
     2IBUTION,/10(E9.3,3X)//2X19HTHE TOTAL OUTPUT = ,E9.3,20H PHOTONS PE
     2R SECOND.)
      GO TO 20
130   READ 210,ANN
210   FORMAT ( E9.3 )                                                  IR050010
220   FORMAT (10E6.3)
      GO TO 18
      CALL EXIT
      END                                                              IR000210
```

```
GTRAN COMPILER          MARK NO. 30204          DATE    03/05/72          TIME    10.
      SUBROUTINE PHIC (PHIT,PHIO,PHI,PHIPSX,PHIPSY,PHIS,AN,R,S,CL,SI,B,NIR001015
     2,K,AO,W,TAU,SL,AM,ANO,C,CVX,CVY,ANN)
C TO CALCULATE THE OUTPUT AFTER A FURTHER PASS                              IR00
      DIMENSION PHI(10,100),PHIO(10,100),PHIT(10,100),PHIPSX(100),PHIPSY
     2(10),AN(10),ANO(10)
      CALL AEQUB (PHIT,PHIO)                                                IR001040
C ALL ELEMENTS HAVE A FLUORESCENCE CONTRIBUTION                             IR00
      DO30 NX1=1,10                                                         IR001050
      DO 40 NY1=1,80
C TO CALCULATE Y COORDINATE AFTER A FURTHER PASS.FIND NEAREST INTEGER        IR00
C TO Y
      BN=N
      T=BN*TAU
      Y1=NY1
      Y=2.0*(AO+W*(T-TAU/2.0))*CVY+Y1
      NYA=Y
      NYB=Y+1.0
      YA=NYA
      YB=NYB
C SAME AS PREVIOUS SUBROUTINE FOR X COORDINATE
      X1=NX1
      X=X1+(CL-SL*(AM-1.0)/AM)*(Y+Y1-80.0)*CVX/CVY
      NXA=X
      NXB=X+1.0
      XA=NXA
      XB=NXB
      IF((NXA.LT.1).OR.(NXB.GT.10)) GO TO 40
      IF ((NYA.LT.1).OR.(NYB.GT.80)) GO TO 40
      G=R*S*PHI(NX1,NY1)*EXP(2.0*SL*(SI*AN(NX1)-B))                         IR001105
      PHIT(NXA,NYA)=PHIT(NXA,NYA)+(G*(XB-X)*(YB-Y))/((XB-XA)*(YB-YA))
      PHIT(NXA,NYB)=PHIT(NXA,NYB)+(G*(XB-X)*(Y-YA))/((XB-XA)*(YB-YA))
      PHIT(NXB,NYA)=PHIT(NXB,NYA)+(G*(X-XA)*(YB-Y))/((XB-XA)*(YB-YA))
      PHIT(NXB,NYB)=PHIT(NXB,NYB)+(G*(X-XA)*(Y-YA))/((XB-XA)*(YB-YA))
40    CONTINUE
30    CONTINUE
      CALL AEQUB (PHI,PHIT)
C TO SUM PHI OVER X
      DO 50 NY=1,80
      PHIPSX(NY)=0.0
      DO 60NX=1,10
      PHIPSX(NY)=PHIPSX(NY)+PHIT(NX,NY)
60    CONTINUE
50    CONTINUE
C TO SUM PHI OVER Y
      DO 110NX=1,10
      PHIPSY(NX)=0.0
      DO 120 NY=1,80
      PHIPSY(NX)=PHIPSY(NX)+PHIT(NX,NY)
120   CONTINUE
110   CONTINUE
C TO CALCULATE INVERSION DENSITY AFTER ANOTHER PASS
      PRINT 280,AN(5)
      DO 70NX=1,10
      AN(NX)=AN(NX)-(R*S*TAU*PHIPSY(NX)*(EXP(2.0*SL*(SI*AN(NX)-B))-1.0)
     2*CVX**2)/(SL*10.0*(1.0-B/(SI*AN(NX))))
      IF ((ANN*ANO(NX)-AN(NX))/(ANN*ANO(NX)).GT.0.01) K=1
70    CONTINUE
280   FORMAT (//6X,6HAN(5)=,E10.3)
C TO SUM PHI OVER BOTH VARIABLES
      PHIS=0.0
      DO 80 NY=1,80
      PHIS=PHIS+PHIPSX(NY)
80    CONTINUE

      RETURN
      END
```

```
GTRAN COMPILER        MARK NO. 30204        DATE    03/05/72        TIME    10.
      SUBROUTINE AEQUB (A,B)
C SETS TWO ARRAYS EQUAL
      DIMENSION A(10,100),B(10,100)
      DO90 NX=1,10
      DO 100 NY=1,80
      A(NX,NY)=B(NX,NY)
100   CONTINUE
90    CONTINUE
      RETURN
      END
```

APPENDIX II

Program to Find Optimum Parameters of Nd:glass Laser

The simultaneous equations to be solved are:-

$$\beta\ell - \ln D = \frac{\beta \ell_o P}{2Q(P-1)} \qquad \ldots (3.46)$$

$$\frac{2.9\ PQ}{2PQ-2Q+P} = \frac{1}{N}\left[\frac{G_o H_o c \ell_o \sqrt{t_o}(2PQ-2Q+P)}{2P^2Q^2(-\ln S)}\right]^{1.45} + 0.45 \qquad \ldots (3.47)$$

where

$$P = 1 + 0.28 t_o^{c/4}$$

$$Q = 1 + 2.63 \times 10^{-3}\ Ec/\ell_o\sqrt{t_o}$$

$$N = 0.48 \times 10^{-2}\left(\frac{h\nu}{\sigma}\right)^{1.45}$$

and where the rod length (ℓ_o) is given by:-

$$\ell_o = \frac{2.63 \times 10^{-3} Ec^2(P-1)}{\sqrt{t_o}\ (4P-cP+c)} \qquad \ldots (3.48)$$

The parameters to be optimized are:-

rod length ℓ_o; neodymium concentration c; flash duration t_o

(the optima of these being given by the above three equations)

rod radius r_o; mirror reflectivity R; output energy E_{OUT}

the optima of these being given by:-

$$r_o = \frac{E}{400\ell_o\sqrt{t_o}}$$

$$-\ln R = \left[\frac{2Q-P}{2PQ-2Q+P}\right][-\ln S] \qquad \ldots (3.45)$$

and

$$E_{OUT} = \frac{Mk^2(-\ln R)E^2}{\ell_o^2 t_o}\left[F - \frac{N}{F^{0.45}}\right] \qquad \ldots (3.40)$$

where

$$F = \frac{G_o H_o c\ell_o \sqrt{t_o}}{PQ(-\ln RS)} \quad \text{and} \quad M = 3.50 \times 10^{-4}$$

The above is to be calculated at different input energies (E), with the following parameters fixed:-

loss coefficient of rod (β); total of other losses per pass (1-D);

effective radius of output as fraction of rod radius (k)

stored energy per unit gain for the rod material $\left(\frac{h\nu}{\sigma}\right)$

Cavity transfer efficiency (G_o); flash tube efficiency (H_o).

The program calculates the differences X and Y between the left and right hand sides of Equ. 3.46 and Equ. 3.47 respectively, for many pairs of possible values for c and t_o. These differences will both be zero for the correct pair of values. All the other parameters are also calculated for all pairs of c and t_o, and the optimum set of values are those corresponds to zero for both X and Y.

Changes of nomenclature in the program are:-

k becomes V; β becomes B; $-\ln D$ becomes C1; c becomes C;

t_o becomes T; ℓ_o becomes L; $-\ln R$ becomes R1;

E_{OUT} becomes E1

and the program itself is as follows:-

```
RFS111     13:51    G265 A 04/06/73

95  READ J
100 READ N
110 READ E,G,H
120 READ V
130 READ B
140 READ C1
150 READ S1,S2
160 READ T1,K1
170 READ V2
175 LET D=.71*J↑.5
177 LET M=(1.31E-3)/J
180 FOR Q1=1 TO 10
190 PRINT
200 PRINT
210 LET C=Q1*S1+S2
220 PRINT "C = ";C
230 PRINT
240 FOR I1=1 TO 10
250 LET T=T1*(K1)↑I1
260 LET P=1+N*T*EXP(C/4)
265 LET K=EXP(D/(T↑.25))
270 LET L=M*C*C*E*(P-1)/(SQR(T)*(4*P-C*P+C))
280 IF L<0 THEN 500
290 LET Q=1+(M*E*C)/(L*SQR(T))
300 LET X=L*B*P/(2*Q*(P-1-(D*P)/(4*T↑.25)))-L*B-C1
310 LET R1=(2*L*B+C1)*(2*Q-P+.5*P*Q*LOG(K))/(2*P*Q+P-2*Q-.5*P*Q*LOG(K))
320 LET F=G*H*C*400*2*J*L*T↑.5/(P*Q*K*(R1+2*L*B+C1))
330 IF F<0 THEN 500
340 LET Y=.0037*F↑1.45+.9-5.8*P*Q/(2*P*Q+P-2*Q-.5*P*Q*LOG(K))
350 IF R1<0 THEN 500
360 LET E1=V*V*E*E*R1*(((.22E-6)/(J*J))*F-(.117E-3)/(J*J*F↑.45))/(L*L*T)
370 LET T5=INT(T*10↑4+.5)/10↑4
380 LET E5=INT(E1*10↑4+.5)/10↑4
390 PRINT
400 PRINT T5;TAB(8);E5
410 LET X2=ABS(X)
420 LET Y2=ABS(Y)
430 IF X2>V2 THEN 500
440 IF Y2>V2 THEN 500
450 LET X5=INT(X*10↑4+.5)/10↑4
460 LET Y5=INT(Y*10↑4+.5)/10↑4
470 LET Y5=INT(L*10↑4+.5)/10↑4
480 LET R5=INT(R1*10↑4+.5)/10↑4
490 PRINT T5;TAB(8);E5;TAB(16);X5;TAB(24);Y5;TAB(32);L5;TAB(40);R5
500 NEXT I1
510 NEXT Q1
515 DATA .2
520 DATA .66
530 DATA 40,.8,.3
540 DATA .7
550 DATA .006
560 DATA .1
570 DATA .1,7.9
580 DATA .056, 1.04
590 DATA 5
595 DATA 18
600 END

RUN
```

APPENDIX III

A Holographic Photoelastic Study of a Spinning Prism

Introduction

Spinning optical elements have uses which include optical scanning, time resolution of a varying light pattern and Q-switching of lasers. These applications often require as high a rotation speed as possible and by rotating the elements on magnetic or air bearings speeds of 300,000 r.p.m. and above have been achieved. An important consideration at these high speeds is the possibility of failure of the stressed material of the optical element as well as the probability of distortion in the material sufficient to alter significantly the optical wavefront transmitted or reflected.

In our programme of research on pulsed lasers for optical applications, we have developed a pentagonal internally reflecting prism integrally mounted within a hollow air-driven turbine running in air bearings for use as a laser Q-switch. The light enters and leaves the end faces at Brewster's angle and is reflected from one of the side faces (Fig. III.1). In this application optical wavefront distortions can seriously affect the mode of operation of the laser. Contributions to the deformation could come from:

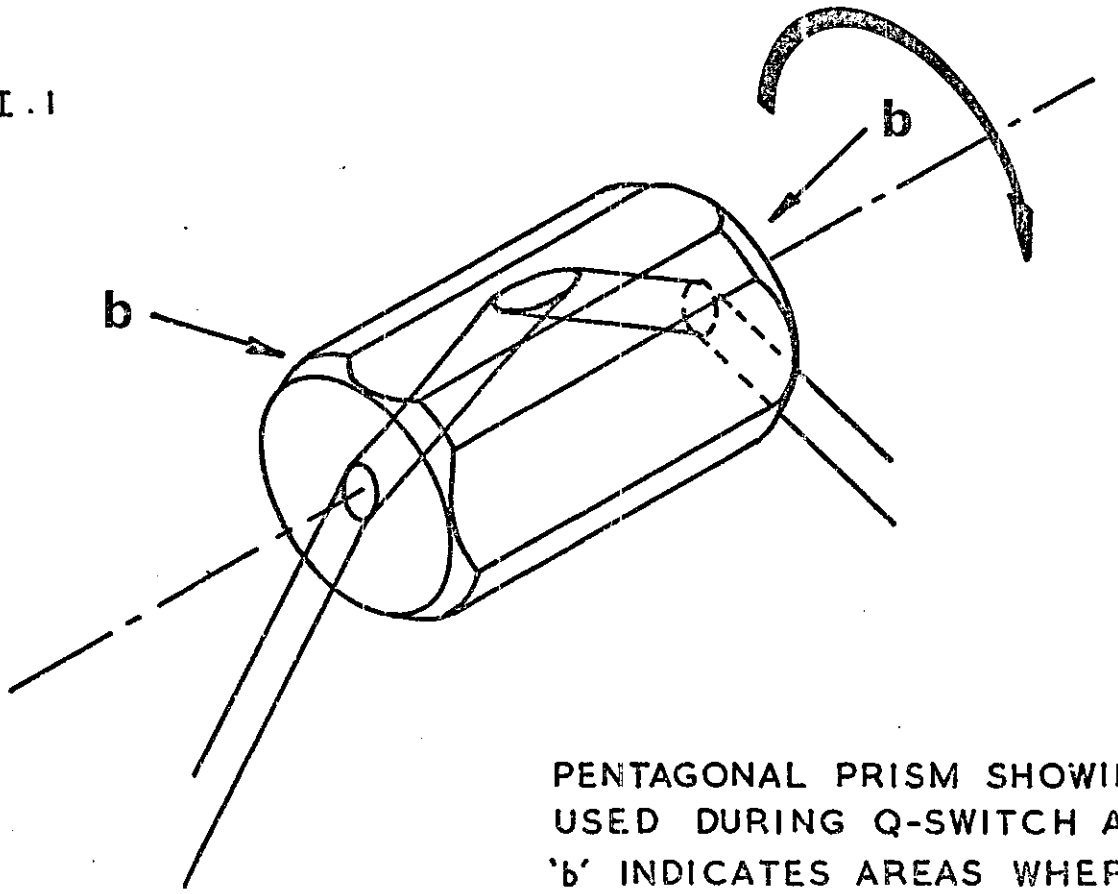
(i) distortion of the shape of the prism surfaces

(ii) refractive index gradients

(iii) stress birefringence, both throughout the prism and, more particularly, in the regions near the points of external constraint where there may be local stress concentrations.

Particular importance is attached to the last of these, namely, the effect at the mounting areas (b) of the prism where differential expansion

FIGURE III.1



PENTAGONAL PRISM SHOWING THE LIGHT PATH USED DURING Q-SWITCH ACTION.
'b' INDICATES AREAS WHERE PRISM IS MOUNTED.

DIVISION OF OPTICAL METROLOGY, NATIONAL PHYSICAL LABORATORY, TEDDINGTON, MIDDLESEX.	DIMENSIONS		SCALE		TITLE FIGURE 1
	PROJECTION		MATERIAL		
	DRAWN	R.F. STEVENS	FINISH		
	CHECKED		NO. OFF		
	DATE		TOLERANCE		

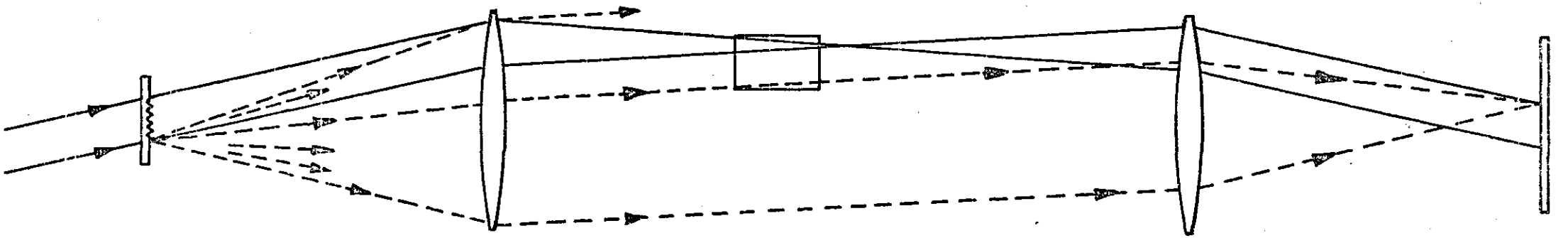
between prism and housing and imperfections in construction may well give high local stress.

It is desirable before putting new prism units into service to subject them to an optical test to discover the extent of these non-uniform regions, if any, and their positions in three dimensions. It is possible to do both of these by (a) using an axially directed monitoring beam which 'sees' all the prism including the regions of high stress concentration which are clear of the path of the beam under conditions of Q-switch operation, (b) using a holographic technique with sufficient discrimination in depth. As it is essentially optical path difference information that we require the double exposure technique of interference holography is used (Burch, Ennos and Wilton 1966). An advantage of this method is that spatial variations of optical path which occur in both exposures are eliminated.

Procedure

A diagram of the system used is shown in Figure III.2. The light source employed was a ruby laser Q-switched with a spinning prism similar to the one under test. For recording the hologram less than 10 mJ was required and the pulse length of 50 ns was sufficiently short to 'freeze' the motion of the prism. The holographic system (Gates 1968) employed a controlled scatter plate as beam splitter; it produced a hologram in a plane conjugate with the plane of the scatter plate and bearing a Fourier transform relationship with a plane very close to the object. In this system the normal requirements on spatial and temporal coherence are relaxed hence imposing fewer restrictions on the laser source. Both signal and reference beam passed through the prism under test. The prism was placed just beyond the focus of the reference beam, at which point this beam was not sufficiently concentrated to break down the material of the spinning prism but was of sufficiently small area for the phase variations across the reference wave

FIGURE III.2 DIAGRAM OF HOLOGRAPHIC SYSTEM



a Scatter plate beam splitter

b,d Lenses

c Prism under test

e Hologram plate

Full lines are reference rays

Dotted lines are examples of scattered rays

DIVISION OF OPTICAL METROLOGY, NATIONAL PHYSICAL LABORATORY, TEDDINGTON, MIDDLESEX.	DIMENSIONS		SCALE		TITLE
	PROJECTION		MATERIAL		
	DRAWN	R. S.	FINISH		FIGURE 2.
	CHECKED		NO. OFF		
	DATE	JAN. 2. 1970	TOLERANCE		

due to the prism to be negligible. These phase variations can be considered negligible when the resulting decrease in visibility of the interference pattern reconstructed from the hologram is small.

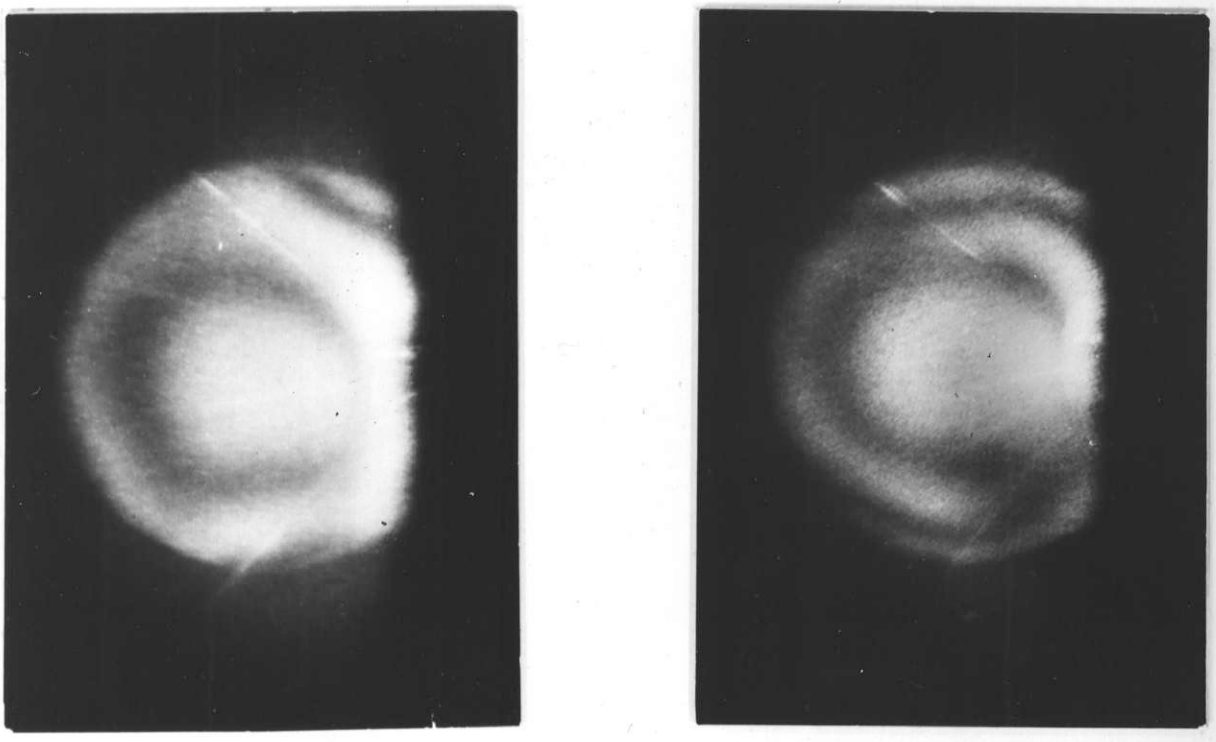
The hologram plate was given two exposures: one exposure was made with the prism stationary and the other with the prism at the required speed. There was no control over the relative positions of the prism in the two exposures. This was not necessary because the tolerances on the construction of the prism ensured that the wavefront transmitted by the prism when stationary was aberration-free to a small fraction of a wavelength. Consequently, a rotation of the prism did not disturb the transmitted wavefront. Even in less well corrected prisms having regular distortions such as tilt or lens it is still unnecessary to provide rotational synchronization since these distortions merely result in no modification of the transmitted wavefront or one which can be allowed for. Irregular static optical distortion however could only be eliminated by correctly phasing the prism and ruby laser source.

The doubly-exposed and processed hologram, when re-illuminated with the reference wave, creates two coherent reconstructed waves which interfere showing fringes across the prism aperture. These represent the change in optical path across the aperture. By taking holograms at different speeds from zero to the maximum of 120,000 r.p.m. the optical path length changes in the prism were determined as a function of position in the prism and speed. Examples of reconstructions at two speeds are shown (Fig. III.3).

Three-dimensional information

The 3-dimensional information in the hologram is revealed by either observing the parallax effects of translating the hologram across a small viewing aperture or by reconstructing from the entire hologram and focussing on different planes in the reconstruction. For the purposes of testing the

Figure III 3



90,000 r.p.m

120,000 r.p.m

Holographic interferograms showing distortion in a spinning silica 5-sided prism at two different rotational speeds.

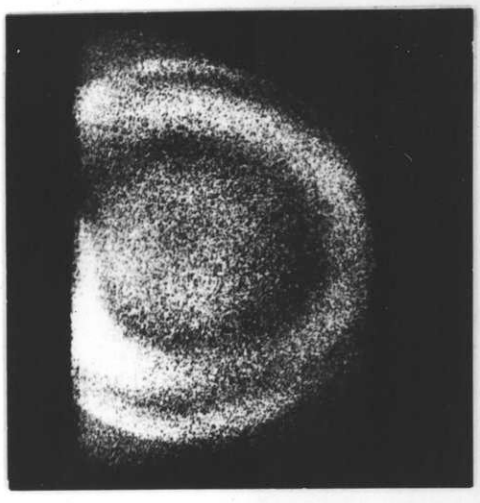
prism only a visual qualitative examination by either of these methods was necessary to check for freedom from local changes of refractive index. The quantitative determination of the variation of refractive index in three dimensions is more difficult but a simplified approach can be made using the parallax method mentioned above.

This method, of using separate small areas of the hologram for reconstruction, is equivalent in our optical system to viewing the prism from different directions. Variation of the refractive index in 3-dimensions results in general in a variation of integrated optical path with the ray direction through any given point of the prism. Corresponding variations of the observed interference fringe pattern are seen for a movement across the hologram, and an example is shown in Figure III.4.

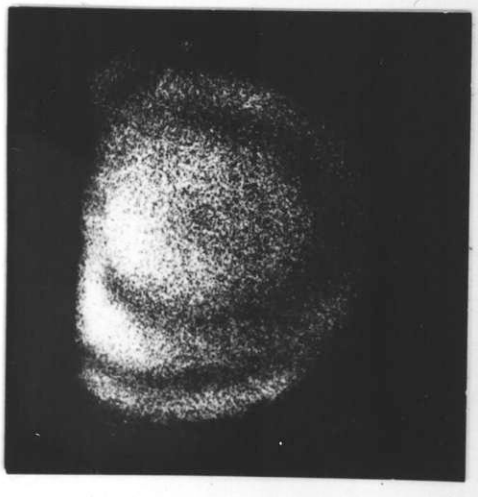
In deriving a relationship between the 3-dimensional refractive index variation and the variation of the observed fringe pattern with a movement across the hologram plate, we will assume the refractive index to be a scalar quantity. Birefringence, which leads to a polarization dependant refractive index, will be ignored here although some qualitative discussion is given later on one aspect of its effect. The following is valid then if no birefringence is present and is otherwise a valuable approximation in so far as the birefringence is generally small in comparison with other refractive index changes.

The derivation will be given for the two-dimensional case, see Fig. III.5. In our optical system the wavefront which focusses at a point P on the hologram passes through the object at an angle θ to the axis. The interferogram reconstructed from a small area at P gives the optical path difference $L_p(x)$ (path difference between a particular ray, coordinate x, of the signal beam, and the reference beam) as a function of the coordinate x in the mid-plane of the prism. Now since the value of

Figure III 4

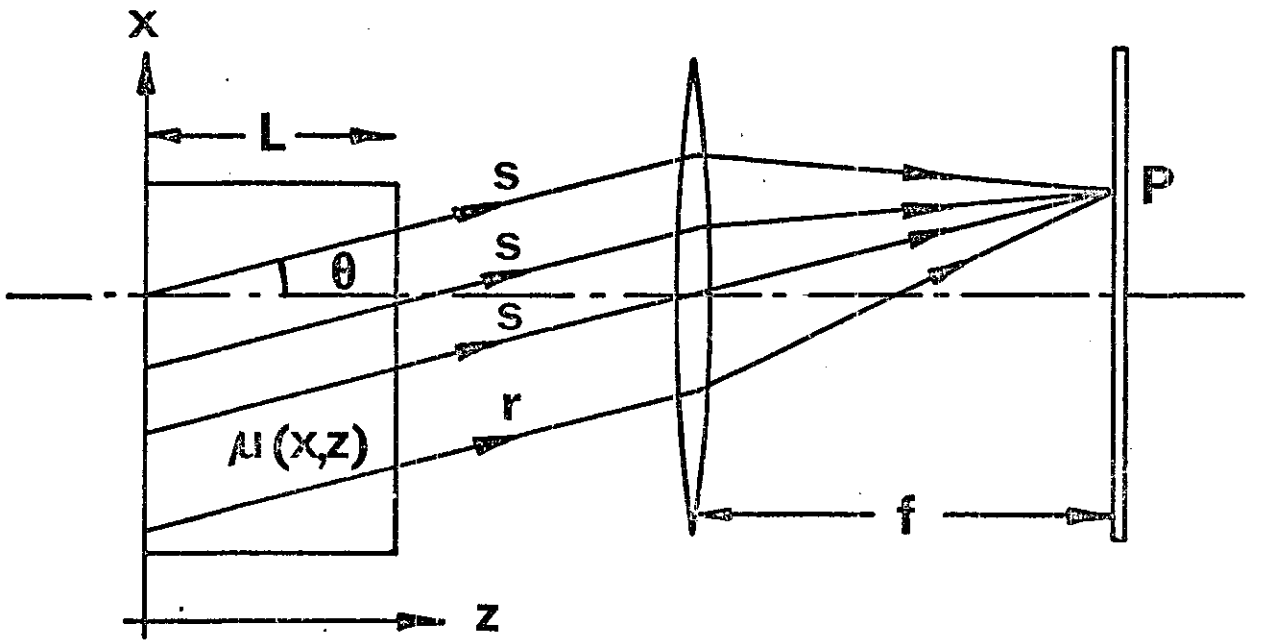


Reconstruction using a small area at the top of the hologram.



Reconstruction using a small area at the bottom of the hologram.

FIGURE III.5



DIVISION OF OPTICAL METROLOGY, NATIONAL PHYSICAL LABORATORY, TEDDINGTON, MIDDLESEX.	DIMENSIONS		SCALE		TITLE
	PROJECTION		MATERIAL		
	DRAWN	R. F. STEVENS	FINISH		FIGURE 5
	CHECKED		NO. OFF		
	DATE		TOLERANCE		

θ is uniquely determined by P, $L_P(x) \equiv L_\theta(x)$. Thus by using small areas at different points of the hologram we are able to plot out $L_\theta(x)$ for different values of θ. The information obtained can thus be denoted by $L(x,\theta)$. $L(x,\theta)$ is related to the refractive index distribution $\mu(x,z)$ by:-

$$L(x,\theta) = \int_0^{\ell} \mu(x + z\ \tan\theta, z)\ \frac{dz}{\cos\theta} - \frac{\mu_o \ell}{\cos\theta} \qquad \ldots \text{III.1}$$

where μ_o is the mean refractive index in the reference beam.

This expression is, of course, only valid for small variations in the index μ such as would not change the ray directions appreciably. We can re-write this in the form:-

$$M(x,t) = \int_0^{\ell} \mu(x + tz, z)\ dz + C \qquad \ldots \text{III.2}$$

where $M(x,t)$ is written for $L(x,\theta)\ \cos\theta$ and $t = \tan\theta$ and the constant $\mu_o \ell$ is written as C.

This is a non-linear integral equation for the distribution of the refractive index as a function of position in the prism. We note first that an arbitrary function of z only can be added to the integrand without changing the result, since it would merely change the value of the constant C. Thus a solution to the integral equation is not unique but can have superimposed upon it a refractive index variation which is a function of z only. The solution obtained does however contain information about the distribution of refractive index and can for example pinpoint localised distortions. To obtain a unique solution, it is necessary for the z-distribution of refractive index to be known at one point in the field and it is in fact generally true that information of this nature is available.

A practical method of solving the equation is to transform it into a set of simultaneous equations and solve these by matrix methods on a computer. This is in principle no less accurate a method than solving the equation analytically because the variables x and t are governed by an uncertainty relation and cannot be measured at an infinite number of points. If, for example, the area of the part of the hologram from which measurements are taken is reduced, the precision of θ is increased but, because that part now contains less information, the precision of x is decreased.

Details of the transformation need not be given here: it is sufficient to state that $M(x,t)$ is measured at a rectangular grid of points in (x,t) space and the values of μ in (x,z) space are treated as unknowns.

Theory of Spinning Cylinder

Let us now consider the symmetrically distributed deformation due to rotation of the prism. To determine what is to be expected for the contributions to this deformation, we make the simplifying assumption that the prism approximates to a solid cylinder rotating about its axis.

By considering an element of the spinning prism (Figure III.6a) and assuming that stresses along the axial direction are negligible, the radial equation of motion can be shown to be:-

$$p_\phi - \frac{d}{dr}(rp_r) = \rho r^2\omega^2 \qquad \ldots \text{ III.3}$$

where: p_ϕ = hoop stress: ρ = density

p_r = radial stress: ω = angular velocity

If the element moves out a distance u under the stresses (Figure III.6b) then we have,

$$\text{radial strain, } e_r = \frac{du}{dr}; \quad \text{hoop strain, } e_\phi = \frac{u}{r}$$

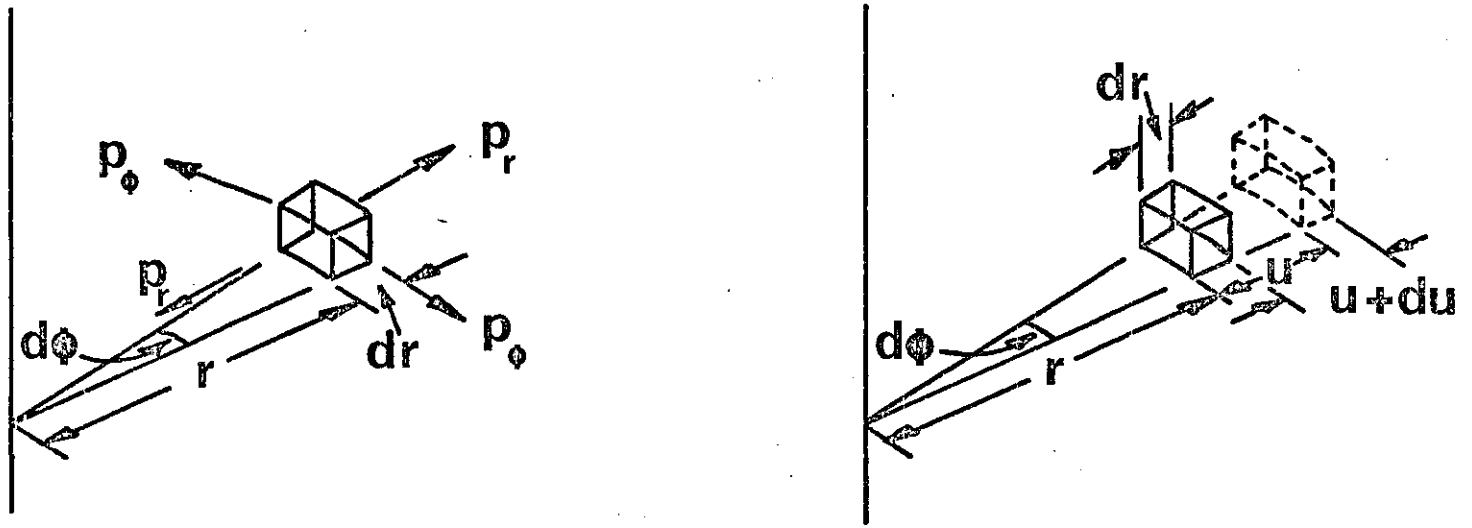


FIGURE III.6

DIVISION OF OPTICAL METROLOGY, NATIONAL PHYSICAL LABORATORY, TEDDINGTON, MIDDLESEX.	DIMENSIONS		SCALE		TITLE
	PROJECTION		MATERIAL		FIGURE 6
	DRAWN	M. STEVENS.	FINISH		
	CHECKED		NO. OFF		
	DATE		TOLERANCE		

but $$e_r = \frac{1}{Y}\left[p_r - \sigma p_\phi\right] \; ; \; e_\phi = \frac{1}{Y}\left[p_\phi - \sigma p_r\right] \qquad \ldots \text{III.4}$$

where Y = Young's modulus and σ = Poisson's ratio.

Consequently, we can solve the above five equations for p_r and p_ϕ using the boundary conditions that $p_r = 0$ at $r = a$ (perimeter) and that there is no discontinuity at $r = 0$. We obtain:-

$$p_r = \frac{1}{8}(3 + \sigma)\rho\omega^2(a^2 - r^2) \qquad \ldots \text{III.5a}$$

$$p_\phi = \frac{1}{8}(3 + \sigma)\rho\omega^2\left(a^2 - \frac{1 + 3\sigma}{3 + \sigma} r^2\right) \qquad \ldots \text{III.5b}$$

(i) There is a lens effect due to a variation of length (ℓ) across the prism aperture. We define the fringe number (n) as the optical path length change from the static path length divided by the wavelength (λ).

For the lens effect:- $n = \mu\Delta\ell/\lambda$

where $\frac{\Delta\ell}{\ell}$ = axially directed strain, $e_z = -\frac{\sigma}{Y}(p_r + p_\phi)$

This experiment measures the difference between the fringe number at the perimeter and the fringe number at the centre.

Using the above equations and inserting values appropriate to our prism, this fringe number difference is calculated to be + 1.9 at 120,000 r.p.m.

(ii) There are refractive index (μ) gradients due to stress gradients in the material. The difference in refractive index between the centre and perimeter of the cylinder gives rise to a fringe number difference similar to that in (i). For this effect:- $n' = \ell\Delta\mu/\lambda$.

It can be shown (Morey 1954) that n' is proportional to n.

The calculated fringe number difference was + 2.5 at 120,000 r.p.m.

(iii) The stress birefringence leads to an asymmetric change in the optical path length through the prism. The principal stresses in a uniform cylinder rotating about its axis are directed radially and tangentially and the difference between the two gives rise to a different optical path length for an incoming ray polarized along the radius and one polarized along the tangent, perpendicular to the radius. As the beam incident on the prism is uniformly polarized in one direction there is one radius for which the polarization is perpendicular to it and another radius for which the polarization is parallel to it. Thus there are observed to be different numbers of fringes along these two radii, i.e. the fringes are not circular. The fringe number difference is:- $n_\phi - n_r = t\delta\mu/\lambda$ where $\delta\mu$ is the birefringence and the subscripts refer to the direction of polarization. In a similar way to (ii) above, it can be shown that

$$n_\phi - n_r \text{ is proportional to } p_\phi - p_r.$$

In our case, calculation gives $n_\phi - n_r = 0.6$ at 120_0^0,000 r.p.m.

The stress birefringence has a further effect. Consider a radius of the prism orientated at 45° to the input polarization and consider a point on the radius at which the birefringence is equivalent to half a wavelength. Then the prism acts as a $\frac{1}{2}$-wave plate at this point and the polarization of the emerging beam is 90° to that of the ingoing one. As it is also at 90° to that of the reference beam the interference between these two beams gives no intensity variation on the hologram plate. Thus no hologram is formed and this point of the prism cannot be reconstructed. Since our fringes are obtained by interference between two reconstructions they do not appear at points in the reconstruction at which one of the reconstructions is not present. This is the case we have postulated. Moving away from these

points increases the intensity of the corresponding reconstruction and the fringe visibility increases.

It is important to know where and how big the regions of low fringe visibility are. For our prism there are calculated to be four regions at a radius of 8 mm (prism radius = 8.5 mm) and on radii all making 45° to the direction of the input polarization. Their extent for a fringe visibility 0.1 is calculated to be ~ 0.4 mm and is considered small enough not to be troublesome in the evaluation of the hologram. The estimate given is pessimistic since the presence of a range of angles in the object tends to fill in these regions of low visibility.

Conclusions

The object of the experiment was principally to detect possible non-uniform distortions in the prism, as these would be most detrimental to its operation as a Q-switch. It can be seen from Figure III.3 that such effects are not detectable; the fringes are symmetrical and the transverse optical path gradient is small. This gradient is about half that indicated from the calculation but varies with turbine speed as expected. In view of the assumption of cylindrical shape and the limited accuracy of values for Y, and in particular the stress-optical coefficients, the results may be regarded as satisfactory.

When the fringe pattern was reconstructed through the entire hologram (angular range = 4°), there was no perceptible change in the fringe structure on focussing through the reconstruction. When the reconstruction was viewed successively through different parts of the hologram a fringe shift of perhaps a quarter-fringe was the most that could be detected. These results suggest that there is very little variation in the axial direction. The sensitivity of the system as a whole however would need to be increased, by widening the range of θ, to be able to put a figure on

this. No effect was found which could have been measured with enough accuracy to use in solving Equation III.2.

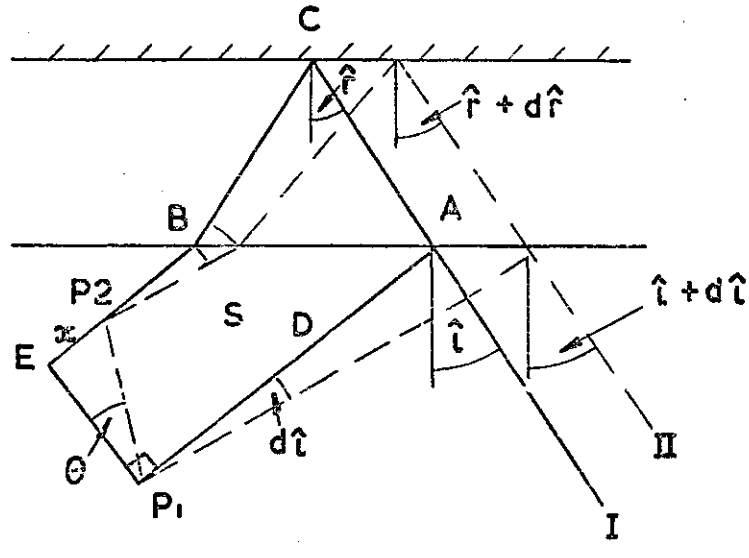
The fact that the observed fringes are roughly in accord with the theory verify that the material is stressed well below its yield point since the maximum stress as given by Equation III.5 is 10^7 Newtons/m^2 and the breaking stress in tension is 3 to 4 $\times$ 10^7 Newtons/m^2.

Summary

An experiment has been described which gives information on the optical distortions present in a spinning prism. The reconstructed interference fringes were those expected for the prism in a freely spinning state, thus showing that stresses at the points at which the prism is mounted did not adversely affect its optical performance.

APPENDIX IV

Exposure Plate



Rays I and II originating from the same point of the object come to a focus at P_1 and P_2 in the first and second images respectively.

Assuming the object (or intensity distribution to be recorded) is normal to the optical axis, and if $d\hat{i}$ is small, then the plane of $P_1E (\perp P_1A)$ is the plane in which the image is in focus.

θ is therefore the angle between the plane in which a point of the object is in focus in all the images, and the plane of each image. It is necessary, if the imaging plate is to operate successfully, for these two planes to coincide; i.e. $\theta = 0$.

Calculation of θ

Now $\tan\theta = x/s$

and $x = (P_1A - DA) - P_2B = P_1A - P_2B - 2t \tan\hat{r} \sin\hat{i}$

and $s = 2t \tan\hat{r} \cos\hat{i}$

$$\therefore \quad \tan\theta = \frac{(P_1A - P_2B)}{2t\tan\hat{r}\cos\hat{i}} - \tan\hat{i}$$

To calculate $P_1A - P_2B$, we proceed as follows:-

$$P_2B = \frac{1}{d\hat{i}} \times \text{ray separation at B in air}$$

$$= \frac{1}{d\hat{i}} \times \frac{\cos\hat{i}}{\cos\hat{r}} \times \text{ray separation at B in glass}$$

$$= \frac{\cos\hat{i}}{d\hat{i}\cos\hat{r}} \left[\text{ray separation at A in glass} - \frac{2t\, d\hat{r}}{\cos\hat{r}} \right]$$

$$= \frac{\cos\hat{i}}{d\hat{i}\cos\hat{r}} \times \frac{\cos\hat{r}}{\cos\hat{i}} \times \text{ray separation at A in air} - \frac{2t\cos\hat{i}}{\cos^2\hat{r}} \frac{d\hat{r}}{d\hat{i}}$$

$$= \frac{\text{ray separation at A in air}}{d\hat{i}} - \frac{2t\cos\hat{i}}{\cos^2\hat{r}} \frac{d\hat{r}}{d\hat{i}}$$

$$= P_1A - \frac{2t\cos\hat{i}}{\cos^2\hat{r}} \frac{d\hat{r}}{d\hat{i}}$$

$$\therefore \quad P_1A - P_2B = \frac{2t\cos\hat{i}}{\cos^2\hat{r}} \frac{d\hat{r}}{d\hat{i}}$$

but $$\sin\hat{i} = \mu \sin\hat{r}\,.$$

$$\therefore \quad \frac{dr}{di} = \frac{\cos \hat{i}}{\mu \cos \hat{r}}$$

$$\therefore \quad P_1A - P_2B = \frac{2t\cos^2 \hat{i}}{\mu \cos^3 \hat{r}}$$

$$\therefore \quad \text{By substitution:} \quad \tan \theta = \frac{2t \cos^2 \hat{i}}{\mu \cos^3 \hat{r}.2t \tan \hat{r} \cos i} - \tan \hat{i}$$

$$\text{Or} \quad \tan \theta = \frac{\cot \hat{i}}{\cos^2 \hat{r}} - \tan \hat{i} .$$

$\therefore$ The condition for $\theta = 0$ is just $\tan \theta = 0$

$$\text{or} \quad \frac{\cot \hat{i}}{\cos^2 \hat{r}} = \tan \hat{i} \quad \text{i.e.} \quad \cos^2 \hat{r} = \cot^2 \hat{i}$$

The solution of this equation, for a glass of refractive index 1.5, is:-

$$\hat{i} = 49^\circ$$

Maximisation of image separation S

$$S = 2t \tan \hat{r} \cos \hat{i}$$

Maximum S occurs when $\frac{d}{dr}(S) = 0$

Differentiating the equation for S, and rearranging the resulting equation leads to:-

$$\cos^2 \hat{r} = \cot^2 \hat{i} .$$

Being the identical equation, we again have the solution, $\hat{i} = 49^\circ$

APPENDIX V

The Coherence between Two Points in a Radiation Field

The two points are designated P_1 and P_2 (Fig. 5.1). Let the disturbances at P_1 and P_2 be $V_1(t)$ and $V_2(t)$ respectively where the scalar notation of field is sufficient in this case.

An interference experiment is performed as shown in Fig. 5.2 The disturbance $V(t)$ at Q is the sum of disturbances from P_1 and P_2 and is thus given by:-

$$V(t) = k_1 V_1(t-t_1) + k_2 V_2(t-t_2) \qquad \ldots (V.1)$$

where k_1 and k_2 are appropriate attenuation factors, and are purely imaginary, since there is a $\pi/2$ phase shift at initiation of the secondary waves from P_1 and P_2, and where $x_1 = ct_1$ and $x_2 = ct_2$ are the distances of P_1 and P_2 from Q.

The disturbance at Q is measured by the energy density E at that point, the energy density being related to the disturbance $V(t)$ by the relation:-

$$E = \int_t CV(t)V^*(t)dt \qquad \ldots (V.2)$$

where C = constant.

Substituting for $V(t)$ from Equ. V.1:-

$$E = C\int [k_1 V_1(t-t_1)+k_2 V_2(t-t_2)]\,[k_1 V_1(t-t_1)+k_2 V_2(t-t_2)]^* dt$$

$$= C\int k_1 k_1^* V_1(t-t_1) V_1^*(t-t_1)dt + C\int k_2 k_2^* V_2(t-t_2) V_2^*(t-t_2)dt \quad \ldots (V.3)$$

$$+C\int k_1 k_2^* V_1(t-t_1) V_2^*(t-t_2)dt + C\int k_2 k_1^* V_2(t-t_2) V_1^*(t-t_1)dt$$

This equation can be simplified by noting that the energy density at Q from P_1 alone would be

$$E_1 = C\int k_1 V_1(t) k_1^* V_1^*(t)dt \quad \ldots (V.4a)$$

and the energy density at Q from P_2 alone would be:-

$$E_2 = C\int k_2 V_2(t) k_2^* V_2^*(t)dt \quad \ldots (V.4b)$$

and since both these integrals are invariant to a change in the origin of time and $V_1(t)$ and $V_2(t)$ can consequently be replaced by $V_1(t-t_1)$ and $V_2(t-t_2)$ respectively, Equ. V.3 becomes by substitution:-

$$E = E_1 + E_2 + C\int k_1 V_1(t-t_1) k_2^* V_2^*(t-t_2)dt + C\int k_2 V_2(t-t_2) k_1^* V_1^*(t-t_1)dt$$

$$\ldots (V.5)$$

Further simplification can be introduced as follows:-

The third and fourth terms in Equ.V.5 are complex conjugates of each other and their sum is just twice the real part of each. Thus Equ. V.4 can be rewritten:-

$$E = E_1 + E_2 + 2Ck_1 k_2^* \,\mathrm{Re}\left[\int V_1(t-t_1) V_2^*(t-t_2)dt\right] \quad \ldots (V.6)$$

Now Equations 5.3 and 5.4 of Chapter 5 can be combined to eliminate V_{12} and we get:-

$$E = E_1 + E_2 + 2\sqrt{E_1}\sqrt{E_2}\ \mathrm{Re}\left[\gamma_{12}\ e^{-2\pi i\nu\tau}\right] \qquad \ldots (V.7)$$

where $\tau = t_2 - t_1$

Comparison of V.6 and V.7 yields:-

$$\gamma_{12} = \frac{e^{2\pi i\nu\tau}\int V_1(t-t_1)V_2^*(t-t_2)dt.k_1k_2^*}{\sqrt{E_1}\sqrt{E_2}} \qquad \ldots (V.8)$$

Substituting for E_1 and E_2 from Equ.V.4, remembering that k_1 and k_2 are purely imaginary and hence $k_1^* = -k_1$ and $k_2^* = -k_2$ respectively :-

$$\gamma_{12} = \frac{e^{2\pi i\nu\tau}\int V_1(t-t_1)V_2^*(t-t_2)dt}{\sqrt{\int V_1(t)V_1^*(t)dt}\ .\ \sqrt{\int V_2(t)V_2^*(t)dt}} \qquad \ldots (V.9)$$

The next step is to eliminate t_1 and t_2 from this equation, since we know that the coherence is independent of the method of measurement.

Let the disturbances be represented in terms of their spectral compositions i.e. as a Fourier integral:

Thus $$V(t) = \int_0^\infty v(\nu)\ e^{-2\pi i\nu t}\ d\nu \qquad \ldots (V.10a)$$

where $v(\nu)$ = amplitude of the component of frequency ν

and, by the Fourier inversion formula:-

$$v(\nu) = \int_0^\infty V(t)\, e^{2\pi i\nu t}\, dt \qquad \ldots (V.10b)$$

Let $V_2^*(t-t_2)$ of Equation V.9 be replaced by its Fourier integral:-

$$\therefore \gamma_{12} = \frac{e^{2\pi i\bar{\nu}\tau} \int V_1(t-t_1)\left[\int v_2^*(\nu) e^{2\pi i\nu(t-t_2)} d\nu\right] dt}{\sqrt{\int V_1(t)V_1^*(t)dt} \cdot \sqrt{\int V_2(t)V_2^*(t)dt}}$$

where $\bar{\nu}$ = mean frequency

$$\therefore \gamma_{12} = \frac{e^{2\pi i\bar{\nu}\tau} \int \left[\int V_1(t-t_1) e^{2\pi i\nu(t-t_1} dt\right] v_2^*(\nu) e^{-2\pi i\nu\tau} d\nu}{\sqrt{\int V_1(t)V_1^*(t)dt} \cdot \sqrt{\int V_2(t)V_2^*(t)dt}}$$

and from the Fourier inversion formula with respect to $V_1(t-t_1)$:-

$$\gamma_{12} = \frac{e^{2\pi i\bar{\nu}\tau} \int v_1(\nu) v_2^*(\nu) e^{-2\pi i\nu\tau}\, d\nu}{\sqrt{\int V_1(t)V_1^*(t)dt} \cdot \sqrt{\int V_2(t)V_2^*(t)dt}}$$

$$= \frac{\int G_{12}(\nu) e^{-2\pi i(\nu-\bar{\nu})\tau}\, d\nu}{\sqrt{\int V_1(t)V_1^*(t)dt} \cdot \sqrt{\int V_2(t)V_2^*(t)dt}} \qquad \ldots (V.11)$$

where $G_{12}(\nu)$ = 'Mutual Spectral Density'

At this point we assume that the spectral bandwidth is small:-

$$\text{i.e.} \quad (\nu-\bar{\nu})\tau << 1$$

$$\therefore \quad e^{-2\pi i(\nu-\bar{\nu})\tau} = 1$$

$\therefore$ Equ. V.11. becomes:-

$$\gamma_{12} = \frac{\int G_{12}(\nu)d\nu}{\sqrt{\int V_1(t)V_1^*(t)dt}\sqrt{V_2(t)V_2^*(t)dt}} \qquad \ldots (V.12)$$

The numerator can now be converted back in terms of $V_1(t)$ and $V_2(t)$ by an identical proof to that given above, and we get:-

$$\gamma_{12} = \frac{\int V_1(t)V_2^*(t)dt}{\sqrt{\int V_1(t)V_1^*(t)dt}\cdot\sqrt{\int V_2(t)V_2^*(t)dt}} \qquad \ldots (V.13)$$

Transverse coherence function

This is the coherence between P_2 and P_3 of Fig. 5.1 and can immediately be written down from Equ. V.13 :-

$$\gamma_{32} = \frac{\int V_3(t)V_2^*(t)dt}{\sqrt{\int V_3(t)V_3^*(t)dt}\cdot\sqrt{\int V_2(t)V_2^*(t)dt}} \qquad \ldots (V.14)$$

Temporal coherence function

This is the coherence between P_1 and P_3 of Fig. ., where the two disturbances are related by:- $V_3(t) = V_1(t-t_o)$

where t_o = temporal separation of P_1 and P_3 = x_o/c.

Equ. V.13 is now:-

$$\gamma_{13} = \frac{\int V_1(t)V_1(t-t_o)dt}{\sqrt{\int V_1(t)V_1^*(t)dt}\sqrt{\int V_1(t-t_o)V_1^*(t-t_o)dt}} \quad \ldots (V.15)$$

By the same proof again, it is shown that:-

$$\int V_1(t)V_1(t-t_o)dt = \int G(\nu)e^{-2\pi i\nu t_o}\,d\nu$$

where $G(\nu)$ = 'Spectral density' or 'Power Spectrum', and is just the measured intensity at frequency ν

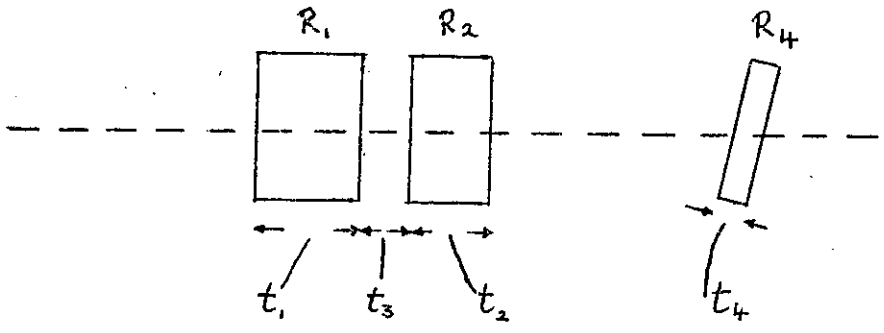
also $\int V(t-t_o)V^*(t-t_o)dt = \int V(t)V^*(t)dt = \int G(\nu)d\nu$ and Equ. .

finally becomes:-

$$\gamma_{13} = \frac{\int G(\nu)e^{2\pi i\nu t_o}\,d\nu}{\int G(\nu)d\nu} \quad \ldots (V.16)$$

APPENDIX VI

Reflectivity of Resonant Reflector



The amplitude reflectivity of the two reflector plates are, from Equ. 5.45:-

$$R_1 = \frac{(\delta_1 - 1)R}{(1-\delta_1 R^2)} \qquad \ldots (VI.1)$$

where $\delta_1 = \exp i\phi_1 = \exp i\left(\frac{4\pi\mu t_1}{\lambda}\right)$; $R = \frac{\mu-1}{\mu+1}$

$$R_2 = \frac{(\delta_2 - 1)R}{(1-\delta_2 R^2)} \qquad \ldots (VI.2)$$

where $\delta_2 = \exp i\phi_2 = \exp i\left(\frac{4\pi\mu t_2}{\lambda}\right)$

and, using the relations preceding Equ. 5.54, along with Equ. 5.50, the amplitude transmissivities of the same reflector plates are:-

$$T_1 = \frac{(1-R^2)\delta_1^{\frac{1}{2}}}{(1-\delta_1 R^2)} \qquad \ldots (VI.3)$$

$$T_2 = \frac{(1-R^2)\delta^{\frac{1}{2}}}{(1-\delta_2 R^2)} \qquad \ldots (VI.4)$$

Equ. 5.49 is now used to calculate the amplitude reflectivity (R_T) of the resonant reflector pair by substituting the above equations into it and by making use of the symmetry equalities,

$R_1 = R_1'$; $T_1 = T_1'$; $R_2 = R_2'$; $T_2 = T_2'$. Equ. 5.49 then becomes:-

$$R_T = \frac{R_1 + (T_1^2 - R_1^2)R_2\delta_3}{1-R_1R_2\delta_3}$$

$$= \frac{\dfrac{(\delta_1-1)}{(1-\delta_1R^2}R + \dfrac{(\delta_1-R^2)}{(1-\delta_1R^2)}\dfrac{(\delta_2-1)}{(1-\delta_2R^2)}R.\delta_3}{1 - \dfrac{(\delta_1-1)}{(1-\delta_1R^2)}R.\dfrac{(\delta_2-1)}{(1-\delta_1R^2)}R.\delta_3}$$

which, after some rearrangement becomes:-

$$R_T = \frac{(\delta_1-1)(1-\delta_2R^2)R-(\delta_1-R^2)(\delta_2-1)\delta_3R}{(1-\delta_1R^2)(1-\delta_2R^2)-(\delta_1-1)(\delta_2-1)R^2\delta_3} \qquad \ldots (VI.5)$$

We now transpose this into the form:-

$$R_T = \frac{A + iB}{C + iD} \qquad \ldots (VI.6)$$

whence the intensity reflectivity (ρ) is given by:-

$$\rho = \frac{A^2 + B^2}{C^2 + D^2} \qquad \ldots (VI.7)$$

R_T is complex due to the terms δ_1, δ_2 and δ_3 being complex.

$$\begin{aligned} \text{Let } \delta_1 &= X_1 + i\,Y_1 \quad \therefore\ X_1 = \cos\phi_1\ ;\ Y_1 = \sin\phi_1 \\ \delta_2 &= X_2 + i\,Y_2 \quad \therefore\ X_2 = \cos\phi_2\ ;\ Y_2 = \sin\phi_2 \qquad \ldots (VI.8) \\ \delta_3 &= X_3 + i\,Y_3 \quad \therefore\ X_3 = \cos\phi_3\ ;\ Y_3 = \sin\phi_3 \end{aligned}$$

by substituting Equ. VI.8 in Equ. VI.5 and collecting up real and imaginary parts:-

$$A = [Y_1Y_2R^2-(1-X_1)(1-R_2X_2)]R+[(R^2-X_1)(1-X_2)-Y_1Y_2]RX_3+[(1-X_2)Y_1+(R^2-X_1)Y_2]RY_3$$

$$B = [(1-R^2X_2)Y_1+(1-X_1)Y_2R^2]R+[(R^2-X_1)(1-X_2)-Y_1Y_2]RY_3-[(R^2-X_1)Y_2+(1-X_2)Y_1]RX_3$$

$$C = (1-R^2X_1)(1-R^2X_2)-Y_1Y_2R^4-[(1-X_1)(1-X_2)-Y_1Y_2]R^2X_3-[(1-X_1)Y_2+(1-X_2)Y_1]R^2Y_3$$

$$D = (1-R^2X_1)Y_2R^2-(1-R^2X_2)Y_1R^2-[(1-X_1)(1-X_2)-Y_1Y_2]R^2Y_3+[(1-X_1)Y_2+(1-Y_2)Y_1]R^2X_3$$

Substituting these equations into Equ. VI.7 and noting that X and Y depend on the wavelength enables the reflectivity (ρ) of a two plate resonant

reflector to be calculated as a function of wavelength (or wavenumber).

To calculate the further effect of the rejector plate, ρ must be multiplied by the square of the transmissivity (τ) of the rejector plate (the square, because the beam reflected from the resonant reflector passes through the rejector plate twice, once before and once after reflection).

The amplitude transmissivity (T_4) of the rejector plate is given by an equation analogous to Equ. VI.3:-

$$T_4 = \frac{(1-R_4^2)\delta_4^{\frac{1}{2}}}{(1-\delta_4 R_4^2)}$$

where $\delta_4 = \exp i\,\phi_4 = \exp i \left(\frac{4\pi\mu t_4}{\lambda} \right)$

R_4 = amplitude reflectivity of the surface of the plate

$$\therefore \quad \tau = T_4 T_4^* = \frac{(1-R_4^2)^2}{1+R_4^4-2R_4^2X_4} \qquad \ldots (VI.9)$$

where $X_4 = \cos \phi_4$.

The reflectivity of the combined resonant reflector and rejector plate is:

$$\rho\tau^2 = \frac{A^2+B^2}{C^2+D^2} \cdot \frac{(1-R_4^2)^4}{(1+R_4^4-2R_4^2X_4)^2} \qquad \ldots (VI.10)$$

A small computer program written in BASIC language for use with an on-line telephone linked computer enabled the reflectivity of any design of two plate reflector and rejector plate to be calculated as a function of wavenumber.

The program itself is listed below.

```
100 READ Z1,Z2,Z3,Z4
110 READ L1,L2,L3,L4
120 READ M,W
130READ K1,K2,S
140 LET R=(M-1)/(M+1)
150 LET P=12.5664
160 PRINT "REFLECTIVITY FROM OPTIMUM TO OPTIMUM +";K;"CM-1"
170 PRINT "          IN STEPS OF ";S;"CM-1"
180 FOR F=K1 TO K2 STEP S
190 LET X1=COS(Z1+P*M*L1*F)
200 LET Y1=SIN(Z1+P*M*L1*F)
210 LET X2=COS(Z2+P*M*L2*F)
220 LET Y2=SIN(Z2+P*M*L2*F)
230LET X3=COS(Z3+P*L3*F)
240 LET Y3=SIN(Z3+P*L3*F)
250 LET X4=COS(Z4+P*M*L4*COS(W)*F)
260 LET A1=(Y1*Y2*R↑2-(1-X1)*(1-R↑2*X2))*R
265 LET A2=((R↑2-X1)*(1-X2)-Y1*Y2)*R*X3
270 LET A=A1+A2+((1-X2)*Y1+(R↑2-X1)*Y2)*R*Y3
280 LET B1=((1-R↑2*X2)*Y1+(1-X1)*Y2*R↑2)*R
285 LET B2=((R↑2-X1)*(1-X2)-Y1*Y2)*R*Y3
290 LET B=B1+B2-((R↑2-X1)*Y2+(1-X2)*Y1)*R*X3
300LET C2=(1-R↑2*X1)*(1-R↑2*X2)-Y1*Y2*R↑4
305 LET C1=C2-R↑2*X3*((1-X1)*(1-X2)-Y1*Y2)
310 LET C=C1-R*R*Y3*((1-X1)*Y2+(1-X2)*Y1)
320 LET D2=-(1-R↑2*X1)*Y2*R↑2-(1-R↑2*X2)*Y1*R↑2
325 LET D1=D2-R↑2*Y3*((1-X1)*(1-X2)-Y1*Y2)
330 LET D=D1+R*R*X3*((1-X1)*Y2+(1-X2)*Y1)
340 LET R1=((A*A+B*B)*(1-R*R)↑4)/((C*C+D*D)*(1+R↑4-2*R*R*X4)↑2)
350 PRINT F,R1
360 NEXT F
370DATA 3.1416,3.1416,3.1416,0
380 DATA 4.31E-2,4.31E-2,6.25E-2,4.31E-2
390DATA 1.449,0.01
400DATA 0,8,1
410END
```

Bibliography

A. Akmanov, S.A., 1968; Sov.Phys.Uspekhi, 11, pp.609-636.

Alcock, A.J., 1971; Modern Optical Methods in Gas Dynamic Research (Plenum, London), pp.119-135.

Aleksandrov, E.B. et al. 1966; Sov.Phys., JETP, 22, pp.986-992.

Anliker, P. et al. 1972; Opt.Comm. pp137-138.

Aprahamian, R. et al. 1971; Experimental Mechanics pp1-6.

Armstrong, J.A. et al. 1962; Phys.Rev. 127, pp 1918-1939.

Arnold, D.H. and Hanna, D.C. 1969; J.Phys.D., 2, pp1174-1176.

Arecchi, F.T. et al. 1964; Il Nuovo Cimento, 34, pp6506-6520.

B. Barjot, G., 1971; J.App.Phys., 42, pp 3641-3642.

Bass, M. and Andringa, K., 1967; IEEE J.Quant.Electr. QE3, pp 621-626.

Beamish, J.K. et al. 1969; AIAA Journal, 7, pp 2041-2043.

Bhawalkar, D.D. et al. 1970; Opto-Electronics, 2, pp 90-97.

Biedermann, K., 1968; Optik, 28, pp 160-176.

Biedermann, K., 1969; Phot.Science and Eng., 13, pp 361-370.

Bjorkholm, J.E., 1966; Phys.Rev., 142, pp 126-136.

Bloembergen, N., 1965; Nonlinear Optics (Benjamin, New York).

Born, M. and Wolf, E., 1965; Principles of Optics (Pergamon, Oxford).

Borrelli, N.F. and Charters, M.L., 1965; J.App.Phys., 36, pp 2172-2174.

Boyd, G.D. and Gordon, J.P., 1961; Bell Syst.Tech.J., 40, pp 489-508.

Boyd, G.D. and Kogelnik, H., 1962; Bell Syst.Tech.J., 41, pp 1347-1369.

Boyd, G.D. and Kleinman, D.A., 1968; J.App.Phys., 39, pp 3597-3639.

Bradley, D.J. et al. 1968; Phil. Trans., 263A, pp 209-223.

Bradley, D.J., 1971; Digest of Technical Papers - IEEE/OSA CLEA Washington (New York IEEE), p 12.

Bradley, D.J., et al. 1972; 10th Int. Conf.High Speed Photography, Nice pp 117-121.

Brandewie, R.A. and Telk, C.L., 1967; JOSA, 67, pp 1221-1225.

Bret, G. and Gives, F., 1964; App.Phys.Lett., pp 175-176.

Burch, J.M. and Palmer, D.A., 1961; Optica Acta, 8, pp 73-80.

Burch, J.M., 1964; Proc. 3rd Int.Quant.Electr.Conf. pp 1187-1202.

Burch, J.M. et al. 1966; Nature, 209, pp 1015-1016.

C. Chesler, R.B., et al. 1970; Proc.IEEE, 58, pp 1899-1914.

Cirkovic, L., et al. 1968; App.Opt., 7, pp 981-982.

Collins, R.J., et al. 1961; J.App.Phys., 33, pp 2009-2011.

Collins, S.A., 1964; App.Opt., 3, pp 1363-1275.

Connes, P., 1956; Revue d'Optique, 35, pp 37-43.

Cooke, C.H., et al. 1964; App.Opt., 3, pp 957-961.

D. DeShazer, L.G. and Komai, L.G., 1965; JOSA, 55, pp 940-944.

Ducuing, J. and Bloembergen, N., 1964; Phys.Rev., 133, pp A1493-1502.

E. Eckhardt, G., 1966; IEEE J.Quant.Electr., QE2, pp 1-8.

Edgerton, H.E., et al. 1964; 6th Int.Conf.High Speed Photography, The Hague, pp 143-151.

Edgerton, H.E., 1970; Electronic Flash; Strobe (McGraw-Hill).

Edwards, J.G., 1967; App.Opt., 6, pp 837-843.

Edwards, J.G., 1968; J.Phys.D., 1, pp 449-456.

Edwards, J.G., 1969; J.Opto-Electronics, 1, pp 1-8.

Edwards, J.G., 1969; J.Phys.,E.(Sci.Instrum.), 2, pp 1126-1129.

Ericsson, K.G., 1968; App.Opt., 7, p 211.

F. Findlay, D. and Clay, R.A., 1966; Phys.Lett. 20, pp 277-278.

Fox, A.G. and Li, T., 1961; Bell Syst.Tech.J., 40, pp 453-488.

Fox, A.G. and Li, T., 1963; Proc.IEEE, 51, pp 80-89.

Franken, P.A. et al. 1961; Phys.Rev.Lett. 7, pp 118-119.

G. Gates, J.W.C., et al. 1968; 8th Int.Conf.High Speed Photography, Stockholm pp 299-303.

Gates, J.W.C., 1968; J.Sci.Instrum., 1, pp 989-994.

Geusic, J.E., et al. 1964; App.Phys.Lett., 4, pp 182-184.

Geusic, J.E., et al. 1968; App.Phys.Lett., 19, pp 306-308.

Goncz, J.H. and Newell, P.B., 1966; JOSA 56, pp 87-92.

Grütter, A.A., et al. 1969; Phys.Rev., 185, pp 629-643.

H. Hagen, W.F. and Magnante, P.C., 1969; J.App.Phys., 40, pp 219-224.

Hanna, D.C., 1970; Optics and Laser Technology,, pp 122-125 and 126-178.

Hattori, S. and Goto, T., 1968; J.App.Phys., 39, pp 5998-6003.

Hercher, M., 1965; App.Phys.Lett. 7, pp 39-41.

Hercher, M., 1967; App.Opt., 6, pp 947-954.

Hercher, M., 1968; App.Opt., 7, pp 951-966.

Hercher, M., 1969; App.Opt., 8, pp 1103-1106.

J. Jahoda, F.C., 1971; Modern Optical Methods in Gas Dynamic Research (Plenum, London), pp 137-154.

Johnson, L.F. and Nassau, K., 1961; Proc.Inst.Rad.Eng., 49, pp 1704-6.

Jones, E. and Wall,B., 1971; EE Annual Rep.RP2-44, No. 9/46-2.

K. Kafri, O., et al. 1971; IEEE J.Quant.Electr. QE7, pp 122-125.

Kahn, W.K., 1966; App.Opt., 5, pp 407-413.

Kalinin Yu, A., et al. 1969; Sov.Phys., JETP, 29, pp 624-627.

Kelley, P.L., 1965; Phys.Rev.Lett., 15, pp 1005-1008.

Kingston, R.H. and McWhorter, A.L., 1965; Proc.IEEE, 53, pp 4-12.

Kleinman, D.A., 1962; Phys.Rev., 128, pp 1761-1775.

Kogelnik, H., 1965; Bell Syst.Tech.J., 44, pp 455-494.

Kogelnik, H., 1966; Lasers, Levine (Arnold, London) pp 295-347.

Kogelnik, H. and Li, T., 1966; App.Opt., 5, pp 1550-1567.

Kushida, T. et al. 1968; Phys.Rev., 167, pp 289-291.

L. Lankford, J.L., 1970; 9th Int.Conf.High Speed Photography Denver, p 97-103.

Livshitz, B.L. and Tursunov, A.T., 1967; Sov.Phys., JETP, 25, pp 975-979.

Lurie, M., 1968; JOSA, 58, pp 614-619.

M. Magnante, P.C., 1972; IEEE, J.Quant.Electr. QE8, pp 440-448.

Magyar, G., 1969; Optics Technology, pp 231-237.

Magyar, G., 1970; Opto-Electronics, 2, pp 68-72.

Maiman, T.H., 1960; Nature, 187, pp 493-494.

Maker, P.D., et al. 1962; Phys.Rev.Lett., 8, pp 21-22.

Markiewicz, J.P. and Emmett, J.L., 1966; IEEE J.Quant.Electr. QE2, pp 707-711.

Marling, J.B., 1970; App.Phys.Lett., 17, pp 527-530.

McClung, F.J. and Hellwarth, R.W., 1962; J.App.Phys., 33, pp 828-829.

McClung, F.J. and Weiner, D., 1965; IEEE J.Quant.Electr., QE1, pp 94-98.

McClung, F.J. et al. 1970; App.Opt., 9, pp 103-106.

McMahon, J.M., 1969; IEEE J.Quant.Electr., QE5, pp 489-495.

Michelis, C.De., 1969; IEEE, J.Quant.Electr., QE5, pp 188-202.

Michelis, C.De., 1970; IEEE. J.Quant.Electr. QE6, pp 630-641.

Michelson, A.A., 1892; Phil.Mag., 34, p 280.

Michon, M., 1966; IEEE J.Quant.Electr. QE2, pp 612-616.

Midwinter, J.E., 1965; Brit.J.App.Phys., 16, pp 1125-1133.

Miller, R.C., et al. 1965; App.Phys.Lett., 6, pp 77-79.

Morey, G.W., 1954; Properties of Glass (Reinhold), pp 442-447.

Murray, J.E. and Harris, S.E., 1970; J.App.Phys., 41, pp 609-613.

N. Nath, G. and Haussühl, S., 1969; App.Phys.Lett., 14, pp 154-156.

Nelson, D.F. and Sturge, H.D., 1965; Phys.Rev., 137, pp 1117-1130.

Noble, E. et al.1971; ILC R and D Technical Rep. ECOM-0035-F.

North, R.J., 1966; Wehrtechnische Monatsheste, 63, pp 154-167.

O. Osterink, L.M. and Foster, J.D., 1968; J.App.Phys., 39, pp 4163-4165.

P. Patek, K., 1970; Glass lasers, (Iliffe, London).

Pavitt, K.W., et al. 1970; J.Phys.E. (Sci.Instrum.), 3, pp 971-5.

Pendleton, W.K. and Guenther, A.H., 1965; Rev.Sci.Instrum. 36, pp 1546-50.

Pershan, P.S., 1966; Progress in Optics, 5, (New York), pp 85-144.

R. Riedel, E.P. and Baldwin, G.D., 1967; J.App.Phys., 38, pp 2720-2725.

Roess, D., 1964; App.Opt., 3, pp 259-265.

Roess, D., 1966; App. Phys.Lett., 8, pp 109-111.

Roess, D., 1969; Laser Light Amplifiers and Oscillators, (Academic Press, London).

Rowlands, R.E., 1969; Exp.Mech., 9, p 385.

S. Schaak, G., 1967; IEEE J.Quant.Electr. QE3, pp 130-131.

Shank, C.V. et al. 1970; App.Phys.Lett., 16, pp 405-406.

Siebert, L.D., 1971; App.Opt., 10, pp 632-637.

Siegman, A.E., 1965; Proc.IEEE, 53, pp 277-286.

Siegman, A.E. and Arrathoon 1967; IEEE J.Quant.Electr. QE3, pp 156-163.

Simmons, W.W., 1970; IEEE J.Quant.Electr. QE6, pp 466-469.

Smigielski, P. et al. 1970; 9th Int.Conf.High Speed Photography, Denver, pp 322-326.

Snavely, B.B., 1969; Proc.IEEE, 57, pp 1374-1390.

Snitzer, E., 1961; Phys.Rev.Lett. 7, pp 444-446.

Snitzer, E. and Young, C.G., 1968; Lasers, Levine (Arnold, London) pp 191-256.

Soncini, G. and Svelto, O., 1967; App.Phys.Lett. 8, pp 261-263.

Sooy, W.R., 1965; App.Phys.Lett. 7, pp 36-37.

Sorokin, P.P. and Lankard, J.R., 1966; IBM J.Res.And Dev. 10, pp 162-163.

Staselko, D.I., et al. 1969; Optics and Spectroscopy, 3, pp 225-229.

Stetson, K.A. and Powell, R.L., 1966; JOSA, 56, pp 1161-1166.

Stockley, C.M., 1966; IEEE J.Quant.Electr. QE2, pp 511-518.

Stroud, J.S., 1968; App.Opt., 7, pp 751-757.

Surget, J., 1970; La Recherche Aerospatiale, 1970-3, pp 167-174.

Swift, H.F., 1972; 10th Int. Conf.High Speed Photography, Nice, pp 262-266 (Arnold, London).

T. Terhune, R.W. and Maker, P.D., 1968; Lasers, Levine Vol. 2 (Arnold, London) pp 295-370.

Thornton, J.R., et al. 1969; App.Opt., 8, pp 1087-1102.

Toraldo di Francia, 1966; Optica Acta, 13, pp 323-342.

V. Volosov, V.D. and Rashchektaeva, M.I., 1969; Optics and Spectroscopy, 28, pp 53-56.

W. Wagner, W.G. and Lengyel, B.A., 1963; J.App.Phys., 34, pp 2040-2046.

Wang, C.C., 1966; Phys. Rev.Lett., 16, pp 344-346.

Watts, J.K., 1968; App.Opt., 7, pp 1621-1623.

Weber, H.P., et al. 1966; J.App.Phys., 37, pp 3584-3586.

Weber, M.J. and Bass, M., 1969; IEEE J.Quant.Electr. QE5, pp 175-188.

Welford, W.T., 1966; App.Opt., 5, pp 872-873.

Wenzel, J.H., 1966; J.App.Phys., 37, pp 3100-3110.

Withrington, R.J., 1968; Engineering Uses of Holography, Strathclyde, (Cambridge Univ.Press) pp 267-278.

Wright, J.K., 1963; Proc. IEEE, 51, p 1663.

Acknowledgements

The work described has been carried out at the National Physical Laboratory, under the scheme for the registration of persons working at Research Institutions as internal students of London University.

I wish to thank Professor W.T. Welford at Imperial College and Dr. J.M. Burch of the National Physical Laboratory for their constructive criticisms and suggestions and for their encouragement throughout this project. There has been much valuable discussion with various memebers of the Division of Mechanical and Optical Metrology, in particular Mr. J.W.C. Gates within whose group and under whose guidance the work was carried out, Mr.R.G.N.Hall who was responsible for the equipment, and Mr.R.F.Stevens who assisted with the experimental work and computer programs.

The calculation of the distribution of excited ions in a Nd:glass rod due to pumping was worked out jointly with Dr. J.G. Edwards. Mr. D. Hibbins-Butter was responsible for this particular computer programme.

Most of all I am indebted to my wife for her patience and encouragement and to my children for their failure, despite all attempts, to destroy the manuscript.

NATIONAL PHYSICAL LABORATORY

Repetitive Q-switched laser light sources for interferometry and holography

J.W.C. Gates, R.G.N. Hall and I.N. Ross
Division of Optical Metrology

Paper presented at the 8th International Congress on High Speed Photography at Stockholm June 23-29, 1968 and published in the proceedings "High Speed Photography" edited by N. Robert Nilsson and Lars Högberg, John Wiley & Sons, Inc. (New York, London and Sydney) Almquist & Wiksell (Stockholm) pages 299-303.

REPETITIVE Q-SWITCHED LASER LIGHT SOURCES FOR INTERFEROMETRY AND HOLOGRAPHY

J.W.C. Gates, R.G.N. Hall and I.N. Ross

Division of Optical Metrology, National Physical Laboratory

INTRODUCTION

This paper reports on the development of a laser source system which may be of use in a wide range of experimental laboratories or in industrial applications where specialized equipment for high speed photography is not available. A consideration of alternative possible systems indicates that electro-optical components and precise electronic timing may not always be necessary if a repetitive light pulse output can be obtained, and such a system may be very economic, especially in first cost.

Some examples of photographic recording by simple means are given: an account of a more specialized application to holographic recording will be included in another paper to be presented to this Congress (ref. 1).

PULSED LASER SYSTEMS

We have considered and developed lasers based mainly on two materials, ruby and neodymium glass. In the latter case, our interest is based on the conversion of the infra red emission into green light by the process of second harmonic generation in a non-linear crystal, so producing a wavelength with much greater effects on photographic materials, even after allowing for conversion losses.

Both materials are usually employed in rods of the same size, about 100 mm long by 10 mm diameter, and are optically pumped in a comparable way, with up to about 1000J of energy applied to a xenon flash tube in 1 or 2 ms in an elliptical cylinder. In both cases up to about 1J of output is obtainable, depending on the temporal and spatial constraints imposed on the resonator. Resonant reflectors control the temporal coherence (refs.2, 3) and help limit the divergence, giving adequate means for operating ruby in a single mode (ref.4). Neodymium presents a much greater problem because of the greater frequency bandwidth and the liability of the glass to be affected more by temperature variations. The spectral distribution often consists of outputs at a few well separated wavelengths, each of which may be very homogeneous, corresponding to coherence lengths of the order of perhaps a metre, but whose total spread may correspond to a coherence length of 1 cm. In examining the spectral and spatial coherence of such lasers, there are many complicating effects, which are not dealt with in this paper. If time and space permit, some examples may be given of far-field distributions, Fabry-Perot interferograms, wavefront division interference experiments and the measurement of coherence by holography. The last two techniques give information on the spatial and temporal coherence. In the first of these, interference occurs between two parts of an incident wave one of which is reversed with respect to the other (ref. 5). To aehieve this, an adaptation of a Michelson interferometer is used in which one mirror is replaced by a roof reflector and gives a pattern of interference bands with a spatial variation of visibility which is related to the spatial coherence (fig. 1). The second method is to make a hologram in which successive areas of the

reconstruction are associated with increasing path difference between the signal and reference wave of the recording stage. The intensity of the reconstruction and the manner of its variation are related to the temporal coherence of the source employed in recording (fig. 2).

Further control of spatial coherence is essentially a matter of adjusting the ratio of losses which are mode dependent, for example by the use of a pinhole aperture within the optical resonator (ref. 5). Such a method unnecessarily restricts the active volume of the laser material participating optically, and alternatives such as lengthening the cavity and introducing focal power offer better compromises for specific purposes. Some startling improvements may be obtained in this way (refs. 2, 6).

The usefulness of the light may also be affected by frequency drift during the laser pulse (ref. 7) and by a change of frequency or mode between successive pulses in a repetitive system. Time resolved studies have been made (using the technique described later in this paper) to investigate the sources of these instabilities (fig. 3). Our attention has been concentrated on the effects of mechanical vibration and on thermal instabilities resulting from the energy dissipated in the pumping flash. These effects are still troublesome in short-duration Q-switched laser pulses, and may even result from the Q-switching elements themselves.

Q-SWITCHING

Alternative methods are available by which Q switched pulses with durations of 1 to 100 ns may be produced (refs. 2, 8), making possible the photographic recording without a shutter of images moving in relation to the photographic plate at speeds of many km s^{-1}. Perhaps the simplest Q-switch is a bleachable absorbing filter or cell of absorbing dye inserted in the laser cavity, which may also have useful mode selecting properties (ref. 9), although it has the disadvantages that inhomogeneities are introduced into the laser and the timing of the pulse is uncertain to within about 100 μs. Further, mode-locking may occur and this may be either a helpful feature, or may result in the development of dangerously high peak powers (ref. 9). For the recording of some continuous events, such as the interference pattern produced by index variations in a fast-moving gas flow from a flame shown in fig. 4, the timing uncertainty may be acceptable. Recording a fast-moving body, on the other hand, demands some synchronization, and the electro-optical Q-switches (Kerr cells, Pockels cells) provide obvious advantages, although at greater cost and with an increase of electronic complexity. There may be other disadvantages, and, in lasers in which mode control is critical, unwelcome inhomogeneities in the electro-optical materials may result from local heating or from the operating electrical fields themselves.

For these reasons, we have examined more carefully the possibility of using a mechanically rotated reflector as a Q-switch in spite of the rise of threshold which may result from the necessarily limited number of light passes which is possible while the reflector is within a tolerable angle of the optimum position. Subject to this limit, a high speed of rotation is desirable, but mechanical vibration and disturbance of the optical path by air turbulence are increased. The effect of these is avoided in the system we have developed (fig. 5). The reflector is the totally internally reflecting face of a silica prism mounted symmetrically within a rotating cylindrical housing. The light enters the transverse faces of the silica prism obliquely and is refracted at the Brewster angle,

so that there is no loss for plane polarised light, and, after reflection, leaves similarly at the exit face. The prism rotates so that the entry and exit faces move in their own planes, minimizing air disturbance. Protecting (loss-less) windows are set close to the rotating end faces of the prism to isolate the rotating part of the system completely. The prism cylinder is supported in air bearings and is driven by an integral air turbine, and is almost completely free from vibration. The system shown has a design speed of 5000 revolutions per second. Earlier stages of the development of this system, shown sectioned in fig. 6, are larger, having a working aperture of 10 mm, and run at speeds up to 2000 revolutions per second. Alternative multi-sided prisms may be employed, and up to 5 faces may be used without loss of working aperture compared with a single surface prism. The odd number of faces also is helpful in avoiding light circulation within the prism. With pentagonal prisms the designed maximum repetition rate for the smaller system is 25 kHz corresponding to an inter-pulse interval of 40 μs. A typical laser pulse duration is 30 ns so that reasonably well detailed images of a moving body may be obtained without a shutter.

Fig. 7 shows two records of this kind, of a dart moving at about 60 m sec^{-1} (unfortunately the fastest projectile we could find!). A similar system may be employed as a shadowgraph technique for following shock waves (fig. 8).

SPATIAL SEPARATION OF MULTIPLE EXPOSURES

When the event to be recorded is not moving transversely, time-separated recordings may be obtained by an adaptation of the streak camera, in which the complete image is streaked across the plate. The small pulse/interval ratio of the laser output gives sharp well separated records even with a very simple nutating mirror to provide the streaking action (fig. 9). The rotational speed of the mirror is arranged to provide one circle of exposures within the active cycle of the laser, giving the possibility of recording up to 10 or more images if the laser can be effectively Q-switched every time. The access time is not restricted, and <u>any</u> photographic material may be used.

INTERFEROMETRY AND HOLOGRAPHY

Because of the pressure on time and space, remarks on applications of this laser system in this field will be dealt with in another paper to be presented to this Congress (ref.1).

SUMMARY

A relatively simple and compact Q-switched laser which provides 30 ns light pulses at repetition rates up to 25 kHz has been described, with some examples of the way in which this source may be used to record travelling events, or with a simple streak arrangement to give separated images.

ACKNOWLEDGEMENT

The work described above has been carried out at the National Physical Laboratory.

REFERENCES

1. J.W.C. Gates, R.G.N. Hall and I.N. Ross:
"Holographic recording of rapid transient events
and the problems of evaluation of the reconstructions"
8th International Congress on High Speed Photography. (1968).

2. D. Rëss: "Laser Lichtverstärker und Oszillatoren"
Akad. Verlag., Frankfurt a.M., (1966).

3. H. Kogelnik: in "Lasers" (ed. A.K. Levine),
Arnold, London, (1966).

4. G. Magyar: Rev. Sci. Instrum., 38, p.517-9,
(1967).

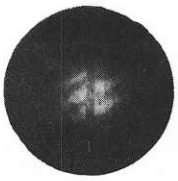
5. L.H. Tanner: J.Sci.Instrum., 44, p.1015-7,
(1967).

6. C.M. Stickley: I.E.E.E. Journal, QE2, p.511-8,
(1966).

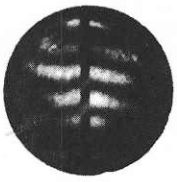
7. D.J. Bradley: Appl. Phys. Letts. 9, 150 (1966).

8. R.W. Hellwarth: in "Lasers" (see ref. 3).

9. J.T. La Macchia and J.E. Bjorkholm: Appl. Phys.
Letts., 12, p.45-6, (1968).

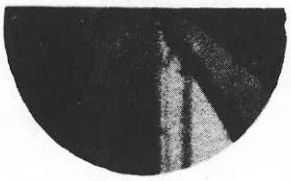


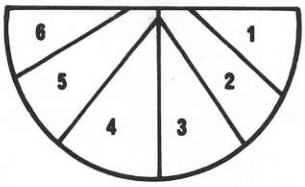
Q-switched Nd: glass laser, 1060 nm, 50ns.
Cavity Fresnel number = 25.



Same laser, Fresnel number = 1.5.

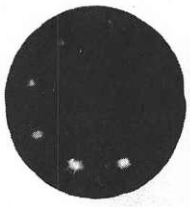
Fig. 1 - Spatial coherence of sources and the effect on the visibility of interference with reversal of one interfering wave.

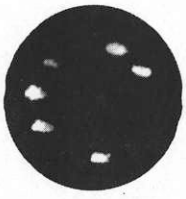




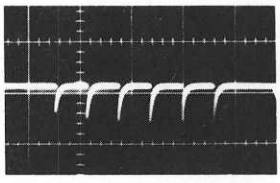
Path differences in mm.
(Stacked 2 mm glass plates)

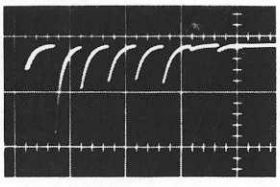
Fig. 2 - The effect of path difference on the recording of a hologram with a source of limited temporal coherence.



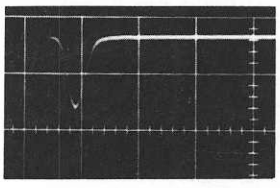


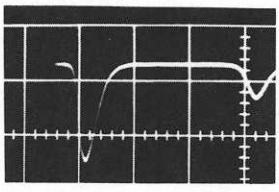
Ruby 694 nm. Neodymium 1060 nm.
1 revolution per ms, anticlockwise





Horizontal: 0.2 ms/sq. Vertical: 0.1 J/sq.





Horizontal: 200 ns/sq. Vertical: 1 MW/sq.

Horizontal: 200 ns/sq. Vertical: 0.5 MW/sq.

Fig. 3 - Time resolved streak records of laser output patterns.



Fig 4 - Interference pattern of the flow of hot gas from a flame. (Ruby laser, bleaching filter Q-switch).

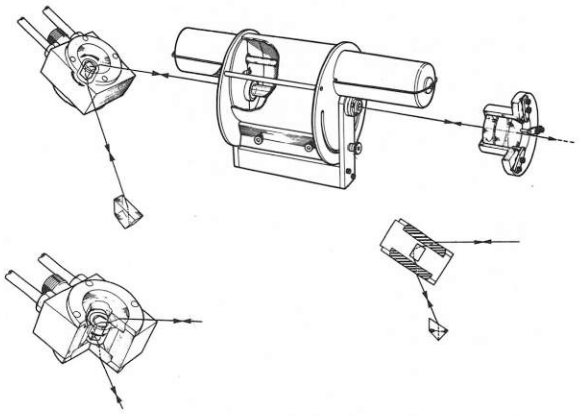


Fig. 5 - Laser system with rotating prism Q-switch.

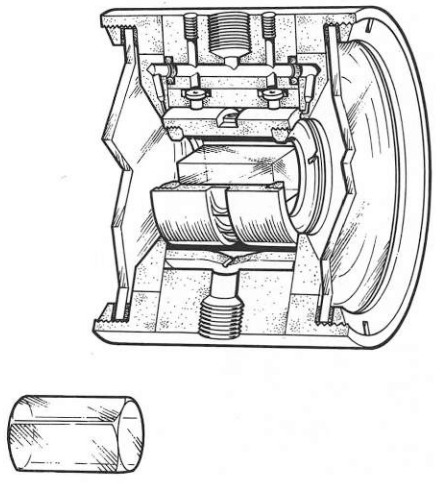


Fig. 6 - Turbo prism Q-switch

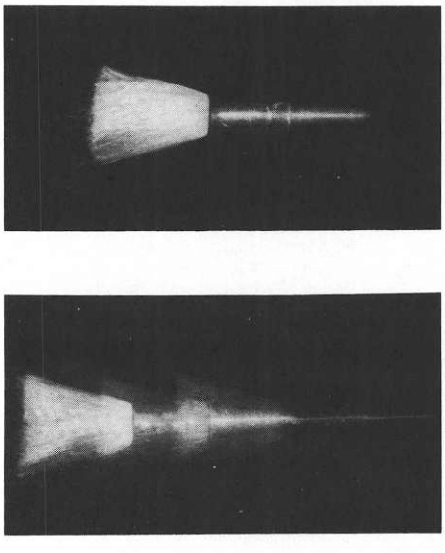


Fig. 7 - Single pulse and triple pulse recording of the flight of an air gun dart. Ruby laser, pulse duration 30 ns, interval 130 µs.

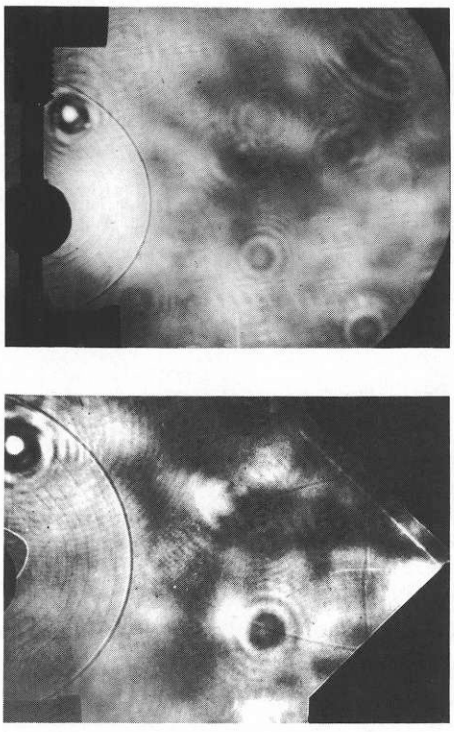
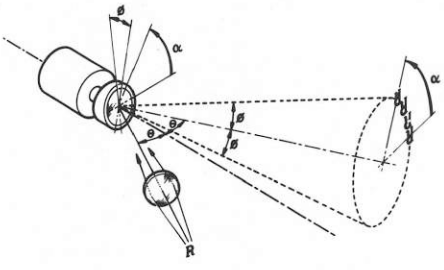


Fig. 8 - Single pulse and double pulse recording of a shock wave. Ruby laser, pulse duration 30 ns, interval 130 µs.



Mirror System - scanning without image rotation

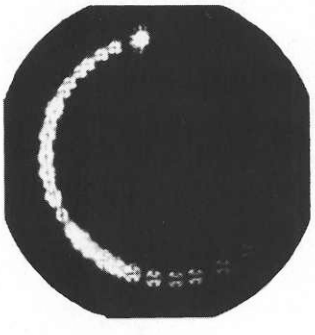


Fig. 9 - Time resolved sequence of laser output patterns by circular-streak nutating mirror.

NATIONAL PHYSICAL LABORATORY

Holographic recording of rapid transient events and the problems of evaluation of the reconstruction.

J.W.C. Gates, R.G.N. Hall and I.N. Ross

Division of Optical Metrology

Paper presented at the 8th International Congress on High Speed Photography at Stockholm June 23-29, 1968 and published in the proceedings "High Speed Photography" edited by N. Robert Nilsson and Lars Högberg, John Wiley & Sons, Inc.(New York, London and Sydney) Almquist & Wiksell (Stockholm) pages 304-308.

HOLOGRAPHIC RECORDING OF RAPID TRANSIENT EVENTS AND THE PROBLEMS OF EVALUATION OF THE RECONSTRUCTIONS

J.W.C. Gates, R.G.N. Hall and I.N. Ross

National Physical Laboratory, Teddington, Middlesex, England

INTRODUCTION

Holography is considerably extending the range of recording techniques now available, but in addition brings several new concepts which may prove to be even more valuable. The modification of Gabor's original proposal (ref.1) made by Leith and Upatnieks (ref.2) demonstrated practical methods for true three-dimensional recording of static objects, and also demonstrated the possibility of powerful optical correlation processes for character recognition and optical coding.

The essential characteristic of a holographic recording is that the phase distribution in the light wave is recorded: this phase distribution may be recoverable on "reconstructing" the hologram and has been directly put to work in the interferometric methods of Collier et al. (ref.3), Brooks et al. (ref.4), and Burch et al. (ref.5). This last investigation has been continued in this Laboratory and includes the holographic study of objects and phase distributions which are moving, or changing form, at high speed (ref.6). This paper reports on some recent work in this field. Examples are presented, but these are only of laboratory-contrived models which may serve to demonstrate the possibility of applying the techniques in industrial or other laboratories.

LIGHT SOURCES

The pioneering work in holography (refs.1 and 2) was carried out with thermal light sources, but the development of the gas laser, more than any other factor, has been responsible for the great extension of the field of study in the last four or five years. In the recording of solid objects by reflected light, there are necessarily large phase variations in the reflected waves, and holography demands a source of adequate temporal coherence so that the modulation-depth of the interference effects which are recorded to form the hologram will be adequate. Coherence lengths of 1 metre or more are available from gas lasers, allowing mismatches of up to 10^6 wavelengths or more, but for recording a hologram it is necessary that the pattern on the sensitive material remains stationary to a small fraction of the spacing of the finest structure in the pattern. This may mean that the object must remain unchanged in form and position to within 1 part in 10^7 of its linear dimensions for the duration of the holographic exposure. Even in the quietest of surrounds the vibration and thermal drift occurring in structures may exceed this limit unless the exposure time is very brief, and the holographic recording of a "static" object may then require some of the techniques of high speed photography. Our claim to take up some time at this conference goes beyond this point, however. If the event to be recorded involves less path variation, or if the optical system can be made to be tolerant of path variations in the object, then the coherence required in the source will be lessened, or the object may be permitted to move at a faster rate for a given exposure time. Our experimental work has demonstrated both possibilities; an optical system has been described with which it has been shown that holograms may be

made even with white light (ref.7), and the examples to be given in this paper suggest the possibilities for high speed photography, using Q-switched solid state lasers with light pulse durations of the order of 30 ns.

OPTICAL SYSTEM

Objects which may be transilluminated are the easiest to record holographically, and the optical system may be designed so that only small path mismatches are introduced between reference and signal waves. One very versatile system we have used extensively employs a scatter plate (fig.1). A collimated light beam from a pulsed laser or other source falls on the scatter plate and is partly transmitted without phase changes, to form a concentration of energy in the central plane of the object region. Light which is randomly deviated at the scatter plate illuminates the object uniformly; phase and amplitude disturbances which are impressed on the constituent waves by the object propagate with them until they are recombined with the reference wave at the back focus of the second lens, where the sensitive material is placed to record the hologram. After processing the photographic plate, a coherent light wave falling upon the resultant hologram can re-create all the attributes of the light waves as affected by the object, making it possible, for example, to photograph separated planes in depth in the reconstructed object (fig.2). If the successive phase distributions from an object which changes in the interval between exposures are reconstructed simultaneously, they interfere and show up the phase variation between successive situations as an interference pattern. The pattern shows changes according to the direction of viewing and the plane upon which the camera is focused, just as a three-dimensional amplitude-modulating object does (fig. 3).

TIME RESOLUTION OF MOVING OBJECTS

In photographic recording, an object which moves transversely across the field of a camera may be recorded on separate areas of the sensitive material by employing a light source emitting a brief flash at intervals. Similarly, in holography, if a moving object is recorded, separated images may be obtained on reconstruction, but the separation may be in three dimensions, not in two (fig. 4). Further, the successive holographic exposures need not be separated on the photographic material. Since the phase disturbances associated with each recording are superimposed, interference effects which show the phase changes may be revealed at the same time. In fig. 5 interference between the reconstructions for two successive recordings of the progress of a shock wave show up the refractive index difference across the shock front.

TIME RESOLUTION OF CHANGES IN STATIONARY FIELDS

When the object is not moving across the field between successive brief exposures, but changes its form, interference effects may be blurred out unless the motion is periodic (ref.8). Generally, it is desirable to be able to separate out the successive records of the object, as in a high speed framing camera. This may be achieved by recording successive holograms on a fresh area of the sensitive material, and if the exposure time is short enough compared with the interval between exposures, a simple streak camera may be employed with a pulsed laser, as described in another paper presented to this Congress (ref. 9). The exposure time must be much shorter in relation to the interval in holography, compared with direct photography, since any blurring of the structure of the hologram, in which

spacings as small as 1 μm may be important, will result in deterioration in the reconstruction, and possibly in the complete disappearance of parts of the field. Typical proportions indicate that the ratio of interval to exposure duration, which is the same as the ratio of the diameter of the hologram to its fine detail (fig. 6), must be about 3×10^4 for the sort of holograms which produced the example given. Thus, repeated laser pulses of 30 ns duration could record holograms in this way at a repetition rate up to 1 kHz. In order to record at a greater repetition rate with this form of streak photography, it is necessary either to use smaller holograms, with reduced information capacity, or to allow them to overlap. The latter possibility has led us to construct a scanning system with which much higher repetition rates can be achieved. The operation of this system depends on the principle that a hologram not only reconstructs the amplitude and phase variations in the original wave as far as these delineate the optical properties of the object which was recorded, but also re-creates the essential characteristics of the complete optical system through which the recording was made. In addition to recording amplitude and phase in a plane corresponding to the object, or in a conjugate, image, plane, the hologram can reproduce the distribution which corresponds to the exit pupil of an optical system through which the image was being projected. Thus a spatial scanning of the plane of the reconstructed pupil could have the same function as scanning across, for example, the lens array of a mirror drum camera, similarly coding the time sequence by pupil position. A simple demonstration of the principle is indicated in fig. 7. The object consisted of a series of ten numerals replacing each other in the same location at intervals, and the plane of the hologram was arranged to be conjugate with this object plane. The pupil of the optical system by which the object was projected was arranged to gyrate virtually about the reference beam by the use of a rotating reversing prism.

The reconstructed ten pupils (duplicated by the "twin image" effect) are shown, with typical reconstructions in the hologram plane from selected pupils.

The reversing prism has been mounted in an air-bearing air-turbine and is capable of rotation at 500 revolutions per second, giving a repetition of the cycle of exposures at 1 kHz (fig. 8). If ten resolved pupils can be produced from the superposed holograms, the "frame" repetition frequency will be 10 kHz, and a similar pulse repetition rate is already available from our repetitively Q-switched laser (ref. 9).

Development of this design is proceeding to a repetition frequency of up to 25 kHz and perhaps beyond. Alternatively, the same system may be useful in exploring time-resolution by spatially separated holograms, simply by changing the inclination of the recording beam (fig. 9).

PROBLEMS OF EVALUATION

Time and space unfortunately do not permit a consideration of the interesting optical possibilities which arise, or of the problems of measurement to which holography may be applied, but these aspects are, perhaps, more appropriate to an optical or engineering forum, and will be presented in these fields in due course.

ACKNOWLEDGEMENT

The work described above has been carried out at the National Physical Laboratory.

REFERENCES

1. D. Gabor, Nature, 161, p.777-8 (1948).

2. E.N. Leith and J. Upatnieks, J. Opt. Soc. Amer, 53, 1377 (1963).

3. R.J. Collier, E.T. Doherty, and K.S. Pennington, App. Phys. Lett., 7, p.223, (1965).

4. R.E. Brooks, L.O. Heflinger, and R.F. Wuerker, App. Phys. Lett. 7, p.248, (1965).

5. J.M. Burch, A.E. Ennos, and R.J. Wilton, Nature, 209, p.1015 (1966).

6. J.M. Burch, J.W.C. Gates, R.G.N. Hall, and L.H. Tanner, Nature, 212, p.1347-8 (1966).

7. J.W.C. Gates, J. Sci. Instrum. (in the press).

8. E. Archbold and A.E. Ennos, Nature, 217, p.942-3 (1968).

9. J.W.C. Gates, R.G.N. Hall and I.N. Ross, "Repetitive Q-switched laser light sources for interferometry and holography" 8th International Congress on High Speed Photography.

SUMMARY

Examples have been given of a sequence of development in applying holography to high speed recording of amplitude and phase disturbances, using pulsed lasers. The advantages in three dimensional recording, in revealing progressive phase changes, and in recording short sequences of separable records without a specialized high speed camera are described.

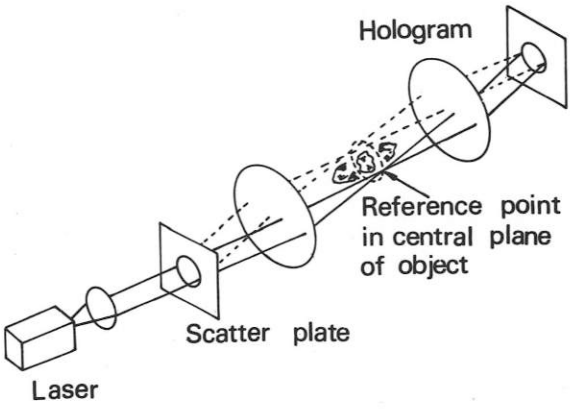


Fig. 1 - Holography of trans-illuminated objects using scatter plate.

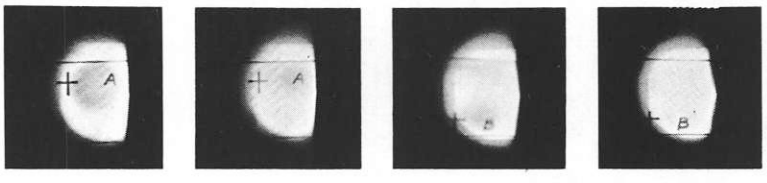


Fig. 2 - Reconstructions from one hologram to show the three dimensional image. (Pulsed neodymium glass laser with second harmonic generation of green light, wavelength 530 nm. Pulse duration 30 ns).

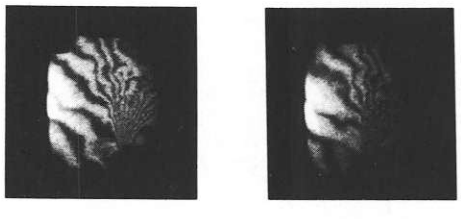


Fig. 3 - Reconstructions from a hologram exposed twice, once with a three-dimensional phase disturbance (a turbulent jet of gas) and once without. Parallax and changes of pattern are shown by views photographed through different portions of the hologram. (Ruby laser, pulse duration 30 ns).



A "snapping" rubber band, moving upwards and away at about 100 ms^{-1}. 3 reconstructions from a single plate, refocussing on the loop of the band recorded in successive positions.

Fig. 4 - Reconstruction from a single area of a plate bearing a series of superimposed holograms, showing a spatially resolved movement. (Ruby laser, pulse duration 30 ns, pulse repetition rate 6 kHz).

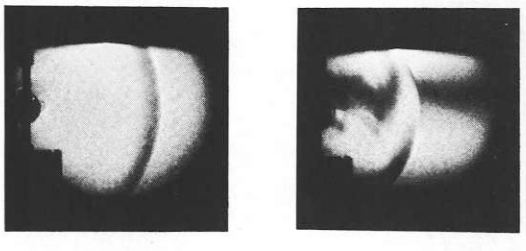


Fig. 5 - Reconstructions from two holograms of shock waves in air from sparks. Each hologram was doubly exposed so that the initial exposure occurs before the spark is triggered, thus providing a reference background wave and giving interference on reconstruction. (Ruby laser, pulse duration 30 ns, pulse repetition rate 6 kHz.)

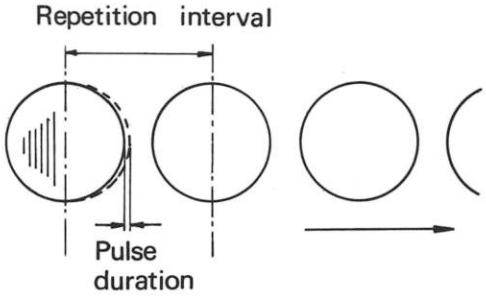


Fig. 6 - Relation of the separation and the permissible movement of holograms in a streak camera.

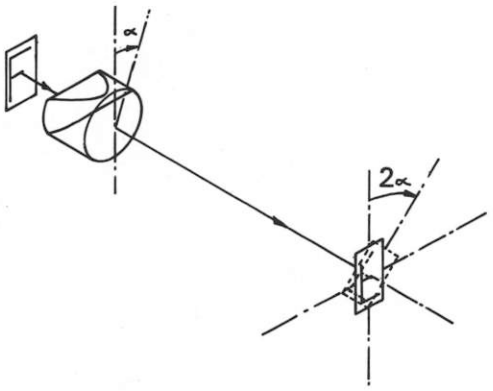
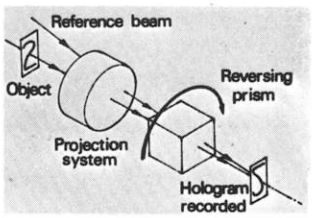


Fig. 8 - Recording superposed holograms with a turbo-driven image-reversing prism.



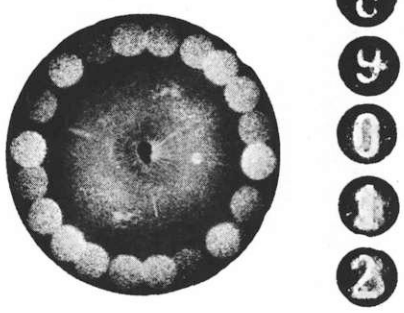


Fig. 7 - Recording successive superimposed holograms. Photograph of the reconstruction pupil plane and examples of the reconstruction obtained through selected pupils.

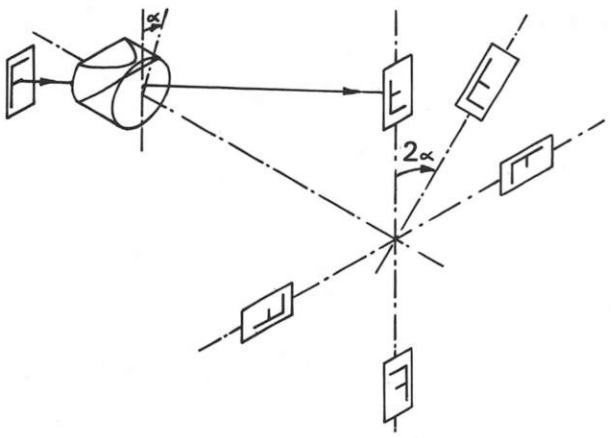


Fig. 9 - Recording time-separated holograms with the turbo-driven image-reversing prism.

LECTURE DEMONSTRATIONS

At the time of presentation of this paper, reconstructions of a number of holograms were demonstrated from the platform by television, and other holograms were demonstrated in another room at other times.

Although it is felt that a proper appreciation of the three dimensional reconstructions can only be obtained from a "live" presentation, the following photographs of reconstructions from holograms recorded consecutively at a high rate, which were demonstrated at the Congress, are offered as a record of the proceedings.

The object recorded in each case was a small washer mounted in a dental drill (figure 10) by means of which it was rotated at 1200 revolutions/second.

Figure 11 shows a superposed sequence of holograms recorded by the method of Figure 8, using the ruby laser at a pulse rate of 7 kHz, and Figure 12 shows three spatially separated reconstructions from these holograms.

Figure 13 shows four successive holograms produced with the same repetitive ruby laser, using the streaking technique of Figure 9. Figure 14 shows four reconstructions, one from each hologram.

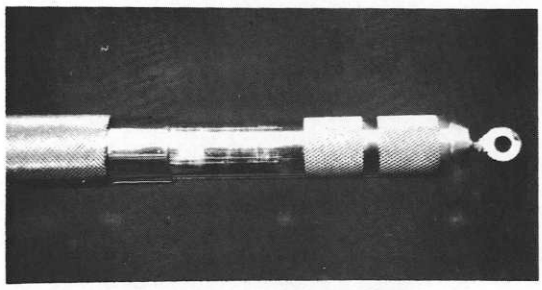


Fig. 10 - Washer mounted in dental drill.

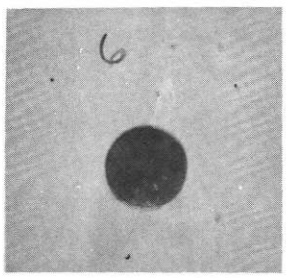


Fig. 11 - Superposed successive holograms, recorded by the method of Figure 8.



Fig. 12 - Spatially separated reconstructions of the successive holograms in Figure 11.

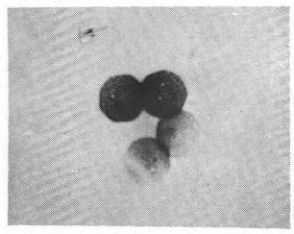


Fig. 13 - Four successive holograms, recorded by streaking as in Figure 9.

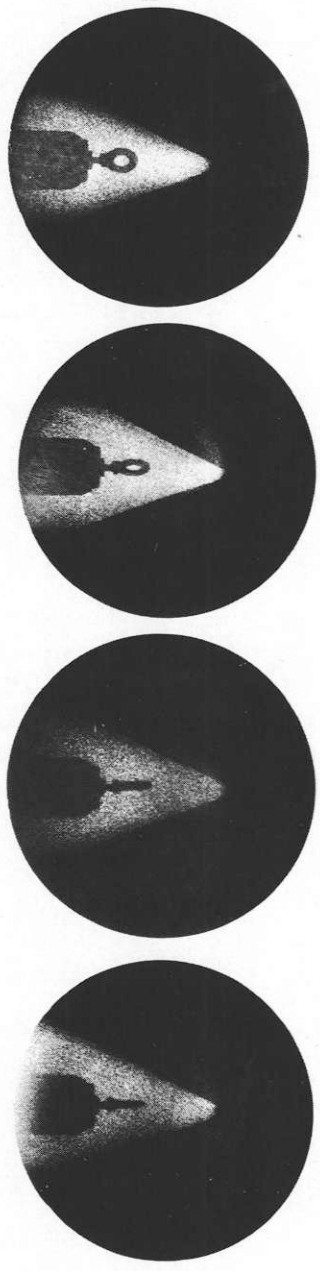


Fig. 14 - Reconstructions from each of the holograms of Figure 13.

Holographic recording using frequency-doubled radiation at 530 nm

J W C Gates, R G N Hall and I N Ross
Division of Optical Metrology, National Physical Laboratory, Teddington, Middlesex

MS *received 16 October 1969*

Abstract This paper sets out some arguments for the use of the green second harmonic (frequency doubled) radiation from a pulsed neodymium laser as the light source in recording transilluminated objects by holography, and gives in some detail a description of one experimentally realized embodiment of the idea. Examples of photographs of reconstructions of complicated three-dimensional shock waves in air are included.

1 Introduction

Lasers with emission at wavelengths shorter than the (red) 632·8 nm emission of the helium-neon laser most often used offer several advantages for holographic recording. A greater choice of light sensitive materials is open, and the shorter wavelength makes possible a more favourable resolving limit for fine detail with an optical system of given aperture. A similar advantage occurs in techniques of hologram interferometry, where changes of optical path are interpreted as the number of bands (or as the fraction of a band) of displacement in an interference pattern. Even the small difference in red and green wavelengths can result in significant improvements, and is partly the reason for the increasing use in holography of argon gas lasers at a wavelength of 514·5 nm. Greater power also, up to a few watts, is available from argon lasers, but may, even so, not be sufficient for applications in which very brief exposures must be used to avoid the effects of rapid motion. In such cases, an effective source is provided by the use of the radiation, at a wavelength of 530 nm, derived from the emission at 1060 nm from a pulsed neodymium laser, by conversion in a suitable nonlinear material to the second harmonic. Solid state lasers of this type can produce single pulses of only a few nanoseconds duration. Others, which are repetitively pulsed, or operated continuous-wave, could possibly rival argon lasers in applications involving only static situations, and may be used in reconstructing a visible image from the hologram for evaluation.

There are advantages in using green light in visual assessment and measurement. The eye is at its most perceptive near the wavelength of 530 nm and is thus best able to analyse and interpret critically.

Recording the hologram and reconstructing from it at the same wavelength avoids changes of scale; other distortions (such as those which may arise from chromatic effects in uncorrected lenses when the same system is used in recording and reconstruction) are not so likely. Subsequent photography of the reconstructions is facilitated because there is a wider choice of photosensitive materials sensitive to green than to red light.

In cases where shorter wavelengths are required, frequency-doubled radiation from a ruby laser could be employed, as reported by Wuerker, Heflinger and Briones (1968). Higher harmonics might also be employed.

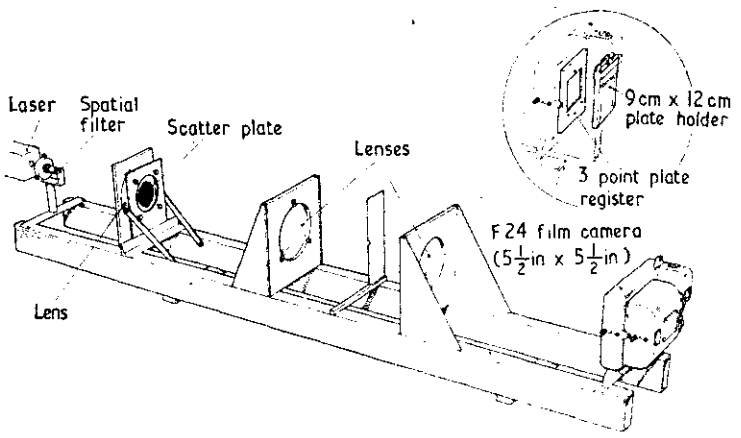
2 Laser

In our experiments we have used a laser which is commercially obtainable (Laser Associates Ltd, Rugby). The basis of the system is a neodymium doped crystal of calcium tungstate pumped by a xenon flash tube and producing either a single output pulse or a continuous repetition of pulses up to a rate of 10 per second. The Q-switch is a Pockels electro-optic cell producing a higher power pulse of about 15 ns duration. The output of the basic laser at 1060 nm would be about 100 mJ per pulse if suitable transmitting mirrors were fitted, but both mirrors forming the resonant cavity are made highly reflecting for the infrared radiation, inducing within the cavity a high level of power density. This infrared radiation is converted into green radiation of twice the frequency in a temperature-controlled intracavity lithium niobate crystal. One of the resonator mirrors is made transmitting for the frequency-doubled radiation, giving a maximum pulse output energy of about 10 mJ at 530 nm with a pulse half-width of 15 ns. This output may be regarded as a 10% conversion of energy from infrared to green light. Much more efficient systems have been reported, and there is every prospect that with development, conversion may approach even 100% (Geusic *et al.* 1968). Repetitively pulsed and continuous wave systems have been reported with average output powers of from 350 mW to several watts in the green. Some of these systems are much more efficient than gas lasers in converting electrical energy into green light, and have more potential for development to even greater power output.

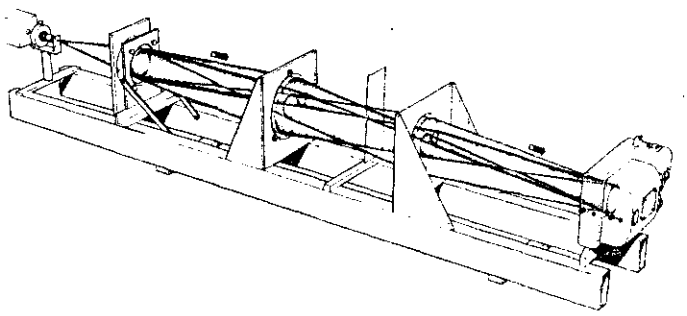
3 Holographic system

Pulsed lasers of the types which may be purchased have rather poor lateral and longitudinal temporal coherence at the present stage of development and are not well suited for some techniques of holography. However, a system of holography whereby satisfactory holograms of transilluminated objects can be obtained using sources of minimal coherence has been previously employed (Gates 1968, Gates, Hall and Ross 1968). The arrangement of the system now used is similar and is shown in figure 1(*a*). The optical arrangement comprises two lenses of similar focal length, a scatter plate, and a means of recording the hologram, on either photographic plates or film. The scatter plate is a specially made diffusing layer on a glass plate which allows part of an incident beam of light to be transmitted and scatters some of the

(a)



(b)



(c)

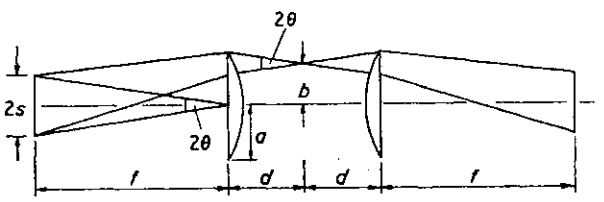


Figure 1 (*a*) Holographic scatter plate apparatus. (*b*) Working volume and reference beam volume. Diagrammatic representation of ray-cones of scatter plate apparatus. (*c*) Geometry of scatter plate system.

remainder randomly over the entire aperture of the first lens, which is positioned with the scatter plate in its first focal plane. The photosensitive material upon which the hologram is to be recorded is set in the second focal plane of the second lens, and the space between the two lenses contains the volume in which the event to be recorded is arranged. The part of the beam of light incident on the scatter plate which is transmitted without scattering converges to form a distribution of minimum cross section midway between the lenses and to one side of the volume, and then diverges through the second lens to fill an area of the photosensitive material which is an image of the scatter plate. This beam of light constitutes the 'reference' beam and interferes with other parts of the original incident beam, after these have been scattered through all parts of the working volume, to produce the complicated interference patterns on the surface of the photosensitive material which are recorded to form the hologram.

The size of the scatter plate and the arrangement of the optical system determines the angle of convergence and divergence of the reference beam and thus determines the shape of the remaining volume in the cylindrical space between the lenses which is available as the working volume. In the apparatus shown, the working volume in which maximum optical performance is available has the form of a truncated double cone with a common circular base in the plane of the reference 'spot' (figure 1(*b*)).

This arrangement is capable of wide variation to adapt it for specific purposes. Choosing the most suitable involves considering the values of several parameters (figure 1(*c*)). Using, where possible, the quantities in the form previously described (Gates 1968), these are s, the scatter plate semi-aperture; a, the lens semi-aperture; f, the lens focal length; but now the lens spacing, previously fixed at $2f$, is regarded as variable and equal to a quantity $2d$. The limitations of the photosensitive recording material must also be considered as far as these may set limits to the functions otherwise defined by the parameters given above (for example, by the effect on the choice of lens aperture which is adequate to resolve fine detail if the spatial frequency at the hologram may exceed the limit at which the material can record).

The quantities which characterize the properties of the optical system are functions of the parameters given above.

Illuminated cone angle $2\theta = 2s/f$ This is the maximum angle subtended at an object point by the useful cone of illumination. The smallness of the spacing of separate points which may be resolved depends on this angle θ, for both transversely and axially separated points.

Object field size $2b = 2(a - sd/f) = 2(a - \theta d)$ This is the

lateral extent of the object field which is illuminated by a full cone of angle 2θ, where this is a maximum, ie in the central plane between the lenses. Obviously $2b$ must be greater than the maximum width of the object field to be studied.

Volume of the object field $V=(2\pi/3)(3a^2d-9a\theta d^2+7\theta^2d^3)$ Object points which lie outside the double truncated cone of this volume (see figure 1(*b*)) are not fully illuminated and reduction in resolution may occur. The expression for V is therefore in this sense a *minimum* volume. In some situations an adequate quality of reconstruction may be obtained in a volume of larger cross section.

Aperture ratio of the lenses $2a/f$ The effective value of this function is limited by the angular extent of the scattering function of the scatter plate. Since the maximum spatial frequency presented in the plane of the hologram is dependent on this ratio, its value is also interrelated with the resolving power of the photosensitive material. An additional limitation on the choice of optimum aperture ratio is the increased lens aberration at high values.

Energy required for exposure $E=I\pi s^2$, where I is the energy per unit area of the photosensitive material required to record the hologram at the optimum level. The source must be able to supply sufficient energy, or s must be limited to suit.

These quantities provide various criteria for optimizing the basic parameters, some of which may conflict. In any particular case, the more important quantities must be selected, and the relative effect on the requirements of variations must be studied.

The following example illustrates the optimization of the system to obtain the maximum working volume V for observing detail of a given minimum size. The resolving power required necessitates a minimum cone angle θ. (The numerical factor relating these quantities is discussed later, from the experimental results.) We assume also that the maximum lens aperture a is given.

The condition for maximizing V, given θ and a, is found to be

$$d=\frac{a}{(3+\sqrt{2})\,\theta}=0{\cdot}226\,a/\theta.$$

This result is independent of the focal length f, as long as the scatter plate semi-aperture s is sufficiently large for the prescribed value of $\theta=s/f$. Choice of f will be dictated in some cases by availability of suitable lenses, and by a compromise between the need to limit the lens aperture ratio $2a/f$ in order to keep aberration small, and the availability of suitable photosensitive material in sizes large enough to provide the required value of s.

In cases where there is no limitation on the size of photosensitive material available, the choice of f will depend on the relationship of resolving power and sensitivity of the plate, within limits set by the energy available to produce an adequate exposure.

The energy required to expose an area of radius s is $E=I\pi s^2$, where I is the optimum exposure per unit area.

Since

$$s=f\theta$$

$$E=I\pi\theta^2f^2.$$

Now the maximum spatial frequency in the hologram is of the order

$$N=\frac{2a}{\lambda f}.$$

From these two relations it may be seen that an increase in f results in a proportional decrease in the demand for resolving power N, but in an increase in the demand for total energy E in proportion to the square of f. When the total energy available is limited, increasing f must be offset by finding a more sensitive material, ie one with a smaller value of I. It follows that, provided the spectral sensitivity, contrast and other properties are the same, the best choice for the photosensitive material is that for which N^2/I is a maximum.

4 Choice of experimental apparatus

The procedure outlined above was followed in choosing the proportions of the apparatus. θ was chosen to be 0·05 in the hope that the resolving limit would not be much worse than 10 μm or so that would be expected from a conventional optical system at a corresponding numerical aperture, and the remaining proportions followed from the selection of an existing pair of lenses of 150 mm diameter ($a=75$ mm) and focal length $f=860$ mm, as being near the best compromise between the factors mentioned.

As already described, the maximum working volume is then obtained for a lens separation

$$2d=0{\cdot}452a/\theta=678\text{ mm}.$$

The maximum field diameter is then

$$2b=1{\cdot}548a=116\text{ mm}$$

$$(b=58\text{ mm})$$

and the scatter plate diameter required is

$$2s=2f\theta=86\text{ mm}$$

for which 9 cm × 12 cm photographic plates and film were conveniently available. The apparatus was actually set up, as is indicated in figure 1, with a considerable margin for the possible use of larger scatter plates and holographic material as these might become available. Provision was made for roll film, size 5½ in × 5½ in ($2s=125$ mm), in an F 24 camera, to be used as one alternative.

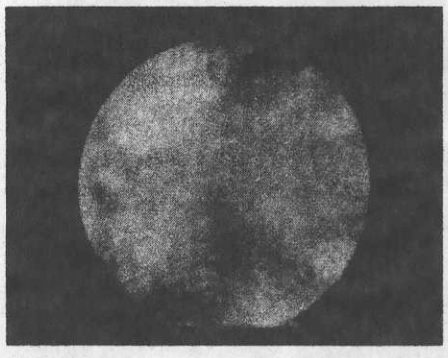
5 Production of scatter plates

The previous paper pointed out the advantages of using scatter plates made holographically in the apparatus in which they were to be used. Details of the procedure for making these plates is repeated here, with developments in technique resulting from experience since the first publication.

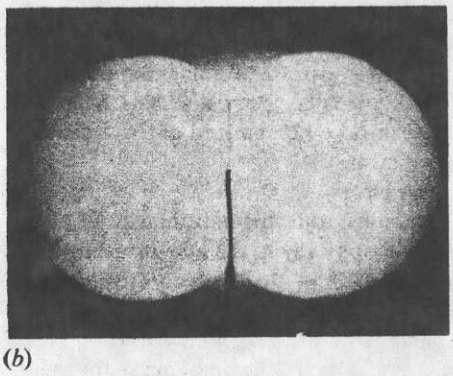
A primary scatter plate is made by smoking a thin glass plate with ammonium chloride to a uniform 'density' of about 2 (measured with a photographic 'contact opal' densitometer). The light scattered by such a 'primary' scatter plate gives a flux integrated over a cone of 10° half-angle of about three times that of the unscattered illumination. This primary scatter plate is placed in the apparatus described in the first focal plane of the first lens and is illuminated with a suitable laser, either continuous wave or pulsed, but preferably of the wavelength with which the main recording is to be made, and preferably with a uniformly illuminated field. The solid angle subtended by the f/5·75 lenses is about a quarter of the 10° cone, so that the relative intensity of scattered and unscattered (reference) beams at the photosensitive material, placed in the second focal plane of the second lens, will be about 3 : 4. Experiments have indicated that the high degree of modulation in the interference pattern produced by near equality of the interfering waves is the optimum choice, producing a result which is relatively insensitive to variations of illumination across the plate and to the ratio of the intensities of the two beams. The interference pattern in the second focal plane of the second lens, which is conjugate with the scatter plate in the first focal plane of the first lens, is recorded on fine-grain holographic photosensitive material. A suitable material is Agfa 10E70, exposed and developed to produce an averaged transmission density of about 0·7, as measured by the integrated transmission in contact with a diffuser. The

silver image is then bleached and removed, leaving a structured gelatin impression which is a 'phase' hologram of high efficiency and durability. Details of development and bleaching are to be found in the appendix.

Scatter plates made in this way (figure 2(*a*)) absorb very little of the incident light and the scattered light nearly all falls within the cone defined by the lens aperture. Twin reconstructions are produced and in the mid-plane of the working volume appear as areas which are centrosymmetric about the reference point (figure 2(*b*)). About 20% of the incident light appears in each of these areas, and the remaining 60% in the 'reference' or 'straight-through' beam. The holographic scatter plate is thus much more efficient than the primary plate. For example, typical measurements of the light transmitted and scattered by an ammonium chloride primary plate at the centre of the hologram image plane show 2·1% in the reference beam and 2·0% in the scattered beam, expressed as percentages of the total incident illumination. The corresponding percentages for a typical bleached holographic copy are 53% and 23% respectively. The holographic scatter plate shown was obtained with the 10E70 Agfa-Gevaert emulsion using laser light of wavelength 632·8 nm from an 8 mW single transverse mode helium–neon gas laser.



(*a*)



(*b*)

Figure 2 (*a*) Photograph of a bleached holographic scatter plate (transilluminated). (*b*) Photograph of twin reconstructions in the mid plane section, produced by a holographic scatter plate. The black line is an obstruction introduced in the photography to eliminate that part of the light left unscattered by the scatter plate

6 Performance of the holographic system

The method and the apparatus described were developed primarily for the observation of phase distributions, and for this purpose resolution is not an overriding criterion. Further, the double exposure technique which is used to make phase disturbances visible by interference cancels out most of the aberrations and distortions caused by the lenses and other optical components. However, for work in which only a single exposure is made, such as the recording of the three-dimensional positions of particles carried in a gas stream, optical distortions and lens aberrations may set the limit to the smallest size of particle which may be resolved, and the number of resolvable volume elements may be reduced.

Some tests were made of the system used in this way. Test objects in the form of glass slides bearing a series of opaque circular areas in a range of sizes from 800 μm down to 25 μm in diameter on each slide were set at a number of positions within the working volume. The slides were obtained from Graticules Ltd and are known as 'new Porton type test graticules'. They happened to be available, but are obviously not intended for use as resolving power test objects, and have a number of undesirable features when used for this purpose. For example, the separation of successive circular areas is rather small, and the surrounding clear area carries a number of fine graticule lines and other markings which spoil a judgement of the resolution limit. Although the tests made are consequently somewhat crude, it is possible to make an attempt to derive a quantitative limit and to examine the relationship between the transverse and longitudinal resolution. Holograms were made on 10E56 plates using the (multimode) frequency-doubled radiation at 530 nm and on 10E70 plates using uniphase 632·8 nm radiation.

The difficulties encountered in assessing the limit of resolution of the reconstructed images need considerable further work to clarify. Some of the difficulty occurs in devising an adequate criterion when the reconstruction is affected by speckle patterns and by the reduction of contrast from stray light. It is to be expected that the limit must be worse than that which would be found in a well-corrected optical imaging system of the same numerical aperture, illuminated incoherently, but the extent of the deterioration is difficult to predict. The speckle effect will have a characteristic size comparable with the diffraction limit, and the effect of optical imperfections in the photographic glass plates and in the lenses is largely unknown. For what it is worth, however,

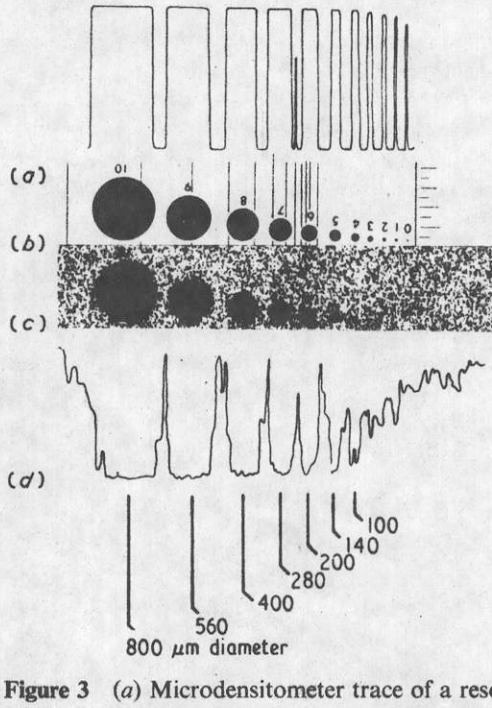


Figure 3 (*a*) Microdensitometer trace of a resolution test graticule. (*b*) Enlarged positive copy of the graticule. (*c*) Photograph of a reconstruction from a hologram. (*d*) Microdensitometer trace of the negative of 3(*c*)

some photographic and microdensitometer evidence is shown in figure 3, and in the circumstances the transverse limit of resolution might be set at 150 μm for a typical hologram. The effect of the limitations was shown by the fact that no improvement in resolution was seen by increasing the area of hologram in use above a circle 20 mm in diameter. (The diffraction limit for a perfect optical system of corresponding aperture is 67 μm.) The resolution limit did not appear to vary axially, though a small but significant decrease was observed for regions transversely distant from the reference beam.

With the geometry chosen and taking the experimentally measured resolution limits for small particles, it may be calculated that more than 5×10^5 resolvable areas may be distinguished in the central cross section. The longitudinal spacing of two small particles which may be distinguished under all circumstances follows from combining the resolving limit with the angular aperture 2θ ($=0{\cdot}1$ radian) of the system. This minimum longitudinal separation should be less than 3 mm and the number of consecutive transverse sections in which pairs of such particles could be distinguished is consequently over 200. Thus the total number of volume elements which may be distinguished should approach 10^8, and it may be expected that a large number of particles, possibly up to 10^6, could be recorded and subsequently reconstructed to give their three-dimensional positions. This procedure needs further experiment, but can only be possible as long as the number and size of the particles are not so large that there is a significant probability of one particle obscuring another. When the population is of mixed sizes, the upper limit is more difficult to calculate, since larger opaque particles will obscure small particles lying within a conical volume of a length equal to about ten times the diameter of the larger particle, both in front and behind.

Finally, it should be pointed out that when the *position* of a particle in a direction parallel to the axis is required, it may be obtained to a closer limit than the 3 mm which is necessary to distinguish two particles axially. Measurement showed that the position could be obtained to within 1 mm.

7 Recording of three-dimensional phase distribution

The system has also been used to examine shock wave phenomena produced by electric sparks, using a technique of interference holography. In figure 4, for example, a double exposure hologram, made by two successive pulses (duration 15 ns) of the frequency-doubled radiation, provided the three reconstructions. Each pulse illuminates the working volume just after the spark is fired. A second shock wave is produced just before the second pulse at a point 300 mm from the first spark. In this example each light pulse provides the background reference wave in reconstruction for the interference with the wave disturbed by the shock in the other exposure. The three photographs are all reconstructions from the *same* hologram. In the first, the camera lens was set at a small aperture so that only a limited area of the hologram was employed, giving maximum depth of field, and showing up both shock waves. In the second and third pictures, the camera is used at full aperture and focused in turn on each shock wave.

A similar example, figure 5, has a series of fringes across the field introduced by displacing the photographic plate in its own plane by a small distance between the two holographic exposures. In the example given the sideways displacement was 50 μm. The difference in density between the undisturbed air and the air within the shock bubble is indicated by the departure of the fringes from a straight line. Although the variation of refractive index across each shock wave is similar, displacements of the interference bands are in opposite directions. This follows from the situation that each exposure provides the background reference wave for the other in reconstruction.

In figure 6 an extended shock wave is shown, interrupted and reflected by a steel plate, which was about 300 mm long and 25 mm wide and set end on to the viewing direction. The reflected portion of the shock wave is seen below the plate. In this example, the first pulse illuminates before the spark and serves to provide the background reference wave in reconstruction for interference with the wavefront disturbed by the shock and recorded by the second light pulse.

8 Further developments

The present paper is intended to serve as a first example of the application of frequency-doubled lasers with scatter plate holography. Apart from the development in progress on the lasers, which may be expected to yield much more economic and useful sources for recording and for subsequent reconstruction and analysis, a number of other features of the system have been briefly discussed, and it may be useful to indicate here some possible developments in several of these.

Firstly, it is our intention to increase the size of scatter plate and hologram to 125 mm square. This will have the effect of improving depth discrimination, although it seems unlikely from the present experiments that transverse resolving power will be simultaneously improved. This somewhat disappointing failure to resolve particles as small as classical optical theory might lead one to expect (as shown up in the



Figure 4 Shock waves in air produced by electric sparks. Frequency doubled radiation at 530 nm, 2 mJ pulses, 15 ns duration. Agfa 10E56 holographic film. Reconstructions from a single hologram: (*a*) using an area of the hologram 15 mm in diameter, the two shock waves were separated by 300 mm; (*b*) using an area of the hologram 70 mm diameter, the camera was focused in the plane of the reconstruction of the far shock wave; (*c*) using an area of the hologram 70 mm diameter, the camera was focused in the plane of the reconstruction of the nearer shock wave



Figure 5 Shock waves in air produced by electric sparks. Frequency doubled radiation at 530 nm, 2 mJ pulses, 15 ns duration. Afga 10E56 holographic film. Reconstructions from a single hologram: (*a*) using an area of the hologram 10 mm diameter, the two shock waves were separated by 300 mm, the hologram plate was displaced between exposures by 50 μm; (*b*) using an area of the hologram 70 mm diameter, the camera was focused on the plane of reconstruction of the far shock wave; (*c*) using an area of the hologram 70 mm diameter, the camera was focused on the plane of reconstruction of the nearer shock wave



Figure 6 Shock wave in air produced by an electric spark and partly reflected by a steel plate 300 mm long and 25 mm wide set roughly end-on to the direction of viewing. Reconstructions from a single hologram: (*a*) using an area of the hologram 10 mm diameter; (*b*) using an area of the hologram 70 mm diameter, the camera was focused on a plane of the reconstruction of the main part of the shock wave; (*c*) using an area of the hologram 70 mm diameter, the camera was focused on the plane of the reconstruction of the part of the shock wave reflected downwards by the steel plate

present photographic results) needs a careful study. A realization of the full resolving power would, of course, constitute a large improvement in the usefulness of the system. The difficulties seem to lie with the effect of speckle, and with the degrading effect of stray light.

The second development in view is to increase the size of field. If the hologram size is not changed, no more energy is required to cover a larger field, and a large aperture mirror system, for example, could be just as easily employed.

Thirdly a great deal remains to be done on the photosensitive materials to optimize the choice of material in relation to the best choice of exposure, contrast and interference modulation depth, both for the production of scatter plates and in the recording of holograms.

Appendix Preparation of scatter plates

A 'primary' scatter plate is made by subliming ammonium chloride on to a suitable glass plate until the transmission density is 2 for red light. The ratio of the scattered flux to the reference flux is then 3 to 1.

This primary scatter plate is placed in the apparatus described and, using a helium–neon laser as the source and leaving the object space empty, a hologram is recorded on Agfa-Gevaert 10E70 plates backed by coating with sprayed black PVC (DCMC Industrial Aerosols Ltd). The exposure required is one giving a density, after processing, of approximately 0·7.

The processing and bleaching is carried out as follows. The plate is developed for 4 minutes in D19b. It is washed for 30 seconds and fixed in 'Hypam' (8 parts to 32 parts of water plus 1 of hardener) for 5 minutes. After a 10 minute wash the plate is bleached for 3 minutes in the dichromate–hydrochloric acid mixture given below, followed by a 3 minute wash and a 5 minute fix in the 'Hypam' hardener mixture as described above. It is then washed for 10 minutes, rinsed in distilled water and finally dried in clean air at room temperature. All processes are carried out at 20°C. The resulting bleached hologram is used as the scatter plate in the experiments described.

Bleach Solution

Solution A Potassium dichromate 40 g l^{-1}.

Solution B 10% solution of hydrochloric acid SG1180.

For use, mix as follows: 1 part A plus 4 parts water plus 4 parts B.

References

Gates J W C 1968 *J. Phys.* E: *Sci. Instrum.* **1** 989–94

Gates J W C Hall R G N and Ross I N 1968 *High Speed Photography* (London: Wiley) pp. 304–8

Geusic J E Levinstein H J Singh S Smith R G and Van Uitert L G 1968 *Appl. Phys. Lett.* **12** 306

Wuerker R F Heflinger L O and Briones R A 1968 *Appl. Phys. Lett.* **12** 302

Journal of Physics E: Scientific Instruments 1970 Volume 3
Printed in Great Britain

HIGH SPEED HOLOGRAPHIC RECORDING OF TRANSILLUMINATED EVENTS

J.W.C. Gates, R.G.N. Hall and I.N. Ross
Division of Optical Metrology,
National Physical Laboratory,
Teddington, Middlesex.

Introduction

This paper reports recent experimental work in recording transient events by the use of the holographic technique described in the 8th Conference[1]. Our own laser system has been further developed to provide repetitive Q-switched pulses at frequencies up to 20 kHz (50 μs interval) and has been applied to further extensions of the method of recording time sequences of holograms. Related work has also been carried out using commercially-available lasers, and a description of the use of our system in studying fuel distribution in an internal combustion engine is included. Our aim has been to provide a reliable low-cost laser holography system which operates without any additional high-speed camera equipment, but is capable of securing single three-dimensional records of transilluminated events, or a train of consecutive records at a high repetition rate.

Holography with scatter plates

The optical system is very simple, and is shown in figure 1. The principles on which it is based have previously been described in detail[1,2,3]. Light from the pulsed laser, cleaned up by spatial filtration, is expanded to fall on the scatter plate. This is a specially made diffuser which allows a large fraction of the incident beam to pass without causing much disturbance to it, but scatters the remainder in a completely random fashion within a well-defined cone which just allows the full aperture of the working field to be evenly illuminated. The volume of the working space (600mm x 150mm diameter) is defined by the two lenses, which are arranged so that all the light scattered from one point of the scatter plate falls on a corresponding point in the plane in which the photosensitive material is placed. The beam which was transmitted without scattering at the scatter plate (the "reference beam") is converged by the first lens to a focus-point (the "reference point") midway between the two lenses, in the mid-plane of the working volume, but to one side of it, and then diverges again to fill an area of the photosensitive material which exactly corresponds with the area illuminated by the scattered beam. Interference between these two beams of light produces a complex interference pattern which is recorded by the photosensitive material to form the hologram.

When the hologram is illuminated, after processing, with a replica of the reference beam, a reconstructed replica of the scattered beam is produced, by means of which all the detail in any object within the working volume which would have been visible at the time of recording is also reconstructed. For example, a stream of opaque particles may be examined as a static three

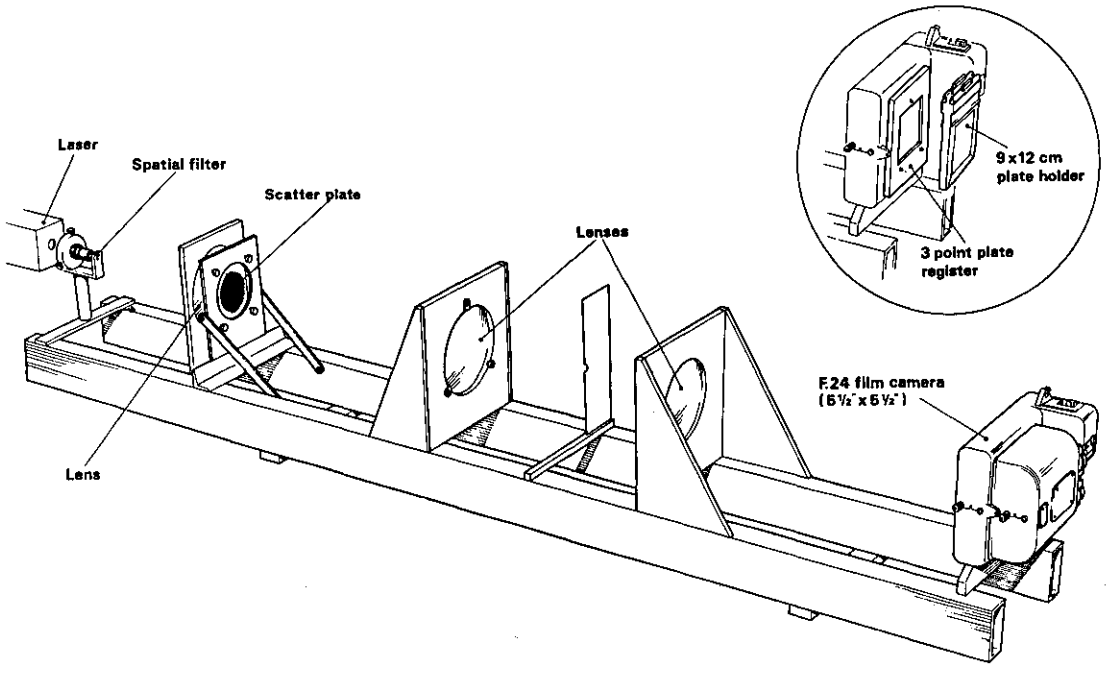


Figure 1

Apparatus for recording holograms. Overall length about 2.5 metres.

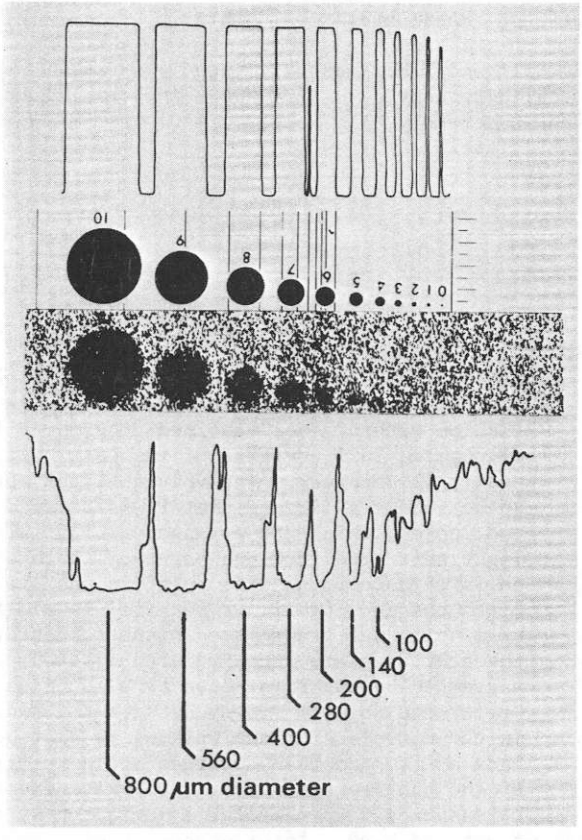


Figure 2
a. Microdensitometer trace of the test object 'b'.
b. Test object.
c. Reconstruction from hologram of 'b'.
d. Microdensitometer trace of 'c'.

(Linear magnification X12 approx)

dimensional distribution. The minimum size of detail which may be resolved depends on the proportions of the apparatus and the scatter plate, but figure 2 gives an indication of what may be recorded. The laser used in recording this holo gram was made by Laser Associates Ltd (Model 252B), and employs neodymium-doped calcium tungstate to produce infra-red radiation which is converted within the resonant cavity into the second harmonic (green) emission at a wavelength of 530 nm, with a pulse duration of about 15 ns.

Recording phase variations

In some cases, the event to be studied may not be directly visible. For example the passage of shock waves through a gas produces variations in the density, pressure, and temperature, but no light is absorbed. Disturbances of this kind which cause changes in refractivity of the gas may be made visible by interference techniques. When holography is employed, an analogous procedure may be followed by making two records on the same photosensitive plate, one with the disturbance, and one without. On reconstruction, the interaction of the two phase distributions results in interference effects which make the disturbance visible in its three dimensional form. Figures 3a,b,c show the patterns resulting from the interaction of four spatially-separated spherical shock waves from four electric sparks, also recorded with second-harmonic pulses from the neodymium-doped calcium tungstate laser.

Photographs give only a very restricted impression of the three-dimensional reconstruction from the hologram. Full discrimination in depth is only obtained by viewing the reconstruction itself.

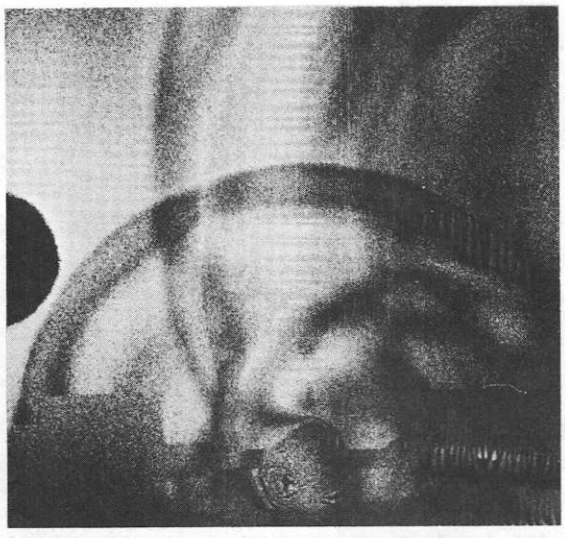


Figure 3a
Reconstruction from a hologram of the shock waves from 4 sparks, separated in depth and fired in sequence. Laser Associates laser Model 252B. Wavelength 530 nm, pulse duration 15 ns. Small camera aperture.

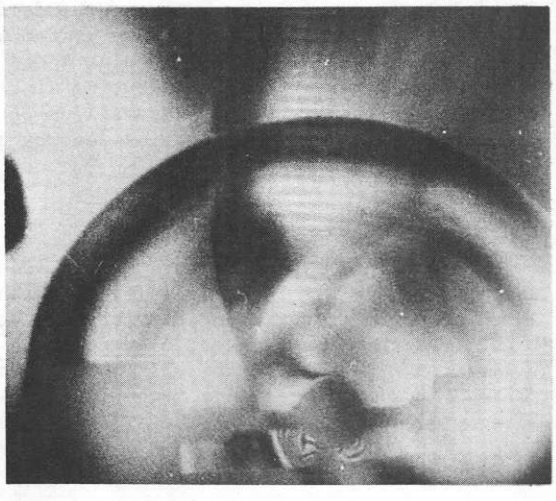


Figure 3b
Reconstruction from the same hologram as 3a. Large camera aperture.



Figure 3c
Same hologram and camera aperture as 3b. Focussed on a different plane in the reconstruction.

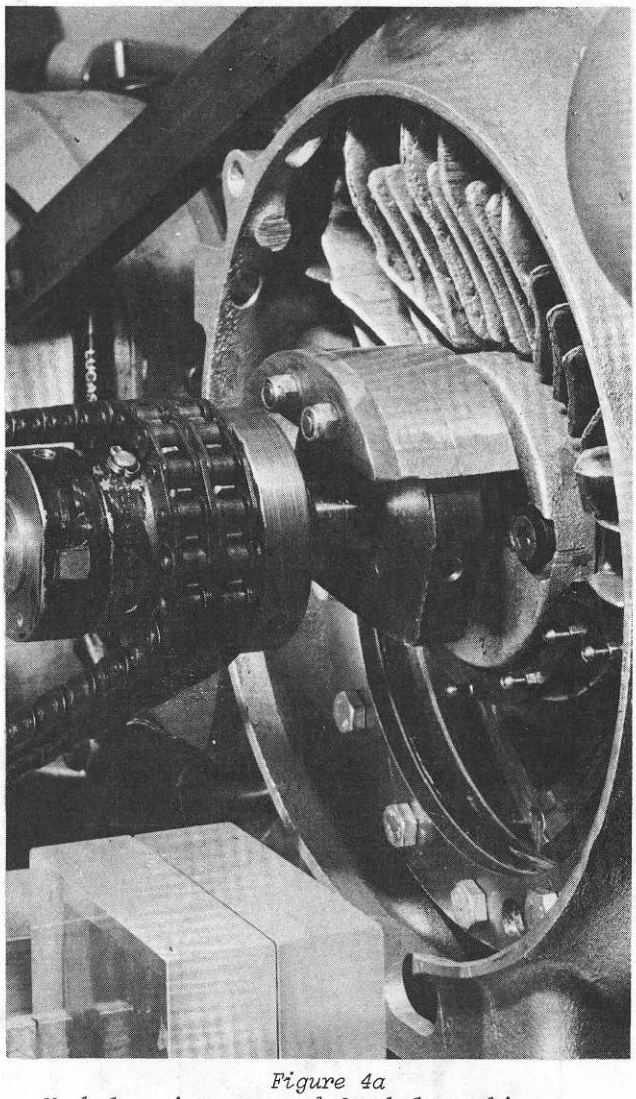


Figure 4a
Wankel engine arranged for holographic recording. Special windows are fitted to the lower part of the engine, and part of the rotor is visible. The reference beam passes through the two compensating plates and below the working volume of the engine. (Photograph by courtesy of RMCS and MVEE).

Application to the study of engines

In experimental work with internal combustion engines, the mixing of the fuel and air, the combustion process, and the distribution of liquid films are all processes which give phase distributions of the kind which can be recorded by double exposure holography, using a sufficiently brief light pulse. The methods we have developed have been most ingeniously employed by B.E. Milsom of the Military Vehicles Engineering Establishment, working at the Royal Military College of Science at Shrivenham, to study the fuel/air distribution in a Wankel engine (figures 4a,b,c). The laser employed was a Laser Associates Q-switched ruby laser Model 211A giving about 1.8J of energy in a 25 ns pulse. The hologram from which the reconstruction was produced was made on an Agfa 8E70 plate.

The deformation in the interference fringes near the lower edge of the window shows a circumferential streaking of a liquid film on one window.

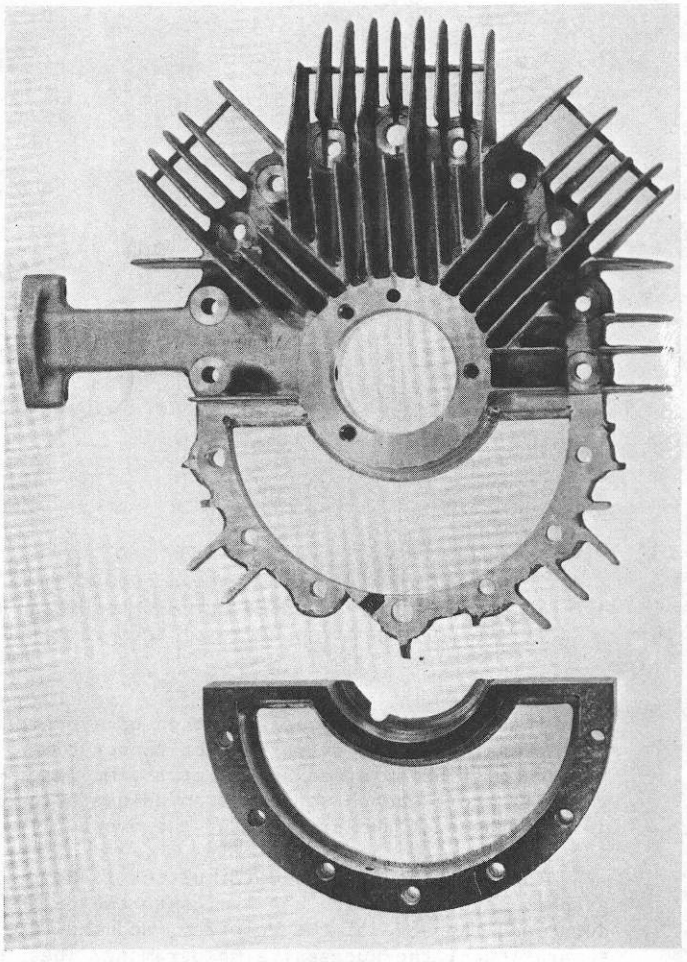


Figure 4b
Front cover of the Wankel engine and the special windows. (Photograph by courtesy of RMCS and MVEE).

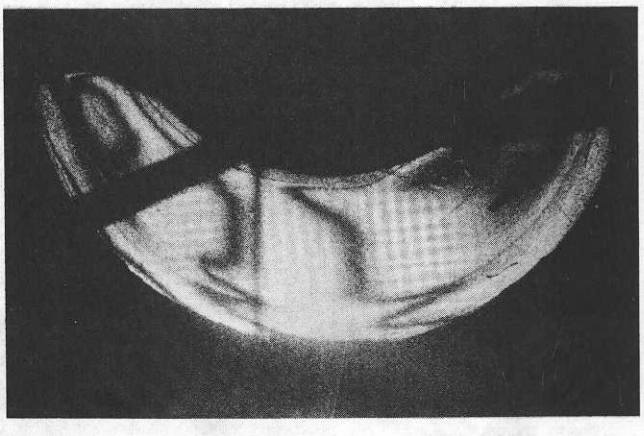


Figure 4c
Reconstruction of a double-exposed hologram, looking through the working volume of the engine while running. The dark shadow on the left is the drive-chain, out of focus. Laser Associates laser Model 211A. Wavelength 694 nm, pulse duration 25 ns, plate Agfa 8E70. (Photograph by courtesy of RMCS and MVEE).

Repetitive recording

In recording transient events, it is obviously necessary to secure an exposure of the hologram at the useful moment, and there are two ways of achieving this which are comparable to the two possibilities in high-speed photography.

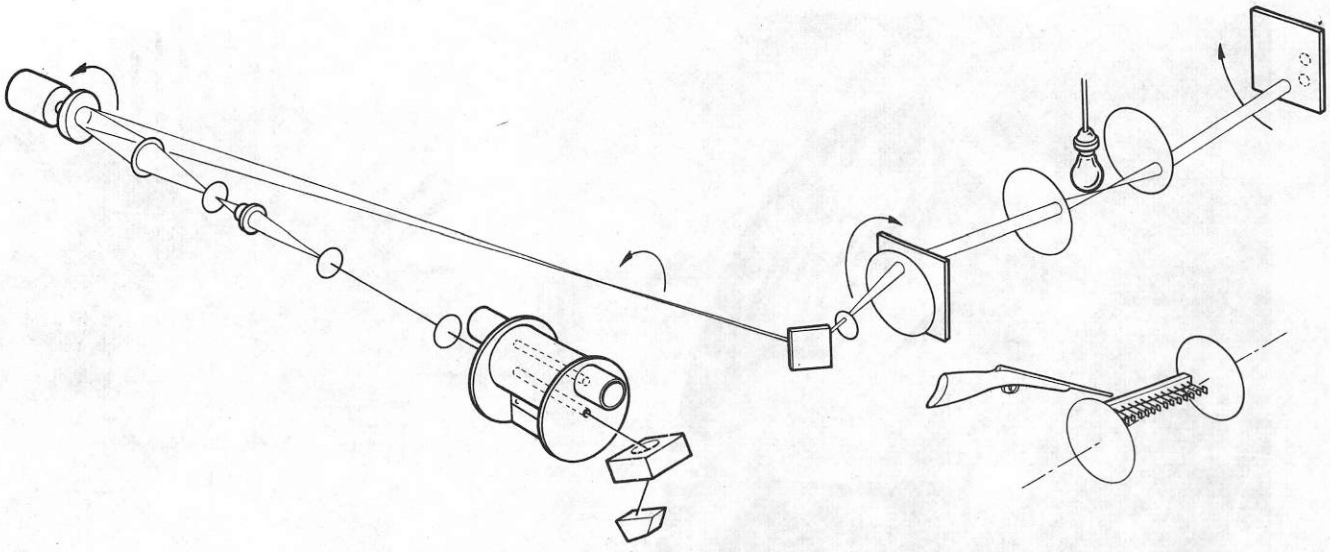


Figure 5

Apparatus for recording a sequence of holograms. The nutating mirror, at the extreme left, produces the circular time-distribution of illuminated patches on the scatter-plate, and the corresponding array of holograms, at the extreme right, and as shown in figure 6a.

Either a sufficiently precise method of synchronizing must be used, or sufficient consecutive records must be obtained spaced at a time interval which is short enough to ensure an adequate record of all stages of the progress of the event.

There may be serious difficulties in holographic recording which set limits to the pulse duration, the size of the hologram, and the time separation of the successive holograms[1]. These difficulties arise when the interference pattern from which the hologram is recorded moves across the plate. By the use of the optical system shown in figure 5, the image of the scatter plate remains relatively stationary upon the plate, and only the patch of illumination changes from pulse to pulse[4]. The nutating mirror causes the illuminated patch to gyrate around the photosensitive plate (figure 6a), so that a sequence of records may be obtained from any starting position on any suitable material. The records shown in figures 6b,c were obtained with a Siemens ruby laser SLR 1P1 operating at a pulse rate of 50 per second, and were recorded on an Agfa 10E75 plate.

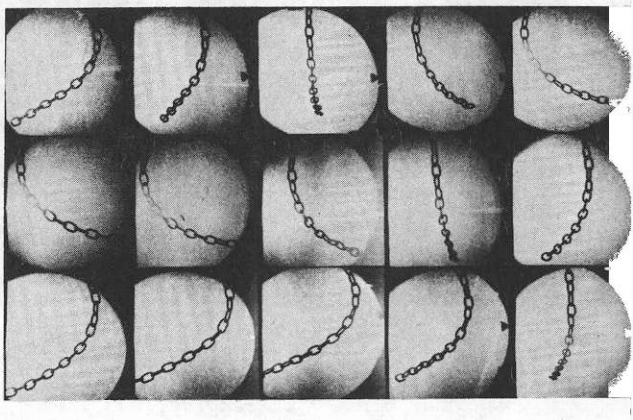


Figure 6b

Reconstructions of a sequence of 15 holograms.

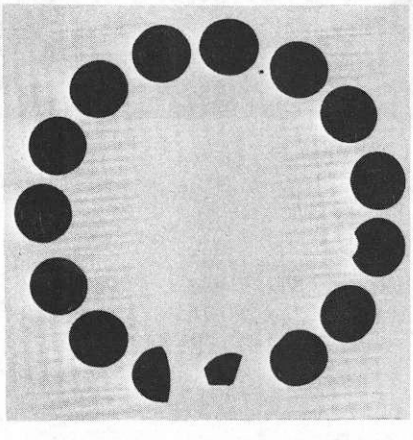


Figure 6a

Sequence of 15 holograms. Siemens laser SLR 1P1, wavelength 694 nm, pulse duration 0.8 ms, repetition frequency 50 per second (interval 20 ms).

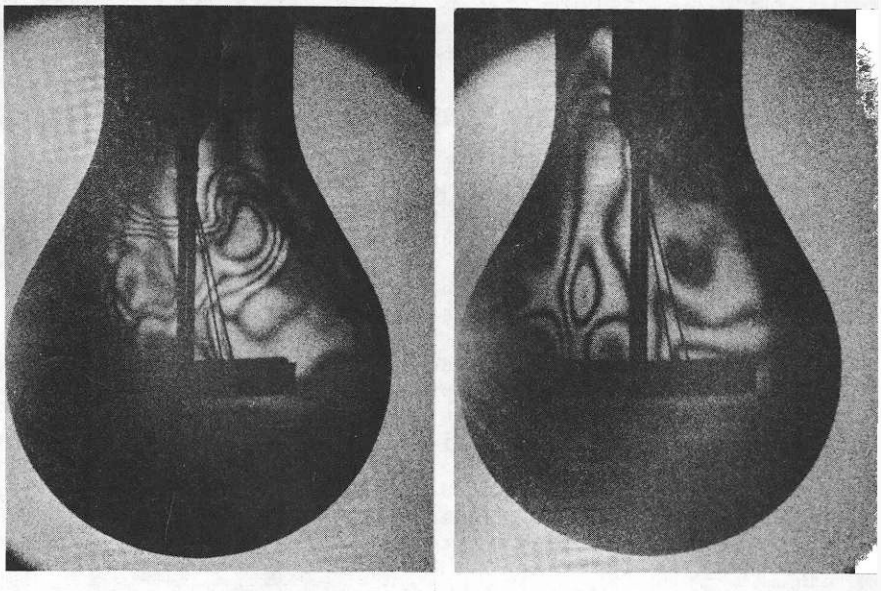


Figure 6c

Two reconstructions from another sequence, made with double exposure of the holograms to record changes in the density distribution of the gas in a lamp as it cools after switching off.

Recording at a high repetition rates

The laser system previously described[1] used as a Q-switch a specially-developed air turbine with an integral reflecting prism, by means of which a ruby laser could be made to emit a train of 7 or more pulses of light each about 30 ns duration, at a repetition frequency of 10 kHz. This system has now been further developed, giving up to 15 successive pulses; and can operate at repetition frequencies up to 20 kHz. Figure 7 shows a typical oscillograph record of the successive light pulses, and figure 8a shows a hologram plate with reconstructions (figures 8b, c,d) from two of the sequence of successive holograms. Two reconstructions from one of the holograms are shown to indicate the possibility that still remains with the holographic recording of choosing the plane of focus to bring out detail over the full depth of the object.

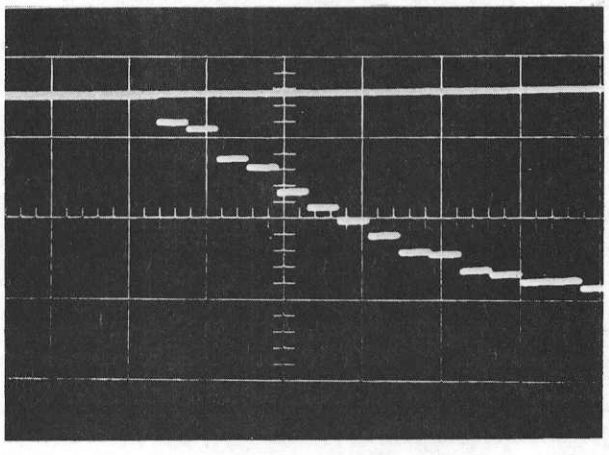


Figure 7
Oscillogram showing 13 consecutive Q-switched pulses from the NPL turbo-prism laser. Horizontal scale of time, 0.2 ms per square. Vertical scale of integrated energy, 0.75 J per square. (Total energy about 1.5 J).

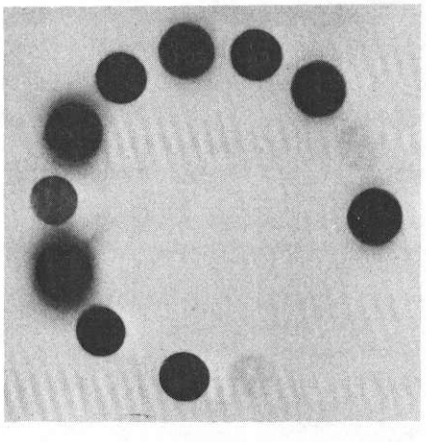


Figure 8a
Sequence of holograms recorded at 11,000 per second. (Some pulses have less energy).

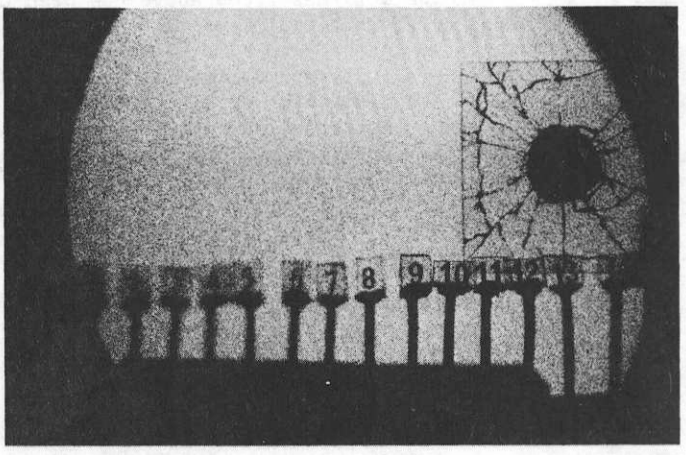


Figure 8b
Reconstruction from the first of a similar sequence of holograms to figure 8a. An air-gun pellet has just struck the glass plate and shattered it.

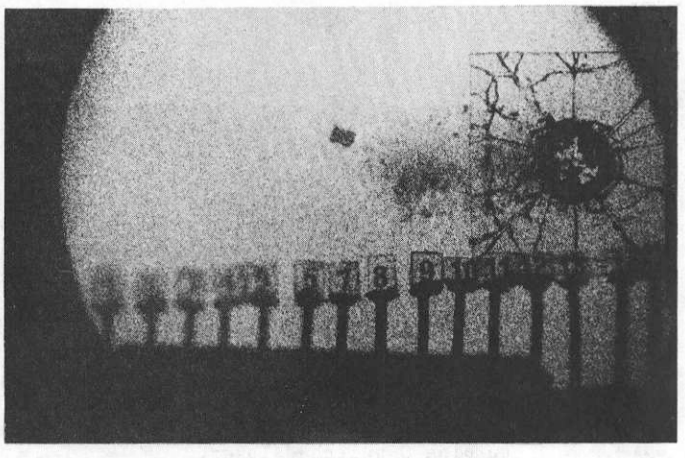


Figure 8c
Reconstruction from the 17th hologram in the same sequence, 1.47 ms after figure 8b. The pieces of the shattered glass plate have not yet moved appreciably, but debris has been carried through by the pellet.

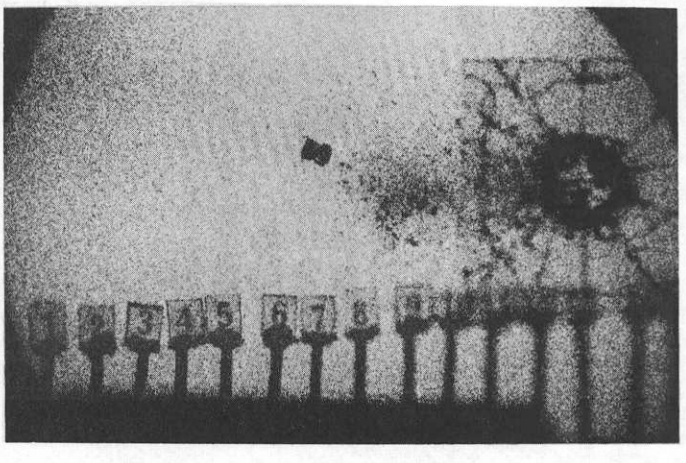


Figure 8d
Another reconstruction from the same hologram as in figure 8c, focussing on the pellet, which was 0.177" (4.5 mm) diameter.

Acknowledgements

The work described above has been carried out at the National Physical Laboratory. We are greatly indebted to B.E. Milsom, to the Dean of the Royal Military College of Science, Shrivenham, and to the Director of Military Vehicles Engineering Establishment, for allowing us to include unpublished photographs from the work on the Wankel engine.

References

1. GATES, J.W.C., HALL, R.G.N. and ROSS, I.N. Proceedings of the 8th International Conference on High Speed Photography, p.299-308, John Wiley & Sons, Inc., 1968.

2. GATES, J.W.C. 1968 J. Phys. E. Scientific Instruments, 1, p.989-94.

3. GATES, J.W.C., HALL, R.G.N. and ROSS, I.N. 1970 J. Phys. E. Scientific Instruments, 3, p.89-94.

4. HALL, R.G.N., GATES, J.W.C. and ROSS, I.N. 1970 J. Phys. E. Scientific Instruments (to be published).

Summary

Further developments in scatter-plate holography are described which illustrate its extension to cover a larger working volume, and to provide more effective three dimensional records of fast-moving objects and phase disturbances. Examples are shown of a simple technique for recording a short sequence of 10-20 holograms at rates up to 20,000 per second, making use, alternatively, of commercially-available lasers and a specially-developed air-turbine Q-switched laser.

Recording rapid sequences of holograms

R G N Hall, J W C Gates and I N Ross
Division of Optical Metrology, National Physical Laboratory, Teddington, Middlesex

MS *received 8 June 1970*

Abstract A simple adaptation of a scatter-plate holographic system provides for the recording of a sequence of 10–20 holograms. Examples are given of records made at a rate of 50 per second of a moving object, and of a changing gas density distribution made visible by interferometry.

1 Introduction

When a rapid transient event is to be studied by optical methods, a ciné camera is often used to record a sequence of images, so that each frame provides information about the object at a single instant of time which can later be analysed in detail. It is frequently the case that only a limited number of frames need be selected for analysis, and often the optimum number is between 10 and 20. Problems of focusing occur when the object is three dimensional or moving unpredictably, and multiple records may then be needed to record sufficient depth of field. The alternative of recording holographically provides a convenient way of recording all the information in a three-dimensional scene, as well as offering a choice of reconstructing techniques; successful experimental demonstrations have been described by Jacobson *et al.* (1969). Apparatus is not yet available commercially, however, and this note describes a simple adaptation of the scatter-plate holographic system (Gates 1968, Gates, Hall and Ross 1970) to record a short sequence of holograms on a single plate or sheet of film.

2 Scatter-plate holography

The basic arrangement (figure 1), as previously described by us, makes use of a 'scatter-plate', which is a specially made diffusing layer on a glass plate, which allows part of an incident beam of light to be transmitted and scatters some of the remainder randomly over the working field. A suitable optical system, which could consist of a pair of lenses as shown in the figure, produces real images of the scatter plate by both the scattered and unscattered light which exactly coincide, in the absence of any gradients of phase disturbance. The photosensitive material is placed in this plane and records the hologram as an interference pattern related to the unscattered light beam as 'reference'. The reference beam usually (but not necessarily) comes to a focus near the central plane of the object to be recorded, so that the volume traversed by the reference beam, which is of minimum diameter in that region, shall not too greatly obtrude into the working space.

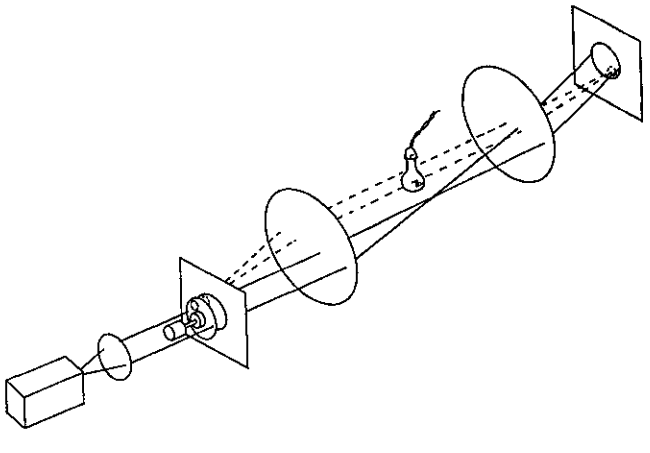


Figure 1 Holographic scatter plate apparatus

After processing the photosensitive material, a replica of the reference beam is made to fall on the resultant hologram, and the transilluminated object is seen as a virtual image through the entire area of the hologram. By employing more or less of the hologram area, and by choosing the position on the hologram, three dimensional effects such as differential focusing and parallax may be employed to discriminate planes at different depths in the object.

3 Hologram-pupil encoding

The transverse extent of the hologram may be employed for other purposes, at the cost of some sacrifice in depth discrimination. For example, it would be possible to record completely different objects at different times, masking either the scatter plate or the conjugate photosensitive material appropriately. Alternatively, simultaneous recordings could be made with different wavelength sources. In these cases the position on the hologram provides means for recording the spatial attributes of the object or objects as a coded array. There are similarities in this principle with some image dissection techniques (Courtney Pratt 1962), and an important extension of the principle may be made for time-resolved recording, in which successively exposed areas of the photosensitive material are used to record a time series of holograms of a transient event. Some attempts to do this were described by us previously (Gates, Hall and Ross 1968), and some success was achieved in recording and reconstructing holograms of a rapidly moving object when the recording frequency was as high as 7 kHz.

In this previous work, the interference pattern formed by the interaction of object beam and reference beam was translated across the photosensitive surface, and this necessarily imposes limits on the size of the hologram, the spatial frequency in the hologram (and consequently the angular

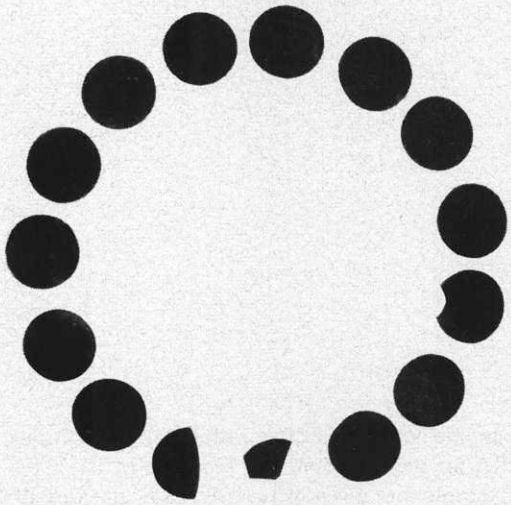


Figure 2 Successively recorded holograms

size of the object which can be recorded), the speed of translation across the surface and the maximum duration of the exposure. The present method, which is based on the previous work but is in fact a simplification, avoids all these limitations, and has been successfully used at repetition frequencies up to 12·5 kHz and higher.

4 Time-resolved recording

As long as the scatter plate and the photosensitive material remain in a conjugate relation without translation of the image of the scatter plate across the photosensitive material, an exposure of any duration may be employed, limited only by considerations of the fastest movements in the object to be recorded, and the effect that the movement will have on the resulting hologram. The effects may well be *less* troublesome than the same amount of movement in conventional ciné photography, and illumination with laser pulses of the order of 1 ms duration causes no problem, compared with the difficulties in the previous method (Gates, Hall and Ross 1968), in which even small holograms necessitated exposures of less than 50 ns duration. The examples given here were recorded using a Siemens ruby laser type SLR 1P1, which gives a continuous train of light pulses less than 1 ms long at the electricity supply mains frequency of 50 Hz. The selection of the area of scatter plate and photosensitive material for each successive holographic record was very simply achieved by rotating a disk pierced with a single aperture at the chosen radius in front of one plane or the other (figure 1). By driving the disk with a synchronous motor, a predetermined spacing of holograms was achieved (figure 2).

The first sequence (figure 3) shows a length of chain whirling in the object space. The second sequence (figure 4) shows the change in the distribution of gas within the envelope of a gas filled lamp after the filament is switched off. The interference patterns are produced by superposing a second set of exposure on the hologram plate while the lamp is at uniform temperature (Ennos 1966, Heflinger *et al.* 1965, Wuerker *et al.* 1968).

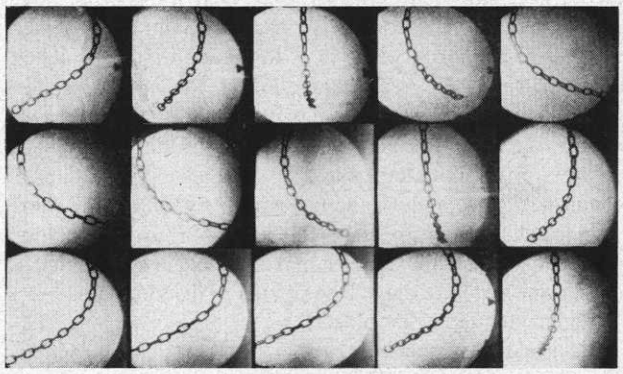


Figure 3 Photographs of reconstructions obtained from successively recorded holograms of a whirling chain; time interval 20 ms

5 Summary

This paper describes the adaptation of the scatter-plate holographic system previously reported for a simple method of recording a sequence of 10–20 holograms at the rate of 50 per second. The same principle can be extended to higher and lower frequencies. Recording at frequencies up to 20 kHz is being reported elsewhere (Gates *et al.* 1971).

Acknowledgments

This work was carried out as part of the research programme of the National Physical Laboratory. The photographs of the reconstruction were made by R F Stevens.

References

Courtney-Pratt J S 1962 *Proc. 5th Int. Congr. on High-Speed Photography* (New York: SMPTE) pp. 197–217

Ennos A E 1966 *Perspective* **8** 276

Gates J W C 1968 *J. Phys.* E: *Sci. Instrum.* **1** 989–94

Gates J W C Hall R G N and Ross I N 1968 *High Speed Photography* (London: Wiley) pp. 304–8

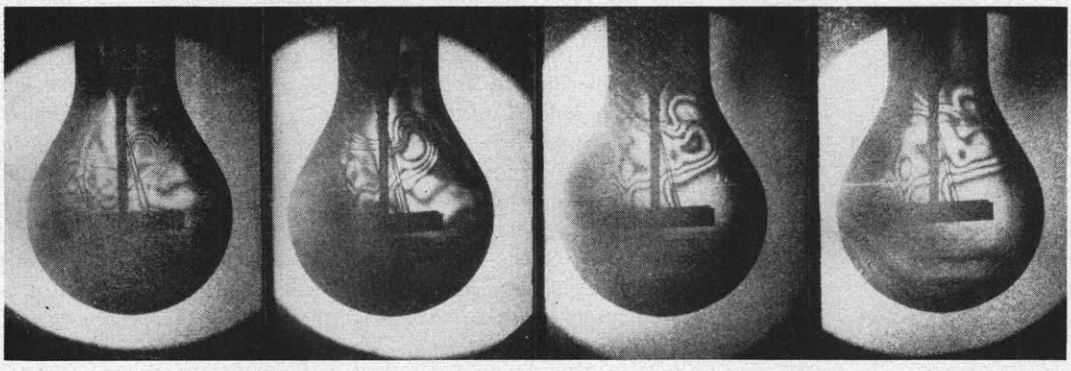


Figure 4 Photographs of reconstructions from a series of successive holograms showing the change in gas distribution in a gas filled lamp when it is switched off

Gates J W C Hall R G N and Ross I N 1970 *J. Phys.* E: *Sci. Instrum.* **3** 89–94

Gates J W C Hall R G N and Ross I N 1971 *Proc. 9th Conf. on High Speed Photography, 1970* (New York: SMPTE)

Heflinger L O Wuerker R F and Brooks R E 1965 *J. Appl. Phys.* **37** 642

Jacobson A D Evtuhov V and Neeland J K 1969 *Appl. Phys. Letters* **14** 120

Wuerker R F Heflinger L O and Briones R A 1968 *Appl. Phys. Letters* **12** 302

Modification for increased efficiency of an intracavity second harmonic neodymium laser

Abstract. The usual method of output coupling for the intracavity-generated second harmonic of 1·06 μm leaves room for improvement of the efficiency by a factor of two. Methods of achieving this factor of two are proposed. The simplest one was tried and gave promising results.

Intracavity second harmonic conversion has been used with high efficiency on both continuous (Geusic *et al.* 1968) and pulsed neodymium lasers. The usual method by which the second harmonic at 0·53 μm is coupled out of the cavity is to employ a suitable dichroic output reflector. This would be a reflector having a maximum reflectivity at 1·06 μm and a minimum reflectivity at 0·53 μm. Such a scheme does, however, suffer from the disadvantage that half of the available energy or power is lost by absorption in the laser material.

Methods of achieving maximum efficiency must introduce between the second harmonic crystal and the laser rod an optical component which separates geometrically the two wavelengths present. It should be completely transmitting at 1·06 μm and must reflect or deviate the green component so that it can leave the laser cavity.

One suitable optical element is another dichroic mirror having the opposite properties to the one already used, i.e. a minimum reflectivity at 1·06 μm and a maximum reflectivity at 0·53 μm. A mirror with these properties is difficult to achieve in practice, particularly with respect to minimizing the reflection losses at the fundamental wavelength.

An alternative method, and one which we have found to operate satisfactorily, makes use, not so much of the difference in wavelength between fundamental and second harmonic, but of the orthogonality of their polarizations. A suitable optical element is the polarizing beam splitting prism.

We have chosen a calcite Glan-Taylor air-spaced prism with a polished side exit face as one which has suitable properties and which is also commercially available.

This prism, in which the optical axes of the two components are parallel, has normal entry and exit faces and does not in consequence deviate the beam passing directly through it. The beam reflected out of the prism which we used emerges at 74° to the axis—a simple and convenient output geometry. Further, this prism has a high damage threshold making it suitable for use in high-power lasers.

Figure 1 shows the reflectivities of the two beams as functions of the angle of incidence on the interface. The optimum operating angle is shown and it will be seen that, whereas the reflection at 0·53 μm is 100%, the transmission at 1·06 μm is not quite 100%. At 98·6% transmission, however, this is not a severe problem. We have assumed that the entry and exit faces are anti-reflection coated and do not introduce losses at either wavelength.

Using this method of output coupling there is no need for transmission through either cavity reflector. A roof prism or coated reflector giving 100% reflectivity at both wavelengths is now required at both ends. Further advantages are that position and angular settings are not critical, and that when in use with an electro-optic Q-switch the polarizing prism serves also as the Q-switch polarizer.

In a preliminary test using the polarizing prism with no anti-reflection coatings, in conjunction with a Laser Associates Q-switched Nd : $CaWO_4$ laser, an increase in total output energy of 60% was immediately obtained at near-maximum output.

Two logical extensions of the above idea may improve the performance at the expense of a loss of tolerance in construction and alignment of the prism.

We have noted a small reflective loss at 1·06 μm. Since there are multiple reflected beams from the prism interface, the possibility is open to us of eliminating this reflected component by destructive interference. For this to occur the air gap between the two

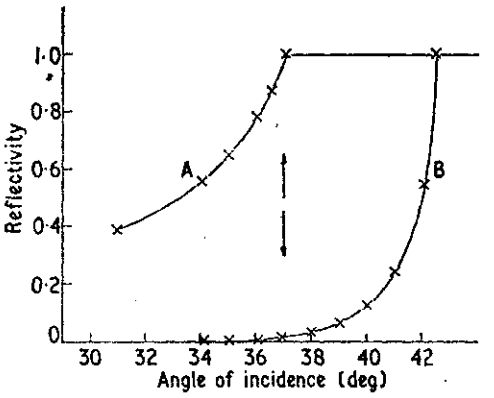


Figure 1. The reflectivity of the interface of the calcite Glan–Taylor prism as a function of the angle of incidence on the interface. Curve A is the ordinary ray at 0·53 μm, curve B is the extraordinary ray at 1·06 μm. The arrow indicates the optimum operating angle.

components of the prism must have constant thickness to a small fraction of a wavelength over the area used, and this thickness must be $(n\lambda/2)\cos\theta$ where n = integer. Theoretically, complete elimination of the reflected component is possible. In practice, incomplete spatial matching of reflected components tends to increase the reflection, but for the calcite polarizing prism this loss will be negligible.

The theoretical complete elimination of the reflection is independent of the single-surface reflectivity, although as the latter increases so do the losses and the criticality of alignment. As a consequence of the former fact it is unnecessary to employ a birefringent material in the beam-splitting prism. With silica for example, the difference in critical angle for 1·06 μm and 0·53 μm is 26′ = 7·6 mrad, and the minimum single-surface reflectivity at 1·06 μm, whilst maintaining 100% at 0·53 μm, is 36%.

Various methods of increasing the intracavity-generated second harmonic of 1·06 μm by a factor two are proposed. The simplest one was tried and gave promising results.

The work described above was carried out at the National Physical Laboratory, Teddington, Middlesex.

Division of Optical Metrology,
National Physical Laboratory,
Teddington, Middlesex.

I. N. Ross
29*th January* 1970

References

Geusic, J. E., *et al.*, 1968, *Appl. Phys. Lett.*, **12**, 306.

Extrait de

APPLICATIONS DE L'HOLOGRAPHIE

Comptes rendus du Symposium International

★

BESANÇON - Juillet 1970

★ ★

Edité par J.-Ch. Viénot, J. Bulabois, J. Pasteur

copie de l'original effectuée par le Service de Reproduction de la Faculté des Sciences de Besançon

THE HOLOGRAPHIC MEASUREMENT OF COHERENCE

by I.N. Ross
National Physical Laboratory, Teddington, Middlesex, England.

Using holographic techniques, coherence measurements have been made on several pulsed lasers. The techniques had many advantages over more conventional coherence experiments and were particularly simple. The results show promise of being able to assign to almost any source accurate numbers for its coherence function.

Introduction

In our work on pulsed holography we are, on the one hand, using commercially available pulsed lasers with compensated optical systems and, on the other hand, improving the coherence properties of both neodymium and ruby systems for use in applications requiring a significant coherence such as reflection holography. It is desirable to assess quantitatively the coherence properties of existing lasers to establish the extent of their limitations and to indicate possible improvements. A single figure of merit is often sufficient to indicate the spatial or temporal coherence of conventional sources and these figures of merit can be obtained quickly and easily by using conventional interference methods. The coherence of multi-mode lasers cannot be specified so easily since it is no longer a simple function and is quite likely, for example, to have a significant value beyond the first zero. It becomes impracticable therefore to carry out the large number of discrete visibility measurements necessary to define the coherence function completely. The need arises for a method which measures the coherence as a continuous function of path difference. This need is satisfied by holography.

Holography offers several further advantages over conventional methods. In it one measures a reconstructed intensity, and this intensity is a direct measure of the coherence. A single hologram can completely record the spatial or temporal coherence of a source, a valuable property when studying pulsed sources. In addition, holography can be economic both in time and equipment and very simple to record. For those workers using lasers for holographic recording, the same method of recording is the natural choice of a means of assessing the performance of the laser.

Several authors (1,2,3,4,5) have performed experiments in which they used holography as a coherence tester, and they showed that the method works well in cases where the coherence function is a simple one. No-one appears to have gone as far as determining the coherence function or mode structure of a laser.

The Holographic Method

The hologram is a two-beam interference recording in which the two beams are, in general, derived from different points in the wave field. The coherence function between these two points (say P and Q) is denoted by $\gamma(P,Q)$, and is defined as a correlation function integrated over a time long compared with $1/c\Delta\nu$.

This element of time in the integration is important when considering laser sources, in particular those which are not stable and have mode structures and power spectrums which are not time invariant. Consequently, the coherence for these systems may be highly dependent on the time of integration; an important consideration when measuring the coherence of a source with a view to using it in a particular application. Further, there follows the possibility of modifying the output parameters of the laser so that its coherence function is better suited to the application and this need not be so drastic and difficult as reduction to single mode and single frequency. The majority of applications do not require complete coherence; a reduced but still fairly uniform coherence is often acceptable.

The visibility of the interference pattern forming a hologram is given by:-

$$V = (2\sqrt{I_1 I_2}/I_1 + I_2)\ |\gamma(P,Q)|$$

(where I_1 and I_2 are the intensities of the two beams at the plate and $|\gamma(P,Q)|$ is the modulus of the coherence function).
The intensity of reconstruction I_r is a function of the fringe visibility V, the mean intensity $\bar{I}$ and the spatial frequency ω of the interference pattern. Thus $I_r = \text{fn}\ (V,\bar{I},\omega)$; this function being dependent upon the emulsion and processing.

For visibilities less than 0.25, the dependence of the reconstructed intensity on V becomes a direct square law to a good approximation, i.e. $I_r = V^2\ \text{fn}\ (\bar{I},\omega)$. We have chosen to work in this regime since, although the efficiency is limited, it is not necessary to calibrate over the whole range of visibility and the signal to noise in the reconstruction is higher.

One of the chief difficulties in obtaining quantitative results is due to variations in intensity across the output beam of the source under test. These variations were intentionally left undisturbed in order not to affect the coherence properties, so it was necessary to make a correction to the experimental results. Two possibilities are open:-
(i) to measure the intensity variations. When doing this, we preferred to pre-expose the hologram. The visibility is then given by:-

$$V = (2\sqrt{I_1 I_2}/I_1 + I_2 + I_0)\ |\gamma(P,Q)|$$

(where I_0 is the effective pre-exposure intensity level)
and the mean intensity is constant and easily controllable. Since the reconstructed intensity is proportional to V,
and only V is affected by intensity changes, the correction can be carried out without recourse to the properties of the emulsion.
(ii) to obtain from the same or a similar hologram another reconstruction for which the source is effectively coherent. The intensity in this other reconstruction can then be used as a normalising factor. It will be seen below how this can be done in practice.

Experimental Methods

It is desirable, to avoid complex analysis, to design the experiment to measure either the spatial or temporal coherence but not a mixture of the two.

One method of measuring the spatial coherence has been demonstrated (1, 2); that of deriving the reference beam from one point of the wavefront, leaving the remainder to act as the signal beam. Only the coherence of the wavefront with respect to a single point in it is thus recorded. Another method, which has been used in this work and which is shown in Fig.1, enables one to record all the coherence information in one hologram. The main component is a scatter-plate beam splitter which causes amplitude division by allowing a fraction of the wavefront through undisturbed and by scattering the rest. The hologram is recorded in a plane where each point of the plate receives, as reference, one ray of the undisturbed beam and, as signal, scattered light from the entire wavefront. Reconstructing through a small area at that point reconstructs only that part of the scattered light coherent with the point of origin of the reference ray. The prism merely creates an off-axis situation so that the twin reconstructions do not overlap. Very little temporal coherence is required if the dimensions are chosen correctly. Furthermore, the second and preferable scheme for correcting for intensity variations can be used by reconstructing from the entire hologram and spatially filtering the reconstructed light.

One way of measuring the temporal coherence continuously over a range of path difference is to make a hologram of a surface inclined at an angle to the viewing or incident direction. A suitable arrangement is to insert a grating into a Twyman-Green interferometer in place of one of the mirrors. Any retro-reflecting surface such as Scotchlite (3) could be used although the

more diffusing it is the less efficient it becomes in getting energy back onto the plate and the more spatial coherence is required. If it is necessary to measure the temporal coherence over a large range or there is little spatial coherence, the grating becomes expensive. An alternative arrangement is shown in Fig.2. This method does not suffer from the disadvantages above, but it does require an emulsion capable of a very high resolution. Unless the plate or film is orientated at the Brewster angle there are inter-reflections from the surfaces, as shown. These are useful in two respects: the two beams I and III form a hologram which reconstructs in a convenient direction and reconstructs more efficiently than that from I and II. The two beams I and IV make a hologram which reconstructs with an efficiency independent of the temporal coherence. This is just the reconstruction required for making a correction to allow for the intensity variations.

Experimental Results

An initial experiment was performed to find out how accurately coherence measurements could be obtained. The spatial coherence of a gas laser emitting simultaneously the TEM_{oo} and TEM_{o_1} modes was measured by the method of Fig.1. Fig.3 shows both the measured intensity across the reconstructed wavefront corrected for intensity variations in the reference and signal beams, and the square of the calculated coherence function for the two-mode output. The result confirms the feasibility of the holographic method as a quantitative measure of coherence, although the accuracy is reduced as the reconstructed intensity approaches the noise level.

The temporal coherences of several pulses lasers with outputs at 0.694μm and 0.53μm were then measured, both suggested methods being used. The grating Twyman-Green method was normally used with a 10E series Agfa plate but, although the efficiency was lower, satisfactory results were obtained with Polaroid 55P/N. Eastman Kodak 649F was used in the second method and gave consistent results in spite of the very high spatial frequency it had to resolve. Fig.4 is a graph showing the temporal coherence of a spinning mirror Q-switched ruby laser using a silica plate as output reflector. The oscillatory nature of the graph corresponds to the spectral filtering properties of the resonant reflector plate.

The spatial coherence was also measured for these ruby and neodymium lasers. Fig.5 shows examples of reconstructions from holograms taken for three of them; the same ruby laser, a small 'pocket flash-gun' ruby laser, and a frequency-doubled Nd:$CaWO_4$ Q-switched laser marketed by Laser Associates. In each case, the upper reconstruction contains the information of the coherence properties of the wavefront relative to a point close to centre of it, and the lower is a reconstruction which differs only by being independent of the coherence function.

The most striking thing to emerge from the measurements made to date is the surprisingly high fraction of the near field pattern of the multimode sources tested over which there is appreciable coherence, especially in view of the non-uniformity of the beam. We infer that considerable interaction exists between modes and it appears to exert an influence across appreciable distances in the near field.

The amounts of spatial coherence which seem to be present in some uncontrolled lasers may be adequate for many holographic uses. It is then unnecessary to apply mode controls, which usually lead to significant reductions in output intensity.

References

(1) LURIE, M. J.O.S.A. 58, 1968, p.614.
(2) MURATA, K., ASAKURA, T. and FUJIWARA, H. Optica Acta 17, 1970, p.5.
(3) McCLUNG, F.J., JACOBSEN, A.D. and CLOSE, D.H. App. Opt. 9, 1970, p.103.
(4) STETSON, K. and POWELL, R. J.O.S.A. 56, 1966, p.1161.
(5) ALEKSOFF, C. App. Opt. 6, 1967, p.2192.

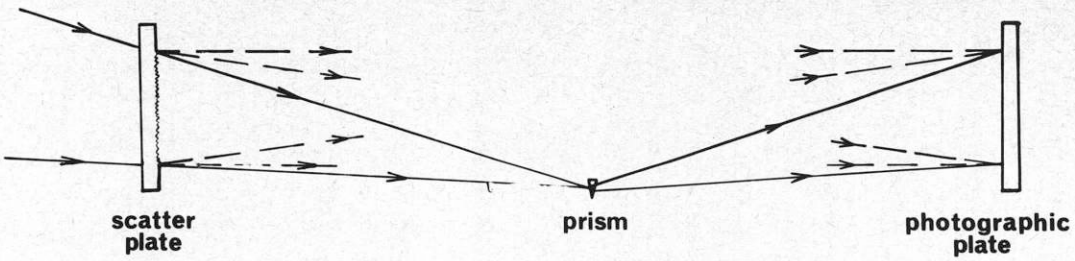
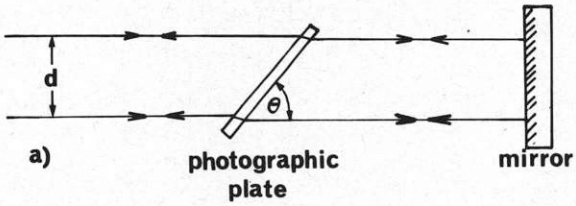


Fig.1 Schematic diagram of the spatial coherence experiment.



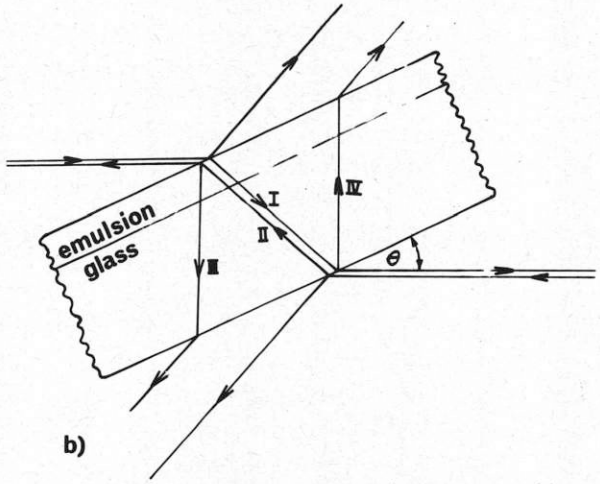
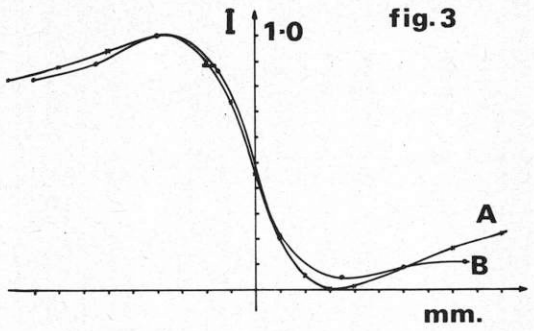


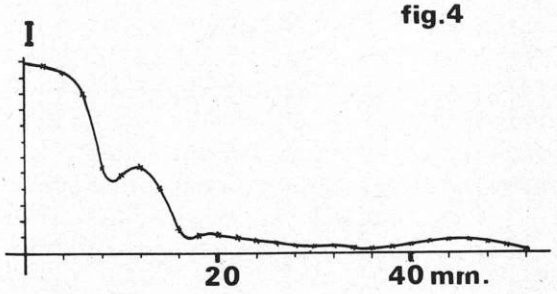
Fig.2 Schematic diagram of the temporal coherence experiment. The various rays in the plate are shown below.

fig.3



Spatial coherence of $TEM_{01}+TEM_{00}$ mode laser
Curve A: normalized reconstructed intensity
Curve B: (calculated coherence function)^2

fig.4



Temporal coherence of ruby laser with resonant reflector.
Reconstructed intensity vs path difference.

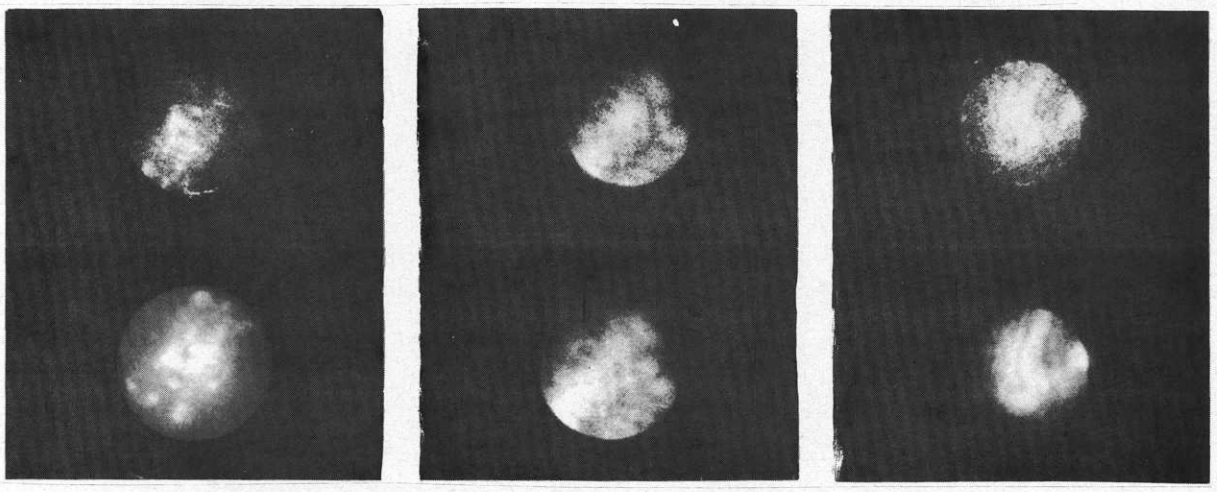


Fig.5 Spatial coherence of three pulsed lasers.
Upper reconstructions depend on coherence with respect to beam centre.
Lower reconstructions are independent of coherence.

Reprinted from Optics and Laser Technology

Holographic interferometry of impact-loaded objects using a double-pulse laser

J.W.C. GATES, R.G.N. HALL, AND I.N. ROSS
National Physical Laboratory,
Teddington, Middlesex, England

Some examples of dynamic holographic interferometry are presented. Two Q-switched laser pulses each of energy 30mJ and separated by 25 μs are used to record holographically the transient impulse response of diffusely reflecting objects occupying volumes of about (30 cm)^3. The laser was of simple form and was not confined to single axial or transverse mode.

Researchers concerned with the investigation of dynamic processes in which high measurement sensitivity is required have been increasingly interested in pulsed holography as a three-dimensional diagnostic method. Its advantages have been demonstrated in fields such as non-destructive testing, plasma research, stress analysis, wind-tunnel investigations and moving-particle distributions, and are becoming increasingly recognized. It has recently become evident that the recording of two or more holograms with short time separations is a powerful method for supplying information about transient phenomena, whether this information be velocity or the rate of change of other parameters[1]. Consequently, there is now a considerable demand for double-pulse lasers with adequate coherence and pulse separations of from 1 μs to 1s.

Using our own laser and holographic system, we have been recording holograms of transient events on diffusely reflecting three-dimensional objects extending in size to about (30 cm)^3, and, in this note, we present some early examples of these double-exposure pulsed holograms with short pulse separations.

The holograms

Figs. 1 - 7 are photographs of reconstructions of holograms, all of which have been recorded using the same laser source and holographic arrangement and, with the exception of Fig. 1, they all show the change in familiar objects over a time interval of 25 μs.

Fig. 1 demonstrates the tilt and bending in a vertical metal plate when a small static force is applied at its upper edge. The two exposures were separated in this case by a time of 5 min and, since the object was relatively stationary, the hologram might have been recorded with a continuous laser. It serves to demonstrate, however, that satisfactory interference holograms can be recorded with the laser running in the double-pulse mode and with a diffuser placed between the laser and the diffusely reflecting plate. The extra diffuser improves the object illumination and reduces the danger of eye damage, but it imposes severe restrictions on the stability of the source, diffuser and object, if good contrast fringes are to be obtained from the double-exposure hologram. These restrictions do not

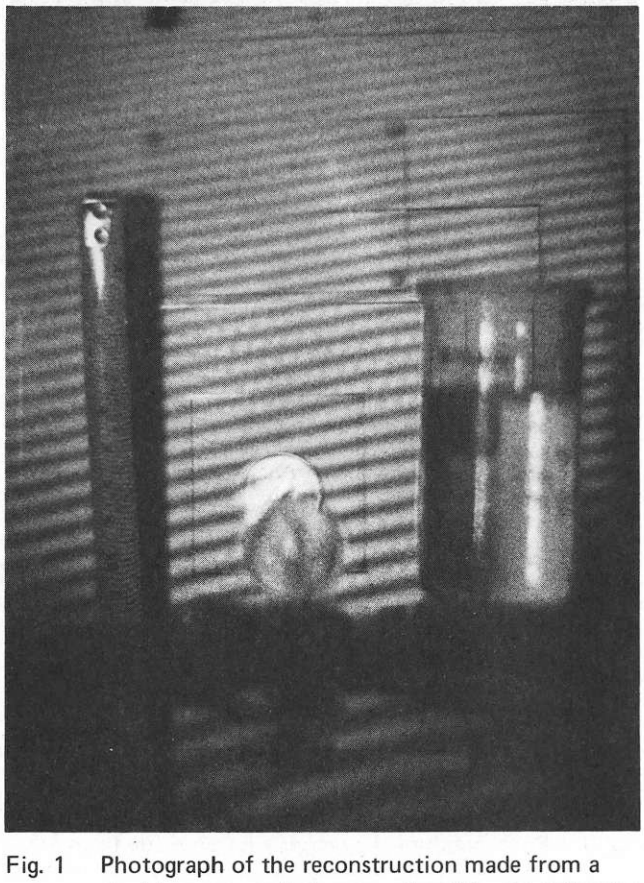


Fig. 1 Photograph of the reconstruction made from a double-exposure hologram of a diffusely reflecting surface illuminated through a diffuser. Plate loaded between exposures: pulse separation 5 min

seem to have been adequately considered in the literature and will be discussed more fully in another communication. Fig. 1 demonstrates that the output of the laser is sufficiently reproducible to give adequate contrast of the fringes, but to avoid the deterioration in fringe quality from the often unpredictable transient in-plane motion of some of the objects, the diffuser was removed for the other examples.

Fig. 2 shows a spinning fan, the blade of which is normal to the line bisecting the illuminating and viewing directions. The top and bottom points of the fan blades have a maximum component of velocity (a maximum distance moved in 25 μs) along this bisector, while all points on the blades lying on a horizontal line have zero component. Straight fringes are expected[2] and these enable the speed of rotation to be calculated. In this case it was 200 r.p.m. There is a limit on speed because of the deterioration of the hologram which results from a path change during the exposure[3], and, by varying the fan speed up to its maximum, the tolerance on path change was shown to be at least 0.3

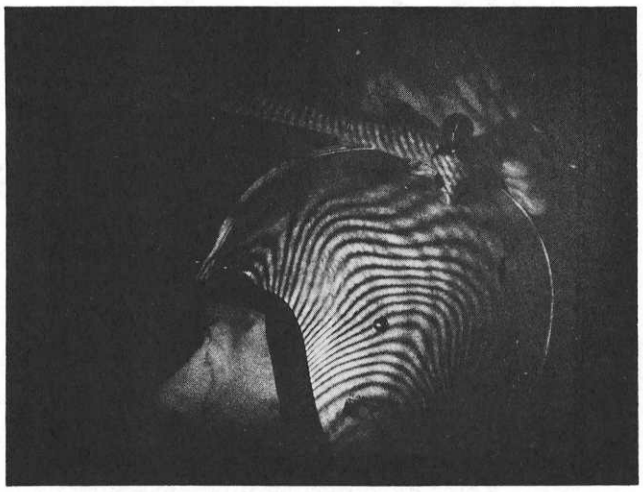


Fig. 4 Photograph similar to Fig. 3 but with a greater delay between the instant of impact of the hammer and the recording pulses

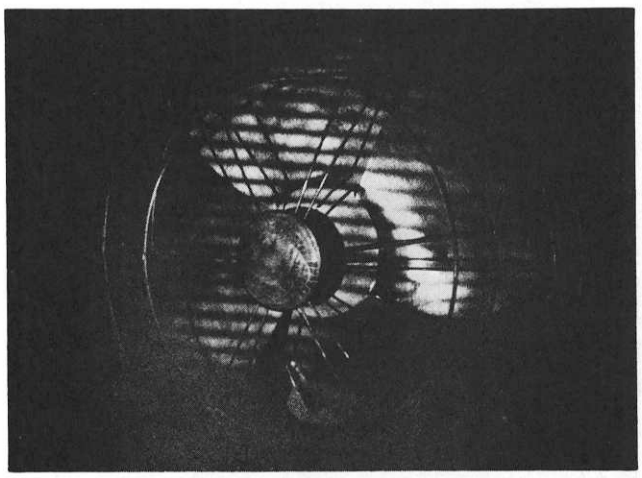


Fig. 2 Photograph of the reconstruction made from a double-exposure hologram of a spinning fan. Rotation speed 200 r.p.m., pulse duration 25 ns, pulse separation 25 μs

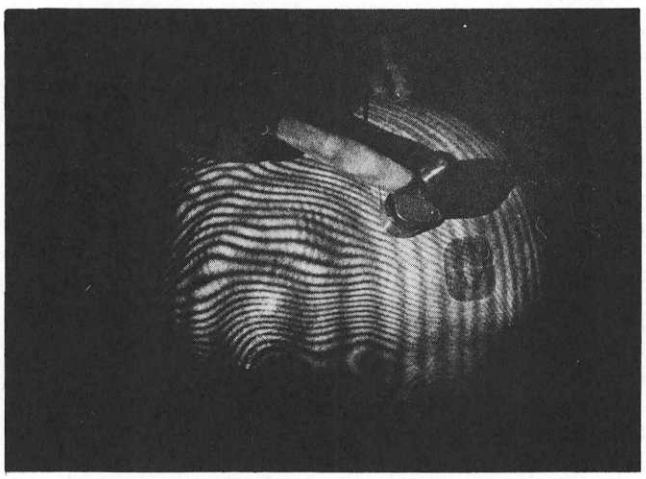


Fig. 5 Photograph similar to Fig. 4, but with the presence of contour fringes as a result of a small component at a different wavelength. Wavelength difference 0·12 Å

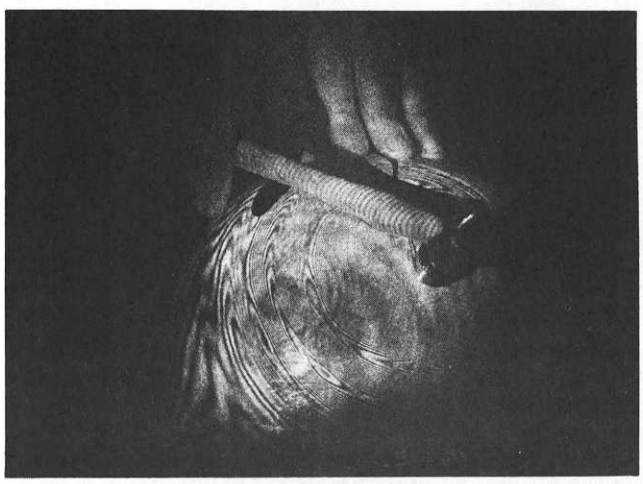


Fig. 3 Photograph of the reconstruction made from a double-exposure hologram of a motor cyclist's crash helmet showing the effect of a hammer blow on its crown. Pulse duration 25 ns, pulse separation 25 μs

wavelengths, which is consistent with the theoretical prediction.

Figs. 3 - 7 show the effect of impact on various objects, the double-exposure hologram being recorded at various times up to 1 ms after impact.

Figs. 3, 4 and 5 show the transient deformation of motor-cyclists' crash helmets after each was struck by a hammer. The hologram from which comes the reconstruction shown in Fig. 3 was recorded immediately following impact and clearly shows the shockwave phenomena. The hologram giving Fig. 4 was recorded a longer time after impact. The helmet on this occasion was untreated in any way (it was not, for example, painted to enhance the reflection). Fig. 5 is included to show that it is possible to contour the object at the same time as observing its deformation. The contour fringes are the result of a small component in the output of the laser with a different frequency and are produced simply by detuning the intracavity tilted etalon. As in the example shown by Fig. 5, these contour fringes can be obtained without seriously affecting the information about

the dynamic disturbance contained in the double-exposure fringes. Even if the interaction between the two sets of fringes were potentially troublesome, there is still the possibility of optically filtering the reconstruction to eliminate one or other of them, since their planes of localization are rarely coincident.

Fig. 6 shows the reaction of one of the authors to a resounding hammer blow on the head—while wearing one of the crash helmets, of course! Care was taken not to allow the undiffused illumination to enter the eye.

Fig. 7 demonstrates the distortional effects in a piece of blockboard which occurred as a nail was being driven into one edge of it.

The holography

The arrangement used is indicated in Fig. 8; it employs a conventional geometry using the Fresnel reflection and transmission at an uncoated surface as beam-spitter, negative silica lenses for beam expansion and mirrors for redirection. Reference and signal beams are expanded to cover uniformly both the photographic plate and an object having a cross-section of about $(30\ cm)^2$, and they have optical path lengths from laser to plate which are contrived to be equal for a point in the centre of the object. The angle between the reference and signal beams at the hologram plane was 20° - 40° and the ratio between their energy densities also at the hologram plane was 5 to 1. Agfa Gevaert 9 x 12 cm 10E75 plates were used and were found to require approximately 50mJ m^{-2} (50 ergs cm^{-2}) for a density of 0.5. The pulse lengths of 25 ns and pulse separations of 25 μs permitted the experiments to be performed without any mechanical stabilization or anti-vibration measures.

The laser

Fig. 9 is a diagram of the laser. A 10 mm x 100 mm ruby is pumped by a linear Xenon flashlamp in an elliptic configuration. Q-switching and double-pulsing is achieved using a 100 000 r.p.m. air turbine rotating prism[4] in conjunction with a double prism assembly. This arrangement allows pulse separations from 10 μs up to 500 μs, the upper limit being determined by the flash duration. It also enables the axes of the two pulses to be separated, resulting in a factor of two increase in total output and a greater ease of achievement of equal energy pulses. Where good contrast interferograms are the main concern, it is usually necessary for the pulses to be co-axial. This was so in our case and equal energy pulses were achieved by increasing the loss per pass for the first pulse. Adequate temporal coherence was achieved using a single-plate, silica, resonant reflector and an intracavity tilted etalon.

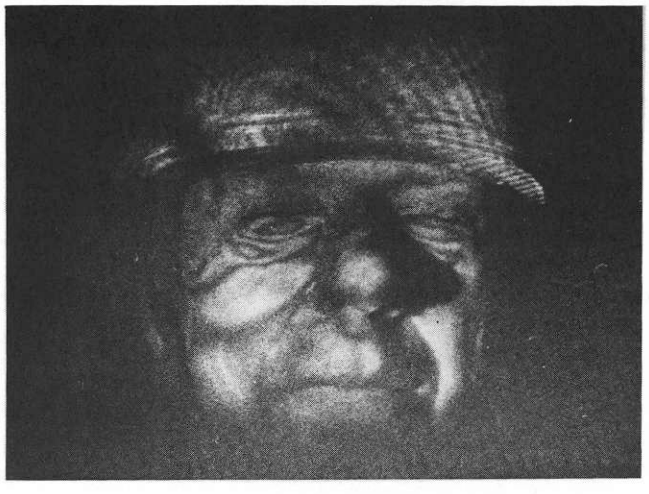


Fig. 6 Photograph of the reconstruction made from a double-exposure hologram of a motor cyclist's crash helmet worn by one of the authors, showing the effect of a hammer blow on the helmet. Pulse duration 25 ns: pulse separation 25 μs

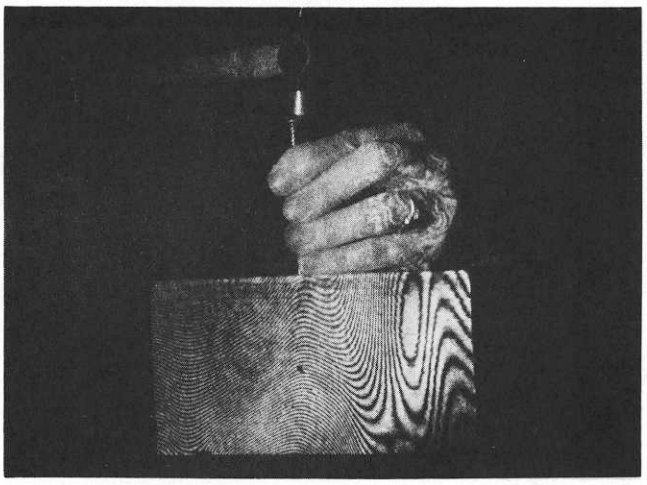


Fig. 7 Photograph of the reconstruction made from a double-exposure hologram of a piece of blockboard, showing the effect of driving a nail into one edge of it. Pulse duration 25 ns: pulse separation 25 μs

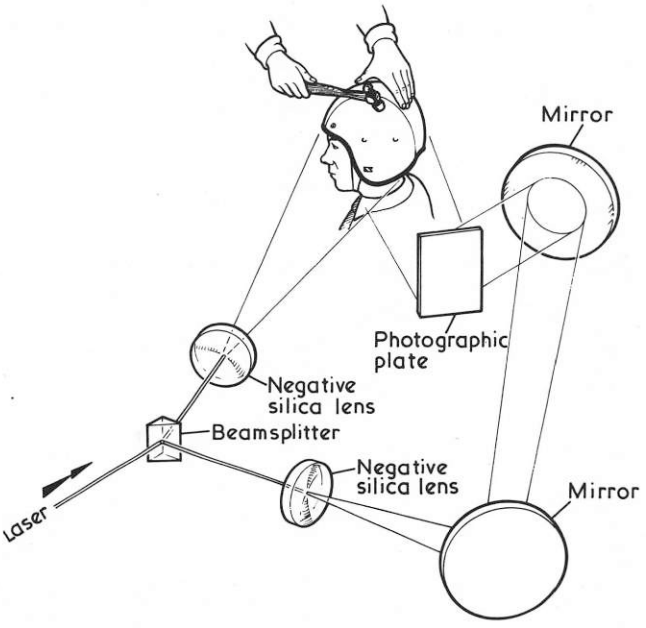


Fig. 8 Hologram recording arrangement

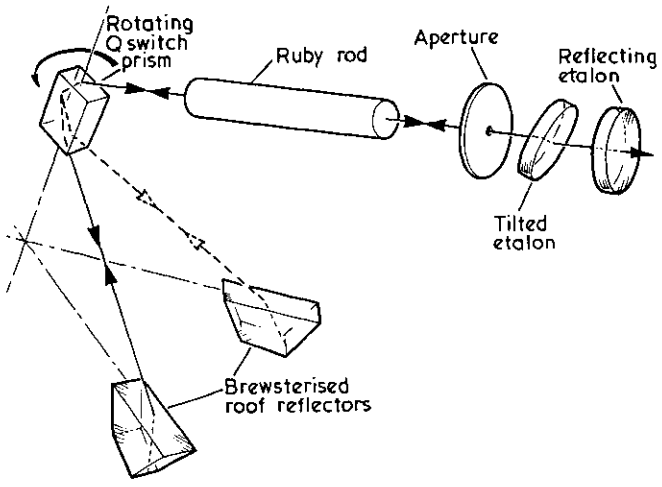


Fig. 9 Laser resonator, showing the Q-switching and double-pulsing arrangement and the coherence controls

Received 8th January 1972

In order to improve the uniformity of the illumination on the object an aperture of 1.8 mm was inserted in the resonator. The resulting Fresnel number of 2.0 had the further effect of restricting the output to just a few transverse modes. Figs. 2 - 7 show that both the transverse and temporal coherence and the object illumination is adequate for differential holographic interferometry of diffusely reflecting objects. The transverse coherence was, in fact, more than adequate as evidenced by Fig. 1 which was obtained in the absence of the intracavity aperture.

References

1 Hirth, A. (1969) C R Acad Sci, Paris **B268**, 961

2 Alexandrov, E.B. and Bonch-Bruevich, A.M. (1967) Sov Phys Tech Phys, **12**, 258-265

3 Neumann, D.B. J Opt Soc Am (1968), **58**, 447-454

4 Gates, J.W.C. and Hall, R.G.N. (1970) Proceedings of the Technical Program, Electro-Optical Systems Design Conference, New York, 387-396

PULSED LASERS FOR OPTICAL MEASUREMENT

by

J.W.C. Gates, R.G.N. Hall and I.N. Ross
National Physical Laboratory
Teddington, Middlesex, United Kingdom

Introduction: Optical Measurement

Measurements of position, length, form or profile, alignment and orientation can be carried out optically, and in some cases, optical measurement may be the best, or the only, method. Physical effects that may cause, for example, changes in refractivity are also susceptible to optical detection and measurement. Allied with electronic technology, or with recording processes such as holography, optical techniques can be considerably extended to measure time (or other) derivatives of these quantities and even more sophisticated quantities such as velocity distributions.

Even when a quantity to be measured is essentially static, only a finite energy is required to make the observation, so there does not seem to be any prima facie argument for choosing a CW laser (with, admittedly, a few exceptions!). Further, it is absurd to use, say an argon laser, running all day and consuming many kw of power, for making a few short exposures, or for visual measurements requiring only nanowatts!

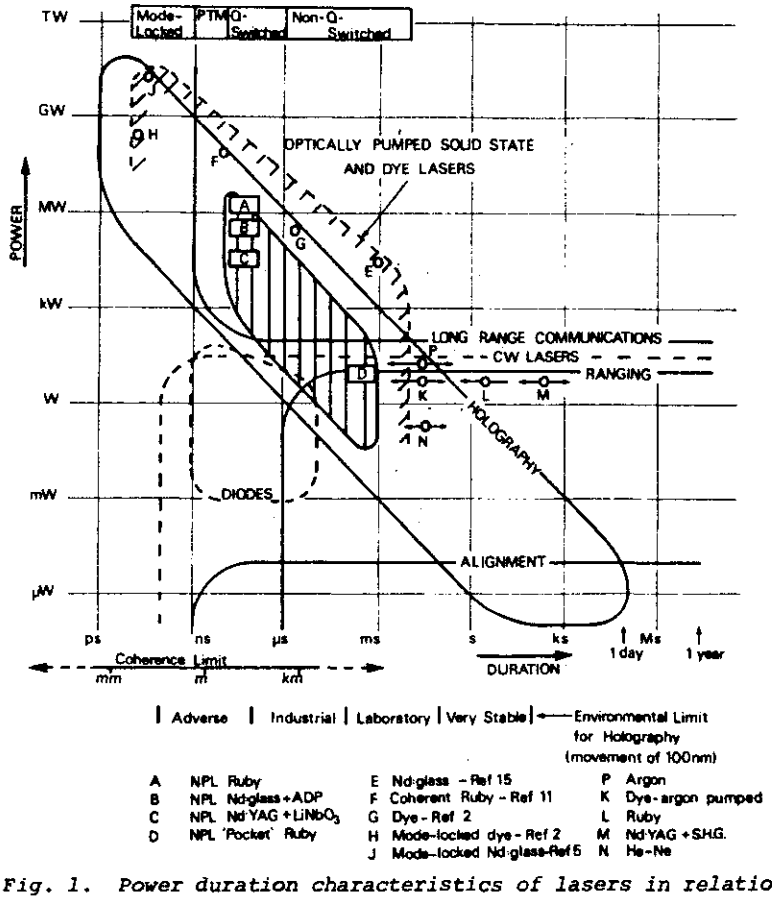


Fig. 1. Power duration characteristics of lasers in relation to potential applications.

Choice Of Lasers

If we therefore include pulsed lasers, there is such a diversity of types of lasers and such an enormous variation in size, power, and function that some types do not overlap at all in capability. Figure 1 shows an attempt to characterize the various types of laser in terms of the peak power plotted against the duration of the laser emission. Lasers with equal energy output are easily distinguished on this diagram, for they lie on straight lines of slope -1 W/s. Continuous-wave lasers are represented, of course, by lines parallel with the duration axis at constant power.

Some areas are indicated that represent the requirements for a number of measurement (and other) applications. The exact positioning of the boundaries leaves much room for argument, but, as an example of the working of this diagram, we can consider the energy required from a laser to record a typical hologram as lying between 1J and 1μJ. Lasers plotted at points below this area cannot be used at the time ordinate that applies; lasers lying above the area are unnecessarily powerful, but could, of course, be used if the output is attenuated.

The maximum exposure time for holography is restricted by movement, vibration, thermal expansion, or other disturbances, and limits are suggested for various environments. Coherence requirements may preclude short duration, limiting the use of lasers on the left of the diagram. We see the region in which lasers most useful for holography should be found, and with [illegible] those lying inside the shaded area are convenient for the holographic recording of most [illegible] interest.

In fact, there are very few lasers available commercially in the favoured area, and the majority of holography so far has been done with CW lasers that have obvious limitations. Similarly, for other measurement applications, it will be seen that there are strong incentives to look more closely at diode lasers[1], at dye lasers[2], and at the smaller varieties of the established ruby and neodymium lasers. We are interested in all of these, but since we have not so far been directly involved with the first two, our paper presents some practical developments of ruby and neodymium systems, with particular reference to uses in holography.

Design Of Lasers For Optical Applications

A given requirement involves a specification of certain laser parameters. These include a) output energy, b) temporal characteristics of the output, c) coherence of the output, d) size and weight, e) output wavelength. Certain combinations of the requirements may prove difficult to meet and this is particularly so in holography when the laser may need to be efficient and lightweight and may be required to deliver a high energy with high tranverse coherence and at a high repetition frequency.

Output energy. The choice of laser parameters for maximum efficiency is made by deriving an equation relating the output optical energy to the input electrical energy and optimizing this equation. Several systems are described later in this paper that have resulted from this analysis. The results show, for example, that one can expect, at best, to obtain 100 mJ (multimode) of light output from ruby and 300 mJ from Nd:glass by optical pumping from a stored electrical energy of 50 J in the capacitor.

Temporal characteristics of the output. Achievement of the required temporal characteristics of the output involves several choices--free running or Q-switched? Type of Q-switch? Method of operating Q-switch (single, double or multiple pulsing, for example)? Continuous or pulsed pumping?

In our work, we have used rotating mirror Q-switches[3] very extensively since they show advantages over other methods in respect to optical quality, insertion loss, and damage threshold. We have also found it possible (perhaps surprisingly) to adapt the rotating mirror for double pulsing, with pulse separations down to a few microseconds, and for multiple pulsing at repetition frequencies up to 25 kHz.

Figure 2 shows some results of comparative measurements on different Q-switches. The rotating mirror is advantageous (see Fig. 2) for high repetition frequency green lasers using Nd:YAG with second harmonic generation and is also capable of producing a higher single mode pulse energy from a ruby laser.

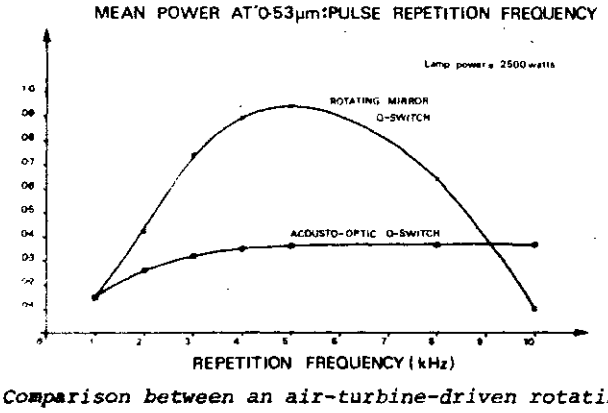


Fig. 2. Comparison between an air-turbine-driven rotating mirror and an acousto-optic crystal as a Q-switch for a high repetition frequency continuously pumped Nd:YAG laser with second harmonic generation.

In applications that entail detection of a highly attenuated signal from the laser, the signal to noise ratio is important and, since this ratio usually increases with peak power, short duration Q-switched pulses are advantageous and pulse-transmission-mode[4] or even mode-locked lasers[5] may be necessary.

Two additional requirements have been considered. A pulsed laser, repetitively fired, can be used very profitably for the preliminary adjustment of auxiliary optical systems and the optimization of the laser itself, and for the visual reconstruction of the pulsed laser hologram. The minimum repetition frequencies required are 2 Hz and 20 Hz respectively.

Coherence of the output. Temporal coherence can be improved to any required degree by the suitable design of a resonant reflector[6], possibly with an intracavity tilted etalon[7], without seriously affecting the laser's efficiency.

The improvement of transverse coherence however is more difficult since attempts to do this with an aperture usually result in a large reduction in laser efficiency[8]. Transverse mode control without such a severe drop in output energy can be achieved by reducing the static and dynamic optical distortions, increasing the ratio of rod length to rod diameter, multiple passing through separated volumes of the rod, designing the resonator to ensure a large single mode volume in the rod.

Attention to these points can lead to a considerable reduction of the size and complexity of the laser. Such a development, however, needs an adequate method of measurement of the coherence of the output, which is often complicated. We have been developing simple measurement techniques using holography[9] that combine a high information storage capability with an intensity readout giving a direct measure of the coherence. An example of such a measurement on a ruby laser is given later and holograms recorded using this laser show that the technique is a valid one.

Size and weight. For many optical applications of pulsed lasers, and particularly those with industrial possibilities, it is usually advisable and often essential to minimize the size and weight of the laser head and its pulsed power supply. One new approach to the fundamentals of the design has produced some significant advances and is incorporated in some of the units described later.

Output wavelength. The wavelength of laser output depends on the active material, so that the choice of laser material is limited by the suitability of its available wavelengths for the requirements of the application and, particularly, by the properties of the detector and recording materials. For some optical applications, the green output obtained by converting the output of a neodymium laser to the second harmonic is more effective than the red output from a ruby laser of comparable input power, in spite of the losses in the conversion process. Further developments of photographic materials and a better choice of existing emulsions may increase further the advantages of the green laser.

Optimum Design For Holography

Achievement of the best holographic performance requires a correct choice of the output energy, its temporal distribution, the coherence, the transverse intensity distribution and the mode stability. There is some flexibility of choice, allowing, for example, a tradeoff between output energy and transverse coherence. This particular tradeoff does not necessarily favour the laser operating in a single transverse mode, as will be shown later in this paper. The requirements for stability have been explored, for example, by Wuerker[10], Ansley[11] and Rogers[12], but our experience suggests that an overrestrictive view is usually obtained.

In one respect, however, published analyses seem to have overlooked one limitation in pulse-to-pulse mode stability that we have found to be most severe in some forms of double-exposure holographic interferometry. When, in the recording process, the optical system comprises two separate stages of diffusion of the illumination (for example, at a diffuser inserted near the source, and at the surface of the object itself), then perfect contrast fringes are only obtainable in the reconstruction if the diffusers are both stationary and the laser mode distribution is exactly repeated.

By the opposite argument, however, there could be a positive advantage in the loss of fringe visibility in some cases. For example, a double exposure hologram without interference effects could be obtained in cases where the change of position of a moving object could be obtained by measuring the coordinates of the images in the reconstruction.

Portable Lasers

It has been demonstrated[13] (Fig. 3) that useful holograms of untreated reflecting objects can be obtained with almost any pulsed solid-state laser, however small or simple.

A laser for such holography can be made, for example, simply by modifying a suitable commercial



Fig. 3. Photograph of the reconstruction from a hologram recorded using a simple pulsed ruby laser. The object, a Stanley knife blade, has a typical engineering surface.

electronic photographic "flash gun," adding only unspecialized components. The original flash tube is retained, but the reflector is replaced by a silvered glass tube surrounding the flash tube and a ruby rod with coated ends, thus forming a small laser head within the body of the unit. A ruby rod 25 mm long by 3 mm in diameter, of no special quality, with its ends coated for 100% and 95% reflectivity at 694 nm, will produce 0.5 mJ of laser output in 500 μs from the 20 J or so stored in the capacitor, using the integral battery. Since the rod is operating near threshold, the output has a useful degree of transverse coherence and a coherence length of about 10 mm. The external dimensions of the flash gun remain unchanged, at 100 x 70 x 40 mm, and the weight of the laser is 300 g. (A laser based on this development will be available from Plasma Electronics Limited, of Slough, Bucks.)

A laser head of this size and design is capable of producing much greater outputs. For example, a capacitor charge equivalent to 50 J stored will produce 7 mJ output. Alternatively, the same rod used in a system fed from a more specialized power supply can be operated repetitively. One such repetitive unit uses an energy storage capacity of 50 J and can be operated at rates up to 20 Hz. The weight is only 12 kg, achieved by using a "transformerless" system charging direct from the 240 VAC mains supply, together with electrolytic capacitors. Cooling permits operation for periods of up to 30 minutes. Another unit, designed to give a flash duration of 150 μs to operate a Nd:YAG laser, charges its capacitors to 20 J at rates up to 25 Hz and weighs only 14 kg.

Laser For Reflection Holography

This laser has been used to record holograms of untreated moving objects having diffusing surfaces and volumes of about 300 mm cube. The basic laser system is shown in Fig. 4. A 100 mm x 10 mm ruby rod (Verneuil grown, of indifferent quality) is pumped by a linear xenon flash lamp in an elliptic cavity, the duration of the flash being between 1 and 2 ms. The resonator is terminated by a roof prism, with Brewster-angle refracting face, at one end and by a single silica-plate resonant-reflector at the other. Temporal mode discrimination is increased further using a tilted intracavity silica etalon, while transverse mode control is introduced when necessary by an aperture. An air-turbine-driven rotating prism[3] running at up to 100,000 rpm Q-switches the laser and results in output pulse lengths of about 25 ns.

The coherence characteristics of this laser are shown in Fig. 5, using one of the methods of Ref. 9, by means of which a direct measure of the transverse coherence is given, representing the distribution of the square of the modulus $|\gamma|^2$ of the normalized function[14] that describes the mutual coherence of the wave field at two selected points. The graph shows that $|\gamma|^2$ nowhere falls below 0.25 in this case, and the Fabry-Perot interferogram indicates a coherence length greater than 500 mm. The energy per pulse is 250 mJ, and holograms of various objects have been recorded on 10E75 plates using this output and a reference to signal ratio of 1.5:1.

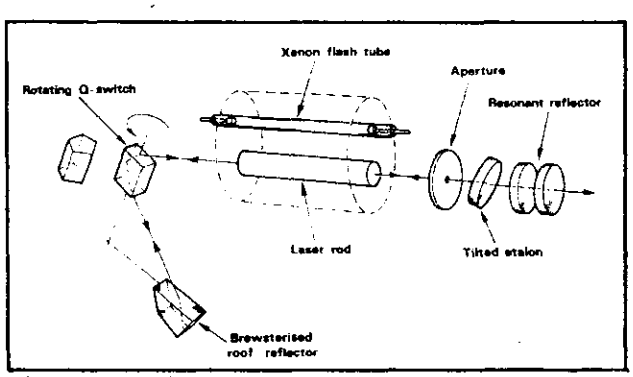


Fig. 4. Basic laser resonator.

The laser described above has been adapted for double pulse operation by using two retro-reflectors

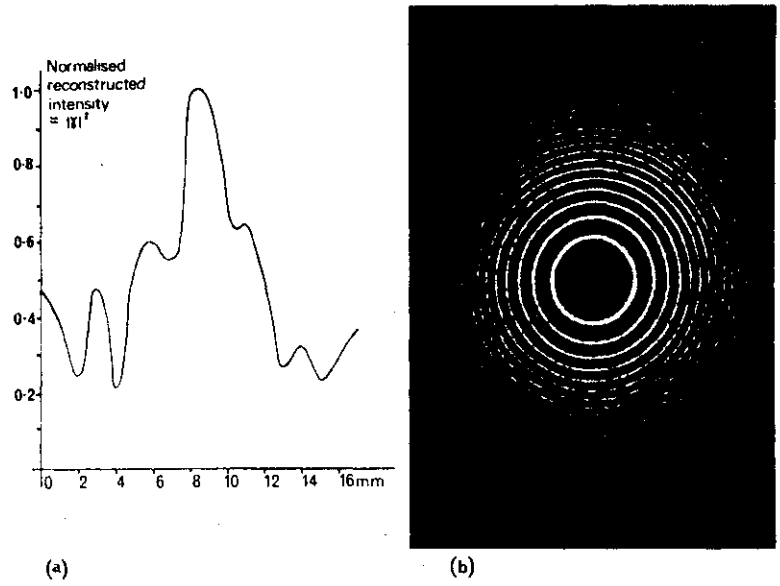


Fig. 5. Coherence of ruby laser used for holography of diffusely reflecting objects. a) Transverse coherence. The square of the modulus of the complex degree of coherence across a diameter of the wave field with respect to the centre point, measured using a holographic technique. b) Temporal coherence. The spectral distribution shown in the Fabry-Perot interferogram (free spectral range = 0.2 cm^{-1}) indicates a coherence length of 500 mm.

with the rotating Q-switch. By varying the angular separation of the roof-prisms and the speed of the Q-switch, pulse separations from a few μs are obtainable. The pulses can be produced from different parts of the rod by a lateral translation of one of the roof-prisms, giving the same energy for each pulse; alternatively, by keeping the two resonators identical but introducing a small loss into the resonator producing the first pulse, two pulses of smaller energy but of identical mode structure are obtained. An aperture of 1.8 mm diameter inside the resonator could be employed in the latter arrangement and was sufficiently small to give even object illumination without a diffuser, while retaining an effective compromise between a need for high output and simple mode structure. The energy per pulse was reduced to about 30 mJ, but this was still sufficient, since the better transverse coherence enabled good holograms to be recorded with less energy at reference-to-signal ratios of 6:1.

Double exposure interference holograms of moving and impact-loaded objects have been recorded, using pulse separations of about 25 μs. Examples of photographs of reconstructions are shown in Fig. 6.

Repetitively Q-Switched Lasers

These lasers enable a series of holograms or photographs to be recorded during a transient event. One of the lasers used is similar to that shown in Fig. 4. The air-turbine rotates an integral five-sided prism at speeds up to a maximum of 300,000 rpm, thus giving a maximum pulse repetition frequency of 25 kHz (pulse separation 40 μs).

A typical pulse train from such a laser with Nd glass as the active material is shown in Fig. 7. The output at 1.06 μm is converted into second harmonic at the more useful wavelength of 0.53 μm in a crystal of ammonium dihydrogen phosphate (ADP), giving a pulse train with 20-30 mJ of green light output. Similar trains of pulses have also been produced from ruby with much higher energy (1-2 J), comparable with the output from a free-running laser of the same dimensions. Both lasers were operated without a restricting aperture.

Figures 8a and 8b show examples of the uses to which these lasers have been put. Photographed reconstructions from holograms of an airgun pellet breaking through a glass plate are seen in Fig. 8a. These reconstructions come from two holograms that are included in a series recorded with a pulse train from the ruby laser. Figure 8b shows a series of photoelastic recordings of a stress wave travelling down a bar of araldite, recorded using the pulse train from a Nd:glass laser converted to the green second harmonic in ADP.

Another laser system investigated has been the CW pumped Nd:YAG laser with second harmonic generation, Q-switched repetitively by the rotating prism turbine shown in Fig. 4. The maximum pulse energy was 0.25 mJ at 3 kHz, and the maximum mean power was 0.9 w at 5 kHz. Mean power above 0.5 w was obtained at all frequencies from 2 kHz to 9 kHz.

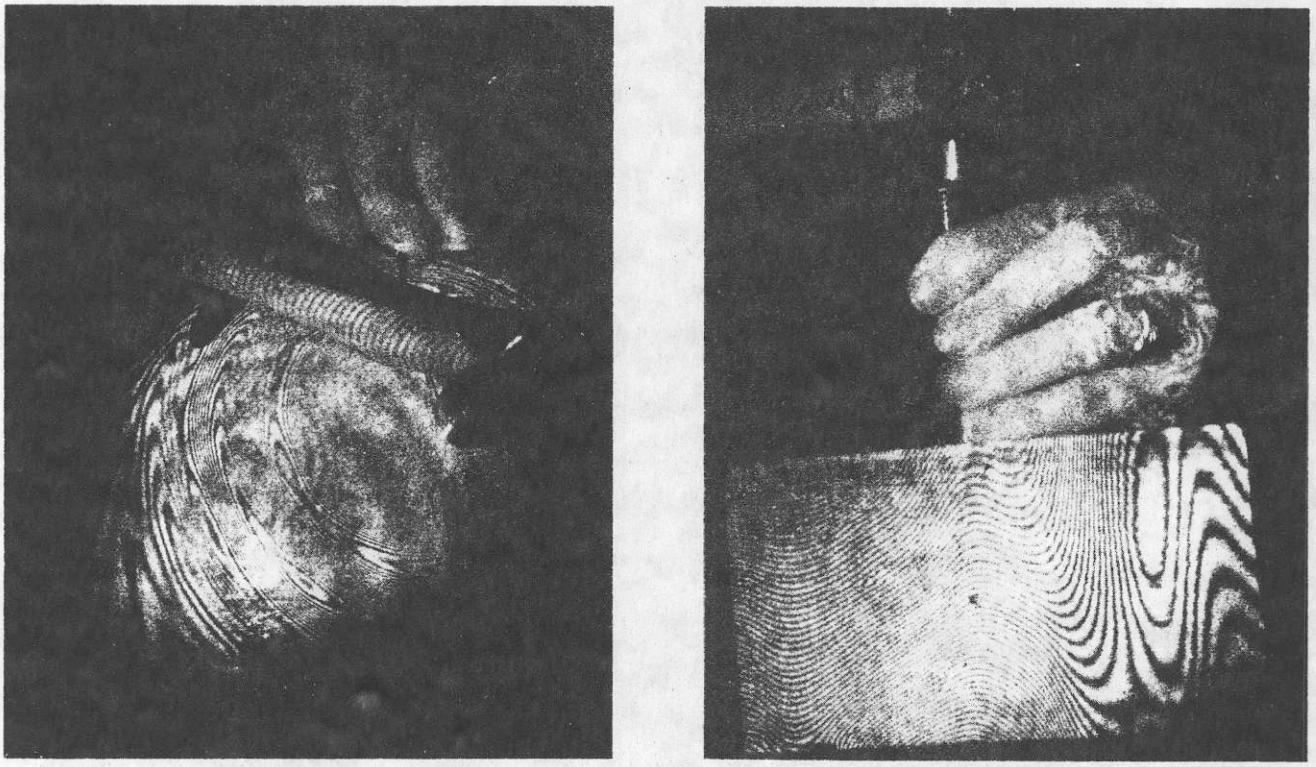


Fig. 6. Double exposure holographic interferograms using double pulse laser. Pulse separation 25 µs. a) Shock waves induced in a motor cyclist's crash helmet by a hammer blow. b) Transient distortion of a piece of blockboard as a result of a nail driven into one edge.

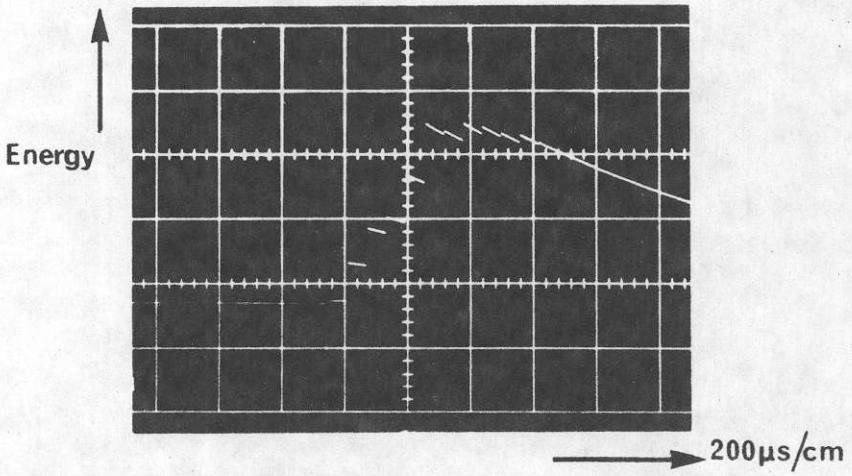


Fig. 7. Oscillogram of a 17 kHz pulse train at 0.53 µm from a repetitively Q-switched Nd:glass laser with second harmonic generation in ADP.

Acknowledgements. The authors acknowledge the assistance of R.F. Stevens and A.S. Butler in the preparation of this paper. They also acknowledge the contribution of R. Penny, Consultants, Chertsey, Surrey, in the design and construction of the portable power supplies and Laser Associates Limited, Rugby, Warks., in the work on comparison of Q-switches.

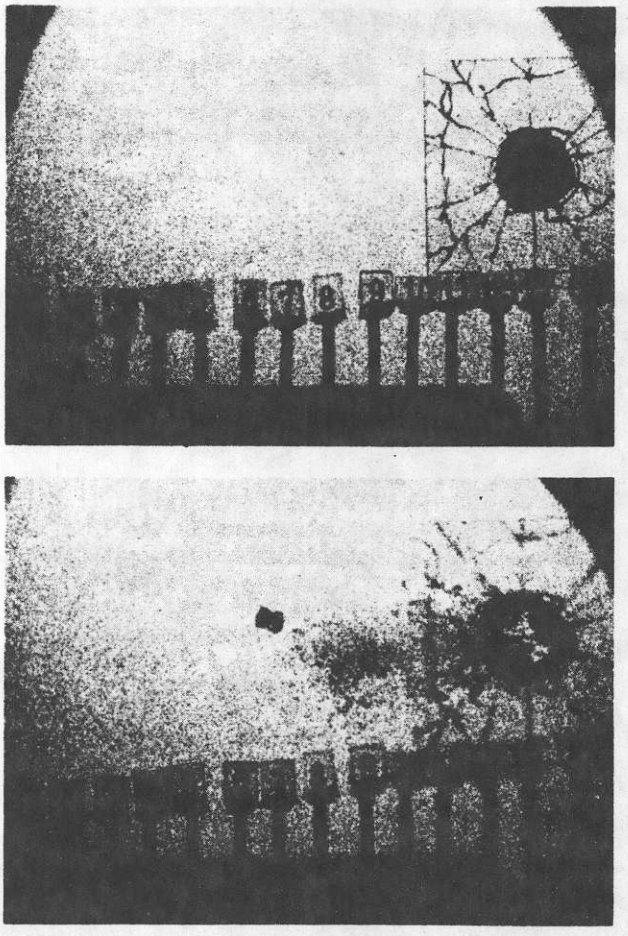


Fig. 8. Examples of optical measurement using a pulse train. a) Photographs of reconstructions from holograms of an air gun pellet fired through a glass plate. The first (top) and seventeenth (middle) holograms were used. b) Photoelastic recordings of the propagation of a stress wave down a transparent bar. Time interval = 55 μs.

References

1. Kressel, H., Lasers, Volume 3, Dekker, 1971.
2. Bradley, D.J., *IEEE Journal of Quantum Electronics, QE7,* p. 270, 1971.
   Bradley, D.J., Proceedings of the Technical Programme, Electro-Optics '71 International Conference, Brighton, England, p. 1, 1971.
3. Gates, J.W.C. and Hall, R.G.N., Proceedings of the Technical Programme, Electro-Optic Systems Design Conference, New York, p. 387, 1970
4. Rundle, W.J., *IEEE Journal of Quantum Electronics, QE.5,* p. 342, 1969.
5. DeMaria, A.J., Glenn, W.H., Brienza, M.J. and Mack, M.E., Proc. IEEE, 57, p. 2, 1969.
6. Burch, J.M., Third International Conference on Quantum Electronics, Paris, *Quantum Electronics, 2,* p. 1187, 1964.
7. Hercher, M., *Applied Optics, 8,* p. 1103, 1969.
8. Hanna, D.C., *Optics and Laser Technology, 2,* p. 175, 1970.
9. Ross, I.N., Proceedings of the Conference on Applications of Holography, Besancon, § 2.4, 1970.
10. Wuerker, R.F., Applications of Holography, Plenum, 1971
11. Ansley, D.A., Applications of Holography, Plenum, 1971
12. Rogers, G.L., *Journal of the Optical Society of America, 61,* p. 784, 1971.
13. Hall, R.G.N., Proceedings of the Conference on Applications of Holography, Besancon, § 9.5, 1970.
14. Born, M. and Wolf, E., Principles of Optics, Pergamon, 1970.

Bibliography

1. Snitzer, E. and Young, C.G., Lasers, Vol. 2, Arnold, 1968.

John Gates is a Senior Principal Scientific Officer at the National Physical Laboratory. His specialities have been interferometry, polarimetry, lasers, and holography.

Roy Geoffrey Noel Hall is Senior Scientific Officer at the National Physical Laboratory. He has been closely concerned with research into pulsed solid state laser design and the application of these devices to engineering holography.

Ian Ross is a Senior Scientific Officer at the National Physical Laboratory and has been a member of the Laser Section since 1966, working on pulsed lasers and holography.

37 SHORT INTERVAL DOUBLE-PULSED HOLOGRAPHY OF REFLECTING OBJECTS

37 HOLOGRAPHIE A DOUBLE IMPULSION A COURT INTERVALLE D'OBJETS REFLECHISSANTS

37 HOLOGRAPHIE REFLEKTIERENDER OBJEKTE MIT HILFE ZWEIER IN KURZEN ZEITABSTÄNDEN AUFEINANDERFOLGENDER IMPULSE

Roy G.N. HALL, John W.C. GATES and Ian N. ROSS
Division of Optical Metrology
National Physical Laboratory
TEDDINGTON, MIDDLESEX, ENGLAND

ABSTRACT

Double exposure holography has proved of considerable value in the analysis of deformation of solid bodies and refractive changes in fluids.

Usually successive exposures have been made with an appreciable time interval, but a much greater range of interesting effects may be observed with a shorter time interval, down to a few microseconds.

A Q-switched laser, giving an exposure time of a few nanoseconds for each pulse, permits the technique to be extended to fast moving events and also allows the examination of objects subjected to impact.

The paper describes some engineering applications and the extension of the method to studying impact loaded regions of the human body.

RESUME

L'holographie à double exposition s'est montrée d'un intérêt considérable dans l'analyse de la déformation de corps solides et des changements d'indice de réfraction dans les fluides.

Ordinairement, on avait fait des expositions multiples avec des intervalles relativement longs, mais on peut observer une gamme plus grande d'effets intéressants avec un intervalle plus court, jusqu'à quelques microsecondes.

Un laser déclenché donnant un temps d'exposition de quelques nanosecondes par impulsion permet d'étendre la technique à des phénomènes rapides et permet l'examen d'objets soumis à un impact.

La communication décrit des applications technologiques et l'extension de la méthode à l'étude de régions du corps humain soumises à des chocs.

ZUSAMMENFASSUNG

Zur Untersuchung der Verformung von Festkörpern und von Brechungsindexänderungen in Strömungen hat sich die Doppelimpulsholographie als sehr nützlich erwiesen.

Normalerweise werden hierzu zwei Aufnahmen in grossen Zeitabständen gemacht. Weit interessantere Effekte sind jedoch nur in kürzeren Intervallen, bis zu einigen Mikrosekunden beobachtbar.

Ein Q-Switch-Laser, der Impulse von einigen Nanosekunden emittiert, gestattet die Ausdehnung dieser Technik zur Beobachtung schnell ablaufender Vorgänge, ebenso ist damit eine Untersuchung stossbelasteter Objekte möglich.

Die vorliegende Arbeit beschreibt einige technische Anwendungen und eine Erweiterung der Methode im Hinblick auf die Analyse von Bereichen des stossbeanspruchten menschlichen Körpers.

INTRODUCTION.

A «frozen fringe» hologram is made by exposing photographic material **twice** to the interference field formed by the interaction between light waves transmitted or reflected by an object and a coherent reference wave. In the reconstruction an interference pattern is formed which reveals any changes that may have occurred between the two exposures. The reconstruction retains all the properties of single exposure holograms, including three dimensional recording, and if a pulsed laser is employed as source, rapidly moving events may be recorded. The advantages of this technique have already been demonstrated in non-destructive testing, stress analysis, plasma research, moving particle distributions and wind tunnel investigations. At previous conferences we have discussed the usefulness of pulsed interferometric holography for the recording of both **transilluminated** events [1-2] and **reflecting** surfaces [3]. Successive exposures have usually been made with an appreciable time interval, but it has become increasingly evident that the recording of two holograms with a very short time separation is a powerful method for obtaining information about transient phenomena, whether this information be velocity, or the rate of change of some other parameter [4-5]. There is, therefore, a demand for double-pulse lasers having adequate coherence for reflection holography and operating with pulse separations from 1 μs to 1 s.

There are advantages in developing the laser source and holographic recording system for such a purpose as a single unit, rather than as two separate units. Varying requirements in the studies to be made (and the variation may be quite large, even in the course of work with one object) are best met by utilising the flexibility of output available from pulsed lasers, and adjusting to the best compromise between pulse duration, output energy, and coherence for each particular requirement. It seems to have been the case frequently in the work of others that specifications for pulsed laser holographic sources have been drawn up to include **all** of the extreme values of the various parameters **simultaneously**, and this has led to performance requirements which are unrealistic, impossible, or at best very costly, to satisfy. We have been successful in recording holograms of transient events on diffusely reflecting three dimensional objects extending in size to about 50 cm^3 using a pulsed ruby laser with just sufficient temporal and transverse mode characteristics.

THE LASER.

The laser (Fig. 1) consists of a 10 mm by 100 mm ruby rod pumped by a linear Xenon flash lamp in an elliptic configuration. Q-switching and double-pulsing is achieved using a 100,000 rpm air turbine rotating prism [6] in conjunction with a double prism assembly [7]. This system provides pulse separations from 10 μs to 500 μs, the upper limit being determined by the duration of the flash envelope. Adequate coherence is achieved by using a single plate silica resonant reflector and a tilted intracavity etalon. We have demonstrated [8] that satisfactory interference holograms can be recorded using this laser in a double-pulse mode with a diffuser placed between the laser and a diffusely reflecting object surface. Although the extra diffuser improves the uniformity of the object illumination and reduces the danger of eye damage it also

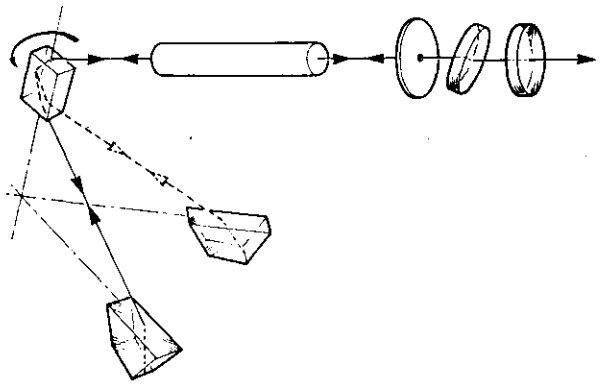


Fig. 1 : Laser resonator, showing Q-switched and double-pulsing arrangement and the coherence controls..

imposes severe restrictions on the stability of the source, the diffuser and the object, if good contrast fringes are to be obtained in the double-exposure hologram.We decided, therefore, to dispense with this first diffuser and to employ an aperture within the laser cavity to improve the uniformity of the illumination on the object. Accordingly, an aperture of 1.8 mm diameter was inserted into the resonator and the resulting Fresnel number of 2.0 had the further effect of restricting the output to just a few transverse modes. The figures 3 to 11, excluding figure 6, show that the transverse, the temporal coherence and the object illumination are adequate for differential holographic interferometry of diffusely reflecting objects.

REFLECTION HOLOGRAPHIC SYSTEM.

The arrangement used is shown in figure 2. It employs a conventional geometry, using the Fresnel reflection and transmission at an uncoated surface as a beamsplitter, negative silica lenses for beam expansion and mirrors for redirection. Reference and signal beams are expanded to cover uniformly both the photographic plate and objects up to half a metre across making the optical path lengths from the laser to plate as nearly equal as possible.

The angle between the reference and signal beams at the hologram is 20°-40° and the ratio between their

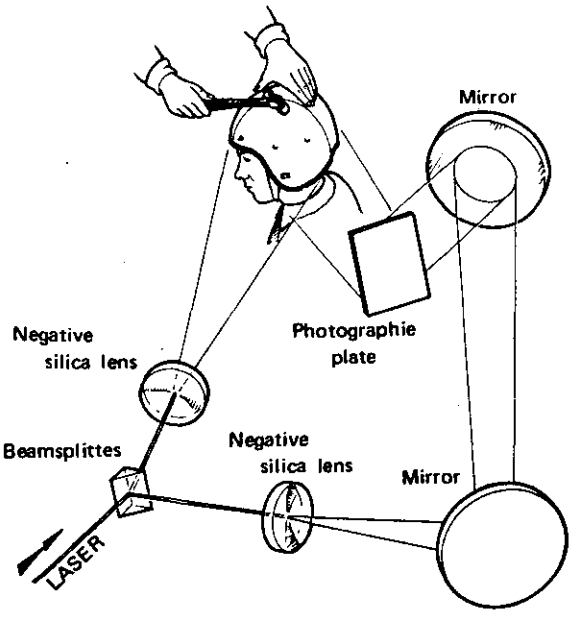


Fig. 2 : Hologram recording arrangement.

energy densities at the hologram plane is about 5 to 1. Agfa Gevaert 9 X 12 cm 10E75 plates have been used and found to require approximately 50 mJm^{-2} (50 erg cm^{-2}) for a density of 0.5. The pulse lengths of 25 ns and pulse separations of 25 μs permitted the experiments to be performed without any mechanical stabilization or anti-vibration measures.

HOLOGRAMS.

Figure 3 shows a spinning fan. The interference pattern is a quantitative indication of the rotational movement of the fan blades. That the fringes are parallel [9] follows from the fact that they are a measure of only the component of motion in the direction bisecting the illuminating and viewing directions. In the example shown the speed of rotation was calculated to be 200 rpm. Loss in contrast of hologram detail occurs if the rate of change of path during the exposure [10] is too high, and, by varying the fan speed up to its maximum, the tolerance on path change was shown to be at least 0.3 wavelength which is consistant with theoretical prediction.

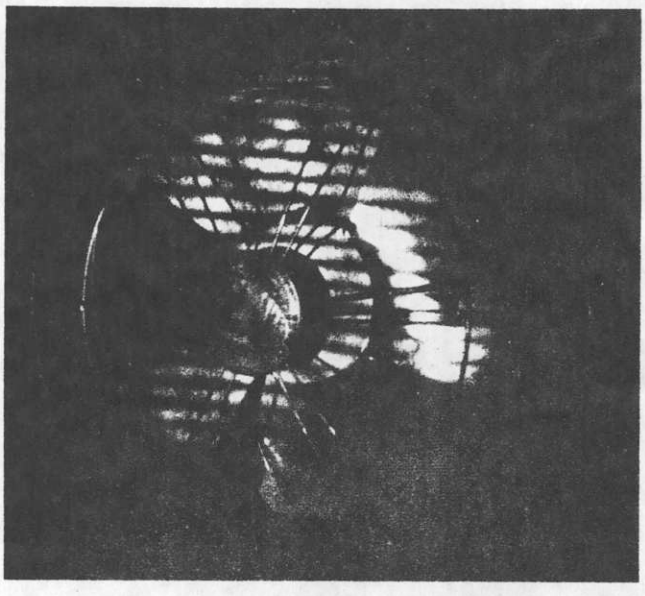


Fig. 3 : Photograph of the reconstruction made from a double-exposure hologram of a spinning fan. Rotation speed 200 rpm, pulse duration 25 ns, pulse separation 25 μs.

Figure 4 shows the transient deformation in a freely suspended mild steel plate, measuring 153 mm wide by 440 mm long and having thickness 6 mm, when struck on its rear face by a light hammer. In this example the first exposure was made just before the plate was struck by the hammer and the second 25 μs later. The amount of deformation (d) present may be calculated from the number of fringes (n) observed, in conjunction with a knowledge of the geometry of the system. In our case, since

$$d = \frac{n\lambda}{2\cos\phi}$$

and $\lambda = 0.6943$ μm and $\phi = 15°$ (half angle between illuminating and viewing directions), the maximum deformation is approximately 10.5 μm.

A 90° vee groove, starting at 9 o'clock at the plate edge and ending in a blind hole centred on the cross was then machined into the metal plate. The form of transient disturbance obtained in this modified structure



Fig. 4 : Photograph of the reconstruction made from a double-exposure hologram of a metal plate showing deformation produced by a hammer blow. Pulse duration 25 ns, pulse separation 25 μs.

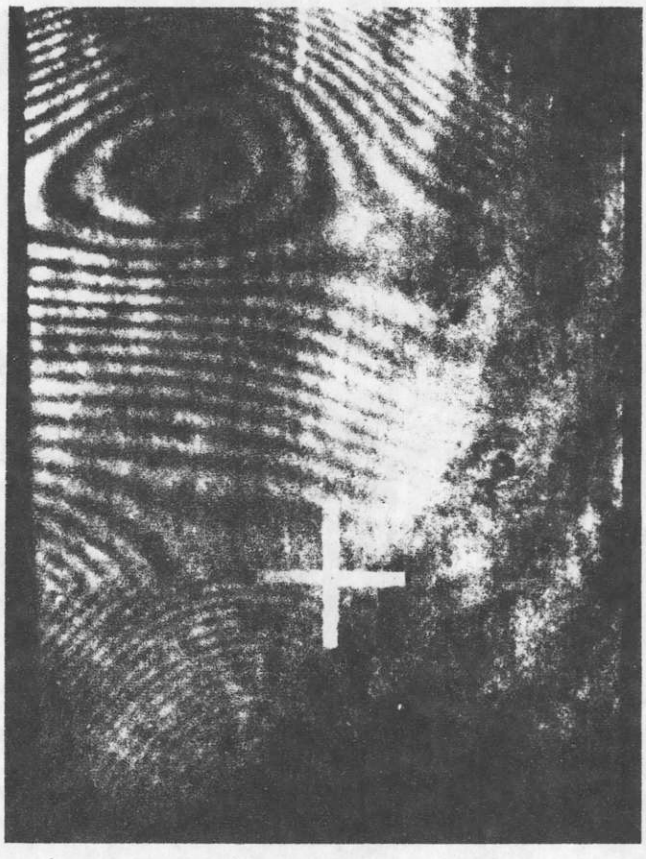


Fig. 5 : Photograph of reconstruction made from double-exposure hologram of metal plate showing deformation produced by hammer blow. Vee groove machined in plate, at rear, 9 o'clock position to cross. Note modified ring system to left of cross indicating groove position. Pulse duration 25 ns, pulse separation 25 μs.

is shown in figure 5 and it is very evident from the fringe discontinuity where the vee groove is located even though it is in the reverse side of the plate and away from the observer.

By way of comparison figure 6 is a photograph of a reconstruction of a conventional time-averaged hologram of this same modified plate. This time, however, the hologram was recorded with a c.w. gas laser and the plate set into a steady vibration mode by means of an electromagnet [11]. The position of the vee groove is indicated by the discontinuity in the fringe pattern to the left of the cross.

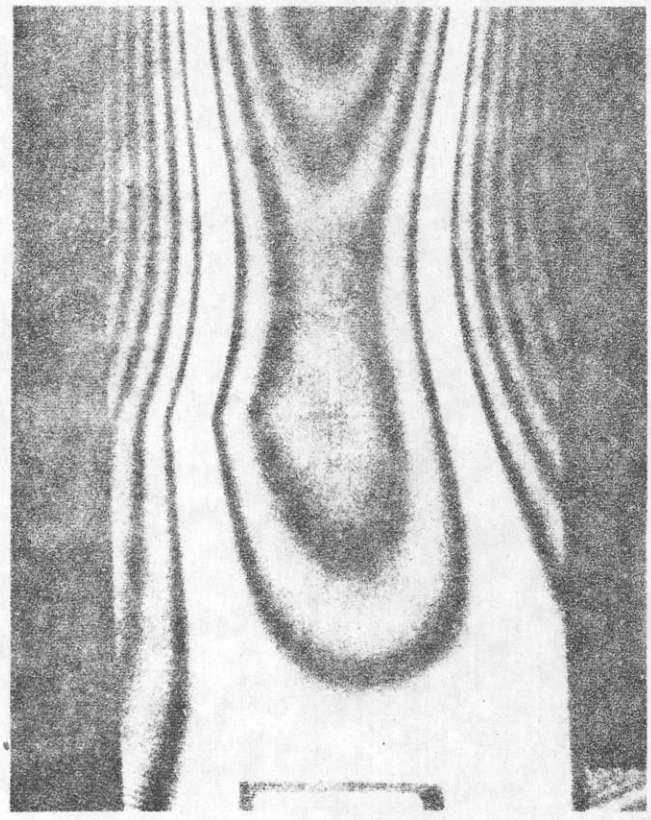


Fig. 6 : Photograph of reconstruction made from hologram produced by conventional time-averaged holography. Plate as in figure 5 and vibrated at 1.5 kHz. Helium-neon laser. Sharp change in fringe pattern to left of cross indicates groove position.

The transient deformation of a motor-cyclist's crash helmet after being struck by a hammer is shown in figure 7. The hologram from which the reconstruction comes was recorded immediately following impact and clearly shows the ripples generated by the hammer blow.

PHYSIOLOGICAL ASPECTS.

Holography when using a Q-switched laser is not limited to inanimate objects and many interesting results can be observed when the double-pulse technique is extended to examine parts of the human body under some form of movement or shock. ZIVI and HUMBERSTONE, for example, have used the technique to examine the chest movement of subjects during inhalation [12]. Figures 8 to 11 show some double-pulse holographic interferograms of live subjects recorded at this laboratory.

Figure 8, for instance, shows the facial movement of one of the authors when struck on the head by a hammer [13] - while wearing a crash helmet, of course ! The movement of the eye ball, under the closed lids, is about



Fig. 7 : Photograph of reconstruction made from a double-exposure hologram of a motor-cyclists' crash helmet showing the effect of a hammer blow on its crown. Pulse duration 25 ns, pulse separation 25 μs.



Fig. 8 : Photograph of a reconstruction made from a double-exposure hologram of a motor cyclists' crash helmet worn by one of the authors, showing the effect of a hammer blow on the helmet. Pulse duration 25 ns, pulse separation 25 μs.

2 μm - a possible method for measuring the shock-absorbing ability of crash helmets !

In figure 9 the head and shoulder of a live subject is shown in the process of breathing out. Body and skin movements are clearly visible.

Figures 10a and 10b are both photographs of reconstructions made of human feet. Figure 10a shows the movement of the parts of the foot when a small jump is executed. The «kinking» in the fringes noticeable on the left foot are presumably associated with ligaments under the skin. In contrast, figure 10b shows skin movements that occur when the board on which the subject is standing is struck sharply by a heavy hammer.



Fig. 9 : Photograph of reconstruction made from a double-exposure hologram of the head and shoulder of a live subject showing the effect on the body of breathing out suddenly. Pulse duration 25 ns, pulse separation 25 μs.

In figure 11 the double-pulsed hologram was made during the course of adjustment of the laser system, and does not involve a separate «object» in the ordinary sense. The recording shows the hand pressing the laser firing button (a plunger switch clasped in the left hand), and a surprising amount of movement of the skin and clothing was revealed.

COMMENTS ON SAFETY ASPECTS.

It is important that extreme care be exercised when making holograms of live subjects to ensure that potentially dangerous levels of illumination are not presented to the eye. The levels recognised as safe are set out in [14] and it is not difficult to keep to these limits for the beams from the object [15] and, more importantly, the reference wave which may be more intense. It is always necessary to make a careful study of the geometry of the system for it is important to realise that laser light may reach type eye by paths other than those of the object beam direction. It has, for example, been pointed out [15] that in certain circumstances the reference beam may be reflected into the eyes of a subject via the surface of the unexposed hologram plate during exposure. A 10 % reflection at such a surface might well result in radiation well above the recommended safety level, reaching the eye.

Once some careful consideration is given to the possible dangers of the proposed experiment it is a simple matter to rearrange the components in such a way that the dangers are completely removed. As a further safeguard it is usually possible to screen the human subjects eyes from potential reflectors of stray radiation, and to provide a non reflecting target on which the gaze is directed.

CONCLUSIONS.

It has been our intention in this paper to show that useful double-pulsed reflection holography can be performed using a fairly simple low output laser. For this reason, the examples have been chosen for their familiarity and the readiness with which the effect can be related to known behaviour. They are not typical, of course, of the kind of studies in which quantitive results are required, but it is inherent in this method that quantitative information can be obtained.



Fig. 10a : Photograph of a reconstruction made from a double-exposure hologram of the feet of one of the authors showing the effect of a small jump. Pulse duration 25 ns, pulse separation 25 μs.

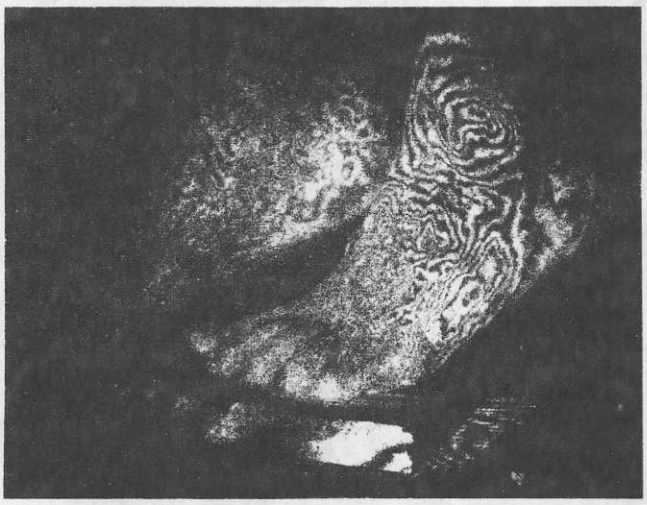


Fig. 10b : Photograph of a reconstruction made from a double-exposure hologram of the same feet, but this time showing the effect produced when the board on which the subject is standing is struck with a hammer. Pulse duration 25 ns, pulse separation 25 μs.

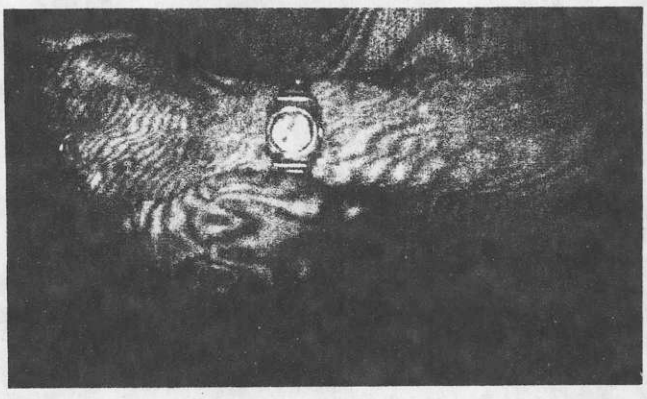


Fig. 11 : Photograph of a reconstruction made from a double-exposure hologram of hands and arm showing the effect produced when the laser firing switch is operated by the left hand. Pulse duration 25 ns, pulse separation 25 μs.

REFERENCES

[1] GATES, J.W.C., HALL, R.G.N., and ROSS, I.N. Proceedings of the 9th International Conference on High Speed Photography, p.5-10, Society of Motion Picture and Television Engineers, (1970).

[2] GATES, J.W.C., HALL, R.G.N., Proceedings of Conference on the Engineering Uses of Holography, p.115-126, Cambridge University Press (1970).

[3] HALL, R.G.N., Proceedings of Conference on Applications of Holography, Besançon, § 9.5, (1970).

[4] HIRTH, A., C.R. Acad. Sci. Paris, B268, 961.

[5] ROTTENKOLBER, H., Werkstatt und Betrieb 103, p.189-193 and 245-246, (1970).

[6] GATES, J.W.C., and HALL, R.G.N., Proceedings of the Technical Program, Electro-Optical Systems Design Conference, New York, p.387-396, (1970).

[7] ROSS, I.N., GATES, J.W.C., and HALL, R.G.N., 10th International Conference on High Speed Photography, (1972).

[8] GATES, J.W.C., HALL, R.G.N., and ROSS, I.N., Optics and Laser Technology p.72-75 (1972).

[9] ALEXANDROV, E.B., and BONCH-BRUEVICH, A.M., Sov. Phys. Tech. Phys. 12, p.258-265, (1967).

[10] NEUMANN, D.B.J., J. Opt. Soc. AM., 58, 447-454, (1968).

[11] STETSON, K.A. and TAYLOR, P.A., J. Phys. E. Sci. Instrum. 4 1009-1015, (1971).

[12] ZIVI, S.M. and HUMBERSTONE, G.H., Medical Research Engineering, p.5-7 (June 1970).

[13] HONEY, R.C., Journal of Occupational Medicine, 10, p.245-246, (1968).

[14] LASER SYSTEMS - Code of Practice, Safety Services Organisation, MoT, (1969).

[15] ANSLEY, D.A., App. of Holography, Plenum Press, New York, London, p.156, (1971).

[16] HALL, R.G.N., GATES, J.W.C., and ROSS, I.N., J. Phys. E. Sci. Instrum, 3, 789-791, (1970).

Appendix to «Short interval double-pulsed holography of reflecting objects» presented at the meeting of the Congress by R.G.N. HALL.

DOUBLE-PULSED STUDIES OF DISTURBANCES IN HORIZONTAL SURFACES.

In the examples of double-pulsed holography prepared before the meeting, the surfaces of the various objects employed were all «diffusing». Light reflected by such surfaces suffers a spatial phase modulation which varies rapidly and randomly across the surface of the object. Motion of the surface between the two recording light pulses is revealed in these examples in the form of a two-beam interference pattern, but good contrast in the pattern is only obtained if the random fine-structure phase variation in the reflected wavefronts remains substantially the same in the two exposures. When the material of the object is not opaque, light is scattered diffusely from the material in a layer below the surface, and if the motion of elements of the material in the layer varies, the contrast may be adversely affected. This may have happened to some extent in figures 8-11 (in the main part of this paper) since the human skin is translucent. Liquids, in which scattering elements may be in rapid random motion, are likely to present some difficulties : for example, the contrast of the interference pattern formed after a double exposure will depend on the duration of each light pulse and on the time interval between the pulses. Figure 12 shows how the previous apparatus was modified to record horizontal surfaces of solid bodies and liquids. The directions of illumination and viewing are equally inclined to the vertical, giving maximum sensitivity to vertical displacements of the surface, and minimum sensitivity to horizontal displacements.

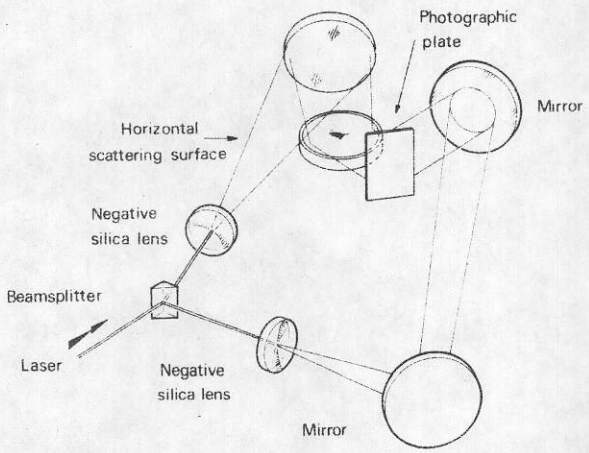


Fig. 12 : Recording holograms of horizontal surfaces.

Figures 13, 14 and 15 show some early experiments to test the effect of motion in liquids. There are obvious qualitative differences in the reconstructions from the holograms, which were all obtained with a time interval of 25 μs and a pulse duration of 25 ns.

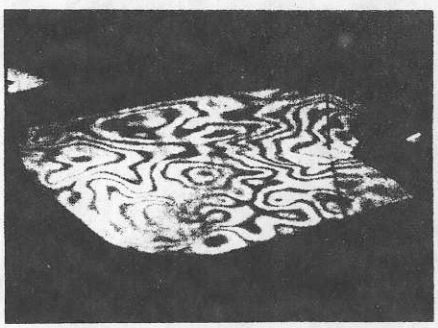


Fig. 13 : Paper surface tapped.

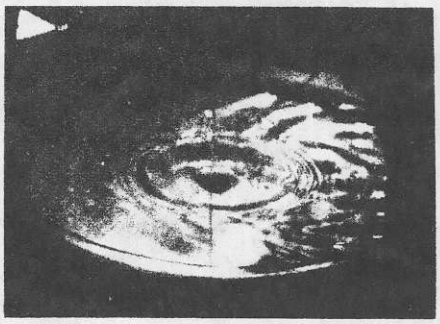


Fig. 14 : Drop of milk, falling into milk.

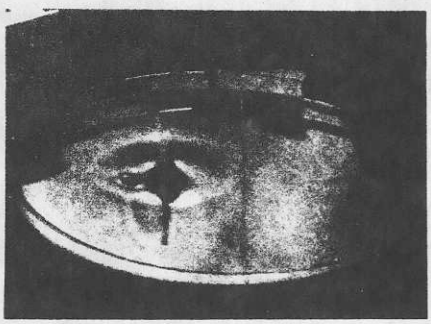


Fig. 15 : Steel ball, into oil/water emulsion.

TIME-SEQUENCE OF MULTI-TIME-DIFFERENTIAL HOLOGRAMS.

A previous paper [16] described a convenient experimental technique for recording a sequence of holograms in order to show (and measure) progressive changes in an object. The same apparatus was used in the present work and employs a holographically - fabricated scatter plate to transilluminate a phase object. Successive areas of the scatter plate are illuminated in sequence, and the hologram is recorded in a plane conjugate with the scatter plate. For convenience the areas may be arranged with radial and circumferential spacing as shown in figure 16.

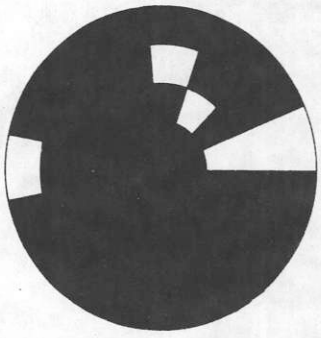


Fig. 16 : Illumination pattern.

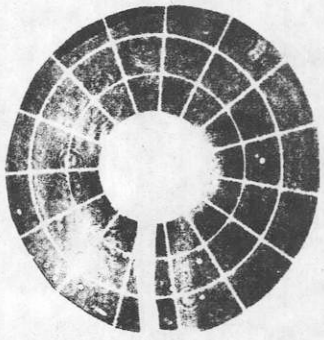


Fig. 17 : Hologram.

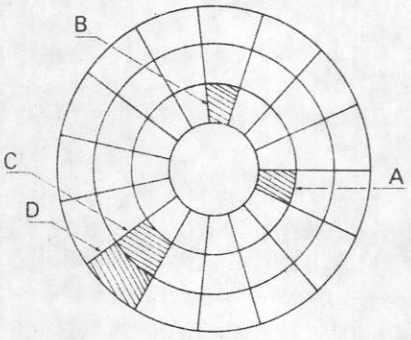


Fig. 18 : Hologram elements selected for (Fig. 19).

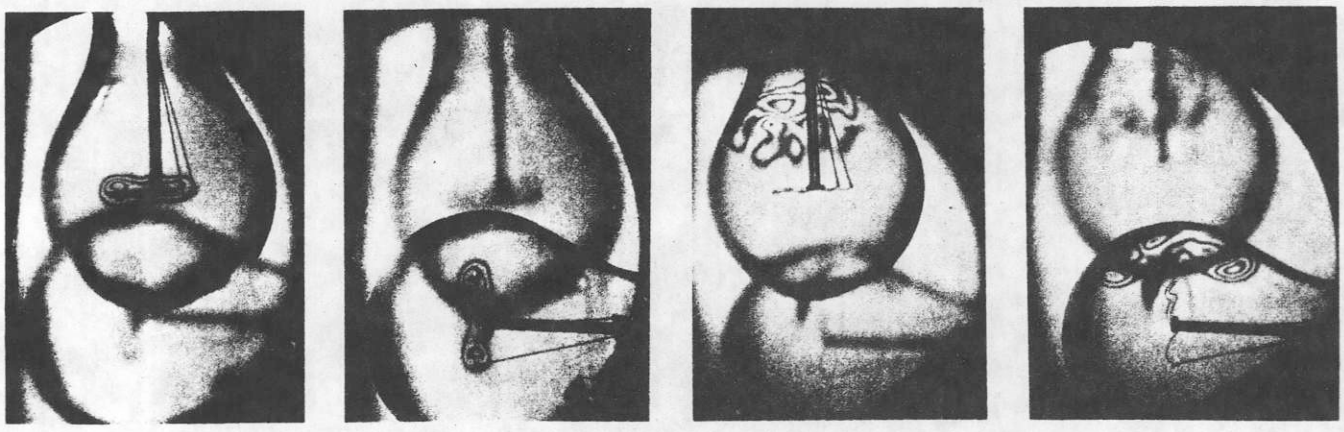
During the exposure, the pattern of illumination (Fig. 16) is rotated one step after each light pulse, giving the record shown in figure 17. The outermost ring has received a sequence of double exposures with an interval of 140 ms. The next ring has received a sequence of double exposures with a 60 ms interval and the innermost ring has received a sequence of double exposures with 40 ms interval.

The three areas on the same radius each received one exposure at the same instant. The spacing round the circle represents a time progression of 20 ms for each interval.

The recording shows the development of gas density changes in a pair of 150 watts gas-filled lamps just after switching on the current through the filaments. The patterns of interference show the different temperature distributions in the two lamps at two stages of the development of the convective flow inside the envelope, and for two simultaneous values of the time-differential of exposure at another stage of the developments.

Thus, the illustration demonstrates a three dimensional record made at successive instants in a time sequence, with three time-differentials. Perhaps it might therefore be claimed that the record is **FIVE-DIMENSIONAL !**

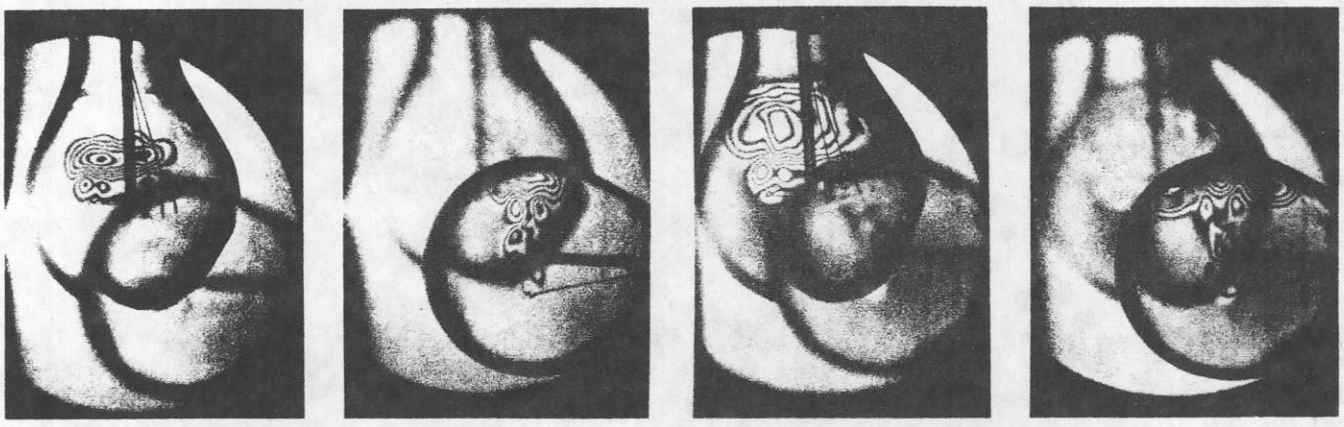
Fig. 19 : Eight photographs of reconstructions from four elements of the hologram shown in figure 17. Each pair of photographs shows two different planes of focus.



Element A ; beginning of sequence.

Element B ; end of sequence.

From the inner ring of hologram elements (Figs 17 and 18), time interval 40 ms.



Element C ; time interval 60 ms.

Element D ; time interval 140 ms.

From elements of the hologram on the same radius (Figs 17 and 18), same elapsed time.

65 PRACTICAL LASERS FOR PHOTOGRAPHIC AND HOLOGRAPHIC RECORDING

65 UTILISATION PRATIQUE DES LASERS POUR ENREGISTREMENTS PHOTOGRAPHIQUES ET HOLOGRAPHIQUES

65 PRAKTISCHE AUSFÜHRUNG VON LASERN FÜR PHOTOGRAPHISCHE UND HOLOGRAPHISCHE AUFNAHMEN

Ian N. ROSS, John W.C. GATES and Roy G.N. HALL
Division of Optical Metrology
National Physical Laboratory
TEDDINGTON, MIDDLESEX, ENGLAND.

ABSTRACT

Pulsed lasers can often be used very profitably as light sources in the study of transient events. Their practicability has often been questioned, however, on grounds of inadequate efficiency and portability, and high costs. These limitations are not insurmountable. Several laser units, we have built and used, are described showing that very useful compact pulsed lasers can be constructed. Requirements on these lasers have come primarily from holographic applications and one of the considerations has been to find the minimum requirements for adequate holographic performance.

RESUME

Les lasers pulsés peuvent souvent être utilisés très utilement comme sources de lumière pour l'étude d'événements transitoires. On a cependant souvent contesté la possibilité de leur utilisation pratique en raison de leur efficacité inadéquate, la difficulté de les transporter, leur prix élevé. Ces limitations ne sont pas insurmontables. Plusieurs unités laser que nous avons construites et mises en œuvre montrent qu'on peut réaliser des lasers pulsés compacts très utilisables. Le besoin pour de tels lasers vient à l'origine des applications holographiques et l'un des buts a été de déterminer les spécifications minimales en vue d'assurer des performances adéquates en holographie.

ZUSAMMENFASSUNG

In vielen Fällen können Pulslaser vorteilhaft als Lichtquellen zur Untersuchung zeitlich veränderlicher Vorgänge eingesetzt werden. Dagegen wurde ihre praktische Verwendbarkeit wegen des geringen Wirkungsgrades, der schlechten Transportierbarkeit sowie der hohen Kostén oft in Frage gestellt. Diese Nachteile sind jedoch nicht unüberwindbar. Es werden einige von uns gebaute und verwendete Lasergeräte beschrieben. Sie zeigen, dass sehr nützliche kompakte Pulslaser gebaut werden können. Die Hauptanforderungen an diese Laser wurden im Hinblick auf die holographischen Anwendungen gestellt, wobei versucht wurde, die für eine geeignete holographische Aufzeichnung minimalen Voraussetzungen zu ermitteln.

INTRODUCTION.

It has been realized for some time that pulsed lasers have much to offer in the field of high-speed recording. The advantages of lasers stem from their capability for high intensity, short duration pulses, from the narrowness of their spectral profile and from the high directionality of their output. Even in situations requiring only one of these properties the laser is often superior to a conventional source. In long distance high-speed photography, for example, the small divergence of the laser output can result in an illuminating and viewing system which is much more efficient with a laser than with a flash source.

In recording techniques requiring a light pulse with not only high directionality but also high monochromaticity and short duration it is often essential to use a pulsed laser. An important technique of this kind is holography and we have been concerned not only with the holographic recording of transient events but also the design of more suitable pulsed lasers for practical applications in this field.

REQUIREMENTS FOR HOLOGRAPHY.

Holography, while placing a stricter requirement on pulse duration and coherence (both spectral profile and directionality are aspects of coherence), also needs greater output energies than is generally required in photography since the fine interference fringe pattern which forms the hologram can only be recorded on slow high resolution recording media. This combination of properties has tended to result in the use of expensive lasers which are so large and heavy that they are not worth moving and only experiments which can be brought to the laser are performed. For many applications of holography, however, the laser should be capable of transportation to the test site, should be robust and should not represent a disproportional capital cost. In our attempts to meet these requirements we have considered the laser and holographic recording technique as an integral unit to be optimized, where the technique can be modified to better suit the laser requirements as well as adjusting the laser parameters to suit the holography. Most of the size and weight of a laser is in the power supply units and as well as minimizing the requirements on the power supplies it has proved to be possible to improve their design so as to give significant reductions in size, weight and cost.

Another requirement of a laser source used in the holographic recording of transient events results from the need, expressed by many workers, for a double-pulse with pulse separations of 1 μs upwards, or even for a pulse train with perhaps ten pulses extending over a millisecond.

In a previous conference [1] we describe the use of a five-sided air-turbine-driven rotating prism Q-switch capable of a millisecond train of up to 20 pulses. An example of the use of such a laser in high-speed photography is shown in figure 1a.

These are photoelastic pictures of a shock wave travelling down a test bar using as the light source a repetitively pulsed Nd : glass laser giving an output at 0.53 μ by virtue of conversion to its second harmonic in a crystal of ammonium dihydrogen phosphate (ADP). A diagram of the laser is shown in figure 1b. The pulse separation in this instance was 55 μs. Further details of this work have been given by Churchward earlier in this conference [2].

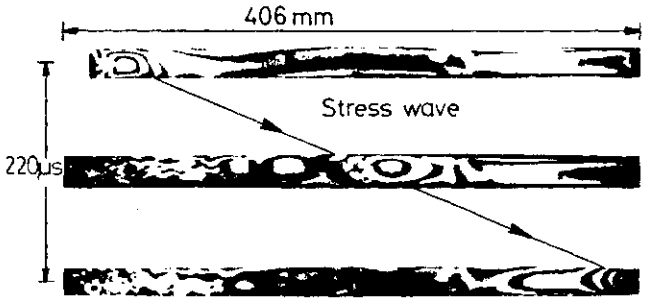


Fig. 1a : Dynamic recordings of a stress wave travelling along a transparent bar (Photoelastic technique).

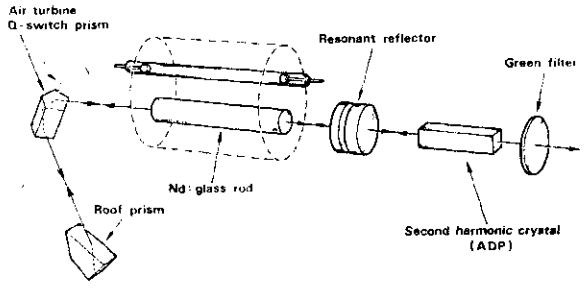


Fig. 1b : Repetitively Q-switched Nd : glass laser with second harmonic generation.

DOUBLE PULSE LASER FOR REFLECTION HOLOGRAPHY.

The usefulness of having a double-pulsing facility with a controllable pulse separation has led us to modify the Q-switch as shown in figure 2. The five-sided prism

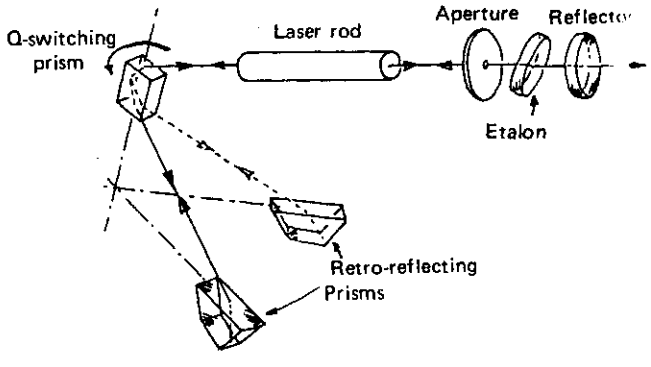


Fig. 2 : Laser design for two Q-switch pulses separated by a short time interval.

is replaced by one of rectangular cross-section having only one polished side face. Two roof prisms are mounted below the spinning turbine so that laser action occurs twice once from each prism, with a time separation equal to the time for the turbine prism to rotate the reflected axial ray from one prism to the other. The time separation can consequently be controlled by changing the angular separation of the prisms with respect to the turbine or by varying the speed of rotation of the turbine. The prism assembly used gave pulse separations down to 10 μs, while the upper limit of 500 μs was set by the duration of the pumping flash. Two methods of obtaining equal pulse energies are possible with this arrangement. A small loss may be introduced in the optical path used for the first pulse only, and, in our case, this was done by placing a wedge (Fig. 3) in front of the appropriate roof prism such that one of the angles of internal reflection in the prism was just below the critical angle. A fraction of the beam is then lost out of the back of the roof prism, this loss being

accurately controlled by rotation of the wedge. In the other method, also illustrated in figure 3, the second prism is translated in a direction normal to the roof-edge and the incident ray so that the axis of generation of the second pulse is translated with respect to that of the first and hence uses a different and yet undepleted volume of the active medium. The second method, although it provides more energy per pulse, cannot be used where exact repeatability of transverse and angular distribution in the output is required from one pulse to the other.

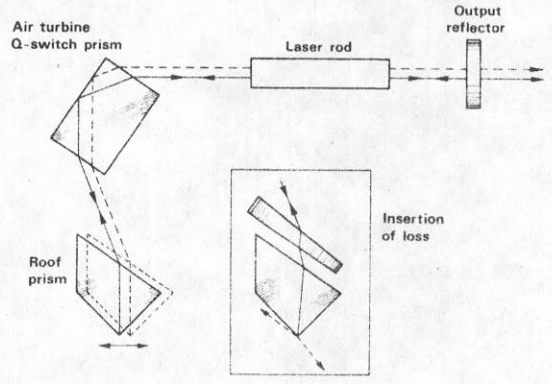


Fig. 3 : Methods of achieving two equal energy pulses from the double-pulse laser.

The use of the turbo-Q-switch laser has been further extended to the holography of diffusely reflecting objects up to 0.5 m across. An increase in coherence length to 25 cm was achieved using a design of resonant reflector as shown in figure 2. This resulted in only a small drop in laser efficiency. The requirement on transverse coherence posed a greater problem since the usual specification for this type of holography is for single transverse TEM_{00} mode (i.e. complete transverse coherence) and the drop in laser efficiency to achieve this coherence was so great (because of the poor optical quality of the ruby rod) that the laser could not supply enough energy. One can show, however, that complete transverse coherence is not essential to the reflection holography of diffusely reflecting

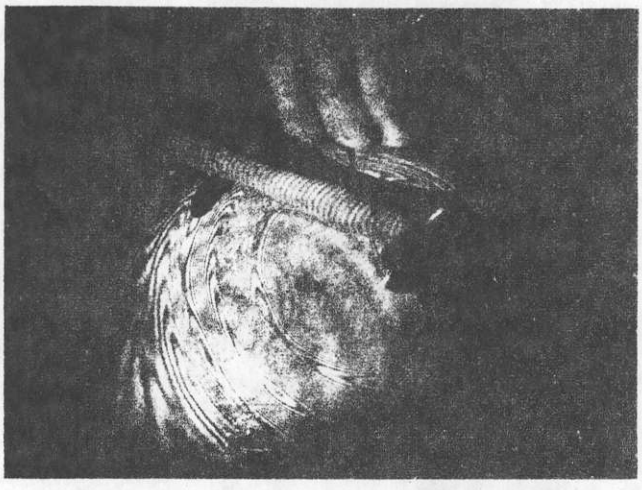


Fig. 4 : Transient disturbance in a motor cyclist's crash helmet following impact from a hammer. Photographed from a double-pulse hologram.

objects and that reduced coherence can be tolerated if more energy is available. Consequently it is possible that optimum operation does not lie with single mode operation if this entails too much reduction in output energy. This is the case with our turbo-Q-switch ruby laser which has a transverse coherence adequate for this holography even in the absence of any aperture mode selection and in this form has an output energy of 250 mJ, again quite adequate for the recording of objects of 0.5 m across. Single exposure holography and double exposure holographic interferometry have been performed with this laser both with and without the double-pulse facility [3]. The double-pulse holography has been described in this conference by Hall [4], and figure 4 shows an example taken from that paper of the stress wave on the surface of a motor cyclist's crash helmet following impact from a hammer.

SMALL LASERS.

It is comparatively rare that holography, or photography, require energies exceeding that possible with the above laser system. The large majority of applications require a very much smaller energy or coherence, as long as proper attention is given to the best design of recording arrangement. Suitable laser sources would be expected to emit in the range 1 to 10 mJ and we have concentrated some effort into designing portable laser systems for operation at these energies. The volume of active material required is small, with rods of length 50 mm or less, and leads to reduced difficulties with respect to heat dissipation, thermal distortion, input power requirements and rod optical quality as well as to increased laser efficiency and lower size and cost. The choice of active material has been left open, the possibilities being ruby, emitting at a wavelenght of 694 nm, Nd : YAG with second harmonic generation emitting at 530 nm and Nd : glass with second harmonic generation also emitting at 530 nm, and the performance of these different media are being compared. The laser can be either free-running or Q-switched depending upon the requirement for pulse duration and the laser must be designed separately for these two alternatives. In particular a simple efficient and reliable Q-switch is required.

The energy to be delivered by and the pulse duration of the power supply vary according to which of the above alternatives is chosen, but there is another important parameter, the charging rate or the pulse repetition frequency. This, along with the energy, determines the mean power requirement which, above any other, determines the size and weight of the unit. For most holographic recording a single shot is used, but if the laser can be repetitively pulsed it can be particularly useful in two ways. The first requires a repetition frequency of > 2 pps and enables the laser to save much time in the initial setting up of the laser itself and of any optical arrangement used in the recording. The second requires a repetition frequency > 20 pps and renders the laser effectively continuous to the eye so that it can be used in the reconstruction of any pulsed holograms particularly those recorded with it. For pumping the small lasers discussed here at more than 20 pps it is necessary to think in terms of a 1 kW mean power capability of the power supply. We have been able to achieve this with very light weight and compact units by (i) eliminating the usual transformer and using direct thyristor controlled charging through a voltage doubler (ii) employing electrolytic capacitors capable of high discharge rates and having low internal losses. Figure 5 shows two such units. One, designed to pump a Nd : YAG laser, delivers 20 J in

150 μs at a maximum repetition frequency of 25 pps and weighs only 14 kg. The other, designed to pump a ruby laser delivers 50 J in 500 μs at a maximum repetition frequency of 20 pps and weighs only 12 kg.

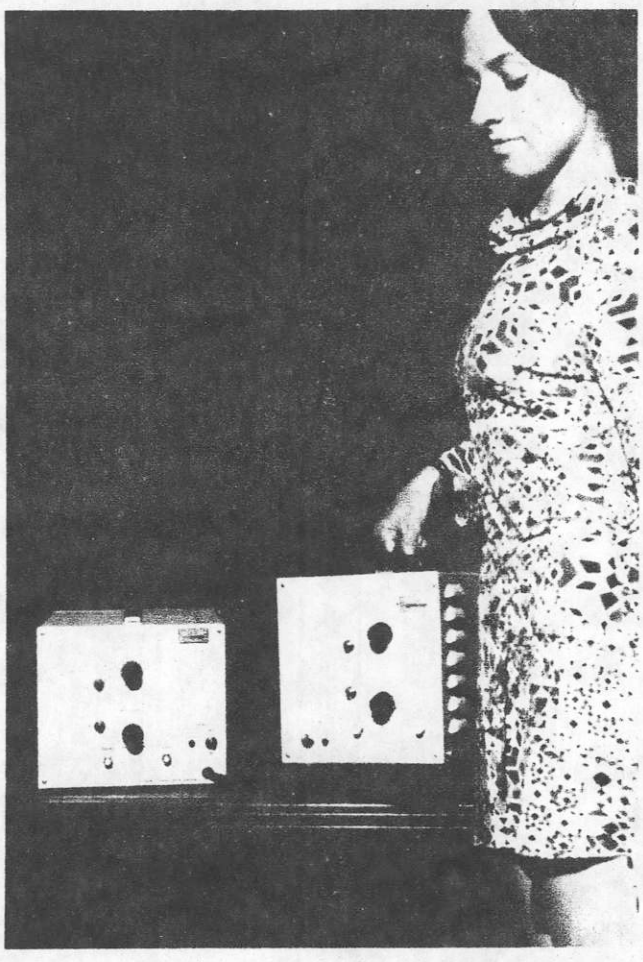


Fig. 5 : Two portable laser power supplies fov repetitive pulsing.

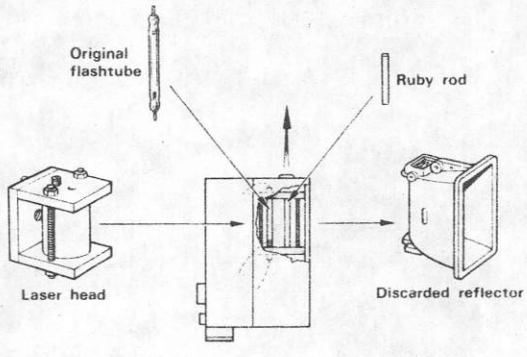


Fig. 6 : Pocket ruby laser.

An example of that can be achieved in producing a useful compact laser of low cost is our "pocket" ruby laser, as shown in figure 6. This single shot device delivers 4 mJ with a useful degree of coherence. It is made simply by modifying a suitable electronic photographic "flashgun". The original flashtube is retained, but the reflector is replaced by a silvered glass tube surrounding the flashtube, while a ruby rod with its ends reflectively coated is inserted parallel to the flashtube inside the glass tube. A small laser head is thus formed within the body of the unit. The ruby rod, 25 mm long by 2 mm diameter made from indifferent quality material and having its ends coated with dielectric multilayers to 100 % and 95 % reflectivity at a wavelength of 694 nm, will produce 4 mJ of laser output in 500 μs from the 25 J stored in the capacitor. Since the rod is operating near threshold its output has a useful degree of transverse coherence and a coherence length of 10 mm. The external dimensions of the "pocket" laser are just those of the original flashgun, 100 X 70 X 40 mm, and its weight is 300 g. The usefulness of this laser is indicated by figure 7 which shows photographs of reconstructions from two holograms ; one, a hologram of a simple engineering surface in reflection (a Stanley knife blade) and the other, a hologram of a fine aerosol of water droplets.

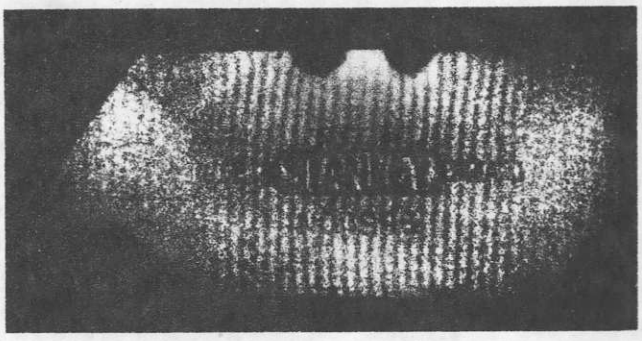


Fig. 7a : Holographic interferogram of a distorted Stanley knife blade. Simple ruby laser recording.

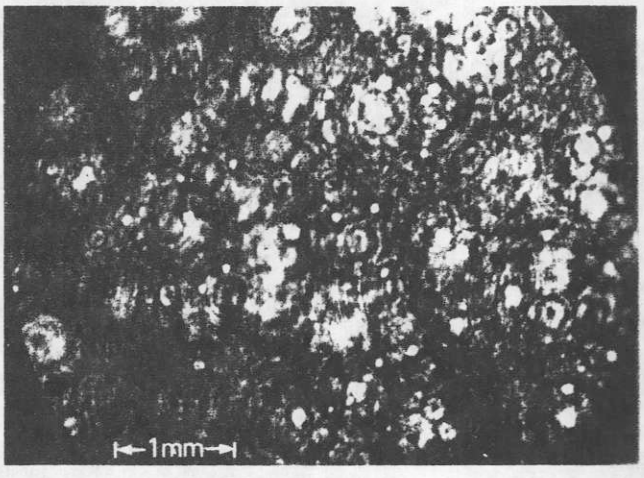


Fig. 7b : Fine water droplets in reconstruction. Hologram recorded using simple ruby laser.

The pulselength of 500 μs was, surprisingly, short enough to record the moving aerosol, but would not of course be short enough for many objects. Further, a very short resonator such as this makes it difficult to achieve a light output with high directionality (the divergence of the pocket laser 5 mrd) and high transverse coherence. Figure 8 shows diagrammatically a laser which incorporates these improvements and is particularly simple and economic [5]. A two inch ruby rod is now used, pumped by a two inch xenon flashtube in an elliptic cylinder cavity. The output reflector is a multilayer dielectric coated

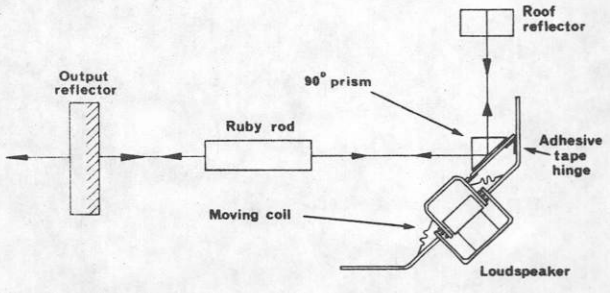


Fig. 8 : Small ruby laser with simple mechanical Q-switch.

to 96% at 694 nm while a good quality roof prism is used as the rear reflector thus making the laser insensitive to angular misalignment when Q-switched with a rotating mirror element. A novel Q-switch of this type is used. It consists of a 90% prism mounted between the moving coil of a small loudspeaker and a fixed support so that the prism is given a rotational impulse when an electrical impulse is sent to the speaker. This electrical impulse is injected simultaneously with the flashtube triggering. The inertia of the prism and moving coil arrangement is adjusted in relationship with the moving coil support (which acts as a restoring force to the deflection) and with the initial angular position of the prism such that the angular velocity is a maximum when the prism brings the resonator mirrors into line and when the gain of the ruby is also a maximum. The Q-switch pulse consequently always occurs at a given time after the flash initiation (jitter ± 10 μs) thus enabling the laser pulse to be timed with respect to an event. This facility is not normally the case with a mechanical Q-switch. The laser when operated in the configuration shown in figure 8 can, with correct adjustment of cavity length, give a single Q-switch pulse of half-width 50 ns and energy 1 mJ. The resonator length was 500 mm. As this length is reduced the number of pulses increases but the output also rises, and when the duration of laser output is 40 μs the output energy is up to 10 mJ. This latter configuration is most useful, when compared to the laser freerunning (20 mJ in 1 500 μs), since with a drop in output of only a factor 2 the duration is reduced by a factor of 38. The power supply for the laser flash tube is a commercial unit built for photographic studios. Although the flash duration is long and results in a long free-running laser pulse and a considerably reduced efficiency (in our case 350 J was being used at twice threshold energy) this disadvantage is more than offset by the cost of the unit (1/10 of typical commercial laser unit) and its weight (5 kg). Other types of Q-switch are possible and have been considered. We have for example tried the natural choice for a simple Q-switch, the bleachable dye. However, at the relatively low powers generated by small lasers, dyes become inefficient and we were not able to achieve a useful energy in single pulse operation.

CONCLUSION.

This paper reports the extension of a laser source to the holography of sizeable objects and to holographic interferometry requiring two pulses separated by a short duration. Also described are two example of simpler, cheaper, and more portable lasers which are useful for a large number of photographic and holographic applications, particularly in the field.

REFERENCES

[1] GATES J.W.C., HALL R.G.N., ROSS I.N. Proceedings of the 8th International Conference on High-Speed Photography, p. 299 - 303, John Wiley & Sons, Inc., (1968).

[2] CHURCHWARD R., (1972), 10th International Conference on High-Speed Photography, Nice.

[3] GATES J.W.C., HALL R.G.N., ROSS I.N. (1972), Optics and Laser Technology, p. 72 - 75.

[4] HALL R.G.N., GATES J.W.C., ROSS I.N. (1972), 10th International Conference on High-Speed Photography, Nice.

[5] ROSS I.N., GATES J.W.C. Submitted for publication.

A small ruby laser with a simple rotating mirror Q switch

I N Ross and J W C Gates
National Physical Laboratory, Teddington, Middlesex

Received 25 September 1972

Abstract A portable Q-switch laser incorporating a simple and inexpensive Q switch and a commercial photographic flashtube power supply is described. This laser has potential uses in high-speed photography and many forms of holography.

1 Introduction

Considerable effort has been put into producing lasers for holography which are capable of meeting all the requirements of this recording technique, however extreme (Ansley 1971). It is possible, for example, to purchase a laser with a Q-switched output of 1 J in a single transverse mode and with a coherence length of several metres. One can also have the facility for double-pulsing the laser, with pulse separations extending from 1 μs upwards and with very high reproducibility of mode. These lasers, however, suffer from the disadvantage of being practically immobile and very expensive. On the other hand, the great majority of photographic and holographic applications (as well as other optical measurement techniques where the detector may be a photodiode or the eye), require very much less energy with greatly reduced requirements on coherence and stability. Such lasers, which should be easily portable and have a price comparable to that of gas lasers, are not commercially available and this note reports on the development of a simple and economic Q-switched ruby laser designed for applications requiring a light pulse of a few millijoules. Possible uses in the field of holography are in the measurement of particle and droplet distributions, in plasma diagnostics and in the nondestructive testing of engineering components. Some examples of these have been given by Wuerker (1971), Pavitt *et al.* (1970), Gates *et al.* (1970) and Hall (1970).

2 The laser

The particular design features of this laser are the mechanical Q switch and the use of a cheap commercial power supply. In other respects the laser design, as shown in figure 1, is not unusual. A 2 in $\times \frac{1}{4}$ in ruby rod of only standard quality is pumped by an E G & G 2 in xenon flashtube in an elliptical cylinder cavity. The rear reflector is a roof prism with a good quality roof edge, and the output reflector is a multilayer dielectric mirror giving a reflectivity of 96% at 694 nm.

2.1 *Power supply*

A particularly lightweight and portable power supply unit can be realized with a ruby laser of this size since (i) the long fluorescent lifetime of ruby ($\sim$4 ms) suggests the possibility of using electrolytic capacitors and (ii) the modest requirement for energy allows the use of a charging voltage less than twice the mains voltage, and this can be achieved by direct charging from the supply without the need for a transformer. Commercial units incorporating both of these features are sold for operating xenon flash lighting in photographic studios. We have selected one suitable to our requirement (Courtenay Majorette Mk III). It delivers up to 400 J in 2–3 ms, weighs 11 lb (5 kg) and costs about one tenth of the price of a typical laser designed unit. It is capable of 100 W mean power output and can, for example, be operated at 50 J and 2 pulses/s. The flashtube was triggered using a third electrode and a larger trigger transformer than is normally used with this power supply unit. A car ignition coil was found to be suitable. The efficiency of pumping the ruby rod was lower than optimum because of (i) dielectric losses in the electrolytic capacitors, (ii) overlong flash duration and (iii) inefficient flashtube operation due both to third electrode triggering and to low charging voltage. This was not a problem, however, since plenty of energy was available from the supply. With the laser non-Q-switched the energy threshold was 170 J stored. At 350 J stored an output of 30 mJ was obtained over a duration of 1·5 ms.

2.2 *Q switch*

The simplest and cheapest type of Q switch is probably the saturable absorber since it consists merely of a cell of dye liquid inside the resonator and requires no external controls. Unfortunately, however, with the low gain and energy available from small lasers such as ours, the dye tends to be inefficient due to incomplete bleaching of the dye absorption. Small residual absorption which cannot be bleached also has a greater effect in a small laser, and if a repetition frequency of more than about 1 pulse/s is required, the dye must be circulated to prevent further reduction in efficiency.

We have in preference devised a simple and inexpensive mechanical Q switch (figure 1). A small 90° prism is mounted between the moving coil and the surrounding metalwork of a small cheap loudspeaker (Radio Spares 2$\frac{1}{2}$ in, 3 Ω general purpose), from which most of the diaphragm is cut away to reduce damping. An electrical signal to the speaker moves one end of the prism out or in and causes the prism to rotate about an axis parallel to its reflecting surface. The Q switch is operated, simultaneously with the triggering of the flashtube, by discharging the energy stored in a capacitor through the speaker coil. A mechanical impulse is thereby given to the

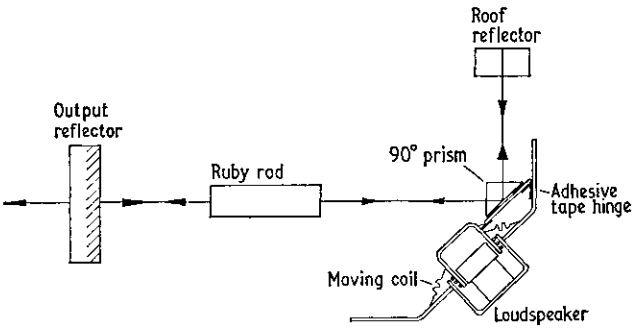


Figure 1 The laser resonator and Q switch

prism, and during the resulting oscillation of the prism it passes through the in-line position and Q switches the laser. Efficient Q switching occurs if the prism comes into line at its maximum angular velocity and at the moment of maximum gain in the ruby rod. These two conditions can be reliably met by correct choice of (i) the rotational inertia of the prism assembly, (ii) its resonant frequency of oscillation, (iii) the restoring force and damping of the oscillation (i.e. the mounting of the moving coil) and (iv) the initial orientation of the prism. With this laser, the maximum gain occurred after 1·2 ms, but this was not critical and the efficiency was approximately constant over the range 1·0–1·5 ms. Figure 2 is a graph of the Q-switch prism's deflection as a function of time and shows that, if the prism is offset by an angle of 11 mrad, the prism has the maximum angular velocity of 28 rad s^{-1} when it Q switches, and this occurs at 1·4 ms. A useful property of this mechanical Q switch is that, unlike most others, satisfactory synchronization of the laser pulse to an event can be achieved. This is because the Q switch is initiated electrically and the laser pulse occurs after a predetermined time which is constant (to within ± 10 μs in our case).

The moving prism is hinged so as to tilt in a predictable and repeatable way, but in any case the use of a roof reflector with two successive reflections at the moving mirror greatly reduces the sensitivity of the system to any displacements of the loudspeaker diaphragm and moving mirror except the rotation required for Q switching.

The relatively low angular velocity of the Q-switching prism tends to give rise to a Q-switch 'open time' long enough to allow multiple pulse operation of the laser. For efficient single pulse operation the open time must be adjusted to be equal to the pulse duration and, in this case, would have to

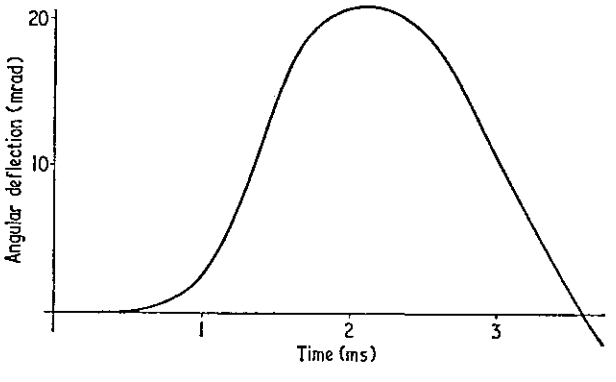


Figure 2 The deflection of the Q-switch prism over the first few milliseconds following initiation

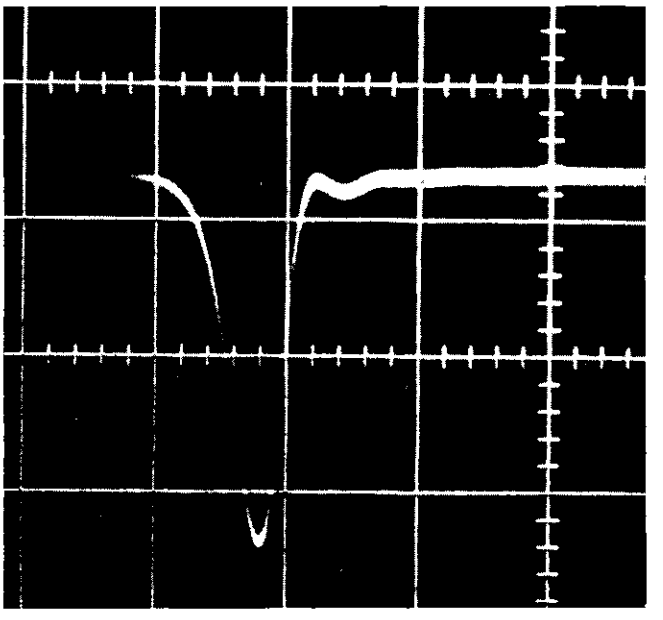


Figure 3 An oscilloscope trace of the laser output power for single-pulse operation: horizontal scale, 100 ns per square; vertical scale, 10 kW per square. The small secondary pulse on the trace is an electrical reflection and should be disregarded

be reduced appropriately. The open time depends on the resonator length and aperture as well as the angular velocity of the Q switch so that if the open time has to be reduced then an increase in the resonator length or a reduction in the aperture are alternatives to an increase in the angular velocity of the Q switch. Figure 3 shows a single Q-switch pulse of half-width 50 ns and energy 1 mJ, obtained when the resonator length was increased to 500 mm.

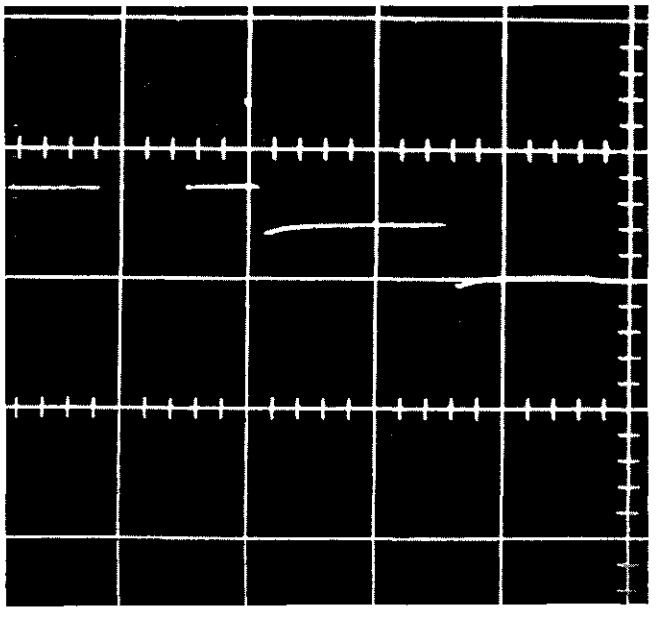


Figure 4 An oscilloscope trace of the integrated laser output for double-pulse operation: horizontal scale, 10 μs per square; vertical scale, 3 mJ per square. The two pulses are represented by the steps in the trace, corresponding to energies of 1·0 and 1·2 mJ respectively with an interval of 15·0 μs. The dimming of the initial part of the trace arises from the triggering process and should be disregarded

If the resonator length or the angular velocity of the prism is reduced, an increasing number of pulses is obtained and the total output energy rises, and although the achievement of a single Q-switch pulse was the primary aim, some of these other forms of output are useful. For example, the laser can be operated to emit two pulses each of energy 1 mJ and with a time separation of 15 μs (figure 4) or, alternatively, if the Q-switch open time is increased considerably, a total output of 15 mJ is obtained in a duration of 50 μs. This represents about half the output energy obtainable with the laser operated without Q switching, but the duration of the pulse train is reduced by a factor of 30.

3 Conclusion

A small Q-switched ruby laser has been designed and built, and is suitable for the many applications in high-speed photography and holography which require only a few millijoules of light energy. The laser incorporates a small moving-coil loudspeaker unit adapted to act as the Q switch, and operates with an inexpensive commercial power supply unit.

Quite a range of modes of operation may be selected by simple adjustments, from a single 1 mJ, 50 ns pulse to 15 mJ, 50 μs pulse train, and double pulsing (1 mJ per pulse, interval 15 μs). There is considerable scope for development in output energy and mode control.

References

Ansley D A 1971 *Applications of Holography* (New York, London: Plenum Press) pp 141–67

Gates J W C, Hall R G N and Ross I N 1970 *Proc. 9th Int. Conf. on High Speed Photography Denver 1970* (New York: SMPTE) pp 4–10

Hall R G N 1970 *Proc. Int. Symp. on Applications of Holography, Besançon* (Besançon: University of Besançon) §9.5

Pavitt K W, Jackson M C, Adams R J and Bartlett J T 1970 *J. Phys.* E: *Sci. Instrum.* 3 971–5

Wuerker R F 1971 *Applications of Holography* (New York, London: Plenum Press) pp 127–39

Journal of Physics E: Scientific Instruments 1973 Volume 6
Printed in Great Britain © 1973